LASER-DOPPLER BLOOD FLOWMETRY

edited by

A.P. Shepherd
P.Å. Öberg

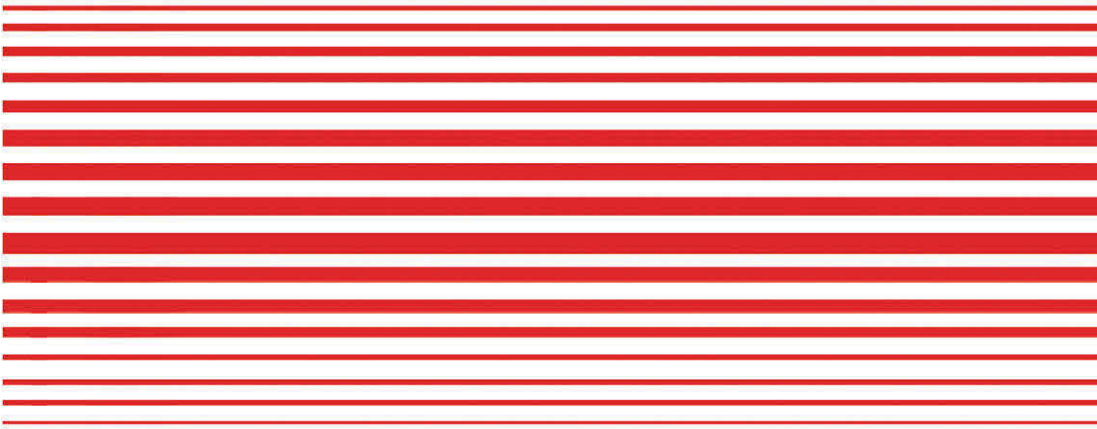

Springer Science+Business Media, LLC

LASER-DOPPLER BLOOD FLOWMETRY

DEVELOPMENTS IN CARDIOVASCULAR MEDICINE

Reiber, J.H.C., Serruys, P.W., Slager, C.L. Quantitative coronary and left ventricular cineangiography. ISBN 0-89838-760-4.
Fagard, R.H., Bekaert, I.E., eds.: Sports cardiology. ISBN 0-89838-782-5. DICM 52
Reiber, J.H.C., Serruys, P.W., eds.: State of the art in quantitative coronary arteriography. ISBN 0-89838-804-X. DICM 53
Roelandt, J., ed.: Color doppler flow imaging. ISBN 0-89838-806-6. DICM 54
van de Wall, E.E., ed.: Noninvasive imaging of cardiac metabolism. ISBN 0-89838-812-0. DICM 55
Liebman, J., Plonsey, R., Rudy, Y., eds.: Pediatric and fundamental electrocardiography. ISBN 0-89838-815-5. DICM 56
Higler, H., Hombach, V., eds.: Invasive cardiovascular therapy. ISBN 0-89838-818-X. DICM 57
Serruys, P.W., Meester, G.T., eds.: Coronary angioplasty: a controlled model for ischemia. ISBN 0-89838-819-8. DICM 58
Tooke, J.E., Smaje, L.H., eds.: Clinical investigation of the microcirculation. ISBN 0-89838-833-3. DICM 59
van Dam, Th., van Oosterom, A., eds.: Electrocardiographic body surface mapping. ISBN 0-89838-834-1. DICM 60
Spencer, M.P., ed.: Ultrasonic diagnosis of cerebrovascular disease. ISBN 0-89838-836-8. DICM 61
Legato, M.J., ed.: The stressed heart. ISBN 0-89838-849-X. DICM 62
Safar, M.E., ed.: Arterial and venous systems in essential hypertension. ISBN 0-89838-857-0. DICM 63
Roelandt, J., ed.: Digital techniques in echocardiography. ISBN 0-89838-861-9. DICM 64
Dhalla, N.S., Singal, P.K., Beamish, R.E., eds.: Pathophysiology of heart disease. ISBN 0-89838-864-3. DICM 65
Dhalla, N.S., Pierce, G.N., Beamish, R.E., eds.: Heart function and metabolism. ISBN 0-89838-865-1. DICM 66
Dhalla, N.S., Innes, I.R., Beamish, R.E., eds.: Myocardial ischemia. ISBN 0-89838-866-X. DICM 67
Beamish, R.E., Panagia, V., Dhalla, N.S., eds.: Pharmacological aspects of heart disease. ISBN 0-89838-867-8. DICM 68
Ter Keurs, H.E.D.J., Tyberg, J.V., eds.: Mechanics of the circulation. ISBN 0-89838-870-8. DICM 69
Sideman, S., Beyar, R., eds.: Activation metabolism and perfusion of the heart. ISBN 0-89838-871-6. DICM 70
Aliot, E., Lazzara, R., eds.: Ventricular tachycardias. ISBN 0-89838-881-3. DICM 71
Schneeweiss, A., Schettler, G.: Cardiovascular drug therapy in the elderly. ISBN 0-89838-883-X. DICM 72
Chapman, J.V., Sgalambro, A., eds.: Basic concepts in doppler echocardiography. ISBN 0-89838-888-0. DICM 73
Chien, S., Dormandy, J., Ernst, E., Matrai, A., eds.: Clinical hemorheology. ISBN 0-89838-807-4. DICM 74
Morganroth, J., Moore, E. Neil, eds.: Congestive heart failure. ISBN 0-89838-955-0. DICM 75
Heintzen, P.H., Bursch, J.H., eds.: Progress in digital angiocardiography. ISBN 0-89838-965-8.
Scheinman, M., ed.: Catheter ablation of cardiac arrhythmias. ISBN 0-89838-967-4. DICM 78
Spaan, J.A.E., Bruschke, A.V.G., Gittenberger, A.C., eds.: Coronary circulation. ISBN 0-89838-978-X. DICM 79
Bayes de Luna, A., ed.: Therapeutics in cardiology. ISBN 0-89838-981-X. DICM 81
Mirvis, D.M., ed.: Body Surface Electrocardiographic Mapping. ISBN 0-89838-983-6.
Visser, C., Kan, G., Meltzer, R., eds.: Echocardiography in coronary artery disease. ISBN 0-89838-979-8. DICM 80
Singal, P.K., ed.: Oxygen Radicals in the Pathophysiology of Heart Disease. ISBN 0-89838-375-7. DICM 86
Iwata, H., Lombardini, J.B., Segawa, T., eds.: Taurine and the heart. ISBN 0-89838-396-X. DICM 93
Mirvis, D.M., ed.: Body surface electrocariographic mapping. ISBN 0-89838-983-6. DICM 82
Morganroth, J., Moore, E.N., eds.: Silent myocardial ischemia. ISBN 0-89838-380-3. DICM 88

LASER-DOPPLER BLOOD FLOWMETRY

Edited by
A.P. SHEPHERD
P.Å. ÖBERG

Springer Science+Business Media, LLC

Library of Congress Cataloging-in-Publication Data

Laser-Doppler blood flowmetry / edited by A.P. Shepherd, P.Å. Öberg.
p. cm. — (Developments in cardiovascular medicine; DICM 107)
ISBN 978-1-4419-4745-1 ISBN 978-1-4757-2083-9 (eBook)
DOI 10.1007/978-1-4757-2083-9

1. Blood flow—Measurement. 2. Laser Doppler blood flowmetry. I. Shepherd, A.P. (Albert P.) II. Öberg, P. Åke. III. Series: Developments in cardiovascular medicine; v. 107.
[DNLM: 1. Blood Flow Velocity. 2. Echocardiography, Doppler. 3. Lasers—diagnostic use. 4. Ultrasonic Diagnosis. W1 DE997VME v. 107 / WG 106 L343]
RC691.6.B55L37 1989
616.1'07543—dc20
DNLM/DLC 89–24473
for Library of Congress CIP

Originally published by Kluwer Academic Publishers in 1990.
Softcover reprint of the hardcover 1st edition 1990

DEDICATION

To the memory of our friend

Sven Malmström

whose vitality, entrepreneurial skills, and generosity
spread the art of laser-Doppler blood flowmetry
around the world.

CONTENTS

LIST OF CONTRIBUTORS

Andreas Bircher
Department of Dermatology
University Hospital
Basel, Switzerland

Robert F. Bonner
Biomedical Engineering and Instrument Branch
National Institutes of Health
Bethesda, Maryland 20014

John A. Borgos
TSI, Inc.
Medical Instruments Group
2963 Yorktown Boulevard
St. Paul, Minnesota 55117

Howard M. Druce
Division of Allergy and Immunology
St. Louis University Medical Center
St. Louis, Missouri 63104

Bengt Fagrell
Department of Medicine, Section of Angiology
Karolinska Institute, Box 60500
S-104 01 Stockholm 60, Sweden

Juan E. Grunwald
Scheie Eye Institute
51 North 39th Street
Philadelphia, Pennsylvania 19104

Richard H. Guy
Department of Pharmacy and Pharmaceutical Chemistry
University of California
San Francisco, California 94143

Per Hedén
Department of Plastic Surgery
Karolinska Hospital
S-104 01 Stockholm 60, Sweden

Sölve Hellem
Department of Oral Surgery
University of Linköping
S-581 85 Linköping, Sweden

G. Allen Holloway, Jr.
Department of Medicine
Maricopa Medical Center, Box 5099
Phoenix, Arizona 85010

John M. Johnson
Department of Physiology
University of Texas Health Science Center
San Antonio, Texas 78284

J.W. Kiel
Department of Physiology
University of Texas Health Science Center
San Antonio, Texas 78284

Julian H. Lombard
Department of Physiology
Medical College of Wisconsin
Milwaukee, Wisconsin 53226

Howard I. Maibach
Department of Dermatology
University of California
San Francisco, California 94143

Josef M. Miller
Kresge Hearing Research Institute
1301 E. Ann Street
Ann Arbor, Michigan 48109–0506

Gert E. Nilsson
Department of Biomedical Engineering
University of Linköping
S-581 85 Linköping, Sweden

Ralph Nossal
Physical Sciences Laboratory
National Institutes of Health
Bethesda, Maryland 20014

Alfred L. Nuttall
Kresge Hearing Research Institute
1301 E. Ann Street
Ann Arbor, Michigan 48109–0506

P. Åke Öberg
Department of Biomedical Engineering
University of Linköping
S-581 85 Linköping, Sweden

Benno L. Petrig
Scheie Eye Institute
51 North 39th Street
Philadelphia, Pennsylvania 19104

Stanley I. Rapoport
Laboratory of Neurosciences
Building 10, Room 6C103
National Institute of Aging
Bethesda, Maryland 20892

Charles E. Riva
Scheie Eye Institute
51 North 39th Street
Philadelphia, Pennsylvania 19104

Richard J. Roman
Department of Physiology
Medical College of Wisconsin
Milwaukee, Wisconsin 53226

E. Göran Salerud
Department of Biomedical Engineering
University of Linköping
S-581 85 Linköping, Sweden

A.P. Shepherd
Department of Physiology
University of Texas Health Science Center
San Antonio, Texas 78284

Michael D. Stern
Division of Cardiology
Johns Hopkins University
Baltimore, Maryland 21205

Karel Tyml
Department of Biophysics
University of Western Ontario
London, Canada N6A 5C1

Kishena C. Wadhwani
Laboratory of Neurosciences
Building 10, Room 6C103
National Institute of Aging
Bethesda, Maryland 20892

PREFACE

The dance along the artery
The circulation on the lymph
Are figured in the drift of stars.
T.S. Eliot

Die Methode ist alles.
Carl Ludwig

In physiology a spirit of finesse
is required.
Claude Bernard

Armed with modern Doppler instrumentation, scientists can now quantify the red blood cell's "dance along the artery" as well as "the drift of stars." In disciplines of science and medicine ranging from cardiology to astronomy, the Doppler principle now provides invaluable velocity measurements in the microcosm of capillary beds and in the cosmos. The newest application of the ubiquitous Doppler principle, laser-Doppler velocimetry, has been used to measure blood flow in tissue for just a few years, but we perceived that, like most new techniques, the birth of laser-Doppler blood flowmetry was not easy, nor was it likely to pass through infancy and reach maturity without difficulty. In physiology and medicine, better techniques for measuring blood flow are constantly in demand, but they often exhibit an unfortunate boom-and-bust cycle: widespread acceptance and uncritical use are soon

followed by studies delineating the limits of the method's validity. The technique is then abandoned for the next more fashionable one, thus proving Ludwig's dictum that a given method is everything or nothing depending upon whether one can believe the data it yields.

Our work on laser-Doppler velocimetry (LDV) measurements of tissue perfusion began soon after the method's inception at the National Institutes of Health in the mid-1970s. In fact, we had the good fortune to learn of it and to begin investigating how it could be used well before commercial instruments became available. After the early publications appeared, what astonished us was the great diversity of applications for which investigators wanted to use LDV blood flowmetry and the enthusiasm with which the method was received by both the scientific and clinical communities. Because our laboratories were among the first to employ this new technique, other investigators contemplating its use sometimes sought our advice. Questions that we were asked to answer were bewildering. Investigators inevitably wanted to know whether the method would measure blood flow in their particular organ or tissue of interest, and they often asked if the fiber optic flow probes could be fashioned into a different configuration for some specialized purpose. We were even asked by instrument manufacturers to estimate the market for clinically applicable LDV blood flowmeters.

This experience convinced us of several things (not the least of which was the need for this book). First, no one could possibly envision the many nascent uses of LDV blood flowmetry. Indeed, in the next several years, many new clinical and research applications were found for LDV blood flowmetry, and we are still convinced that many applications remain yet to be discovered. Second, there was considerable confusion about the technique. Even the instrument manufacturers were unaware that subtle differences in the optical designs of LDV blood flowmeters could profoundly affect their performance in certain tissues. Similarly, many biomedical investigators who wished to use the new technique were unschooled in the relevant physical principles, naive about the method's limitations, and unaware of its untapped potential. These observations led us to fear that because of the conceptual complexity of the method, it could be applied inappropriately, thereby yield invalid data, and be discredited without thorough and fair evaluation.

Our goal in this book is to communicate both the promise and pitfalls of LDV blood flowmetry to the potentially large segment of the biomedical community that will eventually employ the technique. The book begins with a brief overview of the history of the scientific discoveries and technological developments that make laser-Doppler blood flowmetry possible. The chapters that immediately follow provide a firm basis in optical theory and practical guidance for the clinician or beginning investigator. A complete synopsis of commercially available instrumentation provides a useful comparison and contrast of features and technical specifications of state-of-the-art LDV blood flowmeters. Finally, the later chapters of the book contain

descriptions and critiques of identified applications of LDV flowmetry. In choosing topics for these chapters, we did not try to produce an encyclopedic compendium of every identified application of LDV blood flowmetry, but, rather tried to treat only those that were vastly superior to conventional methods or those that by example would light the way for others. With this book, we hope, above all, to secure a permanent place for LDV blood flowmetry in the armamentarium of biology and medicine, so that present and future investigators can measure tissue perfusion with speed, accuracy, convenience—and perhaps even with finesse.

San Antonio and Linköping

LASER-DOPPLER BLOOD FLOWMETRY

1. HISTORY OF LASER-DOPPLER BLOOD FLOWMETRY

A.P. SHEPHERD

The best-known applications of the Doppler principle in biology and medicine are a series of different techniques for assessing blood flow from the Doppler shift that sound waves experience when they travel through the blood flowing in a relatively large blood vessel. One of the chief advantages that Doppler ultrasound techniques such as pulse-echo scanners offer, besides their noninvasiveness, is their ability to produce images of the heart and major blood vessels. However, it is impractical to use Doppler ultrasound methods to measure blood flow in what is arguably the most important part of the cardiovascular system: the microcirculation—in other words, within the tissues nourished by invisibly small blood vessels. Therefore, ultrasound methods are incapable of measuring blood flow at the edge of a healing gastric ulcer, in the torso skin of a burn patient, in the nasal mucosa of an allergy sufferer, or in a skin flap after plastic surgery.

By contrast, these promising applications and many others are possible if laser light is used instead of sound. Light is capable of measuring the velocities of red blood cells even at the relatively slow speeds with which they move through capillaries. Laser-Doppler blood flowmetry thus utilizes the short wavelengths or extremely high frequencies of visible and infrared light to measure tissue perfusion by exploiting the Doppler shifts that moving red blood cells impart to light. The spectral purity of the laser makes it practical to detect the slight frequency shifts produced by the interactions between photons and moving red blood cells. In its relatively short history, the

laser-Doppler principle has been used in several different ways to measure blood flow. The primary implementations of laser-Doppler blood flowmetry are the following instruments or techniques, illustrated in figures 1–1 to 1–4:

Laser-Doppler blood flowmetry in tissue	(figure 1–1)
Laser-Doppler microscopes	(figure 1–2)
Retinal velocimeters	(figure 1–3)
Laser-Doppler catheter velocimeters	(figure 1–4)

The main purpose of this book is to treat at length the most promising and most widely used of these implementations of the laser-Doppler principle: the measurement of tissue perfusion. The chapters that follow treat the principle of the tissue perfusion measurements made by laser-Doppler blood flowmeters, explain the many, varied applications of laser-Doppler blood flowmetry in clinical and research settings, and point out to the potentially interested clinician or researcher the capabilities and the limitations of laser-Doppler blood flowmetry in tissue. The other implementations of laser-Doppler blood flowmetry receive less extensive coverage. Laser-Doppler microscopes are mentioned in this introductory chapter primarily for historical reasons and to contrast them with the other implementations. However, chapter 19 deals with a close relative of the laser-Doppler microscope, the ophthalmic measurement of retinal blood flow. Only chapter 7 is devoted to catheter velocimeters that employ the laser-Doppler principle, because they have not yet found widespread use in either clinical or research applications and because they have not become available commercially. Similarly, analysis of the speckle patterns that are produced on the surfaces of perfused tissue when they are illuminated by laser light may eventually provide a way of mapping blood flow, but the method is not treated in this book because it is still in its infancy.

To understand the present status of the laser-Doppler devices now available for measuring blood flow, it is helpful to consider the contributions that led to the present state of the art. Therefore, the purpose of this first chapter is to provide a historical introduction to laser-Doppler blood flowmetry and to review the scientific principles and technological developments that make modern laser-Doppler measurements of tissue perfusion possible: the Doppler effect, the laser, the combined application of the two into the art of laser-Doppler velocimetry, and the application of laser-Doppler velocimetry to measurements of blood flow.

DOPPLER: MAN AND EFFECT

Johann Christian Doppler (born Salzburg, Austria, 1803; died Venice, Italy, 1853) attended the Polytechnic Institute in Vienna from 1822 to 1825, but found the curriculum too one-sided and returned to Salzburg to pursue his studies privately. After completing the Gymnasium, he was employed as a

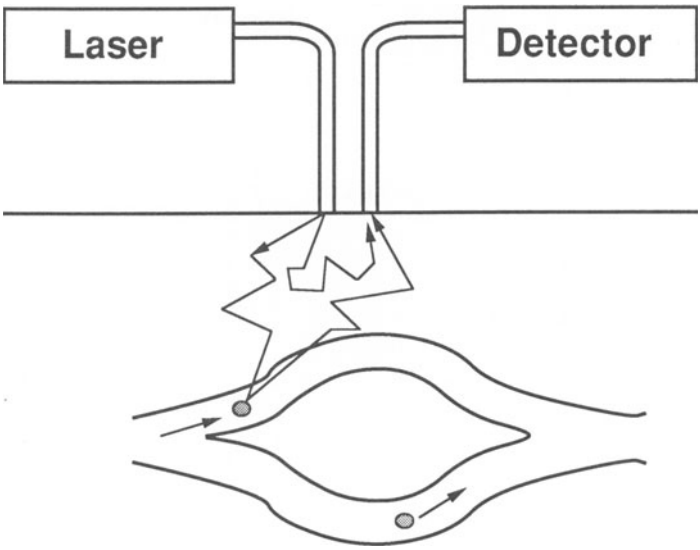

Figure 1–1. Laser-Doppler measurement of tissue perfusion. Laser light is typically delivered to tissue and returned to a detector by fiber optic light guides. Light in tissue is diffusely scattered by stationary tissue. Such light reaches the detector without being Doppler-shifted. Photons that encounter moving red blood cells experience a Doppler shift.

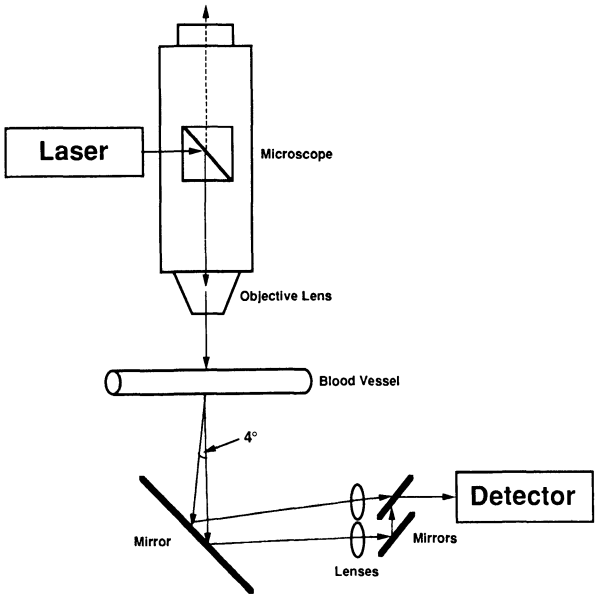

Figure 1–2. Laser-Doppler microscope for measuring red blood cell velocity in a single microscopic blood vessel.

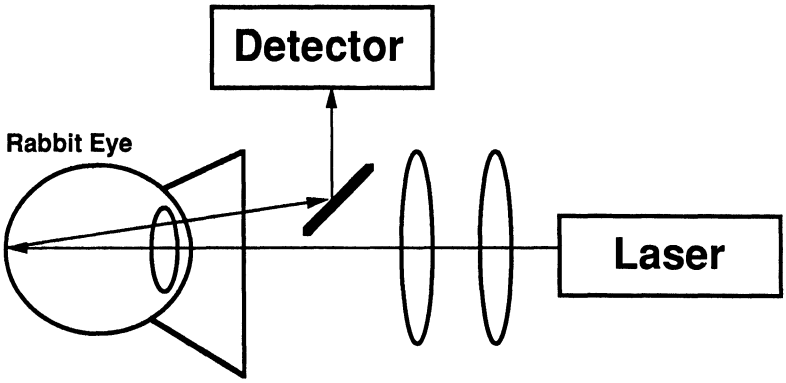

Figure 1–3. Retinal laser-Doppler velocimeter. For details see chapter 19.

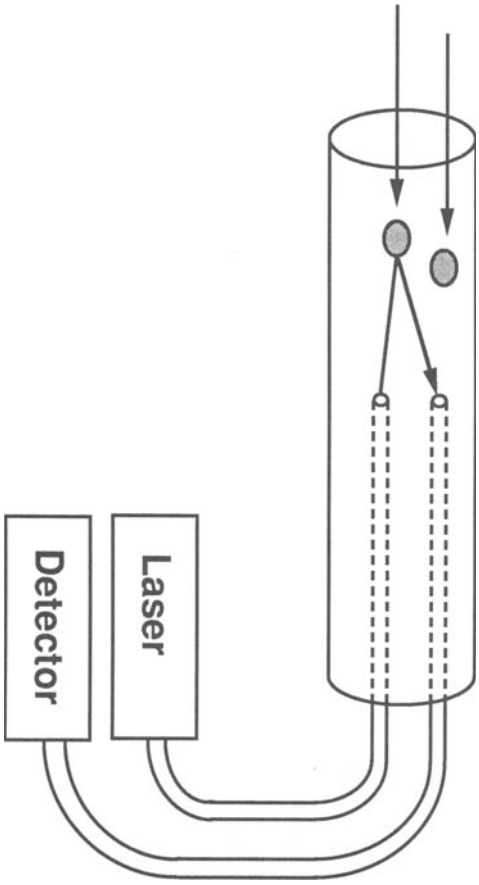

Figure 1–4. Catheter laser-Doppler velocimeter. For details see chapter 7.

mathematical assistant and he began writing on mathematics and electricity. In 1835 he was on the verge of moving to America and had even sold his possessions, but while underway in Munich, he unexpectedly obtained a position at the State Secondary School in Prague. In 1841 he became a professor of elementary mathematics and practical geometry at the State Technical Academy there [1].

On May 25, 1842, he delivered his famous paper, "On the Colored Light of Double Stars and Some Other Heavenly Bodies" to the Royal Bohemian Society of Learning [1,2,3]. In that paper, the correct elementary formula is derived for motion of source or observer along a line between them; the extension to motion of both at the same time appeared in an article in 1846. Doppler mentioned the application of this result both to acoustics and optics. The first experimental verification of Doppler's theory was conducted in 1844 by Buys Ballot, who borrowed a locomotive and a flatcar on which a trumpeter with perfect pitch rode toward a second musician at the train station. The second musician confirmed that as the train approached, he heard the trumpet note one half-tone higher, whereas it was one half-tone lower as the train receded from the station. The astronomical use of the Doppler effect had to wait until proper spectroscopic instrumentation became available, beginning with the work of William Huggins in 1868. Belopolsky first confirmed the optical effect terrestrially. As now modified by the theory of relativity, the Doppler principle has become a major astronomical tool [1].

FUNDAMENTALS OF THE DOPPLER EFFECT

Figure 1–5 illustrates the Doppler effect as it applies to sound waves [2]. Panel A depicts a stationary source of sound with a particular frequency and a listener some distance from the source. If both listener and source and stationary, the listener receives CT/λ waves in T seconds, where C is the speed of sound and λ is the wavelength. Panel B illustrates the situation in which the listener moves toward the sound source at velocity v_L. In this case, the listener will receive an additional $v_L T/\lambda$ waves in time T. Because the frequency the listener experience (f_o) is simply the number of waves per unit time,

$$f_o = (CT/\lambda + v_L\ T/\lambda)/T = (C + v_L)/\lambda.$$

The frequency at the source that the listener hears when stationary is just $f_s = (C/\lambda)$. The difference between the two perceived frequencies defines the Doppler frequency shift (f_d), which can be expressed as

$$f_d = f_o - f_s = f_s\ (1 + v_L/C) - f_s = v_L f_s/C.$$

For sound waves, the motion of the source has a different Doppler shift frequency than the same motion on the listener's part. In other words, it is

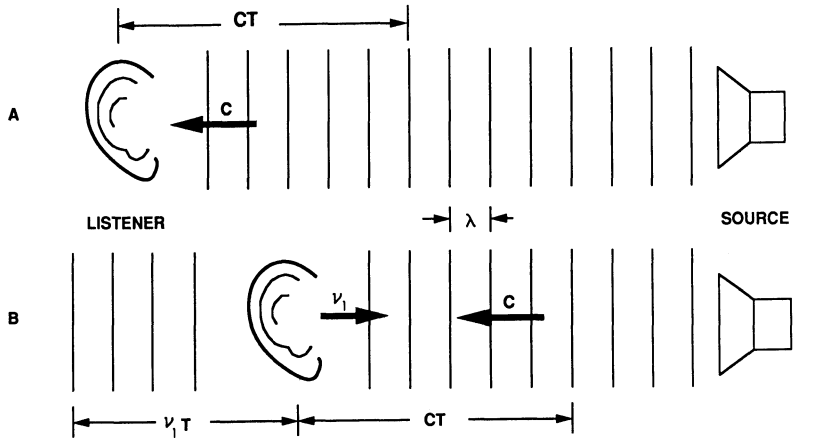

Figure 1–5. Acoustic example of the elementary Doppler principle. (Reprinted from [2] by permission of Hewlett-Packard Journal.)

not just the relative motion between source and listener that is important but which of the two is in motion. In addition, as the velocity of the source approaches the velocity of sound, the Doppler shift frequency becomes infinite. By contrast, the situation is fundamentally different for Doppler effects with light. The difference can be explained in terms of Einstein's theory of relativity, which states that the speed of light is a constant in all reference frames. Light needs no material medium for its propagation, and its speed relative to the source or observer is always the same. Therefore, it is only the relative motion between the observer and the source that determines the Doppler shift frequency. Thus,

$$f_o = [f_s\,(1 - v_{os}/C)/\sqrt{1 - (v_{os}/C)^2}] - f_s,$$

where c is the velocity of light and v_{os} is the relative velocity of the source with respect to the observer [2].

This equation can be applied to light entering tissue, but two other factors must be considered. If light strikes a stationary object and is reflected directly to a receiving detector, the returning light will have the same frequency as the emitted light. However, if the returning light has reflected from an object in motion, such as a red blood cell, the returning light will undergo a Doppler shift that is twice that predicted by the equation. The reason is that the structure reflecting the light acts as both the observer and the source. Because the red blood cell is in motion, the transmitted frequency it receives is Doppler-shifted according to the equation, and the reflected light that leaves the red blood cell is shifted again because the red blood cell also acts as a source in motion relative to the stationary receiver. The second factor to

consider is that only the component of the velocity vector directed toward or away from the receiver (observer) contributes to the Doppler shift frequency. Thus, for direct backscattering, one must actually scale the frequency shift by the cosine of the angle between the red blood cell's velocity vector and the line connecting the object to the receiver. Although the Doppler shifts imparted to light by moving red blood cells are quite small compared to the frequency of light, the method is practical because of the spectral purity of laser light. Chapter 2 provides a detailed explanation of how the Doppler principle is applied to the measurement of tissue perfusion.

DISCOVERY OF THE LASER

For many years, the optical Doppler effect was used almost exclusively in astronomy. What made using the optical Doppler effect feasible in many terrestrial applications was the discovery of the laser. Charles Townes and Arthur Schawlow actually began their work in a region of the electromagnetic spectrum below the operation range of the laser. Their field of interest in the late 1940s and 1950s was microwave spectroscopy, a powerful tool characterizing a wide variety of molecules. This discipline was the common ground on which the two scientists met in 1949, when Schawlow went to Columbia University and began working with Townes [4].

In 1951 Schawlow became a research physicist at AT&T Bell Laboratories, where, during World War II, Townes had worked on radar, another microwave application. Also in 1951, Townes became a consultant to Bell Labs and, in the same year, conceived an idea that would provide the basis for the device that was just a logical jump—though a great scientific leap—away from the laser. Townes knew that as the wavelength of microwave radiation grew shorter, its interactions with molecules became stronger, making it a more powerful spectroscopic tool. However, building a device small enough to generate the required wavelengths was beyond the fabrication techniques of the day. Townes got around that limitation with the idea of using molecules to generate the desired frequencies [4].

In 1953 this innovative concept came to fruition in a device call the maser: Microwave Amplification by Stimulated Emission of Radiation. The device takes advantage of a quantum-mechanical effect that occurs when molecules with excess energy encounter an electromagnetic wave. Under the right conditions, the molecules give up their extra energy to the wave, strengthening it in the process. As the wave encounters one stimulated molecule after another, its strength quickly multiplies. Yet Townes also realized that shorter wavelengths beyond microwave—infrared and visible light—probably offered even more powerful tools for spectroscopy [4].

Townes and Schawlow discussed this possibility, and in the fall of 1957, they began working out the principles of a device that would provide these shorter wavelengths. After eight months of work, they produced the seminal paper "Infrared and Optical Masers" [5]. They received a patent for the laser

in 1960, the same year a working laser was built at Hughes Aircraft Co. Both men received Nobel Prizes, Townes in 1964 and Schawlow in 1981, in part for their contribution to the laser [4].

The first successfully operated laser was a ruby laser built in 1960 by Maiman. The most commonly used laser today is the helium–neon laser that was first operated by Javan in 1961. Both He–Ne lasers and diode lasers are used in laser-Doppler flowmeters. The unique properties of laser light are its high intensity, low divergence, extreme monochromaticity, and its great coherence. The properties of interest in laser-Doppler flowmetry are its monochromaticity, which refers to the narrow range of wavelengths that the laser emits, and its coherence, the fact that the light waves have the same frequency, phase, amplitude, and direction. The principles of laser action are covered in detail in many standard texts [6].

LASER-DOPPLER VELOCIMETRY

Today, when lasers are used throughout modern society and are even found in homes in consumer products such as compact disk players, it is hard to remember that the laser was often criticized as "a solution looking for a problem." Yet, often many years elapse between an important discovery and its practical application. And it was not until 1964 that laser light was used to measure the velocity of fluid flow. Before then, a technique called *light-beating spectroscopy* had emerged [7]. The phenomenon of light beating is directly analogous to the familiar mixing of alternating current electrical signals. Light with two different frequencies, upon falling on a detector, establishes a beat frequency in the detector output proportional to the difference in the two frequencies. In a classic experiment, Forrester et al. [8] demonstrated the phenomenon with a conventional source of monochromatic light, a mercury lamp. Although an experimental *tour de force*, the measurement was extremely difficult because of the low intensity and the large linewidth of the light source. Thus, the technique did not appear to hold great promise. A dramatic change occurred with the advent of lasers. When the output of two independent lasers simultaneously illuminated a single photomultiplier, a beat note was detected at the difference frequency, and it could even be used to determine the stability of the lasers. The high intensity and the narrow linewidth of the laser quickly converted the light-beating phenomenon into a standard laboratory technique [7].

The final step in the development of laser-Doppler velocimetry (LDV) culminated from combining the spectral purity of the laser, the light-beating technique, and the Doppler effect. Light that is scattered by particles or impurities in a moving fluid will be Doppler-shifted by an amount proportional to the local fluid velocity. By mixing the scattered light with unshifted light, Yeh and Cummins [9] succeeded in measuring flow velocities in different regions of a fluid undergoing laminar flow. The art of laser-Doppler velocimetry that was born in these experiments quickly grew into

an industry. Because laser light can traverse with impunity such hostile environments as corrosive fluids and jet exhaust, it can be used where other methods would be destroyed. This and other advantages of laser-Doppler velocimetry gained it widespread use in industrial research, and a wide range of commercial instruments soon became available.

BLOOD FLOW MEASUREMENTS BY LDV

The first LDV measurements of blood flow were made in 1972 by Riva et al. [10], who studied red blood cell velocities in the retinal vessels of rabbits. By improving their system and reducing laser power to safe levels, Tanaka, Riva, and Ben-Sira [11] were able to measure signals that varied with flow velocities in human retinal vessels. Subsequently, Tanaka and Benedek [12] employed a fiber optic catheter to measure velocity-dependent Doppler signals in the femoral artery of the rabbit. These early measurements of blood flow velocity were paralleled by the development of the laser-Doppler microscope. In 1974 and 1975, Mishina et al. [13] and Einav et al. [14] described their attempts to use the laser-Doppler principle to measure the velocities of red blood cells traveling through arterioles and capillaries. Their laser-Doppler microscopes and others [15–18] introduced in the next few years were used to evaluate flow velocities and velocity profiles in a variety of transparent tissues such as the mesentery of rabbit and mouse, the toe-web of frog, and the hamster cheek pouch. The chronology of the developments that led to the present art of laser-Doppler velocimetry are summarized in table 1–1, which also shows when the techniques were used in some of the major organs of the body.

LDV MEASUREMENTS OF TISSUE PERFUSION

The previously mentioned LDV measurements of blood flow were all made in single vessels. Michael D. Stern [19] was the first to suggest that tissue perfusion could be measured by laser-Doppler velocimetry. Stern's work began in 1973 when he was a fellow in Robert Bowman's Laboratory of Technical Development at the National Heart and Lung Institute. Stern, who had studied physics and medicine, wanted to refurbish his physics knowledge and "measure things of medical relevance." In the labs at NIH, he had "piles of antique technical gear" at his disposal. Among the toys in the laboratory was a small helium–neon laser. At the time a group in NHLI was interested in vasospastic diseases such as Raynauds phenomenon. According to Stern's account, "I conceived the idea that something useful might be learned about these conditions by making laser Doppler measurements from nail beds or fingertips. I bravely set up a crude system, with the laser beam shining on a finger, and a reference beam traveling by a separate path. I had little if any understanding of the role of the number of coherence areas collected, and the output device was an ancient spectrum analyzer that produced a scrambled pattern on the oscilloscope when used with a random signal such as the noise

Table 1–1 Chronology of laser-Doppler blood flowmetry

Date	Contribution	Investigator(s)
1842	Velocity-dependent frequency shift	Doppler [1]
1844	Verification of Doppler effect	Ballot [1]
1955	Light-beating spectroscopy	Forrester et al. [8]
1958	Invention of laser	Schawlow and Townes [5]
1961	Light beating with lasers	Javan et al. [32]
1964	Laser-Doppler velocimetry	Yeh and Cummins [9]
1972	Retinal velocimeter	Riva, Ross and Benedek [10]
1974	LDV microscope	Mishina et al. [13]
1975	Catheter velocimeter	Tanaka and Benedek [12]
1975	LDV microscope	Einav et al. [14]
1975	Tissue perfusion	Stern [19]
1977	Cutaneous blood flow	Stern et al. [21]
1977	Fiber optic blood flowmeter	Watkins and Holloway [24]
1979	Blood flow in skeletal muscle	Öberg et al. [33]
1979	Renal blood flow	Stern et al. [22]
1980	Cerebral blood flow	Williams et al. [34]
1980	Noise cancellation circuitry	Nilsson et al. [27]
1981	Theory of LDV in tissue	Bonner and Nossal [29]
1982	Intestinal mucosal blood flow	Shepherd and Riedel [35]
1983	Blood flow in bone	Hellem et al. [36]
1983	Hepatic blood flow	Shepherd et al. [37]
1984	Diode laser blood flowmeter	de Mul et al. [38]
1985	Gastric mucosal blood flow	Kiel et al. [39]
1986	Digital signal processing	Adrian and Borgos [40]

from a photomultiplier. Not too surprisingly, I got nothing. I put the project on the shelf, figuring that it wasn't too surprising that you couldn't make a laser Doppler measurement from something as complex as a fingertip. In the attempt, I had noticed that the diffuse light which was transmitted through the finger did not show a speckle pattern, but I attributed this to the fact that I could not hold my finger sufficiently still."

After conversations with a Navy physicist, Ron Atkinson, about whether multiple scattering in tissue should destroy the temporal coherence of laser light, Stern noted that light that was multiply scattered through both sides of a styrofoam cup still presented a crisp speckle pattern. Atkinson argued that a liquid was a better model for tissue, and put some translucent liquid dish-washing detergent in a beaker. When it was a allowed to sit very still, a faint, rapidly scintillating speckle pattern could be seen near the entry point of the laser beam, but none at all in the diffuse light exiting at the far side. Stern concluded that Brownian motion of the detergent micelles must be responsible. To settle the argument, he got a piece of beef steak, placed it on a little pedestal, and shined the laser on it. There was a perfectly clear speckle pattern. Light scattering in the static tissue had not destroyed the temporal coherence of the light. Could there have been enough microvascular red blood cell motion to completely obliterate the speckle pattern on his finger? If so, why had his laser Doppler measurements failed? He tied a rubber band

tightly around a finger, completely cutting off the circulation, and held it in the laser beam. A speckle pattern appeared! When the rubber band was removed, it was gone.

With the benefit of his speckle observations, Stern realized that the problem lay with his equipment, not his fingertip: "I was very excited. If the naked eye could see the effect of blood flow on the scattered light, it should be easy to measure it with the right hardware." After still more unsuccessful attempts to measure Doppler shifts in his fingertip, Stern obtained help from Ralph Nossal, who had experience with photon-correlation spectroscopy. He also borrowed a low-noise laser and a red-sensitive photomultiplier that was mounted behind a small pinhole. And he talked a salesman into lending him a better spectrum analyzer. As Stern relates, "When the Saicor salesman came with the spectrum analyzer, we all piled into an abandoned darkroom and set up the apparatus. The light from a fingertip showed a clear-cut fluctuation spectrum up to 20 kHz; when the circulation was occluded with a rubber band, it disappeared. I persuaded the Saicor representative to leave his instrument for two weeks while we went through the Federal procurement process to buy it. During that two weeks, all the data in the 1975 Nature paper [19] was gathered."

After collecting and studying the frequency spectra from his fingertip, Stern devised an algorithm to estimate flow quantitatively: the root-mean-square of the spectrum's bandwidth. In July of 1974, Donald Lappe joined the laboratory as a fellow; together he and Stern built a crude instrument for continuously monitoring the flow parameter [20]. A scaling argument indicated that their algorithm should be proportional to flow, if the effective geometry of the microvascular bed did not change too much during changes in flow. The next task was to try to calibrate the instrument, to find out what *too much* meant. In reading about microvascular blood flow in skin, Stern found there were no unimpeachable methods to use as a gold standard. His choice was the xenon washout method that John Chimosky and Allen Holloway used, so he called them and arranged a visit to the Center for Bioengineering at University of Washington. Thus, the first study to compare the LDV flowmeter with another method was attempted in human skin. Unfortunately, the instrument did not work after it reached Seattle. An electronics technician, Dennis Watkins, diagnosed the problem, which was that the signal-processing unit was picking up a television station on the edge of the campus. Thus, the data had to be recorded by the spectrum analyzer and processed off-line. These problems were not mentioned in the ensuing publication [21].

Skin blood flow was of limited interest in the Heart and Lung Institute, so Stern next tried to measure blood flow from the exposed surface of the kidney of a rat. His prototype flowmeter seemed to work very well, and responded dramatically to pharmacological agents applied to the rat renal cortex, but he was not sure that it would work in a microvascular bed that

had a different architecture from skin, so he again looked for a flow-measuring method with which to compare the laser-Doppler device. A search of the literature turned up the microsphere work of Jay Stein's group in the Renal Division at the University of Texas Health Science Center at San Antonio. Stern's visit to San Antonio was an exciting time for all the investigators who saw the prototype laser-Doppler blood flowmeter in use. At that time it still consisted of a He–Ne laser, a mirror to deflect the laser beam vertically down onto the exposed rat kidney, a photomultiplier tube with a pinhole collimator, a box full of home-made electronics, and the spectrum analyzer [22]. The investigators in San Antonio, Jay Stein and A.P. Shepherd, viewed the whole endeavor with both awe and skepticism, and they called in engineers and optical experts from the Southwest Research Institute to hear Stern's seminar on the new technique. To the biomedical investigators, it was gratifying that the optical experts found the device as puzzling as they did. At that time, the optical experts did not even agree on whether fiber optics could be used to replace the pinhole collimation system.

THE COMMERCIAL PHASE

To a large extent, the commercialization of the laser-Doppler blood flowmeter reflects Stern's perigrinations in 1974–1975 with his prototype. At each of the institutions he visited, investigators intrigued and excited about the new technique sought to interest companies in manufacturing the LDV flowmeter. During Stern's Seattle visit, Allen Holloway and Robert Rushmer became acquainted with the technique. Holloway's enthusiasm [21,23,24] for the potential clinical applications of the new technique helped convince a local company, Medpacific, to obtain a license to manufacture the flowmeter patented by Stern and Lappe. P.Å. Öberg visited Seattle shortly after Stern's visit; from Holloway he learned of the new technique and decided to research the method upon his return to Linköping, Sweden. After obtaining financial support from the National Swedish Board of Technical Development, Öberg, together with G. Nilsson and T. Tenland, developed and patented a new LDV flowmeter [25–27] that was subsequently manufactured by Perimed, a company formed by Sven Malmström and the three inventors.

In San Antonio, Stein and Shepherd tried and failed to interest several major American instrument manufacturers in the LDV flowmeter. Later, Shepherd borrowed equipment from TSI, a prominent manufacturer of industrial laser-Doppler instrumentation, and collected the first laser-Doppler spectra from the gastrointestinal tract. Changes in intestinal blood flow clearly altered the frequency spectra in a predictable way, but TSI was not interested in medical instrumentation at that time. Four or five years later, after one of their stockholders brought the new technique to their attention again, TSI sought Shepherd's help in entering the field [28].

When Stern left NIH, Robert Bonner inherited the LDV flowmeter project. Working with Ralph Nossal, Bonner developed a theoretical model of

Table 1–2 Patents on laser-Doppler blood flowmeters for tissue perfusion

Inventor(s)	Title	Patent number	Date
C.C. Johnson	Measurement of Blood Flow Using Coherent Radiation and Doppler Effect	3,511,227	1970
M.D. Stern and D.L. Lappe	Method and Apparatus for Measurement of Blood Flow Using Coherent Light	4,109,647	1978
G. Nilsson, P.Å. Öberg, and T. Tenland	Method and Apparatus for Measuring Flow Motions in a Fluid	7811288–5	1981
R.J. Adrian and J.A. Borgos	Laser Doppler Flow Monitor	4,596,254	1986

Table 1–3 Comparison of laser-Doppler blood flowmeters

Mfg.	Model	Laser	λ (nm)	Signal analysis	Fiber type	No. Fibers[1]	Diam. (μm)	Sep.[2] (μm)	Laser power (mW)	Freq. range[3]	Outputs		
											Flow	RBC vol.[4]	velocity[5]
Med-pacific	LD-5000	He–Ne	632.8	Analog	Graded-index	2	100	500	2	Fixed	+	—	—
Perimed	PF3	He–Ne	632.8	Analog	Step-index	3	120	250	2	Manual	+	+	—
TSI	BPM 403A	Diode	780	Digital	Graded-index	3	50	500	2	Auto	+	+	+
Med-pacific	LD-6000	He–Ne	632.8	Analog/ digital	Graded-index	2	100	500	2	Fixed	+	+	+

[1] TSI and Perimed use one sending fiber and two receiving fibers.
[2] Center-to-center fiber separation.
[3] Medpacific's frequency range is fixed at 100Hz–20kHz.
Perimed's lower limit is 20 Hz. The upper limit can be set to 4 or 12 kHz.
TSI's microprocessor selects the frequency range.
[4] Relative red blood cell (RBC) concentration in tissue.
[5] Average RBC speed.

photon diffusion in tissue [29]. The model served as a useful conceptual framework for further development of laser-Doppler measurements of tissue perfusion. Together with Clem, Bowen, and Bowman, Bonner also designed an LDV flowmeter that employed fiber optics and a new mean-frequency algorithm [30]. Several of the instrument manufacturers studied Bonner's prototype in developing their flowmeters.

The list of patents shown in table 1–2 summarizes the commercialization of the LDV flowmeter. Similarly, table 1–3 compares the various features of the LDV flowmeters that are now commercially available. The names and addresses of the companies that manufacture laser-Doppler blood flowmeters are listed at the end of the book. Chapters 3, 4, and 5 describe the flowmeters made by the major manufacturers, while innovations that have not yet been commercialized are discussed in chapter 6. Terms with which the reader may not be familiar are defined in the glossary at the back of the book.

ACKNOWLEDGMENTS

The brief history of the laser rendered here was excerpted from Laser Focus [4] by permission of the publisher. The explanation of the elementary Doppler principle was taken from the Hewlett Packard Journal [31] and the author's previous treatment of the subject in the Handbook of Physiology (by permission of the American Physiological Society). The author is grateful to Michael D. Stern, Ralph Nossal, Allen Holloway, and P.Å. Öberg for checking the accuracy of the chronology of the developments and applications of the first laser-Doppler blood flowmeters.

REFERENCES

1. Woodruff, A.E. 1971. Johann Christian Doppler. In Dictionary of Scientific Biography, Gillispie, C.C., ed. New York: Charles Scribner's Sons, vol 4, pp 167–168.
2. Magnin, P.A. 1986. Doppler effect: history and theory. Hewlett-Packard J 37:26–31.
3. White, D.N. 1982. Johann Christian Doppler and his effect—a brief history. Ultrasound Med Biol 8:583–591.
4. Kales, D. 1988. Laser inventors Townes and Schawlow—remembrances of things past. Laser Focus (Aug.):75–76.
5. Schawlow, A.L., and C.H. Townes. 1958. Infrared and optical masers. Phys Rev 112:1940–1949.
6. Van Pelt, W.F., H.F. Stewart, R.W. Peterson, A.M. Roberts and J.K. Worst. 1970. Laser Fundamentals and Experiments. Rockville, MD: U.S. Department of Health, Education, and Welfare.
7. Cummins, H.Z., and H.L. Swinney. 1970. Light beating spectroscopy. In Progress in Optics, Wolf, E., ed. New York: American Elsevier Publish Co., vol. 8, pp 135–197.
8. Forrester, A.T., R.A. Gudmunds, and P.O. Johnson. 1955. Photoelectric mixing of incoherent light. Phys Rev 99:1691–1700.
9. Yeh, Y., and H.Z. Cummins. 1964. Localized fluid flow measurements with an He–Ne laser spectrometer. Appl Phys Lett 4:176–178.
10. Riva, C.E., B. Ross, and G.B. Benedek. 1972. Laser Doppler measurements of blood flow in capillary tubes and retinal arteries. Invest Ophthalmol 11:936–944.
11. Tanaka, T., C. Riva, and I. Ben-Sira. 1974. Blood velocity measurements in human retinal vessels. Science 186:830–831.
12. Tanaka, T., and G.B. Benedek. 1975. Measurement of velocity of blood flow (in vivo) using a fiber optic catheter and optical mixing spectroscopy. Appl Optics 14:189–200.

13. Mishina, H., T. Koyama, and T. Asakura. 1974. Velocity measurements of blood flow in the capillary and vein using the laser Doppler microscope. Appl Optics 14:2326–2327.
14. Einav S.H., J. Berman, R.L. Fuhro, P.R. DiGiovanni, J.D. Fridman, and S. Fine. 1975. Measurement of blood flow *in vivo* by laser Doppler anemometry through a microscope. Biorheology 12:203–205.
15. Born, G.V.R., A. Melling, and J.H. Whitelaw. 1978. Laser Doppler microscope for blood velocity measurements. Biorheology 15:163–172.
16. Le-Cong, P. 1976. Development of a laser Doppler velocimeter and its applications to microcirculation studies. Dissertation, University of California, San Diego, University Microfilm Order No. 77–522.
17. Le-Cong, P., and B.W. Zweifach. 1979. In vivo and in vitro velocity measurements in microvasculature with a laser. Microvasc Res 17:131–141.
18. Le-Cong, P., and R.H. Loveberg. 1980. Analysis of dual beam laser velocimeter applied to microcirculation studies. Rev Sci Instr 51:565–574.
19. Stern, M.D. 1975. In vivo evaluation of microcirculation by coherent light scattering. Nature 254:56–58.
20. Stern, M.D., and D.L. Lappe (inventors). 1978. Method and apparatus for measurement of blood flow using coherent light. U.S. Patent 4,109,647.
21. Stern, M.D., D.L. Lappe, P.D. Bowen, J.E. Chimosky, G.A. Holloway, H.R. Keiser, and R.L. Bowman. 1977. Continuous measurement of tissue blood flow by laser-Doppler spectroscopy. Am J Physiol 232:H441–H448.
22. Stern, M.D., P.D. Bowen, R. Parma, R.W. Osgood, R.L. Bowman, and J.H. Stein. 1979. Measurement of renal cortical and medullary blood flow by laser-Doppler spectroscopy in the rat. Am J Physiol 236:F80–F87.
23. Holloway, G.A., and D.W. Watkins. 1977. Laser Doppler measurement of cutaneous blood flow. J Invest Dermatol 69:306–309.
24. Watkins, D.W., and G.A. Holloway. 1978. An instrument to measure cutaneous blood flow using the Doppler shift of laser light. IEEE Trans Biomed Eng BME-25:28–33.
25. Nilsson, G.E., T. Tenland, and P.Å. Öberg. 1980. Evaluation of a laser Doppler flowmeter for measurement of tissue blood flow. IEEE Trans Biomed Eng 27:597–604.
26. Nilsson, G.E., P.Å. Öberg, and T. Tenland (inventors). 1981. Method and apparatus for measuring flow motions in a fluid. Swedish Patent 7811288–5.
27. Nilsson, G.E., T. Tenland, and P.Å. Öberg. 1980. A new instrument for continuous measurement of tissue blood flow by light beating spectroscopy. IEEE Trans Biomed Eng 27:12–19.
28. Shepherd, A.P., G.L. Riedel, J.W. Kiel, D.J. Haumschild, and L.C. Maxwell. 1987. Evaluation of an infrared laser-Doppler blood flowmeter. Am J Physiol 252:G832–839.
29. Bonner, R., and R. Nossal. 1981. Model for laser Doppler measurements of blood flow in tissue. Appl Optics 20:2097–2107.
30. Bonner, R.F., T.R. Clem, P.D. Bowen, and R.L. Bowman. 1981. Laser-Doppler continuous real-time monitor of pulsatile and mean blood flow in tissue microcirculation. In Scattering Techniques Applied to Supra-Molecular and Nonequilibrium Systems, Chen, S.H., Chu, B., Nossal, R., eds. New York: Plenum, pp 685–702.
31. Hunt, B.F., S.C. Leavitt, and D.C. Hempstead. 1986. Digital processing chain for a Doppler ultrasound subsystem. Hewlett-Packard 37:45–48.
32. Javan, A., W.R. Bennett, and D.R. Herriott. 1961. Population inversion and continuous optical maser oscillation in a gas discharge containing a He–Ne mixture. Phys Rev Lett 6:106.
33. Öberg, P.Å., G.E. Nilsson, T. Tenland, A. Holmström, and D.H. Lewis. 1979. Use of a new laser Doppler flowmeter for measurement of capillary blood flow in skeletal muscle after bullet wounding. Acta Chir Scand Suppl 489:145–150.
34. Williams, P.C., M.D. Stern, P.D. Bowen, R.A. Brooks, M.K. Hammock, R.L. Bowman, and G. di Chiro. 1980. Mapping of cerebral cortical strokes in Rhesus monkeys by laser Doppler spectroscopy. Med Res Eng 13(2):3–5.
35. Shepherd, A.P., and G.L. Riedel. 1982. Continuous measurement of intestinal mucosal blood flow by laser-Doppler velocimetry. Am J Physiol 242:G668–G672.
36. Hellem, S., L.S. Jacobsson, G.E. Nilsson, and D.H. Lewis. 1983. Measurement of microvascular blood flow in cancellous bone using laser Doppler flowmetry and ^{133}Xe-clearance. Int J Oral Surg 12:165–177.

37. Shepherd, A.P., G.L. Riedel, and W.F. Ward. 1983. Laser-Doppler measurements of blood flow within the intestinal wall and on the surface of the liver. In Microcirculation of the Alimentary Tract, Koo, A., Lam, S.K., Smaje, L.H., eds. Singapore: World Scientific Publishing Co., pp 115–129.
38. de Mul, F.F.M., J. van Spijker, D. van der Plas, J. Greve, J.G. Aarnoudse, and T.M. Smits. 1984. Mini-laser-Doppler blood flow monitor with diode laser source and detection integrated in the probe. Appl Optics 23:2970–2973.
39. Kiel, J.W., G.L. Riedel, G.R. DiResta, and A.P. Shepherd. 1985. Gastric mucosal blood flow measured by laser–Doppler velocimetry. Am J Physiol 249:G539–G545.
40. Adrian, R.J., and J.A. Borgos (inventors). 1986. Laser Doppler Flow Monitor. U.S. Patent 4,596,254.

2. PRINCIPLES OF LASER-DOPPLER FLOWMETRY

ROBERT F. BONNER and RALPH NOSSAL

Light scattering has long been used to probe properties of bulk matter. In transparent media such as air or clear water, measurements can be analyzed easily and remote sensing can be done over great distances. The basic principles relating the intensity of scattered light to underlying molecular structure were established by Lord Rayleigh in his classic 1871 paper explaining why the sky appears to be blue.

As a medium becomes cloudy—an example being seawater, which contains zooplankton and other microorganisms—only surface layers, having a thickness of a few scattering lengths, can be easily probed. Consequently, due to the extremely strong multiple scattering present in most biological structures, only a very small portion of the light incident on a tissue surface will penetrate very deeply and return to that surface. The penetration depth generally must be measured in millimeters, even when wavelengths are used that fall within the therapeutic window for tissue (600–1200 nm). In this region, absorption by biomolecules is relatively weak. Not only does this strong multiple scattering generally limit accessible optical information to only superfical layers, but also it makes theoretical analysis of light intensity fluctuations due to red blood cell motion much more complicated than the analysis of laser-Doppler effects in clear media (such as Lidar in the atmosphere). Although the theory presented here is complicated, an understanding of the results of the theory and its attendant assumptions can give the user valuable insight into laser-Doppler blood flowmetry. It is easy to make such

measurements with commercial instruments, but it is more difficult to interpret them.

When a substance is illuminated by an electromagnetic field, oscillating dipoles (composed of electrons and nuclei) are induced that themselves become sources of electromagnetic radiations that comprise the *scattered field.* The induced dipoles, oscillating at the frequency of the incident wave, each reradiate energy as spherical waves that interfere with one another. If the illuminating source is coherent in space and time, the instantaneous induced field also will be coherent. By space-time coherence we mean that, if the field intensity is known at one spatial point at any given instant, it can be determined at other nearby points and times. Although the scattered fields thus may be coherent, spontaneous fluorescent emissions do *not* have such a property.

Emissions from CW lasers can have excellent spatial and temporal coherence, in contrast to radiation from incandescent sources. Because incandescent sources have very poor temporal coherence, they can be used only to obtain information about the spatial structure of the scattering medium. In contrast, laser sources can be employed to provide information about both the structure and *motions* of the scattering medium. If one uses a laser source that is coherent over appropriately long periods of time, the scattered field also will appear to be coherent if there are no changes in the structure of the scattering medium. A loss of coherence in the scattered field, with increasing time, arises because the scattering centers are moving with respect to each other. In this way, the spatial and temporal coherence of a laser beam allows one to measure the motion of particles over very small distances (<1 μm) by analyzing changes in the phase or intensity of the scattered light, with a precision similar to that of other optical interferometric techniques. Additionally, intensity fluctuation spectroscopy and laser-Doppler velocimetry are uniquely suited for measuring the characteristic motions of particles *within* a sample.

Such motions will be detectable as changes in the diffraction pattern produced by the scattered field (see figure 2–1). If a small enough region of the diffraction pattern is delimited, e.g., by a set of pinholes, the intensity of the radiation reaching a detector will fluctuate. As the sampled region is reduced in size, the amplitude of the fluctuations will increase relative to the mean amplitude of the detected light. The faster the movements of the scattering centers, the more rapid are the changes in intensity. By suitable theory, the intensity fluctuations can be analyzed to provide detailed quantitative information about the scattering system. Techniques for measuring the speed of flowing particles by laser-Doppler velocimetry are almost as old as lasers themselves [1], and they are made possible by the high temporal and spatial coherence of laser emissions. Biological systems that have been studied in this way include macromolecules in solution (where the diffusion coefficient related to translational motion can be measured), spermatozoa and

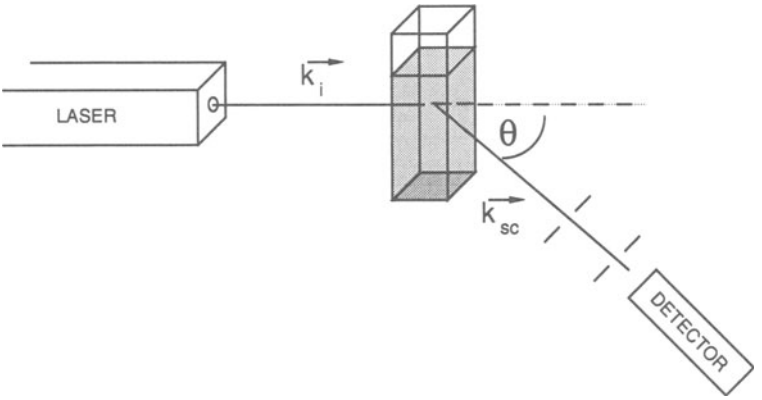

Figure 2–1. Schematic of spectrometer used for performing dynamic light-scattering measurements.

other microorganisms (where one measures the swimming speed), and cross-linked biomacromolecular networks (which are characterized by viscoelastic coefficients). These and other applications are discussed in several texts and reviews [2–7]. Early use of quasi-elastic light scattering to monitor blood flow employed a laser-Doppler slit lamp to make noninvasive, noncontact measurements of Doppler shifts associated with blood flowing in large retinal arteries and veins near the optic disc [8]. Other early techniques required the insertion of optical fibers directly into the blood stream [9]. Also, fluctuations in the laser light scattered from human skin were observed to be related to microcirculatory blood flow [10]. The recognition that Doppler shifts are imparted to laser light as it diffuses through a perfused tissue led to the development of a variety of prototype and commercial instruments for measuring microcirculatory blood flow. The history of these measurements is described in detail in chapter 1. The purpose of this chapter is to describe the principles of laser-Doppler flowmetry in tissue.

Light scattering from biological tissue is very complicated. Therefore it is very difficult to provide a precise picture of the physical processes that occur. A wavelike model for light propagation can be assumed, in which case the scattered field is the result of multiple interactions with an ill-defined, randomly structured medium. Any change in the internal structure of the tissue would be discernible in the emitted field and, in principle, could be calculated in terms of multiply diffracted waves. However, the multiply scattered radiation fields really cannot be well described. A more tractable model is one in which the light field is treated as a collection of discrete photons. This viewpoint underlies the application of photon diffusion theory to tissue optics [11–13]. Such a discrete model generally is a more rewarding starting point for optically dense media. In media that contain moving scatterers,

shifts in the frequency of the scattered radiation can be viewed as the superposition of frequency shifts due to discrete individual scattering events. This assumption forms the basis of a theory of quasi-elastic light scattering that agrees with experimental data obtained from dense colloidal suspensions over a wide range of optical parameters [14].

Two procedures can be used to characterize a time-varying signal arising from temporal variations in the intensity of light falling upon a photodetector: the frequency components $S(\omega)$ of the fluctuating photocurrent can be compared (by using a spectrum analyzer); or equivalently, information can be obtained from the *intensity autocorrelation function*, $\langle i(t)i(t + \tau)\rangle$, which is the joint expectation of the photocurrent at one instant of time and that at later instants delayed by increments τ. This expectation often is referred to as the *photon autocorrelation function*, because photon counting tubes are used when the intensity of scattered light is very low. By the Wiener-Khintchine theorem, the autocorrelation function and the power spectrum, $S(\omega)$, are simple Fourier transforms of each other (see equation 2.17, below). Depending on the intensity of the scattered light signals and the time-scale of fluctuations, in some cases it is more convenient to collect data in the form of autocorrelation functions, whereas in other instances spectral analysis is more appropriate. Currently, practical blood flowmeters use either analog weighting of the spectrum of the fluctuations, or digital weighting of an autocorrelation function, as a method for determining equivalent flow parameters. However, development of the basic theoretical model is most easily carried out in terms of intensity autocorrelation functions, as indicated in the following section.

THEORY OF DOPPLER MEASUREMENT

The classical Doppler effect is the increase of the pitch (or frequency) of a train whistle as it moves towards the observer, and a decrease as it moves away. Doppler ultrasound techniques are easily explained by this analogy: ultrasound principally moves on a straight path through tissue (as does sound in air), and a small fraction is scattered back (i.e., reflected) toward the source by moving red blood cells. If the cell has a velocity $-v_x$ in the direction of the source of the ultrasound and its detector, the ultrasound frequency will be shifted to lower frequencies by an amount $\Delta f = 2v_x/\lambda$, where λ is the wavelength of the ultrasound in the tissue. Thus a Doppler ultrasound probe is sensitive to motion in a specific direction, and it can record the distibution of velocities in that direction. Because the wavelengths of the applied ultrasound field are 0.1–0.3 mm, the relatively high velocities of blood cells moving in large vessels (3–150 cm/sec) result in frequency shifts between 100 and 10,000 Hz. However, the velocities in capillaries are significantly lower (about 1 mm/sec), so the shifts they produce are immeasurably small (about 5 Hz).

For particles suspended in a clear fluid, laser-Doppler backscatter techniques give frequency shifts from which distributions of particle velocities can be determined. Because the wavelengths of light are approximately 500-fold smaller than ultrasound wavelengths, the corresponding Doppler shifts are 500 times greater. More generally, the Doppler shift of scattered laser light is determined by the speed of the particle v, a scale factor $(4\pi n/\lambda)\sin(\theta/2)$, and the cosine of the angle between the velocity direction $\hat{\mathbf{v}}$ and the direction of the Bragg scattering angle $\hat{\mathbf{Q}} = \hat{\mathbf{k}}_{sc} - \hat{\mathbf{k}}_{i}$. (Here, n is the index of refraction of the fluid, λ is the wavelength, θ is the angle that the light is deviated by the scattering, and $\mathbf{k}_{sc}$ and $\mathbf{k}_{i}$ are the wave vectors of the scattered and incident light.) The angular frequency shift is the reciprocal of the time it takes for a particle to move a distance $|1/\mathbf{Q}|$ (or $\lambda/\{4\pi n \sin(\theta/2)\}$) in the direction of $\hat{\mathbf{Q}}$. Although the yardstick of motion, $|1/\mathbf{Q}|$, is dependent on the angle at which the moving particle scatters the light, laser-Doppler techniques are sensitive to motions on the order of 0.3 to 20 μm.

To understand the Doppler shifts of light diffusely scattered from the surface of a tissue in which there is microcirculatory blood flow, it is necessary to enquire how light moves through the tissue. Three critical questions are 1) What are the characteristic scattering angles that determine the relation of Doppler shift to particle speed? 2) What is the optical pathlength within the tissue? 3) What tissue volume is sampled by the detected light? Also, critical to our understanding of in vivo measurements is knowledge of whether these three parameters vary significantly from one tissue or one individual to another. We now review a theory that has been developed to relate laser-Doppler signals to the parameters of mean red blood cell speed, blood flow, and the concentration of red blood cells in tissue. Here we highlight the main points of the derivations; details can be found elsewhere [15–17].

As a photon diffuses through a vascularized tissue, it experiences many collisions with essentially static tissue elements, but only occasional collisions with moving erythrocytes (figure 2–2). The surrounding tissue matrix is assumed to be a strong scatterer of light, so that the tissue basically appears as a turbid medium. Consequently, the transport of light can be accounted for by a diffusion model [11–13] or an equivalent stochastic description of photon migration [18]. The propagating light is considered as a collection of discrete particlelike photons, whose directions of motion at any given point—characterized by scattering vectors $\{\mathbf{Q}\}$—are random. We also assume that the network of microvessels in the tissue, while perhaps having local order, is random on a length scale defined by the mean distance between red blood cell scattering events. Consequently, when calculating the Doppler shifts in scattered photons, one can assume that the blood cell velocities, $\{\mathbf{V}\}$, also are randomly distributed in direction. Either of these assumptions concerning $\{\mathbf{Q}\}$ and $\{\mathbf{V}\}$, by itself, is sufficient to ensure that the change in scattering vector resulting from a collision of a photon with a red blood cell,

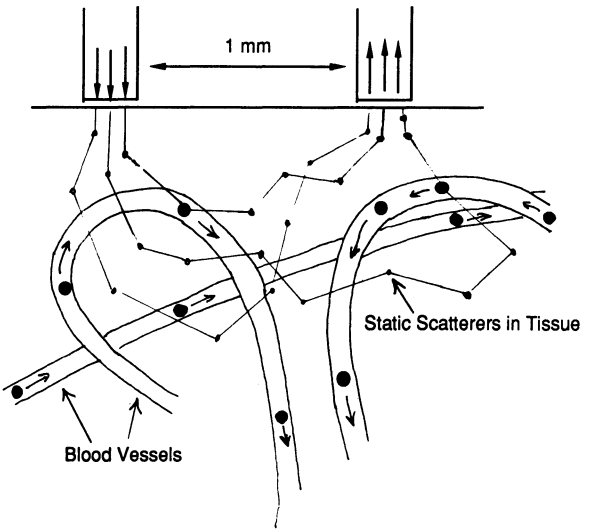

Figure 2–2. Schematic diagram of light diffusing through vascularized tissue.

$\Delta\mathbf{Q}$, is uncorrelated with the direction in which a cell is moving. The cylindrical symmetry of scattering itself is sufficient to cause randomization of the sign of the Doppler shift. Also, multiple Doppler shifts are uncorrelated when a particular photon collides with more than one moving cell. This point can be substantiated by an argument concerning the independence of multiple phase shifts experienced by an electromagnetic wave as it moves through a random medium [15] and, as mentioned above, this point also forms the basis of successful analysis of Doppler-shifted light scattered by turbid colloidal suspensions [14,19,20].

As previously indicated, the intensity autocorrelation function, $\langle i_{sc}(t)i_{sc}(t + \tau)\rangle$, which decays at a rate dependent upon the time scale of the fluctuations, can provide information about motions of scatterers within a sample. The scattered intensity, $i_{sc}(t)$, is proportional to the square of the amplitude of the scattered field, $E_{sc}(t)$, which will contain components $E_{sc}^{(0)}(t)$, $E_{sc}^{(1)}(t)$, $E_{sc}^{(2)}(t), \ldots$. $E_{sc}^{(n)}(t)$ representing photons that have made 0, 1, 2, ... n collisions with moving cells while traversing the tissue. For an assembly whose statistical properties are unchanging, $\langle i_{sc}(t)i_{sc}(t + \tau)\rangle$ is formed by multiplying the value of i_{sc} at a particular time t by that at a later time $t + \tau$, and then repeating the multiplications for other values of t and adding the products. Consequently, the autocorrelation function can be expressed in normalized form as

$$g^{(2)}(\tau) \equiv \frac{\langle i_{sc}(t)i_{sc}(t + \tau)\rangle}{\langle i_{sc}\rangle^2} = 1 + \beta\,[C(\tau)]^2, \tag{2.1}$$

where β is an instrumental constant and $C(\tau)$ is proportional to the joint expectation of the scattered field, $\langle E_{sc}^*(0)E_{sc}(\tau)\rangle$. $C(\tau)$ is given in normalized form [15,17] as

$$C(\tau) = P_o I_o(\tau) + \sum_{m=1}^{\infty} P_m I_m(\tau). \tag{2.2}$$

In equation 2.2, P_m is the probability that a detected photon has been scattered m times from a moving red blood cell ($m = 0, 1, 2, \ldots$), and $I_m(\tau)$ is the contribution that such a photon makes to the autocorrelation function. Each $I_m(\tau)$ is normalized to the value $I_m(0) = 1$. Even if a photon fails to interact with a red blood cell, there might be a measurable time-dependence to the autocorrelation function arising from Doppler shifts imparted by fluctuations in the tissue lattice. Generally, the nonsanguinous tissue elements move much more slowly than red blood cells, and the Doppler shifts they produce can be discriminated against by appropriate electronic filters. In the following we shall assume that $I_o(\tau) \approx 1$ on the time scale appropriate to the motion of the red blood cells.

The time-varying component of $I(\tau)$, i.e., $[I(\tau) - P_o]$, provides a measure of the time it takes for the scattering centers to move a characteristic distance, $1/|\mathbf{Q}|$, along the direction of $\mathbf{Q}$. If everything in the scattering medium were to be frozen in place, the intensity of scattered light, on average, would be invariant with time. In that case, any fluctuations in the number of scattered photons (per unit time) would arise solely from counting statistics, and would be uncorrelated with those at some other time. If, however, the structure of the scattering medium were changing because of the motion of the scatterers, the fluctuations would have an additional component that reflects the structural rearrangements. For very closely spaced time intervals, the scattered light intensities will be nearly identical, whereas, after sufficiently long intervals, the fluctuating components of the intensities will be uncorrelated if the scattering medium is structurally random in time. The $\{I_m(\tau)\}$ individually tend to zero as τ gets large, so from equations 2.1 and 2.2,

$$g^{(2)}(\tau) \approx 1 + \beta P_o^2 \equiv g^{(2)}(\infty), \qquad \tau \gg 0. \tag{2.3}$$

Consequently, once the instrumental factor β has been determined by calibration, the quantity $[g^{(2)}(0) - g^{(2)}(\infty)] = \beta(1 - P_o^2)$ will yield a value for the fraction of photons that are Doppler-shifted.

The relationship given in equation 2.3 does not depend on assumptions about the specific form of the $\{I_m(\tau)\}$, other than that $I_o \approx 1$. The temporal behavior of $g^{(2)}(\tau)$ can be used to infer information about mean red blood cell speed, but interpretation of data depends, in part, on the details of any physical model adopted for further analysis. First, because of the previously

stated assumption that $\underset{\sim}{\mathbf{V}}$ and $\Delta\underset{\sim}{\mathbf{Q}}$ are uncorrelated, it follows that $I_m(\tau) = [I_1(\tau)]^m$, where $I_1(\tau)$ is the normalized single-scatter photon autocorrelation function. Thus, $g^{(2)}(\tau)$ can be written as

$$g^{(2)}(\tau) = 1 + \beta\,[P_o + (1 - P_o)I(\tau)]^2, \tag{2.4}$$

where the normalized time-varying portion of $I(\tau)$ is given as

$$I(\tau) = \sum_{m=1}^{\infty} P_m[I_1(\tau)]^m/(1 - P_o). \tag{2.5}$$

We now note that P_m implicitly is a function of photon path, and can be written as

$$P_m = \sum_n p(m|n)\,\mathscr{P}(n) \tag{2.6}$$

where $p(m|n)$ is the conditional probability that a photon interacts m times with moving erythrocytes, given that it experiences n scattering events in total before exiting the tissue at the detection point. $\mathscr{P}(n)$ is the probability that a photon indeed makes n collisions. Because, for a uniformly distributed microcirculation, the probability of a photon colliding with an erythrocyte is independent of whether it may previously have collided with an erythrocyte, it is reasonable to assume that the probability density $p(m|n)$ is given by a Poisson distribution, viz.,

$$p(m|n) = \frac{[\bar{m}(n)]^m\, e^{-\bar{m}(n)}}{m!}. \tag{2.7}$$

We can assume that the mean number of collisions with a red blood cell (RBC), $\bar{m}(n)$, is proportional to the total number of collisions, in which case

$$\bar{m}(n) \equiv \kappa\, n, \tag{2.8}$$

where

$$\kappa = \frac{\Sigma_{sc}(\text{RBC})}{\Sigma_{sc}(\text{tissue})}. \tag{2.9}$$

Here, Σ_{sc}(RBC) and Σ_{sc}(tissue) represent the blood cell and total tissue scattering cross sections, respectively. Using equations 2.5–2.9, it is a straightforward matter to show that $I(\tau)$ can be expressed [15,17] as

$$I(\tau) = (1 - P_o)^{-1} \sum_n e^{-\kappa n} [e^{\kappa n I_1(\tau)} - 1] \mathscr{P}(n). \tag{2.10}$$

Because $I_1(0) = 1$, we note that $I(0)$ takes the value

$$I(0) = (1 - P_o)^{-1} (1 - \sum_n e^{-\kappa n} \mathscr{P}(n)) = 1, \tag{2.11}$$

as expected, because $\sum_n e^{-\kappa n} \mathscr{P}(n) = P_o$.

Let us now consider the situation where $\mathscr{P}(n)$ is sharply peaked about a value $\bar{n}$ (i.e., all photon paths are approximately of equal length). In this case it is appropriate to write $I(\tau)$ as

$$I(\tau) = [e^{-\bar{m}[1-I_1(\tau)]} - e^{-\bar{m}}] \; / \; [1 - e^{-\bar{m}}]. \tag{2.12}$$

To further investigate the types of signals that one might expect from a measurement, we make the assumption that RBCs move with a Gaussian speed distribution $P(V)$, i.e.,

$$P(V) = \left[\frac{2}{\pi}\right]^{1/2} \left[\frac{3}{\langle V^2 \rangle}\right]^{3/2} V^2 \, e^{-3V^2/2\langle V^2 \rangle}. \tag{2.13}$$

This distribution is peaked about the most probable speed of $(\frac{2}{3})^{1/2} \langle V^2 \rangle^{1/2}$ (see figure 2–3). Although being a reasonable, but not precise, description of blood cell speeds, equation 2.13 leads to simple expressions for the autocorrelation function $I_1(\tau)$ that enable us to examine the general dependence of laser-Doppler measurements on mean RBC speed and concentration. In fact, the shape of the autocorrelation function is almost independent of $P(V)$, and the expressions we derive are reasonable approximations for any speed distribution. On the other hand, it is impossible to learn the shape of $P(V)$ for RBCs by performing this kind of laser-Doppler measurement on tissues.

Similarly, we assume that the form factor, describing the angular dependence of the light scattering from the RBCs, can be well approximated [15] as

$$\mathscr{F}(Q) \approx \exp [-2 \, \xi \, (Qa)^2], \tag{2.14}$$

where $\xi \approx 0.1$ is a constant, a is the equivalent radius of a cell, and Q is the magnitude of the Bragg scattering vector, defined (as above) as $Q = 4\pi n \lambda^{-1} \sin(\theta/2)$, where n is the index of refraction of the plasma, λ is the wavelength of the light, and θ is the angle between the incident and scattered propagation vectors of the photon. From Mie scattering expressions fitted to measured cross sections, $\xi \approx 0.063$ for 633 nm and $\xi \approx 0.080$ for 800 nm [21]. If we make the additional assumption that the incident vectors are

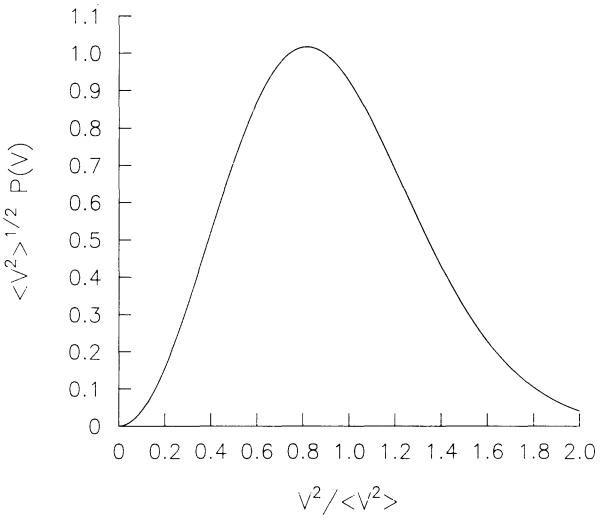

Figure 2–3. Red blood cell speed distribution, $P(V)$, given in equation 2.13, plotted as a function of the ratio of the speed to the rms speed.

completely randomized in direction (which is the essence of the diffusion approximation for light propagation [12], it follows that the single particle autocorrelation function $I_1(\tau)$ can be written [15] as

$$I_1(\tau) \approx \frac{1}{\left[1 + \frac{5}{6a^2} \langle V^2 \rangle \tau^2\right]}. \tag{2.15}$$

This function is shown in figure 2.4, where we plot $I_1(\tau)$ as a function of a reduced variable $T(\tau)$, defined as

$$T(\tau) = \frac{\langle V^2 \rangle^{1/2} \tau}{\sqrt{6}a}. \tag{2.16}$$

Due to the form of equation 2.15, it appears that laser-Doppler flowmetry provides a measure of flow velocity only through the scale factor $\langle V^2 \rangle$. Strictly speaking, the simple dependence upon $\langle V^2 \rangle$ given in equation 2.15 is a consequence of choosing equation 2.13 to describe the RBC speed distribution. In general, however, the function $I_1(\tau)$ for the tissue percolation problem that we are analyzing can be written as a function of the reduced variable $T(\tau) \sim \langle V^2 \rangle^{1/2} \tau / a$, similar in form to that given in equation 2.16, but including correction terms that involve averages of higher-order even powers of V. Since it is impossible to know the details of the flow velocity profile in the tissue bed, not much is lost by using the analytically tractable function given in equation 2.13. However, it must be understood that the flow parameter

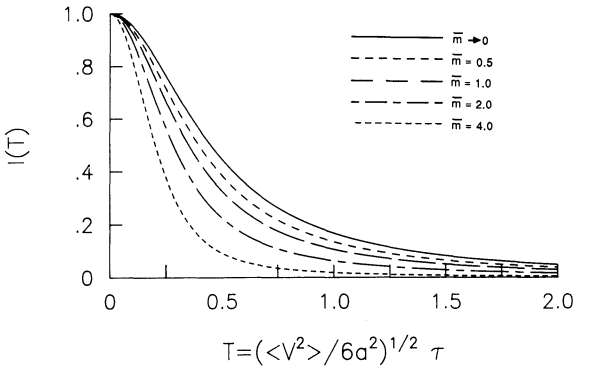

Figure 2–4. Normalized photon autocorrelation function, based on equations 2.12 and 2.15, showing the effect of multiple collisions with moving RBCs (different values of $\bar{m}$). Curves are plotted as a function of the reduced variable given in equation 2.14.

that one measures, which probably is close to the correct value, really is a model-dependent "effective" value.

When equation 2.15 is placed into equation 2.12, the desired autocorrelation function (i.e., that which we expect to measure) can be calculated. As seen from equation 2.12, the shape of the curve depends quite strongly on the value of $\bar{m}$. For small values of $\bar{m}$, $I(\tau)$ tends to $I_1(\tau)$, as expected. In figure 2–4 we show a series of curves for different values of $\bar{m}$. As the mean number of photon–RBC collisions increases, the autocorrelation function tends to sharpen.

As mentioned previously, the information in the time-autocorrelation function can be found, equivalently, in the power spectrum of the detected signal. The significant Doppler-shifted portion of the spectrum, $S(\omega)$, is related to the expression in equation 2.12 [15] as

$$S(\omega) = \frac{1}{\pi} \int_0^\infty \cos(\omega t)\, [g^{(2)}(t) - 1] dt. \tag{2.17}$$

In general, it may be difficult to obtain a closed-form expression for $S(\omega)$. When $\bar{m}$ is much less than 1, $S(\omega)$ tends to $S_1(\omega) + \beta P_0^2 \delta(\omega)$, where $S_1(\omega)$ is given as

$$S_1(\omega) = \frac{2\beta P_0(1 - P_0)}{\pi} \int_0^\infty \cos(\omega t)\, I_1(t) dt. \tag{2.18}$$

This integral can be expressed [15] as an infinite series, each term of which depends on the frequency ω through the scaled variable $W(\omega)$, defined as

$$W(\omega) \equiv (1.2)^{1/2} \omega a \langle V^2 \rangle^{-1/2}. \tag{2.19}$$

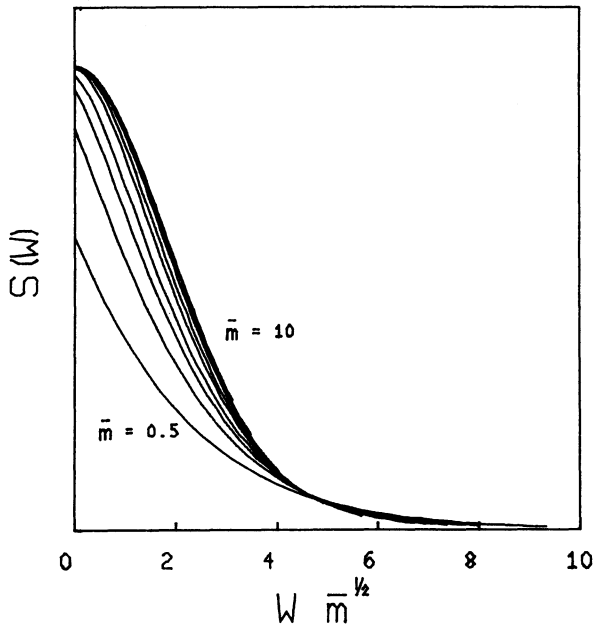

Figure 2–5. Normalized spectra, showing the effect of multiple scattering (different values of $\bar{m}$). Curves are plotted as a function of the reduced variable defined in equation 2.19.

Typical curves, for different values of $\bar{m}$, are shown in normalized form in figure 2–5. For small values of $\bar{m}$, the curves appear to be exponential, whereas for large values they have a Gaussian character.

For present purposes, we wish to focus upon the first moment of the spectrum—a quantity that is closely related to that measured by commercially available blood flow monitors. The first moment of the spectrum here is defined as

$$\langle \omega \rangle = \int_{-\infty}^{\infty} |\omega| \, S(\omega) \, d\omega, \tag{2.20}$$

which, in accordance with equations 2.4 and 2.12, can be expressed [15] as

$$\langle \omega \rangle = \frac{\langle V^2 \rangle^{1/2}}{(1.2)^{1/2} a} \beta f(\bar{m}), \tag{2.21}$$

where $f(\bar{m})$ is given as

$$f(\bar{m}) = \frac{2\exp(-2\bar{m})}{\pi^{1/2}} \sum_{j=1}^{\infty} \frac{(2\bar{m})^j \, \Gamma(j + 1/2)}{\Gamma(j + 1)\Gamma(j)} \tag{2.22}$$

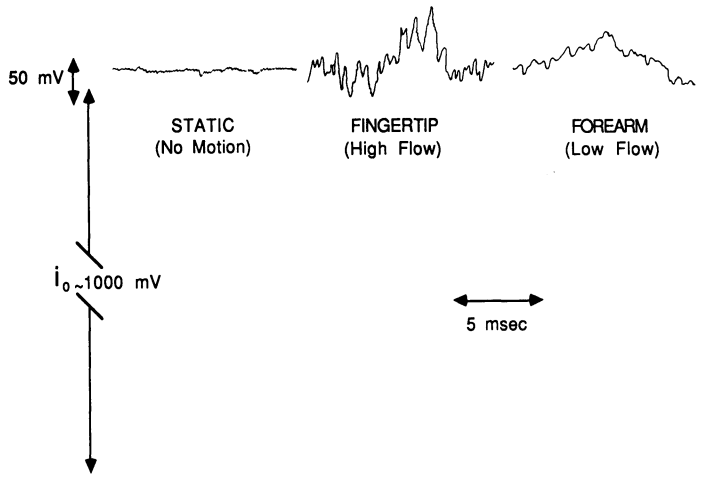

Figure 2–6. Schematic of typical signal detected with a laser-Doppler flowmeter. Phototube current $i(t)$ versus time. The DC (average) component is designated as $\langle i \rangle_{dc}$, so $i_{sc}(t) \equiv i(t) - \langle i \rangle_{dc}$.

The actual form of equation 2.21, and its simple dependence on the root-mean-square speed, $\langle V^2 \rangle^{1/2}$, is obtained because the contributions of the even higher-order moments of the speed distribution in equation 2.13 cancel. Although this is not generally the case, the contribution of the higher-order terms is small even for such extreme cases as a single red blood cell speed or a binary, two-speed distribution [15]. We see from equations 2.21 and 2.22 that, for small values of $\bar{m}$, the moment $\langle \omega \rangle$ is directly proportional to the product of $\bar{m}$ and the mean speed of the cells, thus providing a measure of the flow (see below). For larger values of $\bar{m}$, $\langle \omega \rangle$ cannot be so simply interpreted and corrections may be required, in accordance with equation 2.22, to properly account for the effects of multiple scattering.

In order to apply equation 2.20 to real measurements, it first is necessary to filter out low-frequency artifacts due to tissue motion (e.g., a subject's breathing, muscle twitch, motion of the probe relative to the tissue). Several instruments therefore utilize the following algorithm to calculate the effective Doppler-shift frequency:

$$\langle \omega \rangle_{\text{eff}} \equiv 2\pi \int_{30}^{30,0000 \text{ Hz}} \nu \, P(\nu) d\nu / \langle i \rangle_{\text{dc}}^2, \tag{2.23}$$

where $P(\nu)d\nu$ is the power in the photodetector output current associated with fluctuations in a frequency range $d\nu$ about ν (in Hz), and $\langle i \rangle_{\text{dc}}^2$ is the DC power in the detected signal (see figure 2–6). The average value of the *fluctuating* signal, $\langle i_{sc} \rangle$, here is zero, by definition. By virtue of the low-

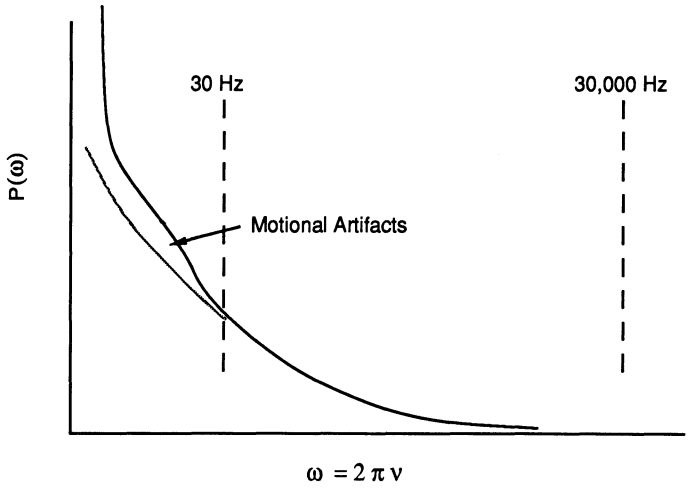

Figure 2–7. Schematic representation of the power spectrum of the detected photocurrent, showing 30 Hz and 30,000 Hz cutoffs.

frequency cutoff, the terms that are associated with tissue matrix movements ($P_0I_0(\tau)$ in equation 2.2) are of no significance, so that it is indeed appropriate to calculate $I(\tau)$ as defined in equation 2.5.

The power $P(\omega)$ is related to the spectrum of scattered light, $S(\omega)$, according to [15]

$$P(\omega) = \langle i \rangle_{dc}^2 [\delta(\omega) + S(\omega)] + \frac{e\langle i \rangle_{dc}}{\pi}, \tag{2.24}$$

where e is a constant and $\delta(\omega)$ is a δ-function (spike) at $\omega = 0$ (figure 2–7). The constant background term that arises from shot noise can be discriminated against and neglected in the following discussion. Thus, the fractional *power* associated with the Doppler-shifted signal can be measured as

$$\chi \equiv \frac{(i - \langle i \rangle_{dc})^2}{\langle i \rangle_{dc}^2} = \int_{30}^{30,000\ \text{Hz}} P(\nu) d\nu / \langle i \rangle_{dc}^2, \tag{2.25}$$

which, from equations 2.1 and 2.3, is seen to be identical to $g^{(2)}(0) - g^{(2)}(\infty)$, i.e.,

$$\chi = g^{(2)}(0) - g^{(2)}(\infty) = \beta(1 - e^{-2\bar{m}}). \tag{2.26}$$

After calibrating an instrument to determine the value of β, it is possible to calculate the mean number of collisions with moving cells, $\bar{m}$, from measurements of the fraction of the power that is Doppler-shifted (e.g., from equa-

tion 2.26). This value of $\bar{m}$ then can be used to determine the concentration of blood cells moving in the tissue, [RBC], according to

$$\bar{m} = \sum_{sc}(rbc) \cdot [RBC]\mathscr{L}, \tag{2.27}$$

where $\mathscr{L}$ is the mean pathlength of the detected light, $\Sigma_{sc}(rbc)$ is the scattering cross section of RBCs, and [RBC] is the number of moving RBCs in a cubic millimeter of tissue.

The mean RBC speed can be calculated from $\langle\omega\rangle/\chi$, using equations 2.21 and 2.26. Strictly speaking, the flow parameter $\langle\omega\rangle$ is the product of $\bar{m}$ (proportional to the red blood cell volume per volume of tissue) and mean speed (cm/sec). Their product has units of flow of blood per unit volume of tissue (i.e., sec^{-1}) times distance (cm). This extra length term arises from measuring all RBCs moving along the length of each sampled blood vessel rather than merely the flow through a cross section of each vessel in parallel. This term represents the mean pathlength of the RBCs' travel through the microcirculation within the volume measured by the laser light. Since the parameter $\langle\omega\rangle$ contains this extra factor, it is frequently called a perfusion parameter. If, for a given tissue, this RBC transit pathlength (i.e., tortuosity) does not vary with physiological changes, then the parameter $\langle\omega\rangle$ will be linear with changes in flow. Since vessel lengths are fixed, the only way in which this RBC pathlength could vary is by changing the distribution of chosen vessel pathways (e.g., shunting) or by changing the size of the sampled volume.

Since the angles between $\mathbf{Q}$ and $\mathbf{V}$ are random, no measure of the directionality of flow or velocity is afforded by this technique. However, unlike normal Doppler measurements such as laser Doppler in clear media or Doppler ultrasound of arteries, one need not know the orientation of the flow relative to $\mathbf{Q}$. All possible angles are measured, weighted by the probability of RBC scattering of light through each angle. Thus, the mean value of $\mathbf{Q}$ used in calibrating the laser-Doppler technique is determined by the optical characteristics of the blood cell (e.g., the equivalent mean radius, a, appearing in equation 2.21).

INFLUENCE OF OPTICAL PATHLENGTH

The mean value of RBC collisions, $\bar{m}$, clearly depends on the paths traversed by the detected photons as they penetrate the tissue. For a homogeneous tissue bed of fixed RBC concentration and blood volume, the value of $\bar{m}$ simply is proportional to the average pathlength of the detected light (equation 2.27). One needs to know how this variable depends, for example, on the distance between the light-delivering and light-detecting fibers (see figure 2–2). If the tissue is inhomogeneous, it also may be important to know how deeply into the tissue the photon penetrates, on average. In certain instances,

one may even wish to know the details of path probability distributions in order to pinpoint the volumes of tissue being sampled. One expects that, the longer the average pathlength, the greater is the dispersion (variance) in individual photon paths (e.g., length and depth). How is the detected signal thereby affected? Can one estimate the necessary tissue parameters by observing the characteristics of the photon emission profiles—i.e., from the diffuse backscattered intensity distribution?

With these questions in mind, we undertook studies to examine, analytically, the properties of photons migrating in turbid biological media [17,18,22,23]. In that work we assumed that the tissue could be modeled by a semi-infinite medium where ρ is taken to designate the distance, along the tissue surface, separating the light-delivering and light-detecting optical fibers. If the medium is homogeneous, an important result, from which several other quantities follow, is an expression for the probability that a photon experiences n collisions with the scattering medium before exiting the tissue (see equation 2.8). If the matrix is modeled by an equivalent isotropic scattering medium, this quantity to a good approximation can be given [15] as

$$\mathscr{P}(n,\rho) = [3/(32\pi^3 n^3)]^{1/2}\,(1 - e^{-6/n})\,\exp(-3\rho^2/(2n) - \mu n). \tag{2.28}$$

where ρ is measured in terms of the mean free path between scatterings (i.e., $\rho = r/L$, where r is the actual physical distance and L is the mean free path of a photon within the tissue). The parameter $\mu = \alpha L$ is the dimensionless absorption coefficient per unit scattering length within the tissue, α being the usual absorption coefficient (units, cm^{-1}).

When equations 2.6, 2.7, and 2.28 are placed into equation 2.5, one immediately finds

$$I(\tau) = A^{-1}\left(\frac{\exp\{-\rho(6\mu)^{1/2}[1 + s(1 - I_1(\tau))]^{1/2}\} - \exp\{-\rho(6\mu)^{1/2}(1 + s)^{1/2}\}}{\rho}\right.$$
$$\left. - \frac{\exp\{-(\rho^2 + 4)^{1/2}(6\mu)^{1/2}[1 + s(1 - I_1(\tau))]^{1/2}\} - \exp\{-(\rho^2 + 4)^{1/2}(6\mu)^{1/2}(1 + s)^{1/2}\}}{(\rho^2 + 4)^{1/2}}\right) \tag{2.29}$$

where s is defined as

$$s \equiv \frac{\kappa}{\mu}, \tag{2.30}$$

and A is a normalization factor, obtained from the quantity in the brackets in equation 2.29 by setting $I_1(\tau) = 1$. When this expression is evaluated with the function given in equation 2.15, generalizations of the curves calculated according to equation 2.12 are obtained in analogy with those presented in

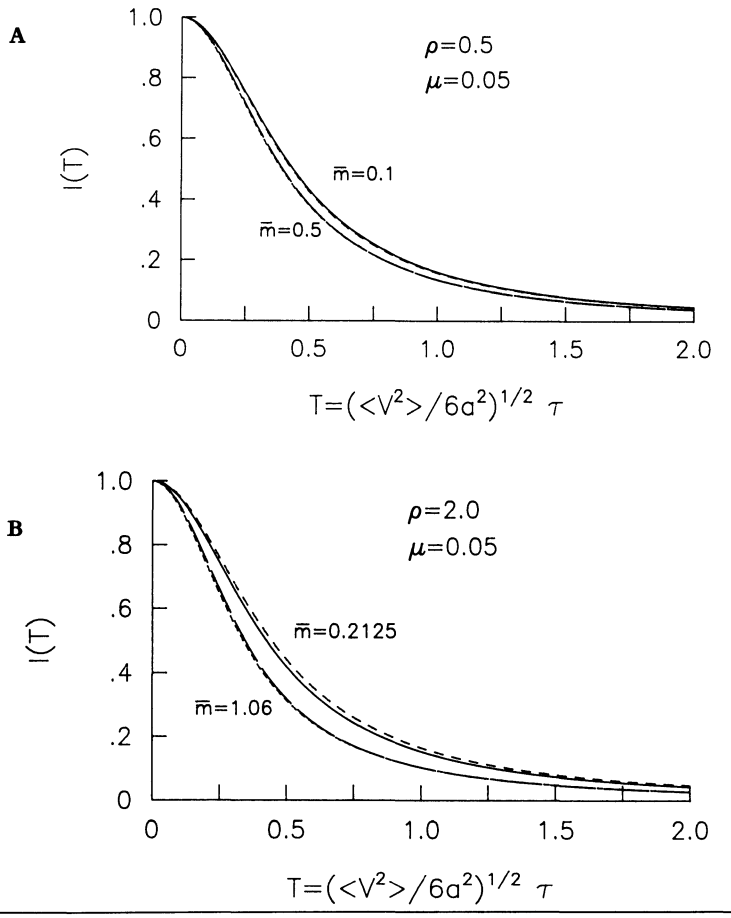

Figure 2–8. Photon autocorrelation functions calculated according to equations 2.15 and 2.29, plotted as a function of the reduced time variable $T = \frac{\langle V^2 \rangle^{1/2} \tau}{\sqrt{6a}}$. Absorption, $\mu = 0.05$.
A. Probe separation $\rho = 0.5$; B. $\rho = 2.0$. Solid lines and long dashes correspond to curves calculated by ignoring pathlength dispersion.

figure 2–5. Some examples are shown in figure 2–8, where curves of $I(\tau)$ are presented for different values of average pathlengths corresponding to differing fiber separations.

The curves in figure 2–8 all were calculated with the value of μ taken to be $\mu = 0.05$, which is a value characteristic of tissue when irradiated with 632 nm light [18]. To obtain the curves shown in figure 2–8A, we chose the probe separation to be $\rho = 0.5$, which corresponds to an actual separation of $\mathcal{R} \approx 1$ mm, a typical value for the probes used in commercial instrumentation. In this case the mean path length, $\langle n \rangle$, was found from figure 8 of [18] to be $\langle n \rangle \approx 4$. The values of $\bar{m}$ that were used, $\bar{m} = 0.1$ and $\bar{m} = 0.5$,

span the range normally to be expected. For figure 2–8B, we chose $\rho = 2.0$, which probably is the maximum value at which data can be acquired without a general redesign of the the instrumentation. In this case, $\langle n \rangle \approx 8.5$.

The quantity s was calculated according to $s = (\bar{m}/\langle n \rangle)(1/\mu)$, which follows from equations 2.8 and 2.30. Curves for $I(\tau)$, calculated according to equation 2.29, are compared with curves for $I(\tau)$, calculated by assuming that all paths have the same length (characterized by a unique value $m = \bar{m}$). In general, one wants to know how a laser-Doppler signal will be affected by differences in pathlength. This is important if different probes are used, or if different tissues are measured, and data are to be compared. In most instances where laser-Doppler techniques are used, the fiber separation is at most only a millimeter. Consequently, the curves shown in figure 2–8A indicate that dispersion in pathlength will not be a large factor in a typical laser-Doppler application that only involves measurement of flow *velocity*. Also, the higher the absorption, the less important are the contributions from long paths and the smaller is the effect of path dispersion. Of course, if the fiber separation is widened or the tissue is very highly perfused, effects of dispersion may have to be taken into account. Some indication of such dependence is seen in figure 2–8B.

Determinations of both the blood *volume* parameter $\bar{m}$ and the *flow* parameter $\langle \omega \rangle$ are more directly affected by fiber separation. One prediction of model studies of photon migration in turbid media is a relationship between average pathlength and fiber spacing, given approximately as

$$\langle n \rangle = 2 + \rho \sqrt{\frac{3}{2\mu}} \left(\frac{1 - \exp\{\sqrt{6\mu}\,[\rho - (\rho^2 + 4)^{1/2}]\}}{1 - \dfrac{\rho}{(\rho^2 + 4)^{1/2}} \exp\{\sqrt{6\mu}\,[\rho - (\rho^2 + 4)^{1/2}]\}} \right), \tag{2.31}$$

where n again is measured in terms of equivalent isotropic scattering lengths (i.e., $nL \Leftrightarrow$ distance). For wider fiber spacing, a linear relationship is obtained from equation 2.31, viz.,

$$\langle n \rangle \approx 2 + 3\rho/\sqrt{6\mu} \qquad \rho^2 \gg 2. \tag{2.32}$$

Thus, as the separation of fibers is increased, the mean number of RBC collisions per photon also increases in a nearly linear manner

$$\bar{m} \approx [2 + 3\rho/\sqrt{6\mu}]\kappa, \tag{2.33}$$

in accordance with equation 2.8. Figure 2–9 shows evidence of this behavior, in which a significant increase in $\bar{m}$ is observed with increasing fiber separation from 0.3 to 3 mm. At even larger fiber separations, the detected intensity falls to such low levels that more powerful lasers would be required to obtain enough light to analyze. Also, at large fiber separations, $\bar{m}$ may become so large (e.g., 1.5 or greater) that virtually all the detected photons

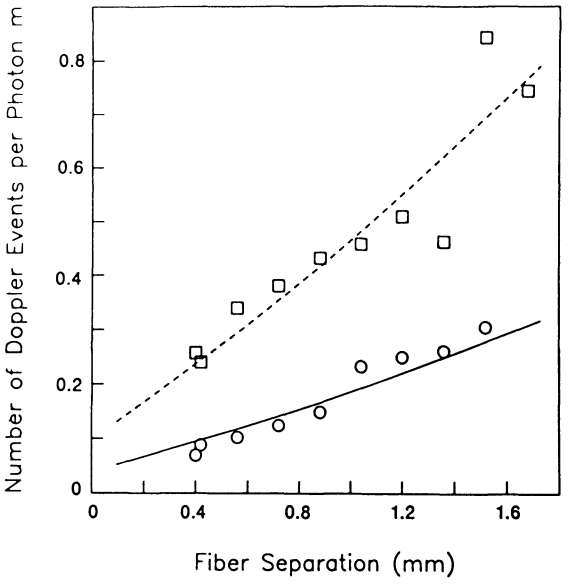

Figure 2–9. Average number of photon collisions with moving red blood cells versus distance along the surface of human forearm skin, measured with a laser blood-flow monitor. Data were obtained with a probe with variable spacing between fibers (○, resting skin; □, vasodilated skin). (Reproduced from [18].)

are Doppler-shifted, many being multiply shifted. In this case, one cannot reliably estimate $\bar{m}$ from the fraction of the photons that are Doppler-shifted (because $e^{-2\bar{m}} \approx 0$ in equation 2.26). As a practical matter, the fiber separation probably should not exceed a millimeter.

An additional complication may occur at larger fiber separations because the optical pathlength decreases as the tissue absorption μ increases. The variation of pathlength with absorption is indicated in figure 2–10, where results of Monte-Carlo calculations of a model of photon migration also are shown. If the tissue absorption at the laser wavelength is predominantly due to absorption by hemoglobin, an increase in blood volume will lead to a decrease in $\langle n \rangle$, partially offsetting the effect of the increase of [RBC] on $\bar{m}$. Such effects should be greatest where hemoglobin absorbance is strongest. With laser wavelengths of 488 and 514 nm (argon laser), these effects are so strong that changes in [RBC] would strongly affect both the pathlength $\langle n \rangle L$ and the volume that is sampled. These effects are much less at 633 nm (He–Ne laser) and even smaller at 785 nm (laser diode). Such a change in average sampled pathlength also could be caused by changes in blood oxygenation (because of differences in absorption between oxyhemoglobin and deoxyhemoglobin). The absorbance of hemoglobin changes dramatically on deoxygenation at 488 nm (from 6000 to 4000 mM^{-1}-cm^{-1}) and at 633 nm

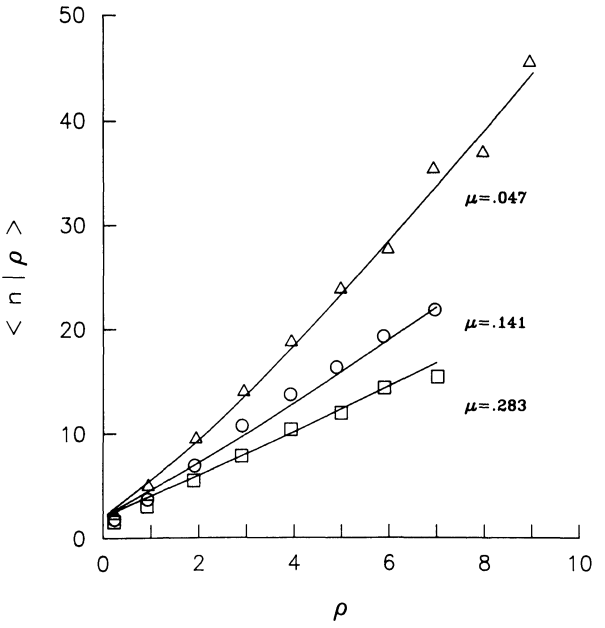

Figure 2–10. The variation of pathlength with probe separation, calculated according to equation 2.31 and compared with Monte-Carlo calculations performed for an isotropic continuum. (Reproduced from [18].)

(from 150 to 1200 mM^{-1}-cm^{-1}), but not significantly at 785 nm (from 190 to 210 mM^{-1}-cm^{-1}).

These effects probably are negligible with a typical fiber separation of 0.5 mm and either a He–Ne or diode laser. However, the use of larger fiber separations or an argon laser (488 or 514 nm) might cause measurements of [RBC] and RBC speed and flow to be affected by the oxygen saturation of hemoglobin.

Another descriptor of photon pathway that may be of interest is the average depth probed by emergent photons before they exit the tissue and are detected. In contrast to the linear relationship with fiber distance shown in equation 2.32, the average depth $\langle z \rangle$ varies as the square root of fiber separation [23], viz.,

$$\langle z \rangle \simeq 0.4\, \rho^{1/2}\, \mu^{-1/4}. \tag{2.34}$$

The dependences on ρ and μ indicated in this equation also have been tested and affirmed by Monte-Carlo calculations [23]. We again note qualitatively reasonable behavior: as the absorption increases, the average depth probed by emergent photons decreases.

To use equation 2.34 for quantitative estimates of penetration depth, it would be necessary to know the tissue absorption coefficient μ and tissue scattering length Σ_{sc}^{-1}. This is perhaps clearer if equation 2.34 is rewritten in terms of real tissue parameters, $\mathcal{R}$ and $\mathcal{Z}$, according to the transformations $\rho = \mathcal{R}L^{-1} = \mathcal{R}L_o^{-1}([1 - \langle\cos\theta\rangle]/[1 + \langle\cos\theta\rangle])^{1/2}$, $z = \mathcal{Z}L^{-1} = \mathcal{Z}L_o^{-1}$ ([1 − $\langle\cos\theta\rangle$]/[1 + $\langle\cos\theta\rangle$])$^{1/2}$ (where $\mathcal{Z}$ is the real-space penetration), and $\mu = ([1 + \langle\cos\theta\rangle]/[1 - \langle\cos\theta\rangle])\nu_o L_o$. We thus obtain

$$\langle\mathcal{Z}\rangle \simeq 0.4\mathcal{R}^{1/2}/(\Sigma_a\Sigma_{sc})^{1/4}. \tag{2.35}$$

Because tissue properties may vary from individual to individual and organ to organ, it may be necessary to estimate the values of the parameters μ and L for specific tissue applications. Fortunately, it appears that this can be done noninvasively for intact tissue by fitting the diffuse surface emission to analytical expressions derived within the context of the theoretical models that lead to equations 2.30–2.35. The diffuse emission intensity about a point located at a distance ρ from the point of photon irradiation, designated as $\Gamma(\rho)$, is given [15] as

$$\Gamma(\rho) = \frac{1}{4\pi\rho}\left\{\exp[-\rho\sqrt{6\mu}] - \frac{\rho}{\sqrt{6\mu(\rho^2 + 1)}}\exp[-\sqrt{6\mu(\rho^2 + 1)}]\right\}e^{-2\mu} \tag{2.36}$$

By fitting surface emission data obtained noninvasively from living tissue to this equation, one in principle can determine the effective scattering and absorption coefficients of the tissue. This was done for human skin [18] as shown in figure 2–11. The values of μ and $L = \Sigma_{sc}^{-1}$ determined for 785 nm, 633 nm, and 516 nm wavelength radiations are $\mu_{785} = 0.048$, $L_{785} = 2.08$ mm, $\mu_{633} = 0.138$, $L_{633} = 1.96$ mm, and $\mu_{516} = 0.697$, $L_{516} = 2.00$ mm, respectively. The dependence of these parameters on wavelength seems to be quite reasonable, in that there is a marked variation of tissue absorption coefficient, but only slight variation of scattering cross section.

The sampled volume can be described by the relative probability of measuring at any given point in the tissue. Values of skin optical coefficients obtained by fitting the data in figure 2–11 to equation 2.36 were used to simulate the sampling distribution of a conventional laser-Doppler blood flowmeter consisting of two 100 μm diameter fibers separated by 0.5 mm. The relative sampling probabilities in human skin are shown in figure 2–12 for 633 nm (He–Ne laser) and 785 nm (laser diode) wavelengths. Most commercial laser-Doppler blood flow monitors use this configuration, for which the signal over short paths is only slightly affected by differences in tissue absorption at 633 and 785 nm. Figure 2–12A shows the fraction of the time that detected photons spend at different depths; Figure 2–12B is a similar indication of the time spent at each distance normal to the plane of the fibers. The equivalent pathlength for most tissues is approximately 2 mm,

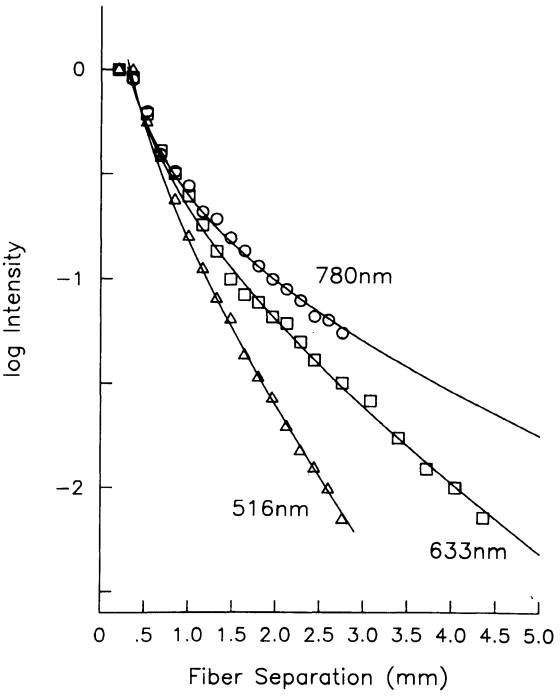

Figure 2–11. Emission intensity measurements for light diffusing within human forearm skin, as a function of probe separation. The solid lines are least-squares fits to the data by equation 2.36. (Reproduced from [18].)

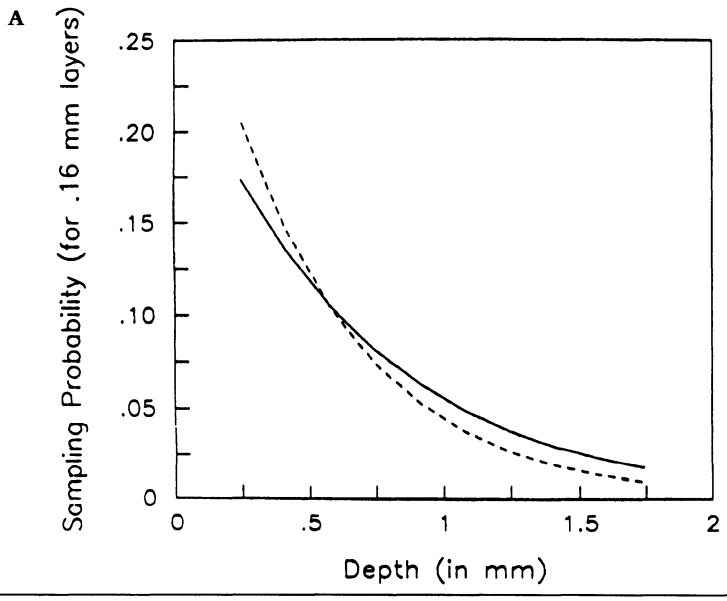

Figure 2–12. Relative probabilities of sampling different layers in human skin, using a laser-Doppler probe consisting of two 0.1 mm fibers separated by 0.5 mm. A. Depth distribution. B. Probability distribution of sampling at a distance perpendicular to the plane defined by the fiber pair. Solid line: 785 nm. Dotted line: 632 nm.

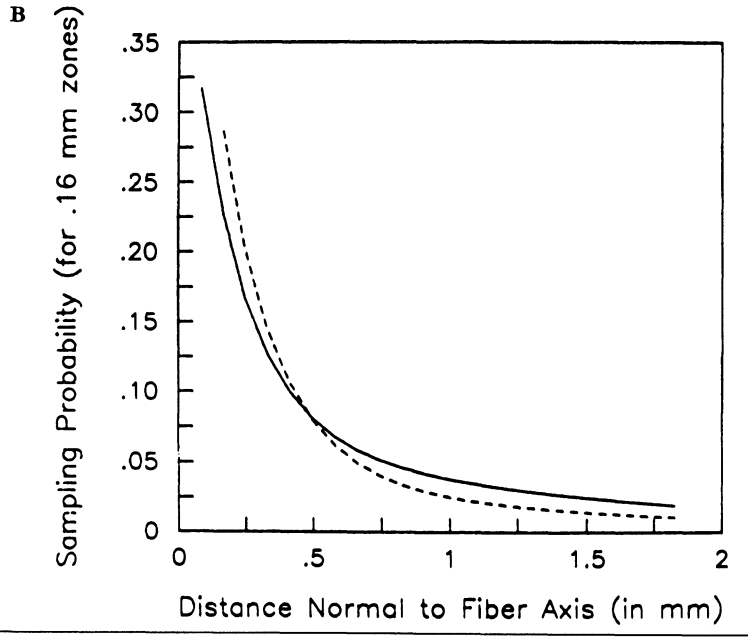

Figure 2–12. (continued)

and the sampling probability falls roughly with an exponential dependence on depth ($1/e$ at $\sim$ 1 mm). Despite the fact that the tissue absorption coefficient at 633 nm is approximately three times that at 785 nm, the sizes of the sampled volumes at 633 nm are only slightly less than those for 785 nm. At shorter wavelengths (for which the absorption μ is appreciable), or much larger fiber separations, changes in tissue absorption may affect both path-length-dependent calibration factors and the volume that is sampled.

At first glance, the values of the scattering length seem to be absurdly high. It must be remembered, however, that the values of μ and L appearing in equations 2.30–2.36 are *equivalent isotropic parameters*. The optical scattering cross-sections in biological tissue actually are strongly peaked in the forward direction, yet the expressions given in equations 2.28, 2.32, 2.34, 2.36, etc. are based on a theory of isotropic random walks [18]. This is an acceptable artifice if, before leaving the sample, a photon makes many collisions with the tissue matrix. In this case, the real scattering lattice can be replaced by one whose scattering centers are separated, on average, by the mean distance that a photon must move before its direction is completely randomized. This can be accomplished [17] by scaling the scattering length that implicitly appears in equation 2.28 (and following equations) by the factor $([1 + \langle\cos\theta\rangle]/[1 - \langle\cos\theta\rangle])^{1/2}$—in other words, replacing the true

scattering cross section Σ_{sc} by an apparent isotropic scattering cross section, Σ'_{sc}, defined as

$$\Sigma'_{sc} = ([1 - \langle\cos\theta\rangle]/[1 + \langle\cos\theta\rangle])^{1/2}\,\Sigma_{sc}, \tag{2.37}$$

where $\langle\cos\theta\rangle = 2\pi \int_0^{\pi} P(\theta)\,\cos\theta\,\sin\theta\,d\theta$ is the expected value of the cosine of the scattering angle. A similar scaling is necessary to obtain values of the effective absorption cross section, $\alpha = ([1 + \langle\cos\theta\rangle]/[1 - \langle\cos\theta\rangle])^{1/2}\,\alpha_0$, where α_0 is the actual absorption cross section (units: cm^{-1}). Consequently, the absorption per equivalent mean free path transforms [17] as $\mu = \alpha L = ([1 + \langle\cos\theta\rangle]/[1 - \langle\cos\theta\rangle])\mu_0$. It is unnecessary to know the actual details of the microscopic scattering processes when information gleaned from surface emission measurements is used to infer pathlengths and depth distributions; if the theory is applied consistently, equivalent isotropic parameters can be used to determine the spatial characteristics of the path distributions.

A common question has been the reliability of measuring flow in heavily pigmented skin. This is a unique case where the pigmented epithelial cells are confined to a thin layer superficial to the microvasculature in the underlying dermis. For a strongly absorbing surface layered on top of a much less strongly absorbing material, our models of light propagation show that light passes directly through the surface layer (being attenuated by the surface absorbers by a nearly constant fraction), and diffuses laterally almost entirely in the lower layer [22]. This means that as the concentration of melanin increases in the epidermis, the total signal collected by the probe decreases, although the volume that is sampled and the pathlengths remain virtually unaffected. Therefore, the dermis is probed in exactly the same manner for dark-skinned individuals as for light-skinned persons, and the laser-Doppler calibration remains unchanged. The insensitivity to epidermal pigmentation or laser attenuation is a consequence of the normalization of the total signal (see equations 2.23 and 2.25).

Similarly, small changes in the absorption or scattering coefficients within tissue layers probably do not have a significant effect on laser-Doppler measurements. Large differences occur when a vascularized pigmented melanoma is compared with normal dermis, since the high absorption coefficient of melanin will greatly reduce pathlength and measurement volume, as well as the intensity of the detected light. Between these extremes, calibration factors may vary when different tissues are compared, such as brain (higher-than-average scattering coefficient), muscle (lower-than-average scattering coefficient), and liver (higher-than-average absorption coefficient). Our understanding of the values of such subtle, yet significant, changes in laser-Doppler calibrations among different tissues is limited. Variations in calibration factors probably are less than 40% for standard probes with a fiber separation of 0.5 mm, but they clearly become larger with increasing fiber separation.

DISCUSSION

A large range of Doppler shifts is observed when laser light is injected at one point on a tissue surface and collected at a nearby point (0.5–1 mm away). Even in Stern's first report [10], it was apparent that a major portion of the light is shifted by much lower frequencies (30–500 Hz) than would be expected to arise from backscatter by red blood cells moving at 1 mm/sec (i.e., approximately 5000–10,000 Hz). In our model, these low-frequency fluctuations are the dominant signal from RBCs in the microcirculation, because the theory takes into account the spectral contributions arising from all scattering angles, weighted by their probability of occurring. Our assumptions are 1) that light is randomized in direction within almost all tissues, independently of blood flow and blood volume; 2) that Doppler shifts due to blood flow principally arise from the scattering of this diffuse light by moving red blood cells; 3) that, since the scattering angle distribution of RBCs is highly anisotropic (mean value only $\sim 6°$ in the forward direction), the magnitude of **Q** is determined by the angular distribution of scattering from RBCs (i.e., 1/20 **Q** for backscatter) and not by the external probe geometry; 4) that the mean number of RBCs by which a typical detected photon is Doppler-shifted increases linearly with the number density of RBCs flowing within the microcirculation; and 5) that the Doppler broadening is increased by multiple scattering from more than one moving red blood cell.

Some comments here are appropriate. First, we note that more than 50% of the long-wavelength (633 or 785 nm) light incident on a tissue surface typically is re-emitted from the surface after being scattered many times within the tissue. Although blood gives well-perfused tissue a pink or red hue, this occurs because hemoglobin absorbs at shorter wavelengths than are used in laser-Doppler flowmetry. Also, the coloration arises from tissue volumes that are much larger than those sampled with typical probes. For a tissue that contains a 10% volume of microvasculature, the tissue optical absorption caused by RBCs is only ~ 0.02–0.03 for 2 mm paths at 800 and 633 nm. At these wavelengths, the diffuse reflectance near the point of incidence is virtually unaffected by the presence of blood (moving or stagnant). Moreover, light principally is scattered by RBCs only through a small angle, with only approximately a one-in-a-thousand chance of backscatter. In contrast, the stationary tissue structures, in aggregate, have much more scattering power and cause much larger angular deviations; thus the diffuse reflection of the laser light back to the detecting fiber depends almost entirely on these stationary tissue structures that do not cause significant Doppler shifts. This may not be the case for some unique tissues such as the retina, which is virtually transparent with a strongly absorbing pigment layer beneath it. In such cases, the diffuse reflectance is much lower, and backscatter from blood may therefore be more significant. Similarly, very thin tissue layers, frequently used in video microscopy of capillary flow, may not be thick enough to diffusely reflect a large fraction of the incident light.

The laser light diffusely reflected from tissue contains two components, one that has been Doppler-shifted by moving blood and one that has not. The fraction of the light that is Doppler-shifted is the ratio of the power in the fluctuating part of the detected signal to its total average power ($\beta\ i_o^2$). For low blood volumes, this fraction is the probability that a typical photon moving through the tissue—from the source fiber to the detecting fiber—will be Doppler-shifted. So long as only a small fraction of the detected light is Doppler-shifted, the actual spectrum of Doppler shifts from tissue will be given by the superposition of spectra for each speed, weighted by the number of the RBCs having that speed within the sampled tissue. This result is very different from the case of ultrasound (or laser-Doppler velocimetry applied to particles moving in clear media). In turbid tissues, one cannot obtain a unique laser-Doppler shift determined by particle velocity and external geometry. Rather, one detects a relatively small symmetric Doppler broadening whose width depends on mean speed and size of the RBC relative to the wavelength of light. Unfortunately this "smearing" of the frequency spectra makes it very difficult to obtain detailed estimates of the *distribution* of RBC speeds, in contrast to determinations in large vessels studied by Doppler ultrasound. On the other hand, the direction of flow relative to the external probe orientation is unimportant, and the mean Doppler broadening is an absolute, rather than relative, measure of mean RBC speed.

The theory outlined here shows explicitly the relationship between the Doppler broadening, $\langle\omega\rangle/\chi$, and the mean speed of the RBCs moving within the sampled volume. The Doppler broadening is proportional to the mean speed, which can be estimated from equations 2.21 and 2.22. When $\bar{m} < 0.4$, this Doppler broadening is virtually unaffected by changes in $\bar{m}$. At higher $\bar{m}$ (longer photon paths or higher [RBC]), $f(\bar{m})/\chi$ is not constant, and the Doppler broadening (mean frequency) increases with $\bar{m}$. This effect is due to multiple Doppler shifts occurring when many detected photons are scattered by more than one moving RBC, an effect which increases the Doppler broadening roughly by a factor of $\bar{m}^{1/2}$. In general, the mean speed can be obtained from the Doppler broadening according to

$$\langle |V| \rangle \approx \langle V^2 \rangle^{1/2} = \langle \omega \rangle \left\{ \frac{(1.2)^{1/2}\ a\ \chi}{\beta\ f(\bar{m})} \right\}. \tag{2.38}$$

As shown in equations 2.25 and 2.26, $\bar{m}$ can be determined from measurements of χ and β. It appears that β is determined by characteristics of the instrument and the fiber optic probe, and possibly can be treated as a constant irrespective of which tissue is measured. The relation of $\bar{m}$ to the number density of flowing RBCs within the tissue sample (given by equation 2.20) depends mainly on the photon pathlength in the tissue. For larger fiber spacings, the theory shows a weak $\mu^{1/2}$ dependence of pathlength on absorption. However, at yet smaller fiber spacing, the dependence on μ seems to be

even weaker, and one probably can ignore any variation of pathlength arising because tissues having different absorption coefficients are measured.

The determination of blood flow from $\langle\omega\rangle$ also depends on $\bar{m}$ and, therefore, on the pathlengths of photons reaching the detector. The variable portion of this calibration factor is $2\bar{m}/f(\bar{m})$, which changes from a value of 1 for small $\bar{m}$ to a dependence on $\bar{m}^{1/2}$ at large $\bar{m}$. Thus, smaller fiber spacings result in relatively constant flow calibrations. However, for values of $\bar{m}$ greater than 2, the quantity χ is close to unity, in which case $\bar{m}$ cannot be accurately estimated, and corrections of the speed, volume, and flow measurements cannot be made. Moreover, the effect of the tissue *scattering* coefficients on pathlengths at small fiber separations may not be accurately described by equation 2.31. This could lead to different calibration factors for both blood volume ($\bar{m}$) and blood flow ($\langle\omega\rangle$) for different tissues. The largest differences in pathlengths are expected to be between brain (low values) and skeletal muscle (high values). If the fiber separation in the laser-Doppler probe is increased, variations in tissue optics (both scattering and absorption) might have large effects on calibration, both in a given tissue and between tissues.

Although the average depth sampled by emergent photons increases as the fiber spacing is widened, the use of light to probe tissue, in effect, limits the depth at which the microcirculatory flow can be measured. Because the detected intensity falls off very rapidly with increases in fiber separation, it is not practical to redesign the probe to measure to any arbitrarily desired depth. Rather, one is restricted to at most a couple of millimeters. Increasing the fiber separation decreases the total signal and increases the fraction that is Doppler-shifted ($\bar{m} \sim \rho$) while increasing the average measured depth only by a factor of $\rho^{1/2}$. Within limits, the loss of signal can be compensated for by increasing the laser power or, perhaps, by increasing the area of the collection fiber (which, however, reduces β). It would be erroneous, though, to presume that increasing the laser power would, in itself, affect the depth that is sampled. The normalizations to the total power that are intrinsic to extracting parameters from the raw data (see, e.g., equation 2.23) have the effect of making all results invariant to changes in laser power.

The theory has ignored detailed effects of tissue motion (both lattice fluctuations and bulk motion of the tissue relative to the laser probe). Under ideal conditions, such motions can be minimized and their frequency contributions will occur below 30 Hz. Therefore, they will be excluded from the RBC Doppler signal, and reliable measures of blood flow and blood volume will ensue. However, in this case some of the low-frequency blood flow signal is also excluded, so the signal measures changes in the concentration of those RBCs that are moving fast enough to cause a Doppler shift greater than 30 Hz. Blood cells that are stagnant or moving very slowly may not be sensed. On the other hand, as the velocity of tissue motion increases, false contributions to the apparent laser-Doppler parameters might occur. For

most measurements, internal motion is quite small (a notable exception being contracting muscle), and the motion of the probe relative to the tissue can also usually be made to be negligible. However, if the fraction of light that is Doppler-shifted by RBCs is small (e.g., $\bar{m} < 0.4$), low-frequency motion artifacts may result in very large errors in determinations of $\bar{m}$ (which increases) and the mean Doppler broadening, $\langle\omega\rangle/\chi$ (which decreases). On the other hand, errors in flow, $\langle\omega\rangle = \int \omega\, S(\omega)\, d\omega$, are not as great because the frequency shifts associated with the extraneous motions are much lower than the mean shifts from the moving RBCs. In extreme cases, such as muscle motion in the beating heart or large motions of the fiber probe relative to tissue, specious motion-induced fluctuations may occur at frequencies as high as those of the blood flow signals. Under such circumstances, all indicated parameters would be considerably greater than those actually relating to the blood flow.

REFERENCES

1. Yeh, Y., and H.Z. Cummins. 1964. Localized fluid flow measurement with an HeNe laser spectrometer. Appl Phys Lett 4:176–178.
2. Chu, B. 1974. Laser Light Scattering. New York: Academic Press.
3. Berne, B.J., and R. Pecora. 1976. Dynamic Light Scattering with Application to Chemistry, Biology, and Physics. New York: Wiley (Interscience).
4. Schurr, J.M. 1977. Dynamic light scattering of biopolymers and biocolloids. CRC Crit Rev Biochem 4:371–431.
5. Nossal, R. 1982. Laser light scattering. Methods Exp Phys 20:299–336.
6. Dahneke, B.E., ed. 1983. Measurement of Suspended Particles by Quasi-Elastic Light Scattering. New York: John Wiley & Sons.
7. Pecora, R., ed. 1985. Dynamic Light Scattering: Applications of Photon Correlation Spectroscopy. New York: Plenum.
8. Tanaka, T., and G.B. Benedek. 1975. Measurement of velocity of blood flow (in vivo) using a fiber optic catheter and optical mixing spectroscopy. Appl Optics 14:189–200.
9. Riva, C., B. Ross, and G.B. Benedek. 1972. Laser doppler measurements of blood flow in capillary tubes and retinal arteries. Invest Ophthalmol 11:936–944.
10. Stern, M. 1975. In vivo evaluation of microcirculation by coherent light scattering. Nature (Lond) 254:56–58.
11. Johnson, C. 1970. Optical diffusion in blood. IEEE Trans Biomed Eng BME-17:129–133.
12. Ishimaru, A. 1977. Theory and application of wave propagation and scattering in random media. Proc IEEE 65:1030–1061.
13. Steinke, J.M., and A.P. Shepherd. 1988. Diffusion model of the optical absorbance of whole blood. J Opt Soc Am [A] 5:813–822.
14. Pine, D.J., D.A. Weitz, P.M. Chaikin, and E. Herbolzheimer. 1988. Diffusing-wave spectroscopy. Phys Rev Lett 60:1134–1137.
15. Bonner, R., and R. Nossal. 1981. Model for laser Doppler measurements of blood flow in tissue. Appl Optics 20:2097–2107.
16. Bonner, R., T.R. Clem, P.D. Bowen, and R.L. Bowman. 1981. Laser-Doppler real-time monitor of pulsatile and mean blood flow in tissue microcirculation. In Scattering Techniques Applied to Supramolecular and Nonequilibrium Systems, Chen, S-H., Chu, B., Nossal, R., eds. New York: Plenum, pp 685–701.
17. Nossal, R., R.F. Bonner, and G.H. Weiss. 1989. The influence of pathlength on remote optical sensing of properties of biological tissue. Appl Optics 28:2238–2244.
18. Bonner, R.F., R. Nossal, S. Havlin, and G.H. Weiss. 1987. Model for photon migration in turbid biological media. J Opt Soc Am [A] 4:423–432.
19. Maret, G., and P.E. Wolf. 1987. Multiple light scattering from disordered media. The effect of Brownian motion of scatterers. Z Phys B 65:409–413.

20. Pine, D.J., D.A. Weitz, P.M. Chaikin, and E. Herbolzheimer. 1989. Features of diffusing wave spectroscopy. In Photon Correlation Techniques and Applications, Abbiss, J.B., Smart, A.E., eds Washington, DC: Optical Society of America, pp 35–43.
21. Steinke, J.M., and A.P. Shepherd. 1988. Comparison of Mie theory and the light scattering of red blood cells. Appl Optics 27:4027–4033.
22. Nossal, R., J. Kiefer, G.H. Weiss, R. Bonner, H. Taitelbaum, and S. Havlin. 1988. Photon migration in layered media. Appl Optics 27:3382–3391.
23. Weiss, G.H., R. Nossal, and R.F. Bonner. 1989. Statistics of penetration depth of photons re-emitted from irradiated tissue. J Mod Optics 36:349–359.

3. MEDPACIFIC'S LDV BLOOD FLOWMETER

G. ALLEN HOLLOWAY, JR.

In December of 1978, an agreement to transfer the then-existing laser-Doppler velocimetry (LDV) technology from the University of Washington to Nuclear Pacific, Inc. was signed, and a few months later the National Institutes of Health signed for an exclusive license for production. Shortly thereafter, design and fabrication of the first-production laser-Doppler flowmeter system began. From the commercial perspective, involvement with this instrument system was a calculated risk because measurement of blood flow in the microcirculation of the skin had been done only by researchers and generally not in clinical settings. The other techniques, e.g., radioisotope clearance and plethysmography, were time-consuming, somewhat costly, and not continuous. Furthermore, they could be used only on certain areas of the skin. Laser-Doppler velocimetry promised to overcome these disadvantages by being noninvasive, continuous, and applicable to any exposed tissue surface.

The meaning of LDV blood flow values recorded from the skin was appreciated only by a few researchers; there were no data available to determine whether significant clinical uses existed for LDV flowmetry in the day-to-day care of ailing patients. However, it appeared that this technology could potentially be of value to clinical medicine and would prove financially rewarding as well.

The basic question confronted by the Medpacific company was how to develop the market for this LDV technology, particularly in clinical settings,

a question that in many respects still remains the biggest problem for manufacturers of the instrument today.

REVIEW OF RELATED HISTORY

As reviewed in chapter 1, the biological use of the laser Doppler began in 1972 with the work of Riva, Ross, and Benedek [1], who studied blood flow velocity in the retinal artery and vein. The development of the method and its first use in the skin was described by Stern [2] in 1975. The first system, created by Stern and coworker Lappe, was transported to the University of Washington in late 1975, where they collaborated with Chimosky and Holloway and made measurements on skin that had been irradiated with ultraviolet light. Independent measurements were made with the ^{133}Xenon radio-isotope clearance technique. The correlation proved good [3] and led to further development of the laser-Doppler system.

While Stern and Lappe continued their work at the National Institutes of Health (NIH), Holloway and Watkins, in early 1976, began developing a clinical laser-Doppler system that would be portable and could be transported to the clinics. This work resulted in a prototype system using a small helium–neon (He–Ne) laser, optical fibers with newly available optical fiber connectors, and a solid-state photodetector. The instrument was portable and could be used on any skin surface [4]. Validation studies with ^{133}Xenon showed a correlation similar to that in the previous studies [5].

In 1978, the parent company of Medpacific, Nuclear Pacific, Inc., expressed interest in manufacturing and marketing this laser-Doppler device. Because a patent had been granted to Stern and Lappe in 1978, Nuclear Pacific negotiated an exclusive license with the NIH for the manufacture of such a system. The technology transfer occurred between Holloway and co-workers at the University of Washington and what became Medpacific, with intermittent additional input from Bonner, then working with the group at the NIH with which Stern and Lappe had previously been associated. An intermediate prototype was assembled at the University of Washington and was additionally modified by Medpacific for production before the first commercial prototype was fabricated. Since then the company has continued to improve the initial model with assistance from both Holloway and Bonner.

Medpacific has recently developed a new, second-generation model. The initial model manufactured was the LD-5000. The newer, second-generation, digital model is the LD-6000. These are both pictured in figure 3–1.

OVERVIEW OF LD-5000 AND LD-6000 SYSTEMS

The LD-5000 and LD-6000 systems function in a similar manner and are based on the principles outlined in chapter 2 and used by other laser-Doppler flowmetry systems. The difference between the two systems is in the signal processing, which is analog in the LD-5000 unit but predominantly digital in

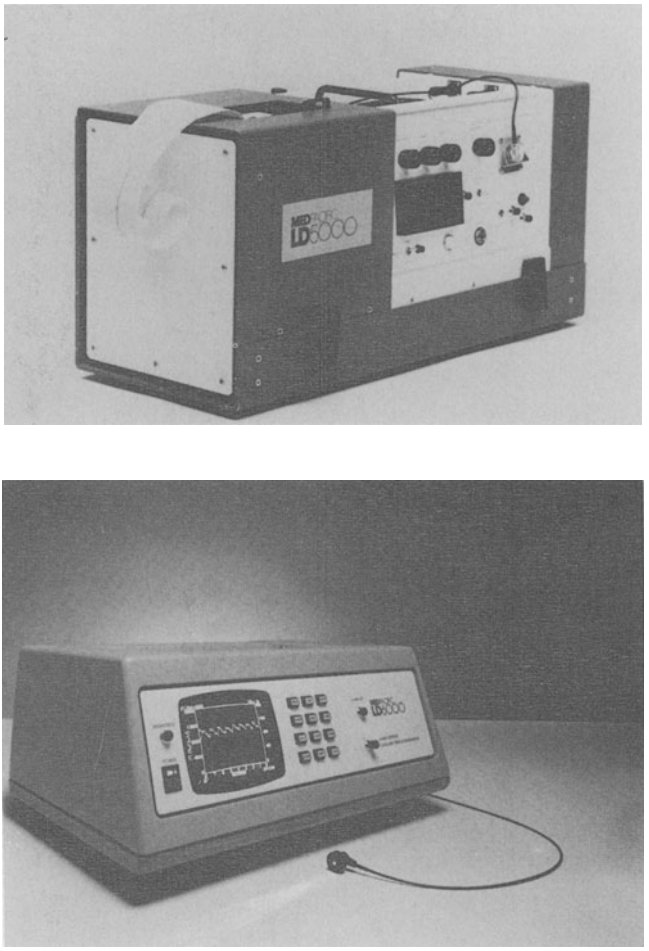

Figure 3–1. Medpacific LD-5000 (upper) and LD-6000 (lower) laser-Doppler flowmeter systems.

the LD-6000 system. The latter system also has an improved output, a CRT display.

A block diagram of the basic configuration of the LD-5000 system is shown in figure 3–2, and that of the LD-6000 system in figure 3–3. The light source in both these systems is a 2 mW helium–neon gas laser. Initially, a 5 mW laser was used, but with the improvement in signal-to-noise ratio that occurred over the first several iterations of the system, an adequate signal could be obtained with a 2 mW source. A 10x microscope objective lens was initially used to focus the laser output into the transmitting optical fiber. However, with the improvement in optical fiber coupling systems, a

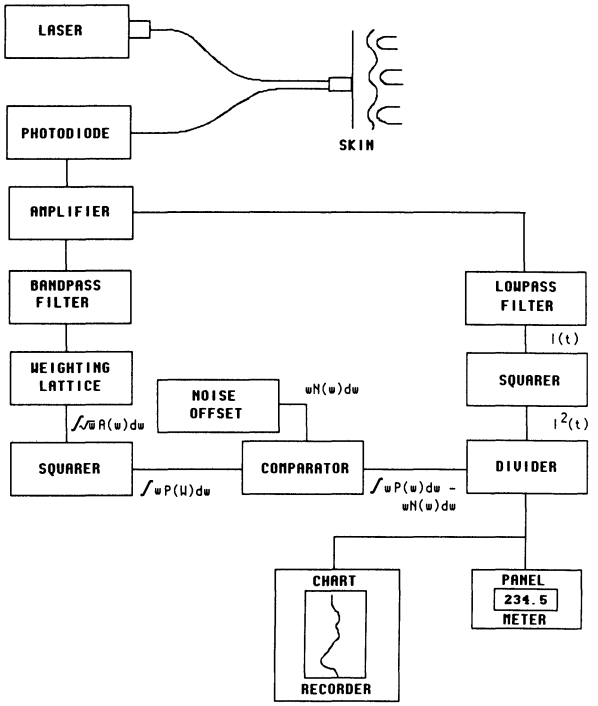

Figure 3–2. Block diagram of the LD-5000 system.

commercially available coupling system was attached to a three-dimensional translation stage, allowing the light from the laser to be coupled into the fiber with greater than 80% efficiency.

The probe is composed of two glass graded-index optical fibers, one transmitting and one receiving, each having a core diameter of 100 μm and an overall diameter, including cladding and coating, of 500 μm. Larger core fibers were tried originally, but they caused excessive noise due to transmission of several longitudinal modes from the laser and their interaction in the fibers and tissue. The resulting high-amplitude mode competition noise resulted in the switch to smaller fibers in the present size range. The smaller diameter essentially eliminated the mode competition noise as well as that caused by fiber motion, eliminating the need for additional common-mode rejection circuitry.

The two fibers enter the probe head parallel to each other and are separated by 0.5 mm at the probe surface, where they are polished. The configuration of the probe head is different for each of the several different types of probes. Each configuration serves to hold the two fibers in their correct orientation and to hold the probe in the proper position to make measurements. The types include hand-held, needle, and flat probes (figure 3–4). The standard

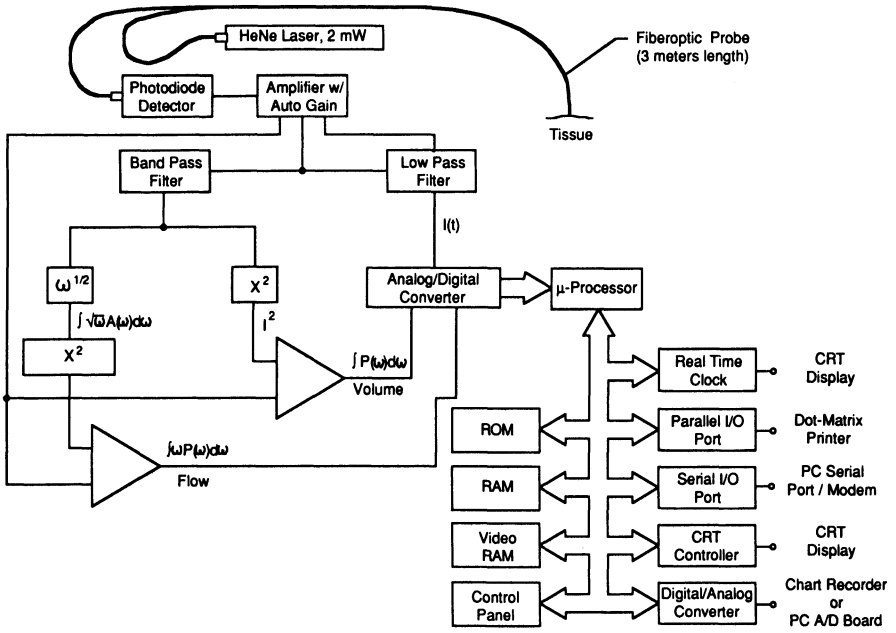

Figure 3–3. Block diagram of the LD-6000 system.

probe has been the hand-held type, which can either be held on the tissue being examined or be glued to it with double-sided adhesive discs. The needle probe consists of the fibers embedded in 18-gauge needle stock, and it can be used in situations where space is limited or inserted into the tissue itself. The third type is a flat probe that is only 2.5 mm in thickness and can be used in situations in which a low probe profile is desired. An additional probe, a heater probe, is the standard hand-held probe with a heater added to permit warming of the skin beneath the probe.

As figures 3–2 and 3–3 show, signal processing proceeds as follows. A portion of the light diffused into the tissue being studied is backscattered and led by the receiving fiber to the surface of a solid-state photodetector. The components of this light from both moving and stationary tissue mix on the surface of the detector.

The output signal is then split, with part of it passing through a low-pass filter. This signal represents the photocurrent or mean backscattered light level, which is then squared and used to normalize the other component of the input signal to permit comparison of signals from tissues with varied pigmentation and backscattering characterics. The other component is bandpass-filtered to within the expected signal bandwidth, fed into the frequency-weighting lattice, and then squared. This process yields an output signal proportional to the first moment of the power spectral density. Early

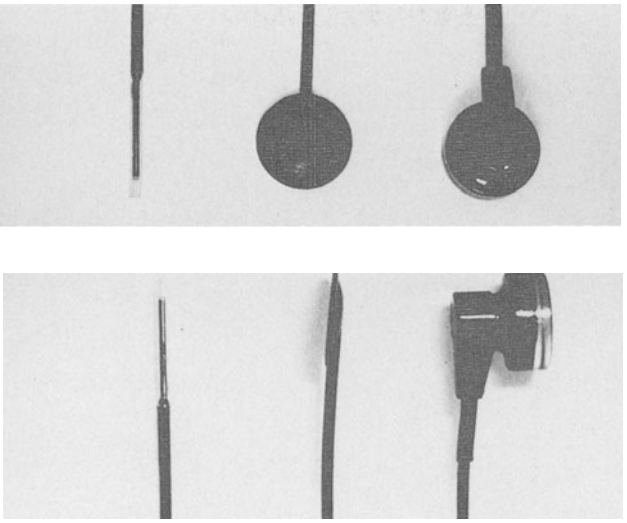

Figure 3–4. Probes for both the LD-5000 and LD-6000 systems. Pictured from left to right are the needle, flat, and standard probes seen from above (top) and from the side (below).

systems used a Root-Mean-Square (RMS) algorithm with weighting by the square of the frequency, but work by Bonner [6] and later work by Nilsson et al. [7] showed that weighting by the frequency itself produced a more linear variation with flow. This algorithm has been used on all subsequent systems. A comparator then allows an offset proportional to system noise to be subtracted, after which the signal is divided by the squared photocurrent in the final normalization process.

The output is fed to either a panel meter, a CRT display, or a self-contained or external strip-chart recorder, depending on the model.

SPECIFICS OF THE LD-5000

The LD-5000 model measures 10″ × 33″ × 8″ and weighs 32 pounds. The construction is a solid design with a metal base and a cover that includes a handle for easy transport. Output is to an LED panel meter that displays values ranging from 0–2000 millivolts. A panel switch selects the display either of the backscattered light level (DC) or of the normalized flow signal (AC). The normalized flow signal is also directed to a built-in strip-chart recorder that records the analog signal at paper speeds of either 5 mm or 5 cm per second. The flow signal and backscattered light level are also available in analog form from BNC connectors on the back panel. Preamplifier gain can be varied by a rotary potentiometer switch to allow for increased gain in tissues with heavy pigmentation.

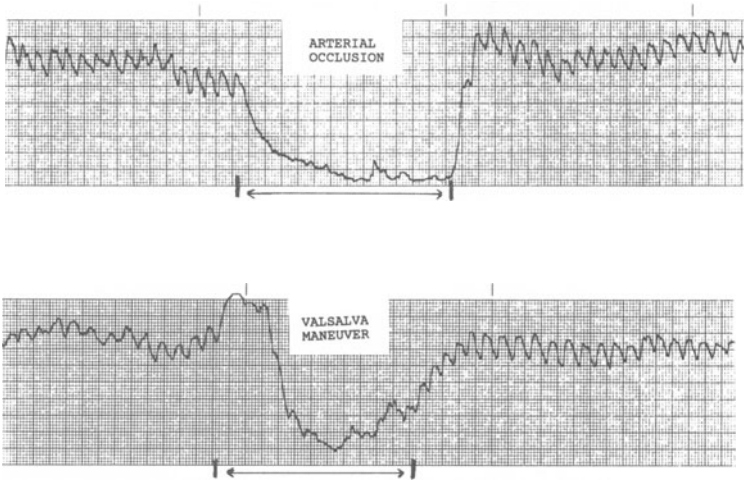

Figure 3–5. Strip chart recording of LD-5000 output. Decrease in flow is seen with arterial occlusion with blood pressure cuff (top), and the Valsalva maneuver (bottom).

The instrument is zeroed by placing the probe on a nonmoving surface that has optical properties similar to tissue and pushing a pushbutton switch. This subtracts the noise component of the signal and gives an absolute zero. The question of what represents a biological zero is still being debated. If arterial inflow to a tissue is halted, red blood cells within the tissue continue to move, and a flow signal, although low, is still present.

SPECIFICS OF THE LD-6000

The LD-6000 model measures 8″ × 17″ × 12″, weighs 24 pounds, and differs in several ways from the earlier LD-5000 model. The most obvious differences are that the instrument is smaller and lighter with a case of plastic rather than metal, and that the output is on a CRT that displays both an analog waveform and a digital value for the normalized flow signal. This display can be set so that the screen will show eight seconds, eight minutes, or eight hours of analog flow data. Digital signal processing includes an automatic gain control (AGC) circuit to compensate for varying pigmentation levels and an automatic zeroing circuit. Also added is an algorithm to determine the relative number of moving red blood cells in the sample volume. This quantity, which is an indicator of the number of red blood cells in the area being evaluated, is also displayed digitally on the CRT. An example of output from the LD-5000 system in response to two different physiological perturbations is seen in figure 3–5.

Outputs for both normalized flow values and red blood cell density are available to the user in both analog and digital form. The latter is in serial

format through an RS-232 connector. An internal strip-chart recorder has not been included in this model, but an external digital printer to capture data from the CRT screen is available as an option.

Probes made for the LD-5000 system can be used on the LD-6000 system but require factory replacement of the optical connectors.

CALIBRATION METHODS

There is no gold standard methodology for the measurement of blood flow to the skin and therefore no standard with which to calibrate laser-Doppler systems. There is also no adequate physical model to represent skin blood flow. As will be discussed in chapter 6, "calibration" of the various systems has involved comparison with results from other methods of measuring cutaneous microcirculatory blood flow such as radio-isotope clearance, venous occlusion plethysmography, and microsphere deposition. Initial studies by Stern [3] and Holloway and Watkins [5] used ^{133}Xenon clearance as the standard. Each manufacturer currently uses different methods of "calibration", so unfortunately results from one machine cannot be quantitatively compared with those of another.

The Medpacific LD-5000 and LD-6000 instruments are calibrated with a standardized suspension of latex microspheres, the Brownian motion of which remains constant at a given temperature. The instruments are adjusted to give the desired fixed flow value when a probe is placed on the surface of a cuvette containing the suspension, which appears to be adequately stable with time and between batches. Each instrument is also set so that when the probe is placed on a nonmoving Delrin surface acting as a nonperfused skin analogue, a reading of zero is obtained. When standardized in this way, the Medpacific flowmeter has yielded results in skin that have compared favorably with results obtained with other methodologies as well as with other laser-Doppler systems.

USE OF THE MEDPACIFIC LD-5000 AND LD-6000 SYSTEMS

As indicated above, the laser-Doppler systems are quite easy to use. The system is zeroed either manually or automatically, and the probe is placed on the surface to be examined. Depending upon the probe configuration, it can be lightly held, set on the surface, or attached using double-sided adhesive discs. Because of slight inherent motion of the hand relative to the skin surface, a spurious flow signal occurs when the probe is hand-held. Therefore, the latter two methods are preferable. Motion of the tissue within reasonable limits does not result in noise with the Medpacific systems, and measurements can be made during activity, including exercise, if reasonable care is taken. Although it is possible to take readings when the probe is not touching the skin surface, such use is difficult because of slight motion of the probe relative to the tissue surface. The small needle probe can be held in a

micromanipulator or similar device and positioned just touching a surface, such as the bowel. This method can achieve a very good, stable tracing.

Although the probe can be moved and multiple readings taken at different locations, most studies necessitate leaving the probe affixed to a single location because it is practically impossible to reposition the probe within the same 1 mm^3 volume and obtain repeatable values for flow. If readings from multiple locations are necessary, it is common to take a number of readings within a small area and determine the average value. This technique has proven useful in many clinical situations such as the evaluation of multiple areas of cutaneous burns to determine perfusion levels in relation to burn depth.

It is also important to realize that skin blood flow is very dynamic and changes in response to a number of physiological variables, only some of which we know. Even though we may intellectually appreciate the volatility of cutaneous blood flow, a wandering baseline is a source of frustration and is often blamed on a faulty instrument. In an awake individual at rest, skin perfusion can vary quite widely in response to emotional input. For instance, a rather marked fall in flow is seen in response to the quiet query between investigators, "Where should we put the needle?" The seemingly random variation is much less when skin blood flow is perturbed, e.g., increased by heating the skin or decreased by local cooling.

Another important point is that the system measures red blood cell motion and is nondirectional. If a blood-pressure cuff is inflated above systolic pressure and flow is measured distally, flow will fall to a very low value, but will not achieve zero, at least initially. Although there is no new nutrient flow into the tissue, there are apparently local pressure differences and vascular activity that cause motion of the red blood cells in the microvasculature in that region. This motion can be easily observed in either the bat wing or hamster cheek pouch preparation under a microscope. When inflow is cut off, one can immediately see this redistribution phenomenon, which can persist for an extended period of time. This has been further demonstrated by Marks and coworkers [8] who have shown that laser-Doppler flow signals fall to zero after a period of several hours or immediately if the experimental preparation is immersed in liquid nitrogen.

As with many instruments, appreciation of what the laser-Doppler flowmeter can and cannot do, pitfalls encountered in different uses, and interpretation of results are a matter of experience in using the particular technique. In biological systems that we do not fully understand, the results frequently do not match our preconceived notions. With repeated use of a laser-Doppler system, appreciation of normal and abnormal flow states is acquired, and results become more interpretable. Our continued combined experience with these various sytems is necessary before we can reasonably evaluate what we are seeing and what the long-term use of these instruments will be.

ACKNOWLEDGMENTS

My thanks to Tom Burnett and Piper Mason of Medpacific, Inc. for their help in obtaining and assembling parts of the information and illustrations for this chapter.

REFERENCES

1. Riva, C.E., B. Ross, and G.B. Benedek. 1972. Laser Doppler measurements of blood flow in capillary tubes and retinal arteries. Invest Ophthalmol 11:936–944.
2. Stern, M.D. 1975. In vivo evaluation of microcirculation by coherent light scattering. Nature 254:56–58.
3. Stern, M.D., D.L. Lappe, P.F. Bowen, J.E. Chimosky, G.A. Holloway, and H.R. Keiser. 1976. Continuous measurement of tissue blood flow by laser-Doppler spectroscopy. Am J Physiol 232(4):H441–H448.
4. Watkins, D.W., and G.A. Holloway, Jr. 1978. An instrument to measure cutaneous blood flow using the Doppler shift of laser light. IEEE Trans Biomed Eng BME-25:28–33.
5. Holloway, G.A. Jr., and D.W. Watkins. 1977. Laser Doppler measurement of cutaneous blood flow. J. Invest Dermatol 69:306–309.
6. Bonner, R., and R. Nossal. 1982. Model for laser Doppler measurements of blood flow in tissue. Appl Optics 20:2097–2107.
7. Nilsson, G.E., T. Tenland, and P.Å. Öberg. 1980. A new instrument for continuous measurement of tissue blood flow by light beating spectroscopy. IEEE Trans Biomed Eng BME-27:12–19.
8. Marks, N.J., R.E. Trachy, and C.W. Cummins. 1984. Dynamic variations in blood flow as measured by laser Doppler velocimetry: a study in rat skin flaps. Plast Reconstr Surg 73(5):804–810.

4. PERIMED'S LDV FLOWMETER

GERT E. NILSSON

Perimed's product line of laser-Doppler flowmeters originated from research activities initiated in 1977 at the Department of Biomedical Engineering, Linköping University in Linköping, Sweden, where a research contract with the Swedish National Board for Technical Development supported a survey of various methods for the assessment of peripheral blood flow. The results of this survey and the early work on tissue laser-Doppler flowmeters by Stern [1] and Holloway and Watkins [2] inspired a project to develop a laser-Doppler flowmeter for use both in clinical settings and in experimental medicine.

The first laser-Doppler flowmeter prototypes utilized 5 mW He–Ne lasers as light sources and thick (700 μm) step-index plastic fibers for conducting the light to and from the tissue. These early prototypes were equipped with ω^2-weighting filters (an ω^2-weighting filter has a power transfer function that is proportional to the square of the frequency) and Root-Mean-Square converters (an RMS converter outputs the effective value of a signal) to produce an instantaneous output signal that could be fed to a pen-recorder for real-time presentation. The initial tests of these prototypes revealed a significant problem caused by mode interference that originated from internal modulation of different longitudinal modes in the multimode lasers [3]. In heterodyne detection by a square-law photodetector, beat frequencies between different laser modes were manifested as intermittent noiselike signals sweeping through the frequency range under study. This problem was overcome

by the introduction of a differential detector technique [4] that will be described in further detail below.

In a subsequent study, the performance of different signal-processing algorithms was tested. The results of this investigation showed that a processor based on an ω-weighting filter gave a linear relationship between the output signal and blood flow through a mechanical model [5]. The performance of this processor also agreed with mathematical theories of dynamic light scattering in perfused tissues at low and moderate tissue hematocrits [5,6]. The processor was later improved so that it yielded a linear measure of blood flow even in high hematocrit tissues that give rise to the multiple scattering of a given photon by several moving blood cells [7]. In addition to the ω-weighting processor, the circuit provided a continuous output signal linearly related to the relative concentration of moving blood cells (CMBC). Because cutaneous blood flow is temperature-dependent, the system included a thermostatic probe holder to clamp the skin temperature to a selected value.

During the various phases of its development, the instrument's performance was examined in flow simulators as well as in in vivo animal models. Comparisons with other measurements of tissue perfusion yielded linear relationships with correlation coefficients up to 0.98 [8,9,10].

Currently, Perimed markets two models of laser-Doppler flowmeters (PF2b and PF3) to which a wide range of probes, intended for various applications, can be connected.

OPERATING PRINCIPLE

Signal-processing features common to both the Periflux PF2b and PF3 are outlined in the block diagram in figure 4–1. Monochromatic light from a 2 mW He–Ne laser is guided through an optical fiber to the tissue, where diffuse scattering, partial absorption, and spectral broadening due to the Doppler effect take place (for further details of this process, see chapter 2). A portion of the scattered light is captured by two separate optical fibers that conduct it to two photodetectors where demodulation automatically takes place. The electrical output signals from the two photodetectors are fed through high-pass filters (HP), amplifiers, and normalizing circuits, and finally into a differential amplifier, the output of which forms the unprocessed Doppler signal. This arrangement rejects laser noise and other sources of in-phase noise common to both channels, whereas the Doppler signals, being two independent realizations of the same stochastic process, pass through the system unsuppressed.

As the lower portion of figure 4–1 shows, the unprocessed Doppler signal is fed into the ω-weighting filter, then squared (X^2) and low-pass filtered (LP), after which a signal proportional to the average photodetector current is subtracted in order to eliminate shot noise. The output signal of this compensator is proportional to the first moment of the power spectral density ($\int \omega P(\omega) d\omega$). The first moment of the Doppler spectrum is linearly

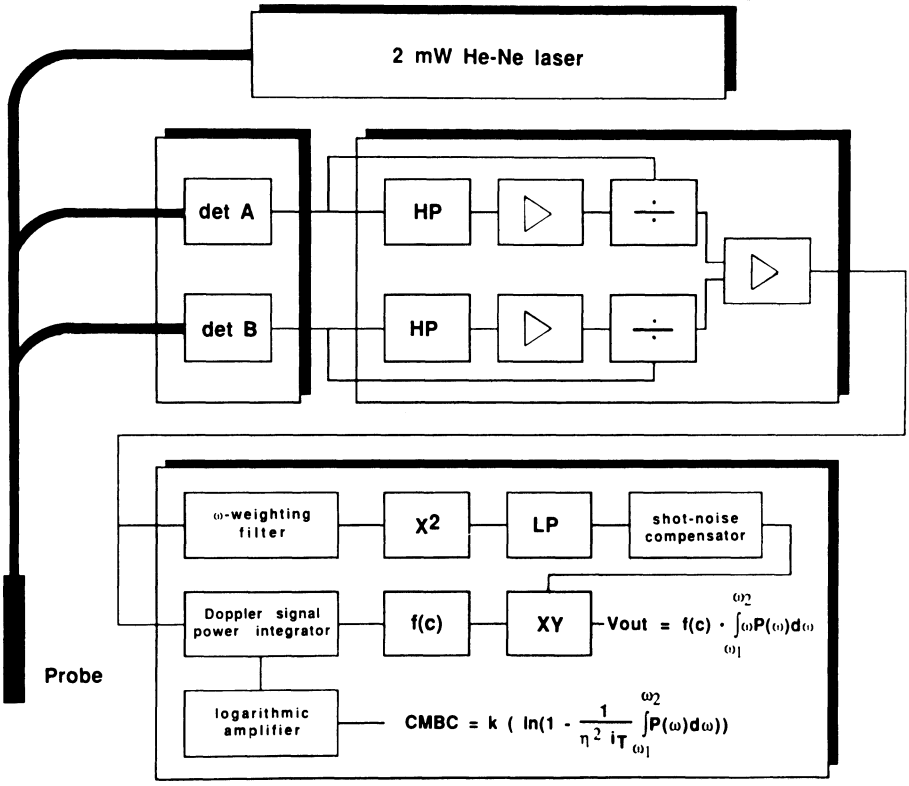

Figure 4–1. Schematic diagram of the basic operating principle of Periflux PF2b and PF3 (for definition of symbols, see equations 4.1 and 4.2 in the text).

related to the tissue perfusion defined as the average blood cell velocity multiplied by the blood cell concentration (c) within the scattering volume, provided this concentration is low enough to generate only a negligible amount of multiple scattering. To make the output signal a linear function of blood flow even at higher tissue hematocrits, the first moment of the power spectral density is multiplied by a compensation factor, $f(c)$, that is derived from the total power of the unprocessed Doppler signal [7], which is related solely to the concentration of moving scatterers. Finally, taking the logarithm of the total power of the unprocessed Doppler signal yields an output that scales linearly with the instantaneous concentration of moving blood cells (CMBC).

INSTRUMENTATION

The *light source* in both PF2b and PF3 is a 2 mW He–Ne laser with a Gaussian beam width of 0.8 mm. The laser tube is suspended in a device that allows

the tube to expand thermally without causing misalignment of the laser beam. After passing through a shutter, the beam is directed through a spatial translation system comprising a precision-moulded female connector into which the male connector of the probe is inserted. The aperture of the shutter is adjusted to give an output power less than 1 mW at the probe tip. Thus FDA regulations (21 CFR 1040.10 and 1040.11) rank these instruments as class II laser products.

The *probe* includes three optical fibers, one to conduct the light from the laser to the tissue and two to carry a portion of the scattered light back to the two photodetectors. All probes utilize a step-index silica fiber with a core diameter of 120 μm, a hard cladding layer of 10 μm, and a numerical aperture of 0.37. This fiber was chosen because of its flexibility, small bending radius and small outer diameter. Because of these characteristics, probes for use on the tissue surface can be constructed in which the fibers run in parallel with the surface. Furthermore, these fibers are sufficiently slender to use in invasive microprobes for measuring deep tissue perfusion.

A microlens that focuses the laser beam onto the transmitting fiber is integrated into the probe connector. The focal length of the lens allows only the lower-order modes of the transmitting fiber to be excited. Thus an effective numerical aperture of about 0.15 is achieved at the probe tip. By exciting only the lower-order modes of the fiber, the fiber-movement artifacts generated mainly by higher-order modes are suppressed. At the probe tip, the three fibers are symmetrically positioned with core center spacings of 250 μm. Widening the distance between the transmitting and the receiving fibers tends to increase the measuring depth from which the scattered light is received, while at the same time the total light intensity impinging on the photodetectors is lowered, decreasing the signal-to-noise ratio. Furthermore, a wider distance between the transmitting and the receiving fiber tips favors the detection of photons that have taken longer pathlengths in the tissue. Consequently, these photons have had a higher probability of suffering multiple Doppler shifts. On the other hand, positioning the fiber ends too close together in the probe tip reduces the average tissue migration distance of the photons that reach the receiving fibers. Reducing the fiber separation yields shallower measuring depth, reduces the fraction of the detected photons that have suffered a Doppler shift, and thus reduces the signal-to-noise ratio. The choice of a fiber spacing of 250 μm is therefore considered a reasonable compromise that will give a measuring volume of about 1 mm^3 and a sufficient signal-to-noise ratio to record even the most minute perfusion rates.

Figure 4–2 shows the power spectra recorded from forearm skin by two identical laser Doppler instruments equipped with probes that contained fibers of different diameters (120 μm and 700 μm). Figure 4–2 also shows the power spectral densities produced by speckle pattern fluctuations mimicking blood flow when the fibers of the two probes are made to

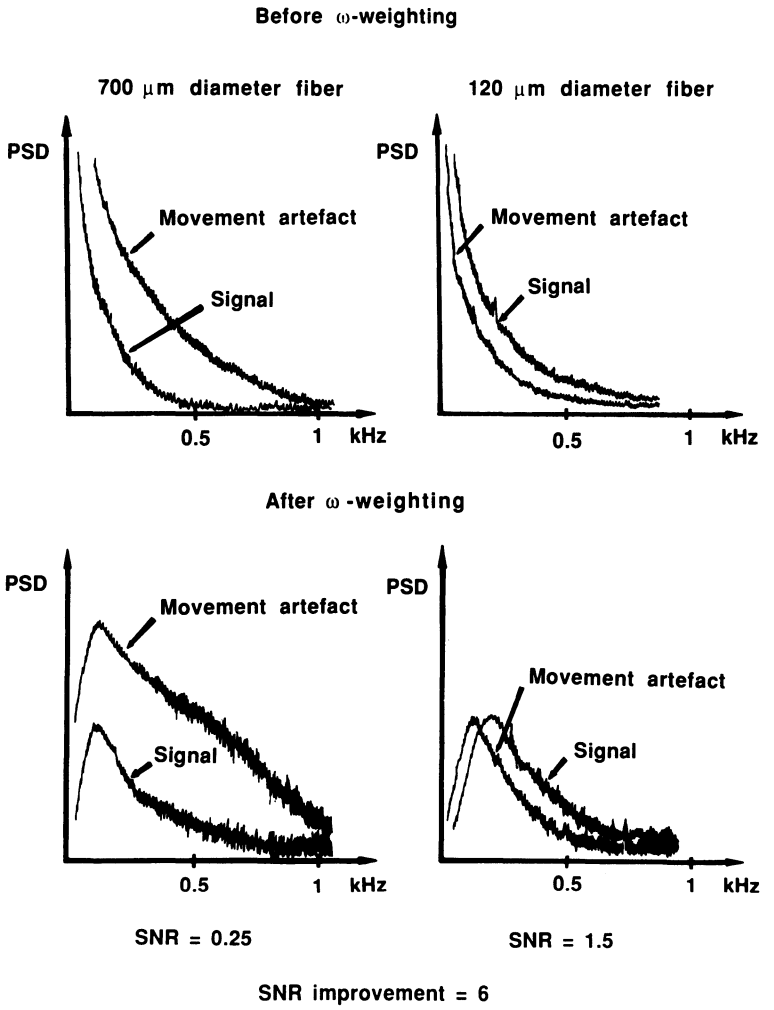

Figure 4–2. Power spectral density (PSD) before and after ω-weighting caused by fiber-movement artifacts and blood flow, respectively, as recorded by laser-Doppler flowmeters equipped with 700 μm and 120 μm step-index fibers. SNR = signal-to-noise ratio.

oscillate slowly with the same frequency and amplitude. Because the power spectra of the signal and the movement artifact overlap, they cannot be separated by simple filtering. The number of modes carried by the optical fiber is proportional to the square of the fiber diameter. Thus substantially more of the light energy is transported by higher-order modes in the 700 μm fiber than in the 120 μm fiber. Therefore, when the fibers are flexed or twisted, the wider difference in pathlength between low- and high-order modes in the 700 μm fiber causes a more rapid fluctuation in the speckle

pattern that appears on the photodetector surface. Consequently, the power spectral density obtained by the instrument equipped with the 700 μm fiber probe is shifted towards higher frequencies. After the signals are fed through the ω-weighting filter, the total energy of the signals related to fiber movements is significantly higher in the probe with the thicker fibers, while the signal energy related to moving blood cells is essentially the same in the two systems. The signal-to-movement artifact ratio was improved by about a factor of six when 120 μm fibers were used instead of 700 μm fibers. Theoretically, using thick fibers would allow the probe to integrate blood flow over a large number of small vessels, but this advantage is offset by the fact that fiber-movement artifacts are suppressed when the diameter of the fiber is reduced.

A further reduction in fiber-movement artifacts can be achieved by using 50 μm graded-index fibers. These fibers, which have significantly fewer modes than step-index fibers, reduce the bandwidth of the movement artifact noise to even lower frequencies. However, they do so at the expense of a higher-magnitude intensity fluctuation when the fiber does move. Further reduction of the fiber diameter may also cause misalignment problems in the probe-to-instrument connector, especially when the probes are exchanged frequently. When the diameter of the fiber is reduced to 50 μm and below, the dimension of the launching and receiving fiber apertures also become smaller than the distance between the capillaries in normal skin (the average capillary density is about 50 capillaries per mm^2). This density implies that even though the entire scattering volume may be on the order of 1 mm^3 and may include a large number of small vessels over which the signal is integrated, the portion of the scattering volume just in front of the receiving fiber may or may not contain a capillary, yet it contributes the greatest weight factor to this integral. Further reductions of the fiber diameter can be made, but only at the risk of losing the integrating ability of the method.

To acheive both an acceptable reduction in fiber-movement artifacts and an integrating ability of the probe, a core diameter of 120 μm was considered a reasonable tradeoff.

To keep the influence of movement artifacts at a minimum, mechanical contact between the probe tip and tissue must be maintained. Physical contact is required not only to avoid relative motion between the probe and the tissue but also to prevent Fresnel scattering of the light speckle in the tissue surface directly into the receiving fibers. During measurements, the probe tip is inserted into a probe holder attached to the skin surface by double-sided adhesive tape, thus ensuring a firm and stable contact between the probe tip and tissue without occlusion of the most minute vessels.

The assortment of Periflux probes ranges from standard probes for recording cutaneous perfusion to flexible probes that can be inserted through a gastroscope. Probes with an outer diameter smaller than 500 μm are intended for measurement of the blood flow in deep tissues. Spatial differences, espe-

cially in skin blood flow, stimulated the development of an integrating probe that averages blood flow in seven adjacent locations [11]. Because probe design is often the key to a successful application, Perimed has a program for constructing custom probes.

The *detector unit* of each channel is composed of a discrete pin-diode followed by a high-input impedance amplifier, operated in a current-to-voltage converter mode. A high signal-to-noise ratio is attained by selecting a high feedback resistor value of 22 Mohm. At the surface of the photodetector, demodulation takes place and results in a photocurrent proportional to the instantaneous light intensity. The fluctuations in the preamplifier output voltage correspond to the Doppler signal produced by the moving scatterers, but they also result from photodetector shot and dark-current noise, thermal resistor noise, and common-mode signals such as laser noise, external lightning, and hum. The magnitude and frequency of the fluctuations produced by the Doppler effect are related to the concentration and velocity of the moving blood cells, respectively. Since the fibers carry numerous modes, the intensity fluctuations are only 1% of the total preamplifier output signal. The photodetector shot-noise power is linearly related to the total photocurrent, which in the signal-processing block is used for automatic noise compensation. The photodetector dark-current noise and feedback resistor thermal noise powers are independent of light intensity.

In the *signal-conditioning unit*, the active third-order high-pass filters with a −3 dB cutoff frequency set to 20 Hz extract the fluctuating portion of the signals, including the Doppler components, from the total preamplifier output signals. It is important to keep the cutoff frequency of these filters as low as possible in order to generate an overall output signal that scales linearly with the velocity of the blood cells in the capillary network (about 0.5 mm/sec). The ratio between the diameter of the moving blood cells and the wavelength of the light is such that most of the light is scattered in the forward direction. Thus, most of the Doppler components are below 100 Hz for these slow-speed scatterers (for details see chapter 2).

To make the blood-flow signal independent of the total light intensity that impinges on the photodetectors, the signal is fed through a normalizer in which the Doppler signal is divided by the preamplifier output signal that is linearly related to the total light intensity. Subsequently, a differential amplifier suppresses common-mode components, thus increasing the signal-to-noise ratio of the unprocessed Doppler signal.

In the *signal-processing unit*, the unprocessed Doppler signal is first fed through an ω-weighting filter composed of four active filters in cascade. By this arrangement, the deviation from the ideal transfer function is below +/−3% within the signal bandwidth 20 Hz–12 kHz. An active third-order low-pass filter with a -3 dB cutoff frequency that can be set to 4 or 12 kHz reduces the influence of high-frequency shot noise and limits the instrument bandwidth to match the bandwidth of the Doppler signal. After this signal is

squared, a voltage proportional to the power of the photodetector shot noise is subtracted to obtain an output signal proportional to the instantaneous value of the first moment of the Doppler power spectral density. Time constants of 0.2, 1, or 3 seconds can be selected by a switch located on the front panel.

To obtain an output signal that is linearly related to tissue perfusion even in tissues with such high concentrations of blood cells that the effect of multiple scattering cannot be neglected, a linearizer circuit is included in the signal-processing block. In this linearizer, the signal proportional to the first moment of the Doppler signal is multiplied by a compensating factor $f(c)$, which is derived from the total power of the Doppler signal. For low concentrations of moving scatterers, this compensating factor is unity, whereas at higher concentrations the value of the factor increases. The mathematical relationship between the compensating factor and blood cell concentration was determined experimentally with a flow simulator [7]. The overall output signal (V_{out}) that is linearly related to tissue perfusion can be expressed by the formula

$$V_{out} = f(c) \int_{\omega_1}^{\omega_2} \omega P(\omega) d\omega, \tag{4.1}$$

where $P(\omega)$ is the power spectral density of the Doppler signal, ω_1 is the lower-frequency cutoff, and ω_2 is the higher limit, selected by the operator. Fiber-movement artifacts can be suppressed by a slew-rate filter connected in series with the output signal through a push button on the rear panel.

The relative *concentration of moving blood cells* (CMBC) is also available as an output signal on the rear panel of the flowmeter. This signal is derived from the total power spectral density of the Doppler signal according to

$$\text{CMBC} = k \left(\ln\left(1 - \frac{1}{\eta^2 i_T} \int_{\omega_1}^{\omega_2} P(\omega) d\omega\right)\right), \tag{4.2}$$

where k is a constant, η^2 is an instrumentation factor dependent primarily on the optical coherence of the signal at the detector, and i_T is the total photocurrent.

It must be emphasized that this signal is related only to the concentration of *moving* blood cells and thus tends to decrease to zero during arterial occlusion experiments, even though the total concentration of blood cells in the tissue under study may be unchanged.

The *temperature module* includes a thermostatic probe holder that contains a heater and a temperature sensor. The temperature of the thermostatic probe holder surface facing the skin can be set to any temperature ranging from 26 to 44°C in steps of 2°C. A separate thermistor monitors the temperature in the heater and automatically switches the power off in case of overheating.

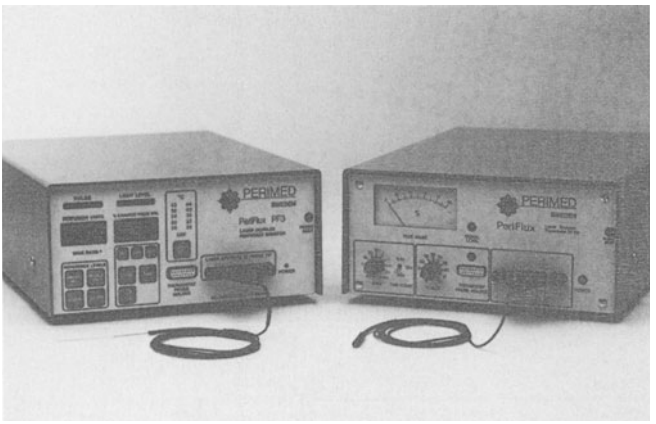

Figure 4–3. The Periflux PF2b laser-Doppler flowmeter and Periflux PF3 laser-Doppler perfusion monitor.

PERFUSION MONITORING

In clinical applications such as postoperative surveillance of the viability of skin grafts, changes in the perfusion of the grafts have proved to give an early warning of failure [12,13]. The Periflux PF3 incorporates monitoring features such as low-perfusion-level detection and alarm settings designed to meet this and other clinical demands. The basic operating principles of the PF3 laser-Doppler perfusion monitor are the same as those previously described for the PF2b laser-Doppler flowmeter. The Periflux PF3 is divided into a flowmeter, a monitoring module, and a temperature-control section (see figure 4–3). The front panel is equipped with touch controls and digital displays. All the processing of information inside the monitor is controlled by a microcomputer, and output data in serial form are available through an RS232 connector on the rear panel.

In the *flowmeter module*, the perfusion value (0.0–999 perfusion units) is displayed on a three-digit display that is updated every two seconds. The time constant of the perfusion value displayed is always five seconds. Autoranging facilitates the display of low perfusion values with one decimal place, while higher perfusion values are given without decimals. Two instantaneous perfusion values can be stored in memory and recalled to the display at any later occasion. It is thus possible to compare the current perfusion value with a reference perfusion value stored in memory at the beginning of an experiment. The flowmeter module can operate in wideband (12 kHz) or narrowband (4 kHz) mode. A separate 11 LED display indicates the magnitude of the pulsatile portion of the perfusion value.

In the *monitoring module*, the digital display indicates the percentage deviation (−99% to +999%) of the instantaneous perfusion value from the refer-

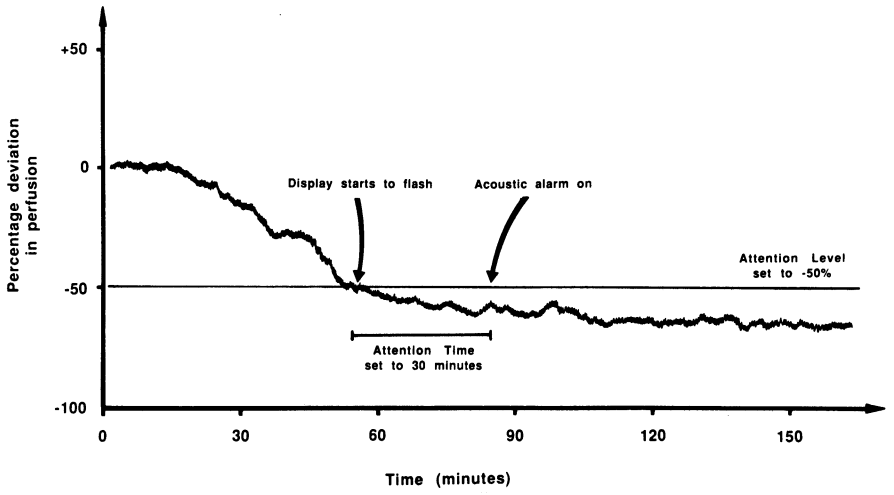

Figure 4–4. Monitoring successive impairment in skin-flap blood flow by the Periflux PF3 laser-Doppler perfusion monitor.

ence value stored in memory. When this percentage deviation decreases below an Attention Level set by the operator (see figure 4–4), the display starts to flash. If this condition persists for a time period longer than an Attention Time value also set by the operator, an acoustic alarm is triggered, calling the attention of the nursing staff. The monitoring module therefore constitutes a tool for the automatic detection of impaired perfusion in a skin flap.

In the monitoring module, an 11 LED display indicates the instantaneous value of the total amount of scattered light impinging on the photodetectors. In monitoring applications, this value decreases during venous stasis but remains virtually unaffected during complete arterial occlusion [14,15].

In the *temperature module*, the target temperature of the heating element in the thermostatic probe holder is set by a touch-control button. The front panel shows both the target temperature and the actual heater temperature, which is brought to the target temperature within ten seconds by the feedback loop. In case of overheating, which is detected by a separate safety circuit, the current to the heater element is automatically switched off, and an acoustic alarm is triggered.

EVALUATION

The choice of an ω-weighting filter as the core of the signal processor is based on mathematical models of dynamic light scattering in tissue (chapter 2). To keep the complexity of these models within reasonable limits, a number of assumptions must be made, and only some of the phenomena involved in the scattering process may be accounted for. Aspects of dynamic

light scattering in tissue that are not included in these models but that can be elucidated by the use of flow simulators and in vivo experiments are discussed below.

Within the conceptual framework of the models, it is assumed that the moving blood cells, regarded as spherical scatterers, are homogeneously distributed in tissue and that the velocity vectors of different scatterers are independent. This is generally not the case in real tissue, where the blood cells may be closely packed together within the minute vessels, and correlated multiple scattering events may occur even though the overall tissue hematocrit is low. Furthermore, the statistical approach to modeling may be questioned when the dimensions of the most sensitive part of the scattering volume, located just in front of the transmitting and receiving fiber apertures, are of the same magnitude as the distance between the individual blood vessels. This is the case when the core diameters of the transmitting and receiving fibers are too small. In addition, the models of dynamic light scattering in tissue do not include other sources of Doppler signals such as the possible contribution from vessel walls moving synchronously with the arterial pulse. These limitations of mathematical models justify the use of flow simulators and in vitro models. Such limitations also necessitate experiments in which the output signal of the laser-Doppler flowmeters can be compared with the results obtained by other methods known to measure the tissue perfusion as accurately as possible.

To verify that an ω-weighting filter in the signal processor provides a laser-Doppler flowmeter with an output signal linearly related to the blood cell average velocity multiplied by the cell volume fraction, a flow simulator (figure 4–5) was constructed [5]. In this simulator, red blood cells passed through a number of fine 300 μm channels in a semitransparent polyacetal disc, which served as a static scatterer, and thus randomized the propagation vectors of the photons. The combination of moving and static scatterers yielded diffusive scattering similar to that in real tissue. The center of the disc was illuminated by the laser light, and the surrounding receiving fibers received a fraction of the scattered and Doppler-broadened light. The average velocity of the blood cells was controlled by a syringe pump. Different hematocrits were produced by diluting the blood cells in saline. Within the velocity range (0–15 mm/sec) and the hematocrit range (0–0.6%), a linear flowmeter response was verified. This linearity persisted regardless of whether the blood cell velocity or the hematocrit was changed. In a successive study [7] in which a linearizer was included in the signal processor, a linear relationship was established up to hematocrits of 1.0%, thus covering the entire hematocrit range that may be expected in real tissue. A similar linear relationship between the CMBC signal and the hematocrit was also obtained. The CMBC output was independent of the average cell velocity. The laser-Doppler output signal showed only a weak dependence (0.06%/mmHg) on the partial pressure of oxygen in the test solution.

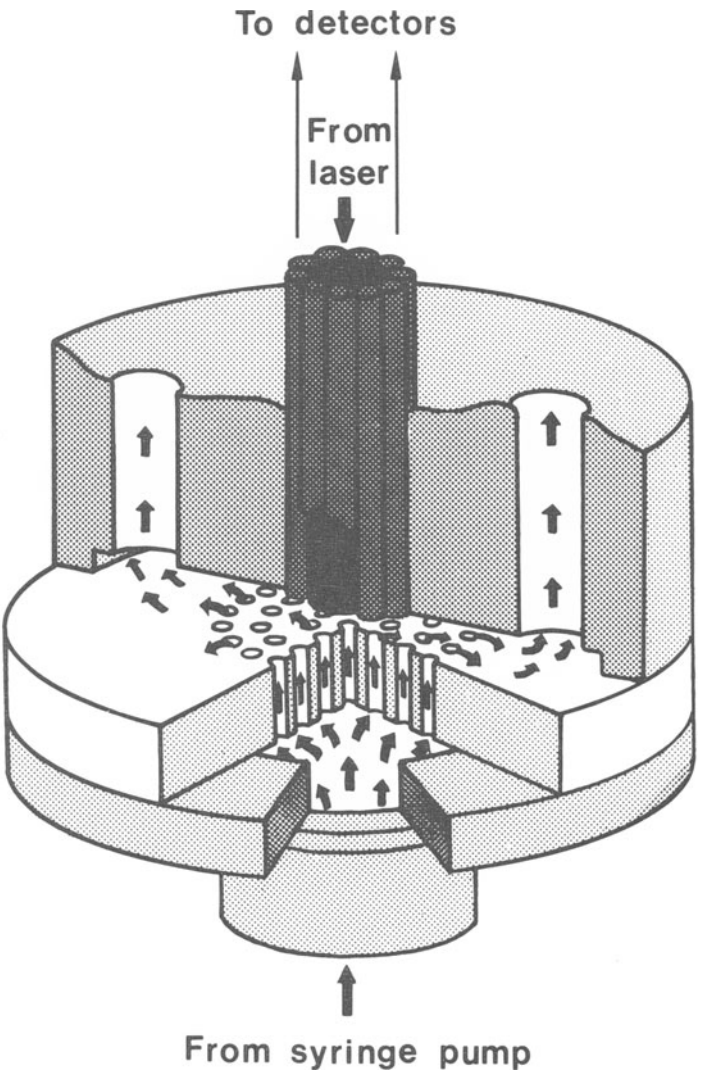

Figure 4–5. Flow simulator for evaluation of the performance of laser-Doppler flowmeters (reproduced from [5] with permission of the Institute of Electrical and Electronics Engineers, Inc.).

The results of these experiments agree in general with the predictions of the mathematical models [6]. A flow simulator, however, does not take into account that in real tissue the blood cells are confined within the vessel walls, thereby violating the assumption of a homogeneous distribution of moving scatterers. Therefore, various investigations with animal models have been performed, most often with the laser-Doppler output signal being compared

with another method for simultaneously measuring perfusion in the same tissue.

The feline intestine has proven to be a suitable animal model for the study of the performance of laser-Doppler flowmeters. It has a uniform and easily controlled perfusion. This model is particularly useful because a specific segment of the intestine is drained through a single vein, the blood flow through which can be accurately determined by a drop-counting technique [8]. A linear relationship between flowmeter output signal and intestinal blood flow has been established for perfusion values ranging from zero to over 300 ml min^{-1} $100g^{-1}$ [10]. However, a calibration in absolute flow units is valid only for the conditions under which it has been obtained, because the optical properties may vary from one tissue to another.

The possible contribution to the Doppler power spectral density from movements of the vessel walls was studied in a separate animal experiment [16]. During anesthesia, the peripheral part of a rabbit's hind leg was perfused with pure saline or with the animal's own blood through a catheter inserted in the femoral artery. Pulsatile flow was obtained in both cases with a syringe pump controlled by a low-frequency (0.5–2 Hz) generator. When the leg was perfused with saline, the laser-Doppler output signal remained at the steady "occlusion zero" baseline level, while with blood perfusion pulsatile flow was recorded. The results of this experiment indicate that the origin of the pulsatile signal is the scattering of light by moving blood cells and that no signal component is produced by surrounding tissue, possibly moving synchronously with flow.

The results with flow simulators and in vivo models generally confirm the mathematical model proposed by Bonner and Nossal [6] for dynamic light scattering in tissue. Multiple Doppler shifts produced by several sequential scattering events inside a vessel do not seem to violate the linear relationship predicted by theory. Neither do internal tissue movements seem to contribute substantially to the output signal, except for the motile tissues discussed in chapters 13 and 14.

TIPS ON THE USE OF PERIFLUX PF2B AND PF3 LASER-DOPPLER FLOWMETERS

Operators of Periflux PF2b and PF3 have found the following information to be helpful in setting up a laser-Doppler flowmetry experiment and interpreting the data. In the present design, laser-Doppler flowmeters are generally better suited for studies of blood flow in which the probe is placed in a fixed position throughout the experiment, rather than investigations involving recordings of blood flow at multiple sites. The reason for this constraint is the high variation coefficients of laser-Doppler output signals recorded from adjacent sites and the spatial differences in blood flow in tissues with apparently homogeneous perfusion [16,17]. Because the scattering volume depends on the scattering and absorption properties of the tissue, blood flow values recorded from different organs generally cannot be compared. For the

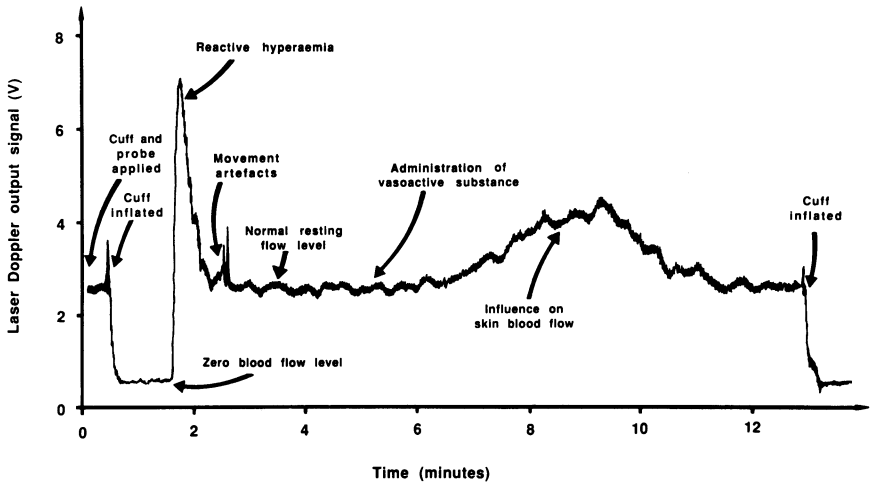

Figure 4–6. Recording of blood flow by laser-Doppler flowmetry in a stimuli–response experiment.

same reason, the output signal of the instrument represents a relative value, and interpretations of the results in terms of $ml \cdot min^{-1} \cdot 100\ g^{-1}$ can be made only for the specific organ for which the relationship has been established.

The sensitivity of the instrument including the probe can be checked and if necessary recalibrated by placing the probe tip in a test suspension of latex particles undergoing Brownian motion. The well-defined velocity pattern of such particles results in a stable and reproducible output of the flowmeter.

Although a laser-Doppler blood flowmeter is often easy to use, the routine outlined below (figure 4–6) will help assure success. A typical situation in which laser-Doppler flowmetry is helpful is the assessment of the influence of vasoactive substances such as sublingually administered nitroglycerin on forearm skin blood flow. Prior to any recordings, the volunteer should rest in a relaxed position for at least 20 minutes. Smoking and ingestion of food or beverages should be avoided for at least two hours before recordings take place. Preparations start by placing a pressure cuff around the upper arm. A probe holder is attached to the forearm skin by two-sided adhesive tape. The probe is placed in the probe holder in such a way that light mechanical contact between the skin and probe tip is attained, and the cable with the fibers is kept still to prevent fiber-movement artifacts during measurements. A strip-chart recorder or a computer connected to the laser-Doppler flowmeter is set to the appropriate voltage input range, offset, and speed. The time constant of the laser-Doppler output signal is set to three seconds to allow for signal averaging, or to 0.2 or 1.5 seconds if the pulsatile components should be included. The pressure cuff is then inflated to above systolic pressure, to obtain a zero flow signal. This stable "occlusive zero" (the

resulting output signal is actually not zero volts), which generally amounts to about 20% of the resting flow value in forearm skin, is recorded for about one minute. The discrepancy between this stable occlusive zero and the true zero output level of the instrument is attributed to the fact that even though blood flow is arrested by the inflated upper arm pressure cuff, the blood cells in the peripheral vessels are still moving randomly and producing minor Doppler components recorded by the instrument. After a one-minute occlusion period and recording of the zero blood flow level, the pressure cuff is released, and a rapid increase in blood flow is recorded due to reactive hyperemia. When the output signal has returned to the preocclusion level, which is considered to represent the normal resting blood flow level in the forearm skin, the value should be recorded for at least one minute. The vasoactive substance may then be administered, and the blood flow recordings may proceed continuously without changing the settings of the instrument or recording system. At the end of the experiment, the pressure cuff should be inflated again to above systolic pressure to verify that the laser-Doppler output signal is still at the same occlusive zero level as recorded at the beginning of the experiment.

The *interpretation* of the results starts with subtracting the occlusive zero blood flow level from the total laser-Doppler output signal. This can be done manually on a recorder chart by a straight line connecting the tracings during the first and the second vascular occlusions. The actual blood flow value is then taken as the difference between the laser-Doppler output signal value and the occlusive zero blood flow value. Because the output signal is in arbitrary units, it is generally better to express changes in blood flow as percentages of the resting flow value. In many situations, the latency time from the administration of a vasoactive substance administration to the onset or peak of the effect on peripheral blood flow may provide useful information. Artifacts generated by bending the fibers are easily identified and may be disregarded if the time constant is set to 0.2 or 1.5 seconds. If the time constant is set to three seconds, however, frequently occurring movement artifacts are integrated and superimposed on the blood flow value, making the interpretation of recorded data more difficult. Temporal fluctuations in tissue blood flow in a given subject, as well as the difference in responses between individuals to similar stimuli, generally require more extensive studies including many individuals to ascertain statistically the specific stimulus–response pattern of a vasoactive substance.

REFERENCES

1. Stern, M.D. 1975. In vivo evaluation of microcirculation by coherent light scattering. Nature 254:56–58.
2. Holloway, G.A., and D.W. Watkins. 1977. Laser Doppler measurement of cutaneous blood flow. J Invest Dermatol 69:306–309.
3. Sargent, M. III, and M.O. Scully. 1972. Theory of laser operation—An outline. In Laser Handbook, Arecchi, F.T., Schulz-Dubois, E.O., eds. Amsterdam: North–Holland, vol 1, pp 45–114.

4. Nilsson, G.E., T. Tenland, and P.Å. Öberg. 1980. A new instrument for continuous measurement of tissue blood flow by light beating spectroscopy. IEEE Trans BME-27:12–19.
5. Nilsson, G.E., T. Tenland, and P.Å. Öberg. 1980. Evaluation of a laser Doppler flowmeter for measurement of tissue blood flow. IEEE Trans BME-27:597–604.
6. Bonner, R., and R. Nossal. 1981. Model for laser Doppler measurements of blood flow in tissue. Appl Optics 20:2097–2107.
7. Nilsson, G.E. 1984. Signal processor for laser Doppler tissue flowmeters. Med Biol Eng Comput 22:343–348.
8. Ahn, H., J. Lindhagen, G.E. Nilsson, E.G. Salerud, M. Jodal, and O. Lundgren. 1985. Evaluation of laser Doppler flowmetry in the assessment of intestinal blood flow in cat. Gastroenterology 88:951–957.
9. Tyml, K., and C.G. Elis. 1985. Simultaneous assessment of red cell perfusion in skeletal muscle by laser Doppler flowmetry and video microscopy. Int J Microcirc Clin Exp 4:397–406.
10. Ahn, H., K. Johansson, O. Lundgren, and G.E. Nilsson. 1987. In vivo evaluation of signal processors for laser Doppler tissue flowmeters. Med Biol Eng Comput 25:207–211.
11. Salerud, E.G., and G.E. Nilsson. 1986. Integrating probe for tissue laser Doppler flowmeters. Med Biol Eng Comput 24:415–419.
12. Svensson, H., and P. Svedman. 1982. On postoperative monitoring of the circulation in flaps. Int J Microcirc Clin Exp 1:326.
13. Jones, B., and B.-J. Mayou. 1982. The laser Doppler flowmeter for microvascular monitoring: a preliminary report. Br J Plast Surg 35:147–149.
14. Svensson, H., P. Svedman, J. Holmberg, and J.B. Wieslander. 1985. Detecting changes of arterial and venous blood flow in flaps. Ann Plast Surg 15:35–40.
15. Johansson, K. 1988. Gastrointestinal application of laser Doppler flowmetry. Thesis No 269, Linköping University.
16. Tenland, T., G.E. Salerud, G.E. Nilsson, and P.Å. Öberg, 1983. Spatial and temporal variations in human skin blood flow. Int J Microcirc Clin Exp 2:81–90.
17. Shepherd, A.P., G.L. Riedel, J.W. Kiel, D.J. Haumschild, and L.C. Maxwell. 1987. Evaluation of an infrared laser Doppler blood flowmeter. Am J Physiol 252:G832–G839.

5. TSI'S LDV BLOOD FLOWMETER

JOHN A. BORGOS

Since its incorporation in 1961, TSI's primary business has been identifying requirements for the measurements of details of fluid flow, and then developing solutions to meet these needs. The company's earliest products were a series of thermal anemometers used for measuring the flow of hot gases. This product line soon expanded into a broad line of hot wire and hot film probes and electronics for fluid flow measurement in research, medical, and industrial applications.

In 1973 TSI introduced its first laser-Doppler velocimeter. This was a major breakthrough at the time, because it allowed for the measurement of the details of fluid motion in a way that was completely noninvasive. Today these LDV products are primarily used in fluid mechanics research, industrial research and product development, and biomedical research and engineering. For example, the development of heart valve prostheses has benefited greatly by the ability of LDV instrumentation to characterize the details of flow in experimental models.

As TSI continued to develop a high level of expertise in the design of optical systems and signal processing, the company began to identify other areas in which laser-Doppler techniques could be applied advantageously for the measurement of fluid flow. One of these areas was the measurement of microvascular blood flow. It was apparent that the ability to quantify levels of capillary perfusion would greatly aid in the diagnosis and evaluation of a wide variety of diseases and injuries, and would greatly improve patient

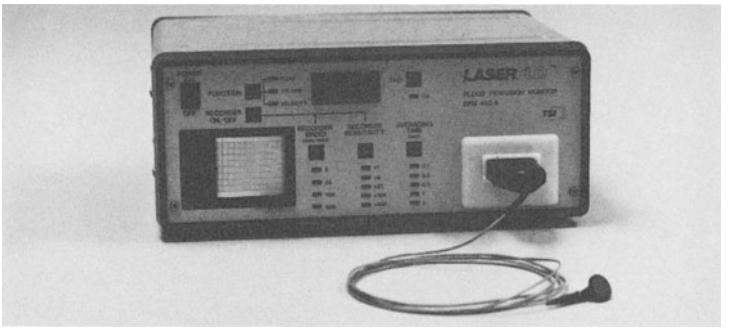

Figure 5–1. The Laserflo Blood Perfusion Monitor.

management in critical situations where therapeutic intervention is required to restore the circulation.

TSI was not the first to introduce a laser-Doppler blood perfusion monitor. Other researchers had developed and tested prototype instruments [1–5], and various early reports seemed to confirm the fundamental capabilities and advantages of the technique [6–11]. Early commercial versions also appeared (see chapters 3 and 4). However, in order for a laser-Doppler instrument to be a truly useful clinical tool, it seemed that three particular requirements had to be met:

1. The results must be quantifiable. In other words, the instrument must be able to measure in absolute flow units, and not arbitrary or simply qualitative values.
2. The instrument must be capable of measurements of microvascular blood volume, velocity, and flow. The volume and velocity parameters have particular relevance in evaluation of microangiopathy, for example.
3. The instrument must be easy to use for clinical personnel.

With these three criteria in mind, TSI began the development of an advanced version of a laser-Doppler instrument, and in 1985 introduced the Laserflo® Blood Perfusion Monitor (figure 5–1). This chapter summarizes considerations that went into this instrument's design. Our objective is to give the reader a greater understanding of its capabilities and limitations and to make him or her more proficient in its use.

THEORETICAL ASPECTS AND ASSUMPTIONS

The theory of laser-Doppler measurements of tissue perfusion is discussed fully in chapter 2. However, a brief summary of several theoretical concepts is included here to facilitate a better understanding of the operation of the instrument. First of all, let us examine the source and nature of the Doppler

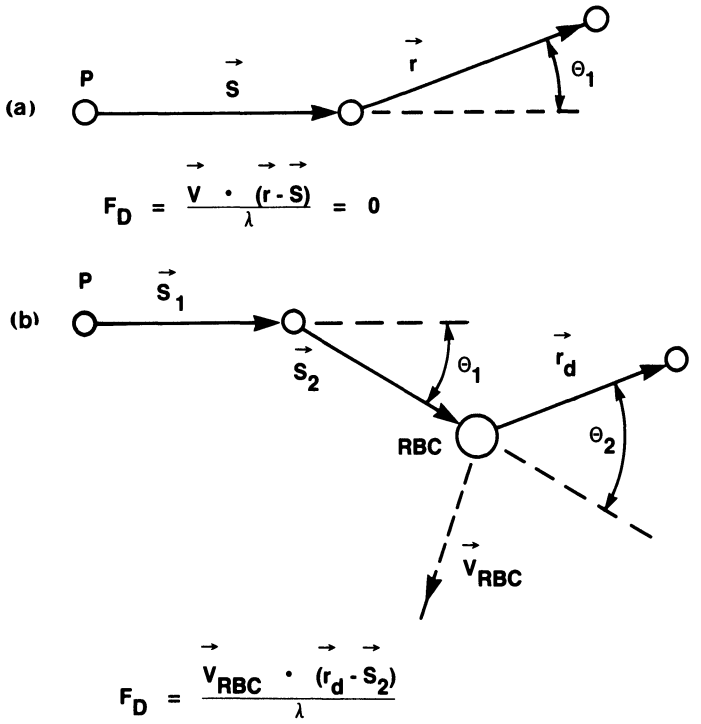

Figure 5–2. Light scattering process in (a) stationary tissue matrix only, and (b) stationary tissue matrix with moving red blood cells. In the first case, a photon (P) traveling initially in direction $\vec{S}$ is scattered by a stationary particle, and proceeds in a new direction $\vec{r}$. Because the velocity ($\vec{V}$) of the particle is zero, the resulting Doppler shift (F_D) is also zero. In the second case, after one or several scattering events with stationary particles, a photon traveling in direction $\vec{S}_2$ is scattered by a red blood cell (RBC) with velocity $\vec{V}_{RBC}$, and proceeds in a new direction $\vec{r}_d$. A nonzero Doppler shift results. The parameter λ is the photon wavelength.

signal itself. Nearly all tissue is relatively opaque, which means that it contains substances which refract (scatter) light in various and random directions. With the exception of the major blood vessels, blood itself occupies only a very small fraction of tissue volume. Therefore, most of the light scattering is accomplished by stationary tissue elements.

On a microscopic level, the scattering process proceeds as shown in figure 5–2. As illustrated in figure 5–2a, light that is scattered only by stationary tissue elements is imparted no Doppler shift. However, as illustrated in figure 5–2b, a moving red blood cell imparts a Doppler shift to the light frequency. Because the scattering angle and red blood cell velocities are variable and can be determined only in a statistical sense, the Doppler shifts from many photons will occupy a broad spectrum of frequencies. However, the only factor in the Doppler equation that will vary with blood flow is the

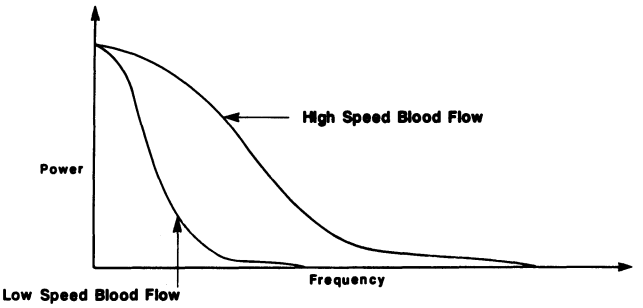

Figure 5–3. Dependence of Doppler spectrum on red blood cell speeds.

red blood cell speed. Therefore, we expect the bandwidth of the Doppler frequency spectrum to scale with red blood cell speeds.

The variation of the Doppler frequency spectrum with mean red blood cell speeds is illustrated in figure 5–3. The lower curve represents a situation with relatively low speeds. If the red blood cell speeds are increased, a spectrum such as the upper curve results. In this situation, the two spectra have the same shape, but different widths, because higher speeds give rise to higher Doppler frequencies.

As illustrated in figure 5–2, the vast majority of scattering events occur when photons interact with stationary tissue. In fact, the red blood cell volume fraction in most tissue is so low that only a small percentage of the detected photons have encountered even one moving red blood cell. In skin, for example, this figure is generally less than 10%. Because of this fortuitous fact, we are able to gain information about the red blood cell volume fraction. If a single red blood cell is scattering light and imparting a Doppler shift, the detectable signal will have a certain small energy level. However, if a second red blood cell is in the measurement volume, the resultant total energy level of the signal will be greater, as illustrated in figure 5–4. The lower curve represents a capillary bed with relatively low red blood cell volume fraction. The total area under the power spectrum, which represents the energy level in the fluctuating portion of the photocurrent signal, is relatively low. The upper curve represents a situation with a relatively high red blood cell fraction, which results in an increase in the energy level or amplitude of the photocurrent fluctuations.

It is important to understand two critical assumptions inherent in this argument. First, we assume that the tissue matrix is relatively stationary and that it dominates the scattering process. In other words, a very sparse collection of red blood cells is somewhat uniformly distributed throughout a tissue matrix. For this reason, these theoretical constructs do not apply to the measurement of blood moving in major vessels. Laser-Doppler techniques

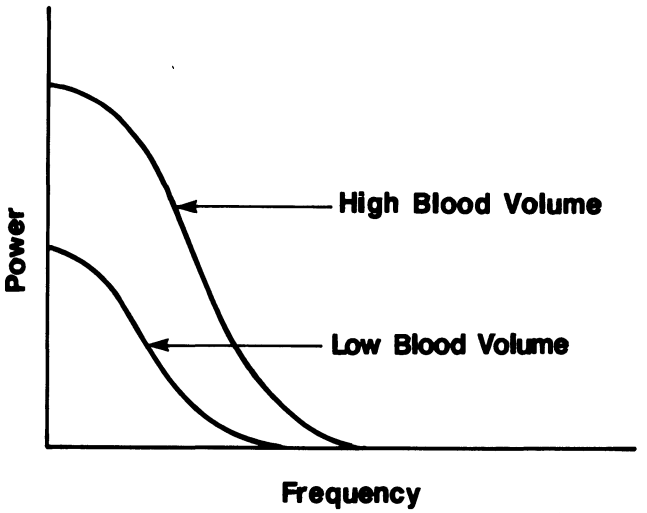

Figure 5–4. Dependence of Doppler spectrum on blood volume.

can indeed be used for the measurement of blood flow in large vessels, but the instrumentation design will be somewhat different (see chapter 7).

Second, we assume that all of the light travels approximately the same distance through the tissue prior to detection. This satisfies the statistical requirement that all detected light has an equal opportunity for a Doppler event.

From these concepts we can define the previously mentioned flow, volume, and velocity terms:

Flow: the number of red blood cells moving through a unit volume of tissue per unit time (e.g., number of red blood cells per minute per 100 grams of tissue)
Volume: the number of moving red blood cells per unit volume of tissue
Velocity: the mean speed of moving red blood cells (i.e., the distance traveled per unit of time)

In practice, it is customary to substitute milliliters of blood for the number of red blood cells in both the flow and volume parameters because these terms are more conventional; however, it must be understood that this substitution implies some assumption about the local microvascular hematocrit.

GENERAL DESCRIPTION

The TSI Laserflo Blood Perfusion Monitor (BPM) incorporates advanced digital and electro-optics technology. A block diagram of the instrument is

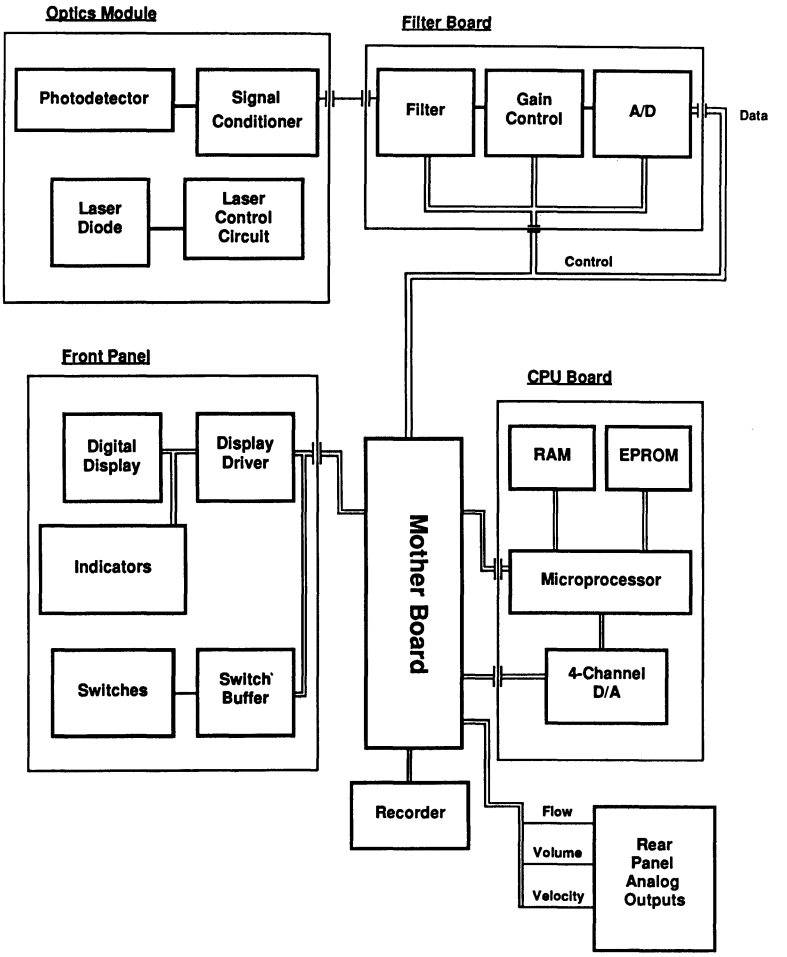

Figure 5–5. Block diagram of Laserflo Blood Perfusion Monitor.

shown in figure 5–5. The laser light source is coupled to an optical fiber, which transmits light to the tissue surface. Two sensing optical fibers collect some of the light that has been scattered through the tissue and return it to a photodetector. The optical mixing of the photons on the photodetector surface generates a photocurrent signal that contains the Doppler frequency information. After initial filtering, the signal is passed through a filter board for bandpass filtering, then digitized, and finally delivered to the microprocessor in which all signal analysis takes place. The signal processor computes the blood volume, velocity, and flow parameters. It then transmits this information to the digital display on the front panel, the built-in trend recorder, and the rear-panel analog outputs. The following sections describe

in greater detail the particular design considerations that enable the Laserflo BPM to satisfy the three design criteria identified above.

OPTICS MODULE

The most critical component of the optics module is the laser source itself. A laser with optimum operating characteristics is of paramount importance because compromises here cannot be corrected anywhere else in the system. The Laserflo BPM incorporates a gallium aluminum arsenide semiconductor laser operating in a single longitudinal mode. The superior coherence properties attainable with these lasers result in two important performance advantages. First, the signal-to-noise ratio is triple that of a helium–neon laser. Second, temporal instabilities can be easily managed, or in some cases eliminated altogether.

The laser wavelength in the Laserflo BPM is nominally 780 nanometers. This wavelength presents several advantages. It is near the isobestic wavelength of oxy- and deoxyhemoglobin (800 nm) so that changes in blood oxygenation have no effect on the measurement. This wavelength is not readily absorbed by tissue pigments, so that measurements can be made on even the darkest tissue. Its propagation in tissue is such that it slightly increases the measurement volume relative to laser-Doppler flowmeters that use helium–neon lasers. The danger of ocular injury is lessened at this longer wavelength, and the low power level permits this instrument to be classified as a class I laser product. The power delivered at the end of the fiber is approximately 2 milliwatts.

The second critical component in the optics module is the photodetector, which is a PIN photodiode. The design of the particular photodiode used is such that its influence on the optical mixing efficiency β[2] is invariable over a wide range of conditions, and from one component to the next. Without this important characteristic, quantitation of flow would not be possible because various instruments would read differently.

The optics module also incorporates a circuit to control the temperature of the laser, which allows the operation of the instrument over a wider variety of environmental conditions. In addition, an optical switch is incorporated that disconnects power to the laser when no probe is connected.

FIBER OPTICS

The fiber optics represent a unique and serious challenge to the design of a laser-Doppler instrument. The best signal-to-noise ratio is obtained with the smallest-diameter fibers, but even the very best fibers do not yield a signal-to-noise ratio that is comfortably high. Consequently, the instrument designer is faced with the necessity of making a tradeoff between signal quality and the difficulty of coupling light into small-diameter fibers.

Small-core-diameter fibers, such as 50 μm or 100 μm graded-index fibers, yield three important performance advantages over large-core step-index fibers.

Table 5–1 Filter settings and digital conversion rates on the Filter Board

Range	Filter bandwidth, Hz	Digital conversion rate, #/Sec
1	30– 1280	3150
2	30– 3280	8012
3	30– 7900	20000
4	30–18500	50000

1. Because of their small numerical aperture, they satisfy the condition that all the detected light has an equal opportunity for a Doppler event. This is because the optical path through the tissue is more precisely defined, and also because the possibility of direct reflections of light from the tissue surface is virtually eliminated.
2. They preserve optical coherence, yielding greater efficiency of optical mixing on the photodetector surface and a consequent increase in the signal-to-noise ratio.
3. They virtually eliminate artifacts caused by motion of the fiber.

The Laserflo BPM utilizes small-core graded-index fibers for its fiber optic probes. Each probe has a 50 μm core fiber for delivery of the light to the tissue and two 100 μm core receiving fibers that return light to a single photodetector. The index gradient in these fibers is selected to be optimal for coherence preservation, and contains no discontinuities or irregular features.

FILTER BOARD

The primary function of the filter board is to improve the signal-to-noise ratio in the photocurrent signal by eliminating noise that is outside the bandwidth of the Doppler frequencies. This module also performs the analog-to-digital conversion of the signal prior to its input to the signal processor.

Two separate filter sections are contained on this module. In the first section, the low-frequency components of the photocurrent signal are eliminated with a 30 Hz high-pass filter. Following this, the signal is passed through a low-pass filter whose cutoff frequency is under software control and depends on feedback from the signal processor. Following this, the signal undergoes analog-to-digital conversion, and the digitized data are sent to the signal processor for spectral analysis. The analog-to-digital conversion rate is also under software control, and is selected to be consistent with the low-pass filter cutoff so as to satisfy the Nyquist criterion. Four filter settings and digital conversion rates are possible, and these are given in table 5–1.

In the second section of this module, the signal is passed through a low-pass filter that eliminates all frequencies higher than 0.5 Hz. The result-

ing zero frequency (DC) signal is proportional to the mean optical power received at the photodetector, and is later used for normalization and also for a calculation of the noise level. This signal is digitized at a rate of 10 Hz, and the digital result is input to the signal processor.

All functions on the filter board are under software control. When the bandwidth of the Doppler signal moves out of the range of a particular filter setting, the signal processor selects the next filter range and digital conversion rate. This process is completely automatic and does not require any interrogation or interruption by the user.

SIGNAL PROCESSOR

All data input to the signal processor are in digital form. This is convenient for the implementation of algorithms designed for spectral analysis, noise compensation, control of the filter board, interrogation of front-panel switch settings, and computation of other parameters. The signal processor in the Laserflo BPM incorporates a patented algorithm for noise compensation and Fourier analysis [12]. It computes a new value for flow, volume, and velocity every 100 milliseconds. Immediately following each computation, it updates all outputs (with the exception of the digital display, which is updated only three times per second). It then also interrogates the front-panel switch settings and makes any changes that have been ordered by the operator.

To compute the blood flow parameters, the signal processor first calculates the noise content in the signal. Because the noise is directly related to the optical power at the photodetector, the zero-frequency signal is the basis for this noise calculation. The next step is to compute the initial estimate of the blood volume, which is based on the normalized mean square high-pass filtered signal from the filter board. As illustrated in figure 5–4, we expect this amplitude to increase as the red blood cell number density increases. The exact nature of this relationship [2] is given by

$$E = \beta\,(1 - \exp\,(-2\bar{m})),$$

where E = normalized mean square of the high-pass filtered signal, β = constant that depends on the optical coherence of the signal at the photodetector, and $\bar{m}$ = mean number of Doppler events per photon.

The factor β depends on the qualities of the fiber optics, the laser, the photodetector, and the tissue matrix itself. Variations in any of these components will result in undesirable variations in this factor. To satisfy the criterion that measurement results be quantifiable, the control of this variable is critical. The TSI Laserflo BPM has been designed so that variations in β are limited to only a few percent, which virtually eliminates instrument-to-instrument and subject-to-subject variation.

Next, the signal processor computes the blood velocity. To obtain an

initial estimate of the velocity, the instrument computes the mean Doppler frequency, $\bar{f}$, according to the following:

$$\bar{f} = \frac{1}{2\pi} \int_0^\infty \omega P(\omega) d\omega \; / \; \int_0^\infty P(\omega) d\omega,$$

where $\bar{f}$ = mean Doppler frequency in kilohertz, and $P(\omega)$ = spectral power at frequency ω.

For most normal levels of tissue perfusion, this initial estimate of the mean Doppler frequency requires no adjustment. However, when the value of $\bar{m}$ exceeds approximately 0.4, a small but important fraction of the light will have been scattered two or more times from moving red blood cells, which results in an upward bias in the mean frequency. Therefore, in these situations the signal processor uses the calculated blood volume ($\bar{m}$) to correct the initial mean-frequency estimate. The result of this correction is the final mean-frequency estimate, expressed in kHz.

The final calculation, blood flow, is the scaled product of the blood volume and the blood velocity values:

$$\text{Flow} = \bar{m} \times \bar{f} \times 60$$
$$= \text{milliliters per minute per 100 grams of tissue } (\text{ml} \cdot \text{min}^{-1} \cdot 100\text{g}^{-1})$$

The computed values for flow, volume, and velocity are retained in memory as 16-bit data values for a period of five seconds, after which they are replaced by freshly computed values.

OUTPUTS

The primary output of the Laserflo BPM is the digital display on the front panel, which can be used to indicate either the flow, volume, or velocity parameter. It automatically adjusts the decimal point location to provide maximum reading sensitivity. The maximum flow value that can be displayed is 400, which is well above the level found in most tissues under most physiological conditions. The maximum blood volume that is displayed by the instrument is 1.6, which is adequate for all but the most highly perfused tissues, such as the renal cortex. The maximum velocity indication is 8.0, which corresponds to red blood cell speeds well in excess of those found in most capillary beds. Units are as defined in the previous section.

A trend recorder on the front panel provides a graphic display of any of the three parameters. The sensitivity of the recorder is adjustable so that a wide range of values can be indicated. For any given parameter selection and sensitivity setting, the full-scale deflection of the trend recorder corresponds to a specific value on the digital display. These relationships are shown in table 5–2.

Table 5–2 Digital panel meter display at maximum deflection of trend recorder

Recorder sensitivity	Flow, $ml \cdot min^{-1} \cdot 100g^{-1}$	Velocity, kHz	Volume, $\bar{m}$
X1	400	8.00	1.60
X4	100	2.00	.400
X20	20.0	.400	.080
X100	4.00	.080	NA
X400	1.00	.020	NA

In addition, the instrument provides analog voltage outputs for each of the three measurement parameters. The maximum voltage attainable is 2.5 volts. For any of the three parameters (flow, volume, or velocity), this full-scale voltage corresponds to full scale on the trend recorder. Therefore, it is possible to obtain quantifiable results by recording data on an external device, noting the sensitivity setting for each parameter and using table 5–2 to translate the output voltage to a parameter value.

TEST SOFTWARE

The microprocessor in the Laserflo BPM incorporates several test software modules that are used for internal diagnostics, fault checks, and calibration tools. These test software modules are accessed by pressing a certain sequence of switches on the front panel, following which the front-panel switch functions are redefined. Details about this are contained in the instrument Service Manual.

The internal diagnostics and fault-check software are normally used only when a malfunction of the instrument is suspected. These diagnostics generally require the expertise of a biomedical engineer to interpret the results. In some cases, test equipment is required also.

There are two types of calibration setup routines that are convenient in certain situations. The first of these is a group of routines that set each of the rear analog outputs to either zero or full scale, so that the user can adjust the zero and span of the built-in trend recorder or an external recorder.

The second series of test routines allows the user to read values for the total photocurrent from the PIN photodiode, commonly referred to as DC. Also, it allows the user to read peak and average values of the fluctuating portion of the photocurrent, commonly referred to as AC. Details for access to these test routines are contained in the Service Manual.

PROBES

In order to obtain quantitative and repeatable blood flow measurements, the design of the fiber optic probes must meet certain requirements. Some of these requirements are, in fact, quite severe, but compromises in these areas will inevitably lead to unpredictable variability in blood flow measurements.

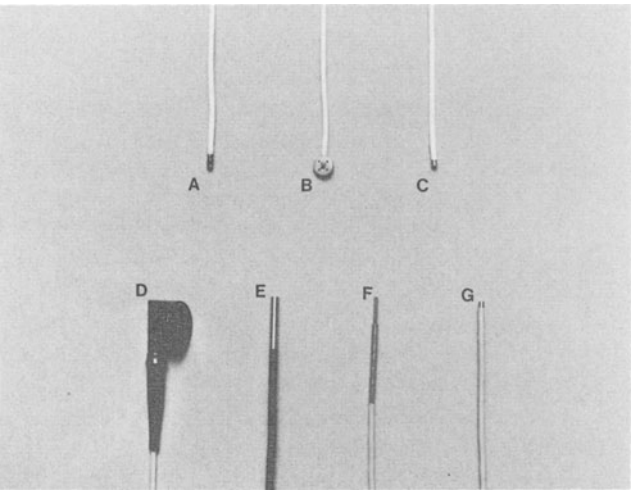

Figure 5–6. Fiber optic blood flow probes. A. Implantable prism probe. B. Implantable disk probe. C. Endoscope probe. D. Right-angle probe. E. Hardtip pencil probe. F. Needle probe. G. Softip pencil probe.

The most important aspects of the fiber optic probes were previously discussed in the section on Fiber Optics.

To obtain repeatable flow measurements, the fiber optic probe is also designed to precisely control the light path in the tissue. The three design features that achieve this are the numerical apertures of the transmitting and receiving fibers, the size of the fibers, and the distance between the fibers. The probe design should ideally be such that the spacing between transmitting and receiving fibers is large compared with the fiber diameter, and the numerical aperture of the fiber should be as small as possible. Unfortunately, the optimization of these parameters tends to decrease the signal-to-noise ratio at the detector. Thus the detector design imposes a fundamental limit on how far these factors can be taken. TSI's fiber optic probes each have two receiving fibers with a core diameter of 100 microns, a numerical aperture of 0.28, and a spacing of 0.5 mm from the transmitting fiber. The transmitting fiber has a core diameter of 50 microns and a numerical aperture of 0.20.

A final requirement of the fiber optic probes is that they be convenient to connect and disconnect, and that the optical alignment be extremely reliable. TSI probes incorporate a patented fiber optic connector design in which the transmitting optical fiber is centered to within 5 μm, thus assuring a reliable transmission of laser power for blood flow measurements [13].

A variety of fiber optic blood perfusion probes is available from TSI to meet different experimental and clinical measurement requirements. Some of the standard probe designs available are shown in figure 5–6.

Standard probe designs fall into three main categories. The first category is general purpose probes, which include the right-angle probe, pencil probes, and needle probes. These probes are used for routine skin perfusion monitoring, experimental measurements in relatively inaccessible areas, and measurements where very precise location of the probe tip is needed.

A second group of probes, designed for temporary implantation, includes the implantable disk and prism probes. These are used primarily for monitoring buried or inaccessible tissue. These probes are made of biocompatible materials and can be sutured in place for temporary implantation for a period of up to 30 days.

A third group of probes, designed for endoscopy, includes the side-view and end-view endoscope probes. These are used primarily in gastric, colonic, and bronchial blood flow measurements. These probes have a stiffened cable, making it easier to insert them in the biopsy channel of an endoscope.

CALIBRATION

The calibration of laser-Doppler flowmeters is inherently difficult because of the unavailability of good reference standards. Other techniques for microvascular blood flow measurements are discontinuous, difficult to use, and often not repeatable. A theoretical approach to calibration could be considered, but this requires a detailed knowledge of the photon path length in the tissue, and our knowledge of optical properties of tissue is not sophisticated enough to provide this information. Therefore, this approach may be useful for obtaining approximate calibration values but requires experimental validation.

In vitro models have been used by many investigators in attempts to calibrate laser-Doppler flowmeters [2,14,15], and these have the advantage of allowing the user to vary the conditions over a wide range of values. They also allow the experimenter to test certain assumptions and approximations about linearity and scaling. However, in order to obtain absolute calibration values, in vitro models must incorporate red blood cells because their size, shape, and refractive index cannot be matched by artificial particles.

This imposes two incompatible requirements that seriously limit the credibility of all in vitro models. The first is that the red blood cells must be sparsely distributed in the model of the tissue matrix. If this condition is compromised, such as by the use of tubes of diameters exceeding 20 μm or so, the probability of multiple scattering events per photon becomes nonnegligible. The result would be an upward bias in the mean Doppler frequencies for a given red blood cell concentration and velocity distribution. Second, the system must allow a continuous and stable situation. The tendency of red blood cells or other particles of similar diameters to aggregate and occlude small lumens necessitates lumen diameters of the order of several hundred microns. Therefore, data from in vitro models should be viewed with considerable skepticism.

The obvious advantage of live-tissue preparations for laser-Doppler calibrations is that there need be no compromise on the physical and optical properties of the subject. Unfortunately, such methods also present a serious challenge—that of finding a suitable technique for independent measurement of microvascular blood volume, velocity, and flow. The particular technique chosen will depend in part upon the tissue type and accessibility, and also upon the measurement objectives of the user.

Perhaps the best technique in most situations is the hydrogen gas clearance method or other similar clearance technique [16–19]. As with laser-Doppler flowmeter, gas clearance measurements sample only the most superficial layers of tissue. Therefore, it is expected that this method will give the most reliable validation of the Laserflo BPM.

The use of radioactive microspheres is a commonly accepted technique for microvascular blood flow measurements [20]. However, the tissue volume sampled by this method is usually larger than that of the laser-Doppler method and may extend to a greater distance from the tissue surface. Because the microspheres become lodged in the capillaries and arterioles, injecting excessive numbers of spheres may alter the flow one is trying to measure. Therefore, it is expected that this method may not correlate well with the laser-Doppler method.

Other methods that essentially yield a measurement of regional blood flow can also be used for validation of laser-Doppler flowmeters. Because of the small tissue volume sampled by laser-Doppler flowmeters, comparison with these techniques requires an assumption about the uniformity of blood perfusion throughout the region of tissue. In certain tissues and under certain conditions, this assumption seems quite reasonable, but in a great many situations it should be made only with great caution. Examples of this kind of approach include the use of a plethysmograph for skin blood flow measurements in the extremities [21], electromagnetic flowmeter measurements of regional blood flow to an isolated organ or region of tissue [8,22], and the collection and weighing of the venous outflow from a tissue specimen [23].

Yet another technique that has been used in attempts to validate laser-Doppler flowmeters is video microscopy [24]. While this method has proven to be very useful in many experimental situations, its ability to give quantitative flow estimates comparable to laser-Doppler instruments is seriously impaired by two limitations. First, its measurement volume is only a single capillary. Second, because the observer generally selects a capillary with relatively high and steady blood cell velocity, the technique tends to overestimate perfusion. Therefore, we do not generally expect good correlations between video microscopy and laser-Doppler flowmetry.

The usefulness of such comparisons with absolute flow values has been widely debated. We have discussed above in some detail the design criteria that must be met in order to obtain repeatable laser-Doppler flow measure-

ments. If these criteria are not satisfied, the possibility of obtaining repeatable and quantifiable measurements is indeed remote. On the other hand, if these conditions are satisfied, as they are with the Laserflo BPM, one can expect good measurement repeatability and quantification of results for microvascular blood flow monitoring.

One must also question whether different tissue types would have varying light-scattering properties, possibly leading to the result that a different calibration factor would be required for each tissue type. In view of the considerable variation in microvascular anatomy among various tissues, this issue certainly deserves consideration. Bonner et al. [25] have developed an analytical model which predicts, among other things, the photon path length through the tissue in a statistical sense. The advantage of this model is that it can be tested experimentally in a very simple way. Although it seems to have limitations with regard to tissues that are very highly vascularized, such as the renal cortex and the liver, or that are atypical in other ways, such as the lung with its air sacs, it nevertheless appears to be suitable for the majority of tissues under normal physiological conditions. Testing of this model has indicated that calibration factors for a wide variety of tissues should not differ substantially (Bonner, personal communication).

As discussed earlier, the Laserflo BPM gives three outputs: volume, velocity, and flow. The volume parameter is defined as the mean number of Doppler events per photon. The velocity parameter is defined as the mean Doppler frequency, expressed in kHz. The flow parameter is the scaled product of the volume and velocity parameters, with the scaling factor being equal to 60.

Several independent investigations in a variety of tissues have yielded scaling factors within 15% of the scaling factor used in the instrument [21,26–28]. As an example, experimental results showing a comparison of the Laserflo BPM with hydrogen gas clearance in gastric mucosa is shown in figure 5–7.

Scaling factors relating the volume parameter to red blood cell (RBC) number density and the velocity parameter to mean red blood cell speeds are approximately as follows:

Volume $\times$ 12,000 = No. of RBCs/mm^3, and
Velocity $\times$ 10 = mm/second.

These scaling factors are approximate and are based on theoretical analysis of the scattering problem. No experimental data have been obtained to verify these factors, yet they do give realistic estimates of these parameters based on accepted physiological values.

In summary, quantitation of blood flow results must begin with suitable instrument design, including strict control of the critical design variables described earlier. Artificial tissue models have serious shortcomings for the

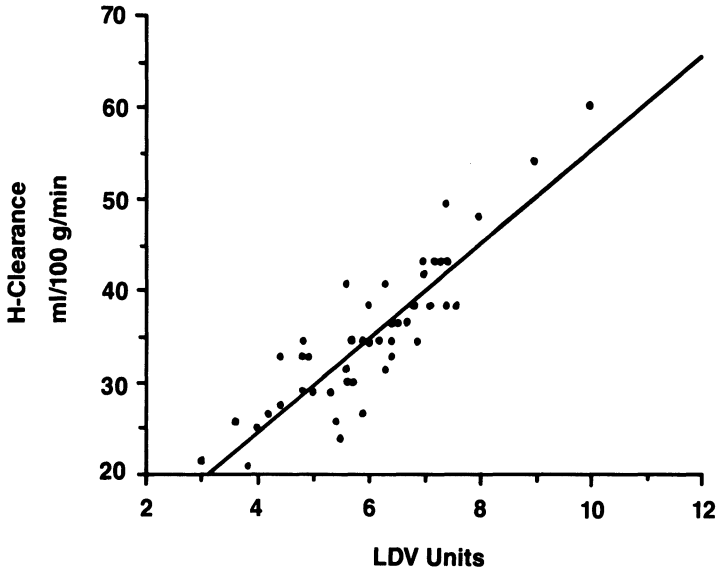

Figure 5–7. Hydrogen clearance versus Laserflo Blood Perfusion Monitor in gastric mucosa. LDV units = volume × velocity × 10. (Reproduced from Chung et al. [26] with permission.)

purpose of calibrating laser-Doppler flowmeters, and in vivo calibrations give the most reliable results. Experimental results have yielded a calibration factor that is valid for a wide variety of tissue types under normal physiological conditions.

GENERAL OPERATING SUGGESTIONS

The Laserflo BPM can be used for continuous microvascular blood flow measurements in any exposed or accessible tissue. Because it measures only in the superficial tissue layers, it cannot ordinarily give information about flow deep beneath the tissue surface; however, in certain situations a needle probe can be inserted beneath the tissue surface, allowing the user to overcome this limitation.

Proper selection of the probe is very important. The probe design should be selected to allow for a stable and immovable contact between the probe tip and the tissue surface. Therefore, when one is making measurements on skin, a probe should be selected that can be taped or otherwise securely attached to the skin surface. For measurements that require a needle probe for proper positioning, the probe should always be held in a micromanipulator in such a way that it cannot move with respect to the tissue surface that is being measured. Probes that are temporarily implanted for longer-term monitoring should always be sutured securely to the tissue under study, and the use of

absorbable sutures is recommended to allow for easy withdrawal of the probe. All standard TSI probes can be sterilized in ethylene oxide gas, using a standard hospital sterilization cycle. In addition, a 2% solution of glutaraldehyde or a 6% solution of hydrogen peroxide may be used. The fiber optic connector itself should never be immersed in any liquid.

Connection of the fiber optic connector to the instrument is easily accomplished by inserting the probe end into the connector port on the instrument and then turning the thumb screw until it is snug. This connection is designed so that the probe cannot be connected backwards, and probes may be connected many hundreds of times with no loss in reliability. Connection of the probe activates the laser, which is turned off when the probe is again disconnected.

When the instrument power is turned on, the digital display immediately indicates the result of a system check. This test is activated on startup in order to indicate whether a continuous optical path exists from the laser to the detector, and also whether a continuous electrical path exists from the detector through the signal processor. Any discontinuity along this path will result in a system-check fail indication, with the code letters SCF. Because the fiber optics component is by far the most vulnerable in the system to damage, the primary purpose of this test is to indicate a fault in that system. Obviously, any failure of the laser or detector would also show a fault condition. When the results of this test are satisfactory, a system-check pass indication will result, with the code letters SCP.

When the user exits from this test, the instrument is in a measurement mode and will continuously measure and display either the flow, volume, or velocity parameter as selected by the user. Under normal operating conditions, the instrument will measure and store in memory a new value every 100 milliseconds for each of the three parameters. The user may select averaging times up to five seconds that allow the digital display and trend recorder to indicate a moving average of the selected parameter. Analog outputs at the rear of the instrument may be connected to an external recorder for simultaneous recording of all three measurement parameters.

The Laserflo BPM is designed to be easy for nontechnical personnel to use. Therefore, it has no external adjustments for zeroing or calibration of the instrument. The instrument's built-in microprocessor automatically selects the correct filter setting, correct gain setting, and correct zero adjustment each time a new measurement is made. The fiber optic connector is designed to be reliable so that no optical alignment by the user is required.

The instrument is also designed to give the user timely information in the event of a fault condition. The system check, which was described in some detail above, can be entered at any time by simply pressing the Test switch on the front panel of the instrument. This immediately interrupts blood flow measurements and gives the user an indication of whether the system fails or

passes the system check. If the user suspects some possibility of damage to the instrument or fiber optic cables, this test allows a simple and convenient check. The user returns to the measurement mode by simply pressing the Test button again, and the recorder settings, function setting, and averaging time return to their previous states.

The instrument is also designed to give a visual fault indication whenever the probe is not in direct contact or close proximity to the tissue surface. A question mark will scroll across the digital display under such a condition, alerting the user to reattach the probe and assure adequate tissue contact before proceeding with measurements.

The reader is referred to the instrument Operator Manual for complete operating instructions.

SUMMARY

Laser-Doppler flowmetry has been shown to be a unique and powerful method for real-time, noninvasive measurement of microvascular blood flow in experimental and clinical situations. To give users the maximum benefit from the potential advantages of this technique, the design objectives of the Laserflo BPM were

1. Capability of providing quantitative and repeatable flow measurements
2. Capability of measuring all three parameters, namely, flow, volume, and velocity
3. Ease of use for nontechnical clinical personnel.

This set of objectives became the driving force behind the selection of the laser, which is a single-mode, semiconductor laser. This laser offers optimum stability, optimum coherence properties, and superior durability.

The design of the fiber optics system is consistent with these objectives also. Small-core-diameter fibers eliminate troublesome motion artifact and optimize measurement repeatability. The fiber optic cable is durable as well as flexible. Notwithstanding the small fiber diameter, the fiber optic connector provides reliable connections every time with no need for alignments by the user.

The low signal-to-noise ratio is a problem inherent with the laser-Doppler technique, but the Laserflo BPM performs real-time noise correction (zeroing) automatically. This requires no intervention on the part of the user, increasing the user-friendliness of the instrument.

Finally, the instrument performs all signal processing digitally, which results in superior instrument repeatability. The patented signal processor design gives improved accuracy of spectral measurements, as well as linearization of the volume and velocity measurements at high red blood cell concentrations, over a very wide range of Doppler frequencies.

REFERENCES

1. Stern, M.D., D.L. Lappe, P.D. Bowen, J.E. Chimosky, G.A. Holloway, Jr., H.R. Keiser, and R.L. Bowman. 1977. Continuous measurement of tissue blood flow by laser-Doppler spectroscopy. Am J Physio 232(4):H441–H448.
2. Bonner, R., and R. Nossal. 1981. Model for laser Doppler measurements of blood flow in tissue. Appl Optics 20(12):2097–2107.
3. Watkins, D.W., and G.A. Holloway, Jr. 1978. An instrument to measure cutaneous blood flow using the Doppler shift of laser light. IEEE Trans BME-25(1):28–33.
4. Nilsson, G.E., T. Tenland, and P.Å. Öberg. 1980. A new instrument for continuous measurement of tissue blood flow by light beating spectroscopy. IEEE Trans BME-27:12–19.
5. Powers, E.W. III, and W.L. Frayer. 1978. Laser Doppler measurement of blood flow in the microcirculation. Plast Reconstr Surg 61(2):250–256.
6. Jones, B.M., and B.J. Mayou. 1982. The laser Doppler flowmeter for microvascular monitoring: a preliminary report. Br J Plast Surg 35:147–149.
7. Larrabee, W.F. Jr., G.A. Holloway, Jr., R.E. Trachy, and D. Sutton. 1982. Skin flap tension and wound slough: Correlation with laser Doppler velocimetry. Otolaryngol Head Neck Surg 90:185–187.
8. Shepherd, A.P., and G.L. Riedel. 1982. Continuous measurement of intestinal mucosal blood flow by laser Doppler velocimetry. Am J Physiol 242(5):G668–G672.
9. Low, P., C. Neumann, P.J. Dyck, R.D. Fealey, and R.R. Tuck. 1983. Evaluation of skin vasomotor reflexes by using laser Doppler velocimetry. Mayo Clin Proc 58:583–592.
10. Tahmoush, A.J., P.D. Bowen, R.F. Bonner, T.J. Mancini, and W.K. Engel. 1983. Laser Doppler blood flow studies during open muscle biopsy in patients with neuromuscular diseases. Neurology 33(5):547–551.
11. Rotering, R.H. Jr., J.A. Dixon, G.A. Holloway, Jr., and D.W. McCloskey. 1982. A comparison of the He Ne laser and ultrasound Doppler systems in the determination of viability of ischemic canine intestine. Ann Surg 196(6):705–708.
12. Adrian, R.J., and J.A. Borgos. 1986. Laser Doppler flow monitor. U.S. Patent 4,596,254.
13. Borgos, J.A., F.J. Bradac, D.J. Haumschild, T.R. Johnson, and R.J. Lee. 1988. Fiber optic connector assembly. U.S. Patent 4,772,081.
14. Nilsson, G.E. 1984. Signal processor for laser Doppler tissue flowmeters. Med Biol Eng Comput 22:343–348.
15. Duteil, L., J.C. Bernengo, and W. Schalla. 1985. A double wavelength laser Doppler system to investigate skin microcirculation. IEEE Trans Biomed Eng BME-32(6):439–447.
16. Engelhart, B., M. Merete, and J.K. Kristensen. 1983. Evaluation of cutaneous blood flow responses by ^{133}Xenon washout and a laser Doppler flowmeter. J Invest Dermatol 80(1):12–15.
17. Kvietys, P.R., A.P. Shepherd, and D.N. Granger. 1985. Laser Doppler, H_2 clearance, and microsphere estimates of mucosal blood flow. Am J Physiol 249:G221–G227.
18. DiResta, G.R., J.W. Kiel, G.L. Riedel, P. Kaplan, and A.P. Shepherd. 1987. Hybrid blood flow probe for simultaneous H_2 clearance and laser-Doppler velocimetry. Am J Physiol 253 (Gastrointest Liver Physiol 16):G573–G581.
19. Durlik, M., R. Benichoux, J. Lopex–Gollonet, and G. Karcher. 1986. A new laser Doppler interface for the continuous measurement of the rat gastric mucosal blood flow. Eur Surg Res 18:41–49.
20. Rundquist, I., Q.R. Smith, M. Michel, P. Ask, P.Å. Öberg, and S.I. Rapoport. 1985. Sciatic nerve blood flow measured by laser Doppler flowmetry and [^{14}C]iodoantipyrine. Am J Physiol 248(17):H311–H317.
21. Winsor, T., D. Haumschild, D. Winsor, Y. Yang, and T. Luong. 1987. Clinical application of laser Doppler flowmetry for measurement of cutaneous circulation in health and disease. J Angiol 38(10):727–736.
22. Spelman, F., P.Å. Öberg, and C. Astley. 1986. Localized neural control of blood flow in the renal cortex of the anaesthetized baboon. Acta Physiol Scand 127:437–441.
23. Ahn, H., J. Lindhagen, G. Nilsson, P.Å. Öberg, and O. Lundgren. 1986. Assessment of blood flow in the small intestine with laser Doppler flowmetry. Scand J Gastroenterol 21:863–870.

24. Tyml, K., and C.G. Ellis. 1985. Evaluation of a laser Doppler flowmeter by video microscopy. IEEE 7th Annual Conf. Engineering in Med. and Biol. Soc.
25. Bonner, R., R. Nossal, S. Havlin, and G.H. Weiss. 1987. Model for photon migration in turbid biological media. J Opt Soc Am [A] 4(3):423–432.
26. Chung, R., D. Bruch, and J. Dearlove. 1988. Endoscopic measurement of gastric mucosal blood flow by laser Doppler velocimetry: Effect of chronic esophageal variceal sclerosis. Am Surg 54(2):116–120.
27. Rosenblum, B., R.F. Bonner, and E.H. Oldfield. 1987. Intraoperative measurement of cortical blood flow adjacent to cerebral arteriovenous malformation using laser Doppler velocimetry. J Neurosurg 66:396–399.
28. Nitzan, M., S.L.E. Fairs, and V.C. Roberts. 1988. Simultaneous measurement of skin blood flow by the transient thermal-clearance method and laser Doppler flowmetry. Med Biol Eng Comput 26:407–410.

6. INNOVATIONS AND PRECAUTIONS

P. ÅKE ÖBERG

Laser-Doppler flowmetry is sometimes referred to as an art. Such an expression indicates that besides the instrument itself, a number of precautions must be considered in order to use the method properly. Therefore, this chapter reviews some important practical precautions regarding the use of laser-Doppler flowmetry. It also describes some innovations and modifications that have been made to laser-Doppler flowmeters and flow probes.

MOTION ARTIFACTS

The laser speckle

Everyone who has worked with laser light has probably observed the *laser speckle* pattern. The speckle phenomenon was recognized for the first time by Rigden and Gordon [1], who described it as a "remarkable granular and peppery nature not present in ordinary light." This pattern can be clearly demonstrated if a laser light beam is directed towards a reflecting surface.

Within a speckle pattern, the microscopic intensity varies from complete darkness to intense bright spots. The random distribution of intensities is formed when coherent light either is reflected from a rough surface or propagates through a medium with random refractive index fluctuations. The statistical properties of speckle patterns depend both on the coherence of the incident light and on the properties of the reflecting surface.

Most surfaces can be considered rough on the scale of the wavelength of light ($\lambda \approx 500$–600 nm). When coherent light is reflected from such a rough

surface, the various component wavelets interfere in a random way. Wavelets in phase at a particular point on the surface amplify each other, resulting in a bright spot, whereas at other locations out-of-phase wavelets cancel each other.

So long as the surface is stationary, the speckle pattern does not vary and will not give rise to intensity fluctuations in the reflected light. As soon as we move the reflecting surface, the laser, or the fiber optics leading the laser light to the surface, the speckle pattern is also changed and causes intensity fluctuations in the light reflected from the surface. What we call movement artifact in laser-Doppler flowmetry is simply intensity fluctuations caused by fiber optic movements or motion of the tissue under study. Because a part of the blood flow information is carried by the intensity fluctuations of the reflected light, we must reduce fiber flexing or surface movements because they contribute error to our blood flow signal.

Several groups have studied the problem of how to reduce the error due to fiber optic movements. Midwinter [2] has covered the theoretical aspects of the problem. Gush and King [3] have suggested several ways to improve existing systems. Newson et al. [4] have studied the Doppler spectrum for several motion amplitudes of the fibers. Öberg, Pettersson, and Rohman (unpublished observations) have studied how the launching of laser light into the fiber can affect the sensitivity to fiber motion.

Ways to reduce motion artifacts

Reduced fiber size

The number of possible modes in an optical fiber is

$$N = kV^2$$

where

$$V = \frac{2\pi a}{\lambda}\sqrt{n_1^2 - n_2^2}$$

and

k = a constant.

N = number of modes in the optical fiber,
V = V-number,
a = core radius [m],
λ = wavelength in vacuum [m]
n_1 = refractive index of the core, and
n_2 = refractive index of the cladding layer.

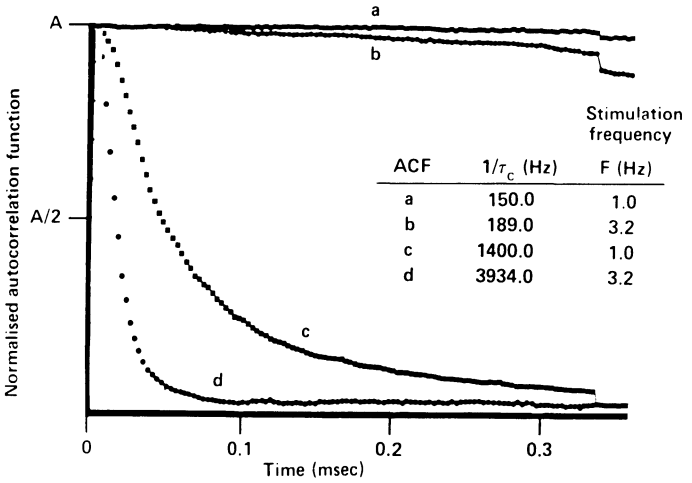

Figure 6–1. Autocorrelation functions (ACF) obtained from the intensity fluctuations produced by manipulated optical fibers: (a) and (b) are from 50 μm core graded-index fiber, and (c) and (d) are from Periflux 763 μm core step-index fibers. The stimulation and mean intensity fluctuation frequencies are tabulated. (From [3] with permission of the International Federation for Medical and Biological Engineering.)

Decreasing the radius of the fibers reduces the number of modes by the square of the radius. Graded-index fibers are also to be preferred over step-index fibers. As indicated by Gush and King [3], the difference between a 50 μm graded-index fiber and a 763 μm step-index fiber is substantial (figure 6–1). Newson et al. [4] have studied the effect of reducing fiber size and have found a reduction in the motion artifact with decreasing diameter of the fibers. But these authors also noted reduced physical dimensions demand increased quality in launching precision and optical surface quality.

Mechanical fiber damping

The movement artifact signal can be greatly reduced by mechanical damping of the optical fibers. Such improvements prevent the fibers from moving fast or going into mechanical oscillations. Damping can be obtained in a variety of ways. The springiness can be reduced by cladding the fiber bundle in a mechanically dead material. Gush and King [3] used aluminium foil to damp the fibers. Öberg, Pettersson, and Rohman (unpublished results) injected vaseline into a plastic catheter containing the optical fibers to obtain the same mechanical stabilization.

A careful general design of the fiber optic system can substantially reduce movement artifact. Optimization of the angle at which the laser beam is launched into the optical fiber, the coupling between the distal fiber end and the tissue, the way the optical fibers are arranged in bundles, and end-surface

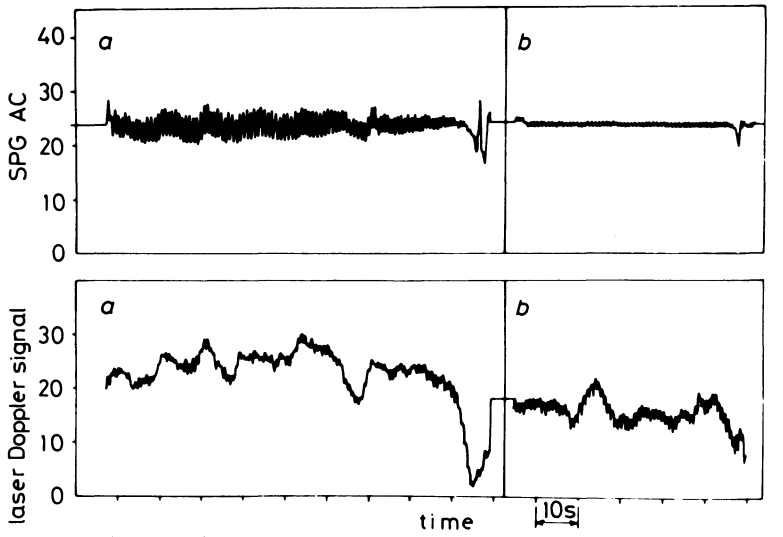

Figure 6–2. Simultaneous measurement of pulsatile flow with LDF (Periflux) and Silastic strain gauge plethysmograph (SPG) (a) on a finger pulp and (b) with a transparent adhesive tape (Sellotape) wrapped around it. (From [3] with permission of the International Federation for Medical and Biological Engineering.)

quality are all examples of practical factors that can considerably reduce fiber-motion artifacts.

Movements of measured site

An overlooked source of movement artifacts is tissue movements at the measured site. Tissue movements occur as a result of working muscles or the pumping action of the heart. The pressure waves in the arterial tree are also transmitted to the surrounding tissue causing pulsating tissue movements. Laser-Doppler measurements in such a moving site contain a signal contribution from the moving tissue that is often indistinguishable from the part of the signal generated by the flux of red blood cells. Gush and King [3] have clearly shown this effect in finger pulp measurements (figure 6–2).

Sometimes the effect can be minimized by selecting stationary tissue areas for blood flow measurements, but mechanically restraining tissue movements may impair blood flow, making this approach less applicable.

Miscellaneous methods

One obvious way of avoiding fiberoptic movements is to design instruments that do not require optical fibers for transmission of laser light to and from the tissue volume under study. de Mul et al. [5] and Jentink et al. [6] have designed such a system (figure 6–3). A semiconductor laser diode in the

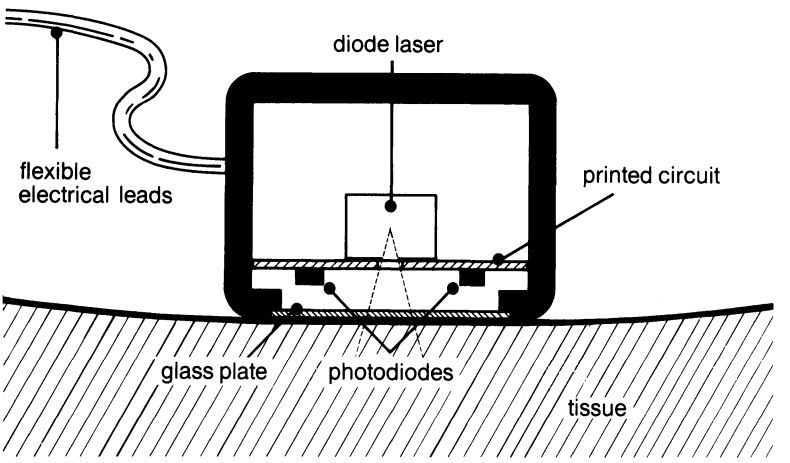

Figure 6–3. Minilaser-Doppler flow monitor without optical fibers. The laser diode is mounted in between the two receiving photodiodes in a housing that is attached directly to the tissue surface under study. (From [5] and [6] with permission from the American Institute of Physics.)

infrared range and two photodetectors were all positioned in a small probe that could be placed directly on the tissue site under study. This way of designing laser-Doppler probes has great advantages in special measurements, including studies in which the movements of the site under study cannot be avoided. The minilaser-Doppler of de Mul et al. [5] and of Jentink et al. [6] later became a commercial product (Diodopp) released by Applied Laser Technology, Asten, The Netherlands, in 1988.

Movement artifacts of optical fibers may also be electronically identified and rejected. This approach has been used in the Perimed PF2 instrument (Perimed, Stockholm, Sweden). An electronic circuit monitors the blood flow signal and switches off the output of the instrument when the rate of change of the signal exceeds a value not likely to be produced by blood flow. The circuit makes the user aware of the presence of movement artifacts but does not eliminate the basic problem, nor does it prevent less rapid fiber-movement artifacts from interfering with the blood flow signal.

STANDARDIZATION AND CALIBRATION OF LASER-DOPPLER FLOWMETERS

Most measurement methods need to be calibrated at regular intervals by comparing them with a standard to maintain accuracy over longer periods of time. The standard usually has a well-specified accuracy and long-term stability. An instrument under calibration is adjusted to give readings coinciding with the setting of the standard. An alternative way is to make up a calibration curve, i.e., a diagram describing the difference between the "true" value (standard) and the reading of the instrument under calibration. The

calibration curve is then used for correcting the actual measurements obtained with the instrument.

Such calibrations are not possible with laser-Doppler instruments, simply because there is no gold standard for measuring blood flow in tissue. Nevertheless, the laser-Doppler method has been compared with a variety of other methods. Such comparisons cannot generally be regarded as calibrations, since the other flow measurements have unspecified accuracies or even measure a different physiological variable related to the flux of red blood cells, but comparisons of this type can give useful information in a specific experiment or preparation.

Calibration

One class of experiments that can be regarded as calibrations of laser-Doppler instruments is that in which isolated or semi-isolated organs are perfused at well-controlled rates with whole blood or a perfusate consisting of physiological salt solutions containing red blood cells.

Shepherd et al. [7] have perfused isolated liver and stomach preparations at known total flow rates. The liver was perfused with canine red blood cells suspended in Krebs Ringer solution by means of a peristaltic pump. The total hepatic volume flow was measured from timed collections of venous outflow.

The perfused dog stomach preparation was kept at 35–37°C by warm Ringers solution. To prevent unpredicted redistribution of blood flow during the experiment, the preparation was vasodilated maximally with isoproterenal. Total blood flow was monitored with an electromagnetic flow meter.

The result for the liver study is shown in figure 6–4 and the gastric blood flow in figure 6–5. A highly linear relation was generally found between the total hepatic flow and the laser-Doppler readings. The calibration factor (the slope of the regression line) varied markedly between preparations and also among different sites on the same preparation. This variability was interpreted as a consequence of the small sampled volume of the laser-Doppler probe versus the heterogeneity of perfusion of the vascular bed. The well-known microvascular variations in hematocrit may also explain the result.

The results of Ahn et al. [8] obtained from the isolated small intestine are also an example of an attempt to calibrate a laser-Doppler flowmeter. In patients undergoing surgery for benign or malignant gastric or colonic disease, an ileal segment was vascularly isolated. One artery supplied the segment with blood and a single vein drained it. Blood flow was estimated by collecting venous outflow. The supplying artery was dissected free and an adjustable clamp around the vessel was used to control the flow in the segment. After resection, the intestinal segment was weighted to allow calculation of flow per 100 g of tissue. A linear relation was found (figure 6–6) for total blood flow rates less than 50 $ml \cdot min^{-1} \cdot 100g^{-1}$. At higher flow rates the flowmeter (Perimed PF1d) underestimated the rate. The in-

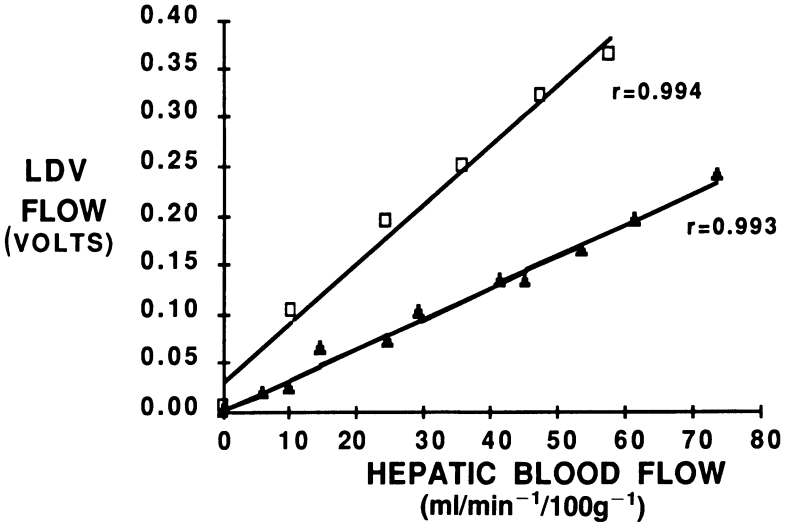

Figure 6–4. Laser-Doppler velocimeter (LDV) measurements versus total hepatic blood flow. Results from two isolated rat liver experiments are shown. Both yielded significant, linear relationships ($r = 0.994$, $y = 0.0061x + 0.0306$; $r = 0.993$, $y = 0.0031x + 0.0001$), but the slopes were markedly different ($p < 0.001$). (From [7] with permission from the American Physiological Society.)

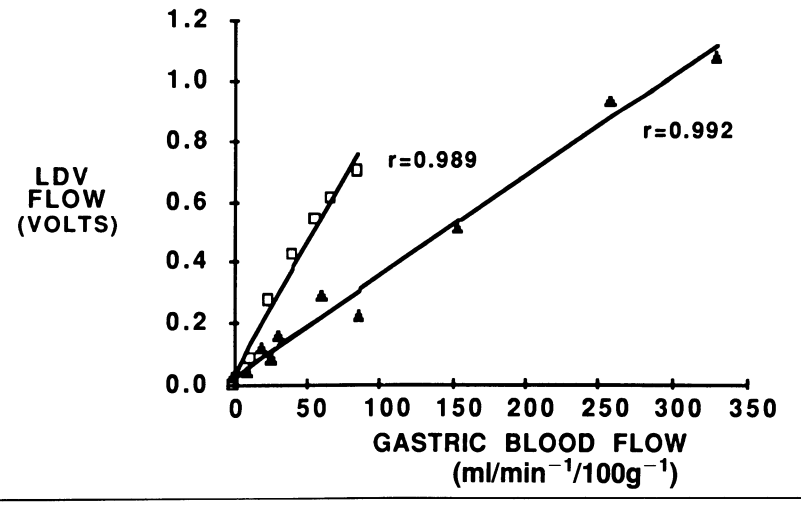

Figure 6–5. Laser-Doppler velocimeter (LDV) measurements of gastric mucosal blood flow versus total perfusion of isolated stomach flaps vasodilated with isoproterenol. Both experiments showed significant linear relationships between local LDV values and total flow ($r = 0.989$, $y = 0.0086x + 0.0027$; $r = 0.992$, $y = 0.0033x + 0.0197$), but slopes were significant different ($p < 0.001$) (From [7] with permission from the American Physiological Society.)

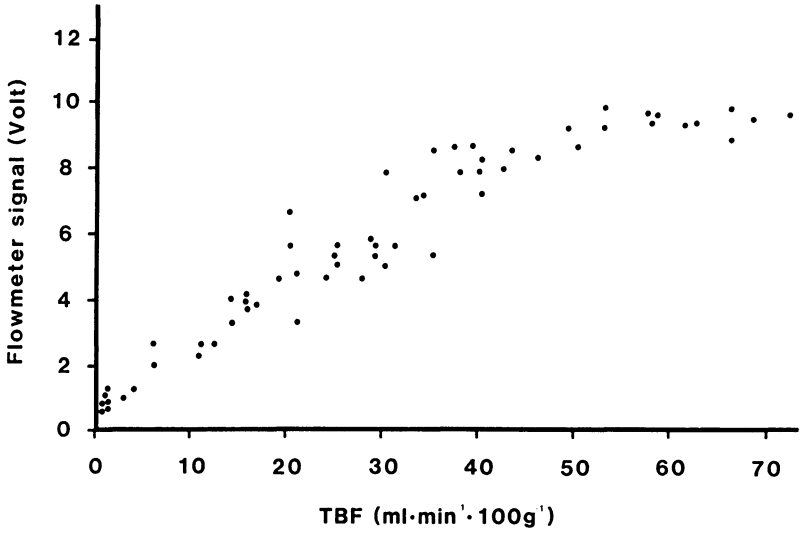

Figure 6–6. The relation between total blood flow (TBF) and laser-Doppler flowmeter signal obtained from the serosal surface of bowel segments in 11 patients. (From [8] with permission from the Scandinavian Journal of Gastroenterology.)

terindividual scattering in data seem to be relatively small in this preparation. When the probe was moved along the bowel segment, the flowmeter signal level varied ±15%.

The conclusion that can be drawn from experiments like these is that the laser-Doppler flowmeter can possibly be calibrated in absolute units ($ml \cdot min^{-1} \cdot 100g^{-1}$) for a particular measurement site on a specific preparation. However, this calibration factor probably cannot be used for other sites on the same tissue or in other tissues. In the light of these results, the attempt by some commercial producers to market factory-calibrated laser-Doppler instruments must be seriously questioned. Their "calibration factors" are based on physical–optical theoretical models and are not necessary valid for various tissues.

Standardization

To standardize an instrument or a method is to make sure it maintains stability, linearity, and reproducibility. However, such standardization does not mean that an absolute value of flow is achievable. Several methods have been suggested for the standardization of laser-Doppler instruments.

Rotating disk

Several authors [7,9,10] have designed rotating disks for the standardization of laser-Doppler instruments. The first three authors used similar devices (figure 6–7). A slowly revolving thin (0.030 inch) disk of fluorocarbon

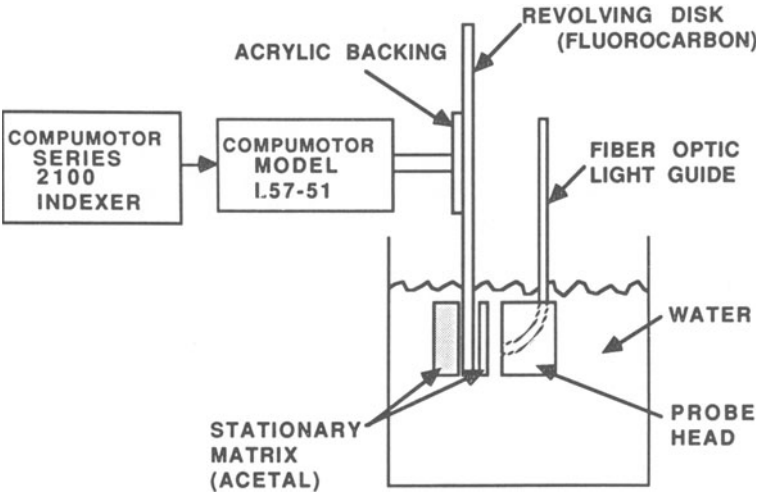

Figure 6–7. Model to simulate perfused tissue. Revolving fluorocarbon disk produced Doppler shifts in light scattered back to fiber optic light guide. Acetal block simulated light scattering by static tissue. Optical fibers delivered light to and carried scattered light back from rotating disk. For clarity, only one fiber is shown. A stepping motor controlled disk velocity precisely. (From [7] with permission from the American Physiological Society.).

(Teflon®, PFTE) simulated moving scatterers. The rotational speed of the disk vertically oriented on the shaft of a computer-controlled stepping motor (Compumotor, model L57-51) was varied over a "wide physiological range." A stationary scatterer of acetal blocks (Delrin) in between the rotating disk and the fiber optic probe simulated the static tissue, which scatters unshifted photons back to the photodetector. The scattering part of the model was submerged in water to facilitate coupling of light though the interfaces. Correlation coefficients between the linear speed of the disk and the flow output of the laser-Doppler instruments were generally close to 1.0 (0.993–0.999).

An even better homogeneity of scatterers than in teflon can be obtained by moulding aluminum dioxide (Al_2O_3) into acrylic plastic (Öberg, Pettersson and Rohman, unpublished results). Al_2O_3 powder from Buehler Micropolish (Buehler, Lake Bluff, U.S.A.) with a particle size of 1 μm was mixed into acrylic plastic Acrifix 90® (Röhm GMBH, Darmstadt, West Germany). Thorough mixing ensured a high homogeneity of scattering particles. Air bubbles in the suspension were eliminated by treatment in a vacuum. The surface of the moulded disk was machined and polished to ensure that surface roughness did not detract from the high homogeneity of scatterers obtained by the moulding process.

In addition to a more homogeneous scatterer distribution, the moulded disks make it possible to vary the slope of the calibration curve to fit a

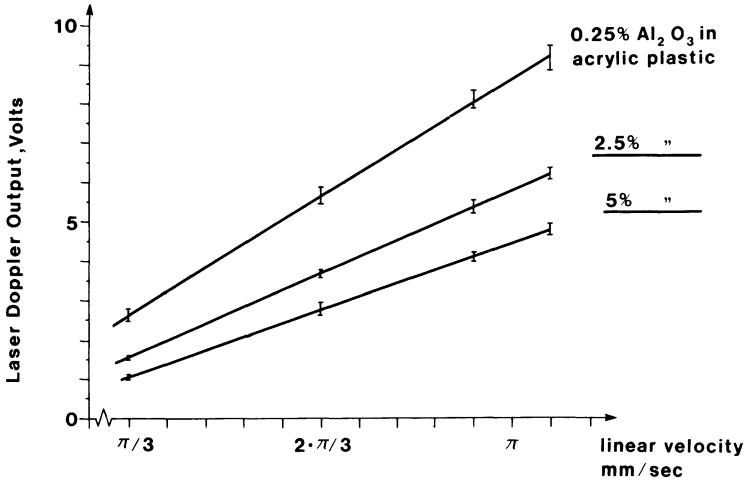

Figure 6–8. The relation between the linear velocity of a rotating disk manufactured from moulded acrylic plastic and laser-Doppler output voltage. Observe the strong influence of the concentration of the scatterers in the moulded disk. (Öberg, Petersson and Rohman, unpublished results.)

particular standardization problem. Figure 6–8 gives the relation between the laser-Doppler flowmeter signal and disk velocity for three different concentrations of scatterers. Observe the nonlinearity in the relations and the effect of the percent Al_2O_3 on the slope of the standardization curve.

Particle suspensions

The Brownian motion of particles in a suspension can be used to standardize laser-Doppler instruments. For short-term use (≈ 1–2 hours), ordinary milk can be used. For standardization during longer periods (≈ 2–3 months), it is important to use a suspension that is not affected by sedimentation or particle aggregation.

A colloidal suspension of latex spheres has been found to have excellent long-term properties. Perimed KB has developed a standard that is a concentrated suspension of latex particles. Under constant temperature conditions (18°–22°C), this standard is a reliable means of quickly checking the performance of laser-Doppler flowmeters. The marketed version of the suspension gives a standard motility of 250 PU (perfusion units) with a coefficient of variation of ±5% depending on random variations in the Brownian motion. Perimed recommends renewing the standard after about a year because the long-term stability is unknown.

Mechanical flow models

A variety of mechanical flow models have been described in the laser-Doppler literature [11–13]. Although most of them were originally used for

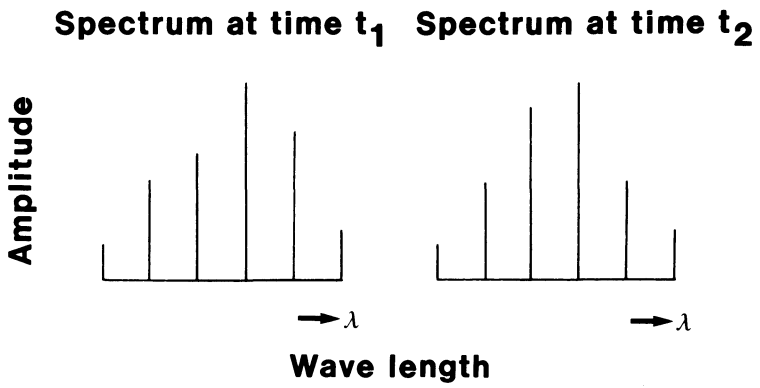

Figure 6–9. Longitudinal mode frequency distribution from a He–Ne laser on two occasions t_1 and t_2. Mode-jump noise occurs when the total energy of the laser is redistributed among the different modes that can exist in the laser cavity.

the study of the principles of laser-Doppler flowmetry, they can all be of great value for standardizing or calibrating laser-Doppler flowmeters. They all seem to give similar results when effects of variations of hematocrit, average velocity, and volume flow are studied. The choice of such models for standardization purposes is therefore very much a question of what can be set up and manufactured locally.

LIGHT SOURCE CONSIDERATIONS

Stabilization of gas lasers

The helium–neon gas laser is the most common light source in commercially available laser-Doppler instruments. Helium–neon lasers in the power range 2–5 mW are multimode lasers, i.e., they oscillate in more than one longitudinal mode. Three to five modes are typical. The difference in frequency Δf between two adjacent modes can be expressed as

$$\Delta f = \frac{c}{2L},$$

where c is the speed of light in vacuum and L is the length of the laser cavity. Typical mode patterns are shown in figure 6–9.

This pattern of fundamental modes is not stable with time but varies with the dimensions of the laser cavity. Because these dimensions change with the temperature of the laser tube, the mode pattern is strongly affected by temperature. Thermal expansion can cause mode jumps, a phenomenon that occurs when a set of modes cannot exist in the laser cavity and is replaced by another set. During this process, the laser beam energy is transferred from the old set of longitudinal modes to the new set. Through internal frequency mixing, noise (sum and difference frequencies) is generated that falls into the

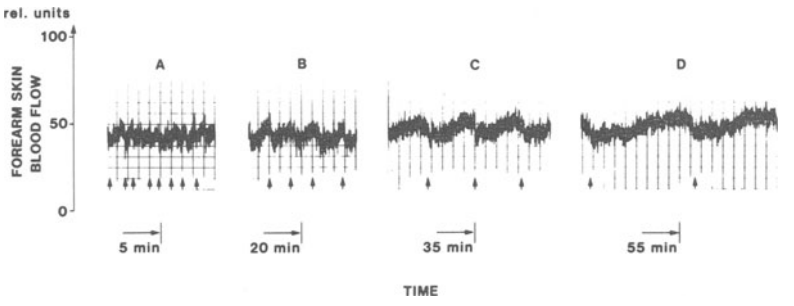

Figure 6–10. Recording of forearm skin blood flow. The blood flow signal mixed with noise from an unstabilized laser-Doppler instrument (Perimed PF1d). The mode jumps occurred at the moments indicated by arrows. The periodicity of the noise varies with the temperature of the laser cavity. This type of noise can easily be misinterpreted as vasomotion. (From [14] with permission from the International Federation for Medical and Biological Engineering.)

same frequency domain as the Doppler signals. This noise can seriously affect blood flow recordings. Figure 6–10 shows a recording of forearm blood flow during the warming-up period of the laser tube (Perimed PF1, Perimed, Stockholm). During the first minutes (figure 6–10A) the mode jumps are frequent, and the noise appears in the blood flow recording as transients that can be misinterpreted as vasomotion. When the temperature of the laser cavity is stabilizing, the mode jumps less frequently, i.e., the time in between the jumps becomes longer. The laser tube never becomes completely stable. The mode-jumping phenomenon is especially marked in certain laser brands and in worn-out laser tubes.

Such laser instability can be eliminated by temperature stabilization of the laser cavity. The principle of such a stabilization circuit is illustrated in figure 6–11. The returning beam from the laser cavity impinges on a Wollaston prism that splits two orthogonal adjacent modes into two separate rays. The vertically oriented mode is focused on one photodetector, and the horizontally oriented mode is focused on the other. Electrical signals proportional to the intensities of the two beams are generated, and the difference between them is formed in a difference amplifier. This difference signal, which is a sensitive measure of the length of the laser cavity, controls the current of a heating coil applied along the laser tube. An electronic network controls the starting conditions and the adjustment of other control parameters.

The result of laser stabilization is shown in figure 6–12. Before stabilization (figure 6–12A), the difference voltage oscillated with decreasing frequency as the laser tube temperature stabilized. After stabilization circuits were connected (figure 6–12B), the oscillations in difference voltage stopped, and a stable mode pattern was reached.

The effect of stabilization can also be seen in the power spectrum recorded from the skin of the lower arm (figure 6–13). The measurement was done with and without stabilization. As the figure shows, a substantial part of the

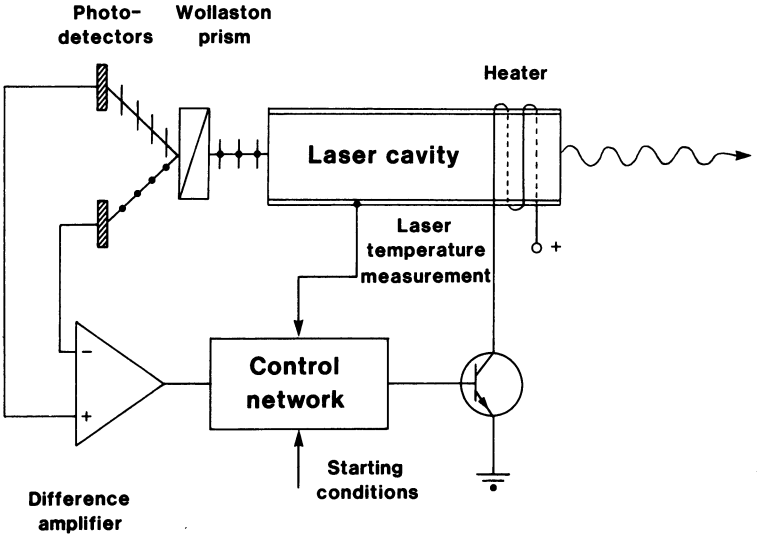

Figure 6–11. Block diagram of the principle for laser temperature stabilization. This type of stabilization can substantially increase the signal-to-noise ratio. (From [14] with permission from the International Federation for Medical and Biological Engineering.)

spectrum before stabilization (contributions from the mode jumps) was eliminated after stabilization [14]. With stabilization, a frequency stability of the order $1{:}10^8$ can be achieved.

Stabilization of diode lasers

During the last two years, laser diodes have increasingly been used in laser-Doppler flowmetry. Laser diodes in the infrared range (750–850 nm) have been used both for experimental purposes and in commercial instruments (Diodopp, AD Asten, The Netherlands; TSI, St. Paul, MN, U.S.A.).

In laser diodes, the central wavelengths of the emission spectrum and the emission wavelength of the monomode laser are strongly temperature-dependent. For relatively small temperature changes, the temperature variation is defined by the change in the Fabry-Perot resonances

$$\left(\frac{d\lambda}{dT}\right)_{FP} = \frac{\lambda}{n}\frac{dn}{dt} \approx 0.1 \text{ nm/°K},$$

where

λ = emission wavelength in nm,

n = refraction index, and

T = temperature in °K.

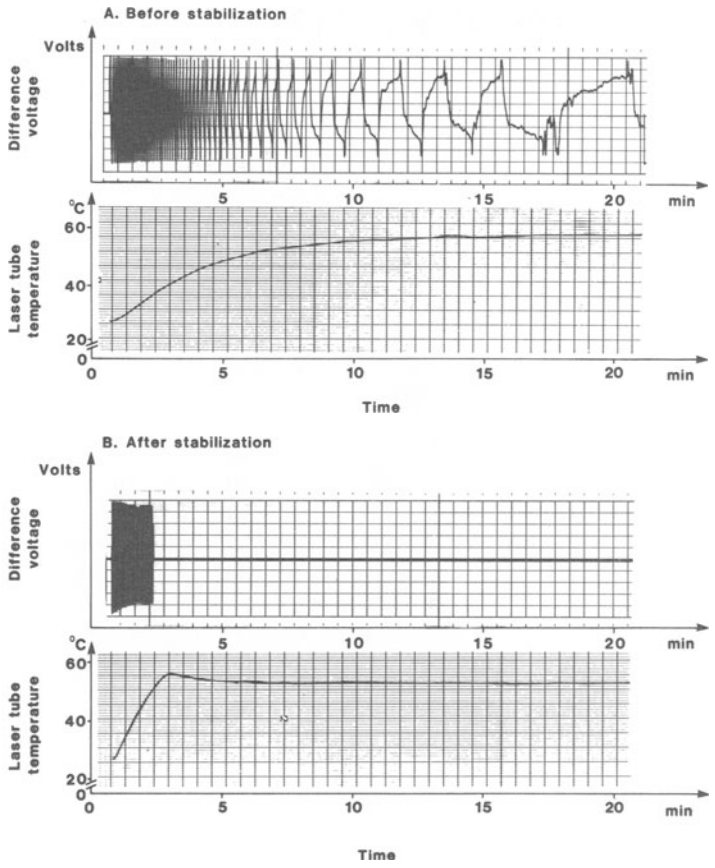

Figure 6–12. Laser performance before (A) and after (B) thermal stabilization of the laser tube. After the initial heating period (B), the closed-loop control of the laser thermal stability completely eliminated the mode-jump noise. (From [14] with permission from the International Federation for Medical and Biological Engineering.)

Over larger temperature intervals, the wavelength change will be determined chiefly by the temperature-dependence of the semiconductor bandgap.

$$\left(\frac{d\lambda}{dT}\right)_g = \frac{hc}{Wg}\frac{dWg}{dT} \approx 0.2\text{–}0.3 \text{ nm/°K},$$

where

Wg = bandgap,

c = velocity of light, and

h = Planck's constant.

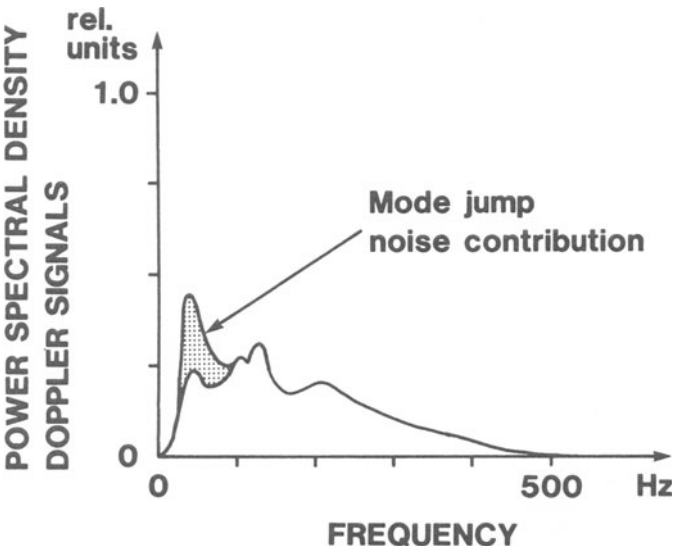

Figure 6–13. Power spectral density of laser-Doppler signals from forearm blood flow with and without thermal stabilization. Each spectral density curve is an average of 200 recordings. Thermal stabilization of the laser cavity eliminated the noise from mode jumps in the low-frequency part of the spectrum. (From [14] with permission from the International Federation for Medical and Biological Engineering.)

To use laser diodes in laser-Doppler flowmetry, they must be stabilized in several ways. The power delivered to the laser must be stabilized by a current control circuit to maintain constant output power. In such a scheme, the PIN-diode that is usually integrated into commercially available laser diodes can be used as a feedback path. In addition, stabilizing the junction temperature is necessary. This can be achieved by mounting the diode laser on a Peltier element to control temperature. Without these precautions, laser diodes are subject to mode-jump disturbances to such an extent that they are useless for laser-Doppler purposes [15].

REFERENCES

1. Rigden, J.D., and E.I. Gordon. 1962. The granularity of scattered optical maser light. Proc IRE 50:2367–2368.
2. Midwinter, J.E. 1979 In Optical Fibers for Transmission. New York: John Wiley and Sons.
3. Gush, R.J., and T.A. King. 1987. Investigation and improved performance of optical fiber probes in laser Doppler blood flow measurements. Med Biol Eng Comput 25:391–396.
4. Newson, T.P., A. Obeid, R.S. Walton, D. Boggett, and P. Rolfe. 1987. Laser Doppler velocimeter: The problem of fiber movement artefact. J Biomed Eng 9:169–172.
5. de Mul, F.F.M., J. Van Spijker, D. Van der Plas, J. Greve, J.G. Aarnoudse, and T.M. Smits. 1984. Minilaser-Doppler (blood) flow monitor with diode laser source and detection integrated in the probe. Appl Optics 23(17):2970–2973.
6. Jentink, H.W., R.G.A.M. Hermsen, F.F.M. de Mul, H.E. Suichies, J.G. Aarnoudse, and

J. Greve. 1988. Tissue perfusion measurements using a mini diode laser Doppler perfusion sensor. SPIE Conference, Vol 904, Microsensors and Catheter-Based Imaging Technology. Los Angeles.
7. Shepherd, A.P., G.L. Riedel, J.W. Kiel, D.J. Haumschild, and L.C. Maxwell. 1987. Evaluation of an infrared laser Doppler blood flowmeter. Am J Physiol 252:G832–G839.
8. Ahn, H., J. Lindhagen, G.E. Nilsson, P.Å. Öberg, and O. Lundgren. 1986. Assessment of blood flow in the small intestine with laser Doppler flowmetry. Scand J Gastroenterol 21:863–870.
9. Haumschild, D.J. 1986. Microvascular blood flow measurement by laser Doppler flowmetry. TSI Application Note. TSI Inc., 500 Cardigan Road, PO Box 64394, St Paul, MN 55164, USA.
10. Smits, G.J., R.J. Roman, and J.H. Lombard. 1986. Evaluation of laser-Doppler flowmetry as a measure of tissue blood flow. J Appl Physiol 61:666–672.
11. Nilsson, G.E., T. Tenland, and P.Å Öberg. 1980. Evaluation of a laser Doppler flowmeter for measurement of tissue blood flow. IEEE Trans Biomed Eng 27:597–604.
12. Roman, R.J., and C. Smits. 1986. Laser-Doppler determination of papillary blood-flow in young and adult rats. Am J Physiol 252:F115–F124.
13. Tamura, T., and P.Å. Öberg. 1988. Studies of scattering volume geometry in laser Doppler flowmetry. Innovation et Techn en Biol et Medecine (ITBM) 9:370–380.
14. Öberg, P.Å. 1988. A method for frequency stabilization of multimode He–Ne lasers in laser-Doppler flowmetry. Abstract. World Congress on Medical Physics and Biomedical Engineering, San Antonio, Texas, August 6–12.
15. Dopheide, G., G. Taux, G. Reim, and M. Faber. 1986. Laser Doppler anemometry using laserdiodes and solid state photodetectors. Third International Symposium on Applications of Laser Anemometry of Fluid Mechanics. Lisbon, Portugal (paper 8.2).

7. CATHETER VELOCIMETERS

MICHAEL D. STERN

The laser-Doppler velocimeter is potentially a very powerful device for measuring intravascular blood flow velocity. Because light can be delivered and collected through optical fibers of very small diameter, the technique lends itself naturally to use through a catheter passed through the blood vessel. The small size of optical fibers also permits high spatial resolution, so that flow velocity at a single point in the cross section of a blood vessel can be measured. However, because catheters disturb the flow of blood in their neighborhood, and because light is multiply scattered in passing through blood, combining the high spatial and temporal resolution of (LDV) laser-Doppler velocimetry with catheter delivery is not straightforward. At the present time, the development of instruments for the practical measurement of blood flow velocity through a catheter is an area of active research. In this chapter, we will present the principles behind this work, and will indicate the present state of the art and the potential uses of catheter LDV systems.

The possibility of measuring blood flow velocity through an optical fiber was explored very early in the development of dynamic light scattering. Tanaka and Benedek [1] showed that it was possible to measure Doppler spectra (actually autocorrelation functions) from flowing blood through a 500 μm optical fiber. The fiber was passed into the femoral vein of a rabbit. The spectra were heterodyne spectra, with the heterodyne reference beam supplied by stray light scattered back from the end of the single fiber, which was used for illumination and collection. When the rabbit was killed, the Doppler spectrum disappeared.

Even in these early experiments, it was noted that direct delivery of light from the end of a perpendicularly cleaved fiber gave unstable spectra whose bandwidth was much less than would be expected from the anticipated flow velocities in a large vein. The authors correctly interpreted this as being due to flow disturbances at the tip of the fiber. When the fiber is directed downstream, a stagnant and possibly turbulent wake forms at the tip of the fiber. Although the size of the stagnation region at the tip of a 500 μm fiber is very small, so is the region from which the signal is collected. Since light is emitted from the same fiber used for collection, the vast majority of the collected photons have been scattered very close to the fiber tip, i.e., in the region of the stagnant wake. Tanaka and Benedek showed that this problem could be overcome by polishing the fiber tip at a 45° angle, so that total internal reflection caused the beam to exit from the side of the fiber, rather than the tip. The flow along the side of the fiber was stable and gave reproducible spectra.

Although most of the important principles in fiber optic blood flow measurement had been demonstrated in this first article, the development of intravascular velocimetry was not pursued at the time, possibly because the motivation for developing the technique did not exist.

In the years since this early work was published, the clinical use of diagnostic and interventional angiography has undergone an explosive growth. The motivation to develop minimally invasive means of intra-arterial flow measurement is now clear, and several groups have explored laser-Doppler velocimetry as an approach.

DOPPLER SPECTRA OBTAINED WITH SINGLE FIBERS

In 1982, Kilpatrick et al. [2,3] and Nishihara et al. [4] published careful measurements of Doppler spectra returned from single optical fibers inserted into large vessels. The fibers used were graded-index communications fibers, substantially smaller than those used previously, having 50 μm core diameter and 125 μm cladding diameter. The experimental configurations used by the two groups were somewhat different.

Kilpatrick used nominal homodyne detection, with a heterodyne reference beam in effect supplied by stray scatter from the fiber end. This configuration does not permit distinction between upward Doppler shifts (blood flowing toward the fiber tip) and downward shifts (blood flowing away from the fiber tip). The fiber was cleaved at right angles and delivered at the end of a 1 mm plastic catheter. With this arrangement, the collected Doppler spectra had greatest intensity at zero frequency shift, with a roughly exponential fall as frequency increased (figure 7–1). No peak was seen in the spectrum. The *maximum Doppler frequency*, determined somewhat arbitrarily as the frequency at which the Doppler spectrum ceased to be detectable above the noise, was found to vary reproducibly with the free-stream flow velocity when the catheter was inserted into model blood flows in plastic tubes.

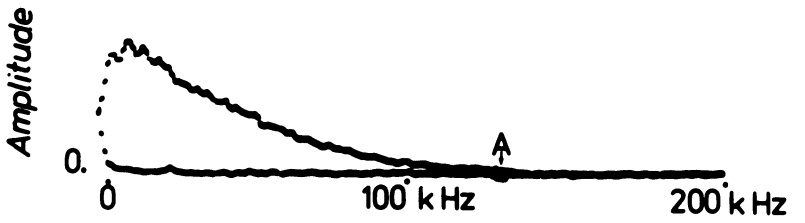

Figure 7–1. Homodyne Doppler spectrum obtained from a single fiber, enclosed in a 1 mm catheter and inserted into a flowing stream of whole blood. The upper spectrum is from flowing blood, and the lower spectrum shows system noise at zero flow. Point A is the *maximum Doppler frequency*, defined as the frequency above which the flow spectrum is indistinguishable from noise. (From Kilpatrick et al. [3], figure 3.)

When flow was directed towards the catheter tip, the relationship between the maximum Doppler frequency and the free-stream flow velocity was relatively linear. However, when the catheter was pointed downstream (as it would be in a branch artery entered during angiography), there was saturation of the maximum Doppler frequency at modest flow velocities (figure 7–2). This was recognized as being due to the stagnant wake formed downstream from the tip of the catheter.

For moderate Reynolds numbers (i.e., flow velocities), this stagnant region is expected to be comparable in size to the diameter of the catheter tip. The cone of light emerging from the fiber tip diverges at an angle which is typically 7° or more; because of the inverse square law, scattered light collected through the same fiber will be dominated by light that has been scattered in the intensely illuminated region within a few fiber diameters of the tip, even in the absence of attenuation by scattering or absorption. Since the catheter diameter is at least an order of magnitude larger than the fiber core, this region is necessarily within the stagnant wake of the catheter when the catheter points downstream.

The system described by Nishihara et al. utilized a frequency-shifted heterodyne reference, making it possible to distinguish upward and downward Doppler shifts. Helium–neon laser light was delivered through a single fiber, and the scattered light was collected through the same fiber. Before detection, the scattered light was mixed with a portion of the primary laser beam that had been passed through a Bragg acousto-optic cell, shifting the optical frequency by 40 MHz. With this scheme, the detected light intensity contains heterodyne components in the neighborhood of 40 MHz. The exact Bragg cell frequency (40 MHz in this case) is surrounded by upper and lower sidebands that are exact replicas of the upper and lower Doppler sidebands that are impressed on the optical waveform (carrier frequency about 4.7×10^{14} Hz) by scattering from approaching or receding blood.

The heterodyne Doppler spectrum was analyzed by a digitally controlled spectrum analyzer, and the maximum Doppler frequency was computed for

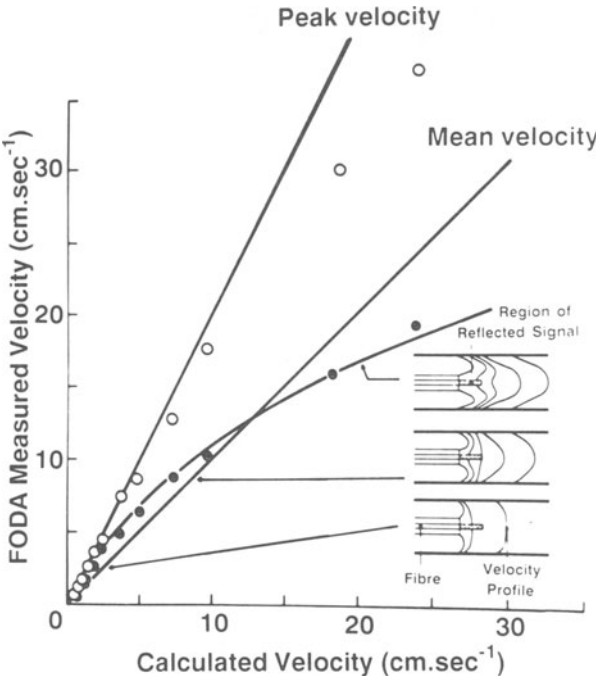

Figure 7–2. The relationship between velocity calculated from maximum Doppler frequency and flow velocity for a fiber/catheter inserted into blood flowing in a tube. The fiber tip was pointed either upstream (open circles) or downstream (closed circles). The straight lines show calculated peak and mean velocities for undisturbed Poiseuille flow in the tube. The saturation of Doppler frequency at high flow rates when the fiber points downstream is due to the development of a stagnant wake at the tip of the catheter, as indicated in the inset. (From Kilpatrick et al. [3], figure 4.)

each sweep of the spectrum analyzer. Rather than pass the fiber through a catheter, it was inserted through the side of the surgically exposed artery through a special holder that held the bare fiber at a 60° angle to the direction of blood flow. With this arrangement, the maximum Doppler frequency was found to correspond accurately to the free-stream flow velocity for flow in either direction (figure 7–3). This made possible the precise space- and time-resolved mapping of the arterial flow velocity profile in, for example, the coronary artery of the dog [5], as shown in figure 7–4.

THEORETICAL PRINCIPLES OF DOPPLER SPECTRA IN BLOOD

The systems described above circumvented the problem of flow disturbance by 1) using geometries in which the light from the fiber avoided the disturbed flow layer as much as possible and 2) measuring the maximum Doppler shift of the broad spectrum, assuming that this frequency represents

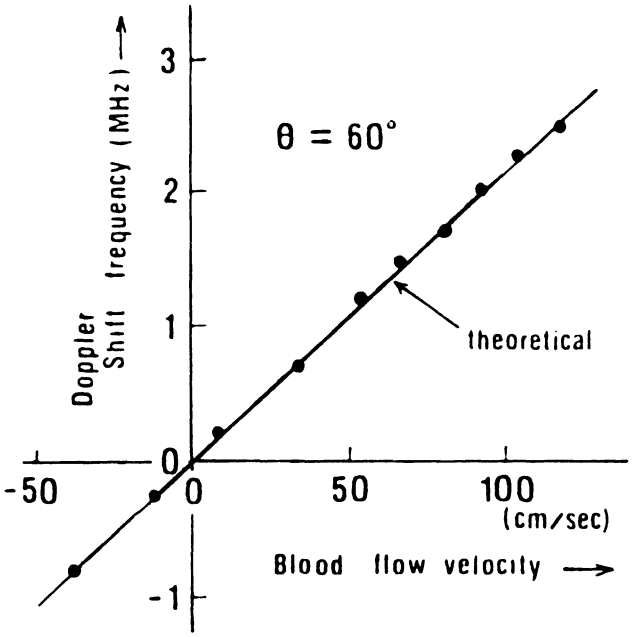

Figure 7–3. Linear relationship between velocity obtained from maximum Doppler frequency and free-stream flow velocity when a bare fiber is inserted into the flow at a 60° angle, avoiding the wake produced by a catheter. Directional Doppler shifts were obtained by a frequency-shift heterodyne method. (From Nishihara et al. [4], figure 8.)

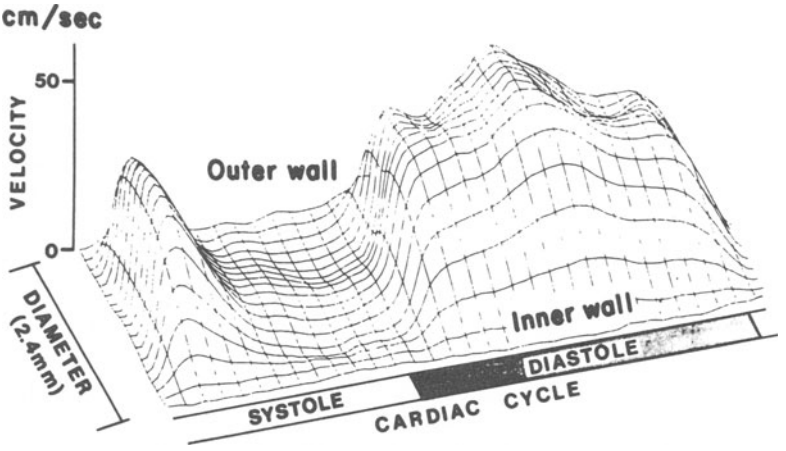

Figure 7–4. Flow velocity profile across a coronary artery of a dog, obtained by positioning a bare optical fiber at different locations in the arterial cross section, displayed as a function of position and time during the cardiac cycle. (From Kajiya et al. [5], figure 7.)

light scattered from the free-stream flow, whereas the (dominant) lower frequencies arise from light scattered in the slower-flowing boundary layer around the fiber tip. For measurements from an intra-arterial catheter, approach (1) is not likely to be very useful, since it is not possible to find a location for the fiber tip that is not at least partly in the boundary layer of the catheter. The assumption in approach (2), that the largest Doppler shift represents the signal from blood distant from the fiber tip, appears superficially reasonable. However, it is difficult to defend rigorously. Blood is a highly multiply scattering medium: the mean free path of a red photon in blood has been estimated to be as short as 7 μm. Therefore, one would not expect any light to return to an optical fiber after scattering at a distance of several hundred μm, without encountering additional scatterings on the way to and from the fiber. Therefore, none of the optical signal can be strictly considered to be arising from any particular location in the flow field, especially one distant from the fiber tip.

In order to clarify this situation, and to determine whether there exists a better optical configuration suitable for use in a catheter-based system, Stern [6] analyzed the theory of laser-Doppler velocimetry in blood. This analysis consisted of three parts: 1) study of the fundamental wave-scattering physics of light in a flowing, optically dense medium; 2) analysis of the penetration depth of Doppler measurements in blood; and 3) analysis using analog signal processing, of the signal-to-noise ratio of a hypothetical fiber Doppler system as a function of the fiber diameter and illumination geometry.

The first part of the study, which will not be described in any detail here, resulted in a nonlocal transport theory for the propagation of Doppler shifts in light diffusing through flowing blood. Because scattering is not localized (due to interaction of scatterers and finite wavelength uncertainty effects) and propagation is not rectilinear (due to diffraction), the nonlocal transport theory is rather difficult to apply to numerical computation. It was shown that, under certain conditions (which are only marginally met in whole blood), the nonlocal transport theory reduces to a local scattering model equivalent to the "photon random walk" described by Bonner and Nossal in chapter 2.

A Monte-Carlo algorithm was developed to solve the local scattering model. Computation of Doppler spectra from a single fiber in blood showed that the experimental shape of the spectra could be explained, provided that the hydrodynamic boundary layer at the fiber tip has the correct thickness, which is comparable to the tip diameter, as expected. The linear relationship between the maximum Doppler frequency and the free-stream flow velocity is approximately valid in the numerical model. This results from the fact that blood is a very strongly forward-scattering material, so that, although the light collected even from one fiber has suffered many scatterings, it is likely that most of these do not alter the direction of propagation very much on the way to and from a site at which a large-angle scattering (which returns the light towards the fiber) takes place. This phenomenon, which may be called

pseudo-first-order scattering, is not fundamental, but depends on a particular combination of scattering properties possessed by dense suspensions of red blood cells, as well as the proper thickness for the hydrodynamic boundary layer. Therefore, the use of the maximum Doppler frequency as a free-stream velocity estimator is questionable on theoretical grounds, although it is well validated experimentally in certain circumstances.

As an alternative to the maximum Doppler frequency, the use of the *algebraic mean Doppler shift* as a velocity estimator was investigated. The algebraic mean Doppler shift is the spectrally weighted average of the Doppler shift (including a negative sign for shifts to lower frequencies than the carrier). We will indicate the algebraic mean Doppler shift by the symbol $\langle\omega\rangle$; it is defined formally by

$$\langle\omega\rangle = \int_{-\infty}^{\infty} \omega S(\omega)\, d\omega \tag{7.1}$$

where $S(\omega)$ is the Doppler spectrum as a function of the signed Doppler shift ω.

It was shown by the Doppler transport theory that, for any fixed geometry of illumination and collection fibers, $\langle\omega\rangle$ is a linear function of the flow velocity field $\mathbf{v}(x)$, given by

$$\langle\omega\rangle = \int \mathbf{P}(x) \cdot \mathbf{v}(x) dx \tag{7.2}$$

where $\mathbf{P}(x)$ is a *sensitivity* vector field that describes the weighting of the contribution of velocity at the point x to the overall algebraic mean Doppler shift. Thus $\mathbf{P}$ describes the sensing profile in space of the fiber configuration (using the algebraic mean Doppler shift as output), even though no particular feature of the spectrum can be associated with any particular flow velocity, due to the effects of multiple scattering.

It can be shown from the transport theory that the Doppler sensitivity field $\mathbf{P}$ can be determined from the irradiance field $I(\mathbf{k}, x)$ describing the intensity at point x in the direction of the unit vector $\mathbf{k}$, produced by the illuminating fiber, together with the reciprocal irradiance field $I^+(\mathbf{k}, x)$, which is the irradiance that *would be produced if the blood were illuminated through the collecting fiber.* For a single-fiber system, of course, I and I^+ are the same. The form of the relationship is

$$\mathbf{P}(x) = \text{div } T, \tag{7.3}$$

where T is a tensor field defined by

$$T_{ij} = C \int \mathbf{k}_i \mathbf{k}_j I(\mathbf{k}, x) I^+(-\mathbf{k}, x) d\Omega(\mathbf{k}), \tag{7.4}$$

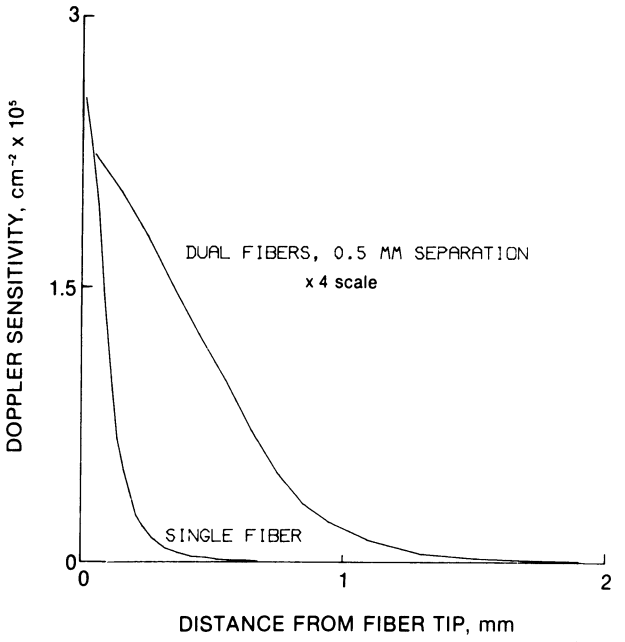

Figure 7–5. One-dimensional plot of calculated Doppler sensitivity fields of single-fiber and two-fiber Doppler systems, as a function of distance from the plane containing the tips of the fiber(s). Sensitivity extends farther from the fiber tips for the two-fiber system.

where C is a constant. the integral is over the directions of light propagation at point x. The presence of the product of I and I^+ indicates that the region of maximum sensitivity will be *where the illumination fields of the illuminating and collecting fiber overlap.*

For a single fiber, this means that the Doppler signal will be dominated by the velocities in the bright region near the fiber tip, which is unfortunately also where flow is the most perturbed. If, however, separate fibers are used for illumination and collection of light, then one would expect the region of sensitivity to move outward into the area where the illumination patterns overlap. To determine quantitatively if this assumption is correct, the Doppler sensitivity profile was calculated for systems of one or two fibers terminating on a plane, with blood flowing parallel to the plane. The sensitivity is plotted as a function of distance from the plane containing the fiber tips (figure 7–5) and confirms that the two-fiber system should sense flow at a greater distance than the single-fiber system.

The geometry used in the above analysis can be mimicked by a pair of fibers terminated on the side wall of a catheter some distance from the tip. In this region flow will generally be laminar, and the streamlines tend to follow the catheter. Such an arrangement is likely to be optimal for making repro-

ducible measurements of relative changes in flow velocity of small arteries such as coronaries.

Using separate fibers for illumination and collection of light markedly reduces the amount of light available for detection. Monte-Carlo simulations indicate that the light collected when two 50 μm-core multimode fibers are spaced 0.5 mm apart in blood is decreased by two orders of magnitude from that collected from a single fiber used for illumination and collection. Of course, most of the extra light collected from the single fiber comes from the bright region at its tip, which is in the disturbed flow. This light is not of value for determining the free-stream flow velocity, hence the rationale for using two fibers. But—the question naturally arises—is there sufficient light available from a dual-fiber system to give an adequate signal-to-noise ratio?

SIGNAL-TO-NOISE RATIO IN LDV SYSTEMS

The signal analysis methods that depend on computing an entire spectrum and determining the maximum Doppler frequency are prone to noise for two reasons. First, ascertaining the maximum frequency at which the spectrum becomes less than the noise is obviously an arbitrary and error-prone technique. Second, most analog spectrum analyzers with bandwidths of several MHz are swept analyzers, which examine only a single frequency at a time. The use of such an analyzer to determine the maximum Doppler frequency f_{max} means that only a fraction of the data contributes to the averaging required to diminish the noise in the vicinity of f_{max}.

The algebraic mean Doppler shift $\langle \omega \rangle$ considered above can be computed continuously by analog means, without any loss of data. Using $\langle \omega \rangle$ as a velocity estimator, the signal-to-noise ratio can be calculated analytically. There are two aspects to signal-to-noise ratio (SNR) for an LDV system. The first is the *input* signal-to-noise ratio, which is the ratio of Doppler signal power from the detector to the total noise due to shot noise, amplifier noise, and laser amplitude-modulation noise. The second is the *output* signal-to-noise ratio, which is the SNR of the velocity estimate output by the processor. The output SNR is the performance criterion of the instrument. The output noise has two sources: the input noise and the intrinsically random nature of the Doppler signal from a particle suspension.

The input SNR can be calculated in a straightforward manner from the collected light intensity, the number of modes collected on the detector (the same as the number of modes supported by the fiber, if all the light from the fiber is detected), the degree of amplitude modulation of the source, and the level of amplifier noise. For a heterodyne system, the optimum number of modes to collect is one, in the idealized case where there are no losses of light. However, the maximum is very flat in the case where the laser and amplifier noise are reasonably small, and the use of multimode fibers with detection of hundreds or thousands of modes is practical, as well as being technically simpler and less prone to losses than the collection of a single mode.

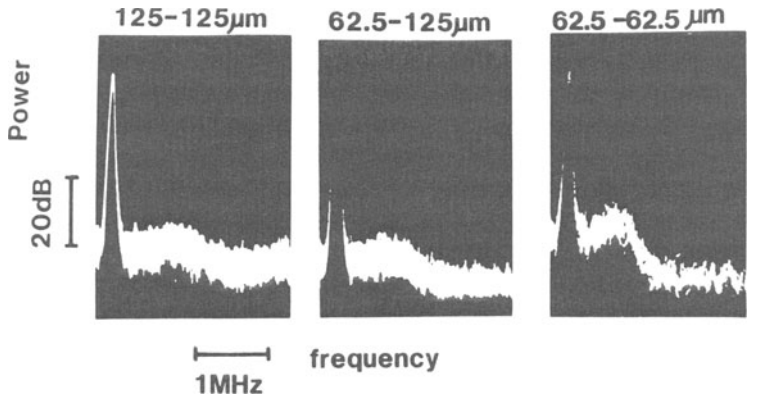

Figure 7–6. Doppler spectra obtained from a dual-fiber heterodyne system for three different fiber spacings, achieved by using pairs of side-by-side fibers of either 125 μm or 62.5 μm outer diameters. The sharp peak at left is the zero Doppler shift point. The broad peaks are the Doppler spectra due to blood flow. (From Kajiya et al. [7], figure 3.)

The output SNR is due both to input noise and to the intrinsic randomness of the signal. It depends on the bandwidth and shape of the signal spectrum, the processing bandwidth of the instrument (which must be wide enough to pass the spectrum for the highest flow velocity), and the input SNR. If the instrument bandwidth, the mean Doppler shift, and the bandwidth of the Doppler signal are comparable (as they are expected to be), then the output SNR is independent of the input noise until the input SNR falls to near unity or below. For practical two-fiber systems, the input SNR will probably be in this low range due to the small amount of light collected. Even so, calculation shows that r.m.s. velocity errors of a few percent should be achievable, in an output bandwidth of 10 Hz, which is quite adequate for clinical applications.

Recently, Kajiya et al. [7] have demonstrated Doppler spectra obtained through dual-fiber systems (figure 7–6). They used pairs of multimode fibers side by side, giving center-to-center distances of 62–125 μm, with a 5 mW helium–neon laser (633 nm) illumination. Only the closest fiber spacing gave "sharply peaked" spectra that were suitable for estimation of flow velocity by peak-tracking. The Doppler shift determined from the peak of the spectrum correlated well with flow velocity in a model uniform flow field (figure 7–7), with only a mild nonlinearity over the range of velocities expected in mid-sized arteries such as coronaries. For greater fiber separations the spectra are broader, as expected from theory. However, they are still well defined and show signal-to-noise ratios compatible with good performance by analog-moment velocity estimation. It is to be expected, therefore, that fiber configurations suitable for use in the stable flow along the sidewall of a catheter can be made to operate effectively, especially by using 800 nm light, which

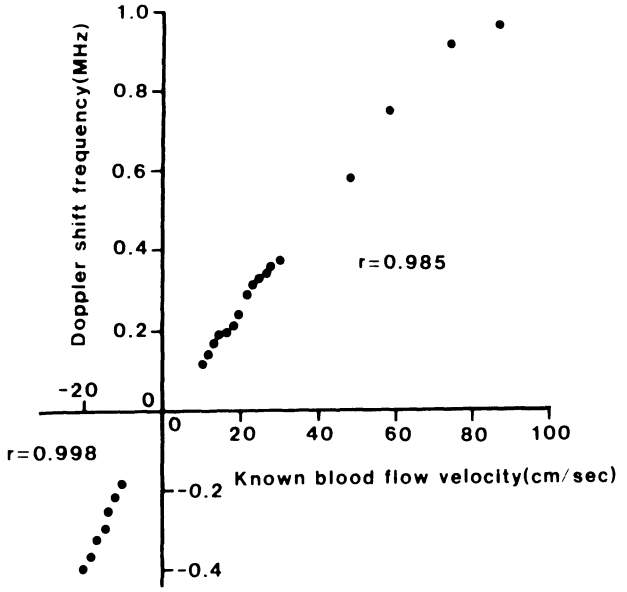

Figure 7–7. Relation between free-stream flow velocity and the Doppler shift frequency at the spectral peak for a dual-fiber system with center-to-center spacing of 62 μm. (From Kajiya et al. [7], figure 5.)

has appreciably better penetration in blood, and is more efficiently detected by solid-state detectors.

The development of such systems is a matter of active research at present. It will make possible the continuous monitoring of blood flow velocity, or at least arterial flow reserve, during the performance of angioplasty. On the basis of present theoretical and experimental evidence, the design criteria for such a catheter-based system might include the following: 1) dual fibers for illumination and collection, respectively; 2) fiber termination along the sidewall of the catheter, some distance from the catheter tip; 3) operation in the neighborhood of 800 nm, using a long coherence-length diode laser producing 20–50 mW of illumination; 4) the greatest possible separation between illumination and collection fibers, as limited by the intensity of collected scattered light; 5) real-time signal processing that makes use of all the information in the scattered spectrum to estimate flow velocity.

REFERENCES

1. Tanaka, T., and G.B. Benedek. 1975. Measurement of the velocity of blood flow (*in vivo*) using a fiber optic catheter and optical mixing spectroscopy. Appl Optics 14:189–196.
2. Kilpatrick, D., T. Linderer, R.E. Sievers, and J.V. Tyberg. 1982. Measurement of coronary sinus blood flow by fiber-optic laser Doppler anemometry. Am J Physiol 242:H1111–H1114.
3. Kilpatrick, D., J.V. Tyberg, and W.W. Parmley. 1982. Blood velocity measurement by fiber optic laser Doppler anemometry. IEEE Trans Biomed Eng 29:142–145.

4. Nishihara, H., J. Koyama, N. Hoki, F. Kajiya, M. Hironaga, and M. Kano. 1982. Optical-fiber laser Doppler velocimeter for high-resolution measurement of pulsatile blood flows. Appl Optics 21:1785–1790.
5. Kajiya, F., G. Tomonaga, K. Tsujioka, Y. Ogasawara, and H. Nishihara. 1985. Evaluation of local blood flow velocity in proximal and distal coronary arteries by laser Doppler method. J Biomed Eng 107:10–14.
6. Stern, M.D. 1985. Laser Doppler velocimetry in blood and multiply scattering fluids: theory. Appl Optics 24:1968–1986.
7. Kajiya, F., O. Hiramatsu, Y. Ogasawara, K. Mito, and K. Tsujioka. 1988. Dual-fiber laser Doppler velocimeter and its application to the measurement of coronary blood velocity. Biorheology 25:227–235.

8. THE CUTANEOUS CIRCULATION

JOHN M. JOHNSON

Laser Doppler flowmetry (LDF) is the latest of a large number of methods designed to study the cutaneous circulation. Theoretical analysis predicts a correspondence of LDF to tissue blood flow, and mechanical/hydraulic models support this prediction (see chapters 2–6). However, because each of these is necessarily idealized with respect to the actual movement of blood in tissue, experimental confirmation is required. This chapter considers the correspondence of LDF with other measures of skin blood flow, the depth of measurement of blood flow in skin by LDF, and examples of uses of LDF that take advantage of its unique attributes.

VALIDATION STUDIES IN SKIN

Verification of the LDF method is a difficult task, because the precise volume of tissue under inspection is unknown and is small relative to other measurement methods. Hence, it has not proved possible to measure tissue perfusion or red blood cell (RBC) flux in an area by LDF and from those same vessels by an independent method. LDF is usually compared with more global measures of tissue blood flow (e.g., flowmeters, microspheres, plethysmography). Even when compared with regionally discrete methods (clearance, videocapillaroscopy), precise conformance to the same volume of tissue is doubtful. Thus, correspondence is as dependent on the degree of parallel behavior among different volumes of the same tissue as it is on the validity of the LDF method per se.

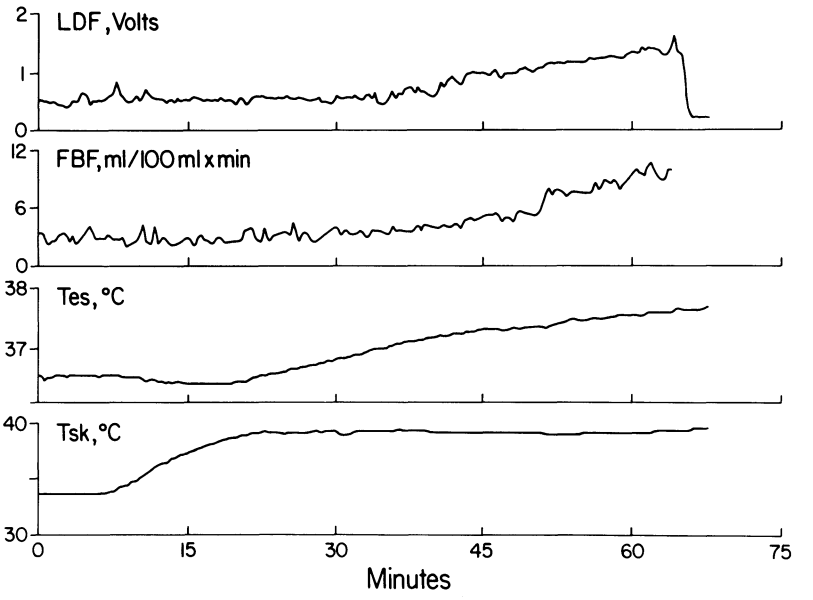

Figure 8–1. Responses in laser-Doppler blood flow (LDF), forearm blood flow (FBF-plethysmography), and esophogeal temperature (T_{es}) to heat stress caused by elevating whole-body skin temperature (T_{sk}). Note the generally parallel response pattern between LDF and FBF. (From [1], by permission.)

PLETHYSMOGRAPHY VERSUS LDF

Venous occlusion plethysmography includes blood flow to both skin and muscle of the forearm. Consequently, changes in forearm muscle blood flow will contribute to the plethysmographic measurement, but not to LDF (see Depth of Measurement below). With this concern in mind, we compared LDF with plethysmographic estimates of skin blood flow using whole-body heat stress to raise skin blood flow [1]. Heating was not applied to the area of blood flow measurement; hence, the increased blood flow was purely of reflex origin. The levels and durations of heating used do not cause any appreciable change in blood flow to resting skeletal muscle, and the increase in forearm blood flow with body heating is directed specifically to the skin [2–4].

Whole-body skin temperature was raised to 38–39°C for one hour. Forearm blood flow and LDF were measured simultaneously throughout. Figure 8–1 illustrates this protocol and the results from one subject. The increase in LDF paralleled that of total forearm blood flow. That these two measures corresponded linearly is illustrated by figure 8–2. Overall, the correlation in a given comparison was excellent, with correlation coefficients ranging between 0.94 and 0.98, averaging 0.96.

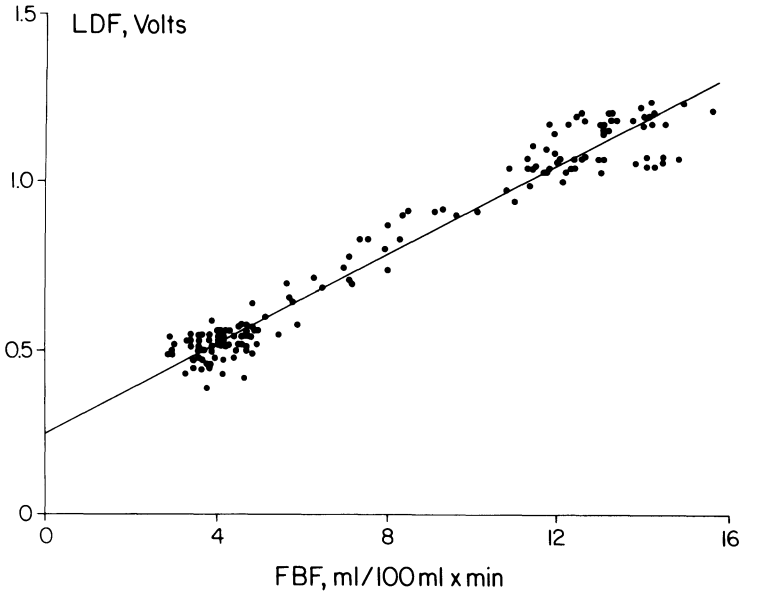

Figure 8–2. Simultaneous values for LDF and FBF during a protocol like that shown in figure 8–1. LDF and FBF were highly correlated during cutaneous vasodilation accompanying heat stress. Note that the extrapolated intercept of the relationship is on the LDF axis, (From [1], by permission.)

Similar findings were made by Saumet et al. [5] in a similar study. Correlation coefficients averaged 0.90, again suggestive of the validity of the LDF method. An important element in the design of these two studies was the examination of the relationship between LDF measured at a single site and total forearm blood flow. Because different small volumes of skin are likely to have different vascularities, basal levels of blood flow, or degrees of response, the relationship between a global measurement of tissue blood flow (plethysmorgraphy) and that from a small region (LDF) may vary as the latter is moved from site to site. That such is the case is illustrated by figure 8–3, in which regressions relating LDF to forearm blood flow during heat stress from five studies are shown along with the correlation coefficient for each individual study [1]. Despite the highly linear relationship between LDF and forearm blood flow in each study, slopes and intercepts of the relationship varied markedly from one study to the next. These also varied when LDF was measured from two sites on the same forearm [7]. In the case of the comparisons illustrated by figure 8–3, the slope relating LDF to forearm blood flow varied from 40 to 122 (averaging 78) mV per unit increase in forearm blood flow [1]. The particular slope will vary with the instrument used, but the three-fold variation in slope should be seen with any instrument [7]. Saumet et al. [5] also noted that the level of LDF at a given

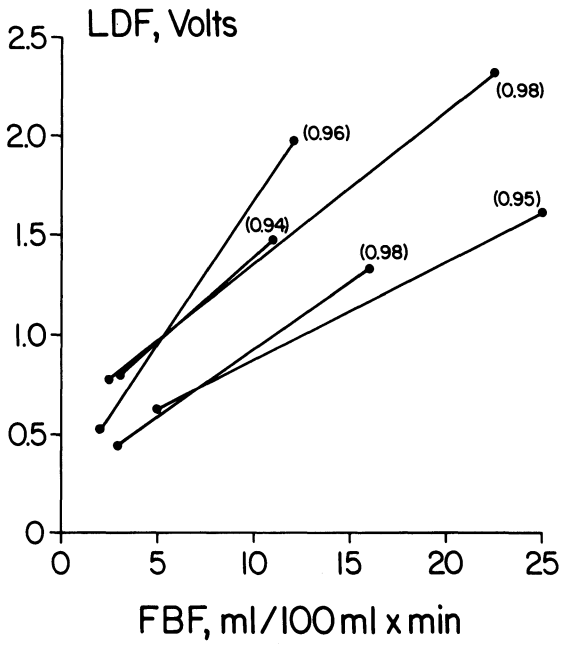

Figure 8–3. LDF–FBF relationship from five separate studies. Lines are drawn over the individual ranges of blood flow. Correlation coefficient for each study is indicated. Although there was a highly linear relationship for each study, slopes and intercepts varied considerably among separate studies. (From [1], by permission.)

level of forearm blood flow varied markedly among studies. Similar marked variability in slope was seen in other tissues and with other standards of measurement [8,9], suggesting that this variability is not unique to skin. The variability is not due to the instrument yielding an inconstant signal for a given blood flow in the field of view of the LDF probe, since the signal proved highly reproducible when obtained with a mechanical model [8] or a calibration standard [10].

Why does such variability exist? The above indicates that there is sufficient heterogeneity in the absolute magnitude of blood flow within the skin that a single small site within that region may have a blood flow well above or well below the average (the latter being indicated by a global measure such as plethysmography). This spatial heterogeneity was first noted by Tenland et al. [10], who obtained widely differing LDF values among six sites on an individual forearm with, presumably, a constant total blood flow. LDF values from individual sites varied from as low as 30% to over twice the average from the six sites. Similar findings were made in our laboratory [1] with roughly the same regional variation, LDF values from individual sites varying from 43% to 248% of the average for a given forearm. Total

forearm blood flow (by plethysmography) was stable. Hence, a major source for the intersubject and intrasubject variability in the forearm blood flow versus LDF relationship [1,5] is the spatial heterogeneity of blood flow within the tissue itself. This heterogeneity extends to the increase in LDF for a given increase in total forearm skin blood flow. It is not clear whether the origin of this variability among different small regions relates more directly to heterogeneity in vasodilator response characteristics of the vessels among regions or to variation in the number of vessels contributing to the LDF measurement, although the likely candidate is the latter of these possibilities [1]. The number of perfused capillaries per mm^2 varies by more than sixfold over the body surface [11] and could account for the variation in the slope of the forearm blood flow versus LDF relationship from site to site [1,5] and the variability in the level of LDF among sites [1,10].

The linear LDF versus forearm blood flow relationship discussed above was not seen by Smolander and Kolari [12]. They found LDF to rise less steeply at higher levels of forearm blood flow. Although differences in protocol and analytical procedures may have contributed to the inconsistency with the studies cited earlier [1,5], a nonlinear relationship may result from saturation of the LDF signal at higher levels of blood flow. Such has been suggested for some instruments when the blood flow exceeded about 45 $ml \cdot min^{-1} \cdot 100g^{-1}$ [13,14], an achievable level for skin blood flow in heat stress. A forearm blood flow of 12 $ml \cdot min^{-1} \cdot 100g^{-1}$ during heat stress is partitioned to skin and muscle by a ratio of about 10:2. Because this value is expressed per 100g of forearm and because skin volume is about 9% of forearm volume [15], the level of blood flow to skin would be over 100 $ml/ml \cdot min^{-1} \cdot 100g^{-1}$ of skin. Also, if the measurement depth of LDF does not include the full thickness of skin, nonparallel increases in blood flow to deep and superficial cutaneous vessels will result in a nonlinear relationship between LDF and forearm blood flow by plethysmography. Such a possibility is raised by Hirata et al. [16] and is discussed in more detail under Depth of Measurement below.

A final comment relates to the intercept of the LDF versus forearm blood flow relationship. In theory, this intercept should occur on the forearm blood flow axis to account for forearm muscle blood flow. However, the intercept is often seen on the LDF axis [1,5]. Why this occurs is not clear, but it presents an analytical difficulty. If a portion of the LDF signal is not related to blood flow, it should be subtracted before assessing fractional changes. With some instruments, a persistent signal during vascular occlusion suggests that a portion of the signal is unrelated to blood flow [1,5,13,17]. Regardless of whether the source is from the tissue or from the instrument itself, caution should be exercised in estimating absolute levels of blood flow or percentage changes from the LDF signal. If the portion of the signal not due to blood flow is of the order of 50%, the fractional change in LDF will be only 50% of the fractional change in skin blood flow.

CLEARANCE VERSUS LDF

Clearance of ^{133}Xe has also been compared with LDF measurements of skin blood flow [18–21]. Stern et al [21] and Holloway and Watkins [19] sampled several LDF values surrounding a depot of ^{133}Xe, and compared the LDF signal to the clearance before and after cutaneous erythema induced by ultraviolet radiation. Averaging LDF from several sites obviates, to some extent, the site-to-site variability identified earlier. These LDF values were from areas of skin adjacent (approximately 7 mm) to the Xe depot, and did not include the hyperemia associated with injection trauma [22]. The correlation between the two methods was especially good in view of the discontinuous comparison and the combination of data from several subjects. The extrapolation of the relationship between tracer washout and LDF gave a positive value on the LDF axis [19,21], again suggesting that a portion of the LDF signal does not arise from tissue blood flow.

As with any such comparison, differences do not necessarily negate the validity of either technique if the methods measure different quantities. For example, ^{133}Xe is cleared by capillary exchange, whereas LDF probably includes blood flow through arteriovenous anastomoses. Engelhart and Kristensen [18] found the maximum reactive hyperemia from the finger to be over seven times control for ^{133}Xe clearance, whereas LDF reached only 1.5 times control. If a major portion of blood flow to the finger in control is through anastomoses that do not participate in reactive hyperemia, such a divergence between clearance and LDF results would be expected. This supposition is supported by the closer agreement between the two techniques during reactive hyperemia in the skin fold between first and second fingers, in which arteriovenous anastomoses may be less abundant. Given this difference within skin, it is hardly surprising that there was a poor correspondence between ^{133}Xe clearance from subcutaneous adipose tissue and LDF from skin [20].

COMPARISON OF LDF WITH THERMAL METHODS

Most of the thermal methods for the measurement of blood flow are based on caloric exchange across the skin. Because temperatures of blood entering and exiting the region of measurement are rarely known and because noncutaneous losses of heat are difficult to quantify, these methods are semiquantitative. Nevertheless, they do generally follow changes in skin blood flow. Saumet et al. [5] compared LDF with thermal clearance during body heating. Thermal clearance was assessed in a slightly different area than the point of application of the LDF probe. The results were similar to their comparison of LDF with plethysmography: consistent linear relationships between thermal clearance and LDF, but slopes and intercepts varying among comparisons. Judging from their results, the variability in the thermal clearance versus LDF relationship was even greater. Enkema et al. [23] compared LDF with the heater power necessary to maintain skin temperature at a selected level

during a variety of procedures, including vascular occlusion, local temperature changes, and environmental temperature changes. The authors found LDF to be the superior of the two methods with respect to both speed of response and being relatively uninfluenced by the thermal environment.

Nitzan et al. [24] compared skin blood flow measured by LDF on one finger with a transient thermal clearance method applied to an adjacent finger. It should be noted that the transient thermal clearance method involves an elevation in temperature by several degrees over several minutes. Because warming the skin has a local vasodilator effect [6,25], the extent to which the act of making the measurement affected the blood flow is unknown. The finger under inspection by the LDF probe was not subjected to the same thermal perturbations. Nevertheless, these two measurements correlated well, with some offset in the LDF values at the extrapolated zero value of blood flow by the transient thermal clearance method.

To summarize the validation studies, comparative studies between LDF and a variety of other methods for measuring tissue blood flow yield good to excellent correlations. Thus the experimental evidence that LDF is a linear measure of skin blood flow is compelling. Analytic difficulties arise from site-to-site variability in the relationship of LDF to other measures of skin blood flow. This variability probably arises from the small amount of tissue sampled by the LDF method, coupled with regional heterogeneity in the number or sensitivity of vessels in any given small volume of skin, and precludes accurate in vivo calibration. With this heterogeneity, accurate calibration in terms of conventional units of blood flow may not be particularly useful, since the absolute level of blood flow of the region of measurement may be unrepresentative of the general level of blood flow. Analytic difficulties also arise from the frequent observation of a positive value for LDF at an extrapolated zero skin blood flow. The origin and, in many studies, the values of the offset are also unknown. A final analytic problem arises from the possibility of a nonlinear relationship at high levels of blood flow. Nevertheless, the pattern of LDF generally faithfully follows that for skin blood flow measured by alternate methods, affording advantages in frequency response, continuity, and tissue specificity unavailable by other means.

DEPTH OF MEASUREMENT

A major advantage of LDF is its proposed specificity to superficial tissues. This specificity is a particular advantage over plethysmography, in which conclusions regarding skin blood flow are dependent on a knowledge of underlying muscle blood flow. Like the theoretical prediction of LDF being a measure of tissue blood flow, the claim of a measurement depth of 0.5–1 mm requires experimental verification.

Only a limited theoretical basis is available for a prediction of depth sensitivity. Although data regarding the penetration of light into skin are

available [26,27], the LDF method relies both on the penetration and the return of light from moving elements within the tissue. Nevertheless, for LDF to be affected by blood flow at a given depth, photons must penetrate to that depth. The primary epidermal pigments tend to have absorption maxima at wavelengths below those used in laser-Doppler flowmeters, e.g., 660–800 nm [26]. Only melanin has significant absorption characteristics above 300 nm, and apparently does reduce the penetration of light through the stratum corneum and epidermis at wavelengths up to 1200 nm. Hence the photoprotection afforded by melanin reduces the penetration of laser light. Hemoglobin gives somewhat different absorption characteristics to the dermis. Again, major absorption peaks appear at wavelengths below 600 nm. In unperfused skin with little melanin, incident light is attenuated to 37% at a depth of 0.55 mm at a wavelength 600 nm and at 1.2 mm at a wavelength of 800 nm [26,27]. However, 37% of the incident light intensity is a significant fraction. Thus, the thicknesses cited above do not define the measurement depth by LDF. Also, melanin and hemoglobin were excluded from the penetration analysis. Those measurements do indicate a slightly greater penetration depth by infrared laser light than by red light. In either case, very little of the incident light penetrated beyond 2 mm. Addition of chromophores could only reduce this value.

Experimental characterization of the depth of measurement by LDF has been approached in several different ways. Nilsson et al. [28] used a polyacetal disc to separate the LDF probe from cells moving within a hydraulic model. They found the sensitivity to become maximal at about 0.6 mm and to fall by about 50% at distances of 0.2 mm and 1.2 mm. A second approach has been to interpose unperfused tissue slices between the LDF probe and the surface of the perfused tissue [21,29–31]. The results have not been uniform. For the rat kidney, Stern et al. [21,31] found unperfused tissue slices of 0.5 mm or 1 mm to eliminate the signal from the underlying renal cortex. Similarly, Kiel et al. [29] found the LDF signal from the canine gastric mucosa to be eliminated by interposition of a layer of unperfused gastric mucosa–submucosa. In the feline intestine, however, Kvietys et al. [30] reduced but did not eliminate the LDF signal with a 3 mm thickness of unperfused jejunum. Whether instrumental differences account for this variability in apparent depth of measurement is unclear [30].

A third approach to definition of the LDF measurement depth has been to change differentially the blood flow to superficial and deeper tissues. For example, Shepherd and Riedel [32] and Kiel et al. [29] found reactive hyperemia usually to be detectable only from the mucosal surface of the canine intestine and stomach, suggesting that the mucosa–submucosa was the site of reactive hyperemia and that the LDF measurement did not include tissues more distant than the thickness of the muscularis layer. Also, isoproterenol was found to vasodilate the canine intestinal mucosa while reducing blood flow to the muscularis, a finding from both microspheres and LDF

[33]. Postprandial hyperemia showed a similar distribution across the bowel wall [34]. Adenosine raised LDF recorded from the serosal surface, but reduced LDF recorded from the mucosal surface in the same preparation [33].

The above studies indicate that in gastrointestinal tissues the LDF method provides a relatively superficial measurement of blood flow. A series of studies by Ahn and colleagues are not in accord with this conclusion [13,14,17] for either the feline or human small intestine or the human colon. They found that LDF had the same correlation to total blood flow whether the probe was placed on the mucosal or serosal surface. Close correlation of LDF values between mucosal and serosal sites suggested that blood flow across the entire bowel wall was monitored. These findings suggest a measurement depth exceeding 6 mm [13].

The conflict noted above and the possibility that the depth of measurement varies among tissues make it necessary to define the depth of measurement for skin. In one approach, local skin temperature in the area of the LDF probe (forearm) was raised to 42°C [35]. This degree of local warming relaxes cutaneous vascular smooth mucle completely [6], with little or no effect on blood flow to underlying skeletal muscle [25]. Vascular occlusion for ten minutes was applied, with the rationale that any reactive hyperemia in LDF would be due to increased subcutaneous (muscle or adipose tissue) blood flow, because the cutaneous vessels were already fully relaxed. Figures 8–4 and 8–5 show LDF and forearm blood flow from that protocol [35]. Unheated skin displayed reactive hyperemia, although to a submaximal level. However, during local heating there was no significant further increase in LDF during the period of reactive hyperemia. The forearm blood flow response indicated a significant vasodilation in underlying skeletal muscle. This muscle hyperemia did not affect the LDF measurement, strongly suggesting that, in skin, LDF does not include blood flow to underlying tissue.

Equally strong evidence for a superficial measurement was provided by a study in which forearm skeletal muscle was preferentially vasodilated by hand exercise [36]. Subjects performed mild hand exercise for three minutes, markedly increasing total forearm blood flow after exercise. As shown in figure 8–6, LDF was unchanged from rest. The increase in the LDF signal during exercise was artifactual, showing the method not to be useful for measuring blood flow to skin over active skeletal muscle. Because the large increase in skeletal muscle blood flow was not detected by the LDF probe, the LDF method is unaffected by blood flow to deeper tissues when applied to skin.

One characteristic of LDF is the variable penetration of laser light into the tissue according to the wavelength [26,27], suggesting that shorter wavelengths might provide measurement from more superficial cutaneous vessels [37,38]. Because the ratio of Doppler shifts of red and blue laser light reflected from skin was not equal (inversely) to the ratio of the wavelengths, Duteil et al. [37] suggested that they were measuring from different regions

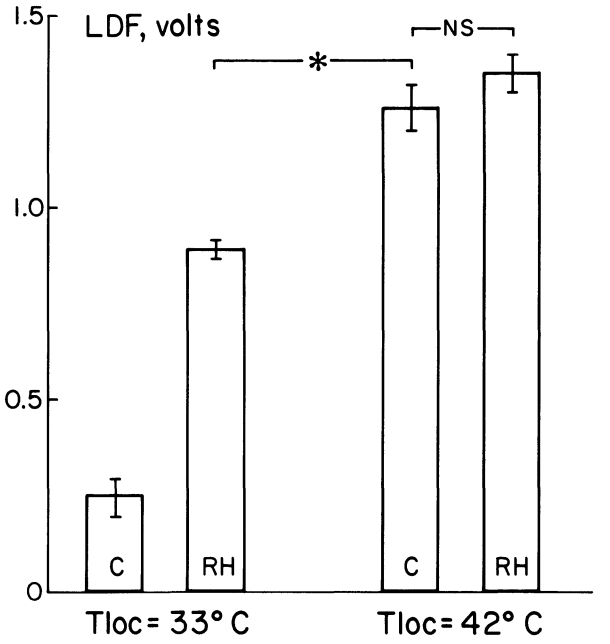

Figure 8–4. LDF responses to reactive hyperemia (RH) at cool (33°C) and warm (42°C) levels of local temperature (T_{loc}). Reactive hyperemia was not detected if the skin was warmed to 42°C. (From [35], by permission.)

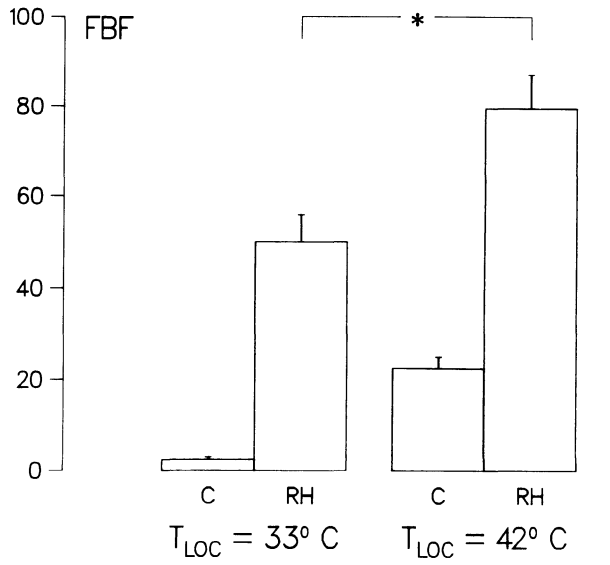

Figure 8–5. Forearm blood flow (FBF) response to reactive hyperemia (RH) at cool and warm local temperatures (T_{loc}). Reactive hyperemia was detected at both arm temperatures. Comparison with figure 8–4 suggests forearm muscle blood flow made no contribution to LDF. (From [35], by permission.)

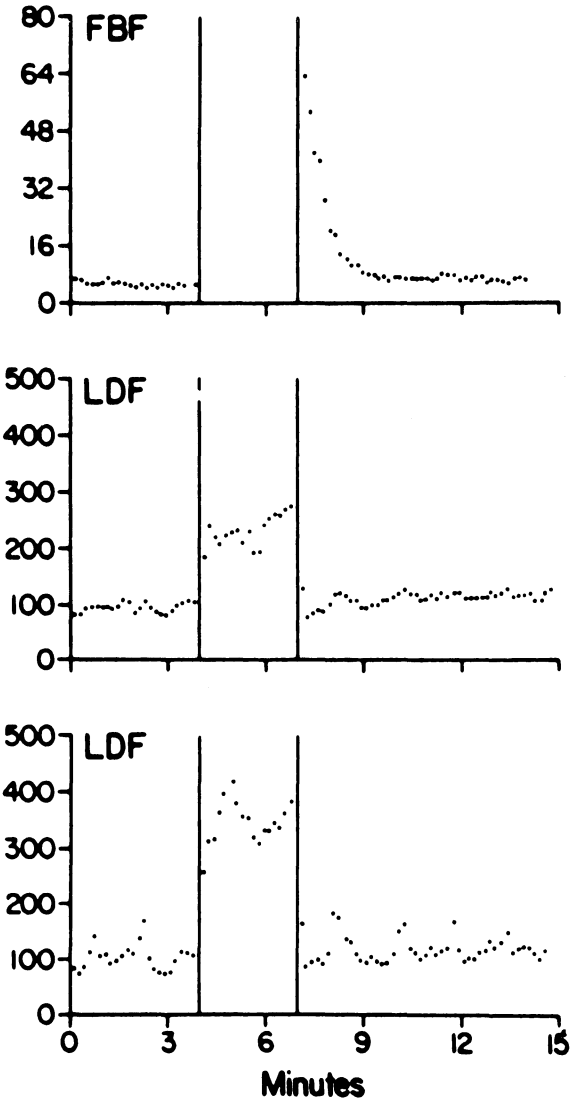

Figure 8–6. Postexercise responses in forearm blood flow (FBF) and in LDF from dorsal (middle panel) and ventral (bottom panel) forearm skin. Mild exercise of forearm muscle was performed from 4 to 7 minutes. Postexercise hyperemia in FBF was not seen in LDF, suggesting no contribution by muscle blood flow to the LDF signal. (From [36], by permission.)

of skin and that the blue light provided a more superficial measurement. Differential effects of intradermal injections of vasoconstrictors supported this suggestion. Similarly, Obeid et al. [38] found the ratios of the mean frequency shifts among three different wavelengths to differ from that which would occur if the same quantities were being measured. This difference was most pronounced for the green–red and green–infrared ratios, suggesting that LDF measurements with green laser light (543 nm) were limited to the upper papillary plexus, whereas deeper dermal blood flow contributed to the red (632.8 nm) and infrared (780 nm) Doppler shifts [38]. The results for the red and infrared were consistent with equal measuring volumes. Most commercially available LDF units use red or infrared light. This approach may prove useful in distinguishing the locus of effects of topical drugs or in characterizing the control of subsections in the cutaneous vasculature.

The separation between transmitting and receiving fibers has also been used in an effort to provide depth discrimination in LDF measurements [16,39]. As the distance between the fibers is increased, the total intensity of the received light decreases and the relative contribution to the received light shifts toward the deeper tissues [39]. Hence, at small fiber separations the detected Doppler shift may be dominated by blood flow in the superficial papillary loops, whereas at greater separations the contribution by blood flow in deeper plexuses may dominate the Doppler shift. Gush et al. [39] found little effect on LDF from the finger as the distance between fibers was increased from 0.8 mm to 2.45 mm. Between 2.45 mm and 3.65 mm, however, there was a sudden increase in the signal, with little further change as the separation was increased to 4.6 mm. This shift was more pronounced for shorter wavelengths. These data suggested that the wider separations (>3 mm) provided a large contribution from deeper dermal structures, whereas at the narrower separations (<2 mm), LDF was dominated by lower-velocity papillary blood flow.

These data suggest that different fiber separations allow different depths of the cutaneous microcirculation to be inspected. Hirata et al. [16] recorded the LDF signal from the finger with fiber separations of 0.3 mm and 0.7 mm, both smaller than the lowest value evaluated by Gush et al. [39]. Hirata et al. [16] found local warming (from 25°C to 35°C) to cause a marked increase in LDF at the narrower (0.3 mm) fiber separation, but only a small increase in LDF at the wider (0.7 mm) separation or in total finger blood flow. The authors reasoned that local warming increased superficial capillary blood flow, but not blood flow through arteriovenous anastomoses [40,41]. It is not clear why a 0.7 mm fiber separation provided a major contribution from deeper cutaneous vessels (anastomoses) in one study [16], but in the other, even wider separations (0.8–2 mm) did not [39]. The ability to sample from different portions of the cutaneous microcirculation would be a major advantage but, until wavelengths and fiber separations are unambiguously defined, such use of LDF will remain speculative.

It currently appears that the red and infrared wavelengths, coupled with fiber separations of about 1 mm, sample most of the thickness of skin without a contribution from underlying muscle. This configuration may miss some of the most superficial blood flow, however. This possibility is raised by the failure of LDF to change when the skin was visibly blanched by topical corticosteroids [42]. Similarly, mild iontophoretic application of norepinephrine to skin caused blanching, but often did not cause a reduction in LDF (D.L. Kellogg and J.M. Johnson, unpublished observations), suggesting in both cases that LDF does not include the most superficial vessels. In keeping with this suggestion, Duteil et al. [37] noted that topical corticosteroid gave a detectable reduction in LDF when blue laser light was used.

CURRENT USES OF LDF IN THE CUTANEOUS CIRCULATION

The major purpose of this chapter is to analyze the utility of LDF as a measurement of skin blood flow and to examine critically the advantages, disadvantages, and uncertain elements inherent in the method. Hence, only a brief and admittedly incomplete listing of current uses will be considered. For the most part, these examples were chosen to underscore the particular advantages of LDF over other techniques.

An obvious advantage of LDF is the ability to measure blood flow in regions other than the limbs. Although ^{133}Xe clearance shares that advantage, the prospect of making 20 or more measurements over the body surface is far more appealing with LDF. Tur et al. [43] recorded LDF from 52 distinct sites and ranked the sites according to the average basal perfusion. Facial sites and finger skin were found to have markedly higher blood flows than the torso, arms, or legs. Comparison of vasomotor responsiveness among various skin locations was addressed by Nilsson et al. [44] who measured LDF responses to thermal stimuli in thigh, palm, and finger skin. The latter two sites showed greater absolute levels but lower fractional responses to these stimuli.

A second advantage of LDF is its frequency response. Not only can LDF be used to examine variations in blood flow through the cardiac cycle, but also, on a somewhat longer time scale, slower rhythms can be observed [10,45–49]. These rhythms, around 5–10 per minute typically, are not obviously linked to respiratory or cardiac rhythms, and are not dependent on autonomic nerve activity, but can be abolished by anesthetic cream applied to the site of measurement [46]. These oscillations in LDF are prominent following vascular occlusion or the application of a chemical irritant to the skin [47–49].

The ability to measure, directly, reactive hyperemia in the skin has proved a productive advantage of the specificity to skin and the wide frequency response of LDF [50]. We found forearm cutaneous resistance vessels were not fully relaxed by ten minutes of occlusion, whereas a local warming to 42°C produced maximal vasodilation [35]. Reactive hyperemia of the toes of subjects suffering from intermittent claudication and of the foot of hyperten-

sive subjects [51,52] showed the vasodilator capacity of those patient groups to be limited relative to healthy controls. Local warming (40°C for five minutes) was also found to cause less vasodilation in primary or secondary Raynaud's phenomenon than in healthy individuals [53]. Since this level and duration of local heating is a submaximal vasodilator stimulus [6,35], the extent to which structural vascular changes are the cause of the abnormally low levels of blood flow remains open.

Hassan and Tooke [54] evaluated the role of local temperature in the cutaneous vasoconstrictor response of the toe when lowered below the heart level. At high local temperatures (>38°C), the response was reversed or abolished. Responses to local stimuli were also seen with LDF by Holloway [22], who measured the cutaneous vascular response to injection trauma. The approximately sevenfold increase in blood flow associated with needle insertion calls into question measurements of skin blood flow provided by the clearance of locally injected tracers.

Cutaneous vascular responses to drugs can be evaluated by LDF with respect to their local effects. For example, minoxidil, a current treatment for hair regrowth on the balding scalp, was found to raise skin blood flow by 2–3 times in the area of application [55] (see chapter 9).

LDF has also been used to study reflex control of blood flow to skin. Documentation of the reflex cutaneous vascular responses to simulated orthostasis, although possible by other methods [25,56,57], was greatly facilitated by the ease of application and specificity of LDF [58]. This use of LDF enables the specific examination of skin blood flow, whereas plethysmography requires having an adequate knowledge of blood flow to muscle. A similar advantage has been used to study the reflex cutaneous vascular responses to dynamic muscular exercise [59]. The ability to measure skin blood flow directly and repeatedly by LDF enabled the conclusion to be drawn that exercise affects the level of internal temperature at which cutaneous vasodilation is initiated. Examination of reflex cutaneous vascular responses to isometric exercise, through the use of LDF, showed that skin blood flow follows a passive course, increasing by the same proportion as arterial pressure [7].

Two new uses of LDF promise a further extension of the method in the exploration of the cutaneous circulation. One use is to enlarge the volume of skin from which LDF measurements are made [60]. A problem with the current use of LDF is the small tissue volume inspected and the regional heterogeneity of skin blood flow [1]. Such heterogeneity denies the use of LDF from a single site to evaluate the general level of skin blood flow, even within a relatively circumscribed area [1,10]. This limitation makes longitudinal studies problematic and denies the utility of an accurate calibration, unless blood flow to a mm^3 of tissue, rather than global levels, is of interest. An approach to this problem was taken by Salerud and Nilsson [60]. By conducting the laser light to the skin through seven separate fibers and

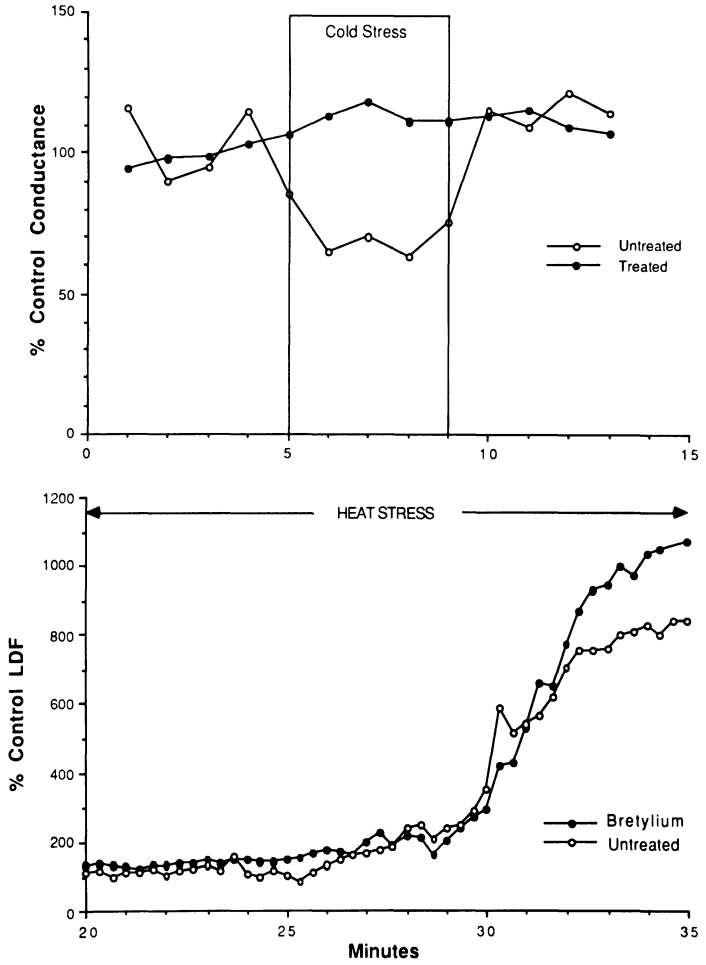

Figure 8–7. Effect of iontophoretic application of bretylium tosylate to a small area of skin on response to whole-body cold stress (upper panel) and to rising internal temperature with exercise (24–35 minutes, lower panel). Bretylium-treated site (closed circles) did not vasoconstrict with cold stress, but showed normal vasodilation with increased body temperature, indicating selective blockade of adrenergic vasoconstrictor nerves but not vasodilator nerves. Laser-Doppler skin blood flow (LDF) was recorded from two adjacent sites on the forearm. (Kellogg, D.L. and J.M. Johnson, unpublished findings.)

returning the reflected light independently from each site, a sevenfold increase in the measuring volume and a significant reduction in the average intrasubject coefficient of variation were achieved. Approaches of this sort should facilitate the quantitative use of LDF in cross-sectional and longitudinal studies.

Another intriguing and relatively new use of LDF includes the ion-

tophoresis of specific agents into a small area of skin [61]. Lindblad and Ekenvall [62], through iontophoretic application of selective alpha adrenergic agonists and antogonists, found both alpha-1 and alpha-2 postjunctional adrenoceptors in skin of the finger. That approach was used to compare alpha-receptor subtype populations between healthy subjects and patients with hypersensitivity to cold [63]. We have recently used the local iontophoresis of bretylium to block the sympathetic vasoconstrictor system, while leaving the sympathetic active vasodilator system [3,15] intact. Figure 8–7 shows that the reflex vasoconstrictor response to cold stress was blocked in sites pretreated by bretylium iontophoresis. Vasodilator responses to subsequent heat stress were not affected (D.L. Kellogg and J.M. Johnson, unpublished results). This combination of iontophoresis of specific agents and LDF is a potentially powerful tool for exploring mechanisms of vasomotor control in the cutaneous circulation.

CONCLUSIONS

The rapidly expanding use of LDF as a method for studying blood flow to skin and other tissues is an indication of the growing acceptance of the technique. Experimental studies generally confirm the theoretical prediction of a linear relationship between LDF and blood flow. The depth of LDF measurement in skin is shallow enough to support the claim of specificity to superficial tissues, giving the technique an advantage over many other methods. The continuous record, relatively broad frequency response, benign effects on the underlying vasculature, and ease of application give a collection of advantages to LDF that is unique. A problem is that the small volume of tissue under the probe may have an absolute level of blood flow well above or below the average. New probe designs are likely to minimize this problem. Further, the use of LDF as a measure of relative responses in skin appears to be valid. The most appropriate use of LDF at this time would appear to be as a continuous measurement from a single site. Recognition of the limitations and appropriate uses of the method coupled with advancements in instrumental design and further elucidation of the depths and volumes of measurement should enhance the use of LDF as an experimental and clinical tool.

REFERENCES

1. Johnson, J.M., W.F. Taylor, A.P. Shepherd, and M.K. Park. 1984. Laser-Doppler measurement of skin blood flow: comparison with plethysmography. J Appl Physiol 56:798–803.
2. Detry, J.-M.R., G.L. Brengelmann, L.B. Rowell, and C. Wyss. 1972. Skin and muscle components of forearm blood flow in directly heated resting man. J Appl Physiol 32:506–511.
3. Roddie, I.C. 1983. Circulation to skin and adipose tissue. In Handbook of Physiology. The cardiovascular system, Shepherd, J.T., Abboud, F.M., eds. section 2, vol. III, part 1. Bethesda, MD: American Physiological Society, pp 285–318.
4. Roddie, I.C., J.T. Shepherd, and R.F. Whelan. 1956. Evidence from venous oxygen

saturation measurements that the increase in forearm blood flow during body heating is confined to the skin. J Physiol (Lond) 134:444–450.
5. Saumet, J.L., A. Dittmar, and G. Leftheriotis. 1986. Non-invasive measurement of skin blood flow: comparison between plethysmography, laser-Doppler flowmeter and heat thermal clearance method. Int J Mircrocirc Clin Exp 5:73–83.
6. Taylor, W.F., J.M. Johnson, D. O'Leary, and M.K. Park. 1984. Effects of high local temperature on reflex cutaneous vasodilation. J Appl Physiol 57:191–196.
7. Taylor, W.F., J.M. Johnson, W.A. Kosiba, and C.M. Kwan. Cutaneous vascular responses to isometric handgrip exercise. J Appl Physiol, in press.
8. Shepherd, A.P., G.L. Riedel, J.W. Kiel, D.J. Haumschild, and L.C. Maxwell. 1987. Evaluation of an infrared laser-Doppler blood flowmeter. Am J Physiol 252 (Gastrointest Liver Physiol 15):G832–G839.
9. Smits, G.J., R.J. Roman, and J.H. Lombard. 1986. Evaluation of laser-Doppler flowmetry as a measure of tissue blood flow. J Appl Physiol 61:666–672.
10. Tenland, T., L.G. Salerud, G.E. Nilsson, and P.Å. Öberg. 1983. Spatial and temporal variations in human skin blood flow. Int J Microcirc Clin Exp 2:81–90.
11. Landis, E.M. 1938. The capillaries of the skin; a review. J Invest Dermatol 1:295–308.
12. Smolander, J., and P. Kolari. 1985. Laser-Doppler and plethysmographic skin blood flow during exercise and during acute heat stress in the sauna. Eur J Appl Physiol 54:371–377.
13. Ahn, H., J. Lindhagen, and O. Lundgren. 1986. Measurement of colonic blood flow by laser-Doppler flowmetry. Scand J Gastroenterol 21:871–880.
14. Ahn, H., J. Lindhagen, G.E. Nilsson, P.Å. Öberg, and O. Lundgren. 1986. Assessment of blood flow in the small intestine with laser-Doppler flowmetry. Scand J Gastroenterol 21:863–870.
15. Greenfield, A.D.M. 1963. The circulation through the skin. In Handbook of Physiology Circulation. Washington, DC: American Physiological Society, vol II, Sect 2, pp 1325–1351.
16. Hirata, K., T. Nagasaka, and Y. Noda. 1988. Partitional measurement of capillary and arteriovenous anastomotic blood flow in the human finger by laser-Doppler flowmeter. Eur J Appl Physiol 57:616–621.
17. Ahn, H., J. Lindhagen, G.E. Nilsson, E.G. Salerud, M. Jodal, and O. Lundgren. 1985. Evaluation of laser-Doppler flowmetry in the assessment of intestinal blood flow in cat. Gastroenterology 88:951–957.
18. Engelhart, M., and J.K. Kristensen. 1983. Evaluation of cutaneous blood flow responses by ^{133}Xenon washout and a laser-Doppler flowmeter. J Invest Dermatol 80:12–15.
19. Holloway, G.A. Jr., and D.W. Watkins. 1977. Laser-Doppler measurement of cutaneous blood flow. J Invest Dermatol 69:306–309.
20. Kastrup, J., J. Bülow, and N.A. Lassen. 1987. A comparison between ^{133}Xenon washout technique and laser-Doppler flowmetry in the measurement of local vasoconstrictor effects on the microcirculation in subcutaneous tissue and skin. Clin Physiol 7:403–409.
21. Stern, M.D., D.L. Lappe, P.D. Bowen, J.E. Chimosky, G.A. Holloway, Jr., H.R. Keiser, and R.L. Bowman. 1977. Continuous measurement of tissue blood flow by laser-Doppler spectroscopy. Am J Physiol 232 (Heart Circ Physiol 1):H441–H448.
22. Holloway, G.A., Jr. 1980. Cutaneous blood flow responses to injection trauma measured by laser-Doppler velocimetry. J Invest Dermatol 74:1–4.
23. Enkema, L., G.A. Holloway, Jr., D.W. Piraino, D. Harry, G.L. Zick, and M.A. Kenny. 1981. Laser-Doppler velocimetry vs heater power as indicators of skin perfusion during transcutaneous O_2 monitoring. Clin Chem 27:391–396.
24. Nitzan, M., S.L.E. Fairs, and V.C. Roberts. 1988. Simultaneous measurement of skin blood flow by the transient thermal clearance method and laser-Doppler flowmetry. Med Biol Eng Comput 26:407–410.
25. Johnson, J.M., G.L. Brengelmann, and L.B. Rowell. 1976. Interactions between local and reflex influences on human forearm skin blood flow. J Appl Physiol 41:826–831.
26. Anderson, R.R., and J.A. Parrish. 1981. The optics of human skin. J Invest Dermatol 77:13–19.
27. Kolari, P.J. 1985. Penetration of unfocused laser light into the skin. Arch Dermatol Res 277:342–344.

28. Nilsson, G.E., T. Tenland, and P.Å. Öberg. 1980. Evaluation of a laser-Doppler flowmeter for measurement of tissue blood flow. IEEE Trans Biomed Eng BME-27:597–604.
29. Kiel, J.W., G.L. Riedel, G.R. DiResta, and A.P. Shepherd. 1985. Gastric mucosal blood flow measured by laser-Doppler velocimetry. Am J Physiol 249 (Gastrointest Liver Physiol 12):6539–6545.
30. Kvietys, P.R., A.P. Shepherd, and D.N. Granger. 1985. Laser-Doppler, H_2 clearance and microsphere estimates of mucosal blood flow. Am J Physiol 249 (Gastrointest Liver Physiol 12):G221–G227.
31. Stern, M.D., P.D. Bowen, R. Parma, R.W. Osgood, R. Bowman, and J.H. Stein. 1979. Measurement of renal cortical and medullary blood flow by laser-Doppler spectroscopy in the rat. Am J Physiol 236 (Renal Fluid Electrol Physiol 5):F80–F87.
32. Shepherd, A.P., and G.L. Riedel. 1984. Differences in reactive hyperemia between the intestinal mucosa and muscularis. Am J Physiol 247 (Gastrointest Liver Physiol 10):G617–G622.
33. Shepherd, A.P., G.L. Riedel, L.C. Maxwell and J.W. Kiel. 1984. Selective vasodilators redistribute intestinal blood flow and depress oxygen uptake. Am J Physiol 247 (Gastrointest Liver Physiol 10):G337–G384.
34. Shepherd, A.P., and G.L. Riedel. 1984. Laser-Doppler blood flowmetry of intestinal mucosal hyperemia induced by glucose and bile. Am J Physiol 248 (Gastrointest Liver Physiol 11):G393–G397.
35. Johnson, J.M., D.S. O'Leary, W.F. Taylor, and W. Kosiba. 1986. Effect of local warming on forearm reactive hyperemia. Clin Physiol 6:337–346.
36. Saumet, J.L., D.L. Kellogg, Jr., W.F. Taylor, and J.M. Johnson. 1988. Cutaneous laser-Doppler flowmetry: Influence of underlying muscle blood flow. J Appl Physiol 65:478–481.
37. Duteil, L., J.C. Bernengo, and W. Schalla. 1985. A double wavelength laser-Doppler system to investigate skin microcirculation. IEEE Trans Biomed Eng 1 BME-32:439–447.
38. Obeid, A.N., D.M. Boggett, N.J. Barnett, G. Dougherty, and P. Rolfe. 1988. Depth discrimination in laser-Doppler skin blood flow measurement using different lasers. Med Biol Eng Comput 26:415–419.
39. Gush, R.J., T.A. King, and M.I.V. Jayson. 1984. Aspects of laser light scattering from skin tissue with application to laser-Doppler blood flow measurement. Phys Med Biol 29:1463–1476.
40. Hales, J.R.S., A.A. Fawcett, J.W. Bennett, and A.D. Needham. 1978. Thermal control of blood flow through capillaries and arterio-venous anastomoses in skin of sheep. Pflug Arch 378:55–63.
41. Hales, J.R.S., C. Jessen, A.A. Fawcett and R.B. King. 1985. Skin AVA dilatation and constriction induced by local skin heating. Pflug Arch 404:203–207.
42. Amantea, M., E. Tur, H.I. Maibach, and R.H. Guy. 1983. Preliminary skin blood flow measurements appear unsuccessful for assessing topical corticosteroid effect. Arch Dermatol Res 275:419–420.
43. Tur, E., M. Tur, H.I. Maibach, and R.H. Guy. 1983. Basal perfusion of the cutaneous microcirculation: measurements as a function of anatomic position. J Invest Dermatol 81:442–446.
44. Nilsson, A.L., L.E. Eriksson, and G.E. Nilsson. 1986. Effects of local convective cooling and rewarming on skin blood flow. Int J Microcirc Clin Exp 5:11–25.
45. Engelhart, M., and J.K. Kristensen. 1986. Raynaud's phenomenon: blood supply to fingers during indirect cooling, evaluated by laser-Doppler flowmetry. Clin Physiol 6:481–488.
46. Salerud, E.G., T. Tenland, G.E. Nilsson, and P.Å. Öberg. 1983. Rhythmical variations in human skin blood flow. Int J Microcirc Clin Exp 2:91–102.
47. Wilkin, J.K. 1986. Periodic cutaneous blood flow during postocclusive reactive hyperemia. Am J Physiol 250 (Heart Circ Physiol 19):H765–H768.
48. Wilkin, J.K. 1987. Cutaneous reactive hyperemia: Viscoelasticity determines response. J Invest Dermatol 89:197–200.
49. Wilkin, J.K. 1988. Periodic cutaneous blood flow during aldehyde-provoked hyperemia. Microvasc Res 35:287–294.
50. Ninet, J., and A. Fronek. 1985. Cutaneous postocclusive reactive hyperemia monitored by laser-Doppler flux metering and skin temperature. Microvasc Res 30:125–132.
51. Del Guerico, R., G. Leonardo, and M.R. Arpaia. 1986. Evaluation of postischemic

hyperemia on the skin using laser-Doppler velocimetry: Study on patients with Claudicatio Intermittens. Microvasc Res 32:289–299.
52. Orlandi, C., M. Rossi, and G. Finardi. 1988. Evaluation of the dilator capacity of skin blood vessels of hypertensive patients by laser-Doppler flowmetry. Microvasc Res 35:21–26.
53. Wollersheim, H., J. Reyenga, and T. Thien. 1988. Laser-Doppler velocimetry of fingertips during heat provocation in normals and in patients with Raynaud's phenomenon. Scand J Clin Lab Invest 48:91–95.
54. Hassan, A.A.K., and J.E. Tooke. 1988. Effect of changes in local skin temperature on postural vasoconstriction in man. Clin Sci 74:201–206.
55. Wester, R.C., H.I. Maibach, R.H. Guy, and E. Novak. 1984. Minoxidil stimulates cutaneous blood flow in human balding scalps: Pharmacodynamics measured by laser Doppler velocimetry and photopulse plethysmography. J Invest Dermatol 82:515–517.
56. Beiser, G.D., R. Zelis, S.E. Epstein, D.T. Mason, and E. Braunwald. 1970. The role of skin and muscle resistance vessels in reflexes mediated by the baroreceptor system. J Clin Invest 49:225–231.
57. Rowell, L.B., C.R. Wyss, and G.L. Brengelmann. 1973. Sustained human skin and muscle vasoconstriction with reduced baroreceptor activity. J Appl Physiol 34:639–643.
58. Tripathi, A., and E.R. Nadel. 1986. Forearm skin and muscle vasoconstriction during lower body negative pressure. J Appl Physiol 60:1535–1541.
59. Taylor, W.F., J.M. Johnson, W.A. Kosiba, and C.M. Kwan. 1988. Graded cutaneous vascular responses to dynamic leg exercise. J Appl Physiol 64:1803–1809.
60. Salerud, E.G., and G.E. Nilsson. 1986. Integrating probe for tissue laser-Doppler flowmeters. Med Biol Eng Comput 24:415–419.
61. Lindblad, L.E., L. Ekenvall, K. Ancker, H. Rohman, and P.Å. Öberg. 1986. Laser-Doppler flowmeter assessment of iontophoretically applied norepinephrine on human finger skin circulation. J Invest Dermatol 87:634–636.
62. Lindblad, L.E., and L. Ekenvall. 1986. Alpha-adrenoceptors in the vessels of human finger skin. Acta Physiol Scand 128:219–222.
63. Ekenvall, L., and L.E. Lindblad. 1986. Is vibration white finger a primary sympathetic nerve injury? Br J Ind Med 43:702–706.

9. SKIN PHARMACOLOGY AND DERMATOLOGY

ANDREAS J. BIRCHER, RICHARD H. GUY, and HOWARD I. MAIBACH

Laser Doppler flowmetry (LDF) has many uses in pharmacologic dermatology. The topics covered in this chapter include cutaneous pharmacology and pharmacodynamics of vasoactive compounds, determination of transcutaneous drug penetration kinetics, and evaluation of the potency of penetration enhancers. Ultraviolet erythema, the effects of inflammatory mediators, irritation from chemical compounds, and patch-test allergens have been studied. Newer applications are the objective measurement of skin lesions, the control of dermatologic therapy, and comparison of the reactivity of the cutaneous microcirculation in different age and ethnic groups. This chapter presents our experience with LDF in the dermatologic and pharmacological investigations and reviews related publications.

CUTANEOUS PHARMACOLOGY

Absorption and elimination

Nicotinic acid and its derivatives have been used to study the reactivity of the microcirculation in normal and diseased human skin [1,2]. These chemicals have served as model substances for the investigation of percutaneous absorption. For example, nicotinic acid and its esters were administered topically and intradermally in humans and the erythematous reaction scored visually [3]. Similarly, vehicle- and temperature-dependent rates of absorption and the duration of action and concentration-dependent intensity of the erythematous reaction were also examined [4]. Further in vivo experiments,

using methyl nicotinate (MN) coupled with sophisticated theoretical interpretation, allowed important deductions about the route and kinetics of percutaneous absorption [5,6].

The mechanism of vasodilative action of nicotinic acid derivatives was studied in the hamster cheek pouch. From the characteristics of the response, a direct drug action on vascular smooth muscle cells and mediation by local nerve conduction was suggested [7]. In a study of the radial spread of erythema following topical MN application in man, the rate of expansion could not be explained by simple diffusion but more likely by transport in the capillaries [8]. Subsequent analysis of this phenomenon [9] indicated that radial diffusion was facilitated in the cutaneous capillary network, thereby indicating rapid uptake, equilibration, and transport of MN. However, there is also evidence for involvement of a second messenger substance. Facial flushing (assessed by skin temperature changes) induced by oral nicotinic acid can be reduced by pretreatment with oral indomethacin [10] and aspirin [11]. As figure 9–1 shows, the cutaneous vascular response (assessed by LDF) to topical application of several MN concentrations was substantially suppressed by oral prostaglandin synthetase inhibitors, but not by histamine antagonists or placebo [12]. This observation was recently confirmed; the erythematous reaction to topical MN, and to other agents inducing irritant contact urticaria, was suppressed by acetylsalicylic acid but not by terfenadine [13,14]. These findings imply that prostaglandins are involved, at least in part, in nicotinate-induced vasodilation.

Photoplethysmography (PPG) and, more recently, LDF have been employed to study the pharmacodynamic effects of vasodilating agents on the cutaneous microcirculation. Thus, local kinetics of skin absorption and elimination have been deduced [15]. Initial studies (table 9–1) compared instrumental and visual determinations of vasodilation and established parameters to characterize dose–response relationships [16]. The pharmacokinetics of percutaneous absorption were investigated by following the cutaneous blood flow (CBF) response to increasing topical doses of aqueous solutions of MN. With increasing concentration, the microcirculatory response was saturable; the duration of the effect, rather than the peak response, was enlarged (figure 9–2). A model of MN transcutaneous kinetics and pharmacodynamics was established, and the data appeared compatible with first-order absorption and elimination and with a saturable interaction of MN with its putative receptor [17].

Although basal perfusion values measured by LDF show considerable spatial variation [18,19], the relative change from basal cutaneous perfusion following application of 1M MN (determined by PPG) was not statistically different for five body sites [20]. This finding agrees with an LDF study, which showed no local difference in CBF changes, stimulated by three concentrations of hexyl nicotinate, at arm and buttock sites [21]. In another PPG investigation, the spatial variability of CBF on the forearm was ex-

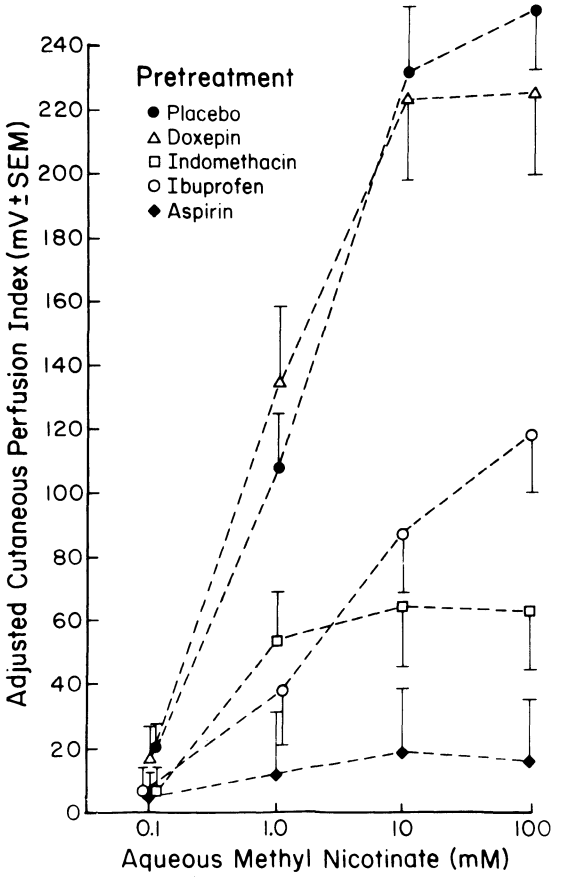

Figure 9–1. The response of the skin microvasculature to different methyl nicotinate concentrations after oral pretreatment with placebo, doxepin, and prostaglandin synthesis inhibitors. Significant inhibition of vasodilation after aspirin, ibuprofen, and indomethacin pretreatment is observed. (Reprinted with permission from [12].)

Table 9–1 Summary of erythema (visual score) and blood flow results (LDF*, PPG**)

Methyl nicotinate concentration (mM)	Onset of LDF response (sec)	Onset of PPG response (sec)	Onset of erythema (sec)
Subject 1			
150	120	125	125
15	160	180	165
1.5	250	270	260
Subject 2			
150	135	150	180
15	300	325	370
1.5	615	635	645

* Laser-Doppler flowmetry.
** Photopulse plethysmography.
(Reprinted with permission from [16].)

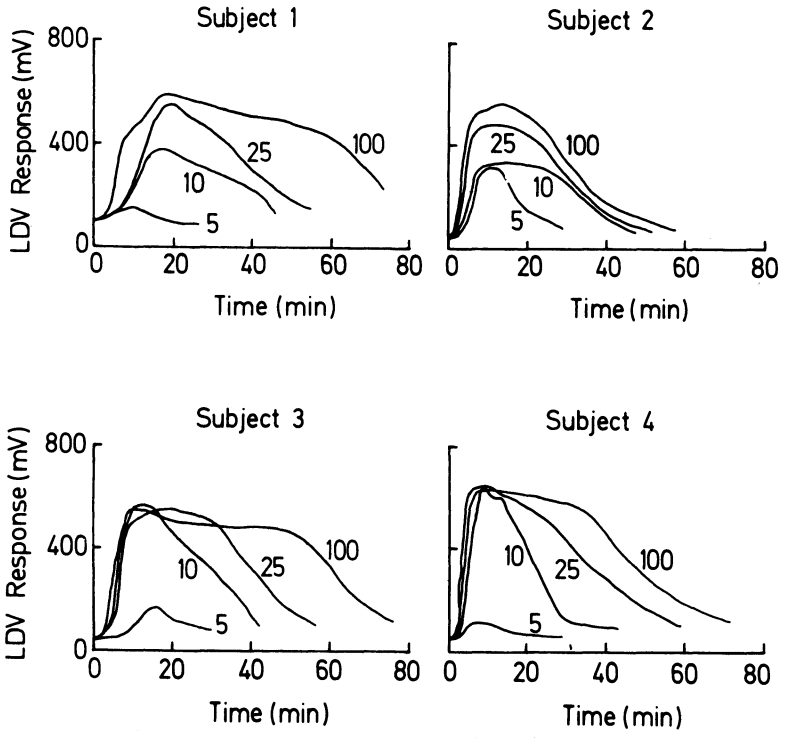

Figure 9–2. CBF response to topical application of four concentrations (in mM) of methyl nicotinate. For concentrations >25 mM, the response was saturable, i.e., further increases in concentration did not increase the maximum response, but instead prolonged the duration (Reprinted with permission from [17].)

amined [22]. There was no difference between left and right and medial and lateral test sites. Vasodilatatory responses in proximal sites, however, were significantly higher than in distal locations. The important issue of spatial and temporal variability of baseline CBF, and the reproducibility of stimuli measured by LDF, has been further addressed. On a given day, highly reproducible results were obtained for several stimuli (inspiration, Valsalva maneuver, venous and arterial occlusion, head-up tilt, and cold pressor test). The authors concluded that, at least for short-term investigations of drugs affecting CBF, LDF is a suitable monitoring method [23]. Similar results were obtained in a recent study [24]. Baseline CBF in forearm skin was determined in healthy volunteers to evaluate temporal, spatial, and individual differences. No significant difference was found between bilateral sites, or between measurements taken in the morning and afternoon. LDF values between medial and lateral sites were different at a borderline significant level ($p = 0.049$). However, CBF values were clearly higher in males than in

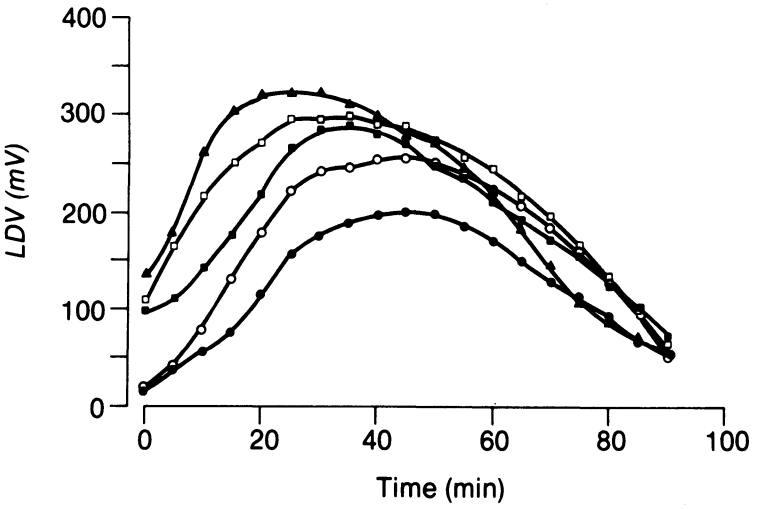

Figure 9–3. CBF response to 10 mM hexyl nicotinate after five different pretreatments: (●) control, (○) occlusion, (■) occlusion plus vehicle, (□) occlusion plus 25% 2-pyrrolidone, (▲) occlusion plus 25% lauracapram. (Reprinted with permission from [26].)

females and greater in proximal than in distal sites (f: $p=0.03$; m: $p=0.006$). To decrease the problem of spatial variation in long-term experiments, a transparent probeholder with multiple holes was used. The device can be accurately repositioned when repetitive measurements are required. Additionally, standardized metal rings up to a height of 4 mm were placed between the probe and the skin surface. By augmenting the probe-to-skin distance, the measured tissue area was increased from a diameter of 3.1 to 19.6 mm and CBF variation was reduced.

Penetration enhancers

One approach to examine the influence of vehicles and penetration enhancers on local skin absorption is to study changes in MN-induced vasodilation after pretreatment. In one study, 200 mM hexyl nicotinate was incorporated into propylene glycol and isopropanol that included either dimethyl sulfoxide or 2-pyrrolidone. Vasodilation by MN was quantified from the peak response and the area under the response versus time curve. Only 2-pyrrolidone significantly promoted penetration [25]. In a more recent study, pretreatment of the skin site with lauracapram or 2-pyrrolidone [26] was followed by challenge with a 10 mM hexyl nicotinate solution. The CBF response was quantified by the following LDF-determined parameters: onset of action, time to peak, peak response, and area under the response versus time curve. CBF was significantly increased by simple occlusion alone and was further elevated by pretreatment with either penetration enhancer (figure 9–3).

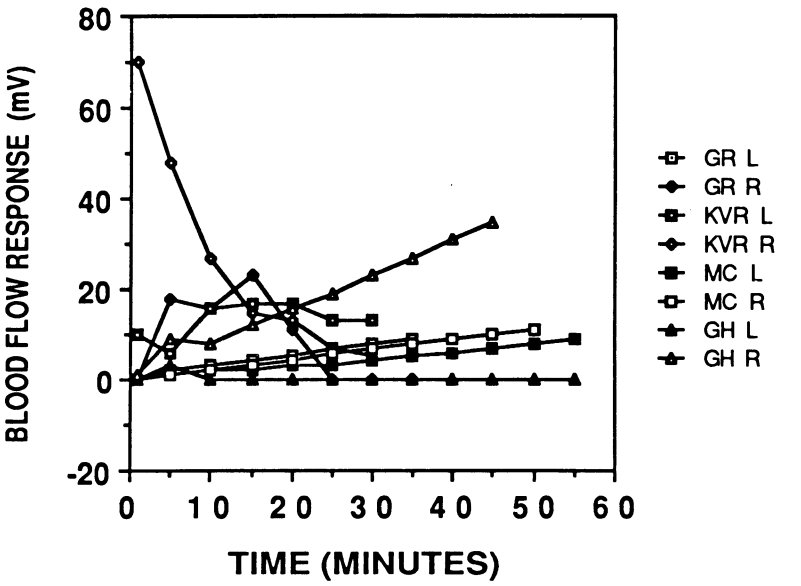

Figure 9–4. CBF response to topically applied water in four subjects. Symmetric sites on the left (L) and right (R) forearm were measured. (Reprinted with permission from [28].)

Vehicles

The influence of supposedly inactive vehicle agents such as water, ethanol, etc. on CBF is controversial. The selection of an appropriate, nonvasoactive vehicle for studies with nicotinates was recently emphasized. Water and lower aliphatic alcohols, but not kerosene, propylene glycol, or polyethylene glycol, elicited an inconsistent and irreproducible vasoresponse [27]. In our experience, water (figure 9–4) [28] and ethanol [29] induce inconsistent changes in CBF. However, these effects are usually of much shorter duration and smaller extent than is the nicotinate-induced change in CBF. Other investigators have reported no influence of water [30,31,32] and, conversely, a significant stimulation of CBF by water [33,34]. It is possible that different skin and vehicle temperatures and occlusive conditions account for the observed variations. To correct for the potential influence of vehicles on CBF, careful planning and performance of the experiment including appropriate vehicle controls are essential.

Age, race, and gender

Human skin undergoes considerable changes with age. Histological and biochemical changes within the tissue have been identified and investigated [35]. Little is known, however, about the reactivity of the microvasculature in aging skin [36]. In an attempt to address this issue, skin reactivity to histamine was determined and shown to be significantly dependent on age,

but not on sex and atopic diathesis [37]. An increase in the response from early childhood to adulthood, which then decreased to a plateau after the age of 60, was found. These observations raise fundamental questions about the effect of age and ethnic background on skin absorption and CBF response to topical stimuli. The point is relevant with regard to skin testing, absorption of drugs, and skin barrier function in general.

For example, in young (20–30 years) white and black and in old (63–80 years) white individuals, 100 mM MN was applied for a short period and the response followed by LDF. Except for the magnitude of the peak response, a remarkable similarity of the response in the different subject populations was found [38]. In another dose–response study using MN in young and old subjects, similar results were obtained [39]. The four MN concentrations used (2.5, 5, 10, and 25 mM in water) stimulated CBF in a dose-dependent manner in both age groups. For each MN concentration, responsiveness in the elderly subjects seemed somewhat attenuated, but the differences were not statistically significant (table 9–2). In young black, Oriental, and Caucasian individuals challenged with three concentrations (0.1, 0.3, 1.0 M) of MN, no difference was seen either in visual erythema scoring or in peak LDF response. The area under the LDF response versus time curve, however, was significantly larger in the black and Oriental groups, indicating that LDF seems to identify grades in erythema not usually differentiated. These results contrast with the perception that black skin has an epidermal barrier that resists irritants better than Caucasian skin [40].

TOPICAL DRUGS

Minoxidil

Several vasoactive drugs have been evaluated by LDF (table 9–3), but the results are not consistent. In one study, 1%–5% minoxidil in a propylene glycol/ethanol/water vehicle increased CBF in balding scalps in a dose-dependent manner. The vehicle control was a 50% ethanol base that also induced CBF. This experiment was suggested to be useful in the direct study of topical minoxidil pharmacodynamics. For the evaluation of the deep perifollicular blood flow that might account for increased hair growth, alternative methods such as the ^{133}Xe washout method were recommended [29]. On the other hand, a recent communication showed that 3% minoxidil in an ethanol/propylene glycol/water base did not increase CBF, whereas 0.1% hexyl nicotinate in the same vehicle triggered vasodilation [41].

Nitroglycerin

Inconsistent findings have also been reported for nitroglycerin (GTN). Topical application of a 2% GTN ointment for various time periods increased CBF significantly over baseline [42]. The peak response, however, did not correlate with the application time, and even repetitive applications

Table 9–2 Stimulation of blood flow by methyl nicotinate in young (n = 6) and old (n = 8) subjects (mean ± SD)

MN concentration (mM)	Age group	Time of onset (min)		Time to peak (min)		Peak response (mV)		AUC (mV × hr)	
2.5	Young	5.6 ± 1.8	N.S.	11.4 ± 2.7	N.S.	333 ± 244	N.S.	179.9 ± 234.3	N.S.
	Old	9.1 ± 4.2		17.6 ± 7.7		250 ± 191		75.6 ± 56.0	
5.0	Young	5.8 ± 2.1	N.S.	11.1 ± 3.9	N.S.	400 ± 240	N.S.	182.9 ± 185.3	N.S.
	Old	6.5 ± 4.3		12.9 ± 7.9		437 ± 267		235.4 ± 192.3	
10.0	Young	4.6 ± 1.7	N.S.	8.9 ± 3.1	$p < 0.03$	609 ± 213	N.S.	377.6 ± 225.7	N.S.
	Old	6.4 ± 2.6		17.9 ± 8.3		564 ± 255		400.8 ± 224.4	
25.0	Young	3.8 ± 1.5	N.S.	10.8 ± 3.2	N.S.	673 ± 111	N.S.	439.0 ± 119.2	N.S.
	Old	6.0 ± 2.6		14.0 ± 6.0		655 ± 212		464.5 ± 171.1	

N.S. = not significant; MN = methyl nicotinate; AUC = area under the response versus time curve.

Table 9–3 Topically administered vasoactive drugs evaluated by laser-Doppler flowmetry

Drug	Method	Vehicle	Concentration	Dose/area/time	Localization	CBF response	Author (reference)
Minoxidil	LDF PPG	Propylene glycol Ethanol/water	0%, 1%, 3%, 5%	0.25 ml/100 cm^2/– Open	Scalp	Concentration-dependent increase	Wester [29]
Minoxidil	Periflux PF2	Ethanol/propylene glycol/water	3%	0.05 ml/1 cm^2/– Open	Scalp	No increase	Bunker [41]
Nitroglycerin (Nitrobid®)	LDF PPG	Ointment	2%	50 µl/2–5 cm^2/10 min Open/occlusion	Forearm	Local increase	Guy [15]
Nitroglycerin (Transderm®)	LDF	TTS	—	–/–/10 hr Occlusion	Chest	Local increase No systemic action	Stevenson [42]
Nitroglycerin	Periflux PF1	TTS	—	25 mg/10 cm^2/24 hr Occlusion	Chest	Local and systemic increase	Sundberg [43]
Fluocinonide	Medpacific	Cream/ointment	0.05%	100 µl/10 cm^2/22 hr Occlusion	Forearm	No change after methyl nicotinate	Amantea [45]
Hydrocortisone HC butyrate Budenoside Clobetasol	Periflux	Ointment — — Ointment	1% 0.1% 0.025% 0.05%	–/0.75 cm^2/1 hr Occlusion	Forearm	Decrease after 4 min of arterial occlusion	Bisgaard [46]

PPG: photopulse plethysmography; CBF: cutaneous blood flow; TTS: transdermal therapeutic system; LDF: laser Doppler flowmetry.

did not further increase the CBF response. It was suggested that GTN is slowly delivered into the dermis with the stratum corneum acting as a rate-controlling membrane. Subsequently, CBF was monitored for ten hours at the application site of a transdermal GTN delivery system. A rapid local increase of CBF to a sustained relatively constant level was found. Despite the occurrence of GTN-induced headache, CBF on the contralateral arm remained at baseline levels, and a systemically mediated action on CBF, therefore, was not demonstrable. On the contrary, during a 24-hour administration of a GTN patch on the chest, a 25% increase of CBF on the forehead was measured throughout the dosing period. The majority of subjects experienced mild to severe headache, indicating systemic GTN action [43].

Corticosteroids

The most common method to assess the potency of topical corticosteroids is the vasoconstriction assay [44], which is based on visual grading of the blanching effect. A first attempt to quantify corticosteroid activity involved challenging a skin area, pretreated with 0.05% fluocinonide, with a 25 mM MN solution. However, no differences in response could be detected between untreated and vehicle-treated skin [45]. In an innovative study, the vasoconstrictive potency of corticosteroids was determined from the postocclusive hyperemic response measured by LDF. Four corticosteroids of different potency were applied for one hour and the hyperemic reaction was determined after four minutes of arterial occlusion (figure 9–5). Significant dose–response behavior with respect to drug potency and to treatment duration was observed. Similar data were obtained in a control experiment using the atraumatic ^{133}Xe washout technique. A possible explanation is that corticosteroids suppress prostaglandin release, causing reactive vasodilation [46]. In an investigation of topical corticosteroid side effects, LDF and stereomicroscopy were used to assess teleangiectasia. Ultrasound was applied to the measurement of skin thickness and evaporimetry determined barrier function [47,48]. Significantly higher CBF was seen on the back than on the forearm. Teleangiectasia was evaluated more reliably by stereomicroscopy than by LDF. The postocclusive rebound dermatitis, however, that occurred in three subjects could be readily quantified by LDF and evaporimetry. Ultrasound measurements revealed significant thinning of the skin at both sites.

INFLAMMATORY MEDIATORS (TABLE 9–4)

Histamine

The visual scoring of the weal and flare response is a standard method to determine 1) cutaneous vasculature reactivity to inflammatory mediators and 2) immediate hypersensitivity reactions. The literature shows that, on the whole, LDF represents a noninvasive and reproducible method to quantify such reactions. The injection trauma itself, however, induces a considerable

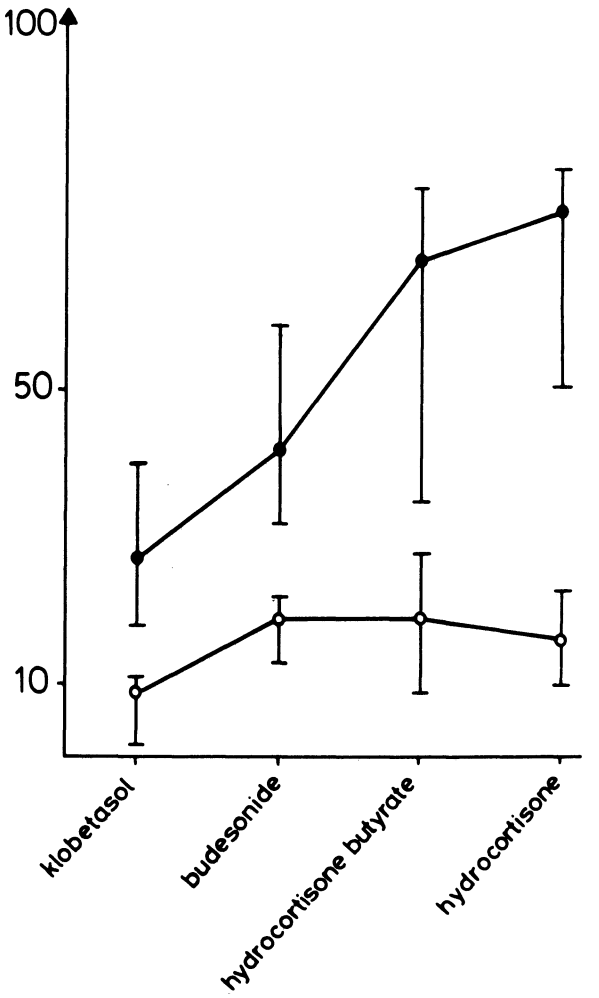

Figure 9–5. CBF in reactive hyperemia (y-axis, arbitrary units) after four minutes (•–•) of arterial occlusion. A significant ($p < 0.01$) dose-response related reduction of the response following a one-hour application of four corticosteroids of different potency was obtained. Two minutes (o–o) of arterial occlusion obscured the difference among the drugs. (Reprinted with permission from [46].)

LDF response (table 9–5). Previously, it had been observed that the LDF-measured CBF increase at the injection site was higher for the needle stick than for saline and histamine [49]. The ability to discriminate between different concentrations of histamine was dependent upon the distance of the measurement site from the injection site and upon the time postinjection [50]. At the injection site, a differentiation of saline and histamine was not possible at any time. However, temporal and spatial measurements permitted

Table 9–4 Intradermally administered inflammatory mediators evaluated by laser-Doppler flowmetry

Agent	Method	Concentration	Dose	Localization	Species	CBF response	Author [reference]
Histamine	Periflux	0.1, 1, 10 mg/ml	Prick	Forearm	Man	Dose-dependent increase	Serup [50]
Histamine	Periflux PF1	$6.5\times 10^{3}-10^{5}$	50 µl	Forearm/back	Man	Dose-dependent increase	Hovell [51]
LTC_4	Perimed	1 µg	0.05 ml	Forearm	Man	Increase	Bisgaard [52]
LTD_4	"	1 µg	"	"	"	"	
Histamine	"	0.375 µg	"	"	"	"	
LTD_4	Perimed	0.04–10 µM	20 µl	Forearm	Man	Dose-dependent increase	Bisgaard [53]
LTD_4	Perimed	3.1–200 pmol	20 µl	Forearm	Man	Dose-dependent increase	Bisgaard [54]
LTB_4, LTE_4	Medpacific	1 ng–1 µg	50 µl	Trunk	Pig	Increase	Chan [55]
LTF_4, PGE_2	"	"	"	"	"	"	
Histamine	"	"	"	"	"	"	
LTC_4, LTD_4	"	"	"	"	"	Up to 100 ng increase/ $\geq$ 1 µg decrease	
Norepinephrine	Periflux	0.1 mM/l	—	Finger	Man	Decrease	Lindblad [58]
Phenylephrine	Periflux	1 µM/ml	—	Finger	Man	Decrease	Lindblad [59]
B-HT 933	"	10 µM/ml	—	Finger	Man	Decrease	
CGRP	Perimed II	10 pM/50 µl	50 µl	Forearm	Man	Increase	Brain [60]

LT: leucotriene; PG: prostaglandin; B-HT 933: α-2 receptor agonist; CGRP: calcitonine gene-related peptide.

Table 9–5 Peak blood flow (in arbitrary units) after intradermal interventions (mean ± SD)

Needle	4.17 ± 0.61
Saline	3.94 ± 0.63
Histamine	2.05 ± 0.52
Epinephrine	1.25 ± 0.32

(Adapted with permission from [49].)

deconvolution of the traumatic and pharmacological actions. Optimal quantification of the weal response was achieved by determinations ten minutes postinjection, 5 mm from the weal center. In a recent comparison of three histamine concentrations, measurement of CBF with LDF was found to be a sensitive and reproducible method to quantify the local response [51]. The LDF response was quantified by integrating the LDF values measured at different distances from the injection site. With this approach, it was possible to differentiate between the three histamine concentrations and the saline control for up to 30 minutes after administration (figure 9–6). Repeat measurements one week later were not significantly different, indicating good reproducibility.

Eicosanoids

Leucotrienes (LT) are potent vasoactive agents and inflammatory mediators. To investigate further the apparent species differences in the response to leucotrienes [52], equimolar concentrations of LTC_4, LTD_4, and histamine were administered intradermally to establish and compare their effect in humans. Discrimination was not possible, which indicated that all agents maximally dilated the vascular bed. The measurements, however, were made twice at a single site over 15–30 minutes, which may be an insufficient period to cover the evolution of the complete response. In a dose–response study of LTD_4, planimetric measurement of erythema, LDF, and ^{133}Xe washout were compared. The latter two techniques were found to be superior to planimetric grading; ^{133}Xe washout was better than LDF in discriminating interindividual differences in CBF [53]. In an extensive investigation [54], intradermal LTD_4 increased CBF equipotently to histamine with a peak response within five minutes and a duration of 60 minutes. Late reactions were not observed. Saline always provoked lower CBF responses of a shorter duration than LTD_4. Pretreatment with H_1- and H_2-antagonists did not alter the CBF response to LTD_4, and the sympathetic nerve action in areas injected with LTD_4 and saline was undisturbed. Local anesthesia with lidocaine, however, abolished local sympathetic nerve activity on cutaneous vessels. These data indicate that LTD_4 acts on the microvasculature in acute inflammation [54].

Similar investigations have been performed in animals. In pig skin, intradermal LTB_4, LTF_4, prostaglandin (PG) E_2, and histamine were tested

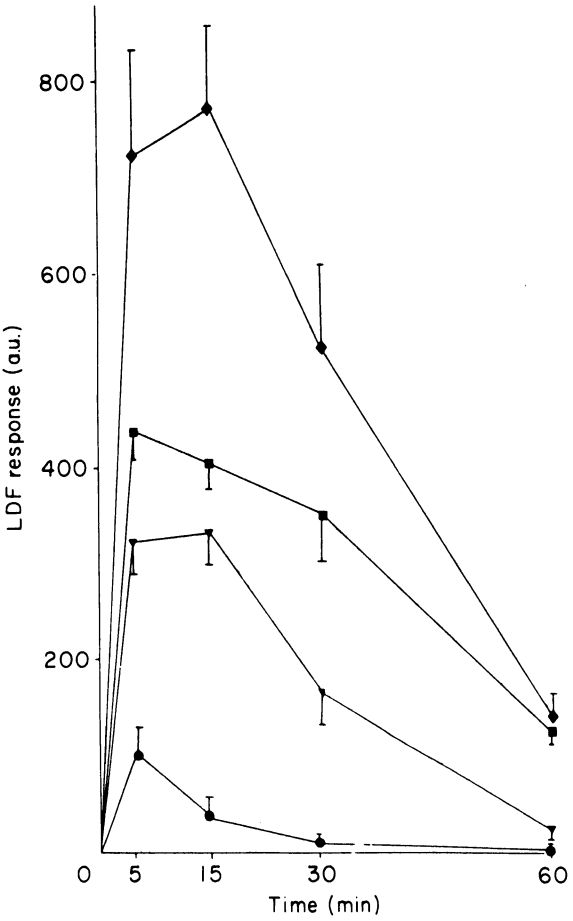

Figure 9–6. Time course of the laser-Doppler response to intradermal injection of three doses of histamine: 6.5×10^{-5} M (▼); 6.5×10^{-4} M (■); 6.5×10^{-3} M (◆); and saline (●). LDF response represents integration of the LDF values measured at different distances from the injection site. (Reprinted with permission from [51].)

[55]. LTC_4 and LTD_4 induced vasodilation at doses of 1 ng and caused vasoconstriction at 1 μg (figure 9–7). Indomethacin did not influence the CBF response to any agent, while saline induced a 200%–300% increase of baseline CBF that persisted for less than three minutes. The differences between human and pig skin are 1) that the duration of the response in the pig is shorter, and 2) that doses of 1 μg LTC_4 and LTD_4 induce vasoconstriction in the pig, whereas vasodilation continues to occur in human skin. However, compared to other animals, such as the guinea pig and the rat, the pig seems to be the model most relevant to human skin in the study of the effects of leucotrienes.

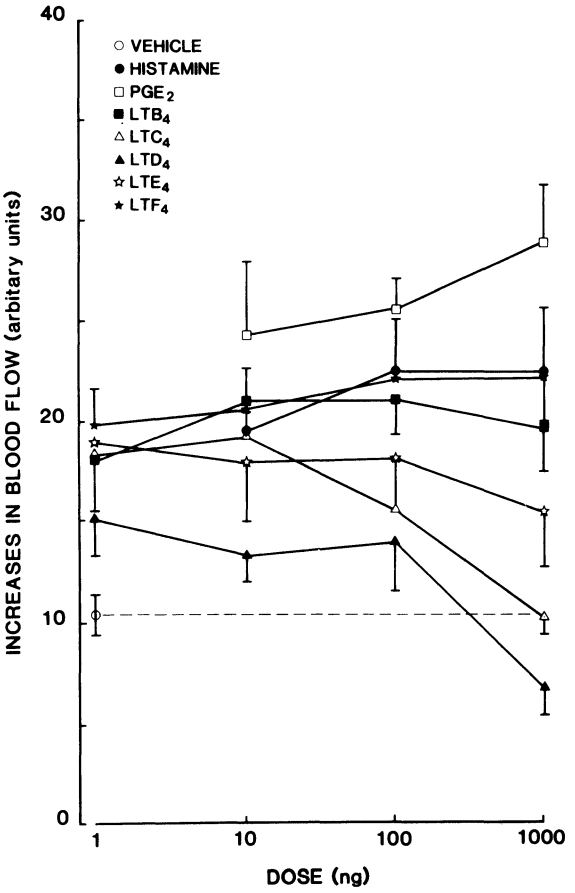

Figure 9–7. Effects of intradermally injected leucotrienes, prostaglandin E_2, and histamine on CBF in pig skin. The response (in arbitrary units) represents the difference between the peak height of the response and resting CBF. (Reprinted with permission from [55].)

Prostacycline is a potent vasodilator that has an opposite pharmacologic action to thromboxane A_2, another powerful arachidonic acid metabolite. To test thromboxane synthetase inhibitors, prostacycline-induced CBF was measured in a rabbit epigastric island flap [56]. The three agents failed to induce any CBF changes beyond those elicited by a saline control.

Because prostaglandin D_2 and histamine are generated in type 1 allergic skin reactions and released into the venous blood in cold and heat urticaria, the interaction between these two weal and flare inducing agents was studied [57]. PGD_2 increased CBF and the area of erythema in a dose-dependent manner. The amount of PGD_2 necessary of elicit a response was higher than its blood levels measured in urticaria, and its injection in combination with

histamine did not significantly enhance the respective effect of either mediator alone on CBF and erythema. An essential role of PGD_2 in the pathogenesis of urticarias was hence believed to be unlikely.

Miscellaneous inflammatory agents

The problems of the injection trauma influencing CBF response measured by LDF and the alterations of CFB by the systemic action of intravenously administered agents have been prevented by the iontophoretic delivery of norepinephrine into finger skin [58]. The technique allows continuous recording of CBF during the administration of the drug without systemic effects. The same technique was employed to identify α-1 and α-2 adrenoceptors in finger skin using specific agonists and antagonists [59]. The action on the cutaneous microvasculature of a newly discovered neuropeptide, calcitonin gene-related peptide, was also monitored by LDF [60]. An increase in CBF was found, which gradually decreased over four hours. Comparison of the weal and flare reaction induced by other vasodilators such as histamine, PGE_2, PGI_2, substance P, and vasoactive intestinal peptide, revealed an inability of calcitonin gene-related peptide to act similarly. However, it elicited the largest and most prolonged erythema.

ALLERGIC AND IRRITANT SKIN REACTIONS (TABLE 9–6)

Visual scoring of allergic and irritant skin reactions is rapid and inexpensive, but heavily dependent on variables such as the examiner's experience, and the subject's skin color and skin type. Noninvasive evaluation of skin reactions by bioengineering techniques may provide quantitative and more comparable data between reasearch groups so that statistical analyses can be performed more rigorously [61]. However, instrumental approaches are expensive and sometimes more time-consuming. Such disadvantages may limit their application to scientific investigations rather than to everyday use [62]. One should note, however, that LDF measurements represent dynamic CBF and do not necessarily correspond to erythema [63,64]. For example, in venous occlusion, healthy-appearing skin color with low perfusion values may be present, whereas, in burnt skin sites, low or no CBF has been measured in the presence of an intensely dark erythema [65].

Patch-test reactions

To study the irritation potential of occlusive patch tests, CBF was measured 48 hours after the application of four allergens (potassium dichromate, wood tars, carbamix, and formaldehyde) from a standard patch-test series [66]. In two nonsensitized individuals, a considerable but transient increase in CBF was found. This result was confirmed for nickel and patch-test chambers from different manufacturers [67]. Again, in nonsensitized individuals the empty chambers did not change CBF, and petrolatum transiently elevated LDF readings, while nickel caused CBF to increase for 96 hours without

Table 9–6 Assessment of allergic and irritant skin test reactions by laser-Doppler flowmetry

Agent	Concentration	Dose	Vehicle	Localization	Application time/type	Species	Evaluation of	Author [ref]
SLS	0.001%–5%	50 µl	Water	Forearm	24 hr/occlusion	Man	Patch-test IR	Nilsson [33]
NaOH	0.1%, 1%	1 ml	Water	Thigh	5 min/open	Man	Irritation	Wahlberg [30]
Anhydrite®	100%	100 mg	—	Forearm	24 hr/occlusion	Man	Occupational IR	Lachapelle [72]
Standard patch tests	—	—	—	Back	48 hr/occlusion	Man	Patch-test AL	Staberg [68]
Propylene glycol	100%	1 ml	—	Thigh	5, 15 min/open	Man	Irritation	Wahlberg [32]
	"	"	—	Thigh	12 days/open	"	"	
	"	"	—	Forearm	24 hr/occlusion	"	"	
4 allergens	0.5%, 2%, 3%, 12%	—	Petrolatum	Back/forearm	48 hr/occlusion	Man	Patch-test IR	Wahlberg [66]
11 solvents	100%	1.5 ml	—	Forearm	5 min/open	Man	Irritation	Wahlberg [31]
Chlorocresol	0.1%, 1%	—	Petrolatum	Flank	24 hr/occlusion	Guinea pig	Patch-test AL	Andersen [71]
Toluene	> 99.5%	Excess	—	Flank	10 min/open	Guinea pig	Irritation	Mahmoud [74]
Nickel/chambers	5%	—	Petrolatum	Back/forearm	48 hr/occlusion	Man	Patch-test IR	Wahlberg [67]
SLS, phenol	0.5%, 1%, 2%, 5%	—	Water	Forearm	24 hr/occlusion	Man	Irritation	Blanken [34]
Tuberculine	1/10000	0.1 ml	—	Forearm	intradermal	Man	Type IV AL	Swanson Beck [111]
SLS	2.5%	100 µl	Water	Forearm	12,24,48 hr/occlusion	Man	Emollients	Blanken [75]
SLS	1%	8 µl	Water	Flank	3 days/open	Guinea pig	Irritation	Frödin [63]
6 contact reactants	—	10 µl	Ethanol	Back	4 hr/open	Man	Contact urticaria	Lahti [13]
SLS	2%, 5%, 7.5%	0.1 ml	Water	Back	6 days repetitive/open	Man	IR hyporeactivity	Lammintausta [80]
	0.5%, 1%	15 µl	Water	Back	24 hr/occlusion	Man		
SLS	2%, 5%, 7.5%	0.1 ml	Water	Back	5 days repetitive/open	Man	IR male/female	Lammintausta [81]
	0.5%, 1%	15 µl	Water	Back	24 hr/occlusion	Man		
7 detergents	100%	—	—	Back	24 hr/occlusion	Man	Irritation	Serup [73]
SLS	1%, 5%, 10%	100 µl	Water	Forearm	48 hr/occlusion	Man	Irritation	Van Neste [76]
Nickel/chambers	5%	—	Petrolatum	Back/forearm	48 hr/occlusion	Man	Patch-test IR	Wahlberg [69]
SLS	2%, 5%	—	Water	Back	24 hr/occlusion	Man	Irritation	Berardesca [79]
Nickel	5%	—	Petrolatum	Upper arm	24, 48 hr/occlusion	Man	Patch-test AL	Staberg [70]
SLS	1%, 2%, 5%, 10%	—	"	"	"	"	Irritation	
7 irritants	—	15–25 mg	Water/paraffin	Forearm	48 hr/occlusion	Man	Irritation	Willis [62]

SLS: sodium lauryl sulfate; IR: irritant reactions; AL: allergic reactions

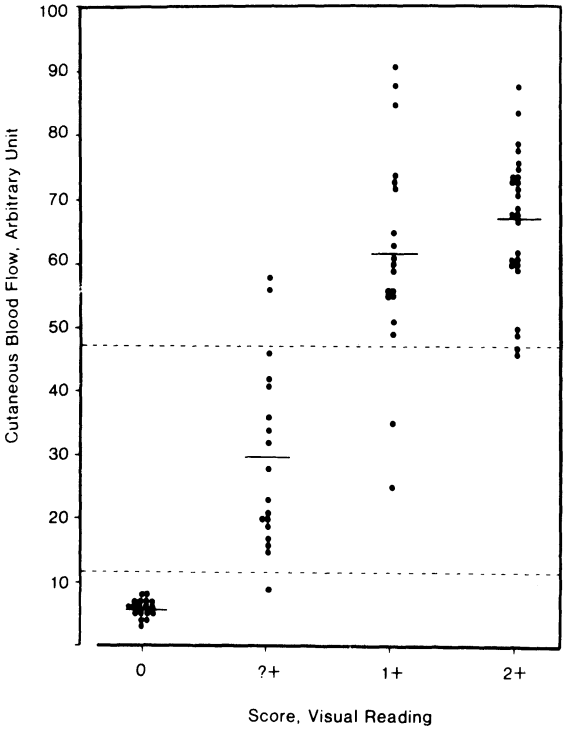

Figure 9–8. Visual grading versus CBF response for standard allergen patch-test reactions. Solid lines represent group means and dashed lines indicate proposed limits to separate negative (0), doubtful (?+), weak positive (1+) and strong positive (2+) reactions. (Reprinted with permission from [68].)

visible erythema at any test sites. In conclusion, late readings at 72 and 96 hours were recommended to prevent false-positive visual and instrumental readings.

In an evaluation of allergic patch-test results, a differentiation between negative and doubtful reactions and between doubtful and 1+ and 2+ responses was clearly possible (figure 9–8). However, doubtful and 1+ readings could not be discriminated [68]. Irritant reactions were excluded from the evaluation, and there was no CBF difference between normal unoccluded skin and negative patch-test sites. The latter is in contrast to other studies [69], where simple occlusion with different brands of test chambers and petrolatum caused transient CBF elevations.

In an attempt to differentiate allergy and irritation, irritant reactions to four sodium lauryl sulphate (SLS) concentrations and to positive nickel patch tests were measured by LDF [70]. The course of CBF was similar for allergic and irritant reactions, and except for some irritant reactions, there was no significant difference between 1+ and 2+ readings. Despite a trend towards lower

CBF values in irritated sites at day 7, the two reactions could not be separated by this method. In sensitized guinea pigs, positive chlorocresol tests were evaluated by visual scoring, LDF, and skin fold thickness [71]. LDF discriminated only between sensitized (grade 2+ and 3+) and nonsensitized (0 and 1+) animals; skin fold thickness differentiated between 2+ and 3+ reactions. Both methods failed to discriminate between every single grade step. On the other hand, the reactions to 1% and 0.1% test concentrations were separable.

Irritation

In initial studies, LDF was established as a suitable technique to quantity irritant skin reactions. SLS, a model skin irritant, was applied on the forearm in concentrations ranging from 0.001% to 5%, for 24 hours under occlusion [33]. An apparent concentration-dependent increase of CBF was observed, with good correlation between visual score and LDF readings. Alkaline solutions also increased CBF in parallel to erythema, whereas a cutting oil, which caused a stinging sensation in workers, elevated CBF slightly without causing visible skin changes [30]. Another occupational irritant, anhydrous calcium sulphate (Anhydrite®), also increased CBF without inducing a visually detectable erythema [72]. Also, undiluted toilet detergents, applied under occlusion on the back, regularly increased CBF but caused few clinical reactions [73].

In humans, open application of solvents (carbon tetrachloride, n-hexane, toluene, trichlorethylene, dimethyl sulfoxide, 1,1,1-trichloroethane, 1,1,2-trichloroethane) for five minutes caused both erythema and increased CBF but distilled water, propylene glycol, ethanol, and methyl ethyl ketone did not change CBF values [31]. Some solvents (methyl ethyl ketone, ethanol, 1,1,2-trichloroethane, carbon tetrachloride) induced skin blanching without reducing CBF. Removal of epidermal lipids and skin structural changes, rather than vasoconstriction, may be responsible for this well-known but poorly understood phenomenon. Evaluation of propylene glycol irritancy did not reveal CBF changes after single and repeated open application; only occlusion increased LDF readings and caused a weak erythema. In patches with water and open control sites, no change in CBF was observed [32]. Assessment of erythema by eye and CBF by LDF in response to seven irritants (benzalkonium chloride, SLS, croton oil, propylene glycol, non-anionic acid in propan-1-ol, dithranol, and sodium hydroxide) showed a close correlation between the two methods [62]. In contrast to the allergic reactions discussed above [64,71], it was possible to discriminate all grades of visual scores by LDF (figure 9–4). CBF in negative patch tests equalled that in normal control skin, making false-negative readings based on visual grading unlikely. Only in three tests was a poor correlation obtained: 1) in two subjects, dithranol stained the skin and the visual scores were less than those expected from the LDF values, and 2) in one individual sodium hydroxide

caused wrinkling, leading to a false-positive visual reading. LDF was more reliable than visual scoring in these cases. In general, however, LDF evaluation of the skin tests was comparable to and more time-consuming than the visual interpretation by a trained observer.

The protective effect of an antisolvent gel was demonstrated in guinea pigs [74]. In the gel-treated sites, CBF response to topical toluene application was significantly attenuated, although a significant increase over baseline values was recorded. In this experiment, LDF was more discriminating than histological evaluation of the test sites. The effect of emollients on irritant skin reactions induced by SLS in human skin were evaluated by visual scoring, LDF and evaporimetry [75]. Apart from a cosmetically pleasing result, none of the emollients quantitatively improved irritation over an observation period of nine days.

The combination of objective techniques measuring different aspects of irritation permits a more differentiated evaluation. For example, 24 hours after application of SLS (0.5%, 1.0%, and 2.0%), phenol, and water, significant increases in CBF, transepidermal water loss (TEWL) and erythema were noted [34]. The LDF results were highly variable, the values in response to 0.5% being higher than those caused by 1% and 2% solutions. This observation could not be explained by individual and substance-related factors alone. Furthermore, after application of 1%, 5%, and 10% SLS, a dose-dependent increase of the measured parameters (LDF, TEWL, visual score) was seen [76], although there was no significant difference between 5% and 10% SLS. TEWL and LDF values had a significant linear correlation after induction and regression of the irritant skin reaction, although CBF values returned to normal within seven days, whereas TEWL normalized only between days 9 to 14. Similar results were obtained in a further investigation with a more rigorous statistical analysis [77]. A good correlation between clinical scoring (erythema, scale formation, roughness), erythema alone, TEWL, and LDF was observed, with an acceptable experimental error of less than 5%. Again, a linear correlation between TEWL and LDF values was obtained. Multiple parameters (visual score, TEWL, LDF, epidermal thickness, and dermal infiltrate) were assessed in a guinea pig model after repetitive SLS application [63]. A progressive increase of all assessed parameters was seen over baseline values, and excellent concordance was obtained between them.

Comparison of black and white skin reaction to SLS by LDF, TEWL, and water-content measurements was performed to address the reportedly [78] lower susceptibility of black skin to irritants [79]. Different responses in the two groups were obtained. Black skin showed less erythema by visual grading and LDF; TEWL and water-content measurements implied a higher irritability of black skin and a different modulation of the defense response. The same techniques were used to investigate gender-related acute and cumulative irritant reactivity to SLS [80]. Both TEWL and water content

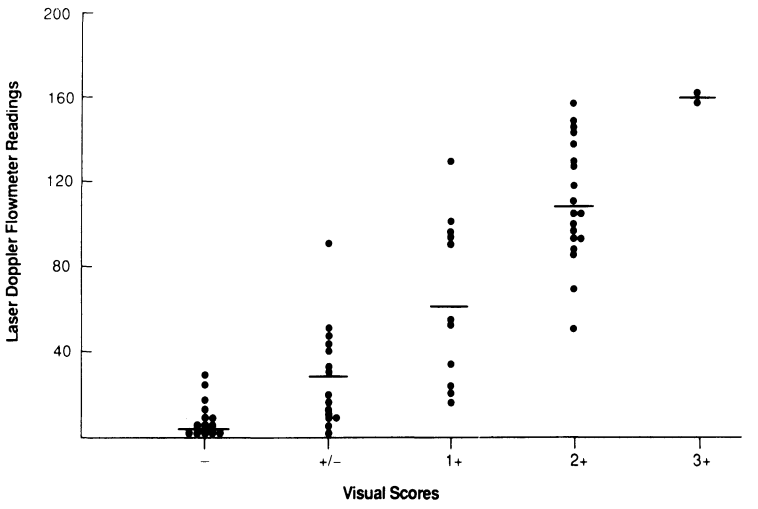

Figure 9–9. Visual grading versus CBF response for erythematous reactions to experimentally induced irritation. Significant differences exist between the different gradings, except 2+ and 3+. (Reprinted with permission from [62].)

increased in response to the repeated open and the single closed application procedure. Only in some closed patches did a visually detectable alteration exist. However, no significant difference between males and females was observed. In a further study [81], after repeated open application of 2%–7.5% SLS, a hyporeactive response to a 1% SLS patch on the contralateral site was surprisingly found, as assessed by LDF and TEWL. Again, great inter-individual variation and significant temporal and spatial variations were found. The interesting finding of a hyporeactive state, after repeated application of SLS, deserves further attention.

Twenty patients with chronic scaling hand eczema were evaluated with evaporimetry, electrical conductance, and LDF [82]. Increased TEWL and decreased electrical conductance were observed, indicating reduced epidermal barrier function and water-holding capacity. CBF was elevated in all but one patient. Correlation among the three techniques, however, was not significant and provided only supplementary information to the clinical findings. In contrast to a defined stimulus,, such as a patch-test chamber with a known concentration of an irritant or an allergen, the heterogeneity and variation in clinically defined disease might be too large to obtain reproducible, correlatable results with such techniques, in typically small patient populations.

ULTRAVIOLET RADIATION

The assessment of acute ultraviolet (UV) effects on skin has typically involved visual grading of erythema and skin temperature measurements.

More recently, techniques such as photopulse plethysmography, ^{133}Xe washout, and skin reflectance have been employed. In several studies, LDF has also been applied to study the time course, intensity, and dose–response of UV-induced erythema and to quantify the protective effect of sunscreens and pigmentation.

For example, 24 hours after irradiation of the forearm with a broad UV spectrum sun lamp, the erythematous response was measured by ^{133}Xe washout and LDF [83,84,85]. Increases of CBF by factors of 2.7 [83] and approximately 2.3 [84,85] compared to the control sites have been found, and a reasonable correlation between the two measuring techniques ($r = 0.88$) has been obtained. The protective value of two sunscreens challenged with a solar simulator was evaluated in pig skin [65]. CBF was enhanced in all irradiated sites including the sunscreen-protected areas, but there was no clear dose–response relationship. Peak values of CBF were measured six hours after irradiation. In the sunscreen-treated sites, reduced CBF values were obtained, but these were significantly different from the untreated controls for only one protecting agent. In burnt areas, i.e., painful sites with deep redness and consecutive epidermal degeneration without bullae, a greatly reduced or absent CBF was observed. In a second trial, three days later, generally lower CBF values were measured, and no significant protetive action of the sunscreens was demonstrated. The postirradiation time course showed that CBF passed two maxima at two and ten hours. A systemic UV protection was suspected to be responsible for this decreased CBF response in the second trial, because local protection mechanisms are not induced in such short periods.

In an extensive study [86], the protective potency of sunscreen components (2-ethylhexylcinnamate and 5-methoxypsoralen) were first tested. Sites were irradiated with a single dose of the complete natural UV spectrum (UVA 15 J/cm^2 plus four minimal erythema doses (MED) of UVB and UVC). Only cinnamate protected against UV; methoxypsoralen had no demonstrable protective value (figure 9–10). In a multiple-exposure experiment to test skin protective mechanisms, five daily doses of UV (10 J/cm^2 UVA and 1 MED UVB/UVC) were administered and followed by a challenge dose (UVA 15 J/cm^2 plus 4 MED UVB/UVC). A smaller CBF response was obtained, thus demonstrating the shielding effect of tanning and epidermal thickening.

The time course and the dose-response of UVB-induced erythema was also measured by LDF [87]. In white skin, a peak at six hours and a persistence of elevated CBF for over 72 hours was observed after irradiation with 2 MED (figure 9–11). In white and pigmented skin, a linear increase in CBF with log (UV dose) over a range of 0.5 to 5 MED was seen. In skin types IV–VI, a shift to the right of the dose–response curve was found, indicating better defense against UV radiation. This result agreed with earlier data [88] showing that skin reflectance also increased linearly with log (UV does) up to 15 MED. In another investigation with the same technique,

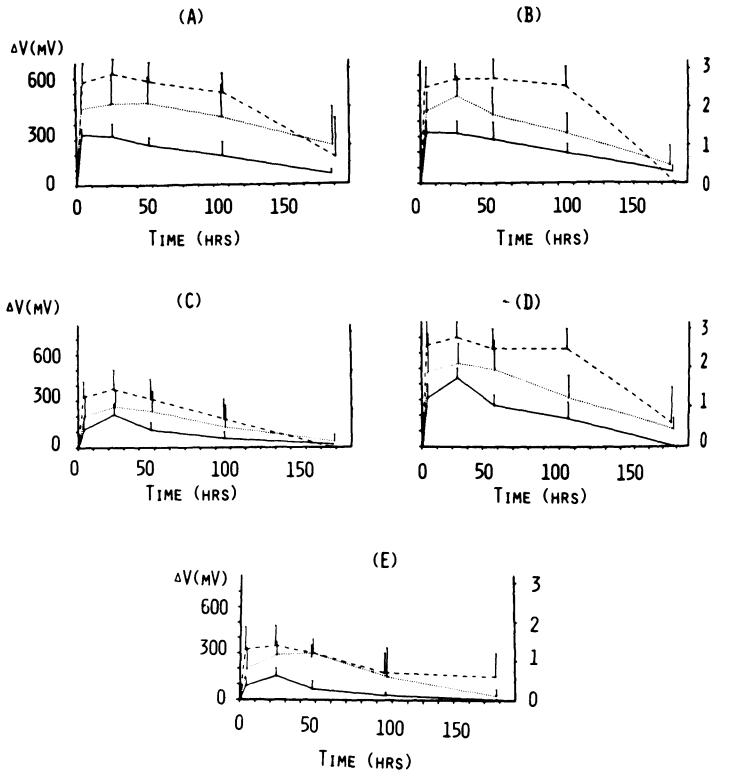

Figure 9–10. CBF response to a single exposure of ultraviolet radiation to skin pretreated as follows: A) control, B) vehicle, C) B+ cinnamate, D) B+ methoxypsoralen, E) B+C+D; readings by Medpacific (——), Perimed (·····), and visual grading (----). Laser-Doppler units on the left, visual score on the right *y*-axis. Significant lower results in sites treated with cinnamate (C, E). (Reprinted with permission from [86].)

however, a linear dose–response was observed, but with a marked plateau between 2 and 3 MED [89]. In further studies, the vascular response to UVB (300 nm) and UVC (254 nm) [90] and to UVA and UVB [91] was measured by LDF and skin reflectance. For UVB a steeper dose–response curve than that for UVC, was determined by CBF and erythema index. However, at both wavelengths a significant increase in CBF occurred, and the dose–response patterns were qualitatively similar. These data indicate that the same dermal vessels are dilated by the different UV wavelengths. For high doses of UVA, a biphasic time course of erythema was seen with a short immediate reaction, a mimimum at four hours, and a plateau phase between 6 and 24 hours [91]. This suggests that, although UVA is 1000–2000 times less erythematogenic than UVB, a common mechanism for both wavelengths and the same vessels are involved in the delayed erythematous response.

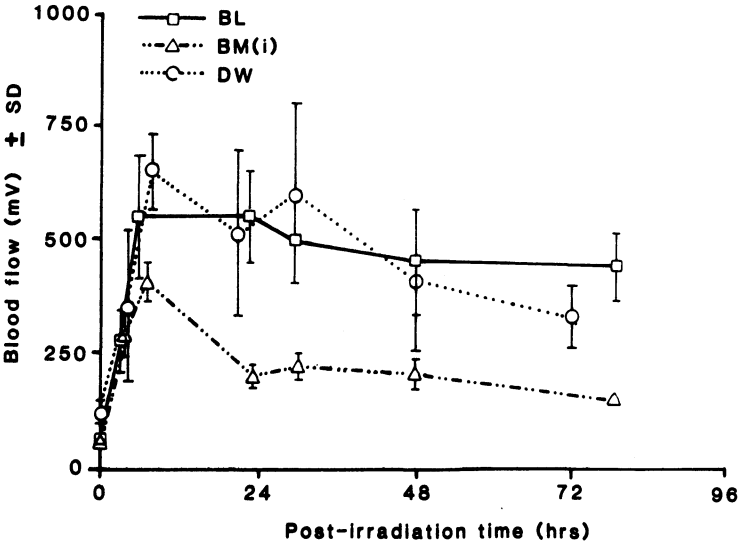

Figure 9–11. Time course of CBF response in three white subjects (BL, BM, DW) exposed to 2 MED of UVB. Each point represents the mean of four replicate exposures. (Reprinted with permission from [87].)

Few studies of UV action on skin have been performed with LDF. A comparison is not possible between studies, in which irradiation sources with different emission spectra and methods other than LDF, have been used to measure erythema. The different parameters measured are one explanation for the conflicting results concerning the induction and evolution of erythema following exposure of the skin to UV radiation.

SKIN DISORDERS

In many skin diseases, inflammatory changes involving the superficial capillary plexus are an important part of the pathologic process. Few systematic investigations employing LDF have been performed. Currently, most emphasis has been placed on quantification of CBF in skin lesions and evaluation of treatment.

Connective tissue disease

A comparison of skin lesions in localized and generalized morphea, an inflammatory disorder of the connective tissue of unknown etiology, was performed [92]. LDF and ^{133}Xe washout showed that the sclerotic plaques and the perilesional lilac rings (i.e., the bluish-colored inflammatory borders) had a significantly greater CBF than normal skin. Older plaques had higher CBF than early lesions. However, in the most advanced "burnt out" plaques, CBF was not different from that in normal skin. It was suggested that the

CBF values represent the grade of inflammation and vascular alteration in the respective stages of the disease.

The successful treatment of acrodermatitis chronic atrophicans, a tick-borne skin disease caused by the spirochete borrelia Burgdorferi, was followed by LDF [93]. The disease passes primarily through an inflammatory stage and progresses, after years without treatment, into irreversible epidermal and dermal atrophy. At the time of diagnosis, CBF in the affected leg was elevated 900% compared to the healthy extremity. After two weeks of therapy with penicillin, CBF was still 200% higher; after five weeks, however, despite a discrete erythema, CBF values were equal in both legs.

Mycosis fungoides

The atrophic form of mycosis fungoides, a malignant T-cell lymphoma, and poikiloderma vasculare atrophicans, a potential precursor of cutaneous lymphoma, have an intriguing affinity to the bathing-trunk area. Based on the low perfusion present in this region [20], it was suggested that this may contribute in an unexplained way to the predilection of these diseases to this site, although certainly other factors such as UV exposure, friction, etc. may play an equally important role [94].

Flushing

Facial flushing is a common sign of emotional distress in humans. On the other hand, it can also be a pathologic reaction due to abnormal enzyme activity or a presenting sign of an underlying hormonal disorder (such as menopause or an endocrinally active tumor). Usually, flushing is transient and difficult to quantify. In individuals of Oriental descent, flushing after drinking alcohol commonly occurs because of a genetically determined low activity of alcohol- or aldehyde-dehydrogenase. To study such reactions and to identify the underlying enzyme abnormality [95], the flushing response was measured by LDF after oral provocation with ethanol. The CBF response was also determined in patch tests performed with different lower aliphatic alcohols and aldehydes. Generally, subjects who had a positive history of flushing also had an elevated cutaneous perfusion index (figure 9–12). This trend was also present in the positive patch-test reactions to primary and secondary alcohols and to aldehydes. The earlier increase of CBF induced by aldehydes in the patch tests and the persistently low CBF values observed at the alcohol patch sites pretreated with an alcohol dehydrogenase inhibitor indicated that aldehyde (not alcohol) is the primary vasodilator. LDF was found superior to thermometry in quantification of alcohol-provoked flushing with regard to sensitivity and specifity. Results from the two methods were significantly correlated with each other and with clinically apparent flushing [96].

Monosodium glutamate (MSG) is thought to cause flushing, one of the reported symptoms of the "Chinese restaurant syndrome" [97]. However,

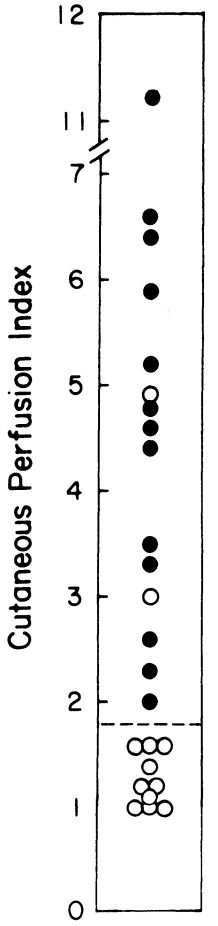

Figure 9–12. Perfusion index (ratio of peak to baseline perfusion) in Oriental subjects after oral challenge with ethanol. Individuals with a flushing reaction (●) had significantly higher values than subjects without a flushing reaction (○). (Reprinted with permission from [95].)

in a study of 18 individuals having a positive history of this reaction, no flushing (as assessed by LDF and thermometry) was provoked by up to 3 g MSG given orally. In a prospective study, up to 18.5 g MSG were tolerated without flushing, although some subjects experience other symptoms. It was concluded that MSG-induced flushing is rare.

Pressure sores

CBF in areas at risk for development of or with already existing pressure sores was measured at ambient temperature [98]. In these sites, values were not significantly different in inpatients with and without pressure sores, but

they were significantly higher than those in healthy subjects. A thermal challenge (40°C) resulted in a singificantly lower CBF response in patients with pressure sores. The effect of massage on CBF, with the aim of preventing pressure sores [99], was also measured by LDF. Since CBF results varied considerably, no significantly CBF change was apparent. Massage, however, is a poorly reproducible stimulus, and CBF changes depend on duration and applied pressure; it is not surprising that CBF varied notably.

The pathogenetic principle of prolonged pressure in the development of sores was proven with the CBF-enhancing effect of a pressure-relieving device [100]. The application of the device resulted in a significant increase in CBF measured by LDF and ^{133}Xe washout. To measure dermal and subcutaneous blood flow, both of which are involved in the pathophysiology of pressure sores, LDF was recommended for CBF and ^{133}Xe washout for subcutaneous blood flow.

TREATMENT EVALUATION

Psoriasis vulgaris

In skin disease, LDF has also been used to follow and assess the response to treatment. The characteristic changes of the capillaries in psoriatic patients has been the subject of considerable research. Only recently have attempts been made to determine the impact of antipsoriatic treatment on the cutaneous microvasculature using LDF and other methods [101].

Goeckerman (topical tar and UVB) and topical tar treatment alone were evaluated using a clinically defined psoriasis index and LDF [102]. The initial CBF in psoriasis was nine times higher than in normal-appearing skin. During therapy, a significant weekly decrease in CBF values was noted that approached uninvolved skin values within 3 to 4 weeks and that correlated linearly with the visual score. This rapid decrease of CBF under therapy was confirmed in a further investigation of eight patients with psoriasis treated with beech tar [103]. Initial CBF in psoriatic plaques was significantly higher than in univolved skin of psoriatic patients and in skin of normal subjects. Again a significant decrease of CBF was seen within the first two days that gradually reached values of the uninvolved psoriatic skin. Comparison of LDF and ^{133}Xe washout measurements showed a reasonable correlation in psoriatic lesions; however, this agreement was not found in either univolved psoriatic skin or the skin of normal subjects. Also, bilateral measurements in normal subjects showed a much higher coefficient of variation for LDF than for ^{133}Xe washout. It was concluded that LDF allows a rough estimate of CBF in highly perfused areas, but is inferior to atraumatic ^{133}Xe washout determination in sites with low CBF.

In a recent investigation of Goeckerman therapy [104], the rapid decrease of CBF in lesional skin measured by LDF was confirmed. Again, a linear relationship between CBF and a visual score was found, but CBF preceded the observed clinical resolution during the first week of treatment (figure

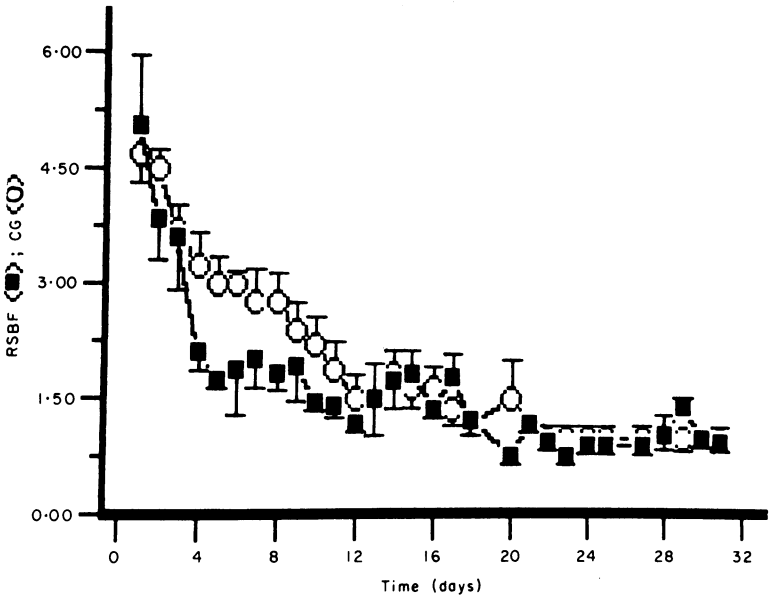

Figure 9–13. Daily assessment of relative CBF (■) and visual score (○) in six psoriatic patients receiving Goeckerman therapy (Tar+Ultraviolet B) until clinical healing was obtained. CBF is significantly lower than visual score between days 4 and 8. (Reprinted with permission from [104].)

9–13). In agreement with the above investigation [103], CBF determined by LDF in uninvolved psoriatic skin was not different from CBF in skin of normal control subjects.

Recently, the importance of the tar component in the Ingram regimen (coal tar bath, UVB irradiation, topical dithranol) for psoriasis was evaluated by LDF and TEWL [64]. Comparable bilateral psoriasis plaques were pretreated with either tar or an oily emulsion. TEWL determinations, LDF values, and clinical scoring paralleled one another and reached normal levels during the observation period of four weeks. The results obtained with coal tar were not different from those obtained with the oil emulsion, suggesting that the coal tar bath is not an essential constituent of the regimen.

Photoaging

Vitamin A and its derivatives have recently attracted much interest because of their alleged efficacy in reversing actinic skin damage. LDF has been proposed as a supplementary method to study vascular alterations, one among numerous epidermal and dermal changes induced by retinoids [105]. In this short, seven-day evaluation of tretinoin, no CBF changes were observed. However, in a placebo-controlled study of photodamaged forearm

skin treated with 0.05% tretinoin for three months, a significantly increased CBF response to trafuril, a nicotinic acid derivative, was obtained [106]. This finding supports the histologically observed increase in vessel density in the upper dermis.

Similar results were obtained in animal experiments. Guinea pig ears were treated for 40 days with topical retinoic acid [107]. Epidermal hyperplasia, as well as collagen and glycosaminoglycan synthesis, were evaluated in biopsies. CBF after eight weeks increased by 81% in retinoic-acid-treated animals. In humans, tretinoin-treated forearms had higher CBF and a higher concentration of erythrocytes, as measured by the new Perimed PF3 [108]. Also, a significantly higher response to challenge with trafuril was seen in the actively treated sites. These results indicate that topical tretinoin induces neoformation and alterations of the cutaneous microvasculature.

Balneotherapy

In balneotherapy, CO_2 is used to induce skin hyperemia. LDF-measured CBF changes to different concentrations of CO_2 and different temperatures were variable. A dose–response relationship was observed that depended on CO_2 concentration and temperature. An objective background for treatment of peripheral vascular disorders with CO_2 baths was given [109].

Portwine stains

Finally, in patients with facial portwine stains, LDF, skin reflectance spectrophotometry, and skin temperature were used to evaluate angiodysplasia objectively [110]. Such determinations may be useful for obtaining a quantitative baseline prior to laser treatment. CBF and hemoglobin content were elevated significantly in the affected skin compared to the normal contralateral site. Cooling caused CBF and temperature to be reduced to the values of the contralateral area, but hemoglobin content did not change.

SUMMARY

LDF is an excellent tool to study changes in the cutaneous microcirculation. It permits noninvasive, in vivo measurements in real time and also allows long-term surveillance of drug action. When well-defined stimuli, such as exact doses of vasoactive substances, a drug, or an inflammatory mediator are used, precise, reproducible, continuous measurement of the effects on skin capillaries is possible. Also, the erythematous response to irritation or allergic reactions of type I and type IV are suitable for LDF evaluation, particularly in combination with other techniques that measure edema (ultrasound), water content, and epidermal barrier function (TEWL). Less clearly defined stimuli, such as UV irradiation, cause more variation in LDF-detected responses. Further, evaluation of clinical disease and the effect of topical treatment on CBF are associated with considerable inter- and intra-individual variations. Occasionally, comparison between studies is not possi-

ble because the exact type of laser-Doppler instrument used is not indicated. Due to technical discrepancies between instruments of different manufacturers and the ongoing improvement of the instruments, some controversial results may be due to different instruments. However, future technical developments of LDF instrumentation may permit more accurate measurements of CBF and determination of other parameters, such as erythrocyte concentration, a potential index for erythema intensity.

REFERENCES

1. Rovensky, J., and A. Preis. 1959. The significance of the trafuril test, with special reference to atopy and rheumatic fever. A capillaroscopic study. Ann Paediat 193:289–303.
2. Murell, T.W. Jr., and W.M. Taylor. 1959. The cutaneous reaction to nicotinic acid furfuryl. Arch Dermatol Syph 79:545–552.
3. Stoughton, R.B., W.E. Clendenning, and D. Kruse. 1960. Percutaneous absorption of nicotinic acid and derivatives. J Invest Dermatol 35:337–341.
4. Fountain, R.B., B.S. Baker, J.W. Hadgraft, and I. Sarkany. 1969. The rate of absorption and duration of action of four different solutions of methyl nicotinate. Br J Dermatol 81:202–206.
5. Albery, W.J., and J. Hadgraft. 1979. Percutaneous absorption: theoretical description. J Pharm Pharmacol 31:129–139.
6. Albery, W.J., and J. Hadgraft. 1979. Percutaneous absorption, in vivo experiments. J Pharm Pharmacol 31:140–147.
7. Fulton, G.P., E.M. Farber, and A.P. Moreci. 1959. The mechanism of action of rubefacients. J Invest Dermatol 33:317–325.
8. Guy, R.H., and H.I. Maibach. 1982. Rapid radial transport of methyl nicotinate in the dermis. Arch Dermatol Res 273:91–95.
9. Albery, W.J., R.H. Guy, and J. Hadgraft. 1983. Percutaneous absorption: transport in the dermis. Int J. Pharm 15:125–148.
10. Svedmyr, N., A. Heggelund, and G. Åberg. 1979. Influence of indomethacin on flush induced by nicotinic acid in man. Acta Pharmacol Toxicol 41:397–400.
11. Wilkin, J.K., O. Wilkin, R. Kapp, R. Donachie, M.E. Chernovsky, and J. Buckner. 1982. Aspirin blocks nicotinic acid-induced flushing. Clin Pharmacol Ther 31:478–482.
12. Wilkin, J.K., G. Fortner, L.A. Reinhardt, O.V. Flowers, S.J. Kilpatrick, and W.C. Streeter. 1985. Prostaglandins and nicotinate-provoked increase in cutaneous blood flow. Clin Pharmacol Ther 38:273–277.
13. Lahti, A., A. Väänänen, E.-L. Kokkonen, and M. Hannuksela. 1987. Acetylsalicylic acid inhibits non-immunologic contact urticaria. Contact Dermatitis 16:133–135.
14. Lahti, A. 1987. Terfenadine does not inhibit non-immunologic contact urticaria. Contact Dermatitis 16:220–223.
15. Guy, R.H., E. Tur, R.C. Wester, and H.I. Maibach. 1985. Blood flow studies and percutaneous absorption. In Percutaneous Absorption, Bronaugh, R.L., Maibach, H.I., eds New York: Marcel Dekker, 393–407.
16. Guy, R.H., R.C. Wester, E. Tur, and H.I. Maibach. 1983. Noninvasive assessments of the percutaneous absorption of nicotinate in humans. J Pharm Sci 72:1077–1079.
17. Guy, R.H., E. Bugatto, B. Tur, C. Gaebel, L.B. Sheiner, and H.I. Maibach. 1984. Pharmacodynamic measurements of methyl nicotinate percutaneous absorption. Pharm Res 1:76–81.
18. Tenland, T., E.G. Salerud, G.E. Nilsson, and P.Å. Öberg. 1983. Spatial and temporal variations in human skin blood flow. Int J Microcirc Clin Exp 2:81–90.
19. Sundberg, S. 1984. Acute effects and long-term variations in skin blood flow measured with laser Doppler flowmetry. Scand J Clin Lab Invest 44:341–345.
20. Tur, E., M. Tur, H.I. Maibach, and R.H. Guy. 1983. Basal perfusion of the cutaneous microcirculation: measurements as a function of anatomic position. J Invest Dermatol 81:442–446.
21. Dowd. P.M., M. Whitefield, and M.W. Greaves. 1987. Hexyl nicotinate-induced vasodila-

tion in normal human skin. Dermatologica 174:239–243.
22. Tur, E., H.I. Maibach, and R.H. Guy. 1985. Spatial variability of vasodilation in human forearm skin. Br J Dermatol 113:197–203.
23. Müller, P., R. Keller, and P. Imhof. 1987. Laser Doppler flowmetry, a reliable technique for measuring pharmacologically induced changes in cutaneous blood flow? Methods Find Exp Clin Pharmacol 9:409–420.
24. De Boer, E.M., P.D. Bezemer, and D.P. Bruynzeel. A standard method for repeated recording of skin blood low using laser Doppler flowmetry. Dermatosen in press.
25. Guy, R.H., E.M. Carlstrøm, D.A.W. Bucks, R.S. Hinz, and H.I. Maibach. 1986. Percutaneous penetration of nicotinates: in vivo and in vitro measurements. J Pharm Sci 75:968–972.
26. Ryatt, K.S., J.M. Stevenson, H.I. Maibach, and R.H. Guy. 1986. Pharmacodynamic measurement of percutaneous penetration enhancement in vivo. J Pharm Sci 75:374–377.
27. Kohli, R., W.I. Archer, and A. Li Wan Po. 1987. Laser velocimetry for the non-invasive assessment of the percutaneous absorption of nicotinates. Int J Pharm 36:91–98.
28. Bircher, A.J., K.V. Roskos, H.I. Maibach, and R.H. Guy. 1980. Laser Doppler velocimetric measurement of skin blood flow: a reply. Int J Pharm 45:263–265.
29. Wester, R.C., H.I. Maibach, R.H. Guy, and E. Novak. 1984. Minoxidil stimulates cutaneous blood flow in human balding scalps: pharmacodynamics measured by laser Doppler velocimetry and photopulse plethysmography. J Invest Dermatol 82:515–517.
30. Wahlberg, J.E. 1983. Skin irritancy from alkaline solutions assessed by laser Doppler flowmetry. Contact Dermatitis 10:111.
31. Wahlberg, J.E. 1984. Erythema-inducing effects of solvents following epicutaneous administration to man studied by laser Doppler flowmetry. Scand J Work Environ Health 10:159–162.
32. Wahlberg, J.E., and G. Nilsson. 1984. Skin irritancy from propylenglycol. Acta Derm Venereol 64:286–290.
33. Nilsson, G.E., U. Otto, and J.E. Wahlberg. 1982. Assessment of skin irritancy in man by laser Doppler flowmetry. Contact Dermatitis 8:401–406.
34. Blanken, R., P.G.M. van der Valk, and J.P. Nater. 1986. Laser-Doppler flowmetry in the investigation of irritant compounds on human skin. Dermatosen 34:5–9.
35. Gilchrest B.A. 1984. Skin and Aging Processes. Boca Raton, FL:CRC Press Inc.
36. Roskos, K.V., R.H. Guy, and Maibach H.I. 1986. Percutaneous absorption in the aged. Dermatol Clin 4:455–465.
37. Skassa-Brociek, W., J-C Manderscheid, F.B. Michel, and J. Bousquet. 1987. Skin test reactivity to histamine from infancy to old age. J Allergy Clin Immunol 80:711–716.
38. Guy, R.H., E. Tur, S. Bjerke, and H.I. Maibach. 1985. Are there age and racial differences to methyl nicotinate-induced vasodilation in human skin? J Am Acad Dermatol 12:1001–1006.
39. Roskos, K.V., A.J. Bircher, H.I. Maibach, and R.H. Guy. 1989. A laser Doppler velocimetric investigation of the cutaneous microcirculation as a function of age. Submitted.
40. Gean, C.J., E. Tur, H.I. Maibach, and R.H. Guy. Cutaneous responses to topical methyl nicotinate in black, oriental and caucasian skin. Arch Derm Res 281:95–98.
41. Bunker, C.B., and P.M. Dowd. 1988. Alterations in scalp blood flow after the epicutaneous application of 3% minoxidil and 0.1% hexyl nicotinate in alopecia. Br J Dermatol 117:668–669.
42. Stevenson, J.M., H.I. Maibach, and R.H. Guy. 1987. Laser Doppler and photoplethysmographic assessment of cutaneous microvasculature. In Models in Dermatology, Maibach, H.I., Lowe, N.L. eds. New York:Karger, vol. 3, pp 121–140.
43. Sundberg, S., and M. Castrén. 1986. Drug- and temperature-induced changes in peripheral circulation measured by laser-Doppler flowmetry and digital-pulse plethysmography. Scand J Clin Lab Invest 46:359–365.
44. McKenzie, A.W., and R.B. Stoughton. 1962. Method for comparing percutaneous absorption of steroids. Arch Dermatol 86:608–611.
45. Amantea, M., E. Tur, H.I. Maibach, and R.H. Guy. 1983. Preliminary skin blood flow measurements appear unsuccessful for assessing topical corticosteroid effect. Arch Dermatol Res 275:419–420.

46. Bisgaard, H., J.K. Kristensen, and J. Søndergaard. 1986. A new technique for ranking vascular corticosteroid effects in humans using laser-Doppler velocimetry. J Invest Dermatol 86:275–278.
47. Serup, J., and P. Holm. 1985. Domoprednate (stermonid®), a topical D-homocorticosteroid, skin atrophy and telangiectasia. Dermatologica 170:189–194.
48. Serup, J., P. Holm, I.-M. Stender, and J. Pichard. 1987. Skin atrophy and teleangiectasia after topical corticosteroids as measured non-invasively with high frequency ultrasound, evaporimetry and laser Doppler flowmetry. Methodological aspects including evaluations of regional differences. Bioeng Skin 3:42–48.
49. Holloway, GA. 1980. Cutaneous blood flow responses to injection trauma measured by laser Doppler velocimetry. J Invest Dermatol 74:1–4.
50. Serup, J., and B. Staberg. 1985. Quantification of weal reactions with laser Doppler flowmetry. Allergy 40:233–237.
51. Hovell, C.J., C.R.W. Beasley, R. Mani, and S.T. Holgate. 1987. Laser Doppler flowmetry for determining changes in cutaneous blood flow following intradermal injection of histamine. Clin Allergy 17:469–479.
52. Bisgaard, H., J. Kristensen, and J. Søndergaard. 1982. The effect of leucotriene C_4 and D_4 on cutaneous blood flow in humans. Prostaglandins 23:797–801.
53. Bisgaard, H., and J.K. Kristensen. 1984. Quantitation of microcirculatory blood flow changes in human cutaneous tissue induced by inflammatory mediators. J Invest Dermatol 83:184–187.
54. Bisgaard, H. 1987. Vascular effects of leucotriene D_4 in human skin. J Invest Dermatol 88:109–114.
55. Chan, C., and A. Ford-Hutchinson. 1985. Effects of synthetic leukotrienes on local skin blood flow and vascular permeability in porcine skin. J Invest Dermatol 84:154–157.
56. Knight, K.R., P.A. Collopy, and B. M. O'Brien. 1986. Response of the rabbit cutaneous microcirculation to prostanoid modifiers as determined by laser Doppler flowmetry. Microvasc Res 31:197–202.
57. Maurice, P.D.L., R.M. Barr, O. Koro, and M.W. Greaves. 1987. The effect of prostaglandin D_2 on the response of human skin to histamine. J Invest Dermatol 89:245–248.
58. Lindblad, L.E., L. Ekenvall, K. Ancker, H. Rohman, and P.Å Öberg. 1987. Laser Doppler flowmeter assessment of iontophoretically applied norepinephrine on human finger skin circulation. J Invest Dermatol 87:634–636.
59. Lindblad, L.E., and L. Ekenvall. 1986. Alpha-adrenoceptors in the vessels of human finger skin. Acta Physiol Scand 128:219–222.
60. Brain, S.D., J.R. Tippins, H.R. Morris, I. MacIntyre, and T.J. Williams. 1986. Potent vasodilator activity of calcitonin gene-related peptide in human skin. J Invest Dermatol 87:533–536.
61. Berardesca, E., and H.I. Maibach. 1988. Bioengineering and the patch test. Contact Dermatitis 12:3–9.
62. Willis, C.M., C.J.M. Stephens, and J.D. Wilkinson. 1988. Assessment of erythema in irritant contact dermatitis. Contact Dermatitis 18:138–142.
63. Frödin, T., and C. Anderson. 1987. Multiple parameter assessment of skin irritancy. Contact Dermatitis 17:92–99.
64. Frödin, T., M. Skogh, and L. Molin. 1988. The importance of the coal tar bath in the Ingram treatment of psoriasis. Evaluation by evaporimetry and laser Doppler flowmetry. Br J Dermatol 118:429–434.
65. Wulf, H.C., B. Staberg, and W.H. Eriksen. 1983. Laser Doppler measurements of blood flow in pig skin after sunscreens and artificial light. Photochem Photobiophys 6:231–237.
66. Wahlberg, J.E., and E. Wahlberg. 1984. Patch test irritancy quantified by laser Doppler flowmetry. Contact Dermatitis 11:257–258.
67. Wahlberg, J.E., and E. Wahlberg. 1985. Skin irritancy from nickel sulfate and test patches. Contact Dermatitis 13:224–225.
68. Staberg, B., P. Klemp, and J. Serup. 1984. Patch test responses evaluated by cutaneous blood flow measurements. Arch Dermatol 120:741–743.
69. Wahlberg, J.E., and E.N.G. Wahlberg. 1987. Quantification of skin blood flow at patch test sites. Contact Dermatitis 17:229–233.

70. Staberg, B., and Serup, J. 1988. Allergic and irritant skin reactions evaluated by laser Doppler flowmetry. Contact Dermatitis 18:40–45.
71. Andersen, K.E., and B. Staberg. 1985. Quantitation of contact allergy in guinea pigs by measuring changes in skin blood flow and skin fold thickness. Acta Derm Venereol 65:37–42.
72. Lachapelle, J.M., M. Mahmoud, and R. Vanherle. 1984. Anhydrite reaction in coal mines. Contact Dermatitis 11:188–189.
73. Serup, J., and E. Ploug. 1987. Testning af sanitetsrengøringsmidler for hudirritation. Ugeskr Laeger 149:472–473.
74. Mahmoud, M., and J.M. Lachapelle. 1985. Evaluation of the protective value of an antisolvent gel by laser Doppler flowmetry and histology. Contact Dermatitis 13:14–19.
75. Blanken, R., P.G.M. van der Valk, J.P. Nater, and H. Dijkstra. 1987. After-work emollient creams: effects on irritant skin reactions. Dermatosen 35:95–98.
76. Van Neste, D., M. Masmoudi, G. Mahmoud, and J.M. Lachapelle. 1986. Regression patterns of transepidermal water loss and of cutaneous blood flow values in sodium lauryl sulfate induced irritation: a human model of rough dermatitic skin. Bioeng Skin 2:103–118.
77. Van Neste, D., G. Mahmoud, and M. Masmoudi. 1987. Experimental induction of rough dermatitic skin in humans. Contact Dermatitis 16:27–33.
78. Weigand, D.A., and G.R. Gaylor. 1974. Irritant reaction in Negro and Caucasian skin. South Med J 67:548–551.
79. Berardesca, E., and H.I. Maibach. 1988. Racial differences in sodium lauryl sulphate induced cutaneous irritation: black and white. Contact Dermatitis 18:65–70.
80. Lammintausta, K., H.I. Maibach, and D. Wilson. 1988. Human cutaneous irritation: induced hyporeactivity. Contact Dermatitis 17:193–198.
81. Lammintausta, K., H.I. Maibach, and D. Wilson. 1987. Irritant reactivity in males and females. Contact Dermatitis 17:276–280.
82. Blichmann, C., and J. Serup. 1987. Hydration studies on scaly hand eczema. Contact Dermatitis 16:155–159.
83. Stern, M., D.L. Lappe, P.D. Bowen, J.E. Chimosky, G.A. Holloway, H.R. Keiser, and R.L. Bowman. 1977. Continuous measurement of tissue blood flow by laser Doppler spectroscopy. Am J Physiol 232:H441–H448.
84. Holloway, G.A., and D.W. Watkins. 1977. Laser Doppler measurement of cutaneous blood flow. J Invest Dermatol 69:306–309.
85. Watkins, D.W., and G.A. Holloway. 1978. An instrument to measure cutaneous blood flow using the Doppler shift of laser light. IEEE Trans Biomed Eng 25:28–33.
86. Drouard, V., D.R. Wilson, H.I. Maibach, and R.H. Guy. 1984. Quantitative assessment of UV-induced changes in microcirculatory flow by laser Doppler velocimetry. J Invest Dermatol 83:188–192.
87. Young, A.R., R.H. Guy, and H.I. Maibach. 1985. Laser Doppler velocimetry to quantify UV-B induced increase in human skin blood flow. Photochem Photobiol 42:385–390.
88. Farr, P.M., and B.L. Diffey. 1984. Quantitative studies on cutaneous erythema induced by ultraviolet radiation. Br J Dermatol 111:673–682.
89. Wan, S., K.F. Jaenicke, and J.A. Parrish. 1983. Comparison of the erythemogenic effectiveness of ultraviolet-B (290–320 nm) and ultraviolet-A (320–400 nm) radiation by skin reflectance. Photochem Photobiol 37:547–552.
90. Farr, P.M., and B.L. Diffey. 1986. The vascular response of human skin to ultraviolet radiation. Photochem Photobiol 44:501–507.
91. Diffey, B.L., P.M. Farr, and A.M. Oakley. 1987. Quantitative studies on UVA-induced erythema in human skin. Br J Dermatol 117:57–66.
92. Serup, J., and J.K. Kristensen. 1984. Blood flow of morphoea plaques as measured by laser Doppler flowmetry. Arch Dermatol Res 276:322–325.
93. Jünger, M., B. Rahmel, G. Rassner, and C. Scherwitz. 1988. Laser-Doppler-Flux zur Therapie kontrolle bei Acrodermatitis chronica atrophicans. Phlebol Proctol 17:136–139.
94. Zackheim, H.S., E. Tur, and R.H. Guy. 1985. Regional blood flow and mycosis fungoides. J Am Acad Dermatol 12:578–580.
95. Wilkin, J.K., and G. Fortner. 1985. Cutaneous vascular sensitivity to lower aliphatic alcohols

and aldehydes in orientals. Alcohol Clin Exp Res 9:522–525.
96. Wilkin, J.K. 1986. Quantitative assessment of alcohol-provoked flushing. Arch Dermatol 122:63–65.
97. Wilkin, J.K. 1986. Does monosodium glutamate cause flushing (or merely "glutamania")? J Am Acad Dermatol 15:225–230.
98. Ek, A.-C, D.H. Lewis, H. Zetterqvist, and P.-G. Svensson. 1984. Skin blood flow in an area at risk for pressure sores. Scand J Rehabil Med 16:85–89.
99. Ek, A.-C., G. Gustavsson, and D.H. Lewis. 1985. The local skin blood flow in areas at risk for pressure sores treated with massage. Scand J Rehabil Med 17:81–86.
100. Karlsmark, T., and J.K. Kristensen. 1987. A method for testing the effect of pressure-relieving materials in the prevention of pressure ulcers. Acta Derm Venereol 67:260–263.
101. Klemp, P. 1987. Cutaneous and subcutaneous blood flow measurements in psoriasis. Dan Med Bull 34:147–159.
102. Staberg, B., and P. Klemp. 1984. Skin blood flow in psoriasis during Goeckerman or beech tar therapy. Acta Derm Venereol 64:331–334.
103. Klemp, P., and B. Staberg. 1985. The effect of antipsoriatic treatment on cutaneous blood flow in psoriasis measured by ^{133}Xenon washout method and laser Doppler velocimetry. J Invest Dermatol 85:259–263.
104. Khan, A., L.M. Schall, E. Tur, H.I. Maibach, and R.H. Guy. 1987. Blood flow in psoriatic skin lesions: the effect of treatment. Br J Dermatol 117:193–201.
105. Marks, R., D. Black, A.D. Pearse, and S. Hill. 1986. Techniques for assessing the activity of topically applied retinoids. J Am Acad Dermatol 15:810–816.
106. Kligman, A.L., G.L. Grove, R. Hirose, and J.J. Leyden. 1986. Topical tretinoin for photoaged skin. J Am Acad Dermatol 15:836–859.
107. Schiltz, J.R., J. Lanigan, W. Nabial, B. Petty, and J.E. Birnbaum. 1986. Retinoic acid induces cyclic changes in epidermal thickness and dermal collagen and glycosaminglycan biosynthesis rates. J Invest Dermatol 87:663–667.
108. Grove, G.L., M.J. Grove, C.R. Zerweck, and J.J. Leyden. 1988. Computerized laser Doppler velocimetry assessment of cutaneous microcirculation: effects of topical tretinoin treatment in photoaged skin. J Cut Aging Cosm Dermatol 1:27–32.
109. Schnizer, W., R. Erdl, P. Schöps, and N. Seichert. 1985. The effects of external CO_2 application on human skin microcirculation investigated by laser Doppler flowmetry. Int J Microcirc Clin Exp 4:343–350.
110. Lanigan, S.W., and J.A. Cotterill. 1987. Objective assessments of portwine stains. Br J Dermatol 117:33–34.
111. Swanson Beck, J., and V.A. Spence. 1986. Patterns of blood flow in the microcirculation of the skin during the course of the tuberculin reaction in normal human subjects. Immunology 58:209–215.

10. PLASTIC AND RECONSTRUCTIVE SURGERY

PER HEDÉN

As early as 700 B.C., reconstructive surgery of nose defects was performed by Susruta in India, and in 1597 the first publication on skin flaps was presented by the Italian Gaspare Tagliacozzi. In spite of this long history, only during the last decades has interest been aroused in the skin flap's circulation. In fact, today it is widely accepted that increased knowledge about skin flap physiology is necessary to improve clinical techniques and to reduce the complication rate in this type of surgery. Because the major cause of flap failure is inadequate blood supply, an accurate assessment of tissue perfusion is of great importance in plastic and reconstructive surgery. However, down through the years the needs and indications for blood flow measurements have changed. At first, efforts were concentrated on estimating the revascularization process and on determining the correct time for the division of flaps destined for transfer as tubes to distant recipient sites in some multistage procedure. When microsurgery was introduced in reconstructive surgery in the early 1970s, a direct one-stage transfer of a flap to a distant recipient area became possible by means of microanastomoses of both the supplying and the draining blood vessels. With this technique, adequate assessment of the flap blood flow became even more crucial, since occlusion of microvascular anastomoses must be diagnosed and rectified promptly to ensure survival of such free flaps. Considering how difficult the clinical assessment of the circulatory status of a free flap can be, it is obvious that reliable monitoring would be of great value. This is obviously also true with

regard to the surveillance of traumatically amputated and microsurgically replanted parts of the body, such as fingers.

As indicated by the observations reported in the following review, laser-Doppler flowmetry (LDF) measurements can be very useful in situations such as those mentioned above. However, many other applications for LDF also exist in modern-day plastic surgery. This is exemplified by modern burn therapy, where the introduction of early wound excision necessitates adequate assessment of the burn depth. LDF may also provide useful information in other clinical situations such as the evaluation of wound healing. However, in plastic and reconstructive surgery it is not in clinical observations but rather in experimental blood flow studies that LDF seems to have its greatest potential.

Numerous other methods for blood flow measurement in plastic and reconstructive surgery have been described and are reviewed elsewhere [1–6]. Even if a there is a broad agreement on the capacity of various instruments, clear-cut differences of opinion also exist. There are several criteria that could be postulated for an ideal monitoring device. However, depending on the field of application, these different criteria are not of equal importance. For example, to judge the circulatory border in a flap at a certain time would not necessitate recordings of rapid flow variations or even a continuous flow value, criteria that would obviously be of greater importance in the surveillance of a replanted finger or a free flap. It should therefore be kept in mind that different monitoring devices all have their advantages and disadvantages and that a particular monitoring device that is suitable for one purpose may be less ideal in another situation. Today, no monitoring device exists that meets all the criteria for an ideal system, and it is likely to be a long time, if ever, before such an instrument becomes available.

LASER DOPPLER FLOWMETRY. EXPERIENCES IN PLASTIC AND RECONSTRUCTIVE SURGERY

Flap monitoring

Prediction of the survival length of flaps

Before the importance of incorporating distinct arterial blood vessels in the base of a flap was formally recognized [7,8], flap elevation was mainly performed with a random blood supply, and the risks of partial flap-tip necrosis were stated to be highly dependent on the length/width ratio. When musculocutaneous, fasciocutaneous, and free flaps incorporating axially supplying blood vessels in the flap pedicle were introduced, the flap length could safely be made much longer, and partial necrosis has since become much less frequent. However, all flaps, be they axially or randomly supplied, that are too long in relation to the amount of blood supplied via the flap pedicle carry the risk of flap-tip necrosis. Thus, the need to predict flap survival is still relevant.

To increase the surviving length of skin flaps with an insufficient blood supply has been the goal of many studies. The treatment can be evaluated by measuring the ultimate flap survival one week after surgery and by predicting this survival by assessing the flap circulation at the time of surgery. For predictions of flap survival, fluorescein measurements of the circulatory border have been the gold standard, but lately LDF measurements have aroused greater research interest [9]. Under standardized conditions with the flap mounted in a frame to avoid movement artifacts, the survival length of critical pedicle flaps has been accurately predicted [10]. Along the center and towards the tip of the flap, the intraoperative LDF value fell rapidly (figure 10–1). A circulatory margin could be estimated, and one week postoperatively the predicted margin was highly correlated with the actual survival margin. In the same study, LDF and the fluorescein angiographic assessment of the circulatory border were also found to correlate well (figure 10–2). With parallel fluorescein and LDF measurements, highly accurate predictions of random pedicle flap survival without false-positive or false-negative results have also been reported by others [11]. The measurements were fairly crude, however, since the rat flaps were divided only into three equal areas; but with this limitation, accurate survival prediction was highly significant and 100% correct [11]. Larrabee et al. [12] also found a high correlation between fluorescein and LDF assessments of random pedicle flap survival, although both methods showed a slight underestimation of flap survival in the immediate postoperative period [12]. However, LDF recordings 24 hours after flap elevation did predict the survival length of flaps exactly.

Other investigators have doubted the usefulness of LDF's capacity for early prediction of the survival of ischemic random pedicle flaps [13]. Variable flow values have been noted, and flow has been recorded in completely devascularized tissue. It was speculated that some of these results represented nonnutritive A-V shunt blood flow. A review of this study does not indicate that movement artifacts have been ruled out. Even if the flow probe was held in a rigid scaffold, the breathing of the animal may have affected the investigated abdominal area profoundly. Secondly, and perhaps more importantly, intermittent recordings were made at several different spots on the abdominal flap. Considering that blood flow can vary significantly in closely adjacent areas, the methodology used by Marks et al. [13] does not lend itself to estimations of circulatory margins in flaps. Lastly, it is well known that recently devascularized tissue has a blood flow higher than zero [14,15], and this is not likely to represent a nonnutritive arterio-venous (A-V) shunt blood flow but rather to-and-fro oscillations of cells within the measuring area.

Other studies have supported the notion that LDF measures not only nutritive blood flow but also perfusion in deeper layers [16]. This A-V shunt flow probably constitutes a significant contribution to the LDF values, especially in areas where the distribution of these shunts is dense, as in fingers [16]. The suggestion that A-V shunt blood flow exists in the distal and

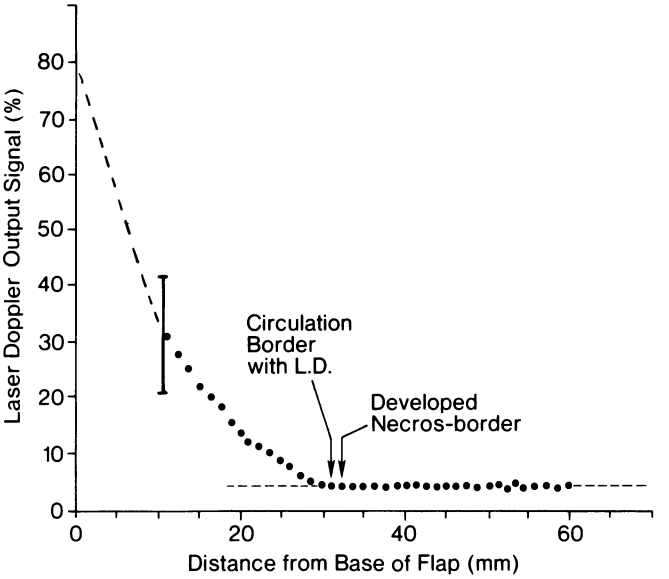

Figure 10–1. Rapidly falling LDF values along the center line of a dorsal pedicle flap of the rat. The curve is a typical tracing. (Reprinted with permission from [10].)

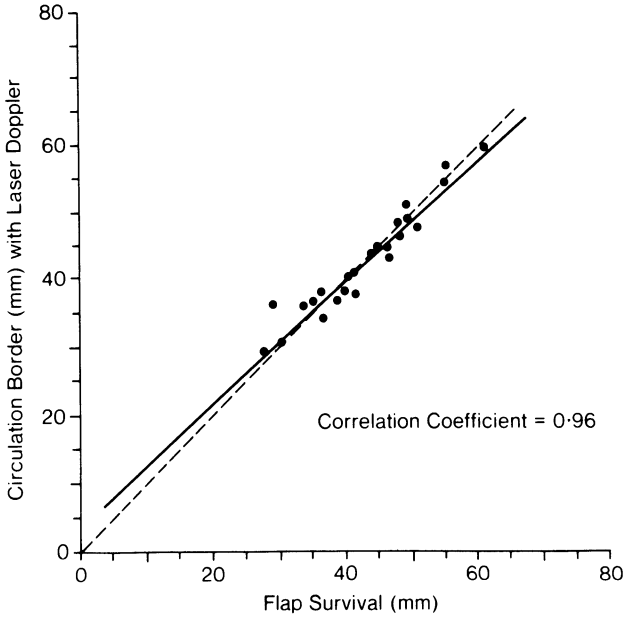

Figure 10–2. Correlation between circulation border measured by LDF and the actual survival of the dorsal pedicle flaps in rats one week after surgery. (Reprinted with permission from [10].)

subsequent dying end of a random pedicle flap [17] and that this shunt flow would result in false-positive LDF values in a dying part of a flap [13,18] has not been convincingly demonstrated. On the contrary, Reinish's shunt theory has been strongly contradicted [19,20]; it is not likely that a significant A-V shunt flow exists in the distal nonsurviving parts of a random pedicle flap.

In their evaluation of several methods for the prediction of flap survival, Sloan and Sasaki [4] reported that LDF was very inaccurate: both great overestimations and underestimations of flap survival were seen during a short time interval. The measuring areas were not well defined, and the well-known spatial variability [21] discussed above is likely to have influenced the results significantly. Another possible explanation of Sloan and Sasaki's findings [4] is that movement artifacts may have blurred the results. It was not reported if and how these were avoided. Sloan and Sasaki's results, as well as those of others [13], emphasize that a broad understanding of the technology and working principles of highly sophisticated equipment like LDF is needed for the correct interpretation of results under certain conditions. The results of these studies also highlight the fact that LDF is most useful for comparative measurements at an exactly defined single site and not for the detection of the circulatory borders of larger areas.

Timing of flap division and assessment of flap neovascularization

With the advent of microvascular free-tissue transfer, the need for multistage tubed flap reconstructions has been reduced remarkably, but even if the need for multiple-stage reconstructions has been markedly reduced, in certain cases assessments of neovascularization still have to be made frequently to judge the accurate time for the division of certain flaps. This could even be true of a free flap that must be trimmed due to bulkiness. Down through the years many methods [22] have been used as guides to assess the correct time for flap division. Nevertheless, the proper time for flap division has been determined more by conventional and personal experience than by objective criteria.

LDF is reported to be a valuable aid in deciding at what stage the base of a pedicle flap can be divided. LDF and also dermofluorometry were able to confirm that the neovascularization of pig island skin flaps was sufficient to supply the tissue between 7 and 10 days after surgery [23]. These results were consistent with the subsequent flap survivals. In a clinical series of 17 myocutaneous flaps investigated in a similar way, the same conclusions were drawn about the ability of LDF to indicate neovascularization [24]. However, it was felt that the dermofluorometer was preferable when early vascular changes were to be detected.

Free-flap monitoring

In the reconstruction of severe tissue defects, microvascular free-tissue transfer has become accepted and reliable. In many ways it is superior to other

reconstructive techniques. This is especially true of the head and neck area and of the distal lower extremity.

More than 15 years have passed since the first successful free-tissue transfer was accomplished [25], but not until the mid-1980s did these procedures become clinically routine in most major plastic surgery centers. However skillful the team performing this type of surgery may be, there is always a risk of occlusion of the vascular anastomoses. For a successful outcome of the procedure, prompt diagnosis and re-establishment of blood flow are necessary. The risk of microvascular compromise is always highest in the early postoperative period, and vascular occlusions after 48 hours are very unusual [3]. It is also well known that neovascularization of a tissue section can support many flaps as soon as after 7–10 days [26]. Therefore, monitoring free flaps is necessary mainly in the early postoperative period.

The failure rate and frequency of postoperative thrombosis varies slightly in different surveys. A postoperative thrombosis frequency of approximately 10% and a failure rate of 6% have been reported [27]. Other studies have shown failure rates as high as 11% in free-flap surgery and 21% in replantation surgery [28]. The aim of using circulatory monitoring devices is to keep or reduce these failures to an absolute minimum.

Following the preliminary report on the usefulness of LDF as a free-flap monitor in 1982 [29], most reports to date have favored LDF as a valuable tool in the surveillance of free flaps [1,2,15,30–33]. Both clinically and experimentally, LDF recordings readily indicate occlusions of the venous or arterial anastomoses (figure 10–3). Experimental island flap studies after prolonged ischemic periods have also concluded that LDF, at any selected time up to 24 hours after revascularization, can reliably predict whether the flap will survive or not [34].

Contrary to most other investigators, Walkinshaw [35] did not find that LDF was a reliable means of diagnosing vascular occlusions. Even though LDF measurements correlated roughly with clinical observations, the latter were more accurate in indicating the need for clinical intervention. A possible reason for these discouraging results is that continuous recordings were not made, but instead intermittent ones were made from a measuring area marked with an ink tattoo. Spatial variability in blood flow, which is known [14,21] to exist in closely adjacent areas (2.5 mm apart), probably influenced the results. It is therefore apparent that free-flap monitoring should be carried out on exactly the same area and preferably should be performed continuously. A probable minimum requirement is to tape, glue, or stitch a probe holder to the flap surface, preferably also indicating the rotation of the probe in this holder. Even a rotation of the probe at the same measuring point is known to alter the measuring areas slightly. If the vascular bed geometry is different in adjacent areas, rotating the probe in the holder may alter the flow values [14].

Different applications of the LDF technique have been advocated for the

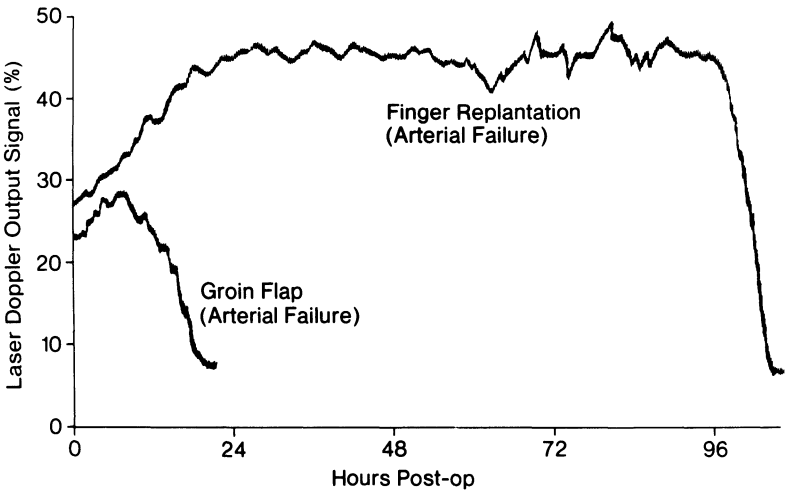

Figure 10–3. LDF flow pattern in two clinical cases with arterial occlusion. (Reprinted with permission from [15].)

monitoring of free flaps. In our own evaluation of the method [15], intraoperative recordings of the LDF value during flap transfer when the flap was devascularized were a valuable guide in judging the postoperative flow values. This was illustrated in a clinical free flap with postoperative edema and a markedly reduced blood flow. The flap showed no clinical signs of perfusion, and without the guidance of the intraoperative devascularized LDF value, the microanastomoses would have been reexplored. The second operation was avoided because the flow values were well above zero flow. The flap survived subsequently without further complications (figure 10–4).

Other investigators have started to monitor flaps postoperatively [30] and have suggested that the flow value after revascularization could serve as a guide in the surveillance [30]. This postoperative flow value was adjusted to a 100% deflection on a recorder, and any reduction during a certain time and below a predetermined level triggered an alarm. During the early postoperative phase after revascularization of free flaps, the normal LDF pattern (figure 10–5) is a steadily increasing flow [15,29,30]. A clear-cut reduction of this flow should thus always give rise to intensified observation to exclude vascular obstruction. A recent development of the Periflux LDF unit (-Pericentry-Periflux PF3) confers the capacity to store both the intraoperative devascularized LDF value and the LDF value after revascularization. Alarm levels can also be set on the instrument to facilitate postoperative monitoring of free flaps. To simplify the interpretation of the flow pattern after a free-flap procedure, other investigators have suggested connecting a microcomputer to the LDF instrument [36]. This has not gained widespread clinical use.

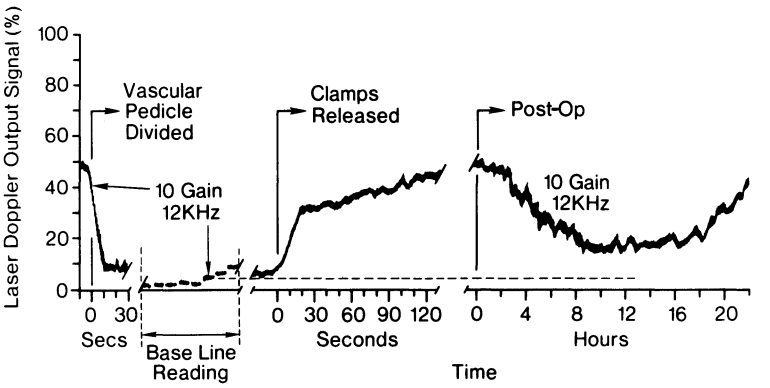

Figure 10–4. Preoperative and postoperative LDF trace in a free forearm flap with postoperative edema, but without vascular occlusion. (Reprinted with permission from [15].)

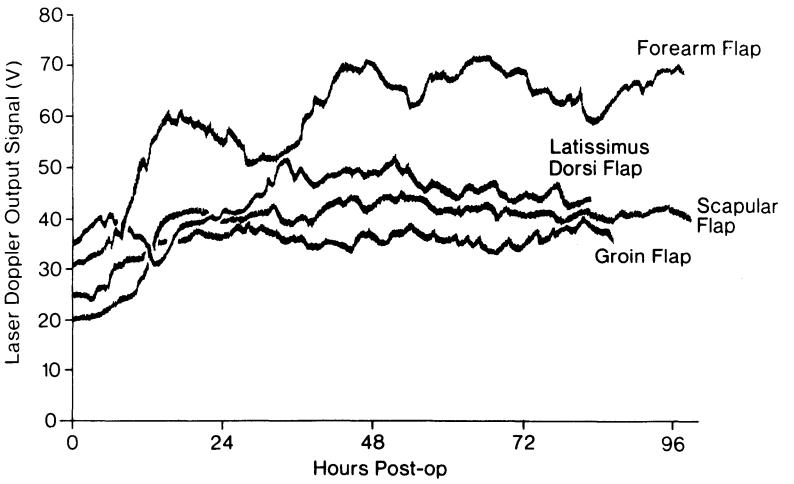

Figure 10–5. Example of normal postoperative flow patterns in complication-free clinical cases. (Reprinted with permission from [15].)

Another application of the LDF technique for the monitoring of free flaps postoperatively was suggested by Jenkins et al. [31]. They advocated that the flap blood flow value be expressed as a percentage of the flow in a control area. In a small clinical series, they found that flaps without postoperative complications had LDF values of approximately 150%, whereas the few cases with complications resulted in LDF values well below 100%. Others have also suggested that LDF values expressed as percentages of control areas made flap perfusion measurements easier to interpret [34]. Once again it should be stressed that moving the flow probe may result in inaccurate flow values. If LDF is measured in a control area, fixed probe holders should be

used. Preferably, two probes should be utilized and, ideally, two laser-Doppler flowmeters. For flap monitoring, a two-channel LDF instrument might be a useful, but probably expensive, development. It should also be remembered that the latest models of LDF instruments can store a flow value from a control area, and flap flow can be expressed as the percentage deviation from this control flow.

Several flowmeters that use helium–neon lasers are commercially available today. These instruments are different in principle in that one operates with a single channel (LD-5000, Med-pacific Co.) and the other has a double channel with a differential amplification detection system (Periflux, Perimed Co). In a limited evaluation of the two devices, this technical difference was not of major importance in monitoring flap perfusion [37]. Both machines could identify arterial as well as venous occlusion. To date, He–Ne lasers have been most widely used, but infrared laser diodes (Laserflow, TSI) have recently been introduced. In preliminary investigations, it has been suggested that the latter machines have certain advantages in the surveillance of flaps [31]; they were easy to handle, and interpretation of the flow curve was found to be simple. In small experimental and clinical series, infrared laser-Doppler flowmeters with implantable miniature probes have also been used successfully to monitor free-muscle transfers [32].

Implantable probes have been developed (figures 10–6 and 10–7) with the main objective of monitoring buried flaps [15,32,33]. The flow probe can be safely mounted on the flap surface with percutaneous stitches, and easy removal after the monitoring period is also possible [15]. Vascularized bone transfers are often completely buried without accessible areas for clinical inspection. Therefore, these grafts present a serious monitoring problem. In two clinical vascularized osteocutaneous fibula transfers, direct bone recordings with buried flow probes produced a flow pattern similar to that of the simultaneously recording flow probes mounted on the skin island [33]. Thus these types of monitoring methods may help solve the difficult problem of surveillance of buried flaps.

In free flaps, venous occlusions are known to be more deleterious than arterial ones; consequently, it is more urgent to revise an obstructed venous anastomosis. Since the arterial and venous anastomoses may be located in different regions, it is also of importance to be able to distinguish between the two types of occlusion. LDF instruments are equipped with a feature that can be used for this purpose. The total amount of backscattered laser light is processed to a direct current, a DC level, also called the laser photometric (LP) value. This level is proportional to the number of moving red blood cells in the measuring area, since congested tissue absorbs more laser light. Consequently, a venous occlusion can be recognized by a reduced DC/LP value. This has been confirmed both experimentally (figure 10–8) and clinically [15,30,38]. The possibility of differentiating between arterial and venous occlusions by means of analysis of the LDF wave form has also been sug-

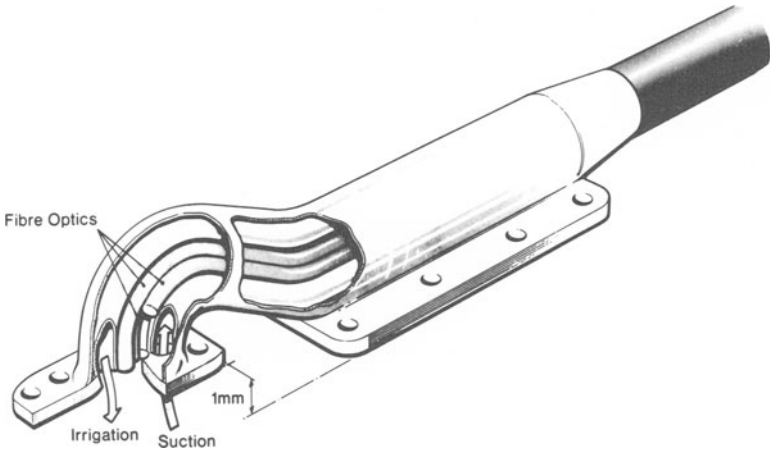

Figure 10–6. LDF flow probe designed for intra-oral or buried use. (Reprinted with permission from [15].)

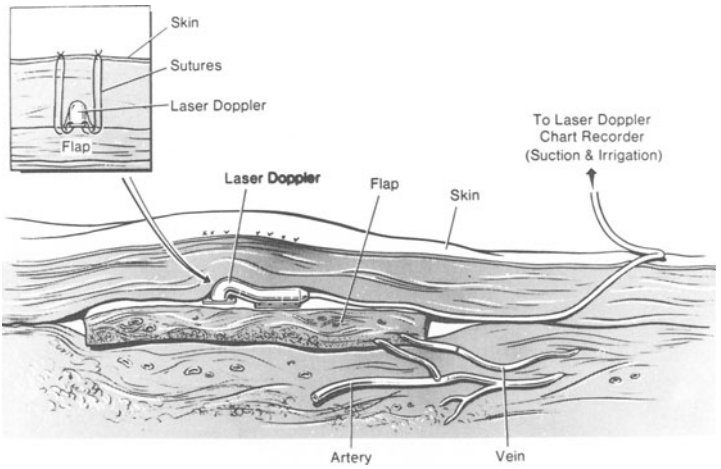

Figure 10–7. Probe attached to buried flap surface. (Reprinted with permission from [15].)

gested [39]. During arterial occlusion, pulsatility decreases, whereas increased pulsatility was seen during venous occlusions.

In the case of vascular occlusions in island or free flaps, LDF has also been compared with other methods for blood flow measurements. Silverman, who popularized the dermofluorometric method [40], has stated that LDF is best suited for continuous monitoring at a single site, as in the surveillance of free flaps, whereas fluorometry is better in producing a multiple-site picture of the flap blood flow. These conclusions were drawn in a comparative study

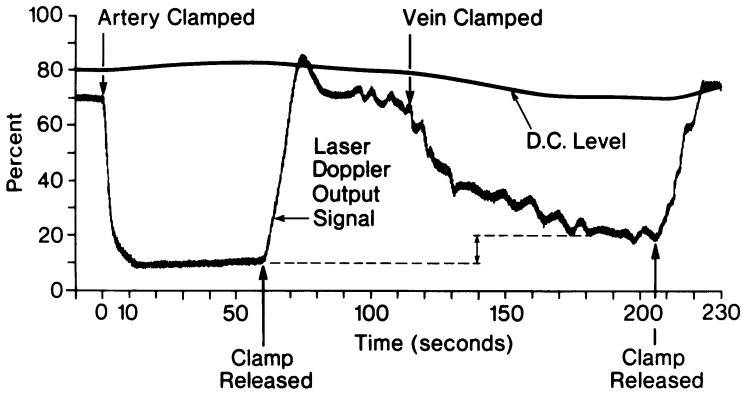

Figure 10–8. LDF and DC (=LP) signal response to arterial and venous occlusion in a rat island flap. (Reprinted with permission from [15].)

of LDF, dermofluorometry, and $P_{tc}O_2$ measurements in canine island flaps subjected to vascular occlusions. Each of the techniques readily identified the clamping insult [41]. Photoplethysmography and LDF have been compared experimentally, and LDF was found to react more quickly to vascular occlusions [3]. The reactivity of transcutaneous oxygen measurements and LDF have also been compared with regard to vascular occlusions in rabbit ear pedicle flaps. Both methods were found to react rapidly [42]. Jones [43] found that the combination of ultrasound Doppler at the time of surgery and laser Doppler postoperatively was a reliable method of monitoring free flaps.

It can be concluded that LDF is a valuable adjunct in the surveillance of free flaps, but flow results may be misinterpreted [35], and superficial skin-flap blood flow is influenced by several other factors than the total blood flow through the pedicle. The most important of these factors is perhaps the surface temperature, which has been found to correlate better with the LDF values than with the total flap blood flow [1]. This has recently led to a modification of the free-flap monitoring technique. An LDF heat-load test has been designed and studied in a series of pig island flaps. During heat load, LDF increased by between 1/3 and 4 times the baseline flow value in all flaps with an intact pedicle blood supply. However, shortly after arterial or venous occlusion, no LDF response was noted. With this modified monitoring technique, it has been possible to distinguish a vascular occlusion with nearly 100% accuracy [44].

Replantations

The success in replantation surgery in the 1960s [45–47] was followed by rapid clinical developments. Today, replantation of amputated parts has become clinical routine in most major plastic surgery centers. Digital re-

plantation in particular is now an established procedure, and success rates between 80% and 90% are reported in clinical surveys. In replantation surgery, postoperative thrombosis at the microvascular anastomosis is more frequent than in elective free-flap surgery. Salvage of the amputated part is possible only with prompt reoperation, which necessitates early detection of the vascular thrombosis. Because of difficulties in clinical assessment, many surveillance systems have been suggested.

Replant monitoring with LDF has been found to be useful, but only limited experiences have been published [15]. Clinically rapid and pronounced flow reductions were seen after arterial thrombosis in a finger replant. In experiments, LDF has also been found to be a reliable parameter in the diagnosis of rejection of allogenic leg transplants in rats. LDF was more accurate in this prediction than analyses of peripheral blood gases, glucose, and lactate levels [48]. It was not possible to use LDF as a predictor of the initial onset of rejection, however.

Burns

The classification of burns has always aroused great interest among burn surgeons, because the diagnosis of burn depth is the guide to the appropriate therapy and prognosis. Growing evidence supports the notion that early excision (3–5 days after the burn) and skin grafting of certain deep burns may increase the survival rate and improve the esthetic and functional results [49]. In this treatment, early and accurate judgment of burn depth is of paramount importance. Inaccurate judgment of burn depth can obviously result in unnecessary and disfiguring surgery of spontaneously healing wounds or delayed surgical intervention that might otherwise have improved the final outcome. The most widely used method to judge burn depth is clinical evaluation of the wound. The cornerstone in this examination is the clinical wound appearance, capillary refill, and preservation of loss of sensation. It is a well-known fact, however, that the clinical assessment of burn depth, especially in the early period after the burn, can be difficult even for the experienced examiner. The accuracy rate of clinical evaluation can be as low as 64% [50]. Thus methods that could measure burn depth with a high degree of accuracy would be of great value. Several methods have been suggested for this purpose: radioisotope clearance, thermography, dye injection, and histological examination. None of many methods has gained widespread clinical use, however.

Burn wound assessment with the LDF technique was described in 1984 [51]. A close relationship was found between LDF values during a heat load of 44°C and the depth of the burn. The vasodilatory capacity of superficial wounds was preserved, whereas deeper burns did not respond to the heat. In a second study by the same group [52], the heat-load test was used to judge burn depth, and a comparison with histological examination showed a high degree of accuracy (92%). No surgical procedures were performed until two

weeks after injury, when the results could be verified by the clinical outcome.

Taking account of the fact that burn wounds are dynamic in the sense that burn depth can change during the first few days, Green et al. [53] adopted another LDF methodology to investigate these wounds. LDF monitoring was performed twice daily for the first three days after the injury. Spontaneously healing, i.e., superficial, wounds showed an increasing blood flow during the first few days, whereas perfusion did not change in deeper nonhealing wounds. A theoretical problem with this method might be the spatial blood flow variability in adjacent skin areas, which is likely to influence intermittent recordings even under normal conditions. This variability was not reported to be a problem with these burn wounds, nor were variable environmental conditions, such as room temperture. Burn depth, expressed as the length of heat exposure, and the LDF reductions were closely correlated in animal studies [53].

A high risk of vascular compromise in the hands or feet is known to exist after circumferential extremity burns. The laser-Doppler technique has been used experimentally to evalauate the accuracy of pulse oximeters in diagnosing upper-extremity ischemia after these types of burns [54]. A close relationship was found between LDF and pulse oximetry, and the decision when to perform escharotomy was facilitated.

In animal experiments, LDF has also been used to follow the circulatory changes after burns. In mouse ears, significant blood flow reductions were seen as soon as 15 minutes after a deep burn. This initial fall was followed by a further flow reduction during the two-hour observation period [55]. Vital microscopy at two hours confirmed that blood flow had ceased.

With the knowledge that clinical assessments of burn depth may have a failure rate of more than 35% and that LDF estimations of burns have had failure rates as low as 8%, it is reasonable to assume that LDF can be a valuable adjunct in the assessment of burn depth. However, several problems will have to be overcome in order to make LDF a valuable tool for the burn clinician, one being the limited measuring area of the LDF probe (1 mm). Such fine resolution cannot provide a representative assessment of the large surfaces that have to be examined in a burn patient. Another factor that has to be assessed is whether reported results are valid in all body areas. It is not unlikely that the thin facial skin may react differently from thick-skinned areas such as the back.

Other clinical applications

The therapy of *chronic ulcers*, especially in the lower leg, can be a difficult problem. Plastic surgeons frequently treat these kinds of wounds with débridement and skin grafting, but before a split skin graft can be applied safely and successfully, the wounds have to be clean and covered with healthy and well-perfused granulation tissue over their whole surface. It is very difficult to make objective assessments of the effectiveness of different wound dres-

sings. Circulatory monitoring devices may aid in making objective assessments of how effective different therapies are in getting a wound clean enough for skin grafting. Effects of other therapies, such as pharmacological treatments, on skin wounds may also be assessed more objectively. Irrigation treatment is indisputably a reliable way of treating wound cavities; with respect to chronic leg ulcers, this type of therapy is fairly new. The treatment has been documented to be more effective than conventional wound dressings, however [56]. The effectiveness was also confirmed by a significantly increased wound blood flow measured by LDF. LDF measurements may be a valuable adjunct in the efforts to make more objective assessments of different wound-healing therapies. *Pressure sores* are another frequently treated type of wound in plastic surgery units. One very important aspect of this therapy is to avoid recurrences. Because circulatory impairment in the pressure area is regarded as a decisive predisposing etiological factor, circulatory monitoring devices may help in objectively evaluating these matters.

With the aid of LDF, the effect of pressure-relieving dressings on local tissue ischemia has been investigated [57]. The patients were resting on a specially manufactured polyacrylate mold through which LDF readings in the pressure area were obtained. LDF has also been used to evaluate the blood flow reactions in patients at high risk for the development of pressure sores [58]. The high-risk group, especially individuals over 60 years of age, showed a poor response to a heat stimulus, a reaction that was suggested to be a possible feature in patients at risk for the development of pressure sores.

These investigations have addressed only a small area of the pressure-sore complex. In the most important group that develops these ulcers, the paraplegics and tetraplegics, little is known today about vasoreactivity, the effect of pressure relief on blood flow or other factors. It is possible that the loss of sensory innervation with depletion of sensory neuropeptides plays an important part in the development of pressure ulcers. These factors are largely unknown and open up new fields of investigation in which LDF may be a helpful tool.

Other experimental investigations

Relationship between total and microcirculatory flap blood flow

Attempts have been made to quantify LDF values in skin flaps during extracorporeal perfusion. Fair correlations with total blood flow (0.63–0.66) were noted in each flap with the flow probe at the same location [59], but it was not possible to quantify the LDF values. During natural perfusion and stepwise arterial occlusion, a high degree of correlation (0.91–0.96) also exists between LDF and total flap blood flow as measured by electromagnetic flowmetry (EMF) [38]. These measurements were also performed on single sites in each individual flap. We have also investigated the correlation between total island flap blood flow and LDF [60] in pigs. Flap manipulations

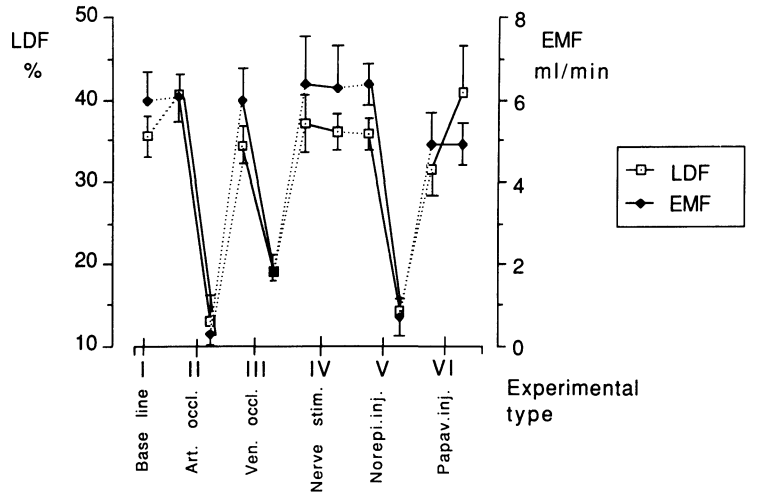

Figure 10–9. Mean variations in LDF (±SEM) and total flap blood flow measured with electromagnetic flowmetry (EMF) during different manipulations of the blood flow in island flaps of the pig. (Reprinted with permission from [60].)

were done to mimic anastomotic complications in a free flap and to produce pronounced changes in flap blood flow. During arterial or venous occlusion or after norephinephrine injection, both LDF and EMF showed highly significant and equally rapid reactions (figures 10–9 and 10–10). However, under stable flow conditions, independent paired observations from different flaps showed poor correlations between LDF and EMF (r ranging between 0.79 and −0.12). Variations in LDF values with time (temporal variability), not coinciding with EMF variations, were seen and may, together with the spatial variability, explain these results.

It is concluded that LDF has a high correlation with the total flap blood flow only if the measurements are made in the same animal and at the same site. It has further been noted that LDF values from independent observations in different flaps showed a better correlation with the surface temperature than with the total flap blood flow as measured by EMF or total venous outflow [1,61].

Events after skin flap elevation

Many suggestions regarding the nature of blood flow reduction after flap elevation have been put forward in the literature. Investigation of the circulatory and metabolic events after elevation of island skin flaps have revealed significant reductions of LDF, total venous outflow (VO), and flap temperatures immediately after flap elevation [61]. Within one hour, total flap blood flow (VO) had returned to preoperative levels, while LDF in the skin surface

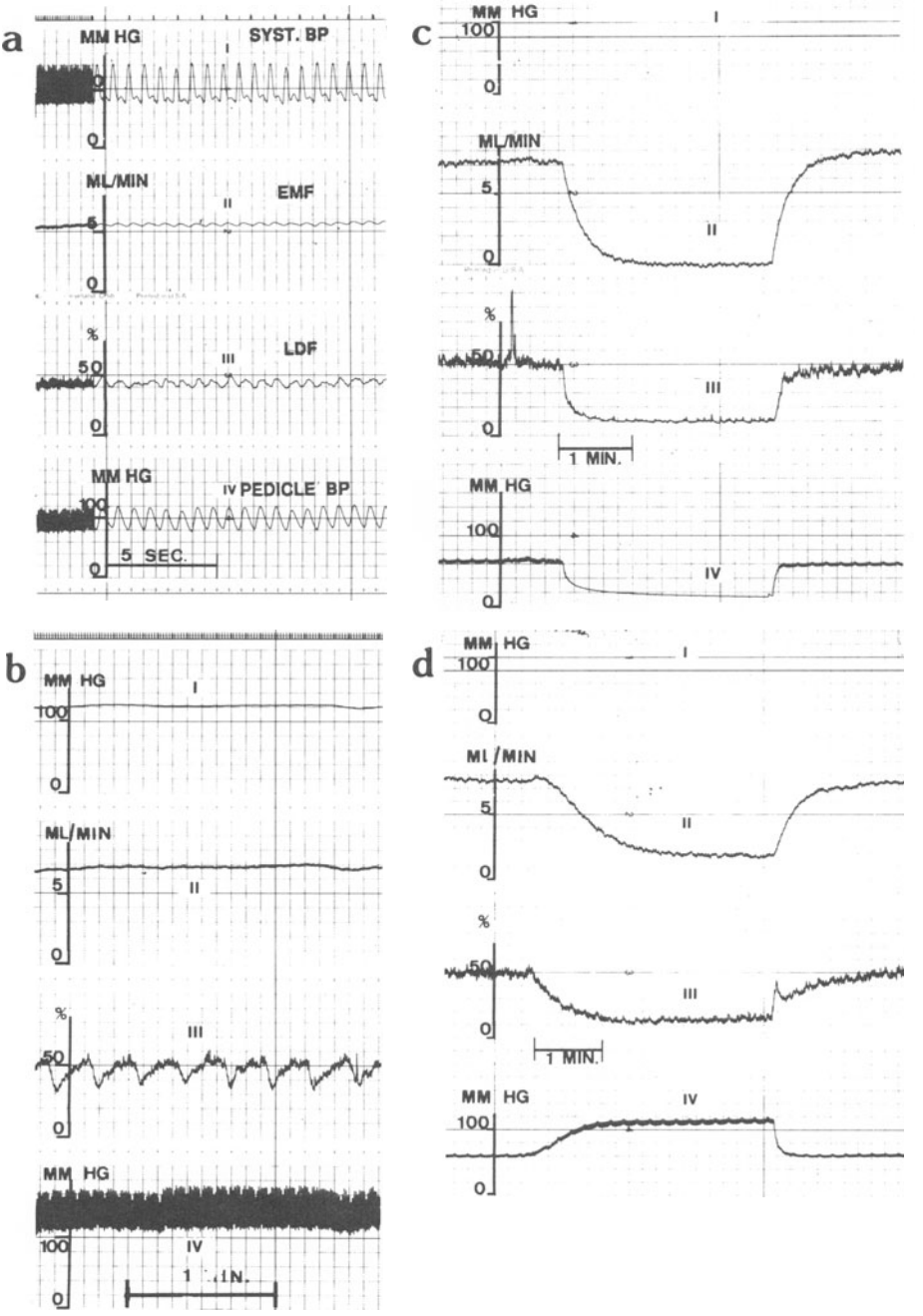

Figure 10–10. Recordings of LDF from the skin surface of pig island flaps and simultaneous measurement of total flap blood flow with electromagnetic flowmetry (EMF).

a. LDF (III) and EMF (ii) variations synchronous with pulse in the systemic blood pressure (I) and pedicle blood pressure (IV).

b. Regular rhythmical variations in LDF (III) not coinciding with EMF (II), systemic blood pressure (I), or pedicle blood pressure (IV).

c. Recordings during complete arterial occlusion.

d. Recordings during total venous occlusion.

(Reprinted with permission from [60].)

continued for four hours to be lower than before flap elevation (figure 10–11a,b,c). There was a significant correlation between LDF and skin-flap temperature throughout the experiments; part of the blood flow reduction after flap construction may have been due to primary hypothermia. In that study [61], norepinephrine (NE) was released into the circulation, and a significant level was noted as soon as four hours after flap elevation. The degenerative release of NE may lead to a reduced blood flow and thus may be deleterious to the survival of randomly supplied areas of the flaps [19,62]. However, at the time of NE release, no blood flow reduction was noted [61].

Events in island flap after arterial or venous occlusion

After one hour of arterial or venous flap occlusion, clear-cut metabolic derangements have been noted, but no significant differences in the magnitude of these changes were seen when venous and arterial occlusions were compared [63]. However, an unexpectedly long-lasting reduction in flap blood flow was seen after venous occlusion, a finding not noted after arterial occlusion (figure 10–12a,b). Both LDF and total flap blood flow showed clear-cut reductions after venous occlusions, and compared to the situation after arterial occlusion, LDF was still reduced one hour after the revascularization. Clinical impressions and experimental results indicate that venous occlusion is more deleterious to the flap than arterial occlusion [64,65]. The striking differences in blood flow noted after arterial and venous occlusion support this view. A more restricted microcirculatory bed after venous occlusion, perhaps due to microthrombotization or swelling of the tissue, may explain these results.

Investigation of pharmacological flap manipulation

Numerous investigations have used different pharmacological treatments in attempts to increase the surviving length of pedicle flaps and, more recently, to increase the ability of island flaps to withstand complete and prolonged ischemia. The final flap survival is the confirmation of the success or failure of the therapy, but the effect of the drugs on the flap blood flow is also of central interest. To date, few skin flap research efforts have been devoted to investigations of the microvascular effects of different drugs, but recently this aspect of pharmacological flap studies has attracted more attention. It has been recognized that a knowledge of the microcirculatory effects of different drugs is an invaluable factor in the evaluation of drug effects and mechanisms of action. Xenon clearance techniques have previously been employed to study flap circulation in these situations [66], but since this method cannot capture the dynamics of blood flow, LDF measurements have recently been suggested [60,67].

The effect of dimethyl sulfoxide (DMSO) on skin-flap survival has not been without contradictions. In an effort to clarify these opposing results, the effect on skin-flap blood flow have been studied by LDF and fluorometry [9].

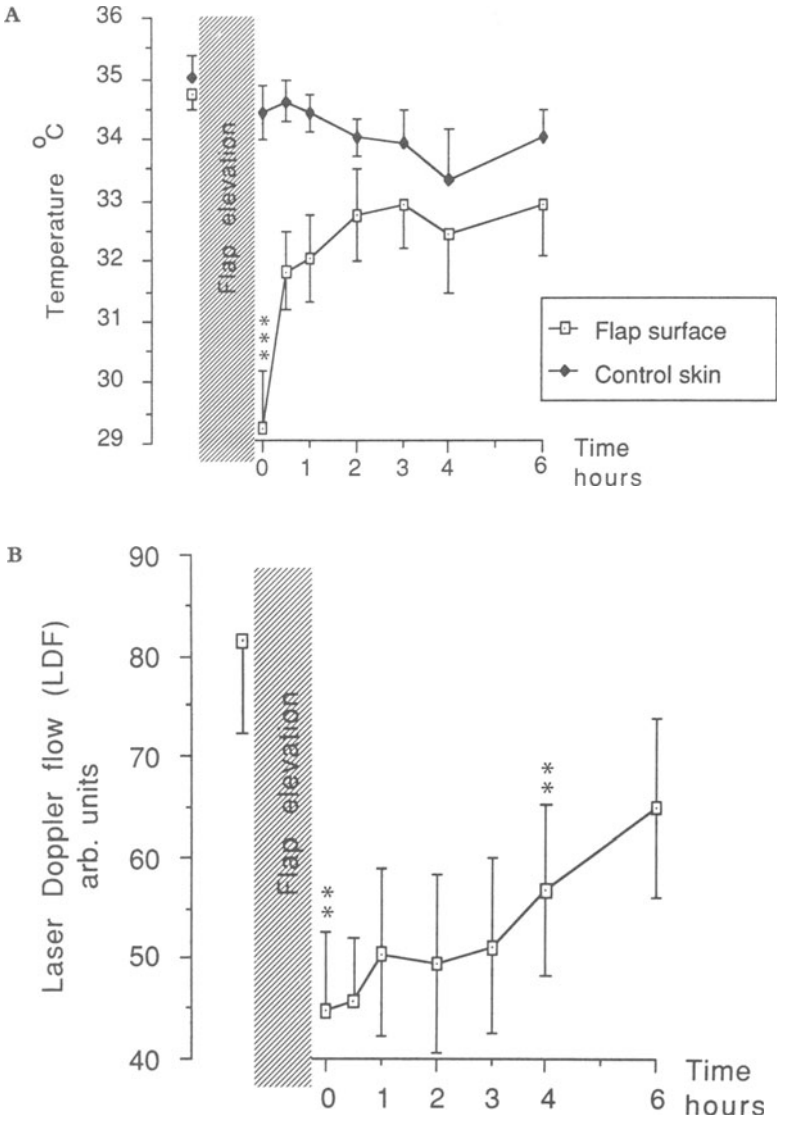

Figure 10–11. Recordings before and 0 to 6 hours after elevation of island buttock flap in pigs. Stars indicate significant differences compared to values before flap elevation. ($p < 0.01$ = **; $p \leq 0.001$ = ***)

A. Temperatures in flap and adjacent control skin (°C ± SE).

B. Laser-Doppler flow (arbitrary units; Mean ± SE) from the surface of the buttock flap.

C. Venous outflow (ml/min; Mean ± SE) from the buttock flap.

(Reprinted with permission from [61].)

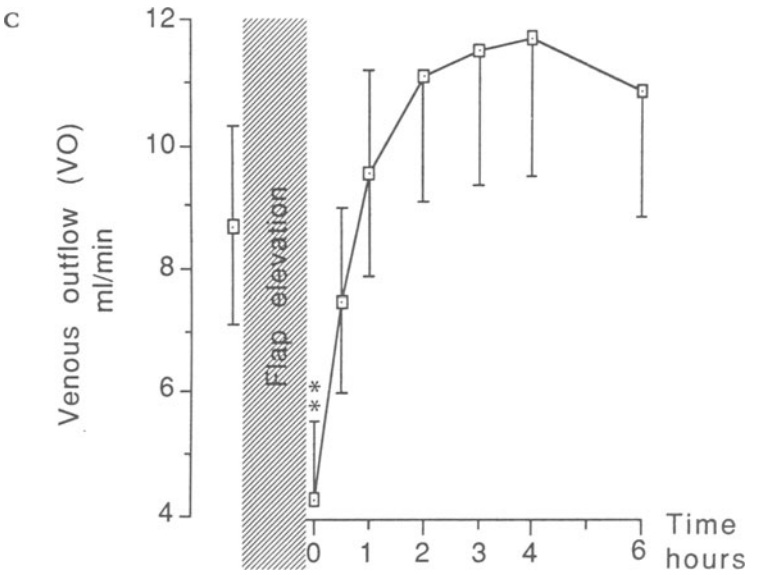

Figure 10–11. (continued)

Both the flap survival and blood flow increased after DMSO treatment, and LDF was found to be a more sensitive method for measuring this blood flow increase than fluorometry.

LDF measurements have been employed to confirm that the well-known and potent vasodilator and platelet disaggregator derived from arachidonic acid, prostacyclin, exerts pronounced vasodilatory effects on rabbit island flaps. However, thromboxane synthetase inhibitors failed to increase the blood flow in such flaps [67].

Calcitonin gene-related peptide (CGRP) is another extremely potent vasodilator. This neuropeptide, found in sensory neurons, prolongs the ability of island flap to withstand ischemia [68]. In another study, we also investigated the effects of CGRP treatment on island flaps blood flow. A significant increase in flap blood flow as measured by LDF was seen up to two hours after injections of CGRP. This increase was unexpectedly short considering the long duration of CGRP treatment in intact skin [69].

Flap elevation necessitates denervation and subsequent development of hypersensitivity to adrenergic stimuli. LDF has been found to be a valuable tool in the investigation of this hypersensitivity. In myocutaneous flaps, increased sensitivity to norepinephrine infusions was confirmed between two and seven days following flap elevation. Alpha blockade with phenoxybenzamine blunted the reactions to norepinephrine [70].

With the introduction of reliable and easily managed blood flow measuring

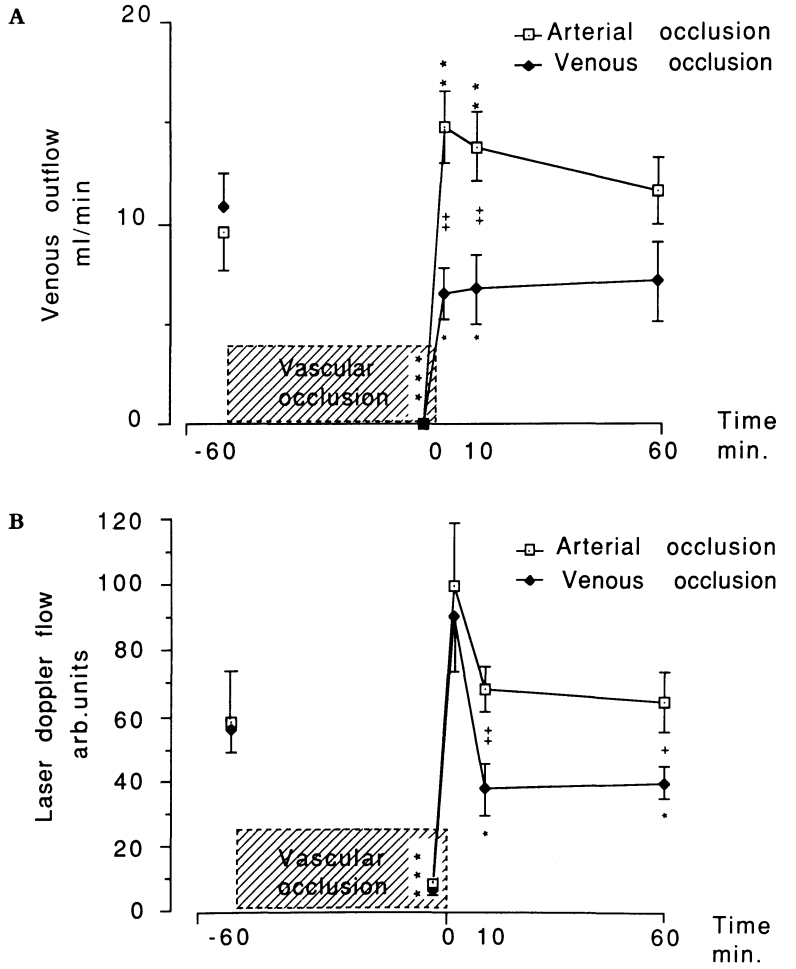

Figure 10–12. Island buttock flaps of the pig exposed to arterial or venous occlusion.

A. Total venous outflow (ml/min; Mean ± SE) from the buttock flap before and after arterial or venous occlusion. Significant differences from preocclusive values are indicated with an asterisk. Significant differences between occlusion types are indicated with a plus sign. ($p < 0.05$ = * or +; $p < 0.01$ = ** or ++; $p \leq 0.001$ = *** or +++.)

B. Laser-Doppler flow (arbitrary units; Mean ± SE) from the surface of the buttock flap before and after arterial or venous occlusion. Significant differences from preocclusive values are indicated with an asterisk. Significant differences between occlusion types are indicated with a plus sign. ($p < 0.05$ = * or +; $p < 0.01$ = ** or ++; $p \leq 0.001$ = *** or +++.) (Reprinted with permission from [63].)

equipment, such as LDF, circulatory studies may become a more frequent element in the evaluation of pharmacological flap manipulations. Undoubtably, these measurements can shed more light on these types of studies, even if the ultimate flap survival will always be a very important component of such studies.

Skin flaps and denervation

Apart from the above-cited studies of CGRP treatment and investigations of the effects of sympathetic denervation, LDF has also been employed to study other aspects of the inevitable denervation of skin flaps. Increasing evidence suggests that not only sympathetic nerves but also sensory ones play an important role in the tissue reactions following trauma. Afferent sensory nerves not only transmit information to the CNS; they are also involved in the so-called *neurogenic inflammation* produced by efferent activity [71]. Antidromic stimulation of sensory nerves releases bioactive mediators from the peripheral nerve endings [72], and this leads to vasodilation and protein extravasation [69,73]. Transcutaneous nerve stimulation (TNS) is known to exert similar effects. We have found that TNS treatment at the base of random pedicle flaps increases the flap blood flow and the LDF-estimated survival border [74]. A beneficial effect of TNS-treatment has also been confirmed in clinical cases [75]. Thus the denervation of sensory nerves after flap elevation may exert circulatory and, possibly, metabolic effects in the flap tissue.

Wound-healing studies

LDF measurements have also been suggested as a means of estimating wound slough resulting from excessive wound tension [76]. In pigs, wound-closing tensions over 250 g resulted in a high incidence of wound sloughs that was correlated with significant blood flow reductions in the distal 1/3 of the flaps.

CONCLUSIONS AND POSSIBLE FUTURE DEVELOPMENTS

A great need for reliable blood flow monitoring equipment exists in modern-day plastic and reconstructive surgery. LDF is clearly a useful addition to the large number of devices that have been described. In many centers, LDF is already a routine method for the surveillance of free flaps, and in a rapidly increasing number of experimental studies, LDF is used to follow the dynamic variations in blood flow. LDF fulfills many of the criteria that can be postulated for an ideal monitoring device, but it has some drawbacks. The small measuring area is one such disadvantage. Because of the great variations in blood flow in adjacent areas, the flow values are difficult to interpret, particularly if independent measurements from different areas are compared. However, a computer-assisted integration of flow values from multiple probes may become a reality in the future. Laser-scanning approaches may also be used to provide a blood flow mapping. Such advanced designs might

greatly increase the indications for LDF in plastic and reconstructive surgery. Many attempts to quantify the LDF values have been made, but only under special and standardized conditions is it possible to express LDF values as a quantitative measurement. Consequently, it is not likely that the LDF technique will ever become a truely quantifiable methodology. However, it is reasonable to assume that future developments will lead to improved accuracy in distinguishing vascular occlusions in flaps and replants. We may even reach a point where preprogramed pharmacological or mechanical regimes are initiated when the flow value drops below a preset value.

REFERENCES

1. Hedén, P. 1988. Monitoring techniques and animal models as guides for free flap surgery. Thesis, Karolinska Institute, Stockholm, Sweden, pp 9–43.
2. Jones, B.M. 1984. Monitors for the cutaneous microcirculation Plast Reconstr Surg 73:843–850.
3. Harrisson, D.H., M. Girling, G. Mott, and T. Eng. 1983. Methods of assessing the viability of free flap transfer during the postoperative period. Clin Plast Surg 10:21–36.
4. Sloan, G.M., and G.H. Sasaki. 1985. Noninvasive monitoring of tissue viability. Clin Plast Surg 12:185–195.
5. Hodges, P.L. 1983. Principles of flaps. Select Read Plast Surg 4:1–20.
6. Cormack, G.C., and B.G.H. Lamberty. 1986. The Arterial Anatomy of Skin Flaps, Cormack, C.G., Lamberty, B.G.H., eds. Edinburgh: Churchill & Livingstone.
7. Fujino, T. 1967. Contribution of the axial and perforator vasculature to the circulation in flaps. Plast Reconstr Surg 39:125–137.
8. McGregor, I.A., and G. Morgan. 1973. Axial and random pattern flaps Br J Plast Surg 26:202–213.
9. Haller, J., R. Trachy, and C.W. Cummings. 1987. Effect of dimethyl sulfoxide on island flap prefusion and survival in rats Arch Otolaryngol Head Neck Surg 113:859–863.
10. Hedén, P., G. Jurell, and C. Arnander. 1986. Prediction of skin flap necrosis: A comparative study between laser Doppler flowmetry and fluorescein test in a rat model. Ann Plast Surg 17:485–488.
11. Lanzafame, R.J., D.Z. Zeiler, J.O. Naim, D.W. Rogers, J.R. Hinshaw, and D. Phil. 1984. A comparison of cutaneous perfusion as determined by laser Doppler velocimetry or sodium fluorescein. Curr Surg 41:271–274.
12. Larrabee, W.R., G.D. Sutton, A. Holloway, and G. Tolentino. 1983. Laser doppler velocimetry and fluorescein dye in the prediction of skin flap viability. Arch Otolaryngol 109:454–456.
13. Marks, N.J., R.E. Trachy, and C.W. Cummings. 1984. Dynamic variations in blood flow as measured by laser Doppler velocimetry: A study in rat skin flaps. Plast Reconstr Surg 73:804–810.
14. Tenland, T. 1982. On laser Doppler flowmetry. Methods and microvascular applications. Thesis, Linköping University medical dissertation no 136. Linköping.
15. Hedén, P.G., R. Hamilton, C. Arnander, and G. Jurell. 1985. Laser Doppler surveillance of the circulation of free flaps and replanted digits. Microsurgery 6:11–19.
16. Svensson, H., and B.-A. Jönsson. 1988. Laser Doppler flowmetry during hyperaemic reactions in the skin. Int J Microcirc Clin Exp 7:87–96.
17. Reinisch, J.F. 1974. The pathophysiology of skin flap circulation: the delay phenomenon. Plast Reconstr Surg 54:585–598.
18. Liu, A.J., C.W. Cummings, and R.E. Trachy. 1986. Venous outflow obstruction in myocutaneous flaps: changes in microcirculation detected by the perfusion fluorometer and laser Doppler. Otolaryngol Head Neck Surg 94:164–168.
19. Pang, C.Y., P.C. Neligan, C.R. Forrest, T. Nakatsuka, and G.H. Sasaki. 1986. Hemodynamics and vascular sensitivity to circulating norepinephrine in normal skin and delayed and acute random skin flaps in the pig. Plast Reconstr Surg 78:75–83.

20. Kerrigan, C.L. 1983. Skin flap failure: Pathophysiology. Plast Reconstr Surg 72:766–777.
21. Tenland, T., E.G. Salerud, G.E. Nilsson, and P.Å. Öberg. 1983. Spatial and temporal variations in human skin blood flow. Int J Microcirc Clin Exp 2:81–90.
22. Gatti, J.E., D. LaRossa, D.A. Brousseau, and D.G. Silverman. 1984. Assessment of neovascularization and timing of flap division. Plast Reconstr Surg 73:396–402.
23. Cummings, C.W., R.E. Trachy, M.A. Richardson, and H.C. Pattersson. 1984. Prognostication of myocutaneous flap viability using laser Doppler velocimetry and fluorescein microfluorometry. Otolaryngol Head Neck Surg 92:559–563.
24. Cummings, C.W., and R.E. Trachy. 1986. Measurement of alternative blood flow in the porcine panniculus carnousus myocutaneous flap. Arch Otolaryngol 111:598–600.
25. Daniel, R.K., and G.I. Taylor. 1973. Distant transfer of an island flap by microvascular anastomoses. Plast Reconstr Surg 52:111–116.
26. Klingenström, P., and B. Nylen. 1966. Timing of transfer of tubed pedicles and cross flaps. Plast Reconstr Surg 37:1–12.
27. Shaw, W.W., and P.M. Parker. 1983. Patency and factors affecting the thrombosis in 400 clinical microvascular anastomoses. The Seventh Symposium of the International Society of Reconstructive Microsurgery New York, June.
28. Davies, D.M. 1982. A world survey of anticoagulation practice in clinical microvascular surgery. Br J Plast Surg 35:96–99.
29. Jones, B.M., and B.J. Mayou. 1982. The laser Doppler flowmeter for microvascular monitoring: a preliminary report. Br J Plast Surg 35:147–149.
30. Svensson, H., H. Pettersson, and P. Svedman. 1985. Laser Doppler flowmetry and laser photometry for monitoring free flaps. Scand J Plast Reconstr Surg 19:245–249.
31. Jenkins, S.D., R.S. Sepka, W.J. Barwick, D. Serafin, and B. Klitzman. 1987. Routine clinical use of laser doppler flowmeter to monitor free tissue transfer: preliminary results. J Reconstr Microsurg 3:281–283.
32. Fernando, B., V.L. Young, and S.E. Logan. 1988. Miniature implantable laser Doppler probe monitoring of free tissue transfer. Ann Plast Surg 20:434–441.
33. Schuurman, A.H., K.E. Bos, and Y.H. Van Nus. 1987. Laser Doppler bone probe in vascularized fibula transfers: a preliminary report. Microsurg 8:186–189.
34. Knight, K.R., P.A. Collopy, and B.M. O'Brien. 1987. Correlation of viability and laser Doppler flowmetry in ischemic flaps. J Surg Res 43:444–451.
35. Walkinshaw, M., A. Holloway, A. Bulkley, and L.H. Engrav. 1987. Clinical evaluation of laser Doppler blood flow measurements in free flaps. Ann Plast Surg 18:212–217.
36. Bruce-Chwatt, A.J. 1986. Free flap monitoring using a microcomputer linked to a laser Doppler flowmeter. Br J Plast Surg 39:229–238.
37. Fisher, J.C., P.M. Parker, and W.W. Shaw. 1983. Comparison of two laser doppler flowmeters for the monitoring of dermal blood flow. Microsurgery 4:164–170.
38. Svensson, H., P. Svedman, J. Holmberg, and J.B. Wieslander. 1985. Detecting changes of arterial and venous blood flow in flaps. Ann Plast Surg 15:35–40.
39. Fisher, J.C., P.M. Parker and W.W. Shaw. 1986. Waveform analysis applied to laser Doppler flowmetry. Microsurgery 7:67–71.
40. Silverman, D.G., D.D. LaRossa, C.H. Barlow, T.G. Bering, L.M. Popky, and T.C. Smith. 1980. Quantification of tissue fluorescein delivery and prediction of flap viability with the fiberoptic dermofluorometer. Plast Reconstr Surg 66:545–553.
41. Silverman, D.G., B.S. Weinstock, D.A. Brousseau, K.J. Norton, S.A. Knifin, and G. Smith. 1985. Comparative assessment of blood flow to canine island flaps. Arch Otolaryngol 11:677–681.
42. Pietilä, J.P., K. von Smitten, and B. Sundell. 1987. The rabbit ear pedicle flap. Scand J Plast Reconstr Surg 21:145–147.
43. Jones, B.M. 1985. Predicting the fate of free tissue transfers. Ann R Coll Surg Engl 67:63–70.
44. Hedén, P., and C. Arnander. The heat load test in laser Doppler surrveillance of free flaps. Scand J Plast Reconst Surg, in Press.
45. Malt, R.A., and C.F. McKhann. 1964. Replantation of severed arms. JAMA 189:716–722.
46. Kleinert, H.E., and M.L. Kasdan. 1963. Salvage of devascularized upper extremities including studies on small vessel anastomoses. Clin Orthop 29:29–38.
47. Komatsu, S., and S. Tamai. 1968. Successful replantation of a completely cut off thumb: case report. Plast Reconstr Surg 42:374–377.

48. Hovius, S.E.R., L.N.A. van Adrichem, P.M.A. Heijden, V.D. Vuzevski, R. van Strik, and J.C. van der Meulen. Postoperative monitoring in allogenic limb transplantation in rats. Ann Plast Surg, in press.
49. Sorensen, B. 1979. Acute excision or exposure treatment. Results of a randomized controlled clinical trial. Scand J Plast Reconstr Surg 13:115–118.
50. Heimbach, D.M., M.A. Afromowitz, L.H. Engrav, J.A. Marvin, and B. Perry. 1984. Burn depth estimation–man or machine. J Trauma 24:373–378.
51. Micheels, J., B. Alsbjörn, and B. Sorensen. 1984. Clinical use of laser Doppler flowmetry in a burns unit. Scand J Plast Reconstr Surg 18:65–73.
52. Alsbjörn, B., J. Micheels, and B. Sorensen. 1984. Laser Doppler flowmetry measurements of superficial dermal, deep dermal and subdermal burns. Scand J Plast Reconstr Surg 18:75–79.
53. Green, M., A. Holloway, and D.M. Heimbach. 1988. Laser Doppler monitoring of microcirculatory changes in acute burn wounds. J Burn Care Rehabil 9:57–62.
54. Bardakjian, V.B., J.G. Kenny, M.T. Edgerton, and R.F. Morgan. 1988. Pulse oximetry for vascular monitoring in burned upper extremities. J Burn Care Rehabil 9:63–65.
55. Blomgren, I., and U. Bagge. 1984. Postburn blood flow, edema, and survival of the hairy mouse ear after scald injury at different temperatures. Scand J Plast Reconstr Surg 18:269–275.
56. Svedman, P. 1983. Irrigation treatment of leg ulcers. Lancet 2:532–534.
57. Karlsmark, T., and J.K. Kristensen. 1987. A method for testing the effect of pressure-relieving materials in the prevention of pressure ulcers. Acta Derm Venereol 67:260–263.
relieving materials in the prevention of pressure ulcers. Acta Derm Venereol 67:260–263.
58. Ek, A.C., D.H. Lewis, H. Zetterquist, and P.G. Svensson. 1984. Skin blood flow in an area at risk for pressure sore. Scand J Rehab Med 16:85–89.
59. Fisher, J.C., P.M. Parker, and W.W. Shaw. 1985. Laser Doppler flowmeter measurements of skin perfusion changes associated with arterial and venous compromise in the cutaneous island flap. Microsurg 6:238–243.
60. Hedén, P., and E. Eriksson. 1989. Skin flap circulation. Simultaneous monitoring with laser Doppler and electromagnetic flowmeters in the pig island buttock flap. Scand J Plast Reconst Surg, 23:1–9.
61. Hedén, P., A. Sollevi, and B. Hamberger. 1989. Early circulatory and metabolic events in island skin flaps of the pig. Plast Reconst Surg. 84:468–473.
62. Jurell, G. 1981. Adrenergic nerves and skin flap survival. Thesis, Karolinska Institute, Stockholm.
63. Hedén, P., and A. Sollevi. 1989. Circulatory and metabolic events in pig island skin flaps after arterial or venous occlusion. Plast Reconstr Surg 84:475–480.
64. Su, C.-T., M.J. Im, and J.E. Hoopes. 1982. Tissue glucose and lactate following vascular occlusion in island skin flaps. Plast Reconstr Surg 70:202–205.
65. Hanashina, T., Y. Sawada, and S. Watanabe. 1977. The relationship between venous occlusion time in island flaps and flap survival. Plast Reconstr Surg 60:92–95.
66. Hendel, P.M., D.L. Lilien, and H.J. Bunche. 1983. A study of the pharmacological control of blood to acute flaps using xenon washout (Part 1). Plast Reconstr Surg 71:387–398.
67. Knight, K.P., P.A. Collopy, and B.M. O'Brien. 1986. Response of the rabbit cutaneous microvasculation to prostanoid modifiers as determined by laser Doppler flowmetry. Microvasc Res 31:197–202.
68. Westin, M., and P. Hedén. 1988. Calcitonin gene related peptide delays the no reflow phenomena in the rat island flap. Ann Plast Surg 21:329–334.
69. Brain, S.D., T.J. Williams, J.R. Tippins, H.R. Morris, and I. MacIntyre. 1985. Calcitonin gene related peptide is a potent vasodilator. Nature 313:54–56.
70. Moor, B.K., R.E. Trachy, and C.W. Cummings. 1986. The effect of alpha-adrenergic stimulation and bockade on perfusion of myocutaneous flaps. Otolaryngol Head Neck Surg 94:489–496.
71. Pernow, B. 1985. Role of tachykinins in neurogenic inflammation. J Immunol 135:812–815.
72. Lembeck, F., and P. Holzer. 1979. Substance P as neurogenic mediator of antidromic vasodilation and neurogenic plasma extravasation. Naunyn-Schmiedeberg's Arch Pharmacol 310:175–183, 1979.
73. Saria, A., J.M. Lundberg, G. Skofitsch, and F. Lembeck. 1983. Vascular protein leakage in

various tissues induced by substance P, capsaicin, bradykinin, serotonin, histamine and by antigen challange. Naunyn-Schmeideberg's Arch Pharmacol 324:212–218.
74. Kjartansson, J., T. Lundeberg, U.E. Samuelson, and C.J. Dalsgaard. 1989. Transcutaneous nerve stimulation (TENS) increases survival of ischemic musculocutaneous flaps. Acta Physiol Scand 134:95–99.
75. Kjartansson, J., T. Lundeberg, U.E. Samuelsoon, C.J. Dalsgaard, and P. Hedén. 1988. Calcitonin gene-related peptide (CGRP) and transcutaneous electrical nerve stimulation (TENS) increases cutaneous blood flow in the dorsal musculocutaneous flap in the rat. Acta Physiol Scand 134:89–94.
76. Larrabee, W.E., G.A. Holloway, R.E. Trachy, and D. Sutton. 1982. Skin flap tension and wound slough: correlation with laser Doppler flowmetry. Otolaryngol Head Neck Surg 90:185–187.

11. PERIPHERAL VASCULAR DISEASES

BENGT FAGRELL

The major symptoms in patients with peripheral arterial occlusive disease (PAOD) are claudication, rest pain, and skin necrosis or gangrene. In these patients the arterial circulation of the limb can be evaluated by a number of different methods, e.g., plethysmography, arterial pressure measurements, and Doppler ultrasound techniques. All these methods are very useful in clinical practice for evaluating the degree and location of an arterial obliteration. However, the local microcirculation of the tissue at risk of ischemia cannot be evaluated by these macrocirculatory methods [1]. For this purpose other techniques, e.g., skin temperature measurements, Xenon clearance, and transcutaneous pO_2 measurements, have been used. Although these methods have also been found to be clinically valuable, most of them are very tedious to use, and they react very slowly to changes in blood flow. Because of their limited frequency response, the normal, rather fast spontaneous fluctuations in tissue blood flow cannot be recorded. Moreover, these methods give only indirect indications of what is happening in the microcirculation of the tissue studied and cannot be used for evaluating the dynamics of the blood flow in the region. New techniques have been introduced during the past decade for studying the skin's microcirculation in clinical practice [1]. One such method is laser-Doppler flowmetry (LDF). The present chapter will deal with the use of LDF for evaluating the tissue microcirculation in patients with peripheral vascular disorders.

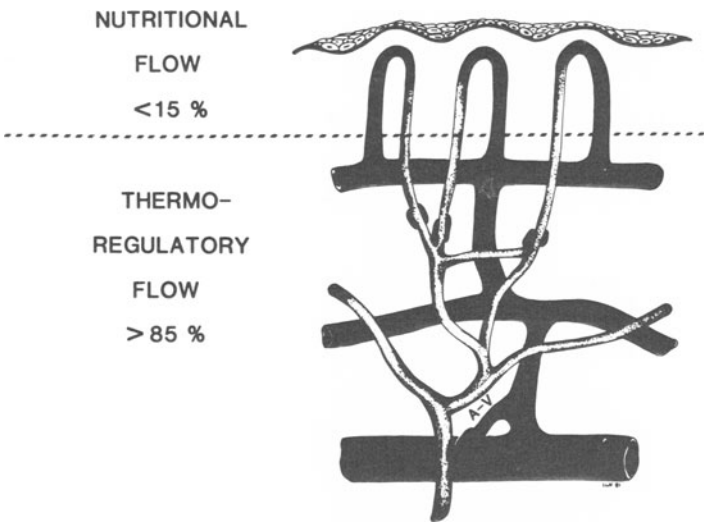

Figure 11–1. Schematic drawing of the human skin microcirculation. Only a small portion of the blood goes through the nutritional, papillary capillaries of the skin. Most of the blood bypasses these capillaries, and enters directly from small arteries and arterioles through the sometimes numerous arterio-venous anastomoses (A-V) into the venous plexuses of the skin.

SKIN MICROCIRCULATION IN HUMANS

The structure of the vascular bed of the skin varies considerably from one area to another in the human body (figure 11–1). In most areas, blood enters the skin through small arteries penetrating the subcutaneous tissue obliquely to the skin surface. One small artery most often branches into several precapillary arterioles (30–80 μm), which pass through one to three layers of venous plexuses that are parallel to the skin surface. The arterioles may divide into as many as ten terminal capillary loops, one to three of which are located in every skin papilla [1].

The main purpose of the skin microcirculation in humans is to regulate the body temperature, and marked variations in the skin flow are necessary to accomplish that function. Only a very small portion of the blood entering the skin is required to meet its metabolic need. The relative distribution of blood between the nonnutritional, thermoregulatory vascular bed and the nutritional papillary capillaries also differs markedly from one area to another. For example, in fingers and toes, more than 90% of the blood flows only through the subpapillary vascular bed, and 10% or less flows through the nutritional capillaries (figure 11–1).

During cold exposure, microcirculatory flow in skin may be extremely low, and it increases successively with skin temperature. A sudden and rather abrupt increase is seen at a temperature of around 31–32°C [1]. The flow in

some areas can vary by a factor of 100–200. These marked variations in skin flow are possible because of the numerous arterio-venous anastomoses, or A-V shunts, that allow the blood to be shunted directly from the small arteries and arterioles into the numerous subpapillary veins and venules (figure 11–1). By this unique arrangement, the temperature regulation of the body may be fulfilled with only a very limited change of blood flow in the nutritional skin capillaries [1]. Other aspects of the physiological control of the cutaneous circulation are covered in chapter 8.

LASER-DOPPLER (LD) MEASUREMENTS OF THE SKIN

Problems of evaluating the LD signal

Signal composition

During the past few years, the LDF technique has been very popular for evaluating the skin microcirculation in humans. In spite of its popularity, it is still uncertain what actually generates the signal recorded from the skin. All moving objects of a certain structure within the measuring volume are recorded, and in the skin of healthy subjects most of the signal is made up by the movement of red blood cells. However, during pathological conditions, e.g., in patients with leukemia or thrombocythemia, a portion of the signal could possibly be produced also by the movements of white cells and platelets, respectively. Consequently, in order to be accurate, it can only be stated that the major part of the signal is produced by the movements of all blood cells in the vascular bed of the measuring volume.

Penetration depth and measuring volume

The penetration depth has been said to be approximately 1.5 mm, but this value cannot be fixed since it must vary with factors like the amount of blood and the composition of the skin in the region investigated. Also, the measuring volume must change with these factors. Consequently, a quantification of flow in $ml \cdot min^{-1} \cdot 100g^{-1}$ can be obtained only if certain specific conditions are fulfilled [1,2], which is not the case for the human skin.

Instrumental and biological zero values

According to the instructions of the manufacturer, the zero value for the instrument is obtained by applying the flow probe to a white surface (Periflux user's handbook). This zero value has been found to be reasonably stable and can be referred to as the *instrument zero*. However, it cannot be used as a zero value for a biological tissue, since marked variations in this value, i.e., the *biological zero*, can be seen from one tissue, and from one area to another. Recently, Caspary et al. [3] reported that significant signals were recorded also from meat slices and the foot skin of deceased patients who had died 8 to 24 hours before the investigation. The signals achieved were also markedly increased by heating the skin surface to 37°C. The zero value during an

arterial occlusion in healthy volunteers and patients with peripheral arterial obliterative diseases (PAOD) varied from 15% to 45% of the resting flux value recorded before application of the arterial occlusion. The highest zero values during occlusion were recorded in patients with moderate PAOD. Consequently, the random portion of the signal became more significant in areas with diminished blood flow. Similar results have also been noticed when external pressure is applied to the skin area where the LD signal is recorded [4,5]. Therefore, it is of utmost importance to record the biological zero value when the LD technique is used in clinical practice. This is especially so when dynamic parameters, such as flow values during postocclusive reactive hyperemia, are used in the calculations. The biological zero values should therefore always be subtracted from the values recorded.

LDF IN PATIENTS WITH PAOD

The skin circulation in patients with PAOD has not been extensively studied with the LDF technique. However, during the last few years, several studies have been performed in patients with PAOD [6–13]. The designs of these studies have all been different. The location of the LD probe has varied from one study to another. It is therefore difficult to get a specific conception regarding the validity of the technique for evaluating the skin microcirculation in patients with PAOD. In the following sections, the different monitored variables will be presented, and their validity for evaluating changes in skin microcirculation in different degrees of obstructive arterial disease will be discussed.

Laser-Doppler resting flux value (rLDF)

Supine position: As already mentioned, the rLDF shows marked spatial and temporal variations. Therefore, it is not surprising that this value has been useless for discriminating between healthy subjects and patients with PAOD [6–8]. In the studies in which rLDF has been recorded in both healthy subjects and patients with PAOD, significant differences have been found between the groups, but the overlap has been considerable [6–8,12,13]. Patients with moderate PAOD can even have significantly *higher* rLDF than healthy subjects. Not even with the multifiber probe described in chapter 8 could these two groups be distinguished (figure 11–2). Furthermore, no difference between young and elderly healthy subjects could be seen. Only when the LD signal was measured at the toe pulp was a significantly lower value recorded in patients with critical ischemia [8].

Sitting position: The reaction to leg dependency has also been tested, and in most healthy subjects rLDF decreased on dependency, most probably due to the so-called venivasomotor reflex [6,11,13]. Most patients with PAOD also react to dependency with a decrease of rLDF, but some patients increase their rLDF values [6,12,13]. In one study, the reaction of rLDF to elevation of the

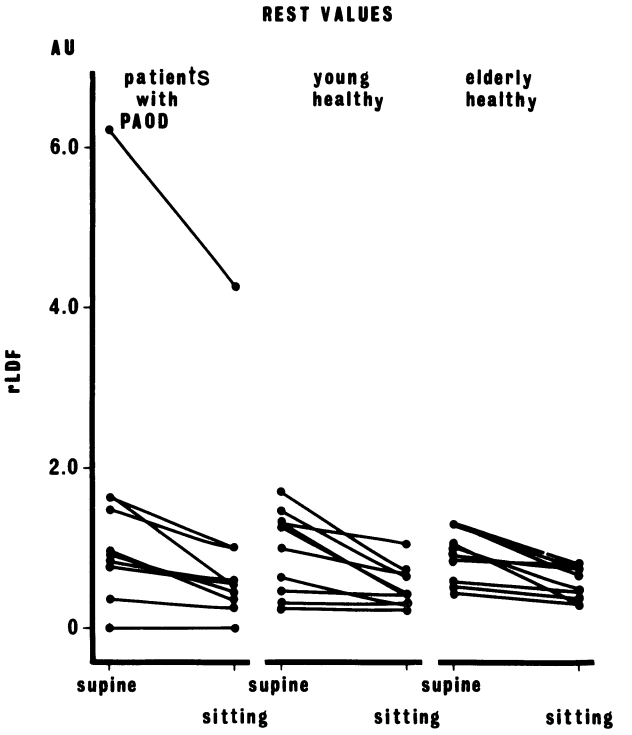

Figure 11–2. Resting LD flux values (rLDF) in young (27–49 years old) and elderly (52–84 years old) healthy subjects, and patients with PAOD (42–78 years old). All investigations were performed in both the supine and sitting position. No discrimination was possible between the healthy subjects and patients with PAOD.

leg 40 cm above heart level was also tested [6]. In this position the rLDF was unchanged or even increased in both patients and healthy subjects, and no difference between the two groups could be seen [1,6]. However, when the skin was heated to 37°C, the reaction of rLDF was significantly impaired in the patients with PAOD.

Reproducibility: The reproducibility of the rLDF values was tested by Creutzig et al. [6] in their patients with POAD, and was found to be very poor. Marked fluctuations from one day to another could be seen within the same area. Mild heating (37°C) of the test area improved the reproducibility.

Conclusion: All studies have shown that the rLDF value is essentially the same in normal subjects and patients with mild to moderate PAOD, i.e., intermittent claudication. Only in patients with critical ischemia has the rLDF been found to be significantly decreased if measured in the big toe [8].

Postocclusive reactive hyperemia (PRH)

One of the most well-known tests in clinical practice for evaluating the functional aspects of the arterial blood flow in a limb is the reactive hyperemic response to a certain period of arterial occlusion. Most such studies have dealt with blood flow in the calf muscle. Very few have examined the response of the skin circulation to such a procedure. However, the laser-Doppler instrument has already been used in several studies for this purpose [5–7,9,10,12–14].

Some pioneering work was done in 1983 by Tooke et al., who reported the PRH response in fingers of healthy controls after occlusions of 15–60 seconds [15]. In 1986, Wilkin reported the reaction of the LDF signal in the forearm of ten healthy subjects before, during, and after a brachial arterial occlusion of six minutes duration [16]. This study was performed mainly to demonstrate the marked rhythmic oscillations that can be seen in the skin during PRH.

The first and largest laser-Doppler study of the PRH response of the skin microcirculation in patients with PAOD was presented by del Guercio et al. in 1986 [7]. They investigated 40 lower limbs of 23 patients with symptoms of intermittent claudication, and 30 limbs of 15 healthy control subjects. The investigation was performed with the patient in the supine position before and after a three-minute arterial occlusion with a cuff applied both around the upper segment of the thigh and around the ankle. The LD signal was recorded from the pulp of the hallux. Since then, several other studies have been performed in which the PRH response was investigated in patients with PAOD [6,9,10,12–14]. In the study by Kvernebo et al. [10], the cuff was placed at three different levels: at the ankle, below the knee, and above the knee. Creutzig et al. [6,17] had it located at the calf level, and Östergren et al. [13] only at the ankle level. Several different variables were investigated in these studies. The terms used to describe these variables are defined and summarized in table 11–1 and figure 11–3.

PRH with cuff at ankle level: The peak flow values are significantly lower in patients with claudication compared to healthy subjects, but the overlap is almost complete between the groups [7,9,13]. The time to peak flux is significantly longer in patients with PAOD, but the overlap is also marked here [7,9]. The same results could be seen in half-time of hyperemia and time of hyperemia [7]. As can be seen in figure 11–3, the time to peak value can sometimes be hard to evaluate because of marked oscillations in flow during the reactive hyperemic response. Because of this, Östergren et al. [18] studied the time to the second peak, which most often also was the highest. The time to reach this peak was >30 seconds in all patients with PAOD and ≤30 seconds in healthy controls when measured in the supine position (figure 11–4). In the sitting position, the time to second peak was longer in all

Table 11–1 The various parameters used for LD evaluation of skin circulation during postocclusive reactive hyperemia (PRH) in patients with PAOD

Parameter	Definition
rLDF	Resting LD flux value
pLDF	Highest LD value after occlusion, peak flow
tpLDF	Time to peak flow
Time of latency, or FRT	Time after occlusion until start of hyperemic response " " " " " " " "
Time of recovery	Time after occlusion until rest LD flux value is reached
Half-time of hyperemia	Time after occlusion to reduction of peak flow to 50%
Time of hyperemia	Time of total duration of the hyperemic response

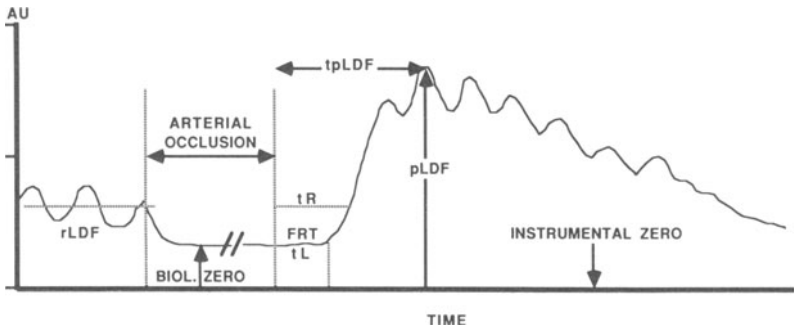

Figure 11–3. Schematic tracing of an LD flux recording during rest (rLDF), arterial occlusion, and postocclusive reactive hyperemia. The following values are indicated: instrumental zero, biological zero, flux reappearance time (FRT) or latency time (tL), recovery time (tR), peak LDF after arterial occlusion (pLDF), and time to pLDF (tpLDF).

severely ill patients than in the healthy subjects, while the less ill patients had values within the normal limit.

PRH with cuff at thigh level: Kvernebo et al. [10] applied the occlusion cuff at several positions (above knee, below knee, and at the ankle), but found that the most useful position was just proximal to the patella. They studied mainly one parameter: the *Flux Reappearance Time* (FRT), which is defined in figure 11–3. FRT is equal to the latency time used by del Guercio et al. [7]. Kvernebo et al. found that with the cuff above knee, all healthy subjects had a FRT value of ≤ 3 seconds. In all patients with critical ischemia, this time was >48 seconds, while no correlation between the ankle pressure or ankle pressure index and FRT could be found in patients with claudication. However, an interesting finding in this last group of patients was that compared with angiography, all claudicants who had significant arteriosclerosis only in the distal vascular bed had significantly prolonged (>15 seconds) FRT values, while those with only proximal obliterations had a normal FRT.

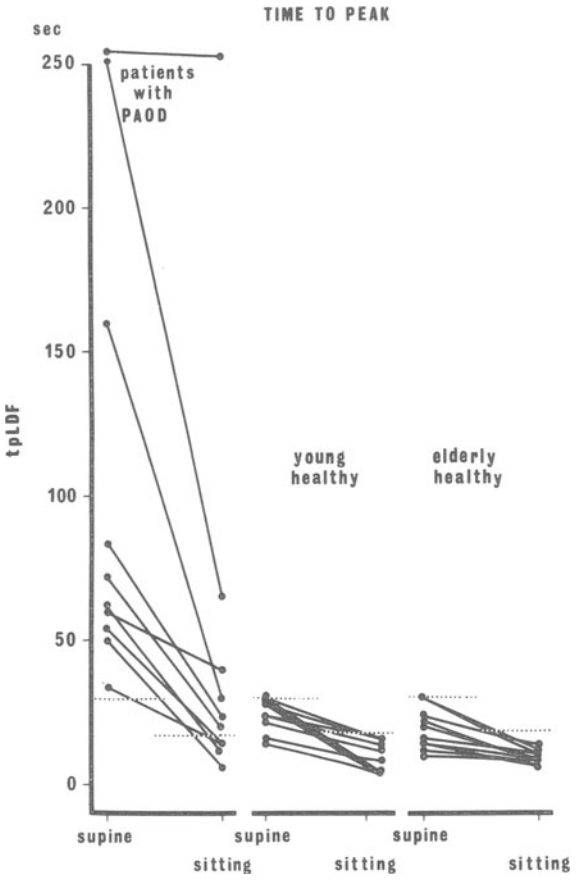

Figure 11–4. Time to peak during postocclusive reactive hyperemia in the same subjects and patients as in figure 11–2. All patients had a significantly longer time to peak LDF (tpLDF) in the supine position than the healthy subjects. In the sitting position, the six most severely ill patients had all a longer tpLDF than the healthy subjects.

Kvernebo et al. drew the conclusion that FRT reflects the vascular resistance in the runoff arteries of the segment between the cuff and the measuring probe. This seems to be the first time that this information, which is of great importance for the results of vascular reconstructive surgery or intraluminal dilatation in patients with PAOD, has been obtained by a noninvasive and clinically applicable technique.

In the study of del Guercio et al., the occlusion cuff was applied high at the thigh level, and at this position there was a complete discrimination between the healthy controls and patients with claudication in regard to the latency time (FRT) and the recovery time [7].

Conclusion: From the results presented, the best values for discriminating between patients with POAD and healthy subjects seem to be (figure 11–3): *Time to peak* (tpLDF; occlusion cuff at ankle level [5,7,10,12,13]), *latency or reappearance time* (FRT; occlusion cuff at thigh level [7,10]), and *recovery time* (tR; occlusion cuff at thigh level [7]).

Predicting healing of ulcerations: Karanfilian et al. [19] have studied the value of the LD method for predicting the healing of forefoot ulcers, and compared LDF measurements with transcutaneous oxygen tension and systolic pressures in the ankle. They conclude that the estimations of skin blood flow by tcP_{o2} and LDF are significantly better than ankle pressure measurements in predicting the healing of forefoot ulcerations and amputations in diabetic and nondiabetic patients.

Oscillatory flow activity

Rhythmic variations in blood flow are a well-known phenomenon that can be found in most animal tissues and are due to variations in the myogenic activity of the smooth muscle cells of the arteries and arterioles [20]. The influence of this myogenic activity on the human skin microcirculation has been of great interest, and it has been studied by different methods [1,21]. The oscillatory flow patterns have been found to be very sensitive to dynamic interventions and to be composed of waves with several different frequencies [1,6,11–16,20–23].

Oscillations in Resting Flow: Creutzig et al. [6] showed that the frequency of the LD flow oscillations in unheated skin of the forefoot was 4.0 ± 0.6 waves/minute in the healthy subjects and 2.6 ± 0.8 in claudicants (<0.01). When the skin was heated to 37°C, the frequency increased in patients to 3.8 ± 1.5 waves/minute, but no change was seen in the healthy volunteers. During leg dependency, the frequency increased in the healthy subjects, but decreased or disappeared in the patients.

Seifert et al. [12] reported LD flow oscillations measured in the forefeet of 12 healthy subjects and 36 patients with various degrees of ischemia due to POAD. They found two different types of waves: large waves and small waves. Large waves with a frequency of 3–4 cycles/minute were presented in 75% to 83% of both healthy subjects and the different groups of POAD patients in the supine position. The prevalence was markedly decreased to between 17% and 42% in the sitting position, the lowest value recorded in the most severe cases.

The small waves, with a consistent frequency of about 22 cycles/minute, were seen in 33%–92% of the patients, but in only 8% of the healthy subjects. The prevalence of these small waves increased successively with the severity of the disease, and there was no major difference between the supine or sitting position. The origin of these small waves is not fully understood,

but Seifert et al. speculate that as arteries and large arterioles dilate in the ischemic areas, the pressure head is transmitted distally into the terminal arterioles, stimulating increased vasomotion in this vascular bed. This hypothesis that the fast small waves reflect the vasomotion in the most terminal arterioles, and that the slow large waves reflect the activity in the arteries or large arterioles, is supported by animal studies. Colantuoni et al. [20] clearly demonstrated in the hamster skin fold preparation that the frequency of vasomotion was lowest (3 cycles/minute) in large arterioles (70–100 μm diameter) and increased successively to about 10 cycles/minute in the terminal, precapillary arterioles (6–15 μm). However, the very fast frequency of about 20 cycles/minute found in human skin is rather puzzling since the highest frequency so far reported in the skin microvascular bed of both animals and humans is about 10 cycles/minute [20,21]. Fagrell et al. [21] also demonstrated this frequency in nailfold capillaries of fingers, and they postulated that this activity was generated in the smallest precapillary arterioles. It is therefore rather surprising that frequencies of 20 cycles/minute can be recorded by the LD technique, since the LD signal arises mainly from the motion of blood cells in the larger, subpapillary vessels of the skin microcirculation [1,6,14]. Another confusing thing is that our group has recently found periodic small waves in the forefoot skin in the majority ($\approx$ 60%) of healthy subjects when recordings were made from five different areas of the forefoot. Consequently, the waves do not seem to be generated only in ischemic areas, although they are much more pronounced in such regions.

Scheffler and Rieger [11] have studied LDF oscillations by Fourier analysis. They report four different types of oscillatory flow patterns: *aperiodical, sinusoidal, small waves,* and *no waves.* They have related these different patterns to the degree of arterial insufficiency (ankle/arm pressure index) in patients with POAD. They found that aperiodic waves decreased, but small waves increased with the severity of the arterial insufficiency.

Flow Oscillations during Reactive Hyperemia (PRH): Marked oscillations have also been seen in the LDF signal during reactive hyperemia. Wilkin [16] described them in the forearm skin of healthy volunteers and also showed that the mean amplitude was highest approximately 30 seconds after a six-minute arterial occlusion, after which they slowly decreased to a minimum in about 1.5 minutes. The frequency of these waves was 6–7 cycles/minute.

A similar pattern of oscillations in the LDF signal has also been recorded in the feet of both healthy subjects and patients with POAD [7,8,10,12,13]. Seifert et al. [12] showed that in 10% of the recordings large waves appeared during PRH, although they were not present at rest. Because of these marked waves during the PRH, it is often difficult to establish the time to peak value during PRH (figure 11–3). Sometimes the first peak is the highest, while at other times the second or third peak is the highest. Östergren et al. [13]

therefore calculated the times to both the first and the highest peak. They found that the time to the highest peak in all patients with POAD was longer than 50 seconds, while all healthy subjects had a value of less than 30 seconds. This limit is much shorter than what del Guercio et al. [7] reported, with values up to 117 seconds in the controls, a difference that may be explained by the location of the occluding cuff. Del Guercio et al. had their cuff at the thigh, and Östergen et al. at the ankle level. The more proximally the cuff is located, the longer the LDF signal takes to reach the PRH peak value.

Conclusion: Some differences in the oscillatory patterns of flow LD seem to exist between healthy subjects and patients with POAD. However, a number of frequency patterns have been reported so far, and further analysis of these different waves in healthy and diseased states should be performed to evaluate their importance in distinguishing health and disease.

LDF IN PATIENTS WITH VENOUS DISORDERS

Only a few papers have been published in which the LDF technique was used in patients with venous disorders of the legs. Belcaro et al. [24] showed that, compared with healthy subjects, the resting LD signal was significantly higher in the skin of postphlebitic limbs with venous hypertension, both in the supine and standing positions. Similar results have been reported by Sindrup et al. [25], who showed a significant increase in LD flux values in the skin surrounding venous leg ulcers. This finding is in full agreement with other studies, using quite different methods, which also have shown that the total skin circulation in patients with venous insufficiency is increased. Creutzig et al. [17] also found that during PRH the LDF value was significantly decreased in comparison to healthy subjects.

Conclusion: The cited studies have shown that the total, resting skin microcirculation of the lower leg, as evaluated by the LDF technique, is increased in patients with venous insufficiency. However, the PRH response is impaired. More extensive studies need to be performed to investigate the value of the LDF technique in patients with venous disorders of the legs.

REFERENCES

1. Fagrell, B. 1984. Microcirculation of the skin. In The Physiology and Pharmacology of the Microcirculation. New York: Academic Press. vol 2, chapter 6, pp 133–180.
2. von Ahn, H.C. 1986. Measurement of gastrointestinal blood flow with laser Doppler flowmetry—An experimental and clinical study. Linköping University Medical Dissertations No 226, VTT-Grafiska, Vimmerby, Sweden.
3. Caspary, L., A. Creutzig, and K. Alexander. 1988. Biological zero in laser Doppler fluxmetry. Int J Microcirc Clin Exp 7:367–71.
4. Castronouvo, J.J., T.S. Pabst, D.P. Flanigan, and L.G. Foster. 1987. Noninvasive determination of skin perfusion pressure using a laser Doppler. J Cardiovasc Surg 28:253–257.

5. Svensson, H. and P. Swedman. 1988. Laser Doppler flow values during completely obstructed flow by occlusion. Int J Microcirc Clin Exp (special issue, August):S90.
6. Creutzig, A., L. Caspary, R.F. Hertel, and K. Alexander. 1987. Temperature dependent laser Doppler fluxmetry in healthy and patients with peripheral arterial occlusive disease. Int J Microcirc Clin Exp 6:381–390.
7. del Guercio, R., G. Leonardo, and M.R. Arpaia. 1986. Evaluation of postischemic hyperemia on the skin using laser Doppler velocimetry: Study on patients with claudicatio intermittens. Microvasc Res 32:289–299.
8. Kvernebo, K., C.E. Slagsvold, E. Stranden, A. Kroese, and S. Larsen. 1988. Laser Doppler flowmetry in the evaluation of lower limb resting skin circulation. A study in healthy controls and atherosclerotic patients. Scand J Clin Lab Invest 48:621–626.
9. Kvernebo, K., C.E. Slagsvold, and E. Stranden. 1989. Laser Doppler flowmetry in the evaluation of skin post-ischemic reactive hyperemia. A study in healthy volunteers and atherosclerotic patients. J Cardiovasc Surg 30:70–75.
10. Kvernebo, K., C.E. Slagsvold, and T. Goldberg. 1988. Laser Doppler flux reappearance time (FRT) in patients with lower limb atherosclerosis and healthy controls. Eur J Vasc Surg 2:171–176.
11. Scheffler, A., and H. Rieger. 1988. Signalverlaufsmuster des Laser-Doppler-fluxes bei peripherer arterieller Verschlusskrankheit und ihre Beziehung zum systolischen Knöchel-druckindex. In Proceedings of the 12th annual meeting of the Schweizerischen Gesellschaft für Mikrozirkulation, Bern.
12. Seifert, H., K. Jäger, and F. Bollinger. 1988. Analysis of flow motion by laser Doppler technique in patients with peripheral arterial occlusive disease. Int J Microcirc Clin Exp 7:223–236.
13. Östergren, J., P. Schöps, and B. Fagrell. 1988. Evaluation of a laser Doppler multiprobe for detecting skin microcirculatory disturbances in patients with obliterative arteriosclerosis. Int Angio 7:37–41.
14. Fagrell, B., M. Intaglietta, A.G. Tsai, and J. Östergren. 1986. Combination of laser Doppler flowmetry and capillary microscopy for evaluating the dynamics of skin microcirculation. In Techniques in clinical capillary microscopy. Progress in Applied Microcirculation, Mahler, F., Messmer, K., Hammersen, F., eds Basel: Karger, vol 11, pp 30–39.
15. Tooke, J.E., J. Östergren, and B. Fagrell. 1983. Synchronous assessment of human skin microcirculation by laser Doppler flowmetry and dynamic capillaroscopy. Int J Microcirc Clin Exp 2:277–284.
16. Wilkin, J.K. 1986. Periodic cutaneous blood flow during postocclusive reactive hyperemia. Am J Physiol 250 (Heart Circ Physiol 19):H765–H768.
17. Creutzig, A., L. Caspary, and K. Alexander. 1988. Disturbances of skin microcirculation in patients with chronic arterial occlusive disease and venous incompetence. VASA 17:77–83.
18. Wilkin, J.K. 1988. Periodic cutaneous blood flow during aldehyd-provoked hyperemia. Microvasc Res 35:287–294.
19. Karanfilian, R.G., T.G. Lynch, V.T. Zirul, F.T. Padberg, Z. Jamil, and R.W. Hobson II. 1986. The value of laser Doppler velocimetry and transcutaneous oxygen tension determination in predicting healing of ischemic forefoot ulcerations and amputations in diabetic and nondiabetic patients. J Vasc Surg 4:511–516.
20. Colantuoni, A., S. Bergtulia, and M. Intaglietta. 1984. Quantitation of rhythmic diameter changes in arterial microcirculation. Am J Physiol 246 (Heart Circ Physiol 15):H508–H517.
21. Fagrell, B., M. Intaglietta, and J. Östergren. 1980. Relative hematocrit in human skin capillaries and its relationship to capillary blood flow velocity. Microvasc Res 20:327–335.
22. Salerud, G. 1986. Laser Doppler tissue flowmetery—fiberoptic methods in microvascular research. Linköping Medical Dissertations No 216, VTT-Grafiska, Vimmerby, Sweden.
23. Tenland, T. 1982. On laser Doppler flowmetry. Linköping Studies in Science and Technology Dissertations No 83, VTT-Grafiska, Vimmerby, Sweden.
24. Belcaro, G., A. Rulo, S. Vasdekis, M.A. Williams, and A.N. Nicolaides. 1988. Combined evaluation of postphlebitic limbs by laser Doppler flowmetry and transcutaneous pO_2 and pCO_2 measurements. VASA 17:259–261.
25. Sindrup, J.H., C. Avnstorp, H.H. Steenfos, and J.K. Kristensen. 1988. Transcutaneous pO_2 and laser Doppler blood flow measurements in 40 patients with venous leg ulcers. Acta Derm Venerol 67:160–163.

26. Fagrell, B. 1986. Microcirculatory methods for evaluating the effect of vasoactive drugs in clinical practice. Acta Pharm Tox 59:103–107.
27. Sundberg, S. 1984. Acute effects and long-term variations in skin blood flow measured with laser Doppler flowmetry. Scand J Clin Lab Invest 44:341–345.
28. Svensson, H. and B.A. Jönsson. 1987. Laser Doppler flowmetry during hyperemic reactions in the skin. Int J Microcirc Clin Exp 7:87–96.

12. BLOOD FLOW IN SKELETAL MUSCLE

KAREL TYML, RICHARD J. ROMAN, and JULIAN H. LOMBARD

With the development of laser-Doppler flowmetry (LDF) (see chapters 1, 2), a new field has opened for quantitative studies of microvascular perfusion in various tissues. LDF allows quick, continuous, and noninvasive assessments of microvascular flow, both in clinical practice and in laboratory animal research. The potential benefits of LDF for the advancement of cardiovascular science have attracted considerable attention among researchers, who have already provided a variety of new insights and applications for this emerging technology. This chapter outlines the applications of LDF for studies of the skeletal muscle circulation. It summarizes existing studies of the skeletal muscle circulation using LDF, and focuses in detail upon comparisons of laser-Doppler flowmeter signals with independent measures of microvascular flow. The final section of the chapter illustrates several new applications of LDF for the study of blood flow in skeletal muscle.

OVERVIEW OF EXISTING LASER-DOPPLER MEASUREMENTS IN SKELETAL MUSCLE

The use of LDF to study the skeletal muscle circulation is particularly attractive, because it involves only a relatively simple preparation for exposing tissue to the laser light. However, relatively few studies to date have employed laser–Doppler flowmetry to assess blood flow in skeletal muscle. The majority of these studies have used either a prototype or the PF1d Perimed laser-Doppler flowmeter [1–9], although a few studies [10,11] have used other instruments.

With the Perimed laser-Doppler flowmeter, resting blood flow signals have been reported in pig hind limb muscles [1,2], triceps brachii of horses [7], rat gastrocnemius [3,4] cremaster [8], and gracilis [8] muscles, and the sartorius muscle of the frog [9]. The resting LDF signal is about 0.2V in mammalian muscle and 0.1V in amphibian muscle. The exact blood flow represented by this signal is unknown, and it depends upon the calibration of the signal versus an independent measure of blood flow.

Because the laser-Doppler flowmeter measures the flux of red blood cells in a discrete volume of tissue, LDF measurements are quite useful in studying spatial variations of blood flow within tissues. The ability of LDF to measure local differences in tissue blood flow has been exploited in several studies of skeletal muscle. For example, LDF has been used to document the extent of ischemic injury in the hind limb of anesthetized pigs following high-energy trauma associated with bullet injury [1,2,5,6]. Changes in the LDF signal across the injured muscle were well correlated with measurements of blood flow made by either ^{133}Xe clearance or radioactive microspheres [1,2,5,6]. All three methods revealed a sharp decline in blood flow at the boundary of the injury. This reduction in blood flow was related to color changes in the muscle [1,5]. The most detailed of these studies [1] demonstrated that blood flow was zero at the margin of the wound, and that very little flow was present in the discolored tissue near the site of injury. Blood flow increased toward normal with increasing distance from the wound. Comparison of blood flow and chemical analyses of tissue samples taken via needle biopsy revealed an excellent correlation between reduced blood flow and biochemical changes in the injured tissue, e.g., reduced ATP, creatine phosphate, K^+, and Mg^{2+} concentrations and elevated tissue levels of Na^+, Cl^-, and H_2O [2]. Based upon LDF measurements in various areas of the tissue, the investigators concluded that the circulation was a major factor determining the fate of traumatized muscle [1].

In another study [7], LDF was used to assess tissue blood flow in the triceps brachii muscles of horses in dorsal and lateral recumbency. The goal of that study was to determine if tissue ischemia occurs in the compressed muscles of anesthetized animals and if it leads to postanesthetic myositis. Blood flow was similar in the paired triceps brachii during dorsal recumbency. However, there was a constant and significant difference in blood flow in the upper and lower muscles when the horses were placed on their sides. During the period following anesthesia, LDF signals in the uppermost muscle were up to four times higher than those in the lower muscle.

Because LDF monitors regional tissue perfusion continuously, it provides a unique opportunity to assess changes in tissue blood flow with time or to evaluate the response of the microcirculation to an experimental perturbation at a single site. A number of studies have employed LDF to demonstrate temporal changes of blood flow in skeletal muscle [3,4,8,9]. LDF signals have provided a useful index of spontaneous changes in muscle blood flow [3,4],

as well as changes in blood flow during reduced perfusion pressure [8], ischemia [3,4], functional hyperemia [9], reactive hyperemia [8,10,11], and following trauma [1,2,5,6].

COMPARISONS OF THE LASER-DOPPLER SIGNAL WITH INDEPENDENT MEASURES OF MICROVASCULAR PERFUSION

Clinical studies

One clinical study employed LDF to assess skeletal muscle blood flow in open biopsies of patients with neuromuscular disease [10]. In that study, Tahmoush et al. utilized a prototype laser-Doppler flowmeter and reported absolute blood flows that were based upon a calibration of the LDF signal against flow measurements with radiolabeled microspheres in the biceps and vastus lateralis muscles of rats. The investigators reported a good linear correlation ($r = 0.88$) between LDF and microsphere measurements in their calibration procedure, and they converted LDF signals to blood flow using the relationship $1\ V = 15.2 \pm 0.9\ ml \cdot min^{-1} \cdot 100g^{-1}$.

Tahmoush et al. [10] reported that mean resting blood flows and post-occlusive reactive hyperemias were similar for control subjects and patients with neuropathic disorders, while patients with myopathic disorders had higher resting muscle blood flows and higher peak flows during reactive hyperemia. These observations lead the authors to suggest that muscle type grouping in neuropathy was not associated with a change in skeletal muscle blood flow, whereas muscle fiber degeneration was linked to an increased flow.

In a recent study, Fernando et al. [11] evaluated the usefulness of an implanted miniature (2.5 mm) probe for the TSI BPM 403 flowmeter to monitor tissue perfusion. In the clinical part of the study, the implanted flowmeter probe was used to monitor blood flow in five different free-tissue transfers in humans. In the experimental part of the study, the authors implanted the miniature probe in the rectus abdominus muscle of four anesthetized dogs. In two of the dogs, LDF measurements were compared with ultrasonic flow probe measurements in the inferior epigastric artery. In the other two dogs, LDF signals were correlated with blood flow when perfusion of the supply artery was controlled with a pump.

In the experimental part of the study, the investigators observed that the LDF signal (reported as the Doppler shift frequency in hertz) responded reproducibly and rapidly to changes in flow in the inferior epigastric artery [11]. The LDF signal decreased tenfold or more within six seconds following arterial occlusion, and decreased to approximately 50% of control within 20 seconds following venous occlusion. Release of the vascular occlusion produced a reactive hyperemia in the muscle that was clearly measurable. The relationship between LDF signal and blood flow during perfusion of the inferior epigastric artery with the pump was linear (approximately 0.87 Hz per $ml \cdot min^{-1} \cdot 100g^{-1}$) up to a computed average blood flow of 10

$ml \cdot min^{-1} \cdot 100g^{-1}$ of tissue, and it was reproducible in different experiments in two dogs. However, the LDF versus blood flow relationship became nonlinear when calculated flow exceeded 10 $ml \cdot min^{-1} \cdot 100g^{-1}$.

In the clinical studies [11], four of the five free-tissue transfers survived and exhibited an adequate flow signal (>20 Hz) during the postoperative period. The flow signals in the flaps ranged between 50–150 Hz before division of the tissue pedicle, and between 50 and 200 Hz in the postoperative period. In several of the flaps, flow decreased postoperatively to a level of 20–50 Hz. This decrease was correlated with the clinical development of edema. In the tissue transfer that failed, the LDF flow signal was inadequate (less than 10 Hz) during surgery. Revision of the arterial anastomosis to the flap restored the blood flow during surgery. However, flow again fell to inadequate levels in the postoperative period, prior to the ultimate failure of the flap.

Fernando et al. [11] concluded that LDF was a sensitive monitor of the muscle microcirculation. Because the implanted miniature probes allowed continuous monitoring of deep tissue perfusion, the authors felt that LDF was useful for predicting the viability of free-tissue transfers [11].

Laboratory studies

Several studies in animals have compared LDF readings with independent measures of blood flow in skeletal muscle, including radioactive microspheres [1,2,5,6,8,10], ^{133}Xe clearance [1,2,4–6], and electromagnetic flow probe measurements [8]. In general, these studies have demonstrated that the LDF signal is closely correlated with independent measurements of muscle blood flow.

Some of the earliest studies of skeletal muscle using LDF demonstrated a close agreement between LDF signals and muscle blood flow measured via ^{133}Xe clearance or radioactive microspheres [1,2,5,6]. Holmstrom and Lewis [1] found a good correlation between LDF and the microsphere technique (mean $r = 0.85$, range = 0.69–0.99), and they noted that LDF permitted more detailed measurements within a smaller area of tissue than either the ^{133}Xe clearance method or radioactive microspheres.

In a later study [4], Nicholson et al. used LDF and ^{133}Xe clearance to study the effect of acute (one hour to one week) and chronic (8 to 12 weeks) femoral artery ligation upon blood flow in the gastrocnemius muscle of rats. These authors concluded that LDF was a useful method to assess tissue blood flow, and that femoral artery ligation produced changes in skeletal muscle blood flow that were similar to those occurring during intermittent claudication in humans.

In the experiments of Nicholson et al. [4], LDF measurements demonstrated a periodic variation (2.1 ± 0.1 cycles/minute) of red blood cell flux in 76 of the 166 normally perfused gastrocnemius muscles studied. These cyclic variations in LDF signal were attributed to vasomotion in the arterioles. The authors stressed that the ability of the laser-Doppler flowmeter to detect

rhythmic changes in red blood cell flux in the muscle indicates that LDF provides a sensitive method for evaluating tissue perfusion.

Both LDF and ^{133}Xe clearance demonstrated a reduction in gastrocnemius muscle blood flow following ligation of the femoral artery [4]. During acute ligation, the reduction of blood flow measured via ^{133}Xe clearance (52%) was greater than that estimated via LDF (41%). The authors felt that this reflected a random difference in the population of animals selected for study by the two techniques. However, they could not rule out the possibility that the differences in the flow reduction observed during acute ligation reflected a difference in the LDF and ^{133}Xe clearance methods, e.g., sampling from different areas of the tissue. They considered this unlikely and stressed that measurement of the effects of acute ligation via LDF and ^{133}Xe clearance in the same animals would resolve the question of any differences in the blood flow measured via the two methods. In contrast to the observations following acute ligation of the femoral artery, ^{133}Xe clearance and LDF provided nearly identical estimates of the reduction in tissue blood flow during chronic ligation of the femoral artery (33% versus 32%, respectively).

Limitations of laser-Doppler flowmetry for measurement of skeletal muscle blood flow

Theoretically, LDF should provide an absolute measure of blood flow that is independent of the tissue studied. However, comparisons of LDF signals against tissue blood flow measurements (e.g., [8]) have demonstrated considerable differences in the relationship between the flowmeter signal and independent measures of blood flow in various tissues. These findings could reflect differences in the optical properties or vascular architecture of tissues, temporal or spatial variation of tissue blood flow sampled by the laser probe, or the limitations and differences of the independent methods used to calibrate the LDF signal.

In a study specifically designed to calibrate the Perimed PF1d laser-Doppler flowmeter, Smits et al. [8] deliberately manipulated tissue perfusion in order to compare the LDF signal with several independent measures of flow. In that study, the authors calibrated spatially averaged LDF readings in the gracilis muscle, cremaster muscle, and renal cortex of anesthetized rats with whole-organ blood flow measured with radioactive microspheres or an electromagnetic flow probe. The authors reported an excellent correlation between the LDF signal and either of the other two independent measures of blood flow ($r = 0.74 - 0.95$). However, the slope of the LDF versus blood flow relationship and the intersection of the calibration lines with the ordinate varied among tissues, and within tissues in which blood flow was measured by both the electromagnetic flowmeter and radiolabeled microspheres. For example, there was a threefold difference in the slopes of the linear regression lines correlating LDF with blood flow measured by radioactive microspheres in the gracilis (figure 12–1) and cremaster muscles (figure 12–2). These

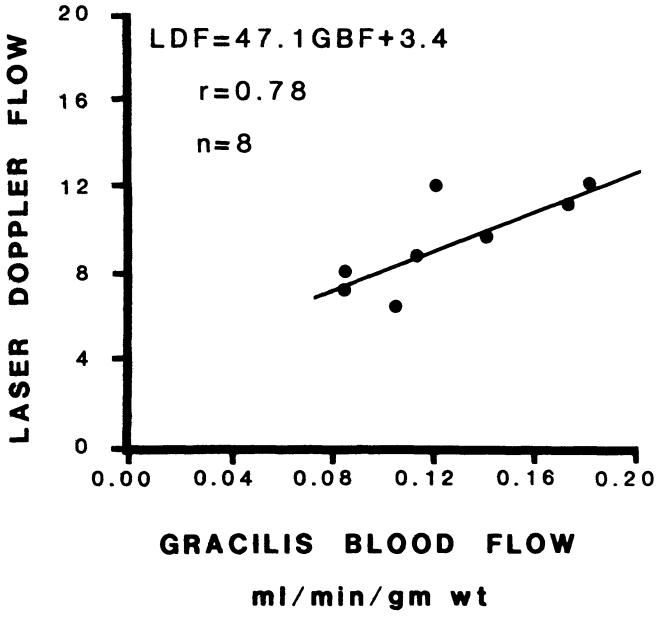

Figure 12–1. Relationship between mean laser-Doppler flow (LDF) signal from Perimed Model PF1d laser-Doppler flowmeter and gracilis muscle blood flow (GBF) measured with radioactive microspheres in eight rats. Laser-Doppler flow signal on ordinate is expressed as LDF units, with the gain set at ×3 (one LDF unit = 0.033V) and the frequency cutoff set at 4 kHz. See text for details. (Reproduced with permission from Smits et al. [8].)

authors concluded that there is probably no universal calibration factor to relate the LDF signal to blood flow in $ml \cdot min^{-1} \cdot 100g^{-1}$ of tissue.

Smits et al. [8] noted that the amplitude of the LDF signal depends upon a number of factors that probably differ among tissues, e.g., hematocrit, red blood cell velocity, vascular architecture, and point-to-point variations of blood flow in the tissue. These authors stressed that any of these factors could prevent calibration factors obtained in one vascular bed from being applied to others. Moreover, any method of blood flow measurement that is used to calibrate the LDF signal has its own characteristics and limitations, so that the calibration factor relating LDF signal to blood flow also depends upon the reference method used to measure tissue blood flow.

The question of calibration was also addressed by Tyml and Ellis [9], who used frog sartorius muscle for a comparison of the LDF signal with actual red blood cell perfusion (red blood cell content × velocity × capillary density) measured via video microscopy. Since frog red blood cells are much larger than mammalian red blood cells, these investigators could visualize red blood cell perfusion at very low magnification. This permitted analysis in a tissue volume (0.84 mm^3) that was of the same order of magnitude as that sampled

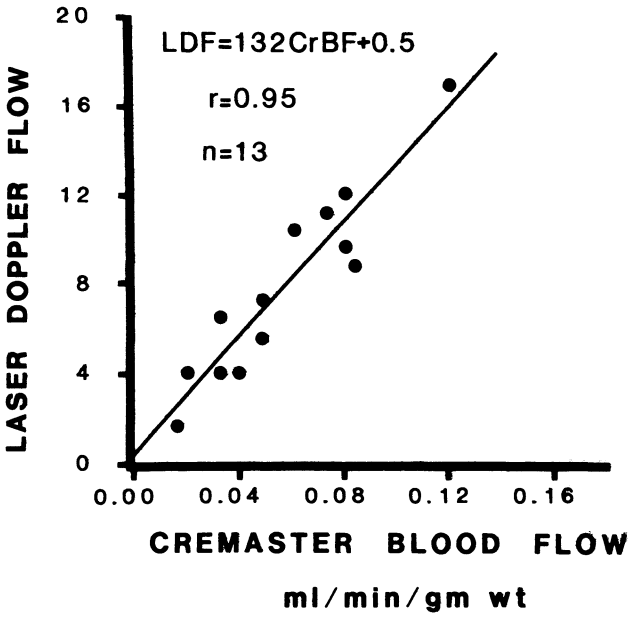

Figure 12–2. Relationship between mean laser-Doppler flow (LDF) signal and blood flow (CrBF) measured with radioactive microspheres in the cremaster muscle of 13 rats. Laser-Doppler flow signal on ordinate is expressed as LDF units, with the gain set at ×3 (one LDF unit = 0.033V) and the frequency cutoff set at 4 kHz. See text for details. (Reproduced with permission from Smits et al. [8].)

by the flowmeter. In the studies of Tyml and Ellis [9], temporal variation of red blood cell flow induced by muscle contraction yielded an excellent correlation between the LDF signal and the actual red blood cell flux (r = 0.83 – 0.98). However, spatial variations of red blood cell perfusion in resting muscle did not correlate with the LDF signal because penetration of laser light to the underlying tissue caused the sampling volumes of LDF and video microscopy to be different. However, when penetration of laser light was limited to 0.3–0.4 mm by inserting a blackened coverslip under the muscle in order to make the sampling volumes more comparable, spatial variations in flow across the tissue correlated very well with the LDF signal (r = 0.76 – 0.95).

Similar to the discrepancy reported by Smits et al. [8], Tyml and Ellis [9] also found that the slopes of regression lines relating LDF signal to tissue perfusion varied by a factor of 2–3 between muscle preparations. The studies of Tyml and Ellis [9] highlighted two problems with LDF calibration. First, it is difficult to provide an independent measure of red blood cell flux in the same tissue volume as that sampled by the flowmeter. Therefore, calibration procedures must rely on the assumption that blood flow in the microenviron-

ment sampled by LDF is proportional to the average blood flow measured independently in the whole tissue. This condition may be satisfied during gross flow changes (e.g., those induced by muscle contraction or ischemia), but will not apply if flow increases due to vascular recruitment or if changes in microvascular hematocrit occur. The second problem of LDF calibration highlighted by the work of Tyml and Ellis [9] also involves the question of sampling volumes. Because of the small volume sampled by the laser probe, there may be differences in the penetration and reflectance of the laser light caused by inhomogeneities in the optical properties of the tissue in the area sampled by the probe. These different optical properties, in turn, could lead to differences in LDF signals obtained from similarly perfused tissues, and they may result in discrepancies in calibration lines.

An additional difficulty encountered in LDF studies of blood flow in skeletal muscle (and other tissues) is that the laser probe detects non-nutritive flow in large vessels. Because of multiple scattering at high-volume fractions of red blood cells and because of frequency shifts that exceed the high-frequency cutoff of the instrument at high-flow velocities, LDF signals obtained from large vessels underestimate true flow and are not linear. Therefore, the possible contribution of larger vessel flow to the LDF signal should always be considered when using this method to assess blood flow in a given tissue.

The differences in the slope of calibration lines obtained in different preparations by the same investigators [8,9] and the observation that a variety of factors can affect either the LDF signal or the independent measure of blood flow used to calibrate the laser Doppler flowmeter call into question the approach of using a single calibration factor to obtain an absolute measurement of blood flow from LDF signals in different tissues. Taken together, these observations suggest that calibration of the LDF signal is needed in each particular tissue studied.

NEW DIRECTIONS FOR LDF STUDIES OF SKELETAL MUSCLE BLOOD FLOW

Effect of mechanical stimulation on microvascular perfusion

One important aspect of microcirculatory work with intravital microscopy is the effect of mechanical manipulation on tissue perfusion. Because surgery and mechanical manipulation are necessary to expose tissue in many preparations, the exposure may upset the microvascular perfusion that is to be investigated. Although a mechanical stimulus can increase flow in mammalian muscle [12], the possibility that exposure of the tissue can potentiate this increase in muscle flow via tissue sensitization during surgery has not been addressed.

Tyml's laboratory has used the Perimed laser-Doppler flowmeter to evaluate the effect of surgical exposure on the response of the microcirculation to mechanical stimulation in the sartorius and gracilis muscles of anesthetized

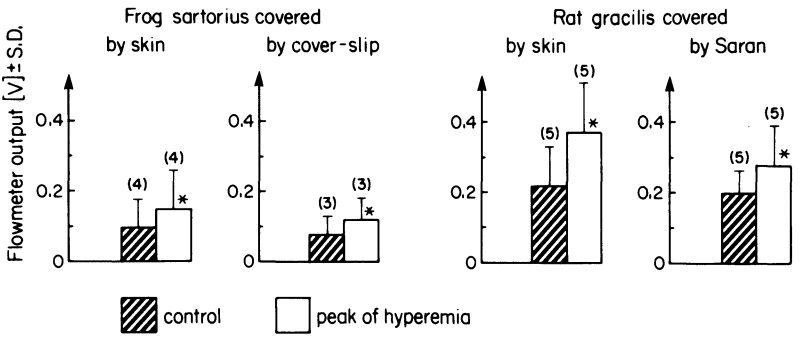

Figure 12–3. Microcirculatory responses to mild mechanical stimulation in frog and rat muscles covered with skin, glass cover-slips, and plastic film. The muscles were tapped ten times with small forceps for a total of five seconds. Each tap was associated with a peak force of 0.20–0.25N. Flow signals were recorded by a Perimed Model PF1d laser-Doppler flowmeter. The peak of hyperemic response was reached in 2.9 minutes and 0.6 minutes in frog and rat, respectively. The duration of response was between 7 and 10 minutes. Asterisks indicate significant increases at $p < 0.05$ using paired t-test; *n* is the number of animals (in parentheses).

frogs and rats, respectively. Since the flowmeter output is sensitive to red blood cell flow in a tissue depth of up to 1 mm, LDF permits analysis of mechanical responses in exposed muscles and in muscles covered by the thin skin in these species (0.2–0.4 mm thick). Figure 12–3 shows that mechanical tapping (0.2–0.25 N force) produced a significant (50%–60%) increase in blood flow. However, this increase in blood flow in response to mechanical stimulation was comparable in exposed and unexposed muscles. Therefore, exposure of a muscle per se does not increase blood flow. Because of the unpredictability of the duration of the response of a muscle to manipulation [12], Tyml's laboratory has recently incorporated LDF into experimental protocols in which the postexposure perfusion is monitored until a steady resting state perfusion is reached [13].

Scanning techniques for assessing regional differences in tissue perfusion in skeletal muscle

The average value of LDF readings taken from multiple sites in a tissue provides a reasonable estimate of blood flow to an organ, since mean LDF readings obtained from scans of rat skeletal muscle are closely correlated to average tissue blood flows measured by either an electromagnetic flowmeter or radioactive microspheres [8]. However, because the laser probe samples from discrete areas of tissue, comparison of the pattern of individual laser-Doppler signals over tissue surfaces may also provide important information concerning the homogeneity of tissue perfusion.

In a series of preliminary studies, Lombard and Roman have assessed the ability of laser-Doppler flowmetry to detect differences in the homogeneity

of tissue perfusion in the skeletal muscle circulation of rats subjected to hemorrhagic hypotensive stress. Because low-flow states may lead to an inhomogeneous perfusion of tissues that could contribute to organ damage in shock [14], LDF scans of the gracilis muscle of spontaneously hypertensive (SHR) and normotensive Wistar Kyoto (WKY) rats were performed to determine if a greater reduction of tissue blood flow or a less homogeneous perfusion of tissues could contribute to the reduced ability of hypertensive rats to tolerate hemorrhage [15].

In these studies, the gracilis muscles of anesthetized SHR and WKY were scanned before and after a hypotensive stress consisting of four individual 1 ml blood-volume withdrawals, separated by 20-minute recovery periods. The laser probe was connected to a micromanipulator and was scanned over the muscle in a precise, reproducible manner. Twenty individual readings were obtained from each muscle during each experimental period.

In nonhemorrhaged animals, the mean LDF readings were similar in SHR and WKY. Two of the seven hypertensive animals exhibited nonperfused sites prior to hemorrhage (one site in one animal and two sites in the other), while none of the six WKY rats exhibited nonperfused sites. In hemorrhaged animals, the mean LDF signal from the gracilis muscle was significantly lower in SHR than in WKY (figure 12–4). Four of the seven hypertensive animals exhibited nonperfused areas of tissue following hemorrhage (1–5 sites per animal), while no unperfused sites were observed in normotensive rats subjected to hemorrhagic hypotensive stress.

These observations suggest that the reduced ability of hypertensive animals to tolerate hemorrhage may arise, at least in part, from a greater reduction of tissue blood flow and a higher incidence of nonperfused areas relative to normotensive animals subjected to the same degree of blood loss. The studies also suggest that LDF scans may provide an effective means to evaluate the homogeneity of microvascular perfusion in large areas of tissue during normal and pathophysiological states.

Indwelling probes for sequential assessment of tissue perfusion in skeletal muscle

In a preliminary report, Gush et al. [16] described a method in which two optical fibers (one for transmitting the laser light and the other for receiving light scattered by the tissue) were sealed in 26-gauge needle stock and implanted in skeletal muscle through a 21-gauge disposable needle. As previously described in detail (see Clinical Studies, above), Fernando et al. [11] recently evaluated an implanted miniature probe for the TSI laser-Doppler flowmeter, and concluded that indwelling probes provide a convenient way to monitor perfusion in the microcirculation of deep tissue in conscious subjects. Preliminary studies (R.J. Roman and A.S. Greene, unpublished results) have suggested that the needle probe for the Perimed PF3 laser-Doppler flowmeter can also be inserted into rat skeletal muscle through a chronically implanted cannula guide. Signals obtained from the implanted

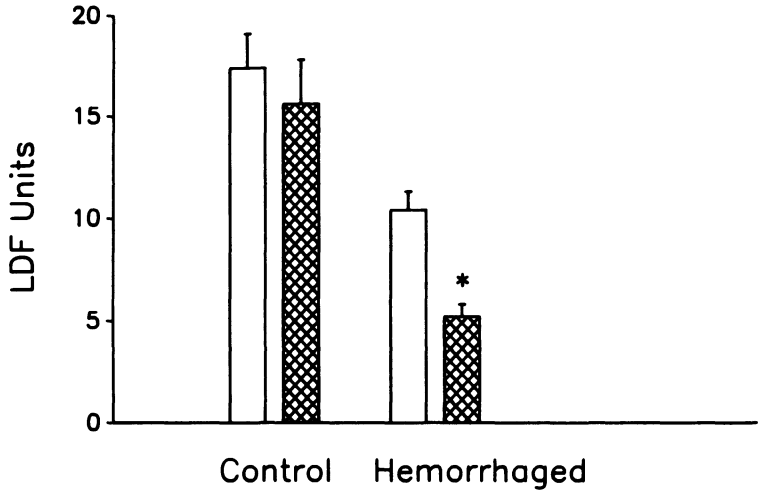

Figure 12–4. Laser-Doppler flowmeter signal (LDF units) in gracilis muscle of seven spontaneously hypertensive rats (hatched bars) and six normotensive Wistar-Kyoto controls (open bars) before and after hemorrhagic hypotensive stress (four 1 ml blood-volume withdrawals separated by 20-minute recovery periods). Data for individual animals were obtained by averaging 20 LDF values per muscle, obtained with a Perimed PF1d laser-Doppler flowmeter at a gain of ×3, a frequency cutoff of 12 kHz, and a time constant of 1.5 seconds. Values are expressed as mean ± SEM, and the asterisk denotes a significantly lower signal following hemorrhage in SHR relative to WKY ($p < 0.05$). See text for details.

probe exhibit reproducible decreases in blood flow in response to norepinephrine and angiotensin, suggesting that sequential readings may be obtained over several days in individual animals. If this technique proves to be feasible, it is possible that sequential changes in skeletal muscle blood flow can be studied in individual animals before and after long-term experimental perturbations, e.g., administration of different pharmacological agents, induction of various types of experimental hypertension, or exposure to simulated high altitude.

CONCLUSIONS

Laser-Doppler flowmetry has been used in a number of studies of skeletal muscle. Although there are difficulties in calibration of the LDF signal to yield an absolute blood flow expressed in $ml \cdot min^{-1} \cdot 100g^{-1}$ of tissue, the instrument provides a meaningful assessment of both temporal and spatial variability of microvascular perfusion under a variety of experimental conditions.

ACKNOWLEDGMENTS

The authors wish to thank Karen Hughes, Blair Williams, and Glen J. Smits for their fine technical assistance, and Ms. Rhoda Adelsen for her excellent secretarial assistance. This work was supported by grants from the National

Institutes of Health (HL-29587, HL-37374, and HL-36279), the American Heart Association (83-853), the Medical Research Council of Canada, and the Heart and Stroke Foundation of Ontario. This work was completed during the tenure of Drs. Lombard and Roman as Established Investigators of the American Heart Association.

REFERENCES

1. Holmstrom, A., and D.H. Lewis. 1983. Regional blood flow in skeletal muscle after high-energy trauma. Acta Chir Scand 145:453–458.
2. Lewis, D.H., A. Holmstrom, G.E. Nilsson, T. Tenland, P.Å. Öberg, and J. Larsson. 1979. Skeletal muscle trauma: Correlation of microcirculatory and biochemical changes. Microvasc Res 18:286 (abstract).
3. Nicholson, C.D. 1984. Blood cell flux in the gastrocnemius muscle of the anesthetized rat. Int J Microcirc Clin Exp 3:433 (abstract).
4. Nicholson, C.D., R.A. Schmitt, and R. Wilke. 1985. The effect of acute and chronic femoral artery ligation on the blood flow through the gastrocnemius muscle of the rat examined using laser Doppler flowmetry and xenon-13 clearance. Int J Microcirc Clin Exp 4:157–171.
5. Öberg, P.Å., G.E. Nilsson, T. Tenland, A. Holmstrom, and D.H. Lewis. 1979. Measurement of skeletal muscle blood flow in bullet wounding with a new laser-Doppler flowmeter. Microvasc Res 18:298 (abstract).
6. Öberg, P.Å., G.E. Nilsson, T. Tenland, A. Holmstrom, and D.H. Lewis. 1979. Use of a new laser Doppler flowmeter for measurement of capillary blood flow in skeletal muscle after bullet wounding. Acta Chir Scand Suppl 489:145–150.
7. Serteyn, D., E. Mottart, C. Michaux, J. Micheels, C. Philippart, L. Lavergne, C. Guillon, and M. Lamy. 1986. Laser Doppler flowmetry: muscular microcirculation in anesthetized horses. Equine Vet J 18:391–395.
8. Smits, G.J., and R.J. Roman, and J.H. Lombard. 1986. Evaluation of laser-Doppler flowmetry as a measure of tissue blood flow. J Appl Physiol 61:666–672.
9. Tyml, K., and C.G. Ellis. 1985. Simultaneous assessment of red cell perfusion in skeletal muscle by laser Doppler flowmetry and video microscopy. Int J Microcirc Clin Exp 4:397–406.
10. Tahmoush, A.J., P.D. Bowen, R.F. Bonner, T.J. Mancini, and W.K. Engel. 1983. Laser Doppler blood flow studies during open muscle biopsy in patients with neuromuscular diseases. Neurology 33:547–551.
11. Fernando, B., V.L. Young, and S.E. Logan. 1988. Miniature implantable laser Doppler probe monitoring of free tissue transfer. Am Plastic Surg 20:434–442.
12. Lindbom, L., R.F. Tuma, and K.E. Arfors. 1982. Blood flow in the rabbit tenuissimus muscle. Acta Physiol Scand 114:121–127.
13. Tyml, K., and C.H. Budreau. 1988. Heterogeneity of microvascular response to ischemia in skeletal muscle. Int J Microcirc Clin Exp 7:205–221.
14. Haljamae, H., E. Jennische, and A. Mendegard. 1977. Transmembrane potential measurements as an indicator of heterogenous distribution of nutritive blood flow in skeletal muscle during shock. Acta Physiol Scand 101:458–464.
15. Burke, M.J., W.J. Stekiel, and J.H. Lombard. 1984. Reduced venoconstrictor reserve in spontaneously hypertensive rats subjected to hemorrhagic stress. Circ Shock 14:25–37.
16. Gush, R.J., T.A. King, and M.I.V. Jayson. 1984. In vivo measurement of subcutaneous and intramuscular tissue blood flow by a laser-Doppler microprobe. Int J Microcirc Clin Exp 3:433 (abstract).

13. GASTROINTESTINAL BLOOD FLOW

J.W. KIEL and A.P. SHEPHERD

Despite the development of numerous methods for measuring gastrointestinal blood flow, important physiological questions remain unanswered regarding the gastrointestinal circulation, its regulation, and its relationship to gastrointestinal function. For example, investigators of the gastrointestinal circulation generally agree that alterations in blood flow participate in the etiology of a variety of gastrointestinal disorders ranging from gastric ulcers to necrotizing enterocolitis. However, the role of blood flow in maintaining mucosal integrity in the stomach and intestine is still poorly understood.

The extensive size of the gastrointestinal system, its functional diversity, and its complex vascular organization constitute the first level of difficulty in studying the gastrointestinal circulation. In research settings, these obstacles have been largely overcome by the development of various experimental preparations (e.g., the isolated stomach flap and gut loop) and techniques for measuring total blood flow (e.g., drop-counters and electromagnetic flow probes). The second and more challenging level of difficulty is the functional and vascular stratification of the gastrointestinal wall. Throughout the length of the gastrointestinal system, the mucosa is specialized for secretion and absorption, whereas the muscularis is specialized for the coordinated propulsion of foodstuffs. Not surprisingly, the intramural vascular organization is equally specialized. Measurements of total blood flow cannot reveal the intramural distribution of blood flow, nor can they illuminate the nuances of blood flow regulation or the relationships between blood flow and function within the layers of the gastrointestinal wall.

A number of techniques can selectively measure blood flow within the different layers of the gastrointestinal tract; however, all of them are either discontinuous, require a long time to complete, are limited to a few measurements, or permit only observations of single vessels. Although most of these methods are quantitative and have yielded significant insights into the gastrointestinal circulation, their inability to provide a continuous measurement precludes investigations of dynamic circulatory events. By contrast, laser-Doppler velocimetry (LDV) provides a continuous measurement of perfusion in a small volume of tissue. Consequently, LDV has the potential to illuminate many previously unexplored aspects of gastrointestinal hemodynamics.

Numerous validation studies show that LDV measurements in gastrointestinal tissue correlate linearly with other established blood-flow-measuring techniques. In addition, several lines of evidence indicate that the depth of the LDV measurement is sufficiently shallow to measure selectively the perfusion in the gastrointestinal mucosa or muscularis. However, LDV has inherent limitations that complicate its use in the gastrointestinal tract. The most serious limitation is the inability to determine the precise volume of tissue in which LDV measures perfusion. LDV is also an exquisite motion detector; its use in the inherently motile tissues of the gastrointestinal tract can be frustrating. However, when used properly, LDV is capable of providing significant new insights into the physiology and pathophysiology of the gastrointestinal circulation. The purposes of this chapter are to describe the studies that validate the use of LDV in the gastrointestinal tract, to highlight the advantages and disadvantages of LDV, and to provide an overview of LDV applications in basic and clinical research.

VALIDATION

Linearity

The comparison with measurements by an established technique is the sine quo non for validating any new method for measuring blood flow. In the earliest attempts to validate LDV in the gastrointestinal tract, LDV measurements on the mucosal or serosal surface were compared with measurements of total blood flow in isolated preparations. Figure 13–1 shows a typical tracing from one of the early studies in the stomach [1]. The figure shows clearly the linear correlation between LDV measurements made on the mucosal surface and electromagnetic measurements of total blood flow.

Shepherd and Riedel [2] were the first to apply LDV in the intestine. In isolated segments of canine jejunum perfused from a pressurized reservoir of arterial blood, they found that LDV measurements made on the mucosal surface correlated linearly with electromagnetic measurements of total blood flow throughout a wide range of perfusion pressures (figure 13–2). To widen the flow range, minimize intestinal motility, and prevent any active redistribution of intramural blood flow, the gut segments were maximally vasodi-

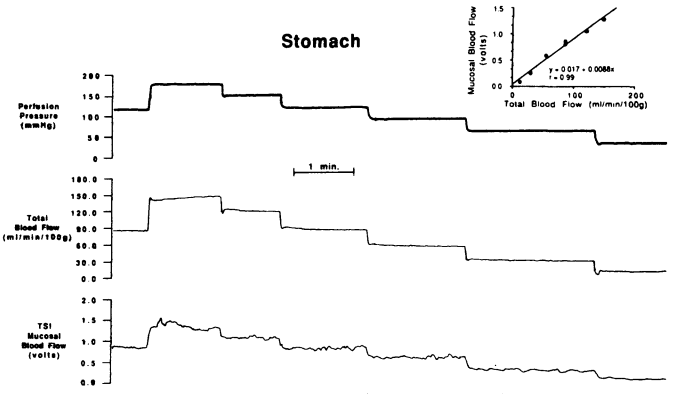

Figure 13–1. Tracings of electromagnetic total blood flow and LDV (TSI, Laserflo BPM 403) signal recorded from mucosal surface during step-changes in perfusion pressure in maximally dilated canine stomach flap. Insert shows linear correlation between flow measurements by the two techniques.

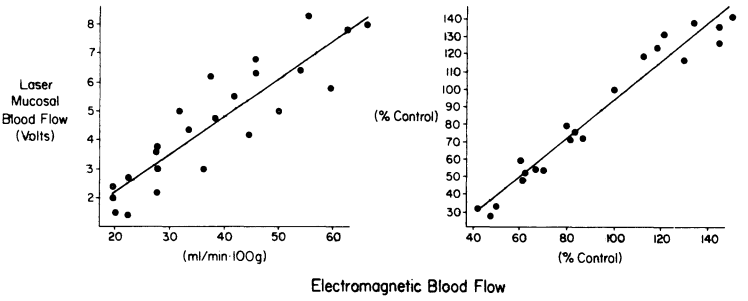

Figure 13–2. Linear correlation between electromagnetic total blood flow and LDV (NIH prototype) mucosal blood flow measurements in vasodilated canine gut loops (n = 4). Total blood flow was altered by changing perfusion pressure. Correlation between the two techniques improved when the data were normalized to control values at perfusion pressure of 120 mmHg (slope = 1.1, r = 0.97). (Reproduced from Shepherd and Riedel [2] by permission of the American Physiological Society.)

lated with isoproterenol. Because commercial LDV flowmeters were not available at that time, the LDV instruments used by Shepherd and Riedel were homemade devices based on the design developed at the National Institutes of Health [3]. Subsequent studies by Ahn et al. [4–6] and Kvietys et al. [7] using the Perimed (PF1d and PF2) instrument also showed a strong linear correlation between LDV measurements and total blood flow in the gut.

Although several earlier gastric validation studies were published in abstract form [8–11], Kiel et al. [12] reported the first comprehensive LDV validation study in the stomach. In chambered canine stomach flaps perfused

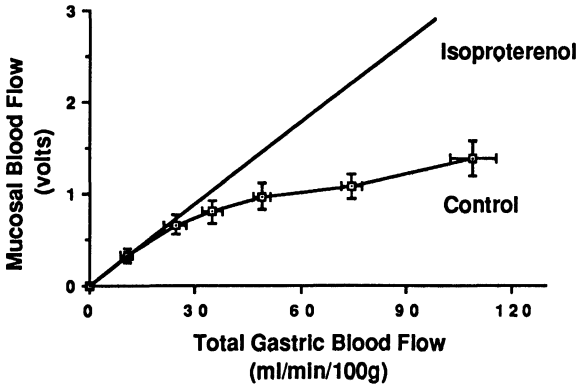

Figure 13–3. LDV (NIH prototype) mucosal blood flow plotted against electromagnetic total blood flow in control ($n = 7$) and vasodilated ($n = 4$) stomach flaps. In control preparations, mucosal flow was independent of total flow at higher flow rates. When intrinsic control mechanisms were paralyzed with isoproterenol, mucosal flow changed in direct proportion to total blood flow ($r = 0.98$). (Reproduced from Kiel et al. [13] by permission of the American Gastroenterological Association.)

by a pressurized reservoir, LDV measurements made on the mucosal and serosal surfaces were both linearly correlated with electromagnetic measurements of total blood flow. As in the study by Shepherd and Riedel [2], the gastric preparations were maximally dilated with isoproterenol. Figure 13–3 shows that in such vasodilated preparations, LDV measurements on the gastric mucosa scaled linearly with total blood flow throughout the entire flow range. However, the figure also shows the results of another study [13] in which the preparations were not vasodilated with isoproterenol. In the nonvasodilated preparations, the LDV signal failed to increase at higher rates of total blood flow, but remained relatively constant at a value well below the saturation level of the LDV instrument. This finding was the first evidence that the mucosa could regulate its blood flow independently of the other layers of the gastric wall.

Selectivity and measurement volume

The precise volume of tissue in which LDV measures blood flow is unknown. According to the LDV theory, the measurement volume is a function of the light-scattering and light-absorbing properties of the tissue and the distance between the fibers delivering light to the tissue and receiving scattered light from the tissue (see chapter 2). More importantly, the measurement volume is assumed to be constant for a given probe geometry in a given tissue: ~1 mm^3 for the currently available LDV instruments in most tissues [14]. Thus, the ability of LDV to measure blood flow selectively in a given tissue depends largely on the tissue thickness. For organs like the stomach or the intestine, the total wall thickness and the thickness of the

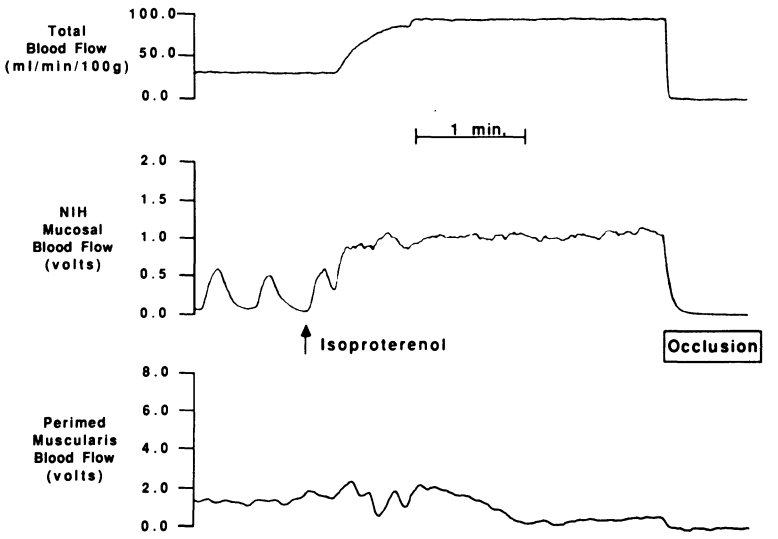

Figure 13–4. Isoproterenol response in canine stomach flap. Increase in total blood flow was detected by LDV (NIH prototype) probe on mucosal surface, but LDV (Perimed, PF1d) probe on serosal surface registered a decrease in perfusion.

component tissue layers vary with the size of the animal. For example, the total thickness of the human stomach is approximately 6 mm, whereas the feline stomach is only 2.4 mm thick [15]. Studies in larger animals such as the dog indicate that LDV provides a selective measurement of mucosal or muscularis perfusion.

In the canine stomach and intestine, simultaneous LDV measurements on the mucosal and serosal surfaces indicate that blood flow in these two layers is regulated independently during a variety of experimental perturbations. In both organs, directionally opposite changes in perfusion are registered by LDV probes on the mucosal and serosal surfaces during administration of selective vasodilators. Figure 13–4 is a representative tracing of the response to isoproterenol infusion in the canine stomach. The tracing shows parallel increases in total and mucosal blood flow and a decline in mucularis perfusion. Figure 13–5 shows a similar response to isoproterenol in the canine intestine [16]. The figure also shows that the intestinal response pattern is reversed during adenosine infusion. Similar redistributions of intestinal blood flow have been recorded with the microsphere technique in response to these two vasodilators [16,17]. Obviously, it would not be possible to register directionally opposite changes in blood flow beneath the mucosal and serosal surfaces if LDV measured blood flow throughout the entire thickness of the gastric or intestinal wall.

More physiologic perturbations also elicit divergent hemodynamic re-

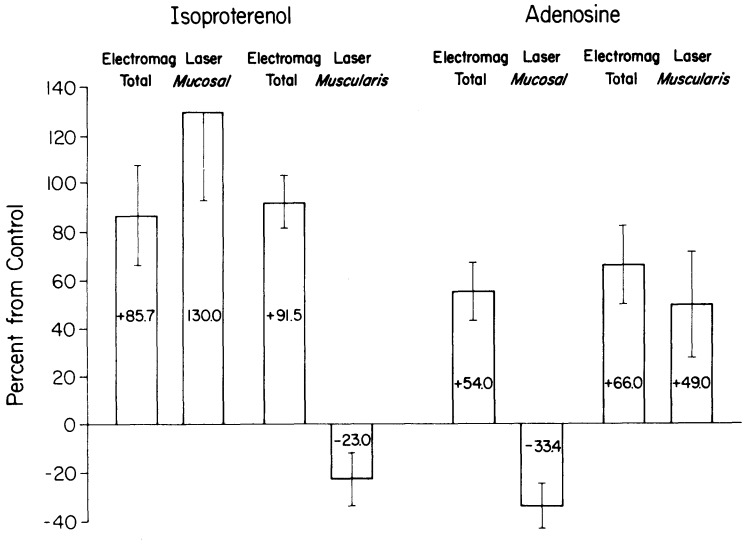

Figure 13–5. Response to selective vasodilators in canine gut segments. LDV (NIH prototype) probes on mucosal and serosal surfaces of intestine registered directionally opposite responses to isoproterenol and adenosine. Both dilators increased total blood flow. (Reproduced from Shepherd et al. [16] by permission of the American Physiological Society.)

sponses that are registered by LDV probes on the mucosa and serosa of the dog stomach and intestine. Figure 13–6 shows the reactive hyperemic responses to two arterial occlusions in the same gastric flap preparation. Following both occlusions, the reactive hyperemia in total blood flow was detected by the mucosal probe but was not registered by an LDV probe on the serosal surface. Two different LDV instruments with different probe geometries and signal processors were used. Both instruments registered the mucosal reactive hyperemia, and both failed to detect the hyperemic response from the serosal surface. Similarly, LDV probes on the serosal surface of the canine intestine [18] seldom register the reactive hyperemic response detected from the mucosal surface (figure 13–7). Moreover, during stimulated acid secretion or glucose absorption, LDV probes on the mucosal surfaces of the canine stomach [19] and intestine [20] register functional hyperemic responses that are not detected from the serosal surface. In both organs, measurements of local perfusion by other techniques also show that functional hyperemia is confined to the mucosal circulation [21,22]. The inability of LDV probes on one surface to detect increased perfusion registered from the opposite surface is inconsistent with a transmural LDV measurement.

Figure 13–8 shows that placing a layer of excised (nonperfused) canine gastric mucosa–submucosa between the LDV probe and the perfused gastric mucosa abolishes the resting flow signal and significantly attenuates the reactive hyperemia that is normally recorded [12]. Kvietys et al. [7] also

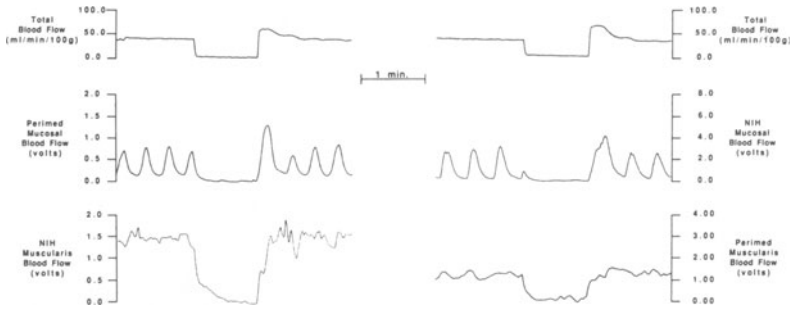

Figure 13–6. Reactive hyperemic responses recorded simultaneously by two different LDV flowmeters (Perimed, PF1d and NIH prototype) following two one-minute arterial occlusions in the same canine stomach flap. Both instruments registered the reactive hyperemia from the mucosal surface. Both instruments failed to detect the reactive hyperemia from the serosal surface.

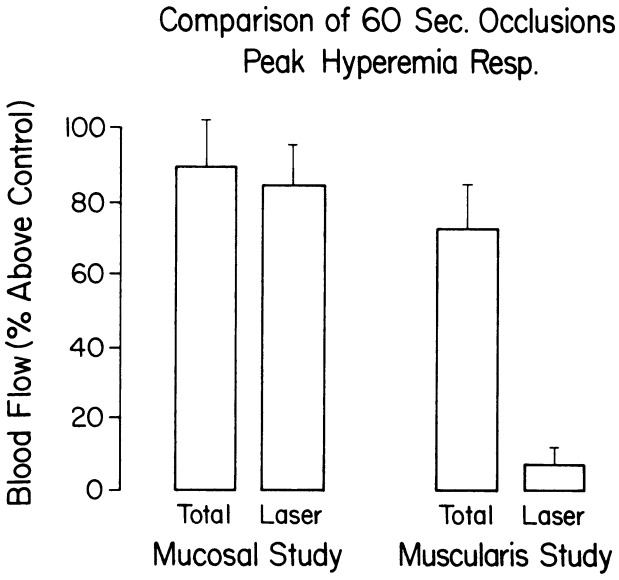

Figure 13–7. Reactive hyperemic response in the intestine is confined to the mucosa and is seldom registered from the serosa. LDV (NIH prototype) probes on mucosal surface of isolated canine gut loops consistently register reactive hyperemia that is undetected from the serosal surface. (Reproduced from Shepherd and Riedel [18] by permission of the American Physiological Society.)

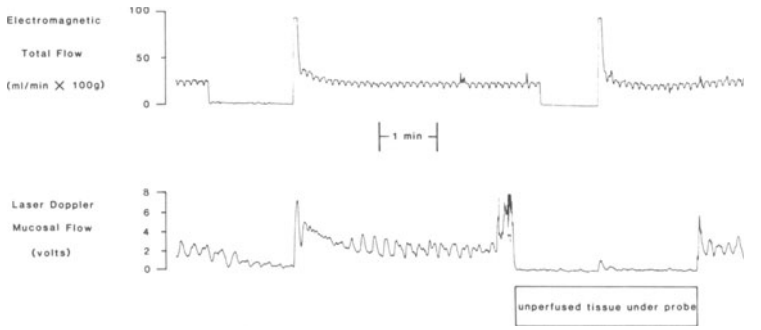

Figure 13–8. LDV signal attenuation by nonperfused tissue. Interposing a layer of nonperfused canine gastric mucosa–submucosa between the LDV (NIH prototype) probe and the perfused canine gastric mucosa abolished the LDV signal and attenuated the normally recorded reactive hyperemic response. (Reproduced from Kiel et al. [12] by permission of the American Physiological Society.)

observed an attenuation of the LDV signal (~80%) when they interposed a nonperfused layer of feline gut between the LDV probe and the mucosal surface of perfused feline intestine. Holm-Rutili and Berglindh [21] obtained similar results in the rat stomach with a nonperfused piece of gastric wall placed between the probe and the mucosal surface (i.e., a 90%–95% attenuation of the LDV signal). Although the optical properties of excised tissue may be different from those of the same tissue when it is perfused normally, the pronounced attenuation of the LDV signal is consistent with a superficial LDV measurement volume.

Additional evidence to support a shallow LDV measurement depth has been obtained by comparing LDV with techniques such as hydrogen clearance or microspheres, which are known to selectively measure mucosal or muscularis perfusion. Gana et al. [23] performed such a comparison and found a strong linear correlation between LDV measurements of canine gastric mucosal blood flow and hydrogen clearance. Similar results were obtained in the canine stomach by DiResta et al. [24] who used the washout of locally generated hydrogen to measure mucosal blood flow. Kvietys et al. [7] measured blood flow in the feline intestinal mucosa with LDV, hydrogen clearance, and microspheres. LDV measurements correlated linearly with flow measurements by both of these conventional, selective techniques for measuring intestinal mucosal perfusion.

The linear correlations between LDV and hydrogen clearance and between LDV and microsphere measures of mucosal blood flow lend further credence to the selectivity of the LDV measurement. However, Ahn et al. [4–6, 9,15,25,26] have concluded that LDV measures perfusion in a much larger volume of tissue and that LDV measures blood flow all the way through the gastrointestinal wall tissue, i.e., to a depth of 6 mm. In their studies, the

mucosal and serosal LDV flow values were identical over a wide range of total blood flow in feline intestine [4] and stomach [15], and in human stomach [9,26] intestine [6] and colon [25]. Moreover, no difference in the reactive hyperemic was registered by LDV probes on the mucosal and serosal surfaces of these tissues. In addition, 6 mm of nonperfused feline intestine was required to attenuate the LDV signal by 77% of the control flow value in the feline stomach. Lastly, when an LDV probe was held against either the mucosa or serosa and a mirror was positioned directly over the probe on the opposite surface, the LDV signal increased roughly twofold with tissue thicknesses less than 6 mm.

Based on their results, Ahn et al. claim that LDV measures blood flow to a depth of at least 6 mm. The results of Shepherd and Riedel [2,16,18,20] and Kiel et al. [12,13,19] indicate a much more shallow LDV measurement depth. One possible explanation for these divergent results is the different LDV instruments used in these studies: the Perimed (PF1d and PF2) was used in the studies by Ahn et al., and two homemade LDV instruments based on the NIH design were used by Shepherd and Riedel and by Kiel et al. Figure 13–9 shows the results of a study in which mucosal and serosal blood flow measurements by the TSI Laserflo (BPM403), the Perimed (Pf-1d), and the NIH prototype LDV instruments in the canine stomach were compared. As the figure clearly shows, all three instruments registered pronounced increases in mucosal perfusion that were not detected from the serosal surface during the reactive hyperemia following one-minute arterial occlusion and during infusion of isoproterenol. Therefore, the discrepancies between the studies by Ahn et al. and those of Shepherd and Riedel and Kiel et al. cannot be explained by differences between the LDV instruments.

Differences in the experimental application of the LDV technique are a more likely explanation for the discrepancy. In the studies by Shepherd and Riedel and by Kiel et al., extensive precautions were taken to isolate the preparations from extraneous sources of motion. As an extreme example, the institutional air conditioning system was turned off on several occasions to verify that building vibrations did not affect the LDV signal. In addition, the LDV probes were positioned at the same location for the duration of the experiments with micromanipulators, clamps, or a specially modified record-player tone-arm. The tone-arm allowed the LDV probe to ride the waves of motility and dramatically reduced the motion noise in the LDV signal [19]. Although motility-induced artifacts occurred occasionally, they were readily distinquished from the normal flow signal. By contrast, in most of the studies by Ahn et al., the LDV probe was hand-held, and the tissue was not isolated from extraneous sources of motion. Indeed, Ahn has stated that "continuous recordings were difficult to obtain, owing to signal artifacts mainly caused by relative motion between the probe tip and the tissue surface," that "breathing movements often caused similar artifacts," and that "the fact that the probe was held manually against the tissue surface also

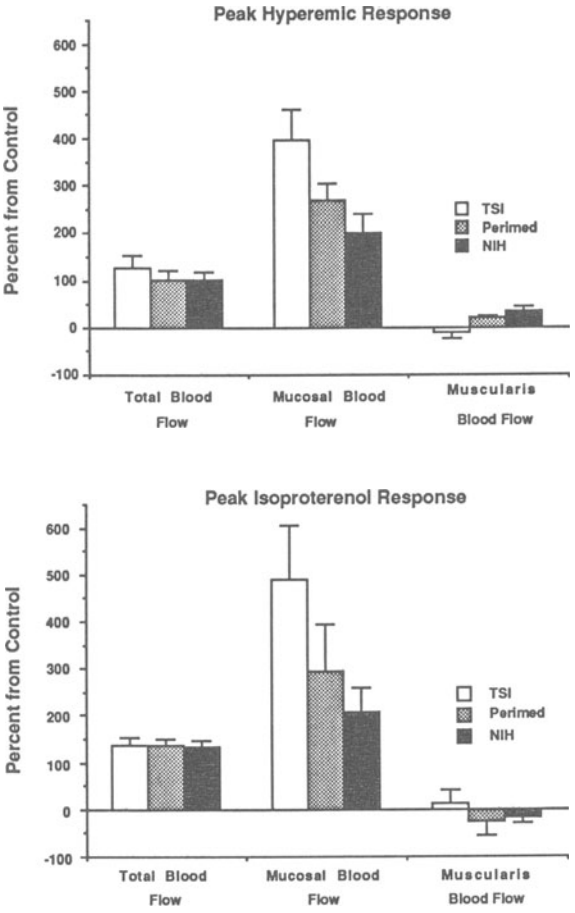

Figure 13–9. Comparison of gastric reactive hyperemia and isoproterenol responses recorded by three LDV instruments: TSI, Laserflo BPM 403; Perimed, PF1d; and NIH prototype. In isolated canine stomach flaps perfused at constant pressure (120 mmHg) from a pressurized reservoir, all three instruments registered qualitatively similar increases in perfusion from the mucosal surface that were not detected from the serosal surface during both interventions.

contributed to the disturbances" [6]. Thus, the disregard for the exquisite motion sensitivity of the LDV technique and the necessarily subjective data analysis by Ahn et al. may account for their results. Moreover, the mirror experiments cast doubt on their understanding of the LDV principle of operation: placing a hand-held mirror on the opposite side of the tissue simply increases the probability of a photon returning to the detecting fiber. The resulting increase in the LDV signal is meaningless.

Motion sensitivity and other problems

The controversy over the depth of the LDV measurement highlights some of the problems inherent in the technique. LDV is an exquisitely sensitive motion detector, and many extraneous sources of noise (e.g., respiratory movements, perfusion pumps, stirrers, and recorder-chart motors) cause mechanical vibrations in the same frequency range as the Doppler shifts produced by red blood cells moving in tissue. Moreover, muscle fasiculations, macromolecular diffusion, vasomotion, red blood cell settling, and any tissue motion relative to the LDV probe may add to the LDV signal. Indeed, a low, positive flow signal often persists even during complete occlusion of the vascular supply to perfused preparations [5,15,27]. Additionally, regression analysis of LDV and total blood flow measurements frequently yields a positive intercept on the LDV axis. However, when tested with mechanical models isolated from extraneous motion, LDV flowmeter readings are reproducible, consistently register zero at zero flow, and extrapolate to a zero intercept [1,28,29]. Therefore, the persistence of the LDV signal in the absence of net blood flow in vivo is not caused by instrument instability but rather originates from an external source of motion that should be eliminated, or from an intrinsic and unavoidable motion source. If the intrinsic noise is assumed to be constant, the problem can be overcome in isolated, perfused preparations by relating the LDV signal to the flow value during an occlusive zero. However, no compensation is possible at tissue loci that preclude vascular occlusion.

Because LDV is highly motion-sensitive and because gastrointestinal organs are inherently motile, it is not surprising that motility-induced artifacts occur during LDV measurements in the stomach and intestine. In fact, rhythmic LDV signal oscillations are commonly recorded in both tissues. However, the oscillations in the LDV signal are not motion artifacts, as figure 13–10 shows. When isolated stomach flaps are perfused with normal blood [12,13], the oscillations in the LDV signal occur at the same frequency as the spikes of electrical activity and the peristaltic waves. However, when the perfusate is switched to a cell-free albumin solution, the reduced viscosity increases total blood flow, but the LDV signal falls to zero since there are no red blood cells to cause Doppler shifts. More importantly, the LDV oscillations are abolished despite the persistence of the electrical activity in the muscularis. Upon reperfusion with normal blood, the LDV signal and the oscillations return. If the LDV oscillations were due to the motion of nonsanguinous tissue, the oscillations should occur in the absence of moving red blood cells, but the magnitude of the signal should be reduced. Therefore, the LDV oscillations are a faithful representation of mucosal blood flow, not motion artifacts. Similar fluctuations in mucosal blood flow have been recorded by thermal clearance techniques [30] and intravital microscopy [31].

Figure 13–10 also underscores the focal nature of the LDV measurement.

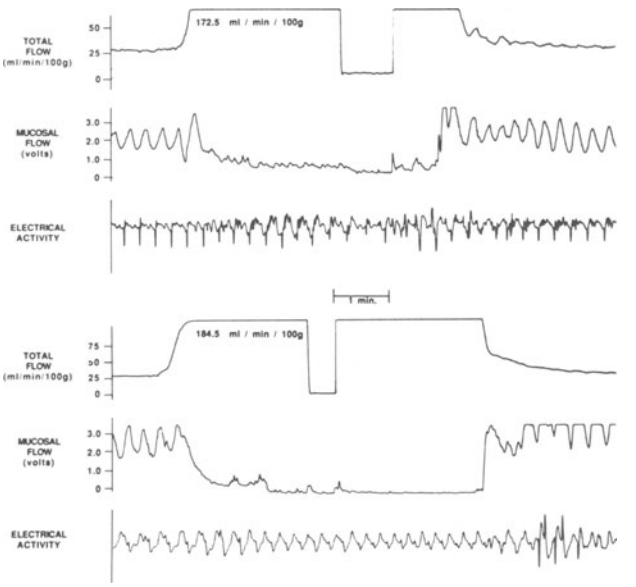

Figure 13–10. Motility-related LDV signal oscillations. In two isolated canine stomach flaps perfused with normal blood (hematocrit ~40%) at constant pressure (120 mmHg), oscillations in LDV (NIH prototype) mucosal flow signal occured at the same frequency as the spikes of electrical activity in the muscularis. When the perfusate was changed to a cell-free albumin solution, total blood flow increased, but the LDV signal was abolished (upper panel). The LDV signal oscillations were also eliminated despite the persistence of the electrical activity in the muscularis. When the perfusate was switched back to normal blood, the LDV signal and the oscillations returned (lower panel). The absence of LDV signal oscillations during cell-free perfusion indicates that the oscillations are not motion artifacts caused by the movement of nonsanguinous tissue. (Reproduced from Kiel et al. [13] by permission of the American Gastroenterological Association.)

As the figure shows, the oscillations in mucosal blood flow coincide with the passage of each peristalic wave of motility at the probe location. In fact, the oscillations registered by two LDV probes placed on the mucosal surface occur at the same frequency, but the oscillations become more phase-shifted as the probes are placed farther apart along the peristaltic axis (authors' personal observation). Because total blood flow is the summation of the local out-of-phase events throughout the preparation, it is not surprising that local flow fluctuations are not apparent in total blood flow (figure 13–10). It is also obvious that flow measurements in a small volume of tissue may not be representative of the entire target tissue. For example, the mean LDV flow signals measured simultaneously at two locations in the same preparation are often different. Moreover, as figure 13–11 shows, the relationships between total blood flow and local blood flow measured by LDV in the same tissue can be characterized by significantly different slopes. The cause of this

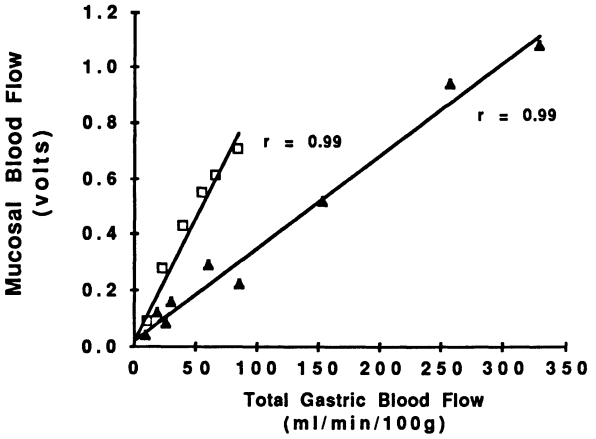

Figure 13–11. LDV (TSI Laserflo BPM 403) measurements of mucosal blood flow in two vasodilated canine stomach flaps plotted against electromagnetic total blood flow. The relationship between LDV mucosal perfusion and total blood flow was linear in both experiments, but the slopes were significantly different ($p < 0.01$). (Reproduced from Shepherd et al. [1] by permission of the American Physiological Society.)

variability is unknown; however, local variations in microvascular organization and capillarity are one plausible explanation [27].

Calibration

Figure 13–11 illustrates a further consequence of the selectivity afforded by LDV. As might be expected, the spatial resolution provided by LDV is both advantageous and disadvantageous. On the one hand, the ability to measure blood flow in a small volume of tissue is desirable for detecting ischemic regions that might precede the formation of an ulcer or other lesions. On the other hand, such a restricted measurement is subject to local inhomogeneities in microvascular organization and may not be representative of blood flow throughout the tissue. Consequently, the slopes of the lines relating the local flow measurements by LDV to total blood flow vary considerably from one animal to another or one location to another (figure 13–11). Moreover, even when LDV is compared with another local flow measurement such as hydrogen clearance [23], the slopes still vary considerably (figure 13–12). Thus, even though the spatial resolution provided by LDV is advantageous in some respects, it also precludes the calibration of the LDV signal in absolute units. The calibration problem is further exacerbated by the ambiguity about the precise LDV measurement volume.

One possible solution to this problem is to make multiple measurements at different locations and average the results. With a single LDV instrument, this approach is tedious and subject to time-dependent flow alterations.

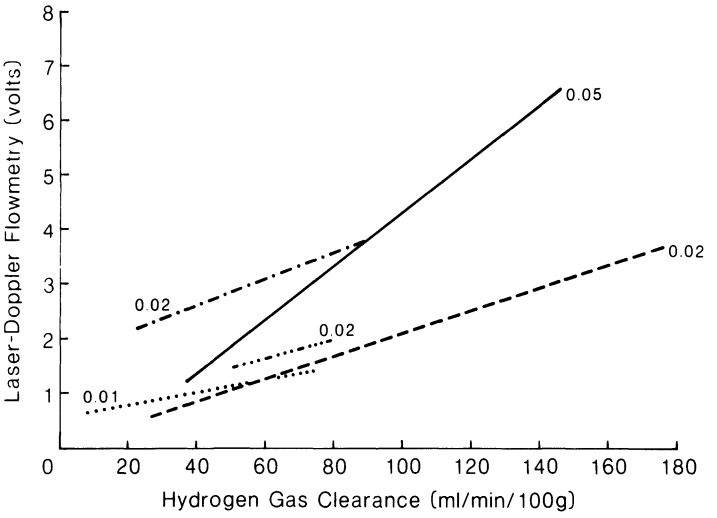

Figure 13–12. Correlation between LDV and hydrogen clearance measurements of mucosal blood flow in canine stomach flaps (n = 5). In each experiment, LDV measurements of mucosal perfusion correlated linearly with hydrogen clearance flow measurements at approximately the same location; however, the slopes were significantly different. (Reproduced from Gana et al. [23] by permission of Academic Press.)

Simultaneous recordings with multiple LDV instruments is another possibility, but an expensive one. Salerud and Nilsson [32] have suggested modifying the standard, single receiving fiber probe used in most LDV instruments. The new probe design consists of seven receiving fibers to collect the light scattered at seven different tissue locations. In preliminary tests, the modified probe significantly reduced the site-to-site variability obtained with a standard LDV probe at adjacent sites on the human forearm.

LDV APPLICATIONS IN BASIC AND CLINICAL RESEARCH

Although calibration of the LDV signal into absolute flow units would greatly enhance the utility of the method, the lack of a universal calibration constant does not preclude its use in studying gastrointestinal hemodynamics. Indeed, because LDV provides a continuous, local measurement, the method has provided new insight into many phenomena inaccessible to more conventional flow-measuring techniques.

Basic research

The ability to record dynamic circulatory events is the main advantage of LDV over the other available techniques for selectively measuring gastrointestinal blood flow. Consequently, the principal application of LDV in physiological studies has been the assessment of transitory phenomena such

as local blood flow regulation within the different layers of the gastrointestinal wall. In isolated stomach and intestine preparations, measurements of total blood flow show many phenomena indicative of local circulatory control: blood flow autoregulation [33,34], reactive hyperemia [35,36], functional hyperemia [22,37], autoregulatory escape from sympathetic stimulation [38,39], and the so-called *myogenic response* to increased venous pressure [40,41]. What was unclear prior to the advent of LDV was whether local control was expressed uniformly throughout the gastrointestinal wall or whether local control was more pronounced in a particular layer. Studies with LDV show that the efficacy of local control is most pronounced in the mucosal circulation, whereas the muscularis is relatively passive.

Local circulatory control is defined as the intrinsic ability of an isolated organ or tissue to regulate its blood flow through active adjustments of vascular smooth muscle tone. Blood flow autoregulation or the relative constancy of blood flow despite changes in perfusion pressure is a classic example of local control. Prior to the development of LDV, the possibility of autoregulation within the separate layers of the gastrointestinal wall had not been investigated. In isolated stomach flaps, Kiel et al. [13,19] monitored mucosal and muscularis blood flow with LDV and total blood flow with an electromagnetic flow probe. Figure 13–13 shows their results. Despite the lack of autoregulation in total blood flow, mucosal blood flow was relatively constant throughout the physiologic range of perfusion pressures. By contrast, blood flow in the muscularis was poorly autoregulated. This LDV study provided the first evidence for autoregulation in the gastric mucosal circulation. The importance of this finding is underscored by the fact that gastric oxygen uptake parallelled the changes in mucosal blood flow and that oxygen uptake became flow-dependent when the mucosa failed to autoregulate. The likelihood that gastric mucosal integrity depends on both metabolic processes and the washout of backdiffusing acid makes the mucosal autoregulation recorded by LDV noteworthy to both physiologists and clinicians.

Autoregulation has been attributed to metabolic and myogenic mechanisms [42–45]. LDV has provided evidence for both mechanisms in the gastric mucosal circulation. Reactive hyperemia is one example of metabolic control that has been investigated with LDV. As noted in the Validation section above, LDV probes on the mucosal and serosal surfaces show that the reactive hyperemic response following the release of an arterial occlusion is confined to the mucosal circulation and seldom occurs in the muscularis (figures 13–6 and 13–9). According the metabolic theory of local control [42], the overshoot in blood flow following the release of an arterial occlusion is caused by vasodilator metabolites that accumulate during the occlusion. Consequently, the magnitude of the reactive hyperemia should vary directly with the duration of the arterial occlusion. Measurements of total blood flow in isolated stomach and intestine preparations show that the magnitude of the

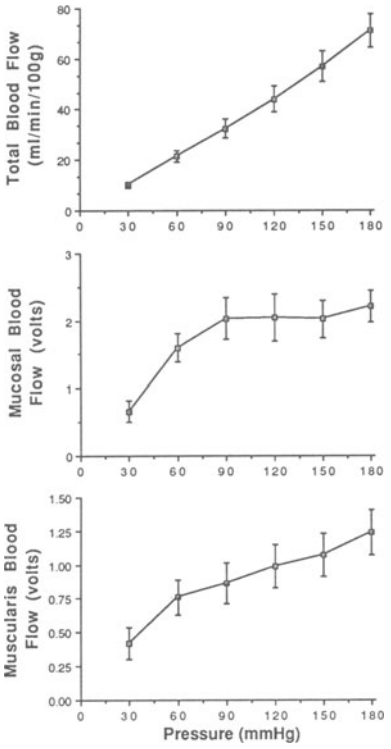

Figure 13–13. Autoregulation of mucosal blood flow in nonstimulated canine gastric flaps (n = 10) perfused from a pressurized reservoir of arterial blood. Total blood flow (upper panel) was not autoregulated. Lack of change in blood flow recorded by LDV (NIH prototype) probe on mucosa (middle panel) indicates pronounced autoregulation in the mucosal circulation over most of the pressure range. Changes in blood flow recorded by LDV (NIH prototype) probe on muscularis (lower panel) indicate limited autoregulation in the muscularis circulation. (Reproduced from Kiel et al. [13] by permission of the American Gastroenterological Association.)

reactive hyperemic response depends on the duration of the arterial occlusion [35,36]. Figure 13–14 shows that, like total blood flow, the magnitude of the mucosal hyperemic response in the stomach increases with increasing occlusion duration [19]. LDV has also shown in the intestinal mucosa that the reactive hyperemic response depends on the occlusion duration [18].

LDV has also provided evidence for myogenic control in the gastric mucosal circulation. According to the myogenic theory of local control [43–45], vascular smooth muscle acts to maintain a constant wall tension in resistance vessels. Thus, an increase in transmural pressure elicited by elevating venous pressure should evoke active vascular contraction and increase resistance. In isolated stomach and intestine preparations, elevated venous

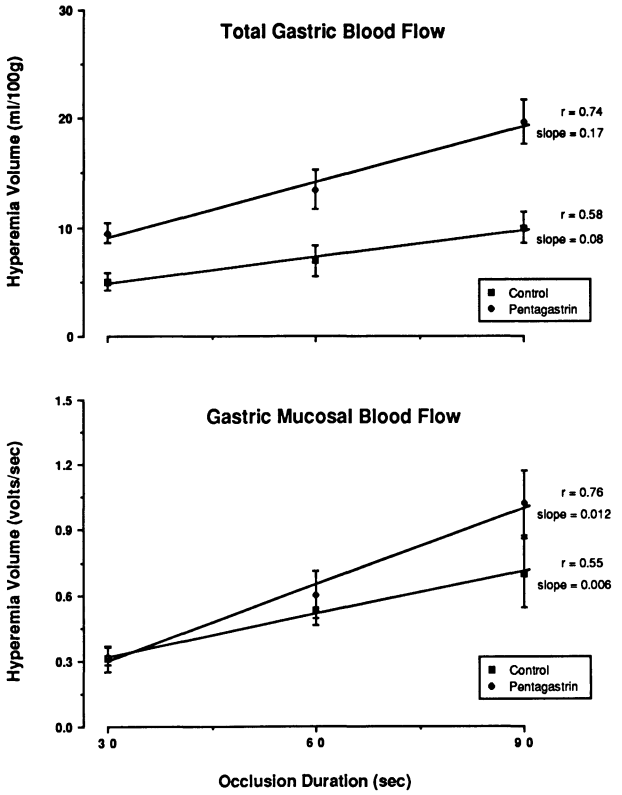

Figure 13–14. Volume of gastric reactive hyperemia plotted as a function of occlusion duration. In control and pentagastrin-stimulated gastric flaps perfused at constant pressure (120 mmHg), magnitude of reactive hyperemic response in total and mucosal blood flow increased with increasing occlusion duration. Total blood flow was measured with an electromagnetic flow probe. Mucosal blood flow was measured by LDV (NIH prototype). (Reproduced from Kiel et al. [19] by permission of the American Gastroenterological Association.)

pressure causes a disproportionate decrease in total blood flow indicative of myogenic reactivity [40,41,45]. During elevated venous pressure in gastric flaps [19], LDV measurements show that, like the reactive hyperemic response, the myogenic response is confined to the mucosal circulation (figure 13–15). In this case, LDV confirmed previous intravital microscopic observations in the rat intestine that indicated that such myogenic reactivity occured in submucosal but not muscularis arterioles [46].

Other examples of LDV findings that confirm results obtained previously with conventional techniques for measuring regional perfusion are 1) the functional hyperemic response that occurs in the gastric and intestinal mucosa during stimulated acid secretion [19,21] and glucose absorption [20,22], 2) the mucosal autoregulatory escape from sympathetic stimulation [47–50],

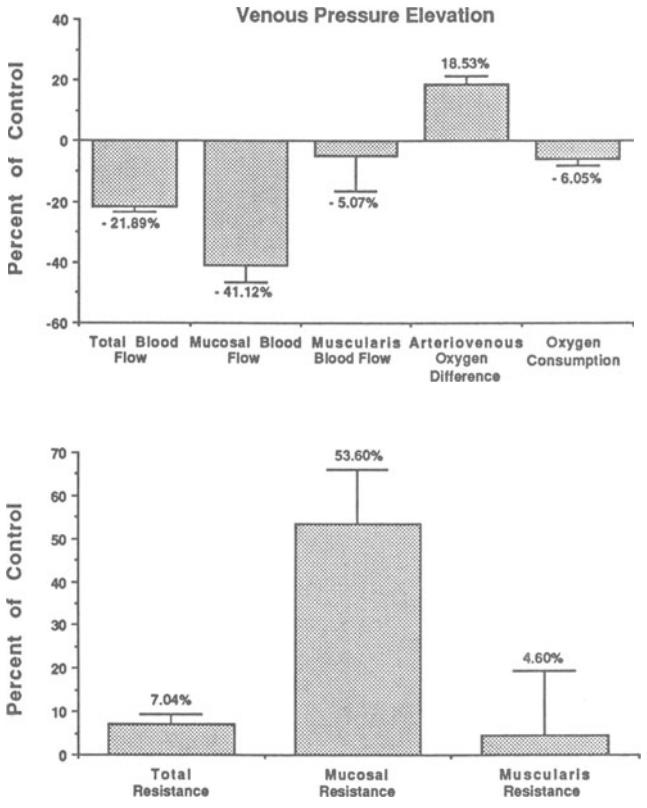

Figure 13–15. Gastric response to venous pressure elevation. In nonstimulated stomach flaps perfused at constant arterial pressure (120 mmHg), elevating venous pressure from 0 to 20 mmHg caused a disproportionate decrease in total blood flow. LDV (NIH prototype) probes on the mucosal and serosal surfaces indicated that the myogenic response was confined to the mucosal circulation. Increased oxygen extraction (as indicated by the arterio-venous oxygen difference) was insufficient to prevent a small but significant decrease in oxygen consumption. (Reproduced from Kiel et al. [19] by permission of the American Gastroenterological Association.)

and 3) the different effects of selective vasodilators on the mucosal and muscularis circulations [12,16,17,51]. What had not been noted previously with conventional, discontinuous techniques was that the different propensities of the mucosal and muscularis circulations to vasodilate can cause one vascular bed to rob blood flow from the other. Simultaneous and continuous LDV measurements of mucosal and muscularis blood flow reveal that a "vascular steal" mechanism occurs within the intestinal wall [16].

As the foregoing examples illustrate, the lack of a calibration constant does not preclude the use of LDV in basic gastrointestinal research. When used properly, LDV is the only available regional blood-flow-measuring technique

that is capable of recording dynamic circulatory events such as reactive hyperemia or the transient flow changes during sympathetic stimulation. However, the validity of results obtained with LDV depends on recognizing the limitations of the technique and taking appropriate precautions. In the types of preparations used in basic research, it is fairly easy to eliminate extraneous sources of motion and to obtain a zero-flow reference point. These precautions are not so easily applied in clinical settings.

Potential clinical applications

In addition to providing a continuous measurement, a further advantage of LDV in clinical applications is that LDV is relatively noninvasive. It is a seemingly simple matter to place an LDV probe at any number of sites on any exposed tissue surface: flow measurements are obtained instantly, and no tissue specimens are required. For the surgeon or gastroenterologist, any technique with these capabilities would be ideal for determining ischemic regions during bowel resection [52] and predicting subsequent tissue viability or for monitoring the healing edge of an ulcer or other lesion through an endoscope. In fact, the potential for combining LDV with endoscopy is one of the most promising clinical applications of LDV. However, LDV's ease of use is deceptive. Because of its extreme motion sensitivity, even measurements obtained with a hand-held LDV probe against a quiescent tissue are questionable. Obviously, it is no simple matter to achieve valid flow measurements using a hand-held endoscope to position an LDV probe against the mucosal surface of an inherently motile organ like the stomach than is also subject to the respiratory, cardiac, and voluntary movements of the patient.

Several investigators have attempted to measure mucosal blood flow through an endoscope. Two of the more thorough feasibility studies were performed by Kvernebo et al. [53] and by Chung et al. [54], who used the Perimed (model not stated) and the TSI (Laserflo, BPM403) instruments, respectively. Both studies found that light-to-moderate probe contact (i.e., a force of 5–20 g/cm^2 that dimpled the mucosal surface by ~1 mm) was essential for obtaining a stable LDV signal. Insufficient contact caused an obvious loss of optical coupling, whereas pushing the probe with too much force against the mucosal surface caused the flow signal to decrease significantly.

Even with appropriate probe contact, both Kvernebo et al. [53] and Chung et al. [54] reported similar, recognizable artifacts in the LDV signal. As shown in figure 13–16, signal fluctuations, synchronous with heart rate, respiration, and peristalic contractions were readily distinguished. The fluctuations synchronous with the pulse and respiration could be minimized by changing the time-constant on the LDV instruments. Obvious motility-induced artifacts could not be eliminated, but could be disregarded. Rhythmic signal oscillations similar to those found by Kiel et al. [11,12] (see figure 13–10) under more controlled conditions were also observed. Kvernebo

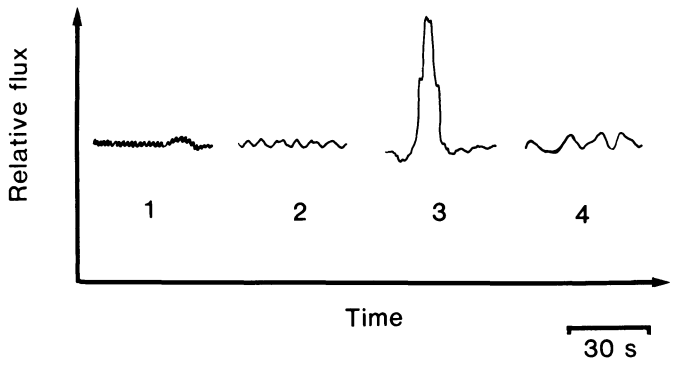

Figure 13–16. Endoscopic LDV recordings. LDV signal fluctuations sychronous with heart rate (1), respiration (2), and motility (3) are readily distinguished from normal oscillatory flow pattern (4). Oscillatory flow pattern recorded by endoscopic LDV is similar to that recorded under more controlled conditions in animal preparations (see figure 13–10). (Reproduced from Kvernebo et al. [13] by permission of the Norwegian University Press (Universitetsforlaget AS), Oslo.)

et al. [53] also assessed the spatial and temporal variability of endoscopic measurements of perfusion by LDV. They found little difference between LDV measurements at adjacent locations (probes placed 0.5–1.0 cm apart) in a given region or between readings taken ten minutes apart at the same location. Moreover, Kvernebo et al. [53] found no change in the LDV signal with angulation of the LDV probe up to 60° away from the perpendicular axis.

Kvernebo et al. [53] and Chung et al. [54] also made clinically relevant LDV measurements during the course of their feasibility studies. In the study by Kvernebo et al. [53], mucosal blood flow was measured at eight different locations in the esophagus and stomach in 23 healthy, fasted volunteers. Their results indicate that in conscious man, mucosal blood flow in the region of the greater curvature is significantly greater than in the lesser curvature. In the study by Chung et al. [54] mucosal blood flow measurements at the juxta-esophageal region of the fundus were compared in three groups of patients: controls without portal hypertension, portal hypertensives with newly developed esophageal varices, and portal hypertensives whose esophageal varices had been successfully treated by sclerotherapy. Their results show that fundic mucosal blood flow is significantly elevated in portal hypertensive patients and that sclerotherapy did not alter fundic mucosal blood flow in these patients.

These two studies indicate that stable measurements of gastric mucosal blood flow can be obtained by carefully applying the LDV probe through an endoscope. However, Chung et al. [54] reported that it was difficult to maintain optical coupling between the probe and the mucosal surface for

periods longer than 30–45 seconds. Moreover, the limited spatial variability noted by Kvernebo et al. [53] conflicts with the previously mentioned site-to-site variability observed in animal preparations under more controlled conditions [32]. These facts, plus the current inability to convert the LDV signal into absolute units, limit the clinical applications of endoscopic LDV. If it is not possible to position the probe in the same location throughout a given intervention, it is difficult to determine whether a subsequent flow change was caused solely by a particular intervention or simply reflects a different microvascular arrangement under the probe at a different location. Furthermore, the lack of a calibration constant and the inability to obtain a zero reference value complicate qualitative assessments of flow changes. Lastly, for diagnostic purposes, endoscopic LDV is constrained by the inability to eliminate extraneous motion or to account for the consequent nonflow component of the LDV measurement: without a reference point, it is difficult to distinguish whether a *steady* LDV signal is an accurate indication of "normal" mucosal blood flow or motility artifacts generated by ischemia. These issues must be resolved before endoscopic LDV can be accepted as a routine clinical procedure.

CONCLUSIONS

The gastrointestinal tract poses unique challenges and opportunities for LDV. The traditional techniques for fractionating gastrointestinal blood flow (e.g., microspheres and hydrogen clearance) are discontinuous and limited to steady-state measurements. By contrast, LDV provides a continuous measurement and is well suited for studying otherwise inaccessible hemodynamic behavior. However, there are several limitations of the technique, notably the unknown volume of tissue in which LDV measures blood flow and the extreme motion sensitivity of the technique. These are relatively minor concerns in homogeneous and immobile tissues, but they become serious problems in the gastrointestinal tract with its different tissue layers and inherent motility.

As we have seen, the ambiguity about the measurement volume not only complicates calibration in conventional flow units but also makes it difficult to ascribe blood flow responses definitively to a particular tissue layer. Moreover, the use of a motion detector like LDV in a motile tissue requires both ingenuity and vigilance to eliminate or at least minimize the nonflow component of the LDV signal. However, we have also seen evidence that LDV provides a superficial measurement in gastrointestinal tissue and that stable LDV signals can be obtained when proper precautions are taken to minimize extraneous sources of motion and to maintain constant optical coupling between the probe and tissue.

LDV is largely past the validation phase of its development. Moreover, some of the problems encountered with LDV in the gastrointestinal system will probably be overcome. The difficulty in stabilizing the LDV probe

during endoscopy might be overcome by a simple modification of the LDV probe: Demling and Wachsmann [30] achieved stable thermal clearance measurements of gastric mucosal blood flow when the probe was held in place with slight negative pressure and a magnet. Moreover, in both research and clinical applications, the multifiber probe proposed by Salerud and Nilsson [32] could be used to reduce the site-to-site variability and provide more representative measurements. Additional optical fibers could also be incorporated into the probe to illuminate the tissue with light at other wavelengths to provide spectrophotometric information about blood in the capillaries (e.g., percent saturation and oxygen content). LDV has already proven its usefulness in gastrointestinal research. As the technique evolves, it will undoubtedly continue to deepen our understanding of the physiology and pathophysiology of the gastrointestinal circulation.

REFERENCES

1. Shepherd, A.P., G.L. Riedel, J.W. Kiel, D.J. Haumschild, and L.C. Maxwell. 1987. Evaluation of an infrared laser-Doppler blood flowmeter. Am J Physiol 252:G832–G839.
2. Shepherd, A.P. and G.L. Riedel. 1982. Continuous measurement of intestinal mucosal blood flow by laser-Doppler velocimetry. Am J Physiol 242:G668–G672.
3. Bonner, R.F., T.R. Clem, P.D. Bowen, and R.L. Bowman. 1981. Laser-Doppler continuous real-time monitor of pulsatile and mean blood flow in tissue microcirculation. In Scattering Techniques Applied to Suptra-molecular and Nonequilibrium Systems, Chen, S.H., Chu, B., Nossal R., eds. New York: Plenum, vol. 73, pp 685–702 (NATO AS 1 Ser B).
4. Ahn, H., J. Lindhagen, G.E. Nilsson, E.G. Salerud, M. Jodal, and O. Lundgren. 1985. Evaluation of laser Doppler flowmetry in the assessment of intestinal blood flow in cat. Gastroenterology 88:951–957.
5. Ahn, H., K. Johansson, O. Lundgren, and G.E. Nilsson. 1987. In *vivo* evaluation of signal processors for laser Doppler tissue flowmeters. Med Biol Eng Comput 25:207–211.
6. Ahn, H., J. Lindhagen, G.E. Nilsson, P.A. Öberg, and O. Lundgren. 1986. Assessment of blood flow in the small intestine with laser Doppler flowmetry. Scand J Gastroenterol 21(7):863–870.
7. Kvietys, P.R., A.P. Shepherd, and D.N. Granger. 1985. Laser-Doppler, H_2 clearance, and microsphere estimates of mucosal blood flow. Am J Physiol 249:G221–G227.
8. Rotering, R.H., K.R. Larsen, J.A. Dixon, and F.G. Moody. 1981. The measurement of canine gastric mucosal blood flow with a laser Doppler velocimeter. Physiologist 24(4):15 (abstract).
9. Ahn, H., K. Johansson, J. Lindhagen, and E.G. Salerud. 1984. Laser Doppler flowmetry in the assessment of gastric blood flow in man. Scand J Gastroenterol 19 (Suppl 98): 33.
10. Murakami, M., H. Saida, M. Seki, M. Inada, and T. Miyake. 1984. Measurements of mucosal blood flow of the esophagus and stomach in humans: regional differences and changes with aging. Gastroenterology 86:1191 (abstract).
11. Saita, H., M. Murakami, M. Seki, and T. Miyake. 1984. Evaluation of the measurement of gastric mucosal blood flow by laser-Doppler velocimetry in rats. Gastroenterology 86:1228 (abstract).
12. Kiel, J.W., G.L. Riedel, G.R. DiResta, and A.P. Shepherd. 1985. Gastric mucosal blood flow measured by laser-Doppler velocimetry. Am J Physiol 249:G539–G545.
13. Kiel, J.W., G.L. Riedel, and A.P. Shepherd. 1987. Autoregulation of canine gastric mucosal blood flow. Gastroenterology 93:12–20.
14. Bonner, R., and R. Nossal. 1981. Model for laser-Doppler measurements of blood flow in tissue. Appl Optics 20:2097–2107.
15. Johansson, K., H. Ahn, J. Lindhagen, and O. Lundgren. 1987. Tissue penetration and

measuring depth of laser Doppler flowmetry in the gastrointestinal application. Scand J Gastroenterol 22:1081–1088.
16. Shepherd, A.P., G.L. Riedel, L.C. Maxwell, and J.W. Kiel. 1984. Selective vasodilators redistribute intestinal blood flow and depress oxygen uptake. Am J Physiol 247:G377–G384.
17. Granger, D.N., J.D. Valleau, R.E. Parker, R.S. Lane, and A.E. Taylor. 1978. Effects of adenosine on intestinal hemodynamics, oxygen delivery, and capillary fluid exchange. Am J Physiol 235:H707–H719.
18. Shepherd, A.P., and G.L. Riedel. 1984. Differences in reactive hyperemia between intestinal mucosa and muscularis. Am J Physiol 247:G617–G622.
19. Kiel, J.W., G.L. Riedel, and A.P. Shepherd. 1987. Local control of canine gastric mucosal blood flow. Gastroenterology 93:1041–1053.
20. Shepherd, A.P., and G.L. Riedel. 1985. Laser-Doppler blood flowmetry of intestinal mucosal hyperemia induced by glucose and bile. Am J Physiol 248:G393–G397.
21. Holm-Rutili, L., and T. Berglindh. 1986. Pentagastrin and gastric mucosal blood flow. Am J Physiol 250:G575–G580.
22. Chou, C.C., C.P. Hsich, Y.M. Yu, P. Kvietys, L.C. Yu, R. Pittman, and J.M. Dabney. 1976. Localization of mesenteric hyperemia during digestion in dogs. Am J Physiol 230:583–589.
23. Gana, T.J., R. Huhlewch, and J. Koo. 1987. Focal gastric mucosal blood flow by laser-Doppler and hydrogen gas clearance: a comparative study. J Surg Res 43:337–343.
24. DiResta, G.R., J.W. Kiel, G.L. Riedel, P. Kaplan, and A.P. Shepherd. 1987. Hybrid blood flow-probe for simultaneous H_2 clearance and laser-Doppler velocimetry. Am J Physiol 16:G573–G581.
25. Ahn, H., J. Lindhagen, and O. Lundgren. 1986. Measurement of colonic blood flow with laser Doppler flowmetry. Scand J Gastroenterol 21(7):871–880.
26. Ahn, H., K. Johansson, and J. Lindhagen. 1986. Local blood flow changes in association with proximal gastric vagotomy. Scand J Gastroenterol 21(8):961–964.
27. Johnson, J.M., W.F. Taylor, A.P. Shepherd, and M.A. Park. 1984. Laser-Doppler measurement of skin blood flow: a comparison with plethysmograph. J Appl Physiol 56:798–803.
28. Nilsson, G.E. 1984. Signal processor for laser Doppler tissue flowmeters. Med Biol Eng Comput 22:343–348.
29. Nilsson, G.E., T. Tenland, and P.Å. Öberg. 1980. Evaluation of a laser Doppler flowmeter for measurement of tissue blood flow. IEEE Trans Biomed Eng BME-27:597–604.
30. Demling, L., and F. Wachsmann. 1961. A new method for measuring blood flow variations in the gastric mucosa. Ger Med Monthly 6:189–191.
31. Holm-Rutili, L., and K.J. Öbrink. 1985. Rat gastric mucosal microcirculation in vivo. Am J Physiol 248:G741–G746.
32. Salerud, E.G., and G.E. Nilsson. 1986. Integrating probe for tissue laser Doppler flowmeters. Med Biol Eng Comput 24:415–419.
33. Shepherd, A.P. 1980. Intestinal blood flow autoregulation during foodstuff absorption. Am J Physiol 239:H156–H162.
34. Perry, M.A., D. Murphree, and D.N. Granger. 1982. Oxygen uptake as a determinant of gastric blood flow autoregulation. Dig Dis Sci 27:675–679.
35. Selkurt, E.E., C.F. Rothe, and D. Richardson. 1964. Characteristics of reactive hyperemia in the canine intestine. Circ Res 15:532–544.
36. Perry, M.A., G.B. Bulkley, P.R. Kvietys, and D.N. Granger. 1982. Regulation of oxygen uptake in resting and pentagastrin-stimulated canine stomach. Am J Physiol 242:G565–G569.
37. Moody, F.G. 1967. Gastric blood flow and acid secretion during direct intraarterial histamine administration. Gastroenterology 52:216–224.
38. Folkow, B., D.H. Lewis, O. Lundgren, S. Mellander, and I. Wallentin. 1964. The effect of graded vasoconstrictor fibre stimulation on the intestinal resistance and capacitance vessels. Acta Physiol Scand 61:445–457.
39. Jansson, G., M. Kampp, O. Lundgren, and J. Martinson. 1966. Studies on the circulation of the stomach. Acta Physiol Scand 68 (Suppl 277):91.
40. Shepherd, A.P. 1977. Myogenic responses of intestinal resistance and exchange vessels. Am J Physiol 233:H547–H554.
41. Lutz, J., and J. Biester. 1971. Die Reaktion der Magengefässe auf venöse und arterielle

Druckreize und ihr Vergleich mit Werten von Milz- und Intestinalstrombahn. Pflügers Arch 330:230–242.
42. Shepherd, A.P., and H.J. Granger. 1973. Autoregulatory escape in the gut: a systems analysis. Gastroenterology 65:77–91.
43. Folkow, B. 1964. Description of the myogenic hypothesis. Circ Res 14 (Suppl 1):279–285.
44. Johnson, P.C. 1967. Autoregulation of blood flow in the intestine. Gastroenterology 52:435–441.
45. Johnson, P.C. 1965. Effect of venous pressure on mean capillary pressure and vascular resistance in the intestine. Circ Res 16:294–300.
46. Davis, M.J., and R.W. Gore. 1985. Capillary pressures in rat intestinal muscle and mucosal villi during venous pressure elevation. Am J Physiol 249:H174–H187.
47. Kiel, J.W., and A.P. Shepherd. 1989. Effects of sympathetic stimulation on gastric blood flow and oxygen uptake. FASEB J 3:A714 (abstract).
48. Shepherd, A.P., and G.L. Riedel. 1988. Intramural distribution of intestinal blood flow during sympathetic stimulation. Am J Physiol 255:H1091–H1095.
49. Guth, P.H. and E. Smith. 1975. Escape from vasoconstriction in the gastric microcirculation. Am J Physiol 228:1893–1895.
50. Guth, P.H., and E. Smith. 1975. Neural control of gastric mucosal blood flow in the rat. Gastroenterology 69:935–940.
51. Archibald, L.H., F.G. Moody, and M. Simons. 1974. Effect of isoproterenol on canine gastric acid secretion and blood flow. Surg For 25:409–411.
52. Rotering, R.H., J.A. Dixon, G.A. Holloway, and D.W. McCloskey. 1982. A comparison of the HeNe laser and ultrasound Doppler systems in the determination of viability of ischemic canine intestine. Ann Surg 196:705–708.
53. Chung, R.S., D. Bruch, and J. Dearlove. 1988. Endoscopic measurement of gastric mucosal blood flow by laser Doppler velocimetry: effect of chronic esophogeal variceal sclerosis. Am Surg 54:116–120.
54. Kvernebo, K., O.C. Lunde, E. Stranden, and S. Larsen. 1986. Human gastric blood circulation evaluated by endoscopic laser Doppler flowmetry. Scand J Gastroenterol 21:685–692.

14. ALLERGY AND RESPIRATORY DISEASE

HOWARD M. DRUCE

RATIONALE FOR USING LASER-DOPPLER FLOWMETRY (LDF) IN THE NOSE

As the principal portal for entry of air into the respiratory tract, the nose is important in serving many critical functions, including conditioning inspired air and protecting the lower airways [1]. The human nose has evolved to meet the specific needs of an upright biped, i.e., the olfactory mucosa is poorly developed, the surface area of mucosal surface is markedly reduced as compared to animals with a great need for heat and water exchange, but the reflex and immune defense components are complex [2]. Almost all the functions of the nose are served by the nasal mucosa (table 14–1). This tissue, in direct contact with the outside air, can produce a limited range of symptoms, i.e. obstruction, fluid secretion, sneezing, itching, bleeding, and abnormalities of odor perception [3]. Of these, obstruction is the most troublesome to patients, since it impedes breathing. It had been considered that nasal obstruction was produced solely by congestion of the capacitance blood vessels (sinusoids) in the nasal mucosa. However, there are several reasons to believe that this is an oversimplification. First, in chronic rhinitis with nasal obstruction, oral vasoconstrictors are poorly effective [4]. Second, visible decongestion has been observed in the absence of nasal mucosal blood flow (NMBF) changes (unpublished observations). Third, cellular infiltration, such as occurs in the mast-cell-mediated *late-phase reaction*, is believed to play a significant role in the nasal obstruction of chronic allergic rhinitis [5]. Attempts have been made to quantify the degree of nasal obstruction by measuring nasal airway resistance [6]. However, an objective measurement of airflow resistance may bear little relationship to the subjective sensation of blockage [7]. Techniques used to measure air flow have included measure-

Table 14–1 Functions of the nasal mucosa

Temperature and humidity control of ambient air
High blood flow (A–V shunts)
Water transudation (fenestrated capillaries)
Changes in airway resistance (venous sinusoids)
Sympathetic autonomic nervous control dominant
Filtration of particulate matter
Mucociliary system
Glandular secretions
Protection of distal (lower) airways from pathogens
Immunologic (IgA, IgE)
Mast-cell mediator production and release
Nonspecific enzymes
Olfaction
Specialized neuroepithelium

Table 14–2 Measurement of nasal microcirculation

Direct observation
Colorimetry
Thermal conductivity
Cannulation (animals)
Radioactive microspheres (animals)
Hydrogen clearance
^{133}Xe washout
Laser-Doppler flowmetry

ments of condensation produced by exhaled air on a mirror placed in front of the nose, xerography, optical measurements, measurements of inspiratory or expiratory flow, plethysmography, computer tomographic scanning, and the flow-pressure measurements of rhinomanometry [8]. Despite advances in rhinomanometric techniques, airflow resistance measurements do not reveal the cause of nasal obstruction. Not only mucosal changes, but also increases in secretions, especially with crusting and synechiae bridging the narrow portions of the nasal cavity, contribute to an elevated nasal airway resistance. Tissue edema contributes to increased volume of mucosal tissue [9].

For these reasons, attempts have been made to separate the components of nasal airway resistance and analyze them independently. Measurement of NMBF has been attempted over the years, utilizing a variety of methods (table 14–2). Initially, simple observations of mucosal color were followed by colorimetry. In animals, invasive studies with radioactive microspheres and vessel cannulation are feasible but are less applicable to humans. Two techniques are currently in active use for human measurements. These are radioactive Xenon washout (XW) and laser-Doppler flowmetry (LDF).

The nose presents other advantages for study of the microcirculation. The nose contains the only human mucous membrane mounted, as it were, on a rigid bony platform and thus amenable to a variety of quantitative proce-

dures of interest to the physiologist. It is thus a model for penetration not only of antigens but also of pollutants and drugs. Its specially adapted microvasculature, with high-speed arterio-venous shunts and large capacity venous sinusoids, makes it an interesting tissue to compare with the skin [10].

ADAPTATION OF LDF INSTRUMENT FOR NASAL MEASUREMENTS

In 1982, a collaboration was established between the laboratories of Michael Kaliner (Allergic Diseases Section, Laboratory of Clinical Investigation, National Institute of Allergy and Infectious Diseases) and Robert Bonner (Biomedical Engineering and Instrumentation Branch, Division of Research Services, NIH). This work was initiated to develop the NIH prototype (LDF) instrument for nasal use. Considerations in this development were

1. The design of a fiberoptic probe for nasal use
2. The stabilization of the probe on the nasal mucosa
3. Assurance that changes in the laser-Doppler signal were not due to movement artifact, e.g., due to respiration
4. Reliability and long-term stability of measurements
5. Obtaining adequate control data with topical nasal provocation challenge of substances known not to perturb NMBF (negative control)
6. Verification of the integrity of the system by use of substances with well-defined activities on NMBF (positive control)

Design of a fiber optic probe for nasal use

Preliminary studies showed that the only feasible access site to place a recording probe in the nose was on the anterior tip of the inferior turbinate mucosa, the portion of nasal mucosa seen on direct inspection through a rhinoscope. Other accessible areas of nasal mucosa, such as the septum, are impracticable because contact with the probe tip stimulates pain and sneeze receptors. Despite the small area of contact, there is good reason to believe that this location is of physiological importance. First, it is the point of contact of inspired air. Second, of all respiratory tract locations, the mucosa has the highest density of mast cells, goblet cells, and glands [11]. These adaptations subserve the critical filtration and defense functions of the nasal mucosa. The turbinate microvasculature is also uniquely adapted to its role of water exchange.

It is crucial that the probe remains in a fixed position relative to the mucosa during studies. Whereas other investigators have elected to keep the head static and use a stereotactic holder, we decided that to provide useful physiologic information, subjects would have to be in a comfortable upright position. It has been clearly demonstrated that changes in head posture change nasal airway resistance, and it is plausible that NMBF is altered as well [12].

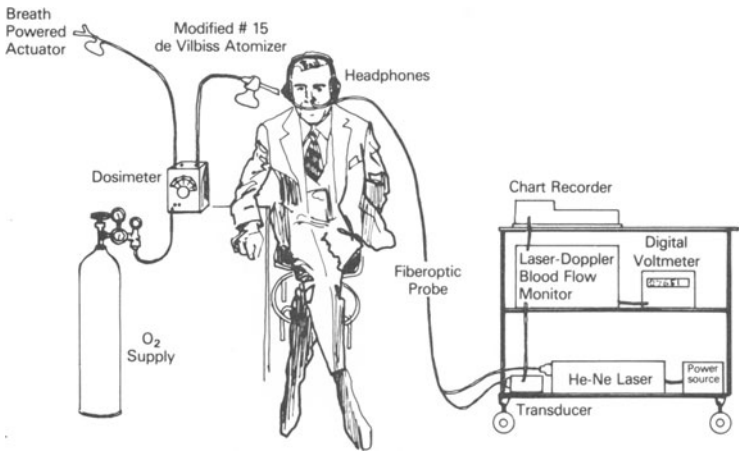

Figure 14–1. General configuration of the NIH prototype laser-Doppler flowmeter as adapted for nasal use, shown together with system for topical nasal provocation challenge using nebulized solutions.

For these reasons, we devised a probe carrier consisting of a set of audio headphones as shown in figure 14–1. (see Stabilization of Fiber Optic Probe, below). The probe consists of two parallel optical fibers each of 0.1 mm diameter separated by 0.5 mm. To maintain separation, the fiber tips are embedded in clear epoxy. The overall probe diameter is 3 mm and the distal 10 cm is enclosed in a plastic sheath. It is important that the fibers are not bent through a tight radius to prevent fracture. However, a slight curve was introduced into the terminal portion so that the probe could be placed gently on the turbinate without contacting the sensitive nasal septum. In the original NIH prototype, the helium–neon laser (632.8 nm) provided sufficient visible red light to place the probe. However, this is not possible using the nearly invisible infrared light produced by the laser diode of the TSI instrument. In consultation with Mr. Victor Kimball of TSI, an illuminated probe was manufactured to our specifications to permit nasal measurements with the TSI instrument. This probe contains a third optical fiber that is connected to a conventional light source. The overall diameter of the probe tip is not increased, and the light source is switched off while LDF readings are taking place. The optic fibers are shielded by a Mylar® encasing for added security. The probe is secured on the headphones as on the original NIH prototype [13].

Stabilization of the fiber optic probe

Since it is necessary to support the tip of the pencil probe against the nasal mucosa for periods of up to an hour, a comfortable yet rigid system is

required. Furthermore, the normal upright anatomic position of the head should be maintained so as not to interfere with other parameters of nasal physiology. To accomplish this, a set of audio headphones (Realistic Pro IIA Model 33–996, Tandy Corp., Fort Worth, Texas) was modified by the placement of a lead bar affixed to each earpiece. The lead bar was coated with heat-shrink plastic and two alligator clips affixed to the center of the bar. The headphones are placed on the subject's head, and the headpiece tightened. The probe is then inserted into the nose under direct vision and clipped to the bar. Two further refinements have since been made to the support system. The flat bar has been replaced by one of circular cross section. The alligator clips are now bonded to a larger-diameter aluminum circle that can be tightened onto the bar. A more rigid headphone has since been substituted (Koss Tech/2, Koss Corp., Milwaukee Wisconsin) (figure 14–2). Second, the subjects now sit in an ENT examination chair equipped with a curved headrest (Storz Maxi Chair Model #6500). This chair does not interfere with the headphones, but further stabilizes the subject's head. In our experience, subjects tend to relax and slouch after 10–15 minutes, or may even fall asleep even if they are undergoing serial topical nasal challenges. To counter this, music of the subject's choice can be played directly through the headphones; alternatively, a cassette player in the laboratory can be heard adequately. To improve comfort for the patient, a $\frac{3}{4}$-inch-thick foam pad is placed between the subjects' head and the headphones. A small soft pillow may be placed behind the subject's neck between the headrest and the top of the chair.

Avoidance of movement artifact

Unlike the tip of the flat probe for cutaneous applications, which is visible during studies, the tip of the pencil probe is within the nasal cavity. Although the area can be illuminated, the precise position and movement during the course of an experiment cannot be determined by direct inspection. For this reason, it was initially decided to output and record the reflected light intensity of the helium–neon laser. Sudden nonphysiological changes in this value imply probe displacement. When this occurs, the probe is gently moved in an attempt to match the previous value of reflected light intensity. If this cannot be achieved, then further readings are suspended. With the TSI Instrument (Model BPM 403), a modification has been made so that the DC output signal of the beam is obtained as a separate output, and this is constantly monitored on a sensitive DC multimeter.

CONTROL DATA

In an initial study [13], 19 nonatopic and 24 atopic subjects were studied. The nonatopic healthy subjects had no systemic disease, were not pregnant, were nonsmokers, and were on no medications. Both saline and water were delivered as inert topical nasal challenge agents. Saline reduced ipsilateral blood flow by an average of 15%, whereas water had no significant effect.

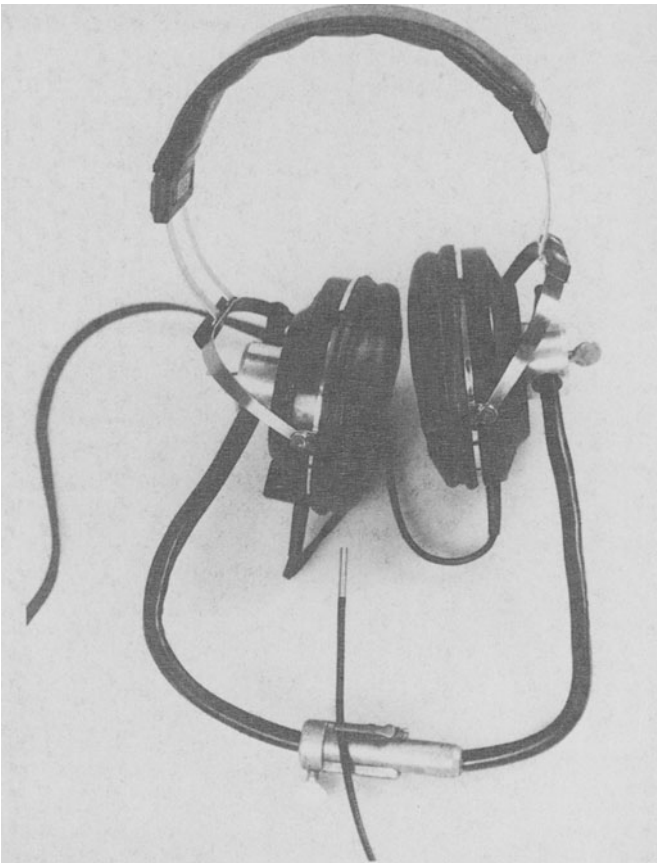

Figure 14–2. Modified headphones adapted to hold tip of laser-Doppler probe against the nasal mucosa.

Neither challenge procedure affected flow measured in the opposite nostril. The 15% value represents the maximum change in blood flow as compared to baseline readings and reflects the cumulative effects of spraying the nose on seven successive challenges at five-minute intervals. Thus it was deduced that NMBF remains relatively constant, varying less than 15% over 35 minutes during frequent contact with saline or by only 2% during contact with water. The measurements were repeated on the contralateral side with 0, 30-, and 40-minute intervals between probe placement, and NMBF varied less than 3% regardless of whether water or saline challenges were being performed on the opposite side. Thus, although day-to-day variations in a subject are considerable, short-term measurements on a particular site remain remarkably stable.

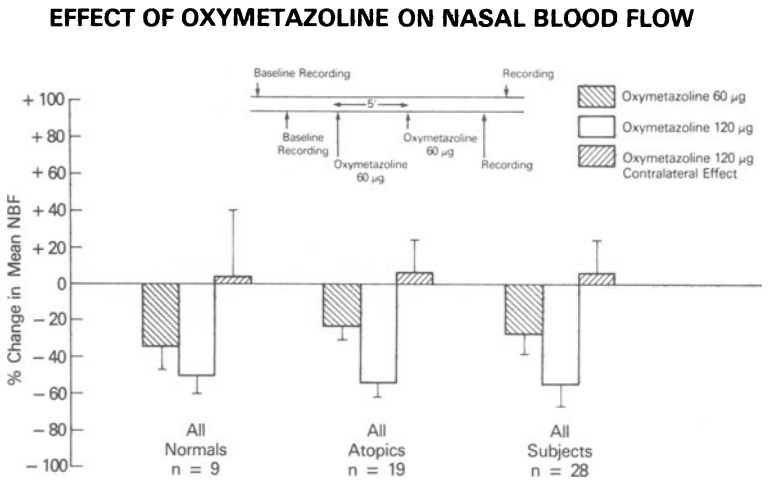

Figure 14–3. Protocol and changes in mean nasal mucosal blood flow after topical nasal challenge with oxymetazoline. (Reprinted from [14] by permission.)

NIH GROUP DATA

Since NMBF is controlled predominantly by sympathetic alpha-adrenergic tone, we decided to challenge the nasal mucosa with topical phenylephrine and oxymetazoline. These are alpha-adrenergic agonist nasal decongestants, and would be expected to produce a fall in NMBF. We also investigated the effects of methacholine hydrochloride, an analogue of acetylcholine on NMBF.

Administration of 60 μg of oxymetazoline hydrochloride by nasal spray reduced NMBF by 35% in nine nonatopic subjects, 22% in 19 atopics, and 26% in the two groups. When a second 60 μg challenge was administered five minutes later, NMBF was further reduced to 50% below baseline in nonatopic subjects, 56% in atopic subjects, and 54% in both groups. Thus oxymetazoline produced a dose-dependent reduction in NMBF. Measurement of contralateral blood flow after oxymetazoline challenge revealed no significant effect (figure 14–3).

Serial provocations with individual doses of 120–1200 μg phenylephrine were given. An average cumulative dose of 1456 μg reduced NMBF by 50%.

Increasing doses of methacholine hydrochloride (0.05–100 mg/ml) were sprayed into the nose at five-minute intervals. Two sets of experiments were performed with six subjects in each. In the first set, methacholine challenge was given without any pretreatment, and no significant effect on NMBF was seen. The second set of experiments was preceded by five minutes with a spray of 120 μg oxymetazoline hydrochloride. Again, methacholine continued to have no appreciable effect on NMBF.

Further development work [14] was undertaken on the NIH instrument, and later applied to the TSI BPM 403. A circuit was incorporated that measures blood volume and mean red blood cell (RBC) speed. By derivation, pulsatility of flow can be determined. Challenges with aerosolized buffered saline or water did not affect these parameters. Nasal application of the alpha-adrenergic agonists reduced NMBF without any significant change in blood volume. This suggests a selective alpha-agonist effect on resistance vessels but not on capacitance vessels. These data are shown in figures 14–4A–D. Topical cholinergic stimulation with methacholine selectively reduced the blood volume without affecting other parameters.

DATA FROM SCANDINAVIAN STUDIES

In 1984, Bisgaard et al. [15] reported a series of nine normal subjects challenged with topical leukotriene D4 to the nasal mucosa. Over the range of 0.063–4.0 nmoles of LTD4, a dose–response increase in NMBF was seen, without corresponding increase in nasal secretion. This study was performed with the Perimed instrument.

The LDF methodology used in this study was explained in more detail in a report by Olsson et al. [16]. Again, nine normal subjects were studied. Subjects were studied resting in the supine position. A stainless steel head probe of outside diameter 1.5 mm was applied at right angles to the mucosa of the anterior part of the inferior turbinate. The probe was fixed in position using a Leyla retractor, which was attached to a hard plastic crown on the subject's head. This crown was held in place with an elastic headband. In this study, after five minutes of stable NMBF recording, the feet were momentarily exposed to cold water (10 ± 1°C) to above the ankles (12 cm), in 12 experiments. The feet were kept immersed in the water for five minutes and were reimmersed for five minutes during subsequent measurement of NMBF. A mean decrease in NMBF of 24% was seen upon exposure to the cold stimulus. The maximum effect occurred 33 seconds after the cold water was applied, and thereafter the blood flow gradually returned to prechallenge values. This correlated with a decrease in nasal mucosal temperature from 35.2 ± 0.9°C (mean ± SD, $n = 6$) to 34.5 ± 0.9°C. These data are consistent with those derived by other methods. The authors concluded that the instrument seemed useful for monitoring changes in NMBF.

The data on leukotriene challenge was expanded by the same group in a 1986 report [17]. The effect of 10 micromolar leukotriene D4 (LTD4) was followed for 14 minutes in seven volunteers. The maximal effect occurred after eight minutes. Concentrations of 0.625, 2.5, 10, and 40 micromolar LTD4 and histamine were applied on separate days to nine subjects. The effect on NMBF was followed for eight minutes after challenge. A dose–response relation was found for LTD4 as well as histamine. The highest concentrations on this occasion caused an increase in NMBF of 10%–15%. The duration of the histamine effects was not described.

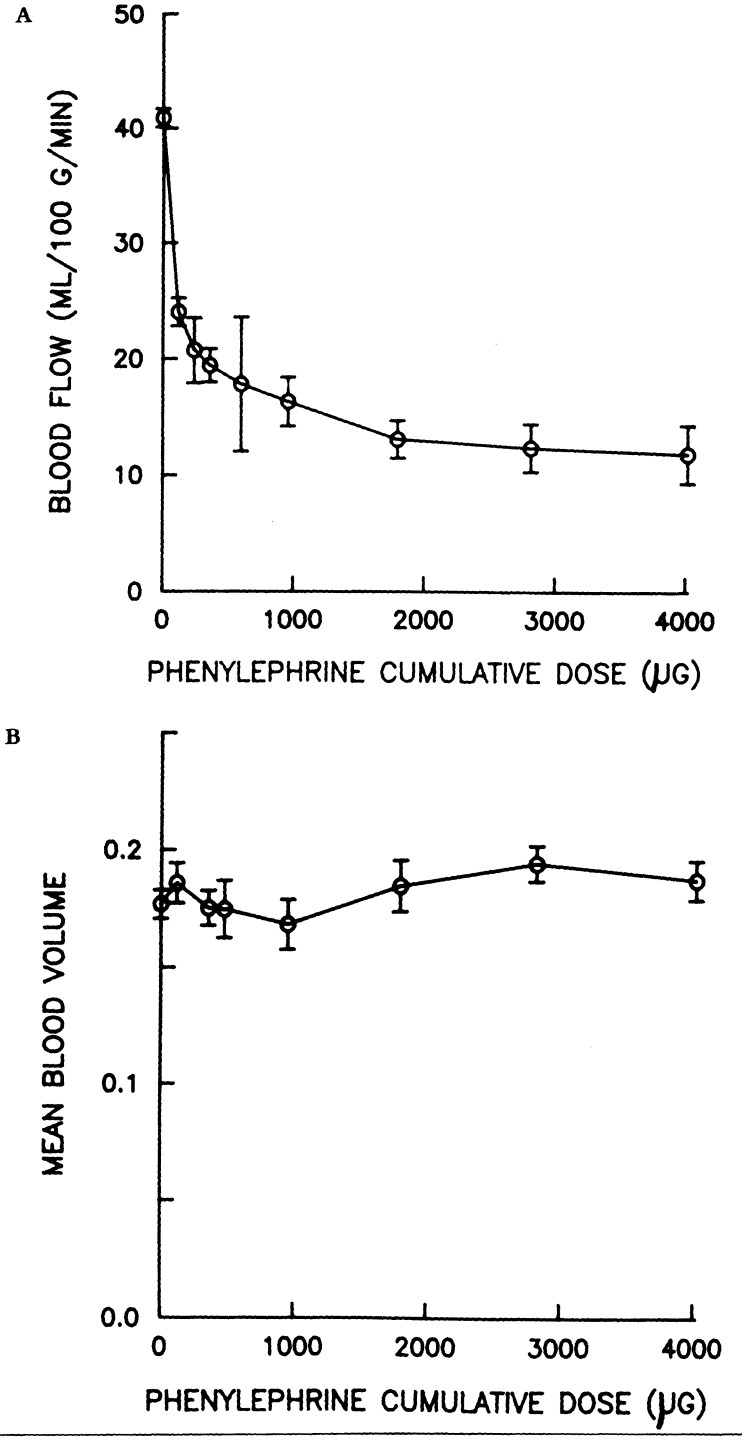

Figures 14–4A–D. The effects of topical nasal provocation challenge with phenylephrine on microcirculatory parameters. A. NMBF in $ml \cdot min^{-1} \cdot 100g^{-1}$; B. Mean blood volume in arbitrary units C. Mean RBC speed in arbitrary units; D. Pulsatility of flow as a ratio of (*maximum* − *minimum*)/(*minimum*) flow at each dose.

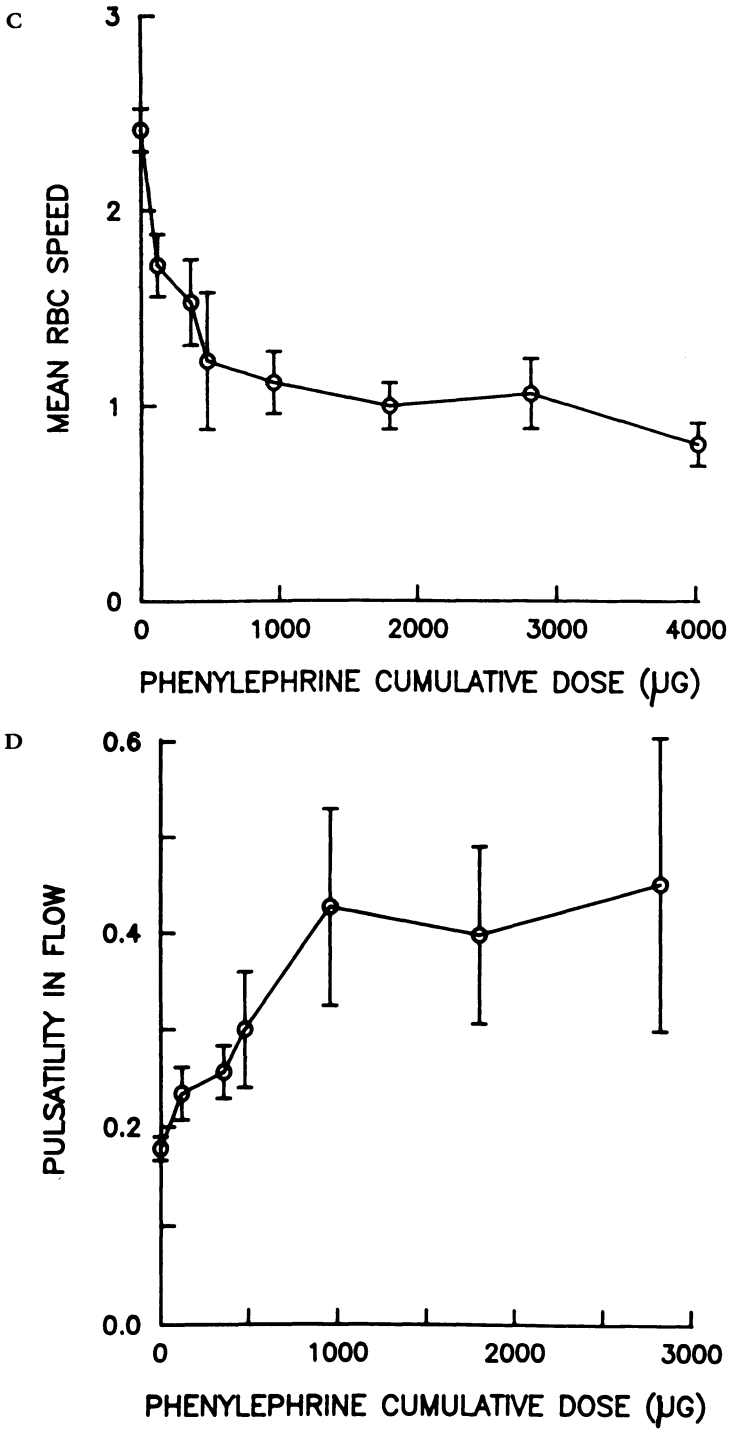

Figure 14–4. (continued)

A similar protocol was adopted by Juliusson and Bende [18]. They studied seven patients who were hypersensitive to birch pollen, but were asymptomatic at the time of the study. Topical provocation challenges were performed by application of 0.05 ml purified aqueous birch pollen extract in serial dilutions of 50–5000 BU/ml applied by a micropipette on the nasal mucosa in front of the laser-Doppler probe. The authors state that most patients experienced nasal irritation and an urge to sneeze after the pollen extract was applied. They do not comment on actual sneezing, which is usually observed after such challenges, and its effect on laser-Doppler readings. They state that the output signal was stable with small oscillations. Placebo caused a mean increase of 26% above baseline values at 30 seconds; thus they did not use these values in calculating their results. The data analyzed represented the area under the curve as a percentage of baseline values. In this fashion, a dose–related increase in NMBF after allergen challenge was demonstrated.

RESEARCH DATA FROM OTHER CENTERS

Olanoff et al. [19] reported a study using the Medpacific LD-5000 instrument. To insure a linear response, the direct current signal amplitude or mean backscattered light level over the tissue section was maintained between 900 and 1500 mV during the entire experiment. In the first experiment, the subjects were supine, and the probe was positioned by the use of a retractor attached to an earphone headset. In the second experiment, the subjects sat, placing their heads on a chin rest secured on a tripod apparatus, with the probe positioned on an adjustable clamp attached to the tripod base. The degree of probe contact with the mucosal tissue was initially adjusted until an optimal midrange direct current signal was obtained (amplitude 1200 ± 100 mV) to provide uniform signal intensity and prevent excess pressure by the probe against the tissue. Ten subjects were challenged with histamine (1, 20, 100, 500 μg) by intranasal spray. Maximal NMBF response demonstrated a significant linear relation to histamine dose. Eight additional subjects received each of the following intranasal treatments: 20 μg histamine followed by 10 μg desmopressin; normal saline followed by 10 μg desmopressin; 20 μg histamine followed by vehicle; or normal saline and vehicle. NMBF was determined before and after each treatment.

Intranasal histamine produced an increase in NMBF that was linearly related to histamine dose. NMBF readings generally peaked within 4–5 minutes after histamine dosing and returned to baseline by the end of the ten-minute recording period. The percent change in NMBF after 500 μg histamine (81 ± 25%) was significantly greater than after normal saline (27 ± 8%). The effect of histamine and desmopressin was greater than desmopressin alone, suggesting that absorption of intranasal desmopressin is enhanced by increasing local NMBF.

In a Japanese study [20], nasal resistance and NMBF were measured con-

secutively before and at several time points up to 30 minutes after exercise in 11 normal subjects and 18 patients with perennial allergic rhinitis. NMBF was measured with the Perimed instrument. Seventy-five patients demonstrated a decrease in NMBF, but no quantitative data were presented. Interestingly, NMBF and nasal resistance did not show a statistically significant correlation. These data differ from those of Paulsen et al. [21] who showed no fall in NMBF as measured by ^{133}Xe washout.

Few studies have applied laser-Doppler flowmetry to the respiratory system in animals. Marling et al. [22] used the Perimed instrument to determine tracheal blood flow in anesthetized cats. Relative changes in tracheal blood flow were measured with a laser probe positioned 1–2 mm from the tracheal mucosa through a small hole in the anterior tracheal wall at the second tracheal cartilage or just above the sternum. The probe faced the posterior tracheal mucosa with a 30° angle from the vertical plane. The data were adequate to permit several inferences on the action of vagal and superior laryngeal nerve stimulation.

An integral part of the workup of the allergic patient is skin testing with allergens, histamine, and saline controls, to determine specific sensitivity [23]. The agents are introduced epicutaneously, and the size of the resulting weal and flare is measured. In a 1985 study, Serup and Staberg [24] induced weals with control substances of saline and histamine in normal volunteers. The cutaneous blood flow was measured in the center of the weals and at several distances from the center, representing the zone of perilesional flare. In the weal center, the blood flow was increased, but neither different concentrations of histamine nor the control reaction could be differentiated. Recordings 5 mm and 10 mm from the center showed significant differences between the different solutions of histamine tested as well as the control reaction.

Olsson et al. [25] evaluated dermal blood flow after skin-prick tests with histamine and allergen in six patients with seasonal allergic rhinitis. Blood flow was recorded for 60 minutes in the weal and flare areas. The prick test procedure by itself induced a transient increase in blood flow that returned to normal after nine minutes. Histamine induced a rapid increase in blood flow in both the flare and weal reactions that returned to baseline values after about 45 minutes. The increase was significantly higher in the flare compared to the weal for the time points from $6\frac{1}{2}$ to 13 minutes. Allergen induced a similar increase; however, this was not noticeable until $2\frac{1}{2}$ minutes after the allergen application and was not completely abolished within 60 minutes. Further, the difference between the flare and weal reaction, with the higher values for the flare reaction, was present for a longer period of time than for the equivalent histamine measurements. These results support the hypothesis that histamine is not the only chemical mediator involved in the genesis of immediate allergic skin reactions.

COMPARISONS BETWEEN LDF AND OTHER MODALITIES

As of this writing, only one study has compared the different ways of measuring NMBF. Olsson [26] compared ^{133}Xe washout and laser-Doppler techniques to evaluate the effect of topical alpha-adrenergic agonists, oxymetazoline, and noradrenaline on NMBF. Xylometazoline was selected because it may selectively constrict the resistance vessels in human nasal mucosa. Noradrenaline was utilized because precapillary sphincters have been shown to be more sensitive to the vasoconstrictor activity of this transmitter than arterioles. The author found that xylometazoline induced a dose-dependent decrease in NMBF, as recorded by both methods. After noradrenaline, a fall in NMBF was seen with LDF but not with ^{133}Xe washout. The author concluded that the two methods estimate blood flow in different parts of the vascular bed. Since the Perimed instrument (Model PF1) measures only flow, it would be of value to obtain further comparative measurements with the TSI instrument, to see how the volume changed.

FUTURE DIRECTIONS

The use of LDF in the respiratory tract has not been as extensive as in skin. However, it has already proven to be a valuable adjunct in assessing nasal provocations. The technique deserves further exploitation in the study of vasoactive agents and specific antagonists within the human nose. Animal studies are technically difficult because of the limited access through the nares. However, the probes can be inserted perioperatively, and areas of tissue not accessible directly can be studied. Examples would include the paranasal sinuses, bronchi and lung parenchyma.

The capabilities of newer LDV instruments, with their ability to measure blood volume and velocity, have yet to be fully realized. The nasal mucosa, with its beds of resistance and capacitance vessels, is a useful model for pharmacologic control of the microcirculation.

REFERENCES

1. Proctor, D.F., and I. Andersen. 1982. The Nose: Upper Airway Physiology and the Atmospheric Environment, Proctor, D.F., Andersen, I. eds Amsterdam: Elsevier.
2. Proetz, A.W. 1953. Structure as a basis for function. In Essays on the Applied Physiology of the Nose, 2nd ed. St. Louis: Annals Publishing Co, pp 30–68.
3. Druce, H.M. 1986. Nasal physiology. Ear Nose Throat J 5:201–205.
4. Mygind, N. 1985. Pharmacotherapy of nasal disease. N Engl Reg Allergy Proc 6:245–248.
5. Dvoracek, J.E., J.W. Yunginger, E.B. Kern, R.E. Hyatt, and G.J. Gleich. 1984. Induction of nasal late-phase reactions by insufflation of ragweed-pollen extract. J Allergy Clin Immunol 73:363–368.
6. Kern, E.B. 1981. Committee report on standardization of rhinomanometry. Rhinology 19:231–236.
7. Eccles, R., B. Lancashire, and N.S. Tolley. 1987. Experimental studies on nasal sensation of airflow. Acta Otolaryngol 103:303–306.
8. Druce, H.M. Measurement of nasal mucosal blood flow. J. Allergy Clin Immunol 81:505–508.

9. Proctor, D.F., and G.K. Adams III. Physiology and pharmacology of nasal function and mucus secretion. Pharmacol Ther 2:493–509.
10. Jafek, B.W. 1983. Ultrastructure of human nasal mucosa. Laryngoscope 93:1576–1599.
11. Tos, M. 1983. Distribution of mucus producing elements in the respiratory tract. Differences between upper and lower airway. Eur J Resp Dis 64 (Suppl 128):269–279.
12. Cole, P. and J.S.J. Haight. 1984. Posture and nasal patency. Am Rev Respir Dis 129:351–354.
13. Druce, H.M., R.F. Bonner, C. Patow, P. Choo, R.J. Summers, and M.A. Kaliner. 1984. Response of nasal blood flow to neurohormones as measured by laser-Doppler velocimetry. J Appl Physiol 57(4):1276–1283.
14. Druce, H.M., M.A. Kaliner, and R.F. Bonner. 1984. Neurohormonal effects on nasal blood flow (NBF) measured by laser-doppler velocimetry. Int J Microcirc Clin Exp 3:479.
15. Bisgaard, H., P. Olsson, and M. Bende. 1984. Leukotriene D4 increases nasal blood flow in humans. Prostaglandins 27:599–604.
16. Olsson, P., M. Bende, and P. Ohlin. 1985. The laser-Doppler flowmeter for measuring microcirculation in human nasal mucosa. Acta Otolaryngol 99:133–139.
17. Bisgaard, H., P. Olsson, and M. Bende. 1986. Effect of leukotriene D4 on nasal mucosal blood flow, nasal airway resistance and nasal secretion in humans. Clin Allergy 16:289–297.
18. Juliusson, S. and M. Bende. 1987. Allergic reaction of the human nasal mucosa studied with laser-Doppler flowmetry. Clin Allergy 17:301–305.
19. Olanoff, L.S., C.R. Titus, M.S. Shea, and R.E. Gibson. 1987. Effect of intranasal histamine on nasal mucosal blood flow and the antidiuretic activity of desmopressin. J Clin Invest 80:890–895.
20. Ohki, M., M. Hasegawa, N. Kurita, and I. Watanabe. 1987. Effects of exercise on nasal resistance and nasal blood flow. Acta Otolaryngol 104:328–333.
21. Paulsen, B., M. Bende, and P. Ohlin. 1985. Nasal mucosal blood flow at rest and exercise. Acta Otolaryngol 99:140–143.
22. Martling, C.-R., B. Gazelius, and J.M. Lundberg. 1987. Nervous control of tracheal blood flow in the cat measured by the laser-Doppler technique. Acta Physiol Scand 130:409–417.
23. Druce, H.M. 1988. Measurement of nasal mucosal blood flow. J Allergy Clin Immunol 81:505–508.
24. Serup, J., and B. Staberg. 1985. Quantification of weal reactions with laser-Doppler flowmetry. Allergy 40:233–237.
25. Olsson, P., A. Hammarlund, and U. Pipkorn. 1988. Weal-and-flare reactions induced by allergen and histamine: Evaluation of blood flow with laser-doppler flowmetry. J Allergy Clin Immunol 82:291–296.
26. Olsson, P. 1986. A comparison between the ^{133}Xe washout and laser Doppler techniques for estimation of nasal mucosal blood flow in humans. Acta Otolaryngol 102:106–112.

15. BLOOD FLOW IN THE CENTRAL AND PERIPHERAL NERVOUS SYSTEMS

KISHENA C. WADHWANI and STANLEY I. RAPOPORT

Blood flow in the central and peripheral nervous systems is regulated by local tissue metabolism, carbon dioxide, circulating vasogenic agents, and probably nerves that innervate blood vessels. An extensive literature exists concerning this regulation. One method for measuring local blood flow, laser-Doppler flowmetry (LDF), has become particularly useful in recent years. In this chapter, we briefly review the structure and function of the vasculature in the nervous system, and then examine major techniques used to study blood flow, particularly LDF.

STRUCTURE AND FUNCTION OF THE VASCULATURE OF THE NERVOUS SYSTEM

The central nervous system

Meninges and blood vessels

MENINGES. The vertebrate brain and spinal cord are protected by three membranes or meninges and are cushioned by a layer of cerebrospinal fluid [1]. The dura mater, the most superficial membrane, is a thick and tough layer of dense collagenous tissue. The intracranial dura consists of two layers, the outer of which is periosteum and the inner the dura proper. Dural venous sinuses are located between the two layers of dura mater, and they receive numerous contributions from intracranial veins.

The arachnoid is a delicate membrane that lies beneath the dura, from

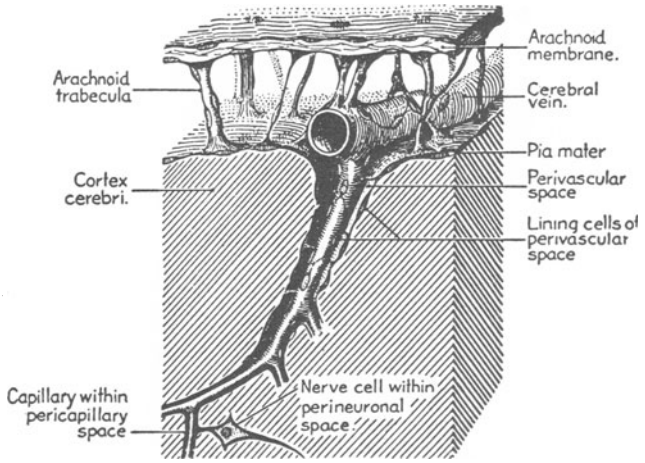

Figure 15–1. Diagram of the arachnoid and pia mater on brain surface. (Reproduced from Ranson [1], with permission.)

which it is separated by the subdural space. As figure 15–1 shows, the arachnoid is separated from another membrane, the pia, by delicate arachnoid trabeculae lying within subarachnoid cerebrospinal fluid (CSF). The arachnoid membrane is avascular; vessels supplying brain and spinal cord run in the subarachnoid space.

The pia mater adheres closely to the brain and spinal cord, and extends down to the depths of the fissures and sulci. Blood vessels from the subarachnoid space ramify within it. As they enter the brain parenchyma, they are accompanied for a short distance by a pial sheath (figure 15–1).

The subarachnoid space is of variable depth, and is expanded in some regions into large cisterns. Arachnoid villi are small tufts of arachnoid that project into venous sinus. Through these one-way valves, cerebrospinal fluid enters the venous sinuses by bulk flow, under a hydrostatic pressure gradient.

BLOOD VESSELS OF THE BRAIN. As figure 15–2 shows, the brain receives its blood supply [2] from the left and right carotid arteries (anterior circulation) and the left and right vertebral arteries (posterior circulation). Each internal carotid artery, originating from a common carotid artery, enters the cranium at the base of the skull and branches into middle and anterior cerebral arteries, which supply blood to cortical territories on the ipsilateral hemisphere, the medial surface of the frontal lobe, and the hypothalamic regions. In addition, the internal carotid artery gives rise to two other branches, the posterior communicating artery, which joins the internal carotid artery with the posterior cerebral artery (from the vertebral artery) at the Circle of Willis, and the choroidal artery, which supplies blood to the choroid plexus.

The vertebral arteries enter the cranial cavity through the foramen mag-

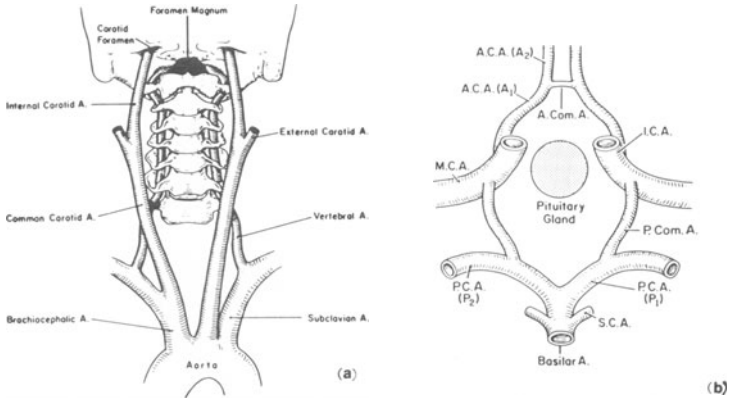

Figure 15–2. Diagrams of major arteries supplying blood to brain (a) and forming the Circle of Willis (b). I.C.A. = internal carotid artery; A.Com.A. = anterior communicating artery; M.C.A. = middle cerebral artery; A_1 = precommunicating segment A.C.A.; A_2 = postcommunicating segment A.C.A.; P.ComA = posterior communicating artery; P.C.A. = posterior cerebral artery; P_1 = precommunicating segment P.C.A.; P_2 = postcommunicating segment P.C.A.; S.C.A. = superior cerebellar artery. (Reproduced from Day [2], with permission.)

num, run rostrally along the ventral surface of the medulla oblongata, and unite at the lower border of the pons to form a common basilar artery. The chief branches of vertebral arteries within the cranium are the posterior inferior cerebellar artery, which supplies the lateral portion of the medulla oblongata, and the basilar artery, which divides into the two posterior cerebral arteries. The posterior cerebral artery sends branches to the medial surface of the occipital lobes and the inferior surface of the temporal lobes.

The Circle of Willis [1,2] is a ring-shaped anastomosis of branches of the major arteries at the base of the brain (figure 15–2), where it surrounds the infundibulum and optic chiasma in the subarachnoid space. This anastomosis provides for collateral circulation if a tributary artery is occluded [1,2].

From the pial surface of the brain, small arterioles enter the brain parenchyma and form an extensive capillary plexus. The unique feature of cerebral capillaries is their continuous belts of tight junctions, which form occluding bands connecting the internal layer of endothelial cells [4]. The tight junctions restrict vascular permeability to proteins, ions, and water-soluble nonelectrolytes. The properties of the blood–brain barrier and how it regulates brain composition have been reviewed elsewhere [5,6].

Blood from the extensive brain capillary plexus (with a capillary surface area of about 140 cm^2/g in gray matter [7]) is collected by intraparenchymal cerebral venules that join the medullary veins or small cortical veins, and then is drained into venous sinuses within the dura mater. The sinuses are divided into postero-superior and antero-inferior groups [3]. Blood from the

former group empties mainly into the internal jugular veins. The anteroinferior sinuses have access to the veins of the orbit and the internal jugular veins. Cerebral veins and dural sinuses differ from veins in other parts of the body. Their walls are thin and lack the three typical layers and valves that usually are found in noncerebral veins. The cerebral venous system helps to regulate brain volume [3].

Function of the cerebral circulation

The brain needs a continuous, highly regulated blood supply for the delivery of oxygen and glucose and the removal of products of metabolism. In man, brain weight is only about 2% of body weight, but the brain receives 15% of cardiac output at rest, consumes 87 mg glucose/min [8,11,12], and consumes about 49 ml/min of oxygen [11,12] or about 20% of the total quantity of oxygen utilized by the body. Normal brain metabolism is completely dependent upon a constant supply of oxygen, and glucose as a sole energy source, although mannose or ketone bodies can partially substitute for glucose under some conditions [5,12]. Four to five minutes of complete cessation of blood flow will result in death of neurons [11].

Although the brain needs an uninterrupted blood flow, this does not mean that the rate of cerebral blood flow (CBF) is constant. At rest, regional CBF (rCBF) is related linearly to the metabolic rates for glucose and oxygen in different brain regions [8,9,12,13]. When glucose consumption is augmented due to increased functional activity, rCBF is augmented as well [13].

Human and animal studies reveal that CBF increases when arterial P_{O_2} decreases [8–10]. On the other hand, steady-state CBF is inversely related to arterial P_{CO_2}; the relation has a sigmoidal shape [8,9]. The linear segment of this curve in man is at P_{CO_2} between 15 and 80 mm Hg [8,9], where CBF changes by about 5% for a 1 mm Hg change in P_{CO_2}. No further change in CBF is observed when P_{CO_2} falls below 20 mm Hg or rises above 100 mm Hg.

It is known that CBF can remain constant despite changes in perfusion pressure [8]. Accordingly,

$$\text{CBF} = \text{CPP}/\text{CVR}, \tag{15.1}$$

where CPP (mm Hg) is cerebral perfusion pressure and CVR (mm $\text{Hg} \cdot \text{g} \cdot \text{min} \cdot \text{ml}^{-1}$) is cerebrovascular resistance. Thus CBF can be kept constant when cerebral blood vessels actively change CVR to oppose the changes in CPP. This phenomenon is termed autoregulation [8–10]. In normotensive man, autoregulation occurs between 50 and 140 mm Hg of systolic blood pressure. In chronically hypertensive subjects, the linear range is shifted to higher systolic pressures [8,9].

A regulated cerebral blood volume is an important condition for maintaining brain volume in the rigid cranium [8,10]. Almost 75% of intracranial

blood is found within the venous bed [8]. Stagnation of cerebral venous blood will increase venous pressure and volume, and thereby cause an increased resistance in major brain arteries, as was discovered by Mchedlishvili et al. [14]. Because intracranial veins respond to sympathetic stimulation and vasoconstrictor agents [15], they probably contribute to the regulation of cerebral blood volume [3].

Blood flow also depends on blood viscosity [8,10], which rises with increased hematocrit or with increased concentrations of plasma proteins. Normally, CBF shows an autoregulatory response that compensates for blood viscosity changes [8,10].

Innervation of blood vessels of the central nervous system

Extensive reviews on innervation of the vasculature of the central nervous system have been published [8,16–19]. Well-developed plexuses of adrenergic and of cholinergic nerves have been observed in pial vessels of humans and animals [8,18,19]. However, the extent of innervation of intraparenchymal capillaries by adrenergic nerve fibers is debatable [18]. Most of perivascular adrenergic nerve fibers within the brain originate from the superior cervical ganglion [18,19], whereas intracerebral adrenergic nerves, which are believed to innervate brain capillaries, originate from the locus coeruleus in the brain stem [17,19]. The vascular distribution of the cholinergic nerves is essentially similar to that of the adrenergic nerves [8,18]; there is a greater number of nerve fibers per vessel diameter in arteries than veins. Appreciable concentrations of acetylcholine, choline acetyltransferase, and acetylcholinesterase have been found in feline cerebral capillaries and arterioles [18], but their relation to cholinergic nerves is unclear, since cholinergic fibers have not been identified in intracerebral vessels [18].

In the mammalian brain, nerve fibers that innervate blood vessels have been reported to contain serotonin, neuropeptide Y, vasoactive intestinal peptide (VIP), and tachykinins (substance P in particular), as well as other neuropeptides (8,16–18]. Humoral factors, i.e., pH, K, and adenosine [8–10], can influence contraction of smooth muscle in the cerebral vasculature, and influence CBF in addition to neuronal influence.

The peripheral nervous system

The nerve sheath and blood vessels

A peripheral nerve consists of a bundle of nerve fibers bound together by a nerve sheath and contains blood vessels [5,20]. Topographic and anatomical features of peripheral nerves have been reviewed extensively [21–24].

THE NERVE SHEATH. As figure 15–3 shows, a peripheral nerve bundle is enclosed by a nerve sheath composed of an epineurium (mostly loose connective tissue) and a perineurium (a series of flat polygonal cell layers with basement membranes on both sides) [21,25]. At the inner layer of the

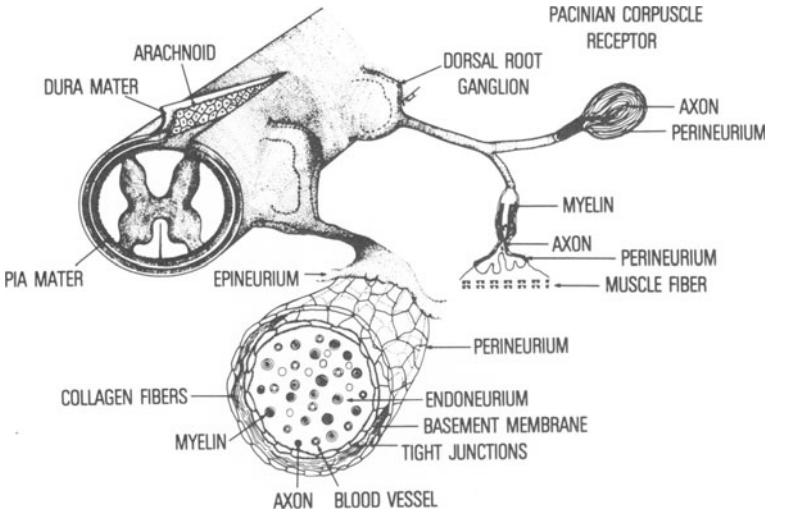

Figure 15–3. Schematic representation of nerve sheaths and their relation to the meninges in the central nervous system.

perineurium, cells are connected by complete belts of tight junctions, which make the perineurium a diffusion barrier [21,25]. Perineurial cells often contain numerous vesicles or caveolae. However, the vesicles do not contribute to transperineurial transport [21]. Where nerves enter or leave the spinal cord, the perineurium is continuous with the arachnoid membrane of the cord, whereas the epineurium is continuous with the dura mater [25].

BLOOD VESSELS SUPPLYING THE NERVE. Blood vessels supplying peripheral nerves have been described in detail [22–24,26,27]. The peripheral nerve is well vascularized, and has two integrated but functionally independent circulations, extrinsic and intrinsic. The extrinsic system consists of segmentally arranged vessels that originate from nearby large arteries and veins as well as from adjacent muscular and periosteal vessels. Extrinsic vessels follow the nerve surface along the length of the nerve [23,24]. As these regional, extrinsic vessels reach the epineurium, they form an anastomotic plexus within the epi-perineurium layers (figure 15–4), which together with the intrafascicular endoneurial vascular bed constitute the intrinsic system or vasa nervorum [23,24]. The epi-perineurial plexus, mostly arterioles, venules, and arterio-venular shunts [23], has numerous communications with the plexus of the endoneurium.

Small vessels, presumably precapillaries [23,24,26], branch from perineurial vessels and penetrate the nerve fascicles to form a capillary bed in the endoneurium (figure 15–4). These intrafascicular capillaries run mostly lon-

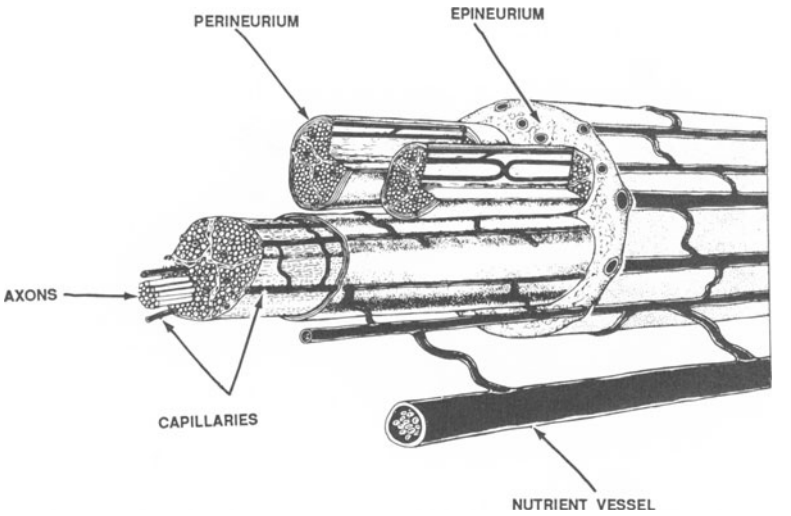

Figure 15–4. Schematic representation of blood vessel networks of the peripheral nerve. Vascular plexuses are present in the epi-perineurium, perineurium, and endoneurium. (From Lundborg [24], with permission.)

gitudinally with nerve fibers throughout the entire length of the nerve. In mammals, including man [27], intrafascicular vessels have larger calibers than does a typical capillary bed (e.g., muscle capillaries), and are more widely spaced.

Like cerebral capillaries, endoneurial capillaries are lined by a continuous layer of endothelial cells connected by belts of tight junctions [28]. This continuous layer and the inner layer of perineurium provide an effective *blood–nerve barrier* [5,22] that restricts blood-borne substances from entering the endoneurium.

Function of the nerve vasculature

Because the nerve at rest normally derives most of its energy from the oxidation of glucose [29], the vasa nervorum is critical in supplying nutrients and oxygen to the peripheral nerve. Acute and profound interruption of the nerve blood supply severely impairs nerve functions [23,24]. However, peripheral nerves generally are considered to be relatively resistant to ischemia [23] because their rich vascular anastomoses contain two integrated but functionally independent vascular supplies [23,26].

If extrinsic vessels are occluded by mobilizing a nerve, the reserve capacity of the intrinsic vessels is sufficient to maintain an adequate blood supply to the nerve [23]. Likewise, if the intrinsic system is interrupted by crushing

or transecting the nerve, the blood supply to the distal nerve segment is preserved by the extrinsic vessels [23,26]. Fluorescence microangiography [24,26] reveals that only part of the endoneurial capillary bed is normally perfused at any given time. Empty capillaries, frequently observed in the endoneurial space, become filled immediately after the nerve is exposed to warm saline or is traumatized slightly.

Autoregulation of nerve blood flow (NBF) has been sought by several investigators [30–33]. In contrast to CBF, there is no evidence that NBF is autoregulated in the arterial blood pressure range of 80 to 160 mm Hg. Observations on the effect of P_{CO_2} on NBF are contradictory. Tchettert et al. [34] showed that NBF increased linearly as P_{CO_2} was varied from 28 to 44 mm Hg. The slope of NBF versus P_{CO_2} curve was about one tenth that of the CBF versus P_{CO_2} curve in the same animals (0.5 versus 4.9 $ml \cdot min^{-1} \cdot 100\ g^{-1} \cdot mm\ Hg^{-1}$). Rechthand et al. [35] reported similar results, and concluded that NBF increased by 1% for a 1 mm Hg increase in P_{CO_2}. In contrast, Low and Tuck [31] failed to demonstrate changes in NBF in rats during acidosis or hypoxia. Hypoxia, as mentioned earlier, decreases the resistance of cerebral blood vessels and thus increases CBF. The lack of change in NBF during hypoxia was explained by the fact that the rate of oxygen consumption by the cerebral cortex is at least 20 times that by the nerve, whereas blood flow in the cerebral cortex is only six times that of the nerve [31]. Thus, NBF may exceed resting metabolic requirements by a considerable margin [31,33]. Relations among NBF, blood volume, metabolism, and blood viscosity have not been examined.

Innervation of the vasa nervorum

Nerve fibers that innervate blood vessels of the peripheral nerve have been identified by both fluorescence and electron microscopy [23,36–41], but their role in regulating NBF is not well understood. Adrenergic nerve fibers are organized into a networklike plexus [37–39]. Adrenergic axon terminals that are adjacent to blood vessels in the epi-perineurium show varicosities typical of innervating adrenergic fibers (figure 15–5). In the endoneurium, adrenergic nerve fibers are seen but rarely are associated with blood vessels [38,39].

In the sciatic and vagus nerves of the rabbit, parasympathetic nerve fibers that innervate the vasa nervorum have been identified [38,41]. In addition, perivascular and nonperivascular nerve fibers containing vasoactive intestinal peptide (VIP), substance P, serotonin, neuropeptide Y, and calcitonin-gene related peptide are found [38,41]. However, no nerve fibers containing these putative neurotransmitters have been shown to innervate veins and capillaries. The origins of perivascular and nonperivascular fibers are not known. However, because their density decreases distally along the nerve trunk and correlates with the caliber and thickness of blood vessels [38], it is thought that they derive from proximal nutrient vessels.

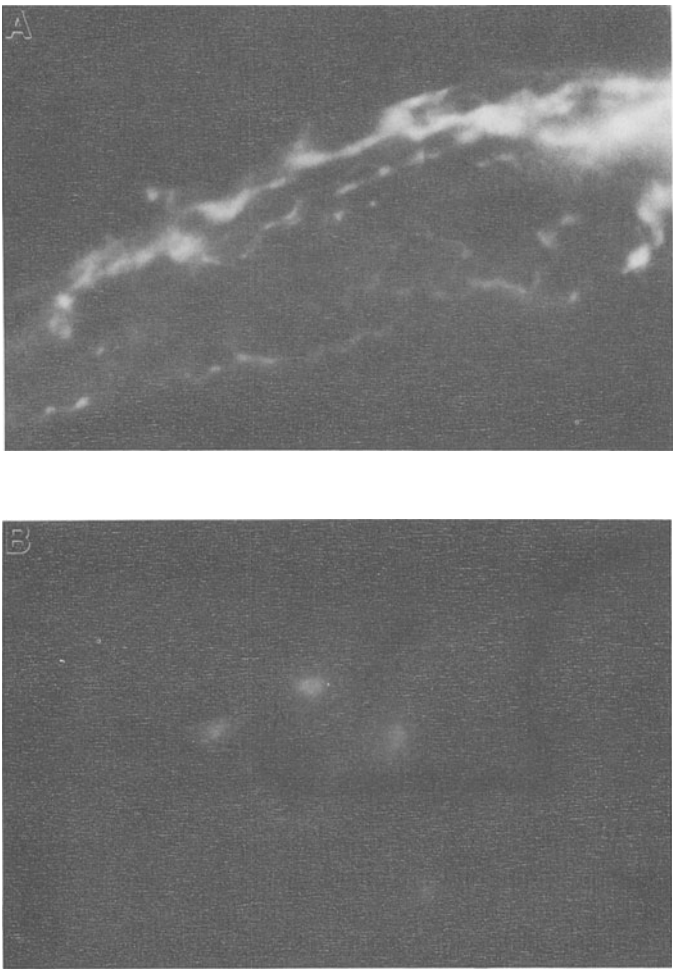

Figure 15–5. Adrenergic nerve terminals that innervate the blood vessels in the epi-perineurium of the rat sciatic nerve as shown by fluorescence histochemistry of whole mount (A) and cross section (B). (Courtesy of Dr. Koistinaho.)

METHODS USED TO MEASURE BLOOD FLOW IN THE NERVOUS SYSTEM

A vast literature treats the techniques for measuring blood flow in the nervous system, particularly CBF. These techniques are summarized in table 15–1.

Laser-Doppler flowmetry (LDF)

Laser-Doppler flowmetry (LDF) is based on the fact that the Doppler shift of a backscattered laser beam from a moving red blood cell is related to the

Table 15–1 Comparisons among methods used to measure blood flow in the nervous system

Technique	Invasive	Repetitive or continuous	Clinical application	Potential errors and/or limitations	Measure	Ref
Freely diffusible tracers:						
Nitrous oxide	Yes	No	Yes	Tracer concentrations in blood and tissue may not be in equilibrium; inaccurate determination of venous tracer concentration	CBF	[65]
^{133}Xe clearance	No	Yes	Yes	Complex clearance curves; inaccurate determination of CBF in small animals	rCBF, NBF	[66, 67]
H_2 clearance	Yes	Yes	No	Complex clearance curves; uncertainty of tip position of electrode; tissue damage	rCBF, NBF	[30, 68, 69]
Heat clearance	Yes	Yes	Yes	Heat may alter flow	rCBF	[70]
Positron emission tomography	No	Yes	Yes	High radioactivity exposure; rCBF and tissue concentration of tracer may not be linear; restricted availability; underestimates blood flow at high flow rate	rCBF	[71]
Tissue uptake of radiotracers	No	No	No	Insensitive to fast flow rates due to limited diffusion of tracer; requires tissue sampling	rCBF, NBF	[72–74]
Indicator trapping (microspheres)	No	Yes	No	Inadequate mixing of microspheres in blood stream; requires tissue sampling	rCBF, NBF	[34, 75]
Venous occlusion plethysmography	No	Yes	Yes	Applicable only to infants	CBF	[76]
Ultrasonic Doppler technique	No	Yes	Yes	Limited resolution; measures blood velocities in large vessels; sensitive to vibration	CBF	[77]
Laser-Doppler flowmetry	No	Yes	Yes	Gives only flow signals, not absolute blood flow values; sensitive to vibration	rCBF, NBF	[47, 60]

velocity of the red blood cells [42,43]. For a complete discussion of the principles of LDF, see Chapter 2. The advantage of LDF over the Doppler ultrasound method is that the output signal reflects not only red blood cell velocity but also red blood cell concentration in a given volume, and hence blood flow [42,43]. LDF provides a noninvasive, instantaneous, and continuous way to measure blood flow. Because its spatial resolution is about 1 mm [42,43], blood flow in capillary beds can be measured. The method has certain disadvantages, however, because a flow signal but not an absolute value of flow is given. On the other hand, the signal can be standardized against flow measured with other techniques [44] (see below). Movements of tissue, vessel wall, or the laser probe will cause erroneous measurements [45,46]. Applications of LDF for measuring blood flow in the nervous system are discussed in the next section.

THE USE OF LASER-DOPPLER FLOWMETRY IN THE NERVOUS SYSTEM

Laser-Doppler flowmetry and CBF

As mentioned in the previous section, LDF allows rapid measurements, provides continuous recording, is not invasive, and can be applied to small tissue regions. Transient changes in blood flow under experimental conditions can be detected. Following is a general review of the literature on the use of LDF to measure CBF.

General review

William et al. [47] first studied rCBF with LDF, following experimental stroke in the rhesus monkey. After an animal was anesthetized and craniotomized, its right middle cerebral artery was ligated. Blood flow on the cortical surface then was mapped with LDF. The results were compared with flow measured with the ^{133}Xe clearance method, although no comparative or quantitative analysis was reported.

In cats, Gyrax and Wiernsperger [48] used LDF to examine the effect of oligemic hypotension on rCBF. Stepwise decreases in arterial blood pressure caused by bleeding elicited no change in the LDF signal, until an average pressure of 60 mm Hg was attained. Below this critical pressure, further reductions in blood pressure led to considerable reductions in the flow signal. Reinfusion of blood to produce a normal blood pressure triggered a short-lasting overshoot in the LDF signal, which became normal after about 30 minutes. This indicated that autoregulation of rCBF was impaired temporarily in the postoligemic period [48].

The effect of local CO_2 on flow velocity in cerebral arterioles of cats was studied by Koyama et al. [49], who used a laser-Doppler microscope with two laser beams. Scattered light reflected from a segment of arteriole was collected via a microscope before impinging upon the photomultiplier. Local elevations in CO_2 increased flow velocity and dilated the arterioles.

In an attempt to find an animal model for ischemic stroke, Chen et al. [50] and Shu et al. [51] used LDF to measure rCBF in rats. An LDF probe was inserted through a burr hole in the skull of an anesthetized rat. rCBF was monitored continuously before and after sequentially ligating the middle cerebral and common carotid arteries [50]. Flow signals at the surface of right hemisphere were reduced to 62%, 48%, and 18% of baseline following successive ligation of the right middle cerebral, right common carotid, and left common carotid arteries, respectively.

LDF also was used to measure rCBF in a cerebral ischemic model in the dog [52]. Through a small window in the left frontal or parietal region, a needle probe (2.5 mm diameter) from a LD flowmeter was positioned epidurally. Blood flow to an entire hemisphere was completely controlled by a perfusion method, using artificial blood to replace the animal's blood [52]. The cerebral hemisphere was brought to a constant level of ischemia for a defined period of time, after which recirculation was instituted. The effects of flow threshold and time threshold of reversibility of cerebral ischemia on brain function were examined, using electroencephalogram and somatosensory evoked potentials. Nearly complete recovery of brain function was found following reperfusion after up to three hours of ischemia (40% normal CBF). No recovery was seen following recirculation if the CBF was reduced to below 20% of normal CBF for more than one hour [52].

LDF also has been used to study rCBF following pharmacological denervation of cholinergic innervation of the cerebral vessels [53]. An LDF probe was placed on the cortical surface of anesthetized, craniotomized rats, whose basal forebrain had been lesioned with ibotenic acid. A 26% decrease in the LDF signal was noted in ibotenic acid-treated rats compared with control animals. In addition, local or systemic administration of physostigmine, carbachol, or papaverine (cholinomimetics) increased the LDF signal in control rats. Atropine (0.8 nmol) prevented the increase in the LDF signal caused by physostigmine, without affecting systemic blood pressure. Thus, cholinomimetics appear to increase cortical rCBF via a local muscarinic cholinergic mechanism [53].

Rosenblum et al. [44] first used LDF to monitor rCBF in humans. A patient with a cerebral arterio-venous malformation underwent craniotomy for excision of her malformation. A LDF probe was used to measure blood flow in the surrounding cortex before and after excision. Using a calibration factor for cerebral cortex (6 $ml \cdot min^{-1} \cdot 100g^{-1}$ per 100 Hz $\times$ 100% of the Doppler-shifted light), mean rCBF, measured in six cortical sites surrounding the lesion, was reported to increase from 35.4 $ml \cdot min^{-1} \cdot 100g^{-1}$ before excision to 103.8 $ml \cdot min^{-1} \cdot 100g^{-1}$ following excision of the lesion.

Laser-Doppler measurements of cerebral blood flow have been compared with those made by other methods [54–56]. LDF output signals from cortical regions of anesthetized rabbits were correlated with rCBF obtained with radiolabeled microspheres in the same animals [54]. Metaraminol (a sym-

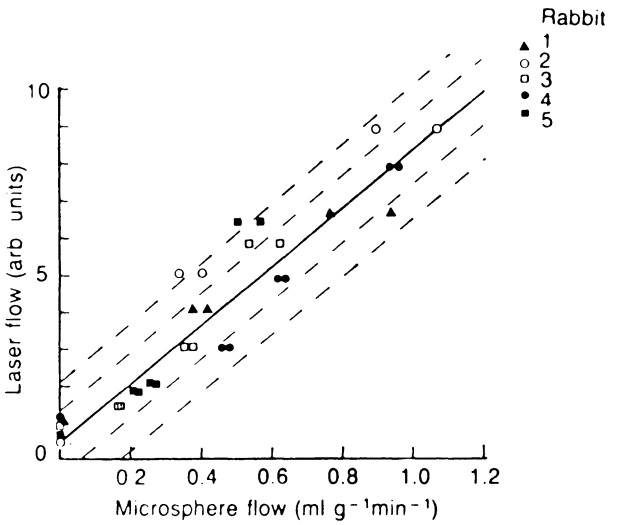

Figure 15–6. Relation between LDF signal at cerebral cortex and rCBF obtained by radiolabeled microspheres in the same rabbits. The solid line is the least-squares best fit; dotted lines are ±1 and ±2 S.D. The pairs of plotted points represent calculated rCBF using microsphere technique in both left and right cerebral hemispheres. (From Eyre et al. [54], with permission.)

pathomimetic) was infused systemically to increase rCBF, whereas hemorrhage was used to decrease rCBF. LDF signals were highly correlated ($r = 0.92$; $p < 0.001$) with microsphere-derived rCBF values (figure 15–6). The LDF method also was compared with the H_2-clearance method in rats by Ellis et al. [55] and Skarphedinsson et al. [56]. Changes in rCBF measured by the two methods were highly correlated ($r > 0.95$) [55]. Skarphedinsson et al. [56] concluded, however, that the LDF signal was correlated better with CBF values corresponding to slow ($r = 0.88$) and weighted mean ($r = 0.88$) components than to the fast ($r = 0.66$) component. Because the slow component, determined by H_2 clearance, may represent blood flow of underlying white matter [56], the authors concluded that the measuring depth of the laser-Doppler flowmeter in the brain was greater than expected (e.g., 1 mm).

Recently, Haberl et al. [57,58] related the cerebral cortical LDF signal to pial arteriolar diameter in rabbits, following induced vasodilation or vasoconstriction. Hypercapnia ($P_{CO_2} = 48$ mmHg) caused the pial arterioles to dilate 19% and LDF signal to increase by 74% [57]. The LDF signal had a relation to the third power of the diameter of the pial arterioles. Intra-arterial indomethacin reduced diameter of the pial arterioles and the LDF signal by a similar degree. Interestingly, topical application of 2-chloroadenosin, a non-metabolizable vasodilator, at a dose that dilated the pial arterioles to the same

extent as 8 μM bradykinin, an enzymatically degradable peptide, produced a much larger increase in the LDF signal than did bradykinin [58]. Furthermore, the LDF signal remained elevated when the pial arteriolar diameter returned to normal after washout of these agents. Thus pial arteriolar diameter on the cortical surface may not always reflect flow within the underlying cortex [58].

Coyle [59] used LDF to study rCBF changes in response to unilateral common carotid artery occlusion in normotensive and hypertensive rats. Whereas the signal did not change in normotensive animals, the collateral flow signal in hypertensive animals was significantly reduced at 15 seconds after occlusion, indicating impairment of the normal vasodilator mechanism [59].

Comparison of the rCBF values obtained from LDF and from other techniques

As mentioned, the LDF method provides a flow signal in the form of voltage output. Therefore, rCBF obtained with LDF must be estimated by calibration with other techniques. Table 15–2 compares LDF-derived rCBF values with those obtained by other methods.

Laser-Doppler flowmetry and NBF

General review

LDF was first used to measure NBF in the peripheral nerve by Rundquist et al. [60]. A segment of sciatic nerve of an anesthetized rat was immobilized in situ and placed on a grooved nerve holder, made of opaque black Perspex, which was fixed to minimize movement. To optimize collection of backscattered light from the illuminated nerve segment, the two afferent optical fibers were positioned 1 mm on each side of the efferent fiber and at an angle of 60° with respect to each other (figure 15–7). LDF signals were correlated with NBF values obtained with ^{14}C-iodoantipyrine on the same nerves (figure 15–8). The correlation coefficient between the two measurements in individual nerves was statistically significant and equaled 0.73 ($p < 0.05$). The slope of the regression line equaled 1.35 ± 0.30 (SE) volts $\cdot$ ml^{-1} $\cdot$ min^{-1} $\cdot$ g^{-1} [60].

The effect of removing the epineurium from the nerve on NBF also was examined. Stripping the epineurial sheath decreased both the LDF signal and ^{14}C-iodoantipyrine radioactivity; each was about 50% less than respective values in intact nerves (figure 15–8). Heterogeneity of NBF was demonstrated by autoradiography of ^{3}H-nicotine-infused nerves and by analyzing the compartmental distribution of ^{57}Co-labeled microspheres in the nerve [60]. As expected from the dual microcirculations of the nerve (see above), NBF was not uniform within the sciatic nerve cross section (figure 15–9). Radiodensity due to ^{3}H-nicotine was greater at the epi-perineurial border than within the endoneurium. Regional NBF in the epi-perineurium, deter-

Table 15–2 Comparison of CBF values obtained with various methods

Method used	CBF ($ml \cdot min^{-1} \cdot 100g^{-1}$)	Species (tissue)	Ref
LDF		Arteriovenous malformation	
	33 ± 2*#	patient (cortex); preoperation	[44]
	106 ± 7*#	Postoperation	[44]
	132 ± 8*	Anesthetized rat (cortex)	[59]
	52**	Anesthetized rabbit (cortex)	[54]
Radiolabeled	45 ± 4	Anesthetized dog (cortex)	[78]
microspheres	76 ± 10	Anesthetized rat (cortex)	[79]
	114 ± 14	Awake rat (whole brain)	[80]
^{133}Xe	65 ± 3	Awake human (whole brain)	[81]
	100 ± 3	Anesthetized rat (cortex)	[82]
Ultrasonic Doppler	61.6***	Awake human (internal carotid artery)	[70]
Nitrous oxide	62***	Awake human (whole brain)	[65]
^{85}Kr	50 ± 5	Awake human (whole brain)	[83]
H_2 clearance	79 ± 22	Awake rat (cortex)	[84]
	45 ± 8	Arteriovenous malformation patient	[68]
	103***	Awake cat (caudate nucleus)	[69]
^{14}C- or ^{131}I-	41 ± 8	Anesthetized rat (whole brain)	[74]
iodoantipyrine	168 ± 0.3	Awake rat (cortex)	[85]
^{14}C-antipyrine	73 ± 0.1	Awake rat (cortex)	[85]
^{14}C-ethanol	122 ± 10	Anesthetized rat (cortex)	[86]

Values are expressed as means ± SEM and are measured or calculated at normotension (100–120 mm Hg) and normocapnia (P_{CO_2} = 39–41 mmHg).

\# Mean and SEM of six different sites surrounding the lesion.

* LDF signals were calibrated to give CBF values.

** CBF value was calculated from the equation $y = 0.47 + 0.08\,x$, given in [54], where x is CBF values obtained from microsphere method in the same animals.

*** no SEM was given.

mined by ^{57}Co-labeled microspheres, was higher than in the endoneurial compartment (0.33 versus 0.23 $ml \cdot min^{-1} \cdot g^{-1}$ wet weight).

In the peripheral nerve, the LDF signal also has been compared with NBF as measured by H_2 clearance technique [61]. The sciatic nerve of an anesthetized rat was bathed in mineral oil at 33–35°C. NBF was measured simultaneously with the LD flowmeter and microelectrode-hydrogen polarography [61]. NBF was altered by exsanguination controlled by an infusion-withdrawal pump. Measurements of NBF by LDF and hydrogen polarography were significantly correlated ($r = 0.74$).

A reduced LDF signal following stripping of the epineurial blood vessels of the rat sciatic nerve also was found by Myers et al. [62]. The signal fell by 58% of control values at one hour after vessel stripping. Subperineurial edema and demyelination that did not extend into the central core fascicles were observed seven days after epineurial stripping. These studies document the importance of the transperineurial circulation for maintaining nerve integrity [62].

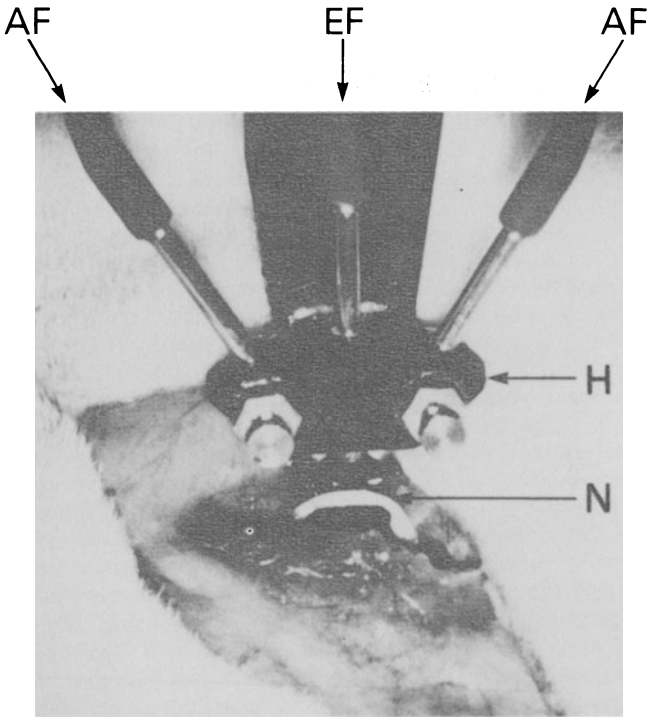

Figure 15–7. Arrangement of LDF probe for measuring blood flow of sciatic nerve in rat. EF, efferent optical fiber; AF, afferent optical fiber; H, nerve holder; N, sciatic nerve. (Reproduced from Rundquist et al. [60], with permission.)

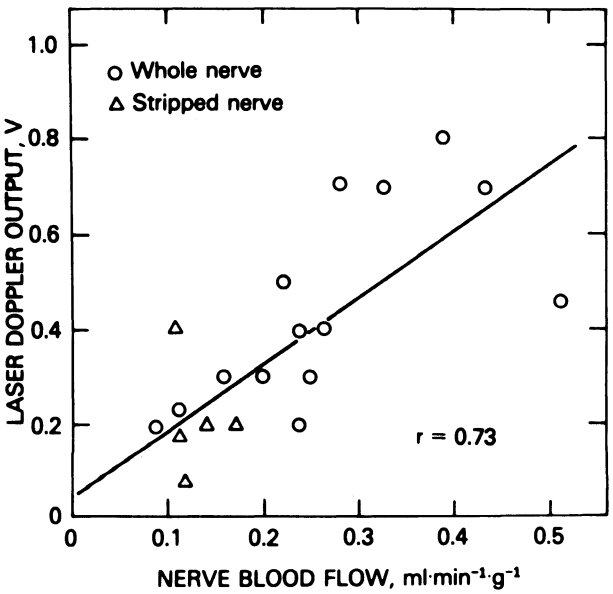

Figure 15–8. Relation between LDF signal and NBF measured by ^{14}C-iodoantipyrine in the rat's sciatic nerve. (From Rundquist et al. [60], with permission.)

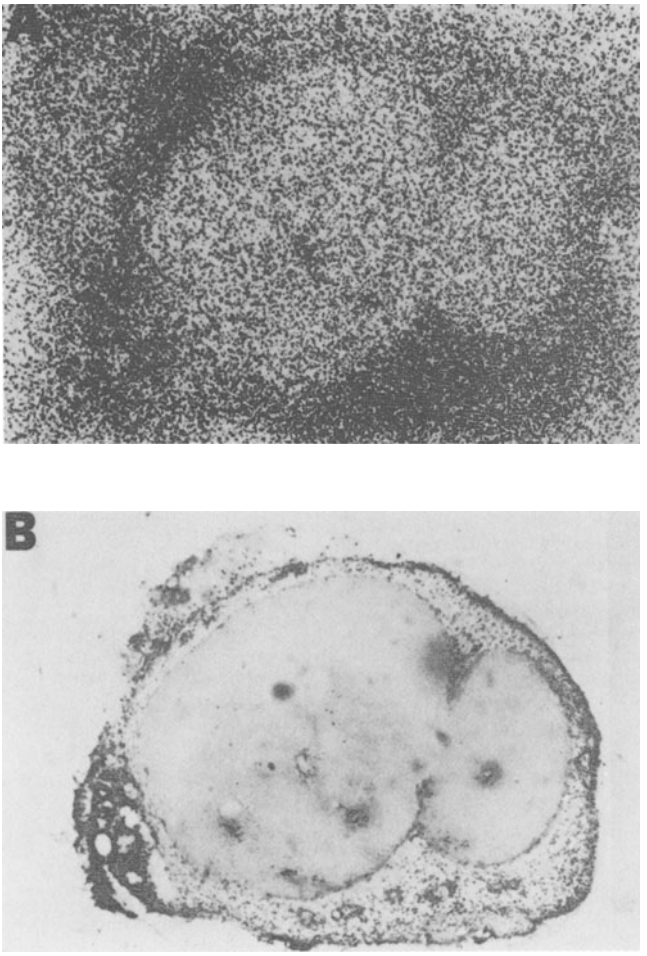

Figure 15–9. ^{3}H-nicotine autoradiograph of rat sciatic nerve (A) and corresponding frozen section stained with cresyl violet (B). Radiodensity due to ^{3}H-nicotine is greater at the epiperineurium than within the endoneurium. (Reproduced from Rundquist et al. [60], with permission.)

The sympathetic innervation of the epineurial and endoneurial blood vessels has been investigated by Zochodne and Low [63], who used LDF and H_2 clearance to examine epineurial NBF and endoneurial NBF, respectively, in the rat sciatic nerve. Intravenous phentolamine, an alpha-adrenergic blocker, at 10^{-4} g·ml^{-1} did not affect the LDF signal but increased NBF as determined by H_2 clearance. Norepinephrine (10^{-6} g·ml^{-1}, i.v.) promptly eliminated the LDF signal, despite a rise in systemic arterial pressure. This reduction, but not the hypertensive response, was blocked by a preceding

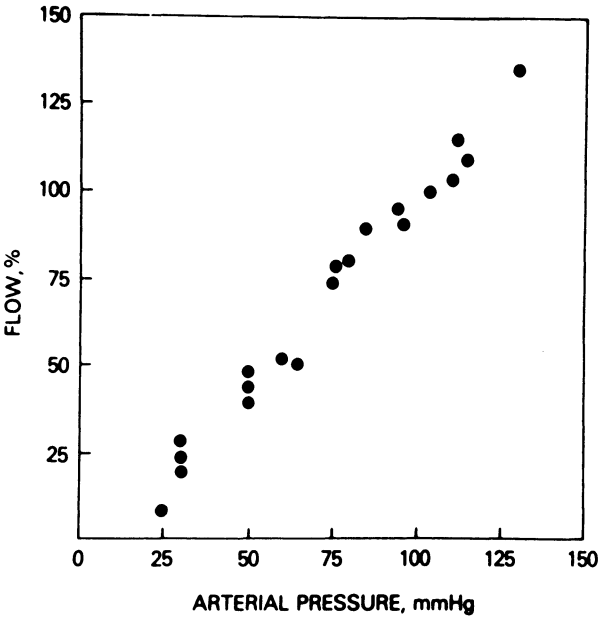

Figure 15–10. Relation between normalized LDF signal (percentage of signal at 100 mm Hg arterial pressure) to arterial blood pressure, in decerebrate unanesthetized rats. (From Sundqvist et al. [32], with permission.)

injection of 10^{-5} g·ml^{-1} phentolamine. These results suggest that the vasa nervorum possesses a heterogenous distribution of alpha-adrenergic receptors [63].

Using H_2 clearance or tracer uptake methods, several investigators have failed to demonstrate autoregulation of NBF in anesthetized animals [30,31]. With LDF, Sundqvist et al. [32] sought to determine whether anesthetic agents could prevent an autoregulatory response in NBF. LDF signals were recorded during graded hypotension caused by exsanguination or aortic clamping of decerebrate unanesthetized rats. LDF signals declined linearly as arterial blood pressure was reduced by graded clamping of the descending aorta (figure 15–10). In addition, the LDF signal versus pressure relation in the sciatic nerve during exsanguination was similar to that during aortic clamping. Results indicated that NBF is not autoregulated during experimental hypotension [32]. However, autoregulation, which is more prominent in sympathetic-denervated than in sympathetic-innervated vasculatures [64], may have been prevented by intrinsic autonomic innervation of the vasa nervorum during the experimental hypotension [32]. Another possibility is that autoregulation during hypotension occurs in one compartment of the nerve vasculature, but is masked by flow changes in the other compartment [60].

Rechthand et al. [35] measured the LDF signal from the sciatic nerve of

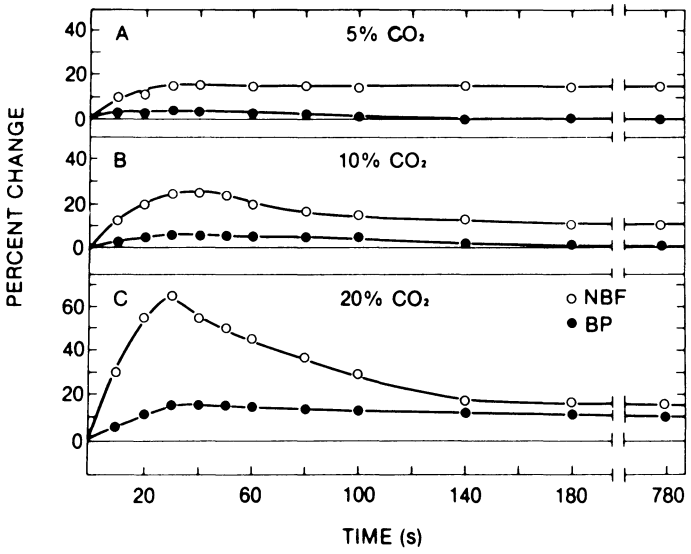

Figure 15–11. Time courses of percent changes in LDF signal, measured from sciatic nerves of unanesthetized decerebrate rats, and of arterial blood pressure, after the start of inspiration of gas mixtures containing 5% (v/v), 10%, and 20% CO_2. Each data point is the mean of 12 observations from different animals. (Reproduced from Rechthand et al. [35], with permission.)

decerebrate rats that inhaled air containing either 5% (v/v), 10%, or 20% CO_2. Figure 15–11 shows the LDF signal and arterial blood pressure as a function of time during inhalation of the different gas mixtures. Inhalation of 5% CO_2 increased arterial pCO_2 by 13 mmHg and increased the LDF signal by 15%, even though arterial pressure returned to baseline after 150 seconds. During inhalation of 10% CO_2, arterial pressure first increased and then returned to baseline after 180 seconds, whereas the LDF signal remained elevated by 15% above control. These results suggest that CO_2 dilates the nerve vasculature, but its vasodilatory effect is much less than in the central nervous system, in which ~ 100% increase would be expected during 10% CO_2 inhalation [8–10].

Comparison of the NBF values obtained from LDF and from other techniques

Table 15–3 presents NBF values from the sciatic nerve of different species. This table facilitates comparison of LDF measurements with those determined by various techniques. NBF values obtained by LDF were derived from figure 15–8 using mean LDF values, which equal 0.44 volts for whole sciatic nerve and 0.21 volts for stripped nerve, in the anesthetized rat [60].

CONCLUSIONS

Laser-Doppler flowmetry (LDF) offers the advantage of dynamic real-time recording of blood flow in the peripheral and central nervous systems. The

Table 15–3 Comparison of NBF values in the peripheral nerve, obtained by various methods

Method used	NBF ($ml \cdot min^{-1} \cdot 100g^{-1}$)	Species (nerves)	Ref
LDF	32*	Rat (sciatic)	[60]
	16*	Rat (desheathed)	[60]
^{14}C-butanol	11 ± 1	Rat (sciatic)	[87]
^{14}C- or ^{131}I-iodoantipyrine	11 ± 6	Rat (sciatic)	[74]
	27 ± 3	Rat (sciatic)	[60]
^{133}Xe	35**	Rabbit (sciatic)	[67]
H_2 clearance	43 ± 2	Cat (sciatic)	[30]
	16 ± 1	Rat (sciatic)	[31]
Radiolabeled microspheres	26 ± 5	Lamb (sciatic)	[88]
	5 ± 1	Dog (sciatic)	[34]
	14**	Dog (vagus)	[34]

Values are expressed as means ± SEM and are measured in normal, anesthetized animals.
* LDF signals are calibrated into NBF values by using the equation $y = 1.35\ x$, where x is the NBF value determined by ^{14}C-iodoantipyrine, given in [60].
** No SEM was given.

technique is also suitable for some clinical as well as basic studies. However, because of the multicompartmental nature of blood flow in the brain and peripheral nerves, LDF signals must be interpreted with caution.

Our understanding of NBF lags behind our knowledge of flow in the central nervous system. Significant questions remain unanswered about the control of NBF by humoral or neurogenic factors, responses of NBF to changes in functional or metabolical activity of the nerve, NBF under pathological conditions, and NBF during development and aging. LDF promises to be a valuable tool to help answer these important questions.

REFERENCES

1. Ranson, S.W. 1953. Meninges and blood vessels of the central nervous system. In The Anatomy of the Nervous System, Ranson, S.W., Clark, S.L., eds Philadelphia: W.B. Saunders, pp 67–81.
2. Day, A.L. 1987. Arterial distributions and variants. In Cerebral Blood Flow. Physiologic and Clinical Aspects, Wood, J.H. (ed). New York: McGraw-Hill, pp 19–36.
3. Capra, N.F., and J.P. Kapp. 1987. Anatomic and physiologic aspects of venous system. In Cerebral Blood Flow. Physiologic and Clinical Aspects, Wood, J.H., (ed) New York: McGraw-Hill, pp 37–58.
4. Reese, T.S., and M.J. Karnovsky. 1967. Fine structural localization of a blood–brain barrier to exogenous peroxidase. J Cell Biol 34:207–217.
5. Rapoport, S.I. 1976. Blood–brain barrier in physiology and medicine. New York: Raven Press.
6. Bradbury, M. 1979. The concept of a blood–brain barrier. Chilchester: John Wiley & Sons.
7. Crone, C., and D.G. Levitt. 1984. Capillary permeability to small solutes. In Handbook of Physiology, sect. 2: The cardiovascular system, vol IV, part 1. Bethesda, MD: American Physiological Society, pp 411–466.
8. Mchedlishvili, G.I. 1986. Arterial behavior and blood circulation in the brain. New York: Plenum Press.
9. Miller, J.D., and B.A. Bell. 1987. Cerebral blood flow variations with perfusion pressure

and metabolism. In Cerebral Blood Flow. Physiologic and Clinical Aspects, Wood, J.H., ed. New York: McGraw-Hill, pp 119–130.
10. McCulloch, J. 1988. The physiology and regulation of cerebral blood flow: In Handbook of Regional Cerebral Blood Flow, Knezevic, S., Maximilian, V.A., Mubrin, Z., Prohovnik, I., Wade, J., eds. Hillsdale, NJ: Lawrence Erlbaum Associates, pp 1–24.
11. Scheinberg, P., and H.W. Jayne. 1952. Factors influencing cerebral blood flow and metabolism. A review. Circulation 5:225–236.
12. Sokoloff, L. 1960. Metabolism of the central nervous system in vivo. In Handbook of Physiology, sect. 1, vol. III, pp 1843–1864.
13. Sokoloff, L. 1981. Localization of functional activity in the central nervous system by measurement of glucose utilization with radioactive deoxyglucose. J Cereb Blood Flow Metab 1:7–36.
14. Mchedlishvili, G.I., V.A. Akhobadze, and L.G. Ormotsadze. 1963. Compensation of cerebral circulation during temporary occlusion of the cranial superior vena cava. Fed Proc 22:T197–T201.
15. Auer, L.M., Kuschinsky, W., Johansson, B.B., and L. Edvinsson. 1982. Sympathoadrenergic influence on pial veins and arteries in the cat. In Cerebral Blood Flow: Effects of Nerves and Neurotransmitters, Heistad, D.D., Marcus, M.L., eds. Amsterdam: Elsevier, North-Holland, pp 291–300.
16. Owman, C., and J.E. Hardebo. 1986. Multiple transmitter amines and peptides in cerebrovascular nerves: possible links in migraine pathophysiology. Cephalalgia Suppl 4:49–62.
17. Owman, C. 1986. Neurogenic control of the vascular system: focus on cerebral circulation. In Handbook of Physiology, sect. 1, vol IV. Bethesda, MD: American Physiological Society, pp 525–580.
18. Edvinsson, L., E.T. MacKenzie, J. McCulloch, and R. Uddman. 1987. Perivascular innervation and receptor mechanisms in cerebrovascular bed. In Cerebral Blood Flow: Physiologic and Clinical Aspects, Wood, J.H., ed. New York: McGraw-Hill, pp 145–172.
19. MacKensie, E.T., and B. Scatton. 1987. Cerebral circulatory and metabolic effects of perivascular neurotransmitters. CRC Crit Rev Clin Neurobiol 2:357–419.
20. Greep, R.O. 1954. Histology. New York: Blakiston.
21. Thomas, P.K., and Y. Olsson. 1984. Microscopic anatomy and function of the connective tissue components of peripheral nerve. In Peripheral Neuropathy, 2nd edition, Dyck, P.J., Thomas, P.K., Lambert, E.H., Bunge, R., eds. Philadelphia: W.B. Saunders, vol I, pp 97–120.
22. Olsson, Y. 1984. Vascular permeability in the peripheral nervous system. In Peripheral Neuropathy, 2nd edition, Dyck, P.J., Thomas, P.K., Lambert, E.H., and Bunge, R., eds. Philadelphia: W.B. Saunders, vol I. pp 579–597.
23. Lundborg, G. 1970. Ischemic nerve injury. Scand J Plast Reconstr Surg Suppl 6:1–113.
24. Lundborg, G. 1988. Intraneural microcirculation. Orthop Clin North Am 19:1–12.
25. Shantha, T.R., and G.H. Bourne. 1968. The perineural epithelium—a new concept. In: The Structure and Function of Nervous Tissue, Bourne, G.H., ed. New York: Academic Press, vol 1, pp 379–459.
26. Lundborg, G., and P.I. Branemark. 1968. Microvascular structure and function of peripheral nerves. Adv Microcirc 1:66–88.
27. Bell, M.A., and A.G.M. Weddell. 1984. A descriptive study of the blood vessels of the sciatic nerve in the rat, man and other mammals. Brain 107:871–898.
28. Olsson, Y., and T.S. Reese. 1971. Permeability of vase nervorum and perineurium in mouse sciatic nerve studied by fluorescence and electron microscopy. J Neuropath Exp Neurol 30:105–119.
29. Greene, D.A., A.I. Winegrad, J.L. Carpentier, M.J. Brown, M. Fukuma, and L. Orci. 1979. Rabbit sciatic nerve fascicle and "endoneurial" preparation for in vitro studies of peripheral nerve glucose metabolism. J Neurochem 33:1007–1018.
30. Smith, D.R., A.I. Kobrine, and H.V. Rizzoli. 1977. Absence of autoregulation in peripheral nerve blood flow. J Neurol Sci 33:347–352.
31. Low, P.A., and R.R. Tuck. 1984. Effects of changes of blood pressure, respiratory acidosis and hypoxia on blood flow in the sciatic nerve of the rat. J Physiol 347:513–524.
32. Sundqvist, T., P.Å. Öberg, and S.I. Rapoport. 1985. Blood flow in rat sciatic nerve during hypotension. Exp Neurol 90:139–148.

33. Sugimoto, H., and W.W. Monafo. 1987. Regional blood flow in sciatic nerve, biceps femoris muscle, and truncal skin in response to hemorrhagic hypotension. J Trauma 27: 1025–1030.
34. Tschetter, T.H., A.C. Klassen, J.A. Resch, and M.W. Meyer. 1970. Blood flow in the central and peripheral nervous system of dogs using a particle distribution method. Stroke 1:370–374.
35. Rechthand, E., S. Sato, P.Å. Öberg, and S.I. Rapoport. 1988. Sciatic nerve blood flow response to carbon dioxide. Brain Res 446:61–66.
36. Hromada, J. 1963. On the nerve supply of the connective tissue of some peripheral nervous system components. Acta Anat 55:343–351.
37. Amenta, F., M.C. Mione, and P. Napoleone. 1983. The autonomic innervation of the vasa nervorum. J Neural Transm 58:291–297.
38. Appenzeller, O., K.K. Dhital, T. Cowen, and G. Burnstock. 1984. The nerves to blood vessels supplying blood to nerves: the innervation of vasa nervorum. Brain Res 304:383–386.
39. Rechthand, E., A. Hervonen, S. Sato, and S.I. Rapoport. 1986. Distribution of adrenergic innervation of blood vessels in peripheral nerve. Brain Res 374:185–189.
40. Hara, H., and S. Kobayashi. 1987. Adrenergic innervation of the vasa nervorum in the cranial nerves and spinal roots in the subarachnoid space. Exp Neurol 98:673–676.
41. Dhital, K.K., and O. Appenzeller. 1988. Innervation of vasa nervorum. In Nonadrenergic Innervation of Blood Vessels, Burnstock, G., Griffith, S. eds. Boca Raton, FL: CRC Press, vol II, pp 191–211.
42. Nilsson, G.E., T. Tenland, and P.A. Öberg. 1980. Evaluation of a laser Doppler flowmeter for measurement of tissue blood flow. IEEE Trans Biomed Eng 27:597–604.
43. Bonner, R., and R. Nossal. 1981. Model for laser Doppler measurements of blood flow in tissue. Appl Optics 20:2097–2107.
44. Rosenblum, B.R., R.F. Bonner, and E.H. Oldfield. 1987. Intraoperative measurement of cortical blood flow adjacent to cerebral AVM using laser Doppler velocimetry. J Neurosurg 66:396–399.
45. Thorne, P.R., A.L. Nuttall, F. Scheibe, and J.M. Miller. 1987. Sound-induced artifact in cochlear blood flow measurements using the laser Doppler flowmeter. Hearing Res 31:229–234.
46. Öberg, P.Å., T. Tenland, and G.E. Nilsson. 1984. Laser-Doppler flowmetry—a non-invasive and continuous method for blood flow evaluation in microvascular studies. Acta Med Scand Suppl 687:17–24.
47. Williams, P.C., M.D. Stern, P.D. Bowen, R.A. Brooks, M.K. Hammock, R.L. Bowman, and G. Di Chiro. 1980. Mapping of cerebral cortical strokes in rhesus monkeys by laser Doppler spectroscopy. Med Res Eng 13:3–5.
48. Gygax, P., and N. Wiernsperger. 1982. Hypotension induced changes in cerebral microflow and EEG and their pharmacological alterations. Acta Med Scand Suppl 678:29–36.
49. Koyama, T., M. Horimoto, H. Mishina, and T. Asakura. 1982. Measurements of blood flow velocity by means of a laser Doppler microscope. Optik 61:411–426.
50. Chen, S.T., C.Y. Hsu, E.L. Hogan, H. Maricq, and J.D. Balentine. 1986. A model of focal ischemic stroke in the rat: Reproducible extensive cortical infarction. Stroke 17:738–743.
51. Hsu, C.Y., S.T. Chen, Y.O. Luk, T.H. Liu, N.L. Banik, R.H. Gadsden, Sr., and E.L. Hogan. 1987. Pathophysiology of focal cerebral ischemia: Studies in a rat model. In Cerebral Vascular Disease 6. World Federation of Neurology 13th Salzburg Conference, Meyer, J.S., Lechner, H., Reivich, M., Ott, E.O., eds. Amsterdam: Elsevier Science Publishers, pp 265–270.
52. Mizoi, K., J. Suzuki, H. Abiko, K. Ogasawara, M. Oba, and T. Yoshimoto. 1987. Experimental study on the reversibility of cerebral ischemia. Residual blood flow and duration of ischemia. Acta Neurochir (Wien) 88:126–134.
53. May, A.M., and S.P. Arneric. 1987. Effects of basal forebrain lesions and cholinomimetics on cerebral cortical microvascular perfusion (CCMP) in rat: Continuous measurement by laser-Doppler flowmetry. Soc Neurosci Abstr 13:1034.
54. Eyre, J.A., T.J.H. Essex, P.A. Flecknell, P.H. Bartholomew, and J.I. Sinclair. 1988. A comparison of measurements of cerebral blood flow in the rabbit using laser Doppler spectroscopy and radionuclide labelled microspheres. Clin Phys Physiol Meas 9:65–74.

55. Ellis, E.F., M.L. Heizer, X. Zhang, A. Marmarou, and R. Haberl. 1988. Laser Doppler flowmetry for the assessment of the cerebral microcirculation. FASEB J 2:A507.
56. Skarphedinsson, J.O., H. Harding, and P. Thoren. 1988. Repeated measurements of cerebral blood flow in rats. Comparisons between the hydrogen clearance method and laser Doppler flowmetry. Acta Physiol Scand 134:133–142.
57. Haberl, R., M.L. Heizer, A. Marmarou, and E.F. Ellis. 1989. Laser Doppler assessment of the brain microcirculation: Effect of systemic alterations. Am J Physiol 256:H1248–H1254.
58. Haberl, R.L., M.L. Heizer, and E.F. Ellis. 1989. Laser Doppler assessment of the brain microcirculation: Effect of local alterations. Am J Physiol 256:H1255–H1260.
59. Coyle, P. 1988. Compromised early development of collateral blood flow to cerebrum in chronic hypertension. FASEB J 2:A507.
60. Rundquist, I., Q.R. Smith, M.E. Michel, P. Ask, P.Å. Öberg, and S.I. Rapoport. 1985. Sciatic nerve blood flow measured by laser Doppler flowmetry and [^{14}C]iodoantipyrine. Am J Physiol 248:H311–H317.
61. Takeuchi, M., and P.A. Low. 1987. Dynamic peripheral nerve metabolic and vascular responses to exsanguination. Am J Physiol 253:E349–E353.
62. Myers, R.R., H.M. Heckman, and H.C. Powell. 1988. Reduced nerve blood flow and subperineurial demyelination following epineurial vessels stripping: Relationship to compression injuries. Peripheral Neuropath Assoc Am Abstr Halifax, Nova Scotia, July 19–23, p 71.
63. Zochodne, D.W., and P.A. Low. 1988. Pharmacologic manipulation of nerve blood flow. Soc Neurosci Abstr 14:996.
64. Green, H.D., C.E. Rapela, and M.C. Conrad. 1963. Resistance (conductance) and capacitance phenomena in terminal vascular beds. In: Handbook of Physiology, sect. 2: Circulation, Hamilton, W.F., Dow, P., eds. Bethesda, MD: American Physiological Society, vol 2, pp 935–960.
65. Kety, S.S., and C.F. Schmidt. 1945. The determination of cerebral blood flow in man by the use of nitrous oxide in low concentrations. Am J Physiol 143:53–66.
66. Ingvar, D.H., and N.A. Lassen. 1961. Quantitative determination of regional cerebral blood-flow in man. Lancet 2:806–807.
67. Selander, D., L.G. Mansson, L. Karlsson, and J. Svanvik. 1985. Adrenergic vasoconstriction in peripheral nerves of the rabbit. Anesthesiology 62:6–10.
68. Gotoh, F., J.S. Meyer, and M. Tomita. 1966. Hydrogen method for determining cerebral blood flow in man. Arch Neurol 15:549–559.
69. Fieschi, C., L. Bozzao, A. Agnoli, M. Nardini, and A. Bartolini. 1969. The hydrogen method of measuring local blood flow in subcortical structures of the brain: Including a comparative study with the ^{14}C antipyrine method. Exp Brain Res 7:111–119.
70. Muller-Schauenburg, W., and E. Betz. 1969. Gas and heat clearance comparison and use of heat transport for quantitative local blood flow measurements. In Cerebral Blood Flow. Clinical and Experimental Results, Brock, M., Fieschi, C., Ingvar, D.H., Lassen, N.A., Schurmann, K., eds. Berlin: Springer-Verlag, pp 47–49.
71. Herscovitch, P., and W.J. Powers. 1987. Measurement of regional cerebral blood flow by position emission tomography. In Cerebral Blood Flow, Wood, J.H., ed. New York: McGraw-Hill, pp 257–271.
72. Landau, W.M., W.H. Freygang, Jr., L.P. Roland, L. Sokoloff, and S.S. Kety. 1955. The local circulation of the living brain; values in the unanesthetized and anesthetized cat. Trans Am Neurol Assoc 80:125–129.
73. Reivich, M., J. Jehle, L. Sokoloff, and S.S. Kety. 1969. Measurement of regional cerebral blood flow with antipyrine-^{14}C in awake cats. J Appl Physiol 27:296–300.
74. Mandel, M.J., F. Arcidiacono, and L.A. Sapirstein. 1963. Iodoantipyrine and Rb^{86} Cl uptake by brain, cord, and sciatic nerve in the rat. Am J Physiol 204:327–329.
75. Tschetter, T.H., A.C. Klassen, J.A. Resch, and M.W. Meyer. 1969. Regional cerebral blood flow in dogs using a particle distribution method. Proc Soc Exp Biol Med 131:1244–1249.
76. Cross, K.W., P.R.F. Dear, M.K.S. Hathorn, A. Hyams, D.M. Kerslake, M.W.A. Milligan, P.M. Rahilly, and J.K. Stothers. 1979. An estimation of intracranial blood flow in the new-born infant. J Physiol 289:329–345.
77. Muller H.R., E.W. Radue, A. Saia, C. Pallotti, and M. Buser. 1985. Carotid blood flow

measurement by means of ultrasonic techniques: Limitations and clinical use. In: Cerebral Blood Flow and Metabolism Measurement. Hartmann, A., Hoyer, S., eds. Berlin: Springer-Verlag, pp 571–592.
78. Fan, F.C., R.Y.Z. Chen, G.B. Schuessler, and S. Chien. 1979. Comparison between the ^{133}Xe clearance method and the microsphere technique in cerebral blood flow determinations in the dog. Circ Res 44:653–659.
79. Mayhan, W.G., F.M. Faraci, and D.D. Heistad. 1986. Disruption of the blood–brain barrier in cerebrum and brain stem during acute hypertension. Am J Physiol 251:H1171–H1175.
80. Tuma, R.F., G.L. Irion, U.S. Vasthare, and L.A. Heinel. 1985. Aged-related changes in regional blood flow in the rat. Am J Physiol 249:H485–H491.
81. Brown, M.M., and H. Pickles. 1982. Effect of epoprostenol (Prostacyclin, PGI_2) on cerebral blood flow in man. J Neurol Neurosurg Psychiatry 45:1033–1036.
82. Eklof, B., N.A. Lassen, L. Nilsson, K. Norberg, and B.K. Siesjo. 1973. Blood flow and metabolic rate for oxygen in the cerebral cortex of the rat. Acta Physiol Scand 88:587–589.
83. Lassen, N.A., and K. Hoedt-Rasmussen. 1966. Human cerebral blood flow measured by two inert gas techniques. Comparison of the Kety-Schmidt method and the intra-arterial injection method. Circ Res 19:681–688.
84. Haining, J.L., M.D. Turner, and R.M. Pantall, 1968. Measurement of local cerebral blood flow in the unanesthetized rat using a hydrogen clearance method. Circ Res 23:313–324.
85. Ohno, K., K.D. Pettigrew, and S.I. Rapoport. 1979. Local cerebral blood flow in the conscious rat as measured with ^{14}C-antipyrine, ^{14}C-iodoantipyrine and ^{3}H-nicotine. Stroke 10:62–67.
86. Eklof, B., N.A. Lassen, L. Nilsson, K. Norberg, B.K. Siesjo, and P. Torlof. 1974. Regional cerebral blood flow in the rat measured by the tissue sampling technique; a critical evaluation using four indicators C^{14}-antipyrine, C^{14}-ethanol, H^{3}-water and Xenon^{133}. Acta Physiol Scand 91:1–10.
87. Sugimoto, H., W.W. Monafo, and S.G. Eliasson. 1986. Regional sciatic nerve and muscle blood flow in conscious and anesthetized rats. Am J Physiol 251:H1211–1216.
88. Hitchon, P.W., J.M. Lobosky, T. Yamada, G. Johnson, and R.A. Girton. 1987. Effect of hemorrhagic shock upon spinal cord blood flow and evoked potentials. Neurosurgery 21:849–857.

16. RENAL BLOOD FLOW

RICHARD J. ROMAN

The microcirculation of the kidney is unique. Most organs are relatively homogeneously prefused by arteries and veins that are interconnected by a capillary bed that supplies oxygen and nutrients to the tissue. In contrast, the perfusion of the kidney is highly heterogeneous. Tissue blood flows range from 700 $ml \cdot min^{-1} \cdot 100g^{-1}$ of tissue in the renal cortex to around 50 $ml \cdot min^{-1} \cdot 100g^{-1}$ of tissue in the renal papilla [1–5]. Moreover, there are structural differences in the microvasculature in various regions of the kidney, and each region contains specialized vascular structures that serve the excretory function of the kidney [6,7]. In this regard, the renal vasculature not only supplies the metabolic needs of the tissue, but it also ultrafilters solutes and water into the tubular system, reabsorbs tubular fluid, preserves the osmotic gradient in the renal medulla, and regulates tubular function by influencing the composition of, and the hydrostatic pressure in, the renal interstitium.

In order to provide a glomerular filtrate and to reabsorb tubular fluid, the renal vasculature has developed unique features. It is the only organ in which two capillary beds are interspersed in series between the arterial and venous circulation. The high-pressure glomerular capillary bed is ideally suited for ultrafiltration, whereas the low-pressure peritubular capillary circulation is designed for the re-uptake of tubular reabsorbate from the renal interstitium. The renal medulla contains the specialized vasa recta capillary circulation, which acts as a countercurrent exchanger and participates in the formation of

a concentrated urine [6,7]. Given the diverse nature of the renal circulation and the influence of renal hemodynamics on the urinary excretion of water and electrolytes, the factors regulating the intrarenal distribution of blood flow have been extensively studied. Unfortunately, the complexity of the renal circulation has limited the usefulness of most of the techniques for measuring tissue blood flow in this organ. Thus, the introduction of laser-Doppler flowmetry for the measurement of tissue blood flow has generated considerable interest in the potential use of this technique in the study of the intrarenal distribution of blood flow.

DESCRIPTION OF THE RENAL CIRCULATION

The kidneys of man and animals weigh less than 0.5% of body mass, yet they receive one fifth of the cardiac output. On a per-gram basis, the kidney is the most highly perfused organ in the body. The arterio-venous oxygen concentration difference measured across the renal circulation is very small. Basal renal blood flow in man and animals is 500 $ml \cdot min^{-1} \cdot 100g^{-1}$ of tissue. It is nearly an order of magnitude greater than the blood flows in other highly perfused vascular beds such as the brain, heart, and skeletal muscle [1]. As can be seen in the cast of the renal vasculature of a rat presented in figure 16–1, the perfusion of the kidney is divided into four distinct vascular regions, i.e., the cortex, the outer stripe of the outer medulla, the inner stripe of the outer medulla, and the papilla.

In the renal cortex, the blood entering the kidney is distributed via the arcuate and interlobular arteries and the afferent arterioles to the glomerular capillary tufts (figure 16–2). Blood leaving the glomeruli via efferent arterioles enters a dense peritubular capillary network that supplies the metabolic needs of the cortical tubules. Approximately 90% of the renal blood flow remains in the renal cortex and perfuses these capillaries [3,6,7]. However, it is important to note that glomeruli are not homogeneously distributed within the renal cortex. The number of glomeruli per unit volume of tissue decreases from the superficial to the deeper layers of the renal cortex [1]. Therefore, cortical blood flow is not homogeneous and declines from around 700 $ml \cdot min^{-1} \cdot 100g^{-1}$ of tissue at the superficial cortex to around 300 $ml \cdot min^{-1} \cdot 100g^{-1}$ of tissue at junction of the cortex and the outer medulla [1–3].

The efferent arteriole of some of the juxtamedullary glomeruli gives rise to the descending vasa recta that supply blood to the outer medulla and the papilla (figure 16–2). Approximately 10% of the blood flow to the kidney enters the vasa recta circulation [6,7]. The vasa recta traverse the outer stripe of the outer medulla in vascular bundles. This region does not contain many secondary capillary networks, which accounts for the avascular appearance of this zone (figure 16–1). In the inner stripe of the outer, medulla, many of the vasa recta branch and perfuse a dense capillary network that supplies the metabolic needs of the medullary thick ascending loops of Henle. This

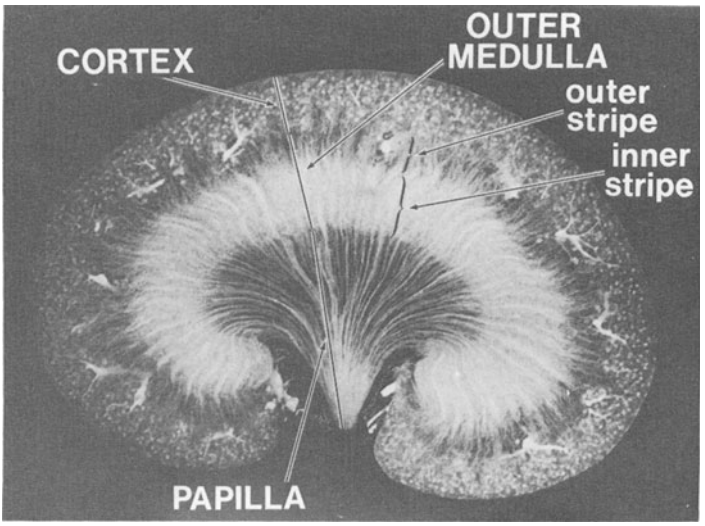

Figure 16–1. Silicone rubber (Microfil) cast of the renal vasculature of the rat.

network, termed the *Frizzled Zone*, accounts for the pronounced filling of the capillaries in the interbundle region in the inner stripe of the outer medulla (figure 16–1). Blood flow in this region is approximately 200 $ml \cdot min^{-1} \cdot g^{-1}$ of tissue [1]. A fraction of the descending vasa recta capillaries enter the inner medulla. Throughout this region, the descending vasa recta regularly branch and give rise to ascending vasa recta. Only about 10% of the descending vasa recta entering the inner medulla reach the tip of the papilla. As a result, the tip of the papilla receives less than 1% of renal blood flow, and the blood flow in this region has been estimated to be 50–100 $ml \cdot min^{-1} \cdot 100g^{-1}$ of tissue [1,3].

MEASUREMENT OF THE INTRARENAL DISTRIBUTION OF BLOOD FLOW

Whole-kidney blood flow can be measured from the renal clearance of para-aminohippurate, a substance that is nearly completely extracted by the renal circulation. Alternatively, renal blood flow can be measured with an electromagnetic flowmeter or radiolabeled microspheres.

Regional blood flow in the kidney has been measured with microspheres [8–10], radiolabeled inert gases [1,3,4], implanted semiconductors [11], hydrogen and thermal clearance techniques [1,3], indicator transit times [12,13], and the accumulation of radiolabeled tracers. Each of these techniques has serious limitations in measuring blood flow in various regions of the kidney.

Microspheres are trapped in the glomerular capillaries and are useful only in determining the distribution of blood flow in the renal cortex. Moreover,

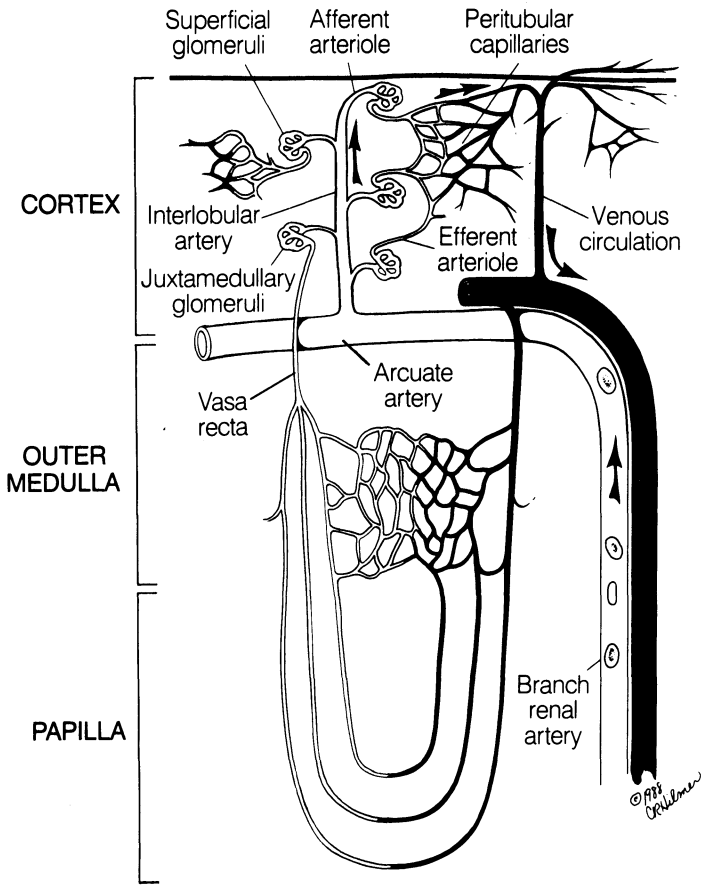

Figure 16–2. Schematic representation of the arterial blood supply to superficial and juxtamedullary glomeruli.

several workers have demonstrated that microspheres overestimate superficial cortical perfusion and underestimate perfusion of the juxtamedullary cortex because of the streaming of these particles in the renal vasculature [9,10].

Measurement techniques based on the clearance of diffusible substances in the kidney are also fraught with problems. Several studies have shown that the loss of diffusible indicators from renal tissue is influenced by changes in the flow rate of tubular fluid, as well as changes in blood flow [1,3–5]. A number of these substances are either trapped or are not uniformly extracted in the medullary circulation [1] because of countercurrent exchange. Therefore, measurement techniques based on the clearance of diffusible substances are of limited value in determining blood flow in the outer medulla and the papilla.

Regional blood flow within the kidney has been extensively studied by dye dilution techniques [12,13]. To evaluate blood flow quanitatively, the volume of distribution and the transit time of the indicator must be determined. Because of the technical difficulties in measuring the volume of distribution, this technique has generally been used qualitatively to study the effects of various maneuvers on the transit time of the indicator in different regions of the kidney.

Papillary blood flow has usually been studied using a variation of the indicator dilution technique developed by Lilienfield et al. [14]. Papillary blood flow is calculated from the accumulation of radiolabeled albumin or red blood cells (RBCs) in the papilla after a bolus injection. The critical assumptions are that the concentration of the indicator entering the vasa recta can be approximated by its concentration in a reference blood sample collected from the femoral artery and that none of the indicator is lost from the kidney prior to collection of the tissue [3,16]. This latter requirement is probably satisfied in the inner medulla of the dog when the tissue is obtained in less than 15 seconds. However, the albumin accumulation technique cannot be used in the renal cortex or outer medulla because the transit times in these circulations are only a few seconds [3]. Moreover, this method has been severely criticized when it has been used to measure papillary blood flow in the rat. Several investigators have argued that the transit time of the medullary circulation of the rat is too short to ensure that the indicator remains in the papilla regardless of when the tissue is collected [3,6]. Another drawback of the accumulation technique is that it does not allow for repeated measurements of blood flow in the same kidney. Despite these problems, the albumin-accumulation technique has provided most of the current information regarding the regulation of papillary blood flow.

Recently, papillary blood flow has been directly studied using videomicroscopy by measuring the velocity of red blood cells in individual vasa recta capillaries [17–20]. This technique has the advantage that blood flow in the same vasa recta capillary can be studied during control and experimental periods. The problem with this technique is that it has been difficult to relate these velocity measurements to tissue blood flow. Calculation of a single vessel blood flow from the measurement of RBC velocity relies on an in vitro calibration factor derived from the flow of blood in glass capillary tubes, a factor that may or may not apply to microvessels [3]. Also, detailed knowledge of the distribution and number of perfused vessels in vivo is needed under each experimental condition to estimate tissue blood flow from measurement of the blood flow in single vessels. Finally, this technique does not allow for the simultaneous study of cortical and papillary blood flow.

The recent development of laser-Doppler flowmetry for the measurement of tissue blood flow provides a new approach to the study of the regional perfusion in the kidney [23–25]. The advantages of this technique are that it provides a continuous measurement of blood flow in discrete areas of tissue

(approximately $1\mu m^3$), and it is relatively noninvasive when flow is measured from the renal cortex or the tip of the renal papilla.

The major limitation of the use of the laser-Doppler flowmeter in the renal circulation is that it has not been possible to calibrate the Doppler flow signal to an independent measure of blood flow in the region of interest [26,27]. Part of the problem, as discussed earlier, is that there is no generally accepted method for measuring tissue blood flow in the kidney. Thus, there is no standard for calibrating the laser-Doppler flowmeter. Moreover, none of the other techniques can measure blood flow in the small volume of tissue studied by the laser-Doppler flowmeter.

An additional problem is that the complexity of the circulation may limit the usefulness of laser-Doppler flowmeters in measuring blood flow in the kidney. Laser-Doppler flowmeters are based on the assumption that the bandwidth of the backscattered laser light broadens in proportion to the velocities of red blood cells and that the amplitude of the signal is proportional to the number of moving blood cells in the tissue [24,25]. These assumptions are probably correct if the fraction of red blood cells in tissue is small in proportion to the total volume of tissue. Using an in vitro model, Nilsson et al. [38] and others [26] have demonstrated that the flow signal obtained from a Perimed laser-Doppler flowmeter is linearly related to red blood cell velocity in the range of 0–10 mm/sec if the volume fraction of red blood cells is less than 1%. At higher RBC volume fractions (1%–10%), the signal was proportional to red blood cell velocity, but it underestimated red blood cell flux because of multiple scattering. This problem was addressed in subsequent models (PF2 and PF3) of the Perimed laser-Doppler flowmeter by the inclusion of a linearizing circuit [25]. However, it is not clear to what extent the correction parameter derived from in vitro experiments applies to the in vivo situation.

In the renal circulation, the volume fraction of RBCs in tissue ranges from 2%–5%, and the velocity of red blood cells is 2–4 mm/sec in the peritubular capillaries and 1–2 mm/sec in the vasa recta [3]. Thus, in this highly perfused organ, calibration factors derived from other tissues, such as skin and skeletal muscle, probably do not apply. Moreover, changes in the Doppler flow signal might underestimate changes in renal perfusion, especially when blood flow increases.

LASER-DOPPLER FLOWMETRY STUDIES OF THE RENAL CIRCULATION

Stern et al. first demonstrated the feasibility of using laser-Doppler spectroscopy to study changes in blood flow in the kidney [21,22]. They showed that norepinephrine decreased the amplitude and the frequency shift of the Doppler signal recorded from the renal cortex of the rabbit [22]. Moreover, the renal cortical blood flow signal, calculated as the root mean square of the Doppler power spectrum, decreased in a dose-dependent manner in response

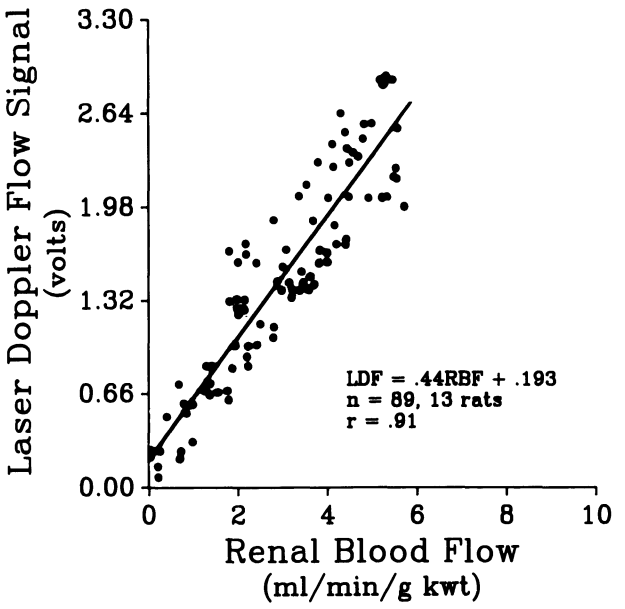

Figure 16–3. Relationships between laser-Doppler flowmeter signal (Perimed Model PF1, Stockholm, Sweden) recorded from the renal cortex and renal blood flow measured using an electromagnetic flowmeter. kwt = kidney weight. (Figure redrawn from the data in [27].)

to intravenous infusions of norepinephrine and angiotensin II [22]. In a subsequent study, changes in cortical blood flow measured with the laser-Doppler flowmeter qualitatively followed changes in renal blood flow produced by reductions in renal perfusion pressure or by the administration of norepinephrine and angiotensin II [23]. However, the changes in the Doppler flow signal underestimated the percent changes in whole-kidney blood flow measured with an electromagnetic flowmeter or microspheres.

More recently, Smits et al. [27] evaluated the Perimed Model PFld laser-Doppler flowmeter for measurement of renal cortical blood flow. The laser-Doppler cortical blood flow signal was well correlated with the renal blood flow (RBF) measured with an electromagnetic flowmeter (figure 16–3) or microspheres (figure 16–4). These studies indicated that the mean laser-Doppler flow signal obtained from several points on the renal cortex can provide a good indication of cortical perfusion even though there is considerable variation in the individual readings. However, the studies also indicate that there is no unique calibration factor for these instruments, since the slopes of the two calibration curves differ and are a function of the technique used to measure RBF.

The designs of the commercially available laser-Doppler flowmeters are quite different. Because few published studies have been performed with

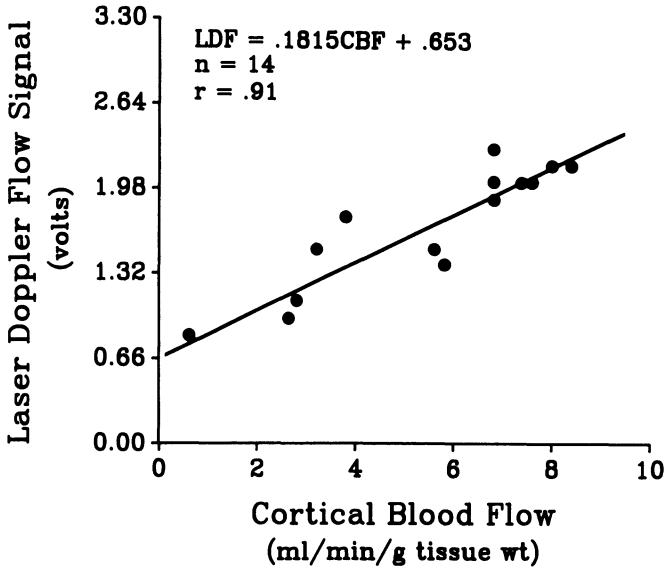

Figure 16–4. Relationships between laser-Doppler flowmeter signal (Perimed Model PF1, Stockholm, Sweden) recorded from the renal cortex and renal blood flow measured using radiolabeled microspheres. (Figure redrawn from the data in [27].)

laser-Doppler flowmeters other than the Perimed model PFl, it was not known whether other instruments could be used to study blood flow in the kidney. Therefore, we recently compared the Perimed models PFld and PF3 with the TSI model BPM 401 laser-Doppler flowmeter. The three flowmeters simultaneously measured renal cortical blood flow in each of several rats. Basal renal blood flow measured with an electromagnetic flowmeter averaged 4.8 ± 0.5 $ml \cdot min^{-1} \cdot g^{-1}$ of kidney while the cortical blood flow signal measured using the Perimed PFl laser-Doppler flowmeter (12 kHz frequency response) averaged 1.76 ± 0.07 volts. The cortical blood flow signal measured by the Perimed model PF3 laser-Doppler flowmeter averaged 2.42 ± 0.44 volts. The difference of 37% is due to the inclusion of a linearizing circuit in the PF3 laser-Doppler flowmeter, which corrects for the multiple scattering of laser light in highly perfused tissue. The degree of compensation in the renal cortex is similar to the signal ratio of 1.32 obtained with these instruments using a calibration standard (PF 100 motility standard, Perimed Corp.) consisting of a suspension of latex microspheres measured at 20°C.

The TSI model BPM 401 laser-Doppler flowmeter was also used to measure cortical blood flow in these animals. It provides a digital display ranging from 0 to 780 units. In skin and in skeletal muscle, one unit is supposed to represent a blood flow of 1 $ml \cdot min^{-1} \cdot 100g^{-1}$ of tissue. Cortical blood flow measured with the TSI laser-Doppler flowmeter averaged 100 ± 23 units

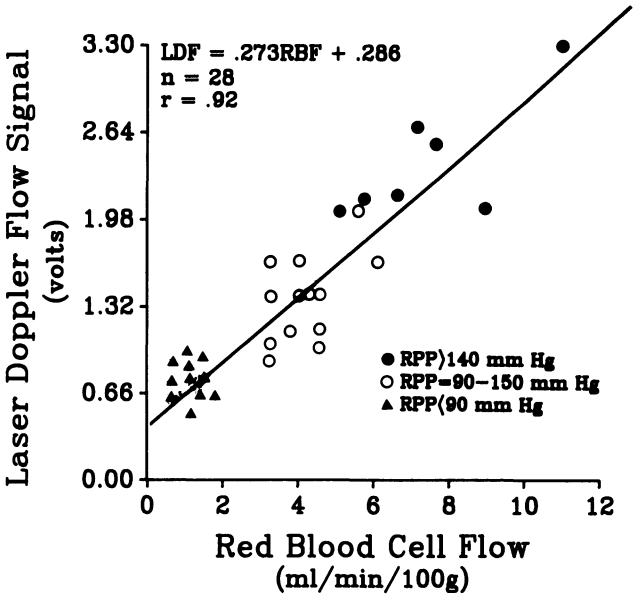

Figure 16–5. Relationship between the laser-Doppler flow signal and red blood cell flow measured in the exposed papilla of rats. (Figure redrawn from data in [26].)

(100 $ml \cdot min^{-1} \cdot 100g^{-1}$ of tissue). The absolute value of cortical blood flow based on this skeletal muscle calibration factor is too low and underestimates blood flow in the renal cortex by a factor of six or seven. Nevertheless, the changes in cortical blood flow measured with the TSI instrument in response to reductions in renal perfusion pressure were linearly related and highly correlated with the changes in renal blood flow that were simultaneously recorded with an electromagnetic flowmeter.

The ability of the Perimed PFld laser-Doppler flowmeter to measure papillary blood flow has also been evaluated [26]. The flow signal recorded from the papilla of rats was linearly related to the blood flow estimated from the accumulation of ^{51}Cr-labeled red blood cells in this tissue (figure 16–5). These studies first demonstrated the utility of laser-Doppler flowmeters for measuring changes in papillary blood flow. The advantages of this technique are 1) it is the only method that provides a continuous measure of papillary blood flow, and 2) changes in cortical and papillary blood flow can be studied in the same kidney. Moreover, it is possible to measure papillary blood flow through the intact ureter [28,29], since the wall of the ureter is thin enough to transmit laser light and blood flow in the ureter is very low in comparison to that in the papilla. A demonstration of this technique is presented in figure 16–6. Papillary blood flow was measured before and 30 minutes after removal of the ureter overlying the papilla. Although papillary blood flow increased 20% immediately after removing the ureter, the flow signal

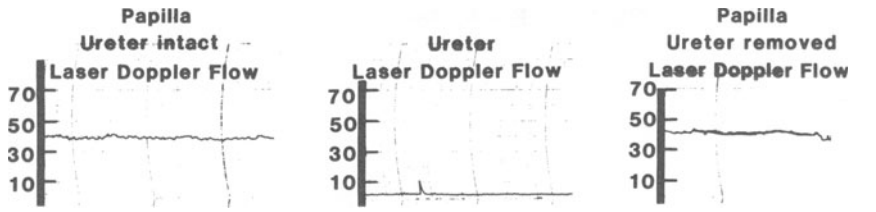

Figure 16–6. Comparison of the laser-Doppler blood flow signal recorded from the papilla of a rat through the intact ureter and 30 minutes are exposing the renal papilla.

returned to control after a 30-minute equilibration period (figure 16–6). The measurement of papillary blood flow through an intact ureter allows for the simultaneous collection of urine while papillary blood flow is monitored. It also avoids the changes in blood flow that are produced by exposing the papilla.

As discussed earlier, the major problem in using the laser-Doppler flowmeter for the measurement of papillary blood flow is the calibration of the signal. Many investigators have argued that papillary blood flow is underestimated when measured by the accumulation of labeled indicators [3] because of loss of the indicator from the medullary circulation. Since the Doppler flowmeter was calibrated for the measurement of papillary blood flow against the accumulation technique, estimates of papillary blood flow using the laser-Doppler technique are probably too low. Another problem is that the Perimed PFld and PF3 instruments yield similar flow signals on the rat renal cortex and papilla even though cortical blood flow is much greater than papillary blood flow. This puzzling result may reflect different calibration factors in these two circulations because of differences in the vascularity, intravascular hematocritis, and optical properties of these regions of the kidney. Alternatively, we have shown that, at the high red blood cell volume fractions found in these circulations, the laser-Doppler flowmeter may simply monitor RBC velocity [26]. The cortical and papillary flow signals may be of the same magnitude because the velocity of red blood cells in peritubular and vasa recta capillaries are not very different [3]. This problem, however, does not preclude the use of laser-Doppler flowmetry for measuring relative changes in blood flow in these circulations because there is little evidence for capillary recruitment in this organ. Thus, changes in blood flow and the velocity of red blood cells are probably directly related in the renal circulations.

APPLICATIONS OF LASER-DOPPLER FLOWMETRY IN THE RENAL CIRCULATION

Several investigators have used laser-Doppler flowmeters to determine whether vasoactive compounds exert a selective influence on vasa recta blood

flow. Hansell and Ulfendahl [30] studied the effects of atriopeptins I and II on renal cortical and papillary blood flow in the rat and correlated the hemodynamic effects with changes in sodium and water excretion. They found that atriopeptin I increased sodium and water excretion without altering cortical and papillary blood flow. Atriopeptin II, which relaxes vascular smooth muscle, increased cortical and papillary blood flow and had a much greater diuretic and natriuretic effect than atriopeptin I. The increase in papillary blood flow produced by atriopeptin II was four times greater than the corresponding change in cortical blood flow. This finding indicates that the renal medullary vasculature is more sensitive to the vasodilatory actions of atriopeptin II than the cortical circulation [30].

Similar findings were reported by Takezawa et al. [28]. These authors found that infusion of low doses of atriopeptin III produced a 20% increase in papillary blood flow in rats, while RBF and cortical blood flow were unaltered. The increase in papillary blood flow was accompanied by an elevation in sodium and water excretion. These results suggest that the diuretic and natriuretic effects of atriopeptin III may in part be related to its effects on vasa recta blood flow.

More recently, we have used the laser-Doppler flowmeter to study the influence of the renin-angiotensin [29], kallikrein-kinin [29], and renal prostaglandin [31] systems on the control of papillary blood flow. Cortical and papillary blood flow were measured before and after 1) blockade of the renin-angiotensin system with captopril, enalaprilat or saralasin, 2) blockade of the kallikrein-kinin system with a kinin receptor antagonist, and 3) blockade of renal eicosanoid synthesis with meclofenamate. These studies indicate that all three of these intrarenal autacoid systems influence papillary blood flow. Kinins and prostaglandins exert a vasodilatory influence on the medullary vasculature, whereas angiotensin II is a vasoconstrictor. Blockade of the renin-angiotensin, kallikrein-kinin, and renal prostaglandin systems had little effect on cortical blood flow measured with the laser-Doppler flowmeter or RBF measured by an electromagnetic flowmeter. These results further support the view that these autacoid systems regulate the intrarenal distribution of blood flow by selectively influencing the vascular resistance of the medullary circulation.

The renal hemodynamic actions of another vasoactive mediator, platelet-activating factor, has recently been studied by Thomas and Navar [32] using laser-Doppler flowmetry. Infusion of platelet-activating factor (PAF) reduced RBF and glomular filtration rate (GFR) by 25% in dogs. Renal cortical blood flow fell by about 10%. Glomerular capillary pressure measured by micropuncture in superficial nephrons fell by the same percentage as the fall in cortical blood flow, indicating that PAF constricts the preglomerular vasculature. One unique feature of this study was that cortical blood flow was measured with the laser-Doppler flowmeter in the same area in which the micropuncture studies were performed, eliminating the possibility that the

micropuncture itself induced a local change in hemodynamics in the area of study.

Nygren et al. [33] recently used laser-Doppler flowmetry to address a clinically relevant problem. The injection of contrast medium for radiological studies often induces a nephropathy. Renal blood flow, however, is generally increased by contrast media. Nygren et al. [33] found that several contrast media lowered papillary blood flow in rats without affecting cortical blood flow. Since the PO_2 in the medullary circulation is normally very low due to the countercurrent exchange of oxygen, it was suggested that contrast-media nephropathy may be due to selective ischemic injury of the renal medulla [33].

Other applications of laser-Doppler flowmetry for the study of the renal circulation have been directed at the heterogeneity of renal cortical perfusion. In a recent study, Pollock and Arendshorst [34] reported that the dopamine DA1 receptor agonist, Fenoldopam, increased renal blood flow. However, the single-nephron glomerular filtration rate measured in superficial nephrons did not increase. Since changes in GFR and renal blood flow are usually coupled, one explanation for these findings is that Fenoldopam may have different effects on the renal vasculatures of superficial and deep cortical nephrons. Using a laser-Doppler flowmeter, these authors demonstrated that superficial cortical blood flow increased by the same percentage as whole kidney blood flow during infusion of Fenoldopam. They concluded that this drug reduces both pre- and postglomerular vascular resistance and thus preserves the single nephron filtration rate in face of an elevation in renal blood flow [34].

A similar study has been reported by Spelman et al. [35]. Changes in RBF and cortical blood flow were compared in response to stimulation of the renal nerves in baboons. In the control period, cortical blood flow measured in different areas of the surface of the kidney were homogeneous. Stimulation of the renal nerves lowered RBF and cortical blood flow. However, the magnitude of the fall in cortical blood flow varied in different locations of the kidney. These authors concluded that the renal cortex is innervated and cortical blood flow is under the control of the renal nerves [35]. The increased heterogeneity of cortical perfusion during stimulation of the renal nerves probably reflects the nonhomogeneous distribution of nerve terminals in the renal cortex [35].

The ability of the laser-Doppler flowmeter to produce a signal proportional to the flux of red blood cells if the optical properties and structure of the vascular beds are similar allows for comparisons of regional blood flow in the kidneys of different animals. Smits and Roman [26] reported that the papillary blood flow signal measured in young rats (3–5 weeks old) was about half the value observed in adult animals (12 weeks old). The laser-Doppler blood flow signals obtained from the renal cortex were not different in the young and adult rats. The reason for the difference in papillary blood flow in

these two groups remains to be explored. It may reflect a difference in the velocity of RBCs in the vasa recta circulation in young and adult rats. Alternatively, it could reflect changes in the vascularity of the papilla as the kidney matures.

Another comparison of papillary blood flow in different groups of animals has been performed in spontaneously hypertensive and normotensive Wistar-Kyoto rats. Roman and Kaldunski [36] reported that papillary blood flow is reduced in spontaneously hypertensive (SHR) rats in comparison to that observed in Wistar-Kyoto rats. The fall in papillary blood flow in the SHR preceded the development of hypertension. This finding eliminates the possibility that the blood flow was reduced by hypertensive vascular injury. These authors suggested that an elevated renal medullary vascular tone may play a role in the development of hypertension in the SHR [36].

Finally, the laser-Doppler flowmeter has been used to address the question of regional differences in the autoregulation of renal blood flow. The original studies of Kramer and Thurau using dye dilution techniques indicated that papillary blood flow is not autoregulated in dogs [12,13]. Subsequent studies using radiolabeled tracers [11] and videomicroscopy [20] suggested that papillary blood flow as well as whole-kidney blood flow was autoregulated. Stern et al. [23] using a laser-Doppler flowmeter also reported that papillary blood flow was autoregulated in response to reductions in perfusion pressure. We have recently reevaluated this question using the Perimed model PFl and PF3 laser-Doppler flowmeters [37]. The results of these experiments (figure 16–7) indicate that cortical and papillary blood flow decrease in parallel in response to reductions in renal perfusion pressure. When renal perfusion pressure was elevated, cortical blood flow was autoregulated; however, papillary blood flow was not. These results suggest that papillary blood flow is not autoregulated over the same range of pressures as cortical blood flow. Apparently, renal medullary vascular resistance reaches its maximal value at the normal level of arterial pressure, whereas renal cortical vascular resistance increases further when renal perfusion pressure is elevated.

CONCLUSIONS

The recent development of the laser-Doppler flowmeter has provided a unique tool for the study of regional blood flow in the kidney. Despite the theoretical problems associated with measuring blood flow in highly perfused tissue, several studies have indicated that the laser-Doppler flow signals obtained from the cortex and papilla reflect changes in tissue blood flow measured with other techniques. The advantages of the laser-Doppler flowmeter are 1) it provides a continuous index of tissue perfusion, 2) it is noninvasive, 3) cortical and papillary blood flow can be measured in the same animal, and 4) it allows for intra-animal comparisons of blood flow in different regions of the kidney. The limitations of the technique are that it may underestimate changes in blood flow when hematocrit or the number of

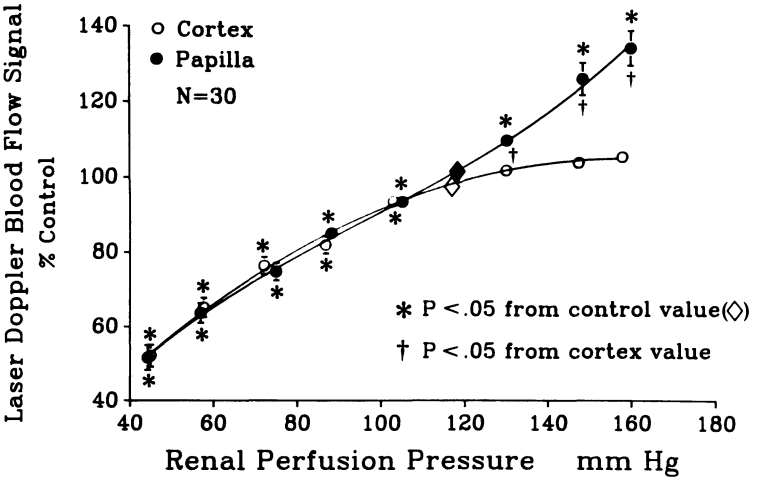

Figure 16–7. Autoregulation of renal cortical and papillary blood flow in volume-expanded rats. Blood flows were measured using a Perimed model PF1 laser-Doppler flowmeter and are expressed as a percent of the control blood flows measured at a renal perfusion pressure equal to the animals' arterial pressure. (Figure reproduced with permission from [37].)

perfused vessels changes in the region of interest, since the laser-Doppler flowmeter apparently responds primarily to changes in the velocity of RBCs in highly perfused tissues. Moreover, it has not been possible to obtain an absolute blood flow calibration of the laser-Doppler signal because there are no accepted techniques for measuring regional blood flow in the kidney in tissue volumes comparable to those sampled by the laser-Doppler flowmeter.

ACKNOWLEDGMENTS

The author wishes to thank Rhoda Adelsen for typing this manuscript and Mr. John Borgos of TSI Incorporated (St. Paul, MN) for providing the TSI laser-Doppler flowmeter used for the comparative studies of cortical blood flow. This work was supported by grants from the American Heart Association (83-853) and the National Institutes of Health (HL-29587 and HL-36279). This work was completed during Dr. Roman's tenure as an Established Investigator of the American Heart Association.

REFERENCES

1. Brenner, B.M., R. Zatz, and I. Ichikawa. 1986. The renal circulations. In The Kidney, Brenner, B.M., Rector, F.C., eds. Philadelphia: W.B. Saunders Company, pp 93–123.
2. Mimran, A. 1987. Regulation of renal blood flow. J Cardiovasc Pharmacol 10(Suppl 5):51–59.
3. Cupples, W.A. 1986. Renal medullary blood flow: its measurement and physiology. Can J Physiol Pharmacol 64:873–880.
4. Knox, F.G., E.L. Ritman, and J.C. Romero. 1984. Intrarenal distribution of blood flow: Evolution of a new approach to measurement. Kidney Int 25:473–479.

5. Aukland, K. 1980. Methods for measuring renal blood flow: Total flow and regional distribution. Annu Rev Physiol 42:543–555.
6. Zimmerhackl, B.L., C.R. Robertson, and R.L. Jamison. 1987. The medullary microcirculation. Kidney Int 31:641–647.
7. Kriz, W. 1981. Structural organization of the renal medulla: Comparative and functional aspects. Am J Physiol 241:R3–R16.
8. McNay, J.L., and Y. Abe. 1970. Pressure-dependent heterogeneity of renal cortical hemodynamics in dogs. Circ Res 27:571–587.
9. Katz, M.A., R.C. Blantz, F.C. Rector, Jr., and D.W. Seldin. 1971. Measurement of intrarenal blood flow. I. Analysis of microsphere method. Am J Physiol 220:1903–1913.
10. Bankir, L., M.M. Trinh Trang Tan, and J.P. Grunfeld. 1979. Measurement of glomerular blood flow in rabbits and rats. Erroneous findings with 15 μm microspheres. Kidney Int 15:126–133.
11. Wolgast, M. 1968. Studies on the regional renal blood flow with labeled red cells and small beta sensitive semiconductor detectors. Acta Physiol Scand Suppl 31:1–109.
12. Kramer, K., K. Thurau, and P. Deetjen. 1960. Hamodynamik des Nierenmarks. I. Mitteilung Capillare Passagezeit, Blutvolumen, Durchblutung, Gewebshamatokrit und O_2-Verbrauch des Nierenmarks in situ. Plugers Arch 270:251–269.
13. Thurau, K. 1964. Renal hemodynamics. Am J Med 36:698–719.
14. Lilienfield, L.S., H.C. Maganzini, and M.H. Bauer. 1961. Blood flow in the renal medulla. Circ Res 9:614–617.
15. Solez, K., E.C. Kramer, J.A. Fox, and R.H. Hepinstall. 1974. Medullary plasma flow and intravascular leukocyte accumulation in acute renal failure. Kidney Int 6:24–37.
16. Rasmussen, S.N. 1978. Red cell and plasma flows to the inner medulla of the rat kidney. Pflugers Arch 373:153–159.
17. Holliger, C., K.V. Lemley, S.L. Schmitt, F.L. Thomas, C.R. Robertson, and R.L. Jamison. 1983. Direct determination of vasa recta blood flow in the rat renal papilla. Circ Res 53:401–413.
18. Zimmerhackl, B., C.R. Robertson, and R.L. Jamison. 1985. Fluid uptake in the renal papilla by vasa recta estimated by two different methods simultaneously. Am J Physiol 248:F347–F353.
19. Zimmerhackl, B., J. Tinsman, R.L. Jamison, and C.R. Robertson. 1985. Use of digital cross-correlation for on-line determination of single vessel blood flow in the mammalian kidney. Microvasc Res 30:63–74.
20. Cohen, H.J., D.J. Marsh, and B. Kayser. 1983. Autoregulation in the vasa recta of the rat kidney. Am J Physiol 245:F32–F40.
21. Stern, M.D. 1975. In vivo evaluation of microcirculation by coherent light scattering. Nature 254:56–58.
22. Stern, M.D., P.D. Bowen, R. Parma, R.W. Osgood, R.L. Bowman, and J.H. Stein. 1987. Measurement of renal cortical and medullary blood flow by laser-Doppler spectroscopy in the rat. Am J Physiol 236:F80–F87.
23. Stern, M.D., D.L. Lappe, P.D. Bowen, J.E. Chimosky, G.A. Holloway, Jr., H.R. Keiser, and R.L. Bowman. 1977. Continuous measurement of tissue blood flow by laser-Doppler spectroscopy. Am J Physiol 232:H441–H448.
24. Bonner, R., and R. Nossal 1981. Model for laser-Doppler measurements of blood flow in tissue. Appl Optics 20:2097–2107.
25. Nilsson, G.E. 1984. Signal processor for laser-Doppler tissue flow meters. Med Biol Eng Comp 22:343–348.
26. Roman, R.J., and C. Smits. 1985. Laser-Doppler determination of papillary blood flow in young and adult rats. Am J Physiol 251:F115–F124.
27. Smits, G.J., R.J. Roman, and J.H. Lombard. 1986. Evaluation of laser-Doppler flowmetry as a measure of tissue blood flow. J Appl Physiol 61:666–672.
28. Takezawa, K., A.W. Cowley, Jr., M. Skelton, and R.J. Roman. 1987. Atriopeptin II alters renal medullary hemodynamics and the pressure-diuresis response in rats. Am J Physiol 252:F992–F1002.
29. Roman, R.J., M.L. Kaldunski, A.G. Scicli, and O.A. Carretero. 1988. Influence of kinins and angiotensin II on the regulation of papillary blood flow. Am J Physiol 255:F690–F698.
30. Hansell, P., and H.R. Ulfendahl. 1986. Atriopeptins and renal cortical and papillary blood flow. Acta Physiol Scand 127:349–357.

31. Roman, R.J., and E. Lianos. Influence of renal prostaglandins on papillary blood flow, renal interstitial pressure and the pressure natriuretic response. Hypertension 13, in press.
32. Thomas, C.E., and L.G. Navar. 1988. Influence of calcium channel blockade on the renal vasoconstrictive actions of platlet activating factor. Kidney Int 33:413.
33. Nygren, A., H.R. Ulfendahl, P. Hansell, and U. Erikson. 1988. Effects of intravenous contrast media on cortical and medullary blood flow in the rat. Invest Radiol 23:753–761.
34. Pollock, D.M., and W.J. Aredshorst. Tubuloglomerular feedback and blood flow autoregulation during DA1-induced renal vasodilation. Am J Physiol, in press.
35. Spelman, F.A., P.Å. Öberg, and C. Astley. 1986. Localized neural control of blood flow in the renal cortex of the anesthetized baboon. Acta Physiol Scand 127:437–441.
36. Roman, R.J., and M.L. Kaldunski. 1988. Renal cortical and papillary blood in spontaneously hypertensive rats. Hypertension 11:657–663.
37. Roman, R.J., A.W. Cowley, Jr., J. Garcia-Estañ, and J.L. Lombard. 1988. Pressure-diuresis in volume-expanded rats: Cortical and medullary hemodynamics. Hypertension 12:168–176.
38. Nilsson, G.E., T. Tenland, and P.Å. Öberg. 1980. Evaluation of a laser Doppler flowmeter for measurement of tissue blood flow. IEEE Trans Biomed Eng 27:597–604.

17. BLOOD FLOW IN BONE

SÖLVE HELLEM and E. GÖRAN SALERUD

The blood supply is recognized as a vital basis of bone growth and remodeling. However, preference has been given to microvascular studies in other tissues. Until recently, bone was a minor topic in the literature of the microcirculation. In 1691, Clopton Havers [1] described "small canals" transversing cortical bone. He assumed a possible vascular pathway in bone, once regarded as a lifeless supporting frame for soft tissues. Some 250 years later, fundamental investigations confirmed Havers's theory of vascular canals and clarified the vascular topography of bone. The physiological aspects of blood flow in bone, however, are still a challenge to microvascular research. As a technique for continuous flow registration in bone, laser-Doppler flowmetry (LDF) has been found to fulfill most of the requirements for experimental research.

GENERAL ASPECTS OF BLOOD SUPPLY AND BLOOD FLOW IN BONE

Concepts of flow direction

Long tubular bones have been the main objects of study regarding microvascular blood flow in bone. In mature bone, the most widely accepted concept of perfusion is that of a centrifugal flow through cancellous and cortical bone, emanating from nutrient medullary vessels [2,3,4]. The vascularity and flow patterns in bone marrow have been extensively described by vital microscopy studies that showed that blood flow to the cortical bone

enters the Haversian canals through marrow arterioles and capillaries and is almost all drained back into the sinusoids and collecting venules of the marrow.

Further studies [5] revealed two distinct vascular pathways in cortical bone. One, containing longitudinal vessels, supplies the Haversian system. The other supplies blood through transverse vessels into the principal vascular and nutrient system of the cortical bone. These findings, based on contrast fluid perfusion of the vascular bed, are in accordance with observations made with vital microscopy [3]. Within this transverse vascular system, vessels are found connecting the central nutrient arteries and venous system in the marrow with the vessels of the periosteum. These medulloperiosteal anastomoses have been demonstrated as most essential when establishing retrograde blood supply distal to a vascular block of the nutrient vessels [6,7].

The course of reestablishment is entirely dependent on the extent of preserved medullary vascularity [8]. A rib transplant with preserved medullary vessels, but supplied only from its periosteal vessels, has been shown to normalize its cortical blood flow within 24 hours [9]. Medullary reaming and nailing of tubular bones, on the other hand, leads to compartmental necrosis of the cortex due to long periods of ischemia or decreased perfusion [6].

Identification of vascular topography in bone

Present knowledge of vascular patterns in bone tissue is based mainly on angiographic or microangiographic studies. The gross vascular architecture has been demonstrated with conventional radiological examination, whereas the microvascular bed is studied in microradiographs made by continuous exposure at low kilovoltage emissions of 200–400 μm thick bone slices in contact with high resolution plates [10].

More detailed studies can be performed on contrast-fluid-perfused specimens observed through light microscopy. On specimens cleared in methylsalicylate or glycerin (Spalteholtz method), a three-dimensional microscopic examination can be achieved. By changing the physical properties of the perfusate and by use of simultaneous injections of different-colored perfusates in selected nutrient vessels, the vascular territories involved can be further differentiated [11].

MEASUREMENT OF MICROVASCULAR BLOOD FLOW IN BONE

Direct visual examination of a functioning microvascular bed in bone was introduced by vital microscopy studies on bone marrow [3]. The technique has also been applied to other parts of the bone [12]. The method enables determination of flow modalities in small vessels within the microscopic field. It is an excellent method for recording qualitative changes in flow within small volumes.

Most techniques for the measurement of blood flow in different parts of the body have been applied to bone tissue as well. These include clearance of

different radioactive isotopes, identification of isotopically labeled microspheres or tagged red blood cells, clearance of hydrogen, bone scintigraphy, and recently laser-Doppler flowmetry [13,14,15]. Of these, the microsphere technique has been the most frequently used method for experimental measurements.

Evidence exists for both a nonnutritive flow, including arterio-venous shunts, and a nutritive or capillary flow in many tissues, including bone. Consequently, analysis of flow recorded from differentiated vascular territories in marrow as well as cancellous and cortical bone should preferably be discussed in terms of total flow and capillary flow. Accordingly, multiple injections of differently labeled microspheres may allow for repeated recordings. The method also measures total arterial inflow to separate parts of the bone. The capillary flow or perfusion may be calculated as a level of nutritive blood flow [16,17], due to intravascular or locally applied diffusible isotopes. The above methods represent sequential recordings of blood flow only. For continuous recordings of flow in bone, however, LDF has been found to be most valuable, and the flow level may be calculated as total flow within the bone area measured [18].

Flow rates and qualitative analysis of blood flow in bone

Blood flow in bone has often been quantified as $ml \cdot min^{-1} \cdot g^{-1}$ tissue both in clinical and experimental studies. The results cover a rather wide range of flow rates, even when comparable parts of bone have been investigated. Recently published data on flow rates in tibial and femoral bones vary from 1.6–7.0 $ml \cdot min^{-1} \cdot g^{-1}$ in cortical bone, 10.0–30.0 $ml \cdot min^{-1} \cdot g^{-1}$ in cancellous bone and 8.9–50.3 $ml \cdot min^{-1} \cdot g^{-1}$ in bone marrow. Corresponding values obtained from the rabbit mandible were 4.9 and 18.3 $ml \cdot min^{-1} \cdot g^{-1}$ for cortical and cancellous bone, respectively [19].

Qualitative analysis of flow is of interest in studies concerning vasomotor activity in bone blood vessels and microvascular response to various stimuli. The medullary pressure in tubular bone has been proposed to be an indirect measure of medullary blood flow, and variations in partial oxygen pressure in bone have been recorded as a function of flow. Besides vital microscopy [3], LDF is regarded as the most reliable method for continuous monitoring of blood flow in bone [18].

Factors controlling microvascular flow in bone

The perfusion pressure gradient and peripheral vascular resistance are two main factors controlling the rate of flow through the microvascular bed. Due to the rigid structures surrounding bone blood vessels, the extravascular pressure may be of particular importance in maintaining adequate nutritive flow, especially in cortical bone.

Peripheral vascular flow resistance, controlled by arteriolar contraction,

pre- and postcapillary sphincters, and arterio-venous anastomoses, has been found to regulate the quantity of blood perfusing the microvascular bed. Studies on pressure–flow relations in the microvascular system generally indicate that arteriolar pressure is maintained despite substantial changes in flow and that precapillary flow can be kept within a narrow range despite wide fluctuations in pressure.

The mechanism controlling these compensatory variations in vasoconstrictor activity has been the subject of several investigations. Regarding bone tissue, considerable evidence for hormonal, metabolic, and neural control has been published. Extensive innervation of bone vessels with unmyelinated C-fibers suggests an autonomic function of these nerves [20]. Variations in vascular resistance by sympathetic stimulation as well as responses to vasoactive drugs have shown the presence of intraosseous vascular α- and β-adrenoceptors [21,22]. Furthermore, norepinephrine and adenosine, producing vasoconstriction and dilation respectively, are found to directly influence the vascular smooth muscles. The response pattern of bone blood vessels was found to be similar to those seen in skeletal muscles [23]. The metabolic control of vascular resistance in bone seems to be potent and strongly responsive to arterial oxygen tension, carbon dioxide tension, and arterial pH.

Arterio-venous shunting is regarded as another regulating factor in microvascular flow. Its presence in osseous tissue has been shown by using different sizes of microspheres, and it has been found to increase with decreased flow levels. Variations in input pressure elicit vascular reactions in different parts of the bone that maintain a stable pressure–flow relationship. Studies on autoregulation of flow in vascular beds have shown that arteriolar dilation follows a decrease in perfusion pressure. Actually, vascular dilation due to hypotension may cause an increase in microvascular flow. Recently, LDF studies have demonstrated this vascular reaction in cancellous bone [24]. Hemorrhagic and medicinally induced hypotension produce quite different vascular reactions in bone. Infusion of a potent vasodilator (adenosine) has been found to produce a significant increase in flow and a decrease in vascular resistance. During hemorrhagic hypotension, however, the opposite vascular reaction was found [23].

Vasomotion, described as the spontaneous and rhythmical dilation and constriction of microvessels, is claimed to have a direct effect on several basic microvascular functions. Rhythmical variations in flow (frequency 1–10 min^{-1}) have been reported in human skin and in several other tissues [25,26,27]. Vasomotion was first demonstrated in bone by LDF [18]. The oscillations ranged from 2 to 11 cycles $\cdot$ min^{-1} and appeared more frequently in areas with increased flow.

In the present literature, however, vasomotion activity and other flow modalities have been infrequently discussed. Consequently, more basic knowledge of different qualitative properties of the microcirculation in bone is highly desirable.

LASER-DOPPLER FLOWMETRY IN BONE

Basic experimental results

Results published in two pioneering reports [28,29] were used to adapt LDF to measure microvascular blood flow in bone. The first results with LDF in bone revealed that microvascular responses to local and systemic constrictors could be continuously monitored [15,24].

The cancellous bone area subapical to the mandibular front teeth in young pigs was chosen. Recordings were made with an early version of the Periflux® Laser-Doppler Flowmeter and with specially designed multifiber flowmeter probes and probeholders [18].

Sensitivity to motion artifacts from the probe and the effect of traumatic probe insertion are two main factors influencing signal interpretation. Both factors have been overcome by tapping the probe holders into the pulp canals of the teeth down in to slight contact with the subapical bone area to be investigated (figure 17–1). The probe holders were designed to hold the laser probe in different angular positions and to illuminate different bone areas (figure 17–2).

The LDF revealed two distinct variations in output signal. A variation of the signal, synchronous with the heartbeat or breathing movements, ranging from 5%–20% of the average flow value, could be discerned and was consistently recorded. A rhythmical variation of the signal (vasomotion), not synchronous with the heartbeat, appeared spontaneously and showed amplitudes up to 75% of the average flow value. Vasomotion was observed in 6% of all recordings made from areas with normal bone tissue and in 34% of bone areas with high flow levels due to inflammatory tissue reactions.

The calculated reproducibility error of 7.4% in the flow recorded with this method was close to the value (6%) achieved by in vitro tests [26]. The error includes both statistical measurement error as well as influences due to limited probe manipulation and inevitable changes in flow and should be considered as the upper limit. A correlation coefficient of 0.98 ($n = 22$) was found between two consecutive recordings from the same probe position compared with marked flow variation following frequent manipulation of the probe [18]. This indicates that continuous flow recording with the probe in a fixed position is preferable when evaluating microvascular reactions from multifiber probes in bone.

Spatial flow variations have been demonstrated in several tissues including cancellous and cortical bone. In the cited study, variations in flow were monitored from four different probe positions, representing four different tissue volumes. The coefficient of variation in blood flow values was calculated to be 24.3%, indicating either a nonuniform vascularity or areas with different perfusion. In bone areas where high flow levels were induced by inflammatory reactions, a decrease in spatial flow variation was found due to an ingrowth of new blood vessels forming a more dense vascularity within the tissue volume illuminated by the laser light.

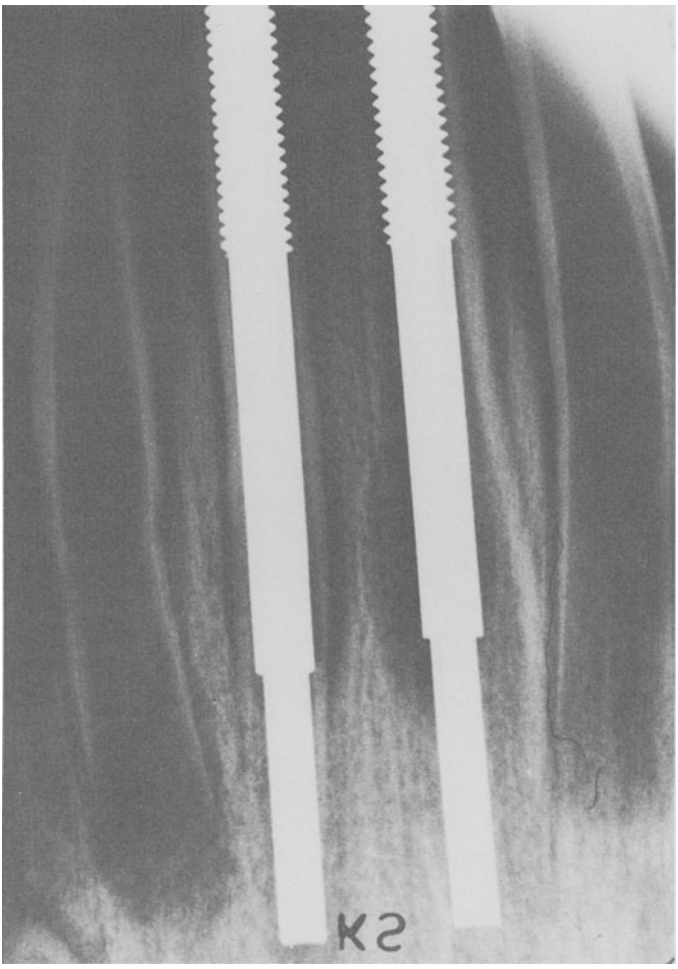

Figure 17–1. Probe-holders, containing a LDF probe, firmly attached and in contact with the subapical bone surface.

The microvascular response to vascular constrictors and to halothane-induced hypotension as recorded by LDF has been mentioned above. Autoregulation of flow has been shown to differ between tissues. In cutaneous vessels, autoregulation does not occur at a perfusion pressure below 100 mmHg. Vessels in skeletal muscles, however, autoregulate within the range of 20–160 mmHg to maintain the capillary pressure constant. Arteriolar dilation and shunting have been demonstrated in different tissues in response

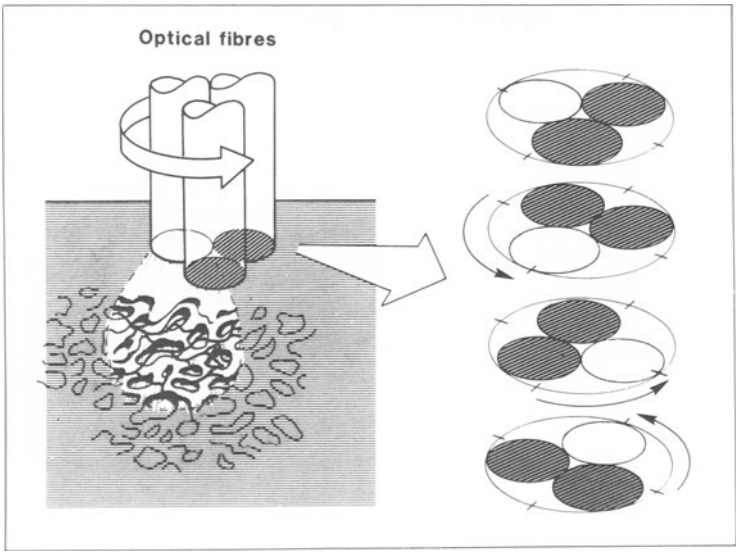

Figure 17–2. Laser-Doppler flowmeter probe in different angular positions, illuminating well-defined bone areas.

to decreases in mean blood pressure (MBP). Autoregulation in bone was demonstrated at MBP levels down to approximately 30 mmHg. Below this level, the autoregulation of flow disappeared.

Furthermore, a local injection of epinephrine reduced cancellous bone blood flow almost to zero within 20 seconds. The expected increase in vascular resistance and MBP in response to an i.v. injection of vasopressin was also recorded. Flow decreased to about 25% of the initial value after approximately three minutes. Within 60 seconds, however, the MBP rose 80%. The discrepancy in time may indicate a sequence of autonomic compensation for the increased intraosseous pressure by arterio-venous (A-V) shunting. An evaluation of microvascular reactions to vasoactive substances or to changes in arterial pressure actually requires controlled studies with continuous recording of MBP and frequent blood gas analysis.

Recent investigations with laser-Doppler flowmetry in bone

During the last five years, further investigations have been performed with LDF in bone, including clinical as well as animal studies. In a study on skeletally mature rabbits, LDF was used to demonstrate a linear relationship between increasing intracapsular pressure and decreasing femoral-head blood flow [30]. Screws, adapted for the laser probe, were placed in the hip joint, and the probe was brought into contact with the articular cartilage of the

femoral head. The subcondral blood flow was then monitored under baseline conditions and under increasing levels of intracapsular pressure produced by infusing dextran through a separate canal in the probe holder. The decrease in the baseline LDF signal was found to adjust to increased intracapsular pressure. Levels lower than the central venous pressure were suggested to have an adverse effect on femoral head blood flow. Histological sections of the femoral heads, perfused with Disulfine blue, revealed different amounts of ischemia proportional to LDF flow levels. In an additional study on four patients with established femoral-head necrosis, the necrotic segment could be defined with LDF.

The clinical use of LDF was further studied in a series of patients treated by osteotomy and revascularized bone grafts for femoral-head necrosis [31]. The LDF was found to be a useful method for continuous measurement of flow and a potential tool for predicting posttraumatic femoral-head necrosis, adding little treatment risk to patients. The need for a laser probe firmly attached to the bone was, however, highly stressed in this study.

In a recent publication, experimental and clinical results of blood flow monitored in vascularized bone grafts were presented [32]. In the experimental series on pigs, significant changes were found in flow values of muscle-pedicled rib grafts compared with vascular-pedicled grafts. Measurements of cortical flow were made with the rib in situ, after osteotomy, and at the end of a three-month healing period. The flow levels correlated well with histological findings.

The second part of the study included flow recordings from free revascularized iliac bone grafts used for mandibular reconstruction. The flow rates, monitored before and after vascular anastomosis, were found to be comparable. Furthermore, the efficiency of anastomosis could be followed postoperatively by percutaneous application of the LDF probe, firmly fixed by a probe-holder screw. Vasomotion effects were not reported in this study. Flow in rib grafts was monitored with a standard Periflux probe (PF-108). The method of standardizing application and fixation of the probe to the bone surface by repeated sequential recordings was described.

Comparison of LDF with other techniques in bone has been reported in three studies [18,24,33]. In a rabbit model, femoral blood flow was measured simultaneously with LDF and ^{85}Sr-labeled microspheres [33]. The correlation coefficients for femoral head and condyle blood flow were calculated to be 0.490 and -0.348 respectively. The discrepancy, especially seen in condylar flow recordings, has been ascribed to bleeding artifacts in the drilling holes in front of the LDF probe. Clotting on the probe tip is usually the main problem in this situation, producing a decrease in the reflected light signal. The surges in the output signal seen in this study may instead reflect irregular shunting, vasomotion effects in the traumatized cancellous bone, or even failure to place the LDF probe in close contact with the area to be measured. The microsphere technique may theoretically reflect flow levels comparable

to LDF. Due to well-known shortcomings, such as A-V shunting and premature tapping of the microspheres in precapillary vessels, however, the recorded flow rates do not represent total input flow to the bone area as "seen" by the optical fiber. Furthermore, samples had to be collected from the bone area illuminated by the LDF probe to achieve comparable results.

According to several authors, isotope clearance reflects effectiveness of flow in minute vessels and thus should not be compared with LDF, which measures total flow levels within an illuminated tissue volume. This argument is in agreement with our own findings comparing ^{133}Xe clearance and LDF in cancellous bone [18,24].

An effort has been made to express the LDF output signal in quantitative units. This may not be of any essential clinical value because of the small probe diameter generally used and the relatively high spatial variation in flow due to the nonuniform vascularity in bone [18].

For low and moderate red blood cell volume fractions, a linear relationship between flow and output signal has been demonstrated for LDF [29]. The moderate flow rates reported for cortical and cancellous bone and results achieved with LDF from tissues with comparable perfusion levels indicate that this method is reliable for blood flow measurements in bone.

Single-fiber laser-Doppler flowmetry in cancellous bone

The diameter of the commercial Periflux® standard probe is not suitable for insertion into tissue. Special needle probes have been manufactured with diameters ranging from 1.2 mm down to 0.5 mm. Because of triangular asymmetry, they record from different microvascular beds, depending on the angular rotation of the probe [18]. Single-fiber laser-Doppler flowmetry lacks axial asymmetry and offers a cross-sectional diameter down to 100–200 μm.

The technique is based on the standard signal-processing unit from Periflux® equipped with a special single-fiber optic waveguide. A He–Ne laser injects laser light (λ = 632.8 nm) into one of three optical waveguides ($\varnothing$ = 0.25 mm). They are bundled and carefully polished and then attached, end-surface to end-surface, to the main single fiber ($\varnothing$ = 0.5 mm). Alignment of the laser and the small efferent waveguide can be achieved through an eccentric coupling or spherical lens. The main waveguide transmits light bidirectionally (figure 17–3) without mixing its inherent frequencies. After light has been backscattered in the cancellous bone tissue, it is once again transmitted through the main fiber and the two afferent small fibers. Finally the photons impinge on two photodetector surfaces and make use of the differential channel operation [34].

Local blood flow in cancellous bone of young domestic pigs was assessed by single-fiber LDF. The aim was to evaluate single-fiber LDF for axial asymmetry and expected responses to vasoactive drugs that had been studied with multifiber probes [18]. The flowmeter probe ($\varnothing$ = 0.5 mm) was guided by the probeholder ($\varnothing$ = 1.0 mm) and could be locked in position. The

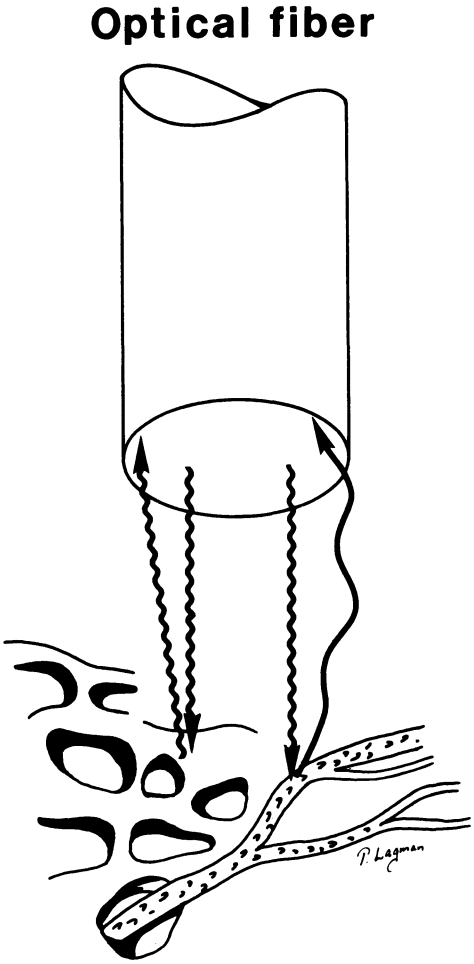

Figure 17–3. Incident light and backscattered, frequency-shifted light are transmitted through one optical fiber.

probeholder technique has been described in a previous publication [18]. Environmental and central influences on blood flow were monitored through simultaneous recordings of skin blood flow and arterial pressure, measured in the lower lip and carotid artery, respectively. A protocol for flow recordings was designed and consecutive measurements were made, each with a sample time of 30 seconds. The angular rotation of the probe was considered random. The average coefficient of variation was calculated to be 8.4% ± 6.2% (mean ± SD). This figure is considerably lower than the value found using multifiber probes. The result shows that single-fiber LDF is less dependent on angular rotation of the probe.

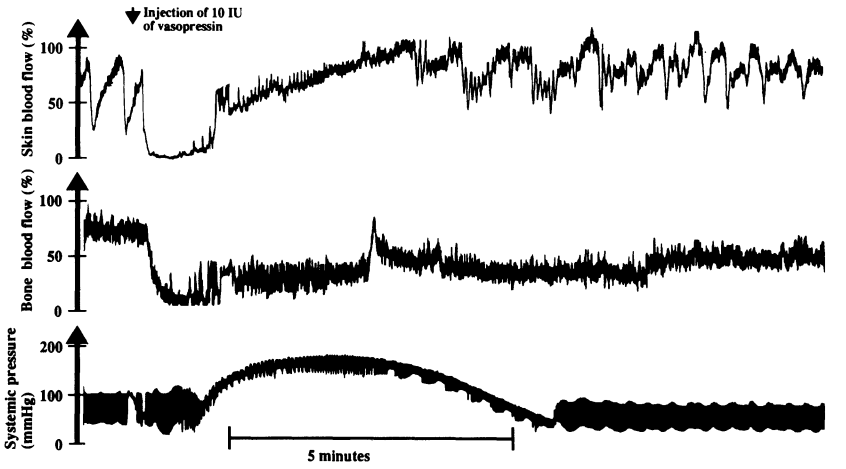

Figure 17–4. Vasopressin (10 IU) i.a. decreased blood flow levels in bone as well as in skin. Bone blood flow is delayed and shows a transient vasoconstriction in comparison to skin.

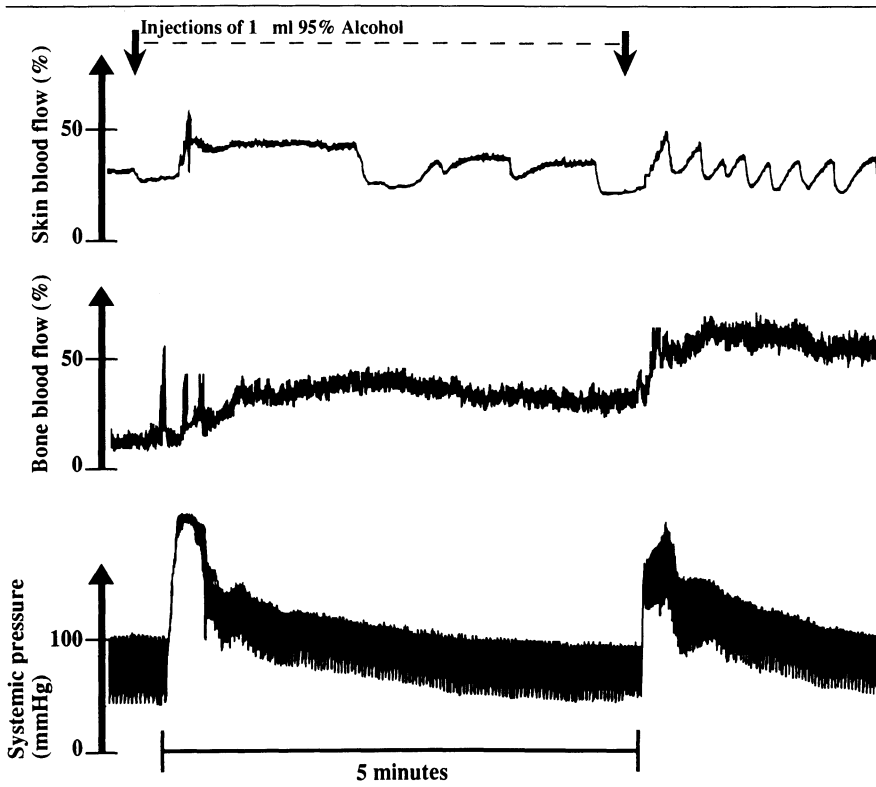

Figure 17–5. The response to alcohol (95% 1ml) i.a. injection is a delayed increase in bone blood flow compared with skin blood flow. A second injection doubled the flow level in bone but caused only increased vasomotion in skin.

Responses of central and peripheral vasoactive agents were studied continuously. Vasopressin injection (10 IU) was performed in the carotid artery for simultaneous LDF monitoring of the vasoconstrictive effects on blood flow in cancellous bone and skin of the lower lip. Figure 17–4 shows an expected decrease in cancellous bone blood flow. The prolonged vasoconstrictive effect in bone contrasts with the vascular reactions in skin. Injections of 1 ml 95% alcohol (figure 17–5) produced a delayed increase in bone blood flow in comparison with skin blood flow. A second injection doubled the bone blood flow but caused only increased vasomotion in skin. This constitutes another example of a quite different reaction in two separate tissues. It also confirms LDF monitoring as a reliable method for measuring bone blood flow.

REFERENCES

1. Havers, C. 1691. Cited from Brookes M., 1971. The Blood Supply of Bone. London, Butterworths.
2. Brookes, M., and R.G. Harrison. 1957. The vascularization of the rabbit femur and tibiofibula. J Anat 91:61.
3. Brånemark, P.-I. 1959. Vital microscopy of bone marrow in rabbit. Scand J Clin Lab Invest 11 (Suppl 38):
4. Rhinelander, F.W. 1968. The normal microcirculation of diaphyseal cortex and its response to fracture. J Bone Joint Surg 50A:784.
5. Trias, A., and A. Fery. 1979. Cortical circulation of long bones. J Bone Joint Surg 61A:1052.
6. Eitel, F., R.K. Schenk, and L. Schweiberer. 1980. Corticale revitalisierung nach Marknagelung an der Hundtibia. Unfallheikunde 83:202–207.
7. Hellem, S., and L.T. Östrup. 1981. Normal and retrograde blood supply to the body of the mandible in the dog II. Int J Oral Surg 10:31–42.
8. Östrup, L.T., and J.M. Fredrickson. 1974. Distant transfer of a free living bone graft by microvascular anastomosis. An experimental study. Plast Reconstr Surg 54:274–285.
9. Berggren, A. 1981. Factors influencing survival of free composite bone grafts revascularized by microvascular anastomoses. An experimental study. Thesis, Linköping University, Sweden.
10. Cunningham, G.J. 1960. Microradiography. In Tools of Biological Research, Atkins, ed. Oxford: H.J.B. Blackwell, vol 2.
11. Hellem, S., and L.T. Östrup. 1981. Normal and retrograde blood supply to the body of the mandible in the dog I. Int J Oral Surg 10:23–29.
12. Albrektsson, T. 1979. Healing of bone grafts. In vivo studies on tissue reactions at autografting of bone in the rabbit tibia. Thesis, Göteborg University, Sweden.
13. Tothill, P., and J.M. MacPherson. 1980. Limitations of radioactive microspheres as tracers for bone blood flow and extraction ratio studies. Calcif Tissue Int 31:261–265.
14. Weiland, A.J., and A. Berggren. 1981. Regional cortical blood flow measured by the hydrogen washout technique in composite canine rib grafts revascularized by microvascular anastomoses. Int J Microsurg 3:13–18.
15. Hellem, S., G.E. Nilsson, and L.S. Jacobsson. 1982. Assessment of cancellous bone blood flow by laser Doppler flowmetry. Int J Microcirc Clin Exp 1:299.
16. Appelgren, L. 1972. Perfusion and diffusion in shock. A study of disturbed tissue–blood exchange in low flow states in canine skeletal muscle by a local clearance technique. Acta Physiol Scand Suppl 378:
17. Töndevold, E., and P. Eliasen. 1982. Blood flow rates in canine cortical and cancellous bone measured with $^{99}Tc^{m}$-labelled human albumin microspheres. Acta Orthop Scand 53:7–11.
18. Hellem, S., L.S. Jakobsson, G.E. Nilsson, and D.H. Lewis. 1983. Measurement of microvascular blood flow in cancellous bone using laser Doppler flowmetry and ^{133}Xe-clearance. Int J Oral Surg 12:165–177.

19. Indresano, A.T., and M.I. Lundell. 1981. Measurement of regional bone blood flow in the rabbit mandible using the hydrogen washout technique. J Dent Res 60:1365–1370.
20. Duncan, C.P., and S.S. Shim. 1977. The autonomic nerve supply of bone—an experimental study of the intraosseous adrenergic nervi vasorum in the rabbit. J Bone Joint Surg 59B:323–330.
21. Tran, M.-A., and J.-P. Géral. 1978. The influence of some vasoactive drugs on bone circulation. Eur J Pharmac 52:109–114.
22. Tran, M.-A. 1980. The effect of lumbar sympathetic stimulation on the vasculature of bone. Br J Pharmac 70:363–366.
23. Gross, P.M., D.D. Heistad, and M.L. Marcus. 1979. Neurohumoral regulation of blood flow to bones and marrow. Am J Physiol 237:H440–H448.
24. Hellem, S., L.S. Jakobsson, and G.E. Nilsson. 1983. Microvascular reactions in cancellous bone to halothane-induced hypotension in pigs. J Oral Surg 12:178–185.
25. Intaglietta, M. 1981. Vasomotion activity, time-dependent fluid exchange and tissue pressure. Mircrovasc Res 21:153–164.
26. Tenland, T. 1982. On laser Doppler flowmetry. Methods and microvascular applications. Thesis, Linköping University, Sweden.
27. Salerud, E.G., T. Tenland, G.E. Nilsson, and P.Å. Öberg. 1983. Rhythmical variations in human skin blood flow. Int J Microcirc Clin Exp 2:91–102.
28. Nilsson, G.E., T. Tenland, and P.Å. Öberg. 1980. A new instrument for continuous measurement of tissue blood flow by light beating spectroscopy. IEEE Trans Biomed Eng 27:12–19.
29. Nilsson, G.E., T. Tenland, and P.Å. Öberg. 1980. Evaluation of a laser Doppler flowmeter for measurement of tissue blood flow. IEEE Trans Biomed Eng 27:597–604.
30. Swiontkowski, M., S. Tepic, R. Ganz, and S.M. Perren. 1986. Laser Doppler flowmetry for measurement of femoral head blood flow. Helv Chir Acta 53:55–59.
31. Swiontkowski, M.F., R. Ganz, U. Schlegel, and S.M. Perren. 1987. Laser Doppler flowmetry for clinical evaluation of femoral head osteonecrosis. Clin Orthop Related Res 218:181–185.
32. Kärcher H., H. Radner, J. Engler, and A. Stenzl. 1988. Die Laser-Doppler-Flowmetrie bei der vitalen Knochentransplantation. Experimentelle und klinische Ergebnisse. Handchir Mikrochir Plast Chir 20:266–270.
33. Swiontkowski, M.F., S. Tepic, S.M. Perren, R. Moor, R. Ganz, and B.A. Rahn. 1986. Laser Doppler flowmetry for bone blood flow measurement: correlation with microsphere estimates and evaluation of the effect of intracapsular pressure on femoral head blood flow. J Orthop Res 4:362–371.
34. Salerud, E.G., and P.Å. Öberg. 1987. Single-fibre laser Doppler flowmetry: A method for deep tissue perfusion studies. Med Biol Eng Comput 25:329–334.

18. COCHLEAR BLOOD FLOW

JOSEF M. MILLER and ALFRED L. NUTTALL

Studies of the cochlear vasculature and cochlear blood flow (CBF) have been of major interest to hearing scientists and otologists for more than a century. Throughout most of that time, this area of research has represented a major technical frustration. From a physiological perspective, it has long been known that the resting and evoked responses of the sensorineural epithelium of the inner ear, as well as its development and maintenance, depend upon the homeostatic environment of the cochlea. The exquisite sensitivity of this receptor to changes in oxygen [1–5] was an early indication of the dominant role of CBF. The recent discovery of a class of metabolically dependent processes determining the micromechanical properties of the inner ear and resulting frequency tuning of the receptor cells has placed greater emphasis on the importance of CBF (see for example [6])

A number of clinical disorders of the inner ear have been presumed to reflect vascular pathology or an inadequate range of responsiveness of the cochlear vasculature. Sensorineural hearing loss from Meniere's disease, presbycusis, some forms of intense noise exposure, and certain conditions of sudden hearing loss may depend to a significant extent upon CBF (7–9). A variety of treatments with vasoactive agents have been used in attempts to deal with such disorders and pathology [10–12]. Two factors complicate their effective application: the first is our lack of knowledge of control mechanisms of CBF and the extent to which local factors (autoregulatory mechanisms) determine vascular responsiveness; the second factor is the high

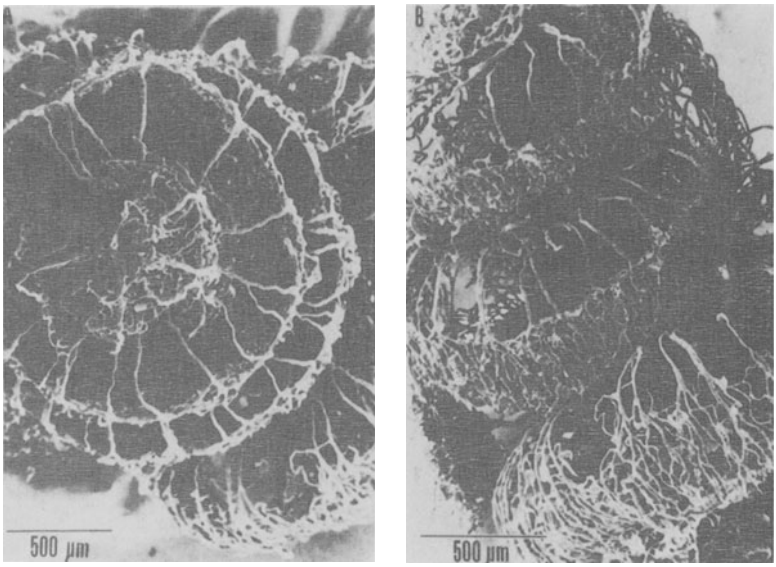

Figure 18–1. Cochlear vasculature as demonstrated by a scanning electron microscopic view of epoxy cast of the inner ear vasculature. (Reprinted with permission from M. Lawrence and American Journal of Otolaryngology.)

rate of spontaneous recovery associated with many of these disease entities of presumed vascular etiology. These factors make the interpretation of clinical results difficult at best. From the perspective of both the basic scientist and the clinical otologist, there is a compelling need for additional knowledge regarding the mechanisms of CBF control and the factors that will permit useful manipulation of the CBF.

To a large measure, the frustrations of studies of CBF stem from the special anatomical characteristics of the vascular system of the inner ear. The enormously rich vascular structure of the inner ear (figure 18–1) is well encased in bone (figure 18–2) that has restricted access to physiological study. Most of our basic knowledge regarding this system has been obtained from anatomical studies performed on postmortem material. The normal characteristics of the inner ear vasculature [13,14], the developing vasculature [15], and changes associated with trauma and pathology (e.g., [16–19] have been well described. However, the postmorten approach has obviously provided a static view of the vasculature. Even in those attempts in which marked care is taken with fixation procedures to use measures that reflect flow in these vessels in the living condition [20], observation may be marred by postmortem artifacts, and the measurements may be only circumstantially related to flow in the living organism.

In the 1950s, intravital microscopy (IVM) was first used to measure CBF

Figure 18–2. Fluid-filled membranous labyrinth of the human otic capsule. (Preparation courtesy of Lars Johnsson.)

[21,22], and it provided our first direct information on CBF. At that time the technical difficulties associated with access to the inner ear vasculature, inadequate optics, and a lack of procedures for quantifying flow characteristics made this approach difficult, and only a few studies were published. More recently, the technique has been reexamined, taking advantage of developments in the field of optical microscopy and digital image processing. It promises to be a major resource for defining the fundamental characteristics of CBF. IVM has the special advantage of providing direct and dynamic information regarding the features of flow in individual vessels of the inner ear [23–31].

Other techniques attempted during the late 1950s and 1960s, such as plethysmography [32,33], have been indirect, and their validity has been questioned [34]. The important quantitative method based on microspheres, on the other hand, can be viewed as a gold standard for direct measures of blood flow in many individual organs. In the inner ear, the technique has been more difficult to apply, requires caution in interpretation and, of course, provides only a few measurements per animal. The chief problem with this technique is the very small percentage of the total cardiac output received by the inner ear and the small number of microspheres that can be captured in its vasculature.

Without doubt a major technical advance in the field of studies of CBF occurred within the last seven years with the introduction and development

of the laser-Doppler flowmeter (LDF) and its application for studies of CBF [7,8,35–42]. This technique is not without its own restrictions (detailed below), but it has overcome some marked technical difficulties and opened up the possibility for convenient real-time dynamic CBF measurements. In combination with other techniques, including the microsphere technique and IVM, it promises to be a tool that will help us elucidate the control mechanisms of CBF. It will also help us identify those agents and manipulations through which CBF can be controlled to produce effective treatments for certain inner-ear disorders.

TECHNICAL AND PRACTICAL CONSIDERATIONS

Anatomy

Laser-Doppler flowmetry (LDF) is one of the most exciting recent technical developments for CBF analysis because it overcomes some difficult measurement problems. The inner ear (which includes both the auditory and vestibular sensory organs) of all mammals is embedded in various amounts of cranial temporal bone. In the human, the temporal bone is dense and very thick, and surrounds the vascular epithelium of both the auditory and vestibular areas. LDF on human bone raises a special set of questions addressed below.

In rodents, nature has modified the bone volume surrounding the sensory epithelium of the inner ear for the purpose of maximizing the size of the air-filled middle-ear spaces. The large airspaces contribute to improve low-frequency hearing in these animals by raising the acoustic compliance of the middle ear. This situation has provided auditory investigators with an excellent model for physiological studies of the cochlea. Figure 18–3 shows histological cross sections of the guinea pig cochlea. One can see that the bone over much of the guinea pig cochlea has been reduced to a thin layer. The human temporal bone, in contrast (figure 18–2), not only has greater bone thickness but provides limited access to the internal vascular areas.

Figure 18–4 compares the sizes of a typical LDF probe and the guinea pig cochlea. It is obvious from Figures 18–1–18–4 that the inner ear is a complex, nonhomogeneous, and anisotropic structure on which to carry out LDF studies. What are the implications of this anatomical structure for LDF studies of CBF in mammals? One implication is the first object encountered by the laser light, the bone itself. There are two issues. First, because if its structure, bone is a relatively good reflector in comparison to the soft tissue of the inner ear. The reflectance of bone raises the amount of backscattered light that is not Doppler-shifted light. This effect and the light attenuation due to the thickness of the bone reduce the signal-to-noise ratio. Fortunately, bone is not opaque, so useable signals are obtained from the guinea pig cochlea, from the human inner ear (Scheibe et al., unpublished observations), and indeed from teeth and skeletal bone. Second, the cochlear otic capsule bone has a circulation of its own. The circulation of the bone around the

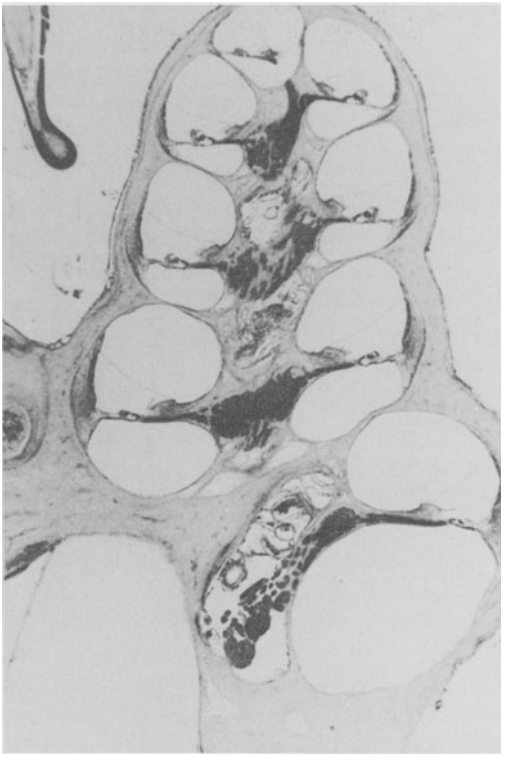

Figure 18–3. A histological cross section of the guinea pig cochlea. The plane of section is through the midline, showing the central core of the cochlea, the modiolus, and the sensory epithelium and vascular structures in the four cochlear turns. The bony shell of the cochlea in the guinea pig is relatively thin, and there is accessability to the vascular structures in all four turns.

cochlea is derived from the external carotid, which also supplies the mucosa of the middle ear. Guinea pig measurements of blood flow with microspheres indicate that total capsular flow is about 10% of total cochlear flow (Nuttall and Brown, unpublished observations). Cochlear epithelial circulation is derived from the vertebral-basilar artery system.

Another implication of cochlear anatomy is a general uncertainty about what internal vascular beds of the cochlea are measured with LDF. At this time no one knows. Figure 18–5 shows diagrammatically the major vascular areas of the cochlea and the intervening optically important structures. An implicit assumption of CBF studies is that the main Doppler signal arises from the membranous lateral wall, which contains the richest areas of vascular density in the cochlea, the stria vascularis. The rationale for this assumption is the great vascular density of the stria, the distance that photons must diffuse to reach the still deeper modiolar layers, the interposed layer of

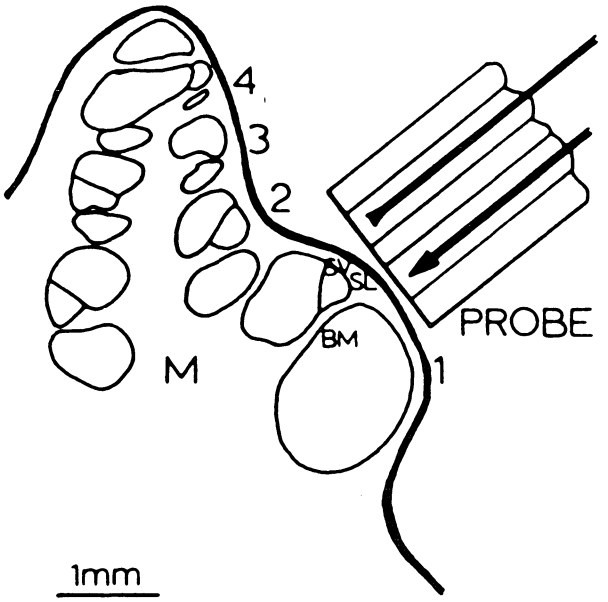

Figure 18–4. A drawing of the midmodiolar section of a cochlea of the guinea pig, shown in relationship to the size of a laser-Doppler flowmeter probe. M = modiolus; SV = stria vascularis; SL = spiral ligament; BM = basilar membrane; 1,2,3,4, = first through forth cochlear turns.

signal-attenuating bone (the otic capsule) encountered by photons before any vascular area is reached, and the notion that the LDF signal comes from a hemisphere of 1 mm radius [43–45].

However, the studies of Kvietys et al. [46] raise an important concern regarding the measurement depth in any vascular system. In these studies [47], vascular flow signals were evident from a depth of 6 mm. In the cochlea, photons that pass directly through the bony capsule into the stria vascularis and the surrounding cellular areas encounter an epithelial tissue only about 100 μm thick. Note in figure 18–5 that once through this region, a photon would not encounter significant scatterers until it has crossed the fluid-filled areas of the cochlea. This indicates that significant signal may arise from the more central, modiolar region of the cochlea.

Since the vascular beds of the cochlea have differing functional roles and possibly differential participation in inner ear pathophysiology, the question of LDF analysis depth is an important issue of future study.

Clearly, a simple methodological matter such as the orientation of the optical fibers (within the probe) in relation to cochlear anatomy could be important. Furthermore, the mechanical arrangements of fibers in the probes from each commercial manufacturer are different. It could matter which configuration is used for a particular physiological study. Preliminary studies

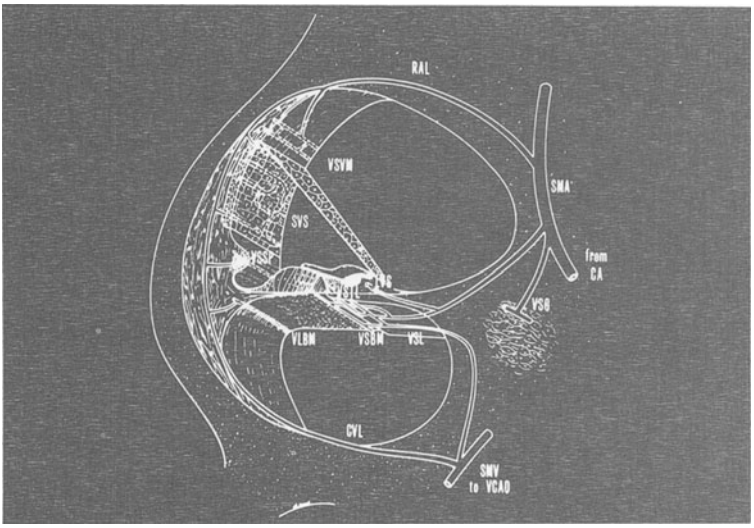

Figure 18–5. A drawing of a vascular network of a single cochlear turn. CA = cochlear artery; SMA = spiral modiolar artery; VSG = vessels of spiral ganglion; RAL = radiating arteriole; VSVM = vessel at vestibular membrane; SVS = stria vascularis; VSSP = vessel of spiral prominence; VSTL = vessel of tympanic lip; VSBM = vessel of basilar membrane; LVS = limbus vessel; VLBM = venules at basilar membrane; VSL = vein of spiral lamina; CVL = collecting venule; SMV = spiral modiolar vein; VCAQ = vein of cochlear aqueduct. (Reprinted with permission from M. Lawrence and Advances in Oto-Rhino-Laryngology, 1973.)

in our laboratory (Baldwin et al., unpublished observations) indicate that different systems yield similar measures of CBF responses to systemically administered hyperosmotic agents. It would seem prudent, in any experimental regimen, to be consistent about probe orientation.

Calibration

For most investigations of cochlea perfusion, it is important to know the blood flow in standard physical units. Cochlear and vestibular blood flow are thought to be implicated in several kinds of inner-ear dysfunction. However, when the LD probe is applied to the cochlea, one cannot yet say whether the actual CBF is normal or pathological. Perhaps the major shortcoming of LDF is the lack of calibration in absolute units.

Considerable work to calibrate LDF has been underway in tissues other than the ear [43,45,46,48–52] (see chapters that speak more directly to this question). Some manufacturers provide flow, velocity, or volume outputs from their instruments, but these should not be naively accepted by inexperienced investigators. For the cochlea, no published studies have addressed the calibration question.

There are perhaps only four appropriate techniques for a quantitative validation of cochlear LDF readings: hydrogen clearance, clearance of

radiolabeled diffusible molecules, microspheres, and intravital microscopy (IVM). In general, these techniques are difficult and time-consuming. Only a few studies have been published on hydrogen clearance [53,54] and autoradiography in the cochlea [55].

The appropriateness of the four techniques for comparison with LDF depends on just how the laser light interacts with the complex structure of the cochlea and how homogeneous the vascular perfusion is in the various vascular beds and in the topographical locations of the cochlea. The problem of quantification is difficult, but it is worth investigating because of its importance to research and clinical questions.

Although no investigations have attempted to quantify the LDF readings of the cochlea, Nuttall et al. [56] used systemic hemodilution to compare the changes in flow determined by radioactive microspheres with the changes in LDF-measured flow. A previous study [57,58] had shown substantially increased LDF readings as a result of either normovolemic or hypervolemic hemodilution in guinea pigs. Reducing systemic hematocrit from 40% to approximately 15% increased LD flow up to 100%. However, when compared to microsphere-measured CBF, the percentage change given by LDF readings was found to be substantially low. An LDF increase of 50% was equivalent to a 150% increase in microsphere-measured CBF. Nuttall et al. [59] attributed the difference to the influence of reduction in hematocrit on the LD signal. In contrast, a comparison of LDF and IVM CBF changes during CO_2 respiration, positive end expiratory pressure, and systemic epinephrine showed similar responses [60]. These procedures do not greatly affect hematocrit.

Hemodilution, hemorrhagic shock, hemoconcentration, and other physiological conditions resulting in hematocrit changes (even including red blood cell redistribution in capillaries e.g., during flow state changes [51,61–63,65]) are important classes of experiments where LDF techniques must be undertaken with extra caution. Such conditions are important, and they demand an effort to understand the LDF signal in these cases.

Nuttall et al. [56] also found that the microsphere-measured CBF was poorly correlated with the LDF-measured CBF. This result stands in contrast to high correlations observed in some other correlative studies [46,49,60]. The difference may be due to the specific procedure of hemodilution. It is also possible that the cochlea presents some unique problems for microsphere-based blood flow measurements. For example, the unusual anatomy of the stria vascularis, where feeder arterioles give rise to capillaries of greater diameter, may give erroneous indications of tissue perfusion as microspheres pass this capillary bed. A second possibility is variability in the trapping of microspheres, which have a critically small mean diameter [59].

In addition to the problem of LDF calibration, there is a second issue often overlooked by users of these instruments, the characterization of the instrument performance. Currently, there are no widely accepted standard tests of instrument linearity, sensitivity to red blood cell velocity, or sensitivity to

red blood cell volume fraction. Thus an investigator has no convenient assurance that performance remains stable or that a given change in some aspect of blood flow (e.g., red blood cell velocity) results in a proportional signal change. If two instruments are used, it is difficult to know whether they act similarly. Obviously, a test model that fulfills the implicit assumptions of the LDF method (or sufficiently closely simulates the actual organ system) is needed.

Interactions of sound with LDF

If CBF is subject to homeostatic regulatory mechanisms, one may expect to find a significant influence of sound on blood flow. Sound is the natural and adequate stimulus for the cochlea. However, whether sound causes a change in CBF, and the role that such a change may have in sound-induced pathology, is controversial. Initially, the indirect measurement technique (intracochlear oxygen tension measured with microelectrodes) showed a large and rapid reduction in oxygen availability with sound exposure [2,66], but later this finding could not be confirmed [67]. Recently, oxygen tension has been found to decrease, but only over a longer time course of sound exposure [68–70]. Short-term (several minute) loud sound exposure has given variable results in microsphere studies. Angelborg et al. [71] found no flow changes while Hillerdal et al. [64] found decreased flow and Prazma et al. [72] observed increased flow.

A decreased CBF or no change to noise exposure is not the regulatory response one would expect if sound increased metabolism, thereby raising the demand for oxygen and leading to accumulation of metabolic byproducts. Indeed, most of the sound exposure experiments are conducted with very loud sounds and may represent a damage condition. Lower levels of sound produced increases in metabolism in all cochlear tissues when assessed by 2-deoxyglucose trapping [35,73–75]. Such increased metabolism may be accompanied by increased CBF. This view is supported in the report on the accumulation of radiolabeled iodoantipyrine indicator with moderate sounds [55].

This important issue of sound-mediated control of blood flow is ideal for LDF studies. Both microspheres and diffusion indicators are essentially discontinuous techniques, while laser-Doppler flowmetry is a continuous and real-time measurement.

Thorne and Nuttall [68] and Thorne et al. [69] have used LDF to study the influence of loud pure tones and of noise on CBF. Figure 18–6 shows a reduction in blood flow measured from the guinea pig cochlea when the probe was placed on the area of the cochlea most affected by the frequency of the sound stimulus. The average decline in LDF reading was 30% for a 110 db SPL pure tone of 12 kHz, but individual cases showed decreases extending to 70%. These general findings were verified by Scheibe et al. (unpublished observations).

For the results shown in figure 18–6 the sound was delivered to the animal

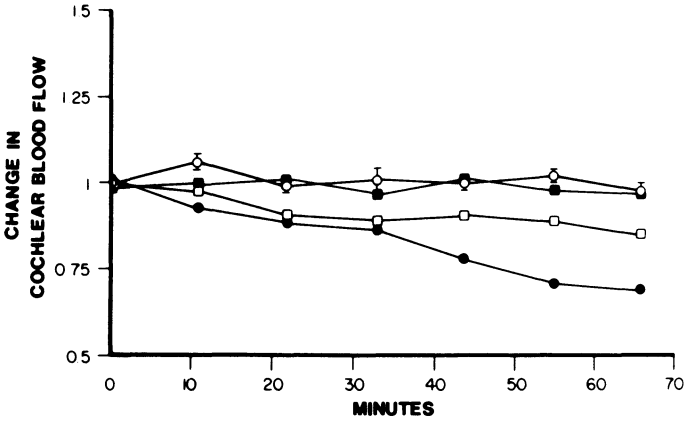

Figure 18–6. The change in CBF measured by LDF occurring during the continuous presentation of loud sound for a period of one hour. The control responses with standard deviations are given by the open circles. In all cases, the guinea pigs were exposed to a 12 kHz pure tone at 90 dB SPL for the closed squares, 103 dB SPL for the open squares, and 110 dB SPL for the closed circles. (Reprinted with permission from P.R. Thorne and Acta Otolaryngologica.)

for a one-hour period but was interrupted for one-minute intervals every ten minutes to allow the LDF measurements. Interrupting the sound exposure was necessary because sound influenced the LDF reading. Figure 18–7A illustrates the strong increase in apparent CBF that occurred almost immediately following onset of the sound. A return to baseline value occurred just as quickly after sound ceased. Thorne et al. [71] tested for the presence of the response in a dead animal and found that the sound response had similar character (figure 18–7B). Thus, the apparent CBF increase during the delivery of loud sound to the guinea pig ear is an artifact.

Thorne et al. [69] explored the nature of the LDF response and determined that it was the result of a portion of the flowmeter photocurrent occurring at the frequency of the sound stimulus. Figure 18–8 gives a power spectrum of the "raw" photocurrent signal from a Periflux PF1 when the probe was placed against the first cochlear turn in the guinea pig. This region of the cochlea is naturally responsive to high acoustic frequencies of 12 to 40 kHz. The portion of the power spectrum below 2 kHz contains the usual Doppler-shifted information caused by moving red blood cells. The sharp spectral peak at 18 kHz is energy at the acoustic stimulus frequency. Since the spectral peak has the same frequency as the acoustic stimulus and does not shift in frequency with acoustic intensity [34], it cannot represent red blood cell velocity information. Rather, it is amplitude modulation of the backscattered laser light.

From the standpoint of interpretation of the LDF response during the administration of loud sound, it is essential to characterize the response and

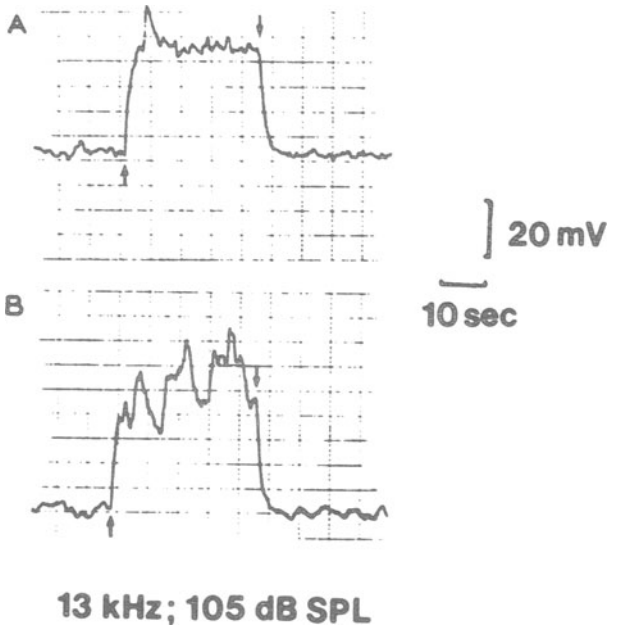

Figure 18–7. A. The changes in LDF signal during the application of a 13 kHz 105 dB SPL pure tone to the guinea pig cochlea. The probe is positioned on the first turn of the cochlea, which is most sensitive to the tone of stimulation. The up arrow indicates the onset of the tone and the down arrow indicating the offset of tone. B. A similar experiment conducted on the postmortem cochlea, showing that the LD BF reading is affected by sound in the absence of real BF.

determine its origin. Thorne et al. [69] showed that the strength of the response was not only a function of the sound intensity but also of the position of the probe on the cochlea and the frequency of the sound stimulus. For these studies, various LD blood flow instruments were used (Periflux PF1, Medpacific Ld-5000, TSI Laserflo). The actual response of the instrument depends also on whether the frequency of the acoustic stimulus is within the analysis passband of the photocurrent processing circuitry.) This result is interesting and surprising. It is interesting because sound naturally activates regions of the cochlea via a traveling wave moving the sensory epithelium. This topographic activity (or some secondary effect) apparently is being seen by the LDF. It is surprising because the actual movements are known to be small, and they are of the deep structures within the cochlea. Indeed, Thorne et al. [69] concluded that it was topographic vibration of the surface of the bony otic capsule that caused the artifact. This is also a surprising situation because it implies a coincidental modal vibration pattern of the bone. If the surface of the bone is driven by internal forces, then this represents energy loss from the local internal activity when precious little can be wasted.

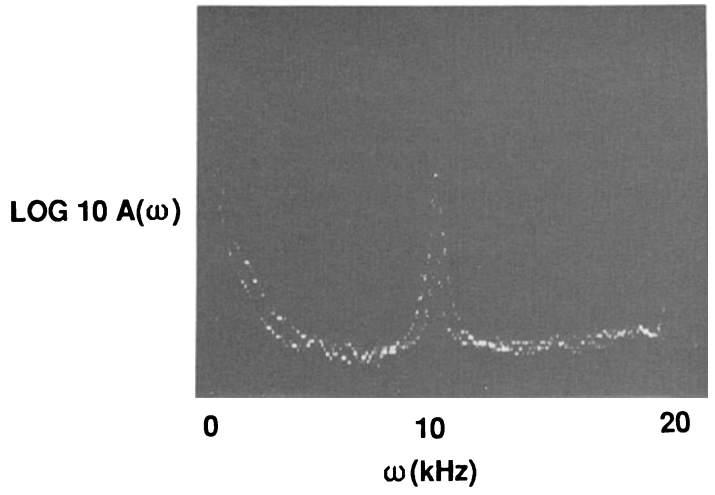

Figure 18–8. The amplitude power spectrum of the raw signal from a Perimed PF1 laser-Doppler flowmeter. In this case the guinea pig cochlea has been stimulated with 10 kHz pure tone at 90 dB or 110 dB SPL. The peaks at 10 kHz indicate the amplitude modulation of a laser light by the 10 kHz pure tone. It is of interest to note that the higher-amplitude sound, while increasing the power spectrum at 10 kHz, decreased the power spectrum in the 0–2 kHz range.

Recently (Nuttall, unpublished observations; Scheibe et al., unpublished observations) it has been determined that the cochlear shell vibration has a peak-to-peak amplitude movement of less than 1 nm for sound intensities less than 100db SPL The topographic pattern present in LDF responses was not seen. By comparison, significant contamination of the LD flowmeter photocurrent required more than 1 nm of surface vibration. These preliminary data point again at the possibility that internal cochlear movements are amplitude-modulating the LD signal. What then can one say about the actual blood flow during sound application?

Observe in figure 18–8 that, in the presence of a peak in the power spectrum at the acoustic stimulus frequency, there was a decrease in spectral energy between 0 and 2 kHZ. If a low-pass electronic filter is applied to the raw photocurrent signal, it is possible to remove the acoustic component. Thus, the LDF would register a decrease in CBF rather than an increase. This is precisely what Scheibe et al. (unpublished observations) noted when the analysis filter of a Periflux PF1 was changed from 12 kHz to 4 kHz and the sound stimulus was a pure tone of 12 kHz.

The question still remains, however, whether the residual response of the filter LDF output is a true flow response. LDF makes use of the principle of heterodyne detection on the surface of a photodiode. The beating of the shifted and unshifted backscattered light leads to small amplitude variations that are detected by the inherent nonlinearity of the photodiode. Adding a third signal (general amplitude modulation of the light) could lead to other

intermodulation components taking energy away from the Doppler shift portion of the spectrum. Since no distinct sidebands are seen around the acoustic component in figure 18–8, this suggests that the residual response of CBF reduction during acute application of loud sound is real. The question needs to be examined with an empirical test. A model system of capillary perfusion could be vibrated while flow is held constant.

Human CBF

At this time only one study has attempted to measure human inner-ear blood flow (Scheibe et al., unpublished observations). The purpose of the study was to determine feasibility, since the human anatomical condition is so different from the rodent models used to study CBF (figures 18–2 and 18–3). During surgical procedures that open the middle ear or when a sufficiently large hole is present in the eardrum, it is possible to place the LD flow probe on the promontory area of the cochlea. This location provides the thinnest layer of bone over the sensory epithelium, the bone being about 1 mm thick. Scheibe et al. (unpublished observations) found, as expected, that the light transmission of this thickness of postmortem human temporal bone was considerably less than the thinner rodent cochlear bone, although the specific attenuation of human temporal bone was less than the rodent.

Nevertheless, the absolute flow reading obtained with a Perimed Periflux PF2 was considerably higher than from rodent ears. Bone blood flow itself is low, as in the rodents, but unlike animal studies, the mucosal lining of the human ear cannot be cleared away before the flow probe is applied. This mucosal component was estimated at 10% of the total flow reading. Thus, human cochlear temporal bone occupies much of the commonly stated 1 mm diameter hemisphere in which LDF measures flow. The large observed LDF signal obviously represents vascular beds within the cochlea. It is likely that these vascular areas are not the usual stria vascularis and lateral wall expected in rodent studies because the promontory area of the human temporal bone covers the scala tympani region of the cochlea. This area should have collecting venules of the basal cochlear turn on the luminal surface of the otic capsule.

Future directions

Chapter 6 addressed the technical developments that the future may hold for assessment of blood flow with Doppler flowmetry. Undoubtedly, these developments will be incorporated into research and clinical measurements of inner ear-blood flow just as they will be for other organ systems. From the current vantage point of experience with commercially produced instrumentation and a knowledge of the unresolved issues of CBF, one of the most obvious areas of hardwave development is probe design.

For human studies, the special shapes required to conveniently measure

from the promontory and look into the round window of the cochlea are simply redesigns of the currently available probe configuration.

For animal experiments, the key issue has always been probe size (chiefly diameter). Currently available sizes extending to as small as 0.5 mm are highly usable for the guinea pig. However, because inner-ear pathological models are uniquely available in rats (e.g., hypertension) and mice (e.g., age and genetic deafness) and because the cochlea has topographic information, further reduction in probe diameter is desirable. Improvements in fiber lightguide technology, laser power, and photodiode sensitivity are readily available at this time to accomplish the above packaging needs.

Animal studies of CBF need to be made in the awake (unanesthetized) condition. The questions of autoregulation, vasomotion, and sympathetic tone are obvious areas of study in the waking state. Thus an implantable, indwelling LDF probe is needed. The anatomy of the skull in rodents and practical considerations of transcutaneous connections will require, again, specially shaped probes. The key new element could be a fiber optic connector on the skull that would make long-term studies more practical. Obviously, the connector needs to be small, convenient, and reliable. Fiber optic communication technology may soon provide for these requirements.

The most important advance for the measurement of CBF by LDF would be the calibration so that one subject could be compared to another. Not only would this enhance our understanding of pathological models of dysfunctional CBF, but it would make feasible the clinical use of this tool. However, practical clinical tests may still be developed based on vascular reactivity and acute systemic manipulations.

An extremely important class of experiments that are immediately before us is the determination of which vascular beds contribute to the LDF output when the probe is applied in various positions on the animal or human cochlea. However, beyond this would be a technical development to enable optical manipulation of the analysis volume. This is already done as part of the design of probes with fiber diameter and interfiber spacing. Perhaps other more sophisticated optical sectioning and digital image-enhancement-type processing techniques could be used to extend this manipulation. One could speculate on the possibility of coupling fluorescence techniques (with intravascular dyes) to enhance vascular signals, allowing deeper analysis volumes while keeping illumination power low. Or the use of different laser frequencies could achieve different analysis volumes. A probe configuration might thus be designed with the specific purpose of use on the human temporal bone promontory and the analysis volume positioned in the modiolus of the cochlea.

In current instrumentation, the problem of extraction of red blood cell volume fraction versus velocity could perhaps be solved by coupling existing technology for determining hemoglobin concentration (or even oxidative state) into the instrument. Combination measurements of several micro-

vascular parameters are already a part of good experimental design in CBF research. Optical analysis of biochemical or biological phenomena offers exciting prospects for novel developments of CBF instrumentation.

MECHANISMS OF CBF CONTROL

As figure 18–2 shows, the soft tissues of the inner ear are surrounded by incompressible fluid and encased in bone. The extent to which the volumes of fluid in the inner ear may be varied are limited. Moreover, the receptor cells of the inner ear are exquisitely sensitive to pressure variations. Therefore, many physiologists think that it is important to isolate the cochlea from pressure changes that may occur systemically in the organism, i.e., blood pressure (BP). The convoluted and tortuous route taken by the main arterial vessels within the central pillar of the cochlea, the bony modiolus, may in part serve as a pressure-damping system, isolating the inner ear from systemic cardiovascular activity.

The high metabolic demand of the inner ear indicates that it requires a high constant blood flow. If so, there may be little need for controlling CBF. Differential (regional) metabolic demands within the inner ear may be met by a redistribution of blood flow within the inner ear [76,77], perhaps accompanied by local environmental factors that affect regional permeability of vessel beds. These suggestions, though largely conjectural, have influenced our thinking and studies of CBF. The notion that CBF is unaffected by systemic factors may now be rejected by observations such as those in figure 18–9, which demonstrates a clear systemically induced change in CBF. Cochlea blood flow potentially may be influenced by changes in systemic blood pressure by neurally mediated changes, humorally induced changes, and by variation of blood hemodynamics.

Systemic BP

Figure 18–9 illustrates changes observed in systemic BP and LDF measured skin blood flow (SBF) and CBF induced by an intra-arterial injection of angiotensin II. As an agent that directly induces a smooth muscle contraction in the arterioles of the peripheral vasculature, injection is followed by a dramatic decrease in SBF, associated with a rapid rise in systemic BP that results from the increased resistance of the peripheral vascular bed. Accompanying this systemically induced increase in perfusion pressure is a dramatic increase in CBF. Figure 18–10 demonstrates a dose–response relationship between these variables and different concentrations of angiotensin II. The systematic relationship observed between changes in systemic BP and CBF demonstrate clearly that CBF can be influence by this systemic blood pressure.

With repeated administration of high levels of vasoactive agents that cause marked changes in systemic pressure, Short et al. [8] observed that the relationship between change in CBF and BP is not proportional and CBF

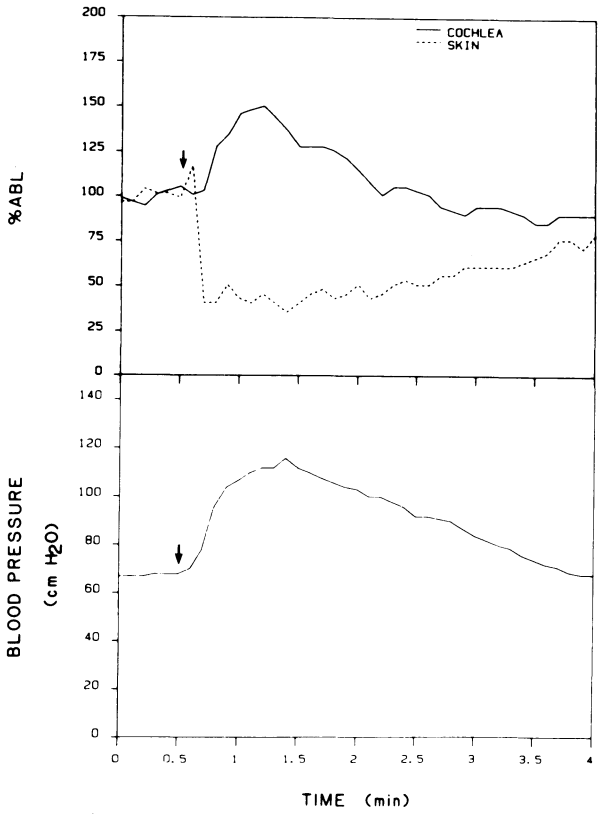

Figure 18–9. Effects of intra-arterially injected (arrow) angiotensin II (100 pm/kg) on CBF and SBF (top) and systemic BP (bottom). (Reprinted with permission with P.C. Goodwin and Acta Otolaryngologica.)

appears to recover to baseline levels before the perfusion pressure. With increasing doses of a systemic α-agonist, such as phenylephrine, it appears that the induced CBF change reaches a limit before the saturating limit is reached by systemic BP. With some agents, like carbon monoxide (figure 18–11), CBF may be dissociated from systemic BP. Obviously, factors other than perfusion pressure may influence CBF.

Neural effects

The studies of Lorento de No and others [78–82] describe a rich adrenergic supply to the inner ear (figure 18–12). One set of these nerves terminates on or near the vessels in the modiolus and on the arterioles radiating from the modiolar vessels. The most compelling data for the presence and potential influence of adrenergic receptors on vessels and flow in the inner ear have been provided by recent work by Ohlsén et al. [83]. Using a new approach

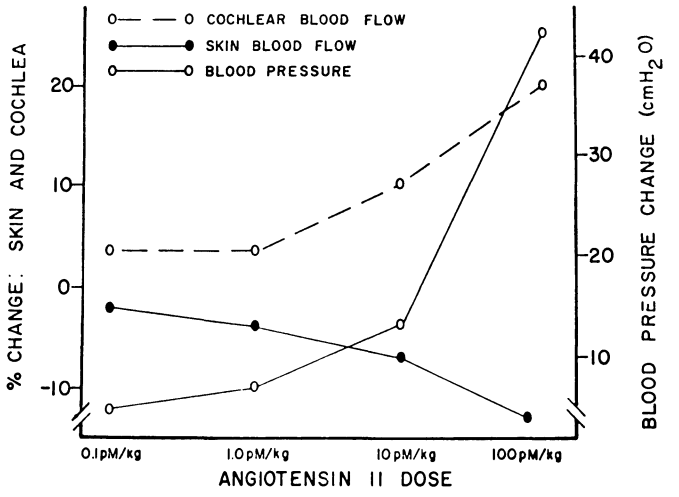

Figure 18–10. Dose–response relationship between angiotensin II and CBF, SBF, and BP. (Reprinted with permission from J.M. Miller and American Journal of Otolaryngology.)

in which vasoactive agents were applied directly to the round window while recording LDF–CBF, they demonstrated the local vasoconstrictive influence of epinephrine, norepinephrine, and phenylephrine. Cochlear blood flow fell as much as 30% within a few minutes of the application of the drug and slowly recovered over 15–30 minutes, depending upon the concentration of the drug used. In some cases (e.g., norepinephrine) an overshoot in CBF was observed during recovery. These changes were observed independent of fluctuations in systemic BP, contralateral CBF, or flow in peripheral vascular beds. A typical example of the changes observed in response to norepinephrine is shown in figure 18–13. With removal of the drug from the round window, the rate of recovery was increased. No effect was observed with isoproterenol or BHT533 (β-agonists). Responses to α-adrenergic agents could be blocked by the phentolamine and even more so by prazosin. A typical dose–response function for norepinephrine and the right shift induced by topical prazosin are illustrated in figure 18–14. The investigation concluded that α-1 receptors were clearly present and effective within the cochlear vasculature. There was evidence of a weak presence of α-2 receptors and no evidence for β-receptors. These findings are consistent with those of Suga and Snow [32,33], who studied various vasoactive agents using plethysmography. They also support the results of microsphere studies [84] indicating a significant sympathetic influence on CBF.

Hormones

An additional class of systemic agents that may influence CBF is circulating hormones. Little work has been done in this area. Circumstantial evidence

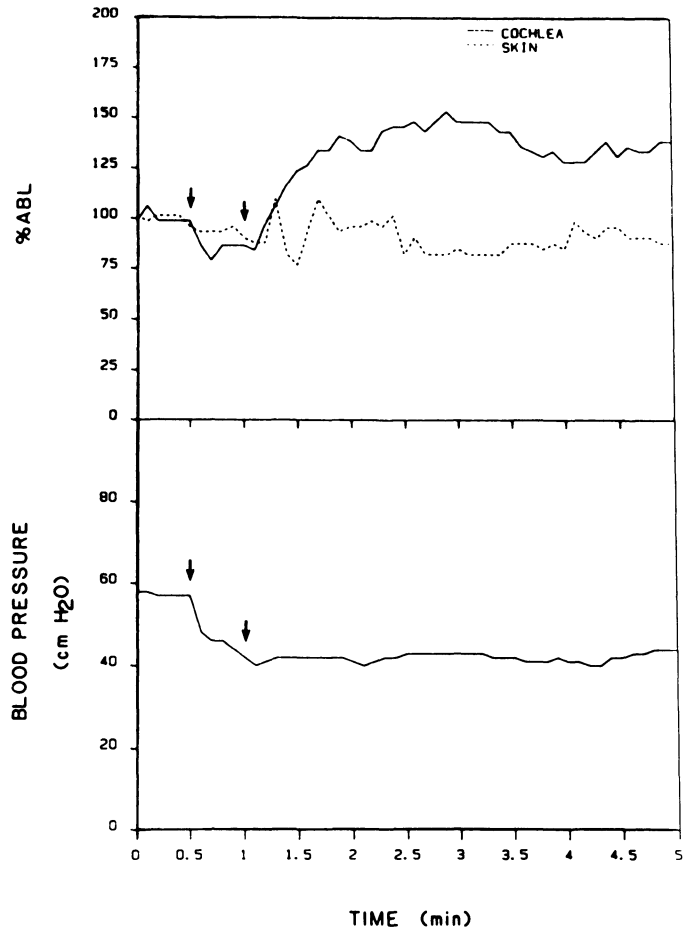

Figure 18–11. Influence of carbon monoxide breathing (30 seconds, 5% CO and 95% air) on CBF and SBF (upper panel) and BP (lower panel). The onset and offset of carbon monoxide breathing is indicated by the arrows. (Reprinted with permission from P.C. Goodwin and Acta Otolaryngologica.)

indicating that circulating hormones may influence CBF include findings of menstrual-cycle-related fluctuations in hearing acuity [85,86], changes in susceptibility to noise-induced hearing loss [87], and suppression of some of these effects with oral contraceptives, which suppress the menstrual cycle. More direct evidence for an influence of ovarian hormones on CBF has been provided by LDF studies of Laugel et al. [88]. They demonstrated that, in overectomized rats, estrogen diminished and progesterone facilitated phenylephrine-induced changes in CBF and the systemic BP responses elicited by phenylephrine and nicotine. In these studies, the form of the re-

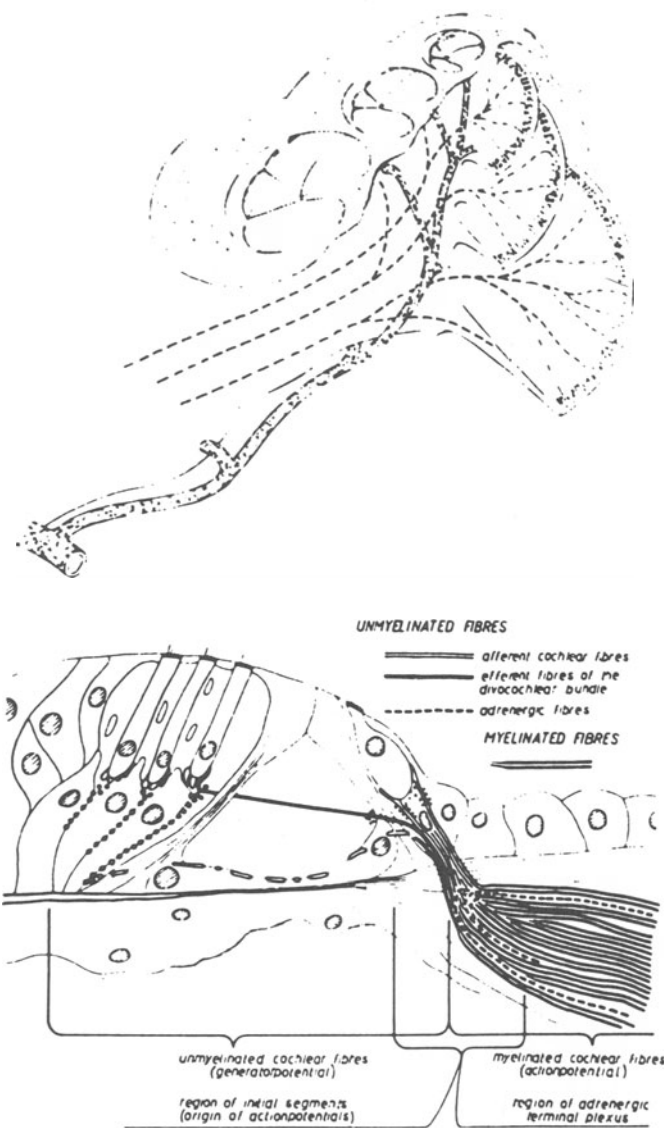

Figure 18–12. Adrenergic innervation of the cochlea, including a perivascular system restricted to the modiolus in a system extending to the lateral wall, independent of cochlear blood vessels. (Reprinted with permission from H. Spoendlin and Annals of Otology Rhinology and Laryngology.)

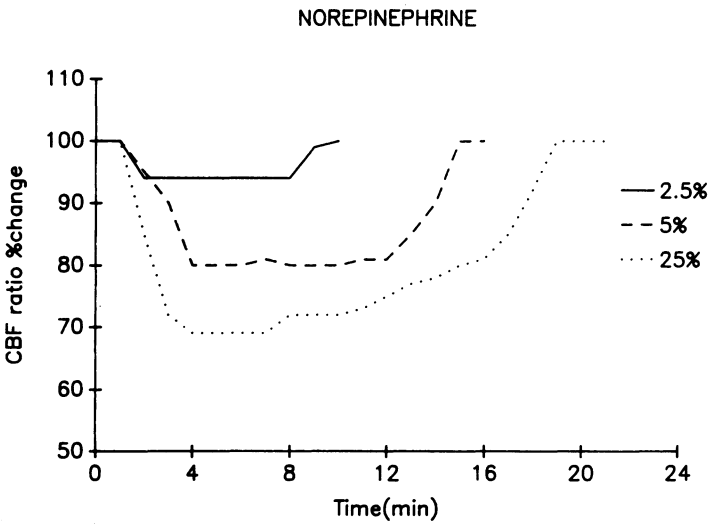

Figure 18–13. CBF response to topical application of 25 μg/kg of norepinephrine applied to the round window niche. (From Ohlsén et al., unpublished observations.)

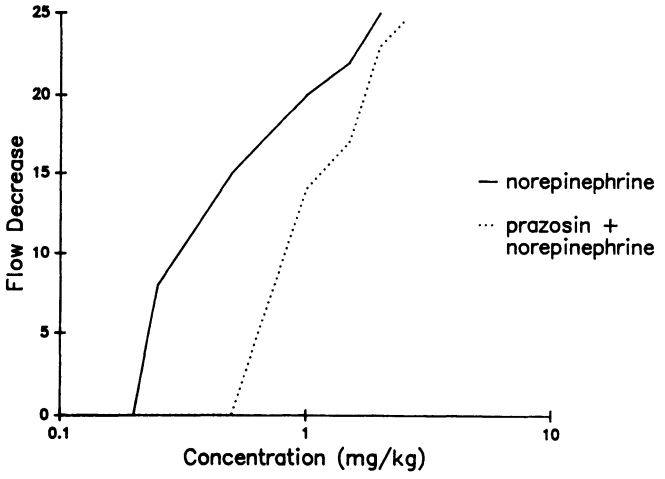

Figure 18–14. Dose–response functions of change in CBF with topical norepinephrine, before and after topical administration of prazosin. (From Ohlsén et al., unpublished observations.)

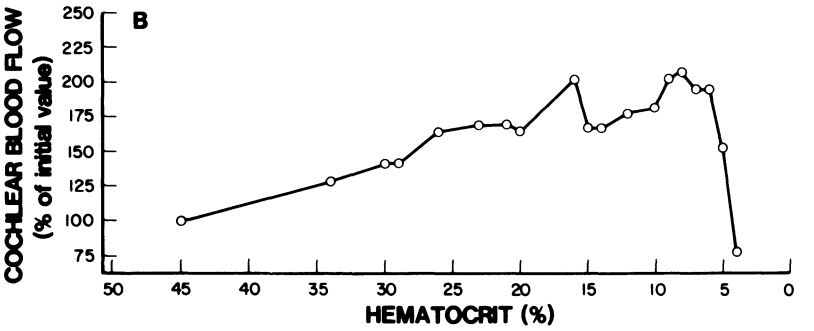

Figure 18–15. LDF-measure changes in CBF in relationship to hematocrit during normovolemic hemodilution with dextran 75. (Reprinted with permission from E. Hultcrantz and American Journal of Otolaryngology.)

sponse is consistent with the view that the CBF change was secondary to systemic influences of the hormones.

Obviously, other chemical agents that influence the major vascular beds, yielding fluctuations in systemic BP, can also produce secondary affects on CBF. LDF investigations of these influences have been performed by Miller et al. [7,36] and Short et al. [8]; however, no systematic investigation of the limits of these effects has yet been performed in the auditory system.

Blood hemodynamics

The powerful effect of changes in the rheological properties of blood on CBF has been well demonstrated in LDF studies. Short et al. [8] showed increases of 100%–150% in CBF, with a reduction in hematocrit. In the anesthetized guinea pig, CBF rises in direct proportion to decreases in hematocrit down to values of 10%–15%, below which CBF decreases (figure 18–15). Typically, CBF increases of 50%–100% can be observed with hematocrits 10%–25% [58]. These LDF findings of an increase in CBF with a decrease in hematocrit have been corroborated by microsphere and intravital microscopy studies [59].

Recently, the effects of the hyperosmotic agents glycerol and urea have been examined in our laboratories (Baldwin et al., unpublished observations). Concentration-dependent increases in CBF were observed. Intravenous infusions of 10%–40% hyperosmotic agents, over three to 15 minutes, yielded increases in CBF up to 300%. CBF peaked at approximately 15 minutes and returned to baseline at 30–40 minutes. The changes observed were correlated with the osmotic agent-induced change in hematocrit; however, the magnitude of the change could not be accounted for entirely by the hematocrit change. We speculate that these hyperosmotic agents not only influence the viscosity of whole blood by increasing the volume of the

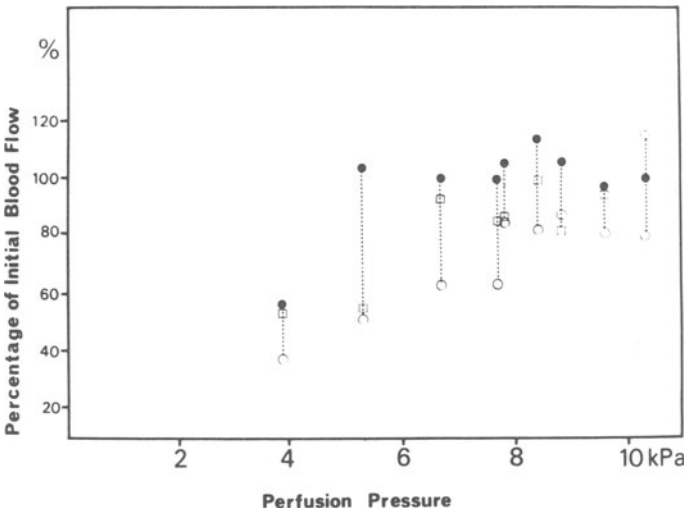

Figure 18–16. Relationship of CBF (close circles), BL in the medulla oblongata (open squares), and cerebral BF (open circles) with perfusion pressure. (Reprinted with permission from H.C. Larson and Acta Otolaryngologica [Stockholm].)

plasma but may also affect surface characteristics of the red blood cells, further decreasing the viscosity of blood.

LOCAL FACTORS

Of the local influences on CBF, local vasoregulation and regional metabolism are classically considered factors. The influence of these factors in autoregulation of the brain have been well demonstrated [89–91]. Evidence from microsphere investigations demonstrating a nonlinearity in the dependency of CBF on perfusion pressure are supportive of the availability of local microvascular mechanisms that may autoregulate flow within the cochlea. Thus, Hultcrantz et al. [84] and Larson [92] showed that over an extended range of perfusion pressure changes, CBF remains relatively constant (figure 18–16). Evidence to support these observations has been recently demonstrated in LDF studies by LaRouere et al. [60]. In their investigations, CBF decreased with positive end-expiratory pressure (PEEP). The change in CBF was directly dependent upon the magnitude of the PEEP, and consistent with the induced change in cardiac output [8] and cochlear perfusion pressure. However, LaRouere et al. [60] demonstrated that CBF returns to baseline with continued presence of PEEP.

Metabolic influences on CBF have been demonstrated only in microsphere investigations, and the data are rather indirect. Hultcrantz et al. [93,94] demonstrated a direct relationship between CBF and systemic blood pH. The pH change was induced by changing the inspired carbon dioxide concentra-

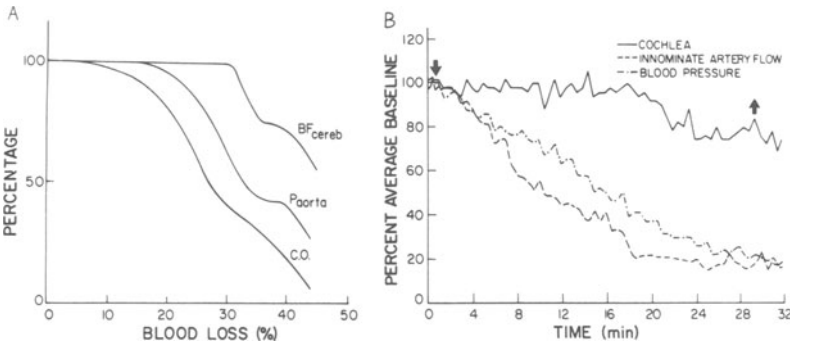

Figure 18–17. A. Changes in cerebral blood flow, aorta pressure, and cardiac output with blood loss. B. Cochlear blood flow, innominate artery flow, and BP over time during exsanguination. (Reprinted with permission from Short and Journal of Otolaryngology Head and Neck Surgery.)

tion. It is clear that these as well as other local mechanisms responsible for the autoregulatory characteristics of the cochlea require further study. The LDF technique certainly affords a strategy that will shed light on these characteristics of CBF. From the variety of data now available, it appears that autoregulation is indeed a powerful influence on CBF. Figure 18–17 illustrates the changes in CBF relative to innominate flow and BP during exsanguination [95] and compares these changes to the changes in brain BF, aorta pressure, and cardiac output expected and observed on the basis of autoregulatory characteristics of the brain. Before our knowledge will be complete and our therapeutic capabilities to manipulate CBF realized, the role played by each of these factors must be understood and the differential effects of vascoactive drugs on the membranes and receptors of cochlear vessel cells must be defined.

THERAPEUTIC MANIPULATION

Although a variety of techniques are now used in patients to manipulate CBF, the data to support the effectiveness of these agents and the clinical success of these therapies are weak. As indicated above, observations in animal studies suggest that hemodilution may be a most effective manipulation [7,8,34,58]. Hultcrantz [98] has argued for the use of hemodilution with Dextran 75 as a palliative in cases in which vascular compromise of the inner ear is suspected. Others [11] have recommended carbogen (95% O_2, 5% CO_2) respiration. This agent has been employed following noise exposure in cases of sudden hearing loss [9]. Animal investigations have indicated that carbogen can increase CBF [38] and reduce the damaging affects of noise exposure [97,98]. LDF studies, IVM studies [60], and microsphere studies [93,94] demonstrate that CO_2 may increase CBF.

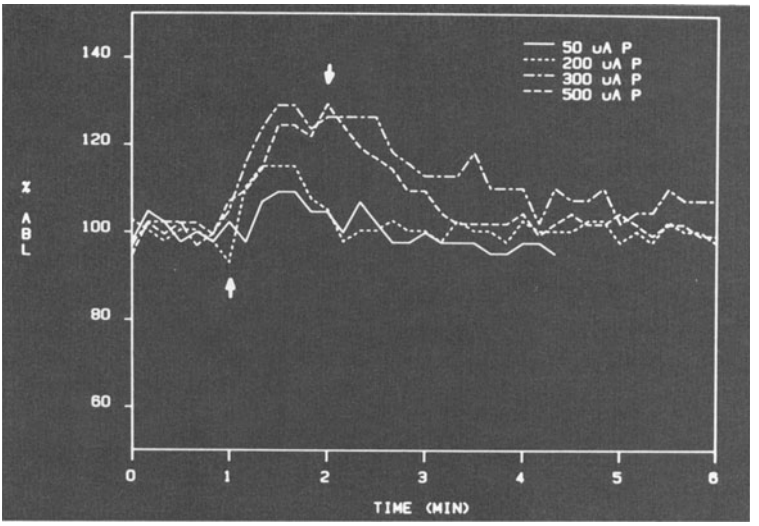

Figure 18–18. Changes in CBF with direct electrical stimulation of the round window with 1000 Hz sinusoidal constant current. Onset and offset of stimulation indicated by arrows.

In the LDF studies of Ohlsén et al. (unpublished observations), which examined adrenergic agents applied topically to the round window, the α-antagonist prazosin alone yielded an increase in CBF, suggesting a blockage of sympathetic tone in vessels of the inner ear. In addition, Ohlsén et al. (unpublished observations) found significant increases in CBF with hydralazine and sodium nitroprusside when they were applied directly to the round window.

Perhaps most intriguing are the recent reports by Sillman et al. [99,100] in which LDF recorded local increases in CBF in response to direct electrical stimulation at the round window (figure 18–18). Cochlear blood flow increased by 20%–30%. These changes were elicited in the absence of systemic pressure changes. These investigations [101,102] suggest that the change may have been mediated by a neuronal loop involving sympathetic or olivocochlear efferent nerves innervating the cochlea. The CBF changes were demonstrable with stimulus levels that were well within the accepted level of cochlear prostheses stimulation. Moreover, we have found that CBF changes may be maintained with such electrical stimulation for periods as long as one hour (Brown, Miller and Nuttall, unpublished observations).

In these studies of the control of CBF and therapeutic manipulations that may modify CBF, it is interesting and reinforcing to note the rate at which our knowledge is changing. Although we have far more questions than we have answers, it is clear that most of the information now available has been

obtained within the last few years. The abundant new data have been made possible by a new dynamic and relatively easy-to-apply technique for assessing CBF. LDF is already having a profound effect on studies of cochlear blood flow.

REFERENCES

1. Davis H., B.H. Deatherage, B. Rosenblut, C. Fernandez, R. Kimura, and C.A. Smith. 1958. Modification of cochlear potentials produced by streptomycin poisoning and be extensive venous obstruction. Laryngoscope 68:596–627.
2. Misrahy, G.A., E.W. Shinabarger, and J.E. Arnold. 1958. Changes in cochlear endolymphatic oxygen availability, actin potential, and micro-phonics during and following asphyxia, hypoxia and exposure to loud sounds. J Acoust Soc Am 30:701–704.
3. Konishi, T., R.A. Butler, and C. Fernandez. 1961. Effects of anoxia on cochlear potentials. J Acoust Soc Am 33:349–356.
4. Nuttall, A.L., and M. Lawrence. 1980. Endocochlear potential and scala media oxygen tension during partial anoxia. Am J Otol 1:147–153.
5. Thalmann, R., T. Miyoshi, and E. Rauchbach. 1973. Biochemical correlates of inner ear ischemia. In Vascular Disorders in Hearing Defects, de Lorenzo ed. Baltimore: University Park pp 219–245.
6. Zenner, H.P. 1988. Motility of outer hair cells as an active, actin-mediated process. Acta Otolaryngol [Stockh] 105:39–44.
7. Miller, J.M., E. Hultcrantz, S.O. Short, and A.L. Nuttall. 1986. Pharmacological effects on cochlear blood flow measured with the laser Doppler technique. Scand Audiol Suppl 26:11–20.
8. Short, S.O., P.C. Goodwin, J.N. Kaplan, and J.M. Miller. 1985. Measuring cochlear blood flow with laser Doppler spectroscopy. J Otolaryngol Head Neck Surg 43:786–793.
9. Cole, R.R., and R.A. Jahrdoerfer. 1988. Sudden hearing loss: An update. Am J Otol 9:211–215.
10. Kellerhals, B., F. Hippert, and C.R. Pfaltz. 1971. Treatment of acute acoustic trauma with low molecular weight dextran. Pract Oto Rhinol Laryngol 33:260–264.
11. Fisch, U. 1983. Management of sudden deafness. Otolaryngol Head Neck Surg 91:3–8.
12. Gieger, H.L. 1979. Therapy of sudden deafness with O2-CO2 inhalation. HNO 27:10–19.
13. Axelsson, A. 1968. The vascular anatomy of the cochlea in the guinea pig and in man. Acta Otolaryngol (Stockh) Suppl 243:1–143.
14. Hawkins, J.E. Jr., and L-G. Johnsson. 1968. Light microscopic observations of the inner ear in man and monkey. Ann Otol 77:608–629.
15. Axelsson, A., A. Ryan, and N. Woolf. 1986. The early postnatal development of the cochlear vasculature in the gerbil. Acta Otolaryngol [Stockh] 101:75–87.
16. Johnsson, L-G., and J.E. Hawkins, Jr. 1972. Vascular changes in the human inner ear associated with aging. Ann Otol Rhinol Laryngol 81:364–376.
17. Jaffe, P.F. 1975. Hypercoagulation and other causes of sudden hearing loss. Otolaryngol Clin North Am 8:395–403.
18. Tange, R.A., and J.L. Bernhard. 1981. A cochlear vascular anomaly in a patient with hearing loss and tinnitus. Arch Otorhinolaryngol 233:177–125.
19. Axelsson, A., and D. Vertes. 1982. Histological findings in cochlear vessels after noise. In *New Perspective on Noise-Induced Hearing Loss*, Hammernik R.P., Henderson, D., Salvi, R. eds. New York: Raven Press, pp 49–67.
20. Vertes, D., and A. Axelsson. 1979. Methodological aspects of some inner ear vascular techniques. Acta Otolaryngol [Stockh] 88:328–334.
21. Weille, F.L., S.R. Gargano, R. Pfister, D. Martinez, and J.W. Irwin. 1954. Circulation of the spiral ligament and stria vascularis of living guinea pig. Experimental study. Arch Otolaryngol 59:731–738.
22. Perlman, H.B., and R.S. Kimura. 1955. Observation of the living blood vessels of the cochlea. Ann Otol Rhinol Laryngol 64:1176–1192.
23. Nomura, Y. 1961. Observations on the microcirculation of the cochlea. Ann Otol 70:1037–1054.

24. Costa, O., and P.-I. Branemark. 1970. Microvascular physiology of the cochlea. Adv Microcirc 3:108–114.
25. Costa, O., and P.-I. Branemark. 1970. Vital microscopic evaluation of the microvessels of the cochlea. Adv Microcirc 3:96–107.
26. Intaglietta, M., and W.R. Tompkins. 1972. On-line measurement of microvascular dimensions by television microscopy. J Appl Physiol 32:546–551.
27. Rhodin, J.A.G., H. Wayland, and Y. Makamura. 1974. Combined intravital fluorescence microscopy and electron microscopy for studying vascular permeability. Proceedings of the Symposium at the Eighth European Conference on Microcirculation. Le Touquet, France. In Modern Methods in Microcirculatory Research, California Institute of Technology.
28. Ellis, C.G., R.G.A. Safranyos, and A.C. Groom. 1983. Television-computer method for in vivo measurement of capillary diameter, based on the passage of red cells. Microvasc Res 26:139–150.
29. Nuttall, A.L. 1986. Distribution of red blood cell flow velocities in capillaries of the guinea pig cochlea. 23rd Workshop on Inner Ear Biology, Berlin (abstract).
30. Nuttall, A.L. 1986. Intravital microscopy for measurement of blood cell velocities in the cochlea. Ninth Midwinter Research Meeting of the Association for Research in Otolaryngology, Clearwater Beach, FL, February, pp 43–44.
31. Miles, F.P., and A.L. Nuttall. 1988. In vivo capillary diameters in the stria vascularis and spiral ligament of the guinea pig cochlea. Hearing Res 33:191–200.
32. Suga, F., and J.B. Snow. 1969. Cholinergic control of cochlear blood flow. Ann Otol Rhinol Laryngol 78:1081–1090.
33. Suga, F., and J.B. Snow. 1969. Adrenergic control of cochlear blood flow. Ann Otol Rhinol Laryngol 78:358–374.
34. Nuttall, A.L. 1988. Cochlear blood flow: Measurement techniques. Am J Otolaryngol 9:291–301.
35. Miller, J.M., N.J. Marks, and P.C. Goodwin. 1983. Laser Doppler measurements of cochlear blood flow. Hearing Res 11:385–394.
36. Miller, J.M., P.C. Goodwin, and N.J. Marks. 1984. Inner ear blood flow measured with a laser Doppler system. Arch Otolaryngol 111:305–308.
37. Goodwin, P.C., J.M. Miller, H.A. Dengerink, J.N. Wright, and A. Axelsson. 1984. The laser Doppler: A non-invasive measure of cochlear blood flow. Acta Otolaryngol [Stockh] 98:403–412.
38. Dengerink, H.A., A. Axelsson, J.M. Miller, and J.W. Wright. 1984. The effect of noise and carbogen on cochlear vasculature. Acta Otolaryngol 98:81–88.
39. Miller, J.M., E. Hultcrantz, S.O. Short, and A.L. Nuttall. 1985. Pharmacological effects of cochlear blood flow (measured with the laser Doppler technique). Abstracts of the Third International Meeting of Medical Audiologists, Visby, Sweden.
40. Wright, J.W., H.A. Dengerink, J.M. Miller, and P.C. Goodwin. 1985. Potential role of angiotensin II in noise-induced increases in inner ear blood flow. Hearing Res 17:41–46.
41. Dengerink, H.A., J.W. Wright, J.M. Miller, and P.C. Goodwin. 1985. The effects of nicotine on laser Doppler measures of cochlear blood flow. Hearing Res 20:31–36.
42. Sillman, J.S., M.J. LaRouere, A.L. Nuttall, M. Lawrence, and J.M. Miller. 1988. Recent advances in cochlear blood flow measurements. Ann Otol Rhinol Laryngol 97:1–8.
43. Bonner, R., and R. Nossal. 1981. Model for laser Doppler measurements of blood flow in tissue. Appl Optics 20:2097–2107.
44. Bonner, R.F., T.R. Clem, P.D. Bowen, and R.L. Bowman. 1981. Laser-Doppler continuous real-time monitor of pulsatile and mean blood flow in tissue microcirculation. In *Scattering Techniques Applied to Supramolecular and Non-equilibrium Systems*, Chew, S.H., Chu, B., Nossal, R. eds. New York: Plenum Press, pp 685–701.
45. Nilsson, G.E., T. Tenland, and P.A. Oberg. 1980. Evaluation of a laser Doppler flowmeter for measurement of tissue blood flow. IEEE Trans Biomed Eng 27:597–604.
46. Kvietys, P.R., A.P. Shepherd, and D.N. Granger. 1985. Laser-Doppler, H2 clearance, and microsphere estimates of mucosal blood flow. Am J Physiol 249:G221–G227.
47. Johansson, K., H. Ahn, J. Lindhagen, and O. Lundgren. 1987. Tissue penetration and measuring depth of laser Doppler flowmetry in the gastrointestinal application. Scand J Gastroenterol 29(9):1081–1088.

48. Nilsson, G.E., T. Tenland, and P.A. Oberg. 1980. Evaluation of a laser Doppler flowmeter for measurement of tissue blood flow. IEEE Trans Biomed Eng 27:597–604.
49. Holmstrom, A. and D.H. Lewis. 1983. Regional blood flow in skeletal muscle after high-energy trauma: An experimental study in pigs, using a new laser Doppler technique and radioactive microspheres. Acta Chir Scand 149:453–458.
50. Smits, G.J., R.J. Roman, and J.H. Lombard. 1986. Evaluation of laser-Doppler flowmetry as a measure of tissue blood flow. J Appl Physiol 61(2):666–672.
51. Swiontkowski, M.F., S. Tepic, S.M. Perren, R. Moor, R. Ganz, and B.A. Rahn. 1986. Laser Doppler flowmetry for bone blood flow measurement: Correlation with microsphere estimates and evaluation of the effect of intracapsular pressure on femoral head blood flow. J Orthopaedic Res 4:362–371.
52. Neufeld, G.R., S.R. Galante, J.M. Whang, D. DeVries, J.E. Baumgardner, D.J. Graves, and J.A. Quinn. 1988. Skin blood flow from gas transport: Helium xenon and laser Doppler compared. Microvasc Res 35:143–152.
53. Maass, B., and J. Kellner. 1984. Hydrogen clearance and cochlear microcirculation at different levels of blood pressure. Arch Otorhinolaryngol 240:295–310.
54. Maass, B., and D. Ludwig. 1984. Effect of pentoxifylline ('Trental') on cochlear blood flow as measured by hydrogen wash-out. Current Med Res Opinion 9:52–55.
55. Ryan, A.F., A. Axelsson, R. Myers, and N.K. Woolf. 1988. Changes in cochlear blood flow during acoustic stimulation as determined by 14C-iodoantipyrine autoradiography. Acta Otolaryngol [Stockh] 105(3–4):232–241.
56. Nuttall, A.L., E. Hultcrantz, H.-C. Larsen, and C. Angelborg. 1987. Cochlear blood flow increases after systemic hemodilution: Comparison of simultaneous laser Doppler flowmetry and radioactive microspheres measurements. Hearing Res 34:215–224.
57. Hultcrantz, E., P.R. Thorne, and A.L. Nuttall. 1986. The influence of cervical sympathetic stimulation on laser-Doppler blood flow measurements from the cochlea. 23rd Workshop on Inner Ear Biology, Berlin, DDR, September.
58. Hultcrantz, E., and A.L. Nuttall. 1986. Effect of hemodilution on cochlear blood flow measured by laser Doppler flowmetry. Am J Otolaryngol 8:16–22.
59. Nuttall, A.L., J. Warner, J.N. Brown, M. Griffiths, E. Hultcrantz. 1988. Estimation of mean capillary size in the guinea pig cochlea from the size distribution of microspheres. XV European Conference for Microcirculation, Maastricht, The Netherlands.
60. LaRouere, M.J., J.S. Sillman, A.L. Nuttall, and J.M. Miller. A comparison of laser Doppler and intravital microscopy measures of cochlear blood flow. Am Otolaryngol Head Neck Surg, in press.
61. Duling, B.R., and C. Desjardins. 1987. Capillary hematocrit—What does it mean? News Int Physiol Soc 2:66–69.
62. McLain, D.H. 1974. Drawing contours from arbitrary data points. Computer J 17:318–324.
63. Sarelius, I.H., and B.R. Duling. 1982. Direct measurement of microvessel hematocrit, red cell flux, velocity, and transit time. Am J Physiol 243:H1018–H1026.
64. Hillerdal, M., B. Jansson, B. Engstrom, et al. Cochlear blood flow in noise-damaged ears. Acta Otolaryngol [Stockh] 104:270–278.
65. Mirhashemi, S. 1987. Microcirculatory effects of normovolemic hemodilution: Analytical and experimental investigations. Dissertation.
66. Maass, B., H. Baumgartl, and D.W. Lubbers. 1976. Lokale pOV2V und pHV2V-Messungen mit Nadelelektroden zum Studium der Sauerstoffversorgung und Mikrozirkulation der Innenohres. Arch Otorhinolaryngol 214:109–124.
67. Nuttall, A.L., E. Hultcrantz, and M. Lawrence. 1981. Does loud sound influence the intracochlear oxygen tension? Hearing Res 5:285–293.
68. Thorne, P.R., and A.L. Nuttall. 1987. Laser Doppler measurements of cochlear blood flow during loud sound exposure in the guinea pig. Hearing Res 27:1–10.
69. Thorne, P.R., A.L. Nuttall, F. Scheibe, and J.M. Miller. 1987. Sound-induced artifact in laser Doppler measurements of cochlear blood flow. Hearing Res 31:229–234.
70. Lamm, K., C. Lamm, H. Lamm, and K. Schumann. 1988. Noise-induced reduction of oxygen tension in the perilymph and simultaneous recording of hearing potentials and blood pressure in guinea pigs. HNO 36:367–372.

71. Angelborg, C., E. Hultcrantz, and M. Beausang-Linder. 1979. The cochlear blood flow in relation to noise and cervical sympathectomy. Adv Otorhinolaryngol 25:41–48.
72. Prazma, J., G.K. Rodgers, and H.C. Pillsbury. 1983. The effect of noise on cochlear blood flow. Abstract Association for Research in Otolaryngology, St. Petersburg, FL, January.
73. Canlon, B., and J. Schacht. 1981. The effect of noise on deoxyglucose uptake into inner ear tissues of the mouse. Arch Otorhinolaryngol 230:171–176.
74. Canlon, B. and J. Schacht. 1983. Acoustic stimulation alters deoxyglucose uptake in the mouse cochlea and inferior colliculus. Hearing Res 10:217–226.
75. Ryan, A.F., F.R. Sharp, N.K. Woolf, and T.M. Davidson. 1983. Deoxyglucose uptake in the cochlea during silence and noise: Localization at the cellular level with T3TH autoradiography. ARO 22:
76. Angelborg, C., A. Axelsson, and H.C. Larsen. 1984. Regional blood flow in the rabbit cochlea. Arch Otolaryngol 110:297–300.
77. Angelborg, C., H.C. Larsen, and N. Slepecky. 1985. Regional cochlear blood flow: A study of observations of microspheres in serial sections. Ann Otol 94:181–185.
78. Lorento de No, R. 1937. The sensory endings in the cochlea. Laryngoscope 47:373–377.
79. Smith, C.A. 1951. Capillary areas of the cochlea in the guinea pig. Laryngoscope 61:1073–1095.
80. Spoendlin, H., and W. Lichtensteiger. 1966. The adrenergic innervation of the labyrinth. Acta Otolaryngol [Stockh] 61:423–434.
81. Densert, O. 1974. Adrenergic innervation in the rabbit cochlea. Acta Otolaryngol [Stockh] 78:345–356.
82. Densert, O., and A. Flock. 1963. An electron microscope study of adrenergic innervation of the cochlea. Acta Otolaryngol [Stockh] 56:587–598.
83. Ohlsén, K.A., A.L. Nuttall, and J.M. Miller. 1989. The influence of adrenergic drugs on the cochlear blood flow. Abstracts of the Midwinter Meeting of the Association for Research in Otolaryngology, vol. 12, pp. 103–104.
84. Hultcrantz E., J. Linder, and C. Angelborg. 1977. Sympathetic effects on cochlear blood flow at different blood pressure levels. INSERM 68:271–278.
85. Cox, J.R. 1980. Hormonal influence on auditory function. Ear Hear 1:219–222.
86. Davis, M.J., and Ahroon, W.A. 1982. Fluctuations in susceptibility to noise-induced temporary threshold shift as influenced by the menstrual cycle. J Aud Res 22:173–187.
87. Petiot, J.C., and J.E. Parrot. 1984. Effects of the ovarian and contraceptive cycles on absolute thresholds, auditory fatigue and recovery from temporary threshold shifts at 4 and 6 kHz. Audiology 23:581–598.
88. Laugel, G.R., H.A. Dengerink, and J.W. Wright. 1987. Ovarian steroid and vasoconstrictor effects on cochlear blood flow. Hearing Res 51:
89. Guyton, A.C. 1981. Textbook of Medical Physiology, 6th ed. Philadelphia: Saunders.
90. Coyle, P., and D. Heistad. 1986. Blood flow through cerebral co-lateral vessels in hypertensive and normotensive rats. Hypertension 8(II):I167–I171.
91. Granger, H.J., M.E. Schelling, R.E. Lewis, D.C. Zawieja, and C.J. Meininger. 1988. Physiology and pathobiology of the microcirculation. Am J Otolaryngol 9:264–277.
92. Larson, H.C. 1982. The effect of intracranial hypertension on cochlear blood flow. Acta Otolaryngol [Stockh] 93:415–419.
93. Hultcrantz, E., H.C. Larson, and C. Angelborg. 1980. The effects of CO_2-breathing on cochlear blood flow. Arch Otorhinolaryngol 228:221–215.
94. Hultcrantz, E., H.C. Larsen, and C. Angelborg. 1980. Effects of the CO_2 inhalation on cochlear blood circulation. ORL 42:304–312.
95. Miller, J.M., and H. Dengerink. 1988. Control of inner ear blood flow. Am J Otolaryngol 9:302–316.
96. Hultcrantz, E. 1988. Clinical treatment of vascular inner ear diseases. Am J Otolaryngol 9:317–322.
97. Brown, J.J., J.A. Vernon, and J.A. Fenwick. 1982. Reduction of acoustically-induced auditory impairment by inhalation of carbogen gas. Acta Otolaryngol [Stockh] 93:319–328.
98. Joglekar, S.S., D.M. Lipscomb, and G.E. Shambaugh. 1977. Effects of oxygen inhalation on noise-induced threshold shifts in humans and chinchillas. Arch Otolaryngol 103:574–578.

99. Sillman, J.S., M.J. LaRouere, R.I. Masta, J.M. Miller, and A.L. Nuttall. Electrically stimulated increases in cochlear blood flow: I. Frequency and intensity effects. Otolaryngol Head Neck Surg, in press.
100. Sillman, J.S., R.I. Masta, M.J. LaRouere, A.L. Nuttall, J.M. Miller. Electrically stimulated increases in cochlear blood flow: II. Evidence of neural mediation. Otolaryngol Head Neck Surg, in press.
101. Thorne, P.R., and A.L. Nuttall. 1989. Alterations in oxygenation of cochlear endolymph during loud sound exposure. Acta Otolaryngol [Stockh] 107:71–79.

19. RETINAL BLOOD FLOW

CHARLES E. RIVA, BENNO L. PETRIG, and JUAN E. GRUNWALD

In ophthalmology, laser-Doppler velocimetry (LDV) has been used for various types of measurements besides those of blood velocity. For example, it has been applied to investigate eye motion during smooth pursuit of a target [1] and the mechanical compliance of the optic nerve head [2]. However, most of the efforts have been directed to investigations of ocular fundus hemodymanics, the subject of this chapter. Some of the readers may not be familiar with the vascular system of the eye. It thus seems appropriate to begin with a brief description of this system. For more details, the reader is referred to the chapter "Ocular Circulation" by Alm and Bill in Adler's *Physiology of the Eye* [3].

The vascular system of the eye is complex. It consists of two components: the retinal and uveal blood vessels. Both are involved in the nutrition of the ocular fundus. In humans, the central retinal artery enters the optic nerve behind the eyeball (figure 19–1A). It then branches into main arterioles (figure 19–1B), each supplying about one quadrant of the retina. These arterioles feed a system of capillaries distributed within the inner two thirds of the retina. The blood is drained out of the retina through a system of venules that merge into the central retinal vein within the optic nerve.

In terms of blood volume, the choroid represents the largest portion of the uveal circulation. It is highly vascularized, with 2–3 arteries (long posterior ciliary arteries) branching from the ophthalmic artery. These arteries subdivide into approximately 20 short posterior arteries that pierce the sclera and

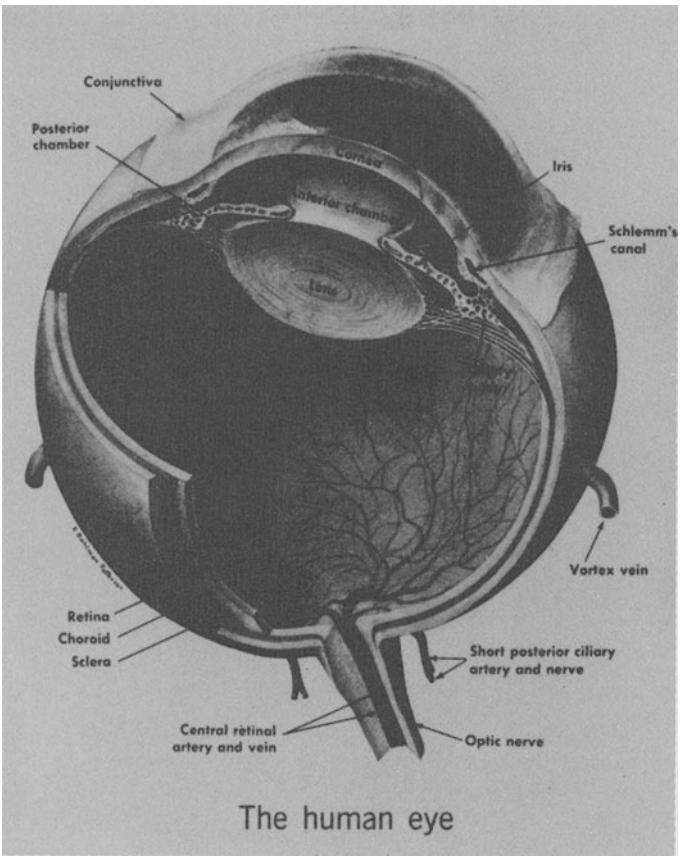

Figure 19–1A. Schematic representation of the human eye. (From Newell, F.W., and J.T. Ernest. 1982. *Ophthalmology: Principles and Concepts*, 5th ed. St Louis: Mosby Co.)

the posterior pole near the optic nerve to form the choriocapillaris, a dense, one-layered vascular network. This layer nourishes the avascular outer retina containing the photoreceptors.

Posterior ciliary arteries also send branches to the optic nerve. These branches supply the optic nerve head and the lamina cribrosa. However, because the vessels of the optic nerve head are anatomically different from those supplying the choroid, the physiology of these blood vessels differs from that of the choroidal vessels. Anatomically, the optic nerve capillary bed resembles that of the inner retina.

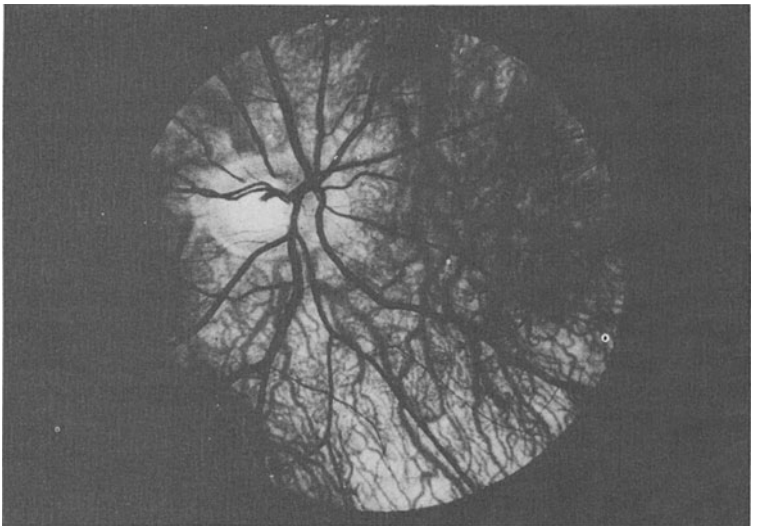

Figure 19–1B. Fundus of a lightly pigmented human eye. The darker vessels in the foreground are retinal arteries and veins. Behind them is the dense net of choroidal vessels with some large choroidal veins. The layer of choriocapillaries is not visible.

MEASUREMENT OF BLOOD FLOW IN THE OCULAR FUNDUS

The measurement of retinal, choroidal and optic nerve blood flow is of substantial value to ophthalmologists because several functional impairments of the visual system are attributed to ischemia. Such measurements also are of great interest to physiologists because of the uniqueness of the vascular system of the eye, which is under local and possibly central nervous control and can be visualized without any invasive procedure.

The visibility of the vasculature in the ocular fundus invites the development of noninvasive optical methods to measure blood flow in this region of the eye. Techniques have been used to time the passage of a dye such as fluorescein in the retinal circulation [4,5,6] or indocyanine green in the choroidal circulation [7]. Although these techniques have provided semiquantitative information on retinal and choroidal blood flow, their value for physiologic studies in humans and for clinical work has been limited. On the other hand, we believe that LDV has proven to be more powerful for physiologic as well as clinical work, as we shall demonstrate in this chapter.

The feasibility of using LDV to measure blood velocity in small tubes and vessels was first demonstrated in 1972 by Riva, Ross, and Benedek [8]. These investigators were able to record Doppler-shift power spectra (DSPS) of laser light scattered by red blood cells (RBCs) flowing in a retinal artery of an

anesthetized rabbit (figure 19–2A), using the optical system shown in figure 19–2B. This work was followed by measurements of blood velocity in retinal vessels of a human subject, using digital correlation techniques [9]. Since then, the technique has progressed considerably and is now applied to the study of the physiology of the retinal and optic nerve circulation in the normal and diseased eye. Its usefulness in the investigation of choroidal hemodymanics is currently being evaluated.

The chief application of LDV to the ocular circulation to date has been the measurement of retinal blood velocity. In the main retinal vessels, the direction of flow and the velocity profile of the RBCs are well defined. In addition, the diameter of these vessels (in man, typically 50 to 120 μm for arteries and 80 to 160 μm for veins) and the high concentration of the RBCs require measurement schemes that differ fundamentally from those used in the measurement of blood flow in tissue. The theoretical treatment that follows has been borrowed to some extent from a previous review of the technique [10].

PRINCIPLES OF LDV FOR RETINAL BLOOD FLOW

Consider a laser beam $\vec{E}_0 \cos\omega_0 t$ incident on a retinal vessel along a direction defined by the wave vector $\vec{\mathbf{K}}_i$ (figure 19–3). It illuminates uniformly the entire cross section of the vessel. Some of the light is scattered by the RBCs and some by the vessel wall. Let us assume that single scattering by the RBCs is predominant. We will validate this assumption later. Light scattered along a direction $\vec{\mathbf{K}}_s$ by a collection of RBCs moving at speed $\vec{\mathbf{V}}$ is shifted in frequency by an amount Δf equal to the scalar product between the scattering vector $\vec{\mathbf{K}} = (\vec{\mathbf{K}}_s - \vec{\mathbf{K}}_i)$ and $\vec{\mathbf{V}}$:

$$\Delta f = \frac{1}{2\pi} \vec{\mathbf{K}} \cdot \vec{\mathbf{V}}. \tag{19.1}$$

$|\vec{\mathbf{K}}_s| = |\vec{\mathbf{K}}_i| = 2\pi n/\lambda$, where n is the refractive index of the flowing medium, and λ is the wavelength of the incident laser light in vacuo.

In a vessel, the RBCs move at various velocities determined by their distance R from the axis. Assuming Poiseuille's law, the relationship between the distance R of an RBC and the velocity $|\vec{\mathbf{V}}|$ of the particle is given by

$$V(\mathrm{R}) = V_{\max}[1 - (R/R_0)^2]. \tag{19.2}$$

R_0 is the radius of the vessel and $V_{\max}$ the maximum centerline velocity of the RBCs.

As previously shown [11], the amplitude of the optical field $E_{sc}(\vec{\mathbf{K}}_s, t)$ of light scattered in direction $\vec{\mathbf{K}}_s$ by RBCs in the illuminated volume is given by

$$E_{sc}(\vec{\mathbf{K}}_s, t) = A_{sc}(\vec{\mathbf{K}}_s) \sum_{i=1}^{N} \cos 2\pi (f_0 + \Delta f_i)t. \tag{19.3}$$

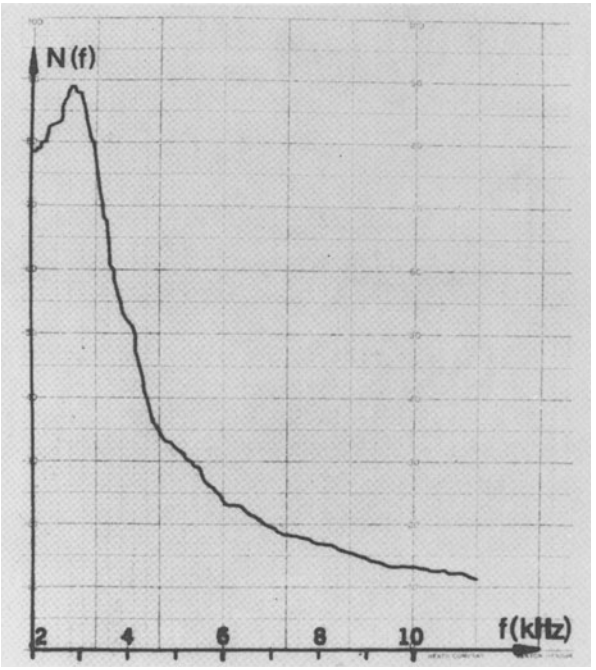

Figure 19–2A. Power spectrum $N(f)$ (= DSPS) of laser light (helium–neon at 632.8 nm) scattered from a retinal arteriole of a rabbit, where f (= Δf in text) is the frequency of the Doppler-shifted light. (From Riva, C.E., B. Ross, and G. Benedek. 1972. Invest Ophthalmol Vis Sci 11:936–944.)

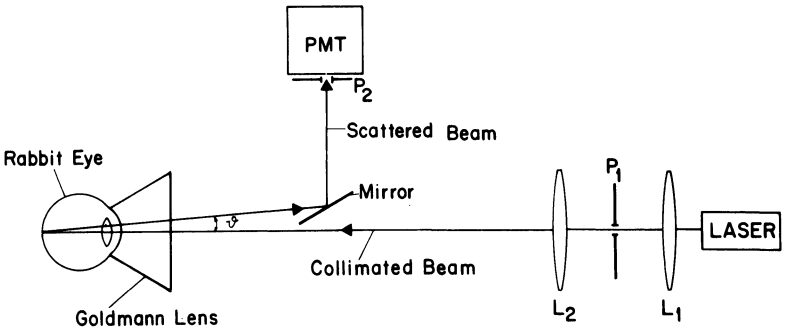

Figure 19–2B. Optical system used for recording the power spectrum shown in figure 19–2A. The Goldmann lens is a contact lens to eliminate refraction of light at the cornea. To obtain the spectrum, the signal from the photodetector (PMT) was amplified and then analyzed by a spectrum analyzer. (From Riva, C.E., B. Ross, and G. Benedek. 1972. Invest Ophthalmol Vis Sci 11:936–944.)

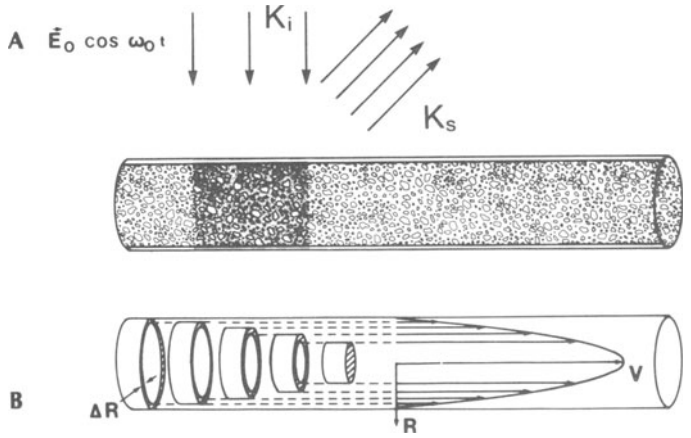

Figure 19–3. A. Schematic representation of a volume of a retinal vessel illuminated by an incident wave defined by $\vec{E}_0 \cos\omega_0 t$ and with direction $\vec{K}_i$. $E_{sc}(\vec{K}_s, t)$ is the light scattered by vessel wall and by the red blood cells along direction $\vec{K}_s$ at time t. ω_0 is the angular frequency of the incident beam.
B. Assumed parabolic velocity profile of red blood cells in the retinal vessels. The cylindrical shell ΔR contains red blood cells moving at velocity V, the value of which is given by Poiseuille's Law. (Adapted from Riva, C.E. and G.T. Feke. 1981. Laser Doppler Velocimetry in the measurement of retinal blood flow. in *The Biomedical Laser: Technology and Clinical Application*, Goldmann, L., ed. New York: Springer–Verlag, pp 135–161.)

It represents a summation of the contributions of N cylindrical shells, which have been obtained by dividing the velocity range from 0 to V_{max} into N equal ranges ΔV. $A_{sc}(\vec{K}_s)$ is the amplitude of light scattered in direction $\vec{K}_s$ by RBCs moving with velocities between V and $V + \Delta V$. A characteristic of Poiseuille's flow is that, if the density of the particles is uniform across the vessel lumen, each velocity range contains the same number of RBCs [8] and therefore $A_{sc}(\vec{K}_s)$ is a constant. Δf_i is the Doppler shift of the light scattered by the RBCs moving at velocity $V_i = i\Delta V$. In addition, the detected light contains light that has been scattered by the vessel wall. It is defined by the amplitude of the optical field $E_{lo}(\vec{K}_s) = A_{lo}(\vec{K}_s)\cos\omega_0 t$. This light is unshifted in frequency. Thus, the optical field scattered from the illuminated volume is

$$E_{sc}(\vec{K}_s, t) = A_{lo}(\vec{K}_s)\cos 2\pi f_0 t + A_{sc}(\vec{K}_s) \sum_{i=1}^{N} \cos 2\pi (f_0 + \Delta f_i)t. \tag{19.4}$$

A_{lo} is the amplitude of the light scattered in direction $\vec{K}_s$ by the vessel wall, which acts as a local oscillator. The power spectral density of the scattered light, $P_E(f)$, is obtained by applying Fourier analysis:

$$P_E(f) = \tfrac{1}{2} A_{lo}{}^2 \delta(f - f_0) + \tfrac{1}{2} A_{ro} A_{sc} \sum_{i=1}^{N} \delta\left[f - \left(f_0 + \frac{i\Delta f_{max}}{N}\right)\right]$$

$$\text{for } f_0 \leq f \leq (f_0 + \Delta f_{max}). \tag{19.5}$$

Δf_{max} is the Doppler shift corresponding to the maximum velocity V_{max} and $\delta(f - f_0)$ is the delta function at the incident laser frequency. Thus the optical density function consists of a delta function at f_0, followed by a flat portion of magnitude $\frac{1}{2} A_{lo}A_{sc}$ from f_0 to $f_0 + \Delta f_{max}$. It is zero beyond $f_0 + \Delta f_{max}$. Since f_0 is approximately 5×10^{14} Hz and a typical Δf_{max} is of the order of 5000 Hz, the required resolution $\Delta f_{max}/f_0 = 10^{-11}$ is far beyond the capability of conventional spectroscopic techniques. By using the technique of optical mixing spectroscopy [12], the information contained in the optical spectral density function can be translated down to sufficiently low frequencies, where adequate resolution can be obtained.

The field given by equation 19.4 is directed onto the photocathode of a photoelectric detector. The photocurrent $\langle i(t) \rangle$ resulting from the emitted photoelectrons is equal to $\int_S \beta E_{sc}(\vec{\mathbf{K}}_s, t) dS$, where S is the illuminated photocathode area. The angle brackets $\langle\ \rangle$ represent the time average.

Following the formalism of Lastovka [13] and the procedure described in detail elsewhere [17], one obtains for the spectral density of the photocurrent

$$P_i(\Delta f) = \tfrac{1}{4} \beta^2 S^2 [A_{lo}^2 + A_{sc}^2]^2 \delta(\Delta f) + \tfrac{1}{2} e\beta S [A_{lo}^2 + A_{sc}^2] + \beta^2 S S_{cohlo} A_{lo}^2 A^2 \sum_{i=1}^{N} \delta\left(\Delta f - \frac{i\Delta f_{max}}{N}\right) \qquad (19.6a)$$

in the range $0 \leq \Delta f \leq \Delta f_{max}$ and

$$P_i(\Delta f) = \tfrac{1}{2} e\beta S [A_{lo}^2 + A_{sc}^2] \qquad (19.6b)$$

beyond Δf_{max}, where Δf_{max} is defined as the cutoff frequency of $S_i(\Delta f)$. e = charge of the electron, β = responsivity of the photodetector, S_{cohlo} = coherence area of the local oscillator at the photocathode. We see that the third term of $P_i(\Delta f)$ in equation 19.6a is a squared replica of the second term of the spectral density $P_E(f)$, but shifted down towards low frequencies so that the RBC velocity can be determined from measurements of $P_i(\Delta f)$. Thus through the mixing of the light scattered by the RBCs and the local oscillator at the photocathode, the power spectrum has been shifted from optical frequencies down to the kilohertz range, allowing high-resolution spectral analysis of the Doppler-shift power spectrum. The term $P_n(\Delta f) = \frac{1}{2} e\beta S(A_{lo}^2 + A_{sc}^2)$ is the photodetector shot noise.

In general, the local oscillator is much more intense than the field scattered by the RBCs, so that $A_{lo} \gg A_{sc}$. As a result, the shot noise is

$$P_n(\Delta f) \cong \tfrac{1}{2} e\beta S A_{lo}^2. \qquad (19.7)$$

In practice, the ability to measure $P_i(\Delta f)$ with high resolution requires that the power spectral density of the signal term be larger than that of the

shot-noise term. A measure of this ability is the intrinsic signal-to-noise ratio (SNR), which is

$$\mathrm{SNR}(\Delta f) = \frac{2\beta}{e} S_{\mathrm{cohlo}} A_{\mathrm{sc}}{}^2 \sum_{i=1}^{N} \delta\left(\Delta f - \frac{i\Delta f_{\max}}{N}\right). \tag{19.8}$$

For a given photocathode efficiency β, RBC volume, and S_{cohlo}, this SNR can be increased only by increasing the intensity of the incident light.

ABSOLUTE RETINAL BLOOD VELOCITY

An absolute measure of $V_{\max}$ could be obtained directly from the measurement of the cutoff frequency $\Delta f_{\max}$ of $P_i(\Delta f)$ and using the Doppler formula (equation 19.1). However, this has not been attempted because of the difficulty of determining the direction of the vessel at the site of measurement. This problem can be circumvented by using a bidirectional detection scheme [14], where Doppler-shift power spectra (DSPS) are obtained for two directions of the scattered light. Each DSPS exhibits a cutoff frequency that is directly related to $V_{\max}$. The difference of the cutoff frequencies is used to obtain $V_{\max}$, independently of the exact orientation of the vessel and of the relative direction of the incident and scattered beams with respect to the flow direction.

The derivation of the relationship between $V_{\max}$ and $\Delta f_{\max}$ proceeds as follows [14]. Consider an RBC at the origin of the coordinate system (figure 19–4) moving with velocity $\vec{\mathbf{V}}_{\max} = (V_{\max,x}, V_{\max,y}, V_{\max,z})$. A laser beam characterized by the wave vector $\vec{\mathbf{K}}_i = (K_{i,x}, K_{i,y}, K_{i,z})$ is incident on this RBC. Light scattered by this RBC is collected along two directions, assumed for simplicity to lie in the (x,y)-plane. The wave vectors of the scattered light along these directions are $\vec{\mathbf{K}}_1 = (K_{1,x}, K_{1,y}, 0)$ and $\vec{\mathbf{K}}_2 = (K_{2,x}, K_{2,y}, 0)$. The laser beams scattered along directions (1) and (2) are shifted in frequency by an amount $\Delta f_1 = \frac{1}{2\pi}(\vec{\mathbf{K}}_1 - \vec{\mathbf{K}}_i)\cdot\vec{\mathbf{V}}_{\max}$ and $\Delta f_2 = \frac{1}{2\pi}(\vec{\mathbf{K}}_2 - \vec{\mathbf{K}}_i)\cdot\vec{\mathbf{V}}_{\max}$. The difference $\Delta^* f_{\max} = \Delta f_2 - \Delta f_1$ is equal to $\frac{1}{2\pi}(\vec{\mathbf{K}}_2 - \vec{\mathbf{K}}_1)\cdot\vec{\mathbf{V}}_{\max}$. From figure 19–4, we find

$$V_{\max,x} = |\vec{V}_{\max}|\cos\beta\cos(\pi - \gamma), \qquad V_{\max,y} = |\vec{V}_{\max}|\cos\beta\sin(\pi - \gamma),$$
$$K_{1,x} = (2\pi n/\lambda)\cos\alpha_1, \qquad K_{1,y} = (2\pi n/\lambda)\sin\alpha_1,$$
$$K_{2,x} = (2\pi n/\lambda)\cos\alpha_2, \qquad K_{2,y} = (2\pi n/\lambda)\sin\alpha_2.$$

It follows that $\Delta^* f_{\max} = (n/\lambda)|\vec{\mathbf{V}}_{\max}|\cos\beta[\cos(\gamma + \alpha_1) - \cos(\gamma + \alpha_2)]$, which can be written as

$$\Delta^* f_{\max} = (n/\lambda)|\vec{\mathbf{V}}_{\max}|\cos\beta[\sin(\pi/2 - \gamma - \alpha_1) - \sin(\pi/2 - \gamma - \alpha_2)]. \tag{19.9a}$$

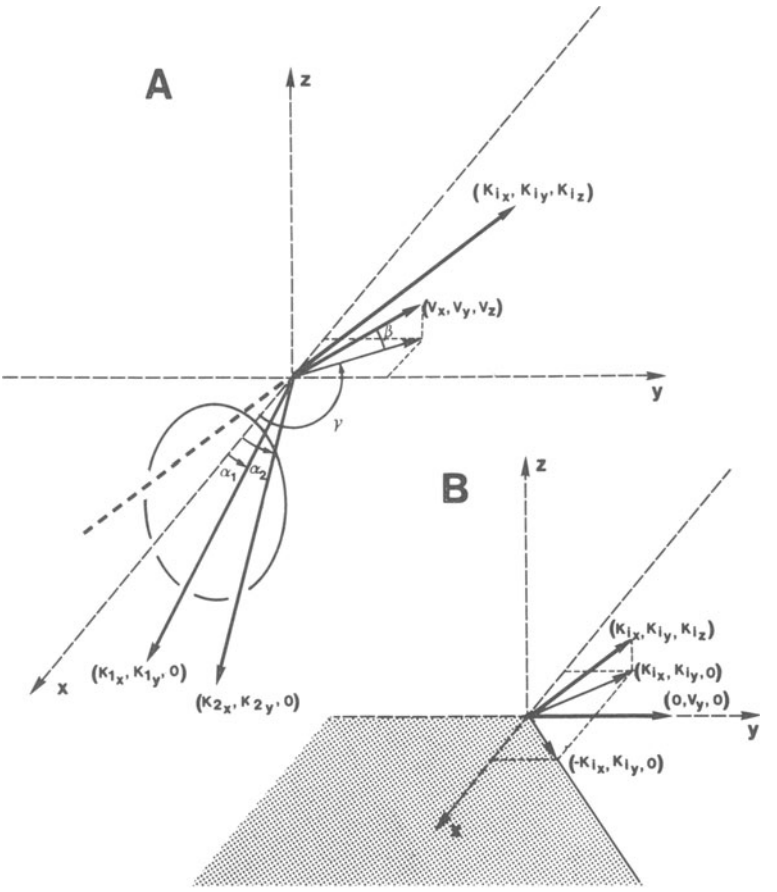

Figure 19–4. A. Bidirectional scattering geometry for measurement of red blood cell velocity in the posterior pole of the eye. Incident beam of direction $\vec{K}_i = (K_{ix}, K_{iy}, K_{iz})$ and scattered beams $\vec{K}_{1s} = (K_{1x}, K_{1y}, 0)$ and $\vec{K}_{2s} = (K_{2x}, K_{2y}, 0)$ are indicated as passing through the pupil of the eye. B. Separation of the (x,y) plane into two regions determined by the direction of zero Doppler shift in the special case of $\vec{V} = (O, V_y, O)$. (From Riva, C.E., G.T. Feke, B. Eberli, and V. Benary. 1979. Appl Optics 18:2301–2306.)

When measurements are performed in vessels at the posterior pole of the eye, γ is approximately equal to $\pi/2$. Therefore, $\pi/2 - \gamma$ is a small quantity. Furthermore, α_1 and α_2 are also small, since they are limited by the size of the pupil. For angles $\pi/2 - \gamma - \alpha_i$ ($i = 1,2$) smaller than 20°, $\sin(\pi/2 - \gamma - \alpha_i)$ can be approximated by $(\pi/2 - \gamma - \alpha_i)$ with an accuracy better than 2%, so that equation 19.9a can be simplified to

$$\Delta^* f_{max} = (n/\lambda)|\vec{V}_{max}|\cos\beta\Delta\alpha, \qquad (19.9b)$$

where $\Delta\alpha = \alpha_2 - \alpha_1$ is the angle between the two scattering directions, and β is the angle between $\vec{\mathbf{V}}_{max}$ and the plane $(\vec{\mathbf{K}}_1, \vec{\mathbf{K}}_2)$. Thus,

$$|\vec{\mathbf{V}}_{max}| = \frac{\lambda \Delta^* f_{max}}{n \Delta a \cos\beta}. \tag{19.10}$$

The LDV instruments that allow the implementation of this bidirectional detection scheme will be described later (see Instrumentation, below).

PROCESSING THE PHOTOCURRENT

For each direction of the scattered light, the photocurrent is amplified and processed for obtaining its DSPS. It is also fed to a loudspeaker and a tape recorder for subsequent analysis. Typically, $\Delta^* f_{max}$ is in the audio range for veins and arteries during diastole. Therefore, during playback, only those portions of the tape are analyzed for which a clearly identifiable pulsatile pitch (for arteries) or a monotonous, high-frequency pitch (for veins) can be heard [15]. These portions correspond to a laser beam that is well focused at the center of the vessel. Until recently, the DSPS were obtained with a hardware spectrum analyzer, one pair at a time, and successively displayed on a oscilloscope screen. An examiner visually determined the cutoff frequency, one channel at a time, by moving a cursor along the frequency axis to the frequency value where a sharp decline in the power spectral density and variance was identifiable. Each estimate of V_{max} (mean and standard deviation) was based on 10 to 20 pairs of DSPS. Such a procedure is time-consuming, especially for retinal arteries for which several V_{max} estimates at different phases of the heart cycle are needed to obtain the exact average blood velocity. In addition, masking of the examiner with respect to the type of patient and experimental protocol is another time-consuming procedure that is needed to eliminate possible bias.

The photocurrent can also be processed with a digital correlator that directly computes the autocorrelation of the photocurrent. This technique was first used to estimate the velocity of blood in a retinal vessel of a human subject [9].

Recently, progress has been made towards on-line, automatic LDV measurements using an array processor coupled with a Masscomp MC5500 computer [16]. A computer algorithm has been developed based on the theoretical model defined by equations 19.6a and 19.6b above. The parallel processing algorithm provides the best fit of this model to a given DSPS using the least-squares criterion. Briefly, this simple model, which is based on single scattering of the laser light by the RBCs, assumes a flat spectral density contribution from DC to some cutoff frequency and includes a constant power spectral density contribution that models the shot noise of the detection system. Under the experimental condition of short measure-

ment time, this model seems to be justified on the basis of previous results obtained in vitro and in vivo [17].

The Masscomp system needs only 80 ms to digitize the signals, calculate the DSPS by fast Fourier transform, and execute the algorithm to determine the cutoff frequency for both scattering directions. At higher cutoff frequencies (large veins) and when the cutoffs are varying in time (arteries), however, this speed is not sufficient to maintain continuous real-time LDV measurements without skipping some of the data. To facilitate measurements in patients, we have adopted an intermittent LDV data collection scheme, where LDV signal acquisition is triggered by the operator to obtain a segment of the entire photocurrent signal for a duration of 3–5 seconds. Analysis of the segment currently takes one to five times as long as the acquisition. During this time, the patient can rest and the operator can replay all the spectra in the segment and review them to determine whether enough data with good laser beam position and focus have been collected from a specific measurement site.

RETINAL BLOOD FLOW

Retinal volumetric blood flow rate is defined as $Q = S\ V_{mean}$, where S is the cross-sectional area of the vessel, which is equal to $\pi D^2/4$, and V_{mean} is the mean velocity of blood. D is usually determined from fundus photographs taken in monochromatic light at approximately 570 nm to obtain the maximum contrast of the blood column relative to the background. The relationship between V_{mean} and V_{max} depends upon the velocity profile of the RBCs, as discussed in detail elsewhere [10].

INSTRUMENTATION

The bidirectional retinal laser-Doppler velocimeter has optical systems to 1) deliver a laser beam to a given site on a retinal vessel, 2) collect the light scattered by the RBCs along two directions, and 3) allow observation of the fundus by the operator. In addition, there is a target for fixation by the subject. The laser delivery and detection systems have been incorporated to a slit-lamp microscope [9,14,18] or a fundus camera [11,19,20].

Laser delivery

The bidirectional LDV system currently used in our laboratory is based on a fundus camera (Topcon, TRC-FE) [20]. Figure 19–5 shows schematically the optical system delivering the laser beam to the retina and collecting the scattered laser light along two directions. When a 0.6328 μm helium–neon laser beam is used (for example, a 0.8 mW, Uniphase 1107P, linearly polarized, diameter 0.5 mm), this beam is first expanded with a 4x expander (EXP, Physitech Corp). This expansion is not necessary, however, if an infrared diode laser with built-in collimator (such as SFS22, linearly polarized, Micro Laser Systems, Garden Grove, CA) provides the incident beam, since this beam is already 2 mm in diameter at the exit of the device.

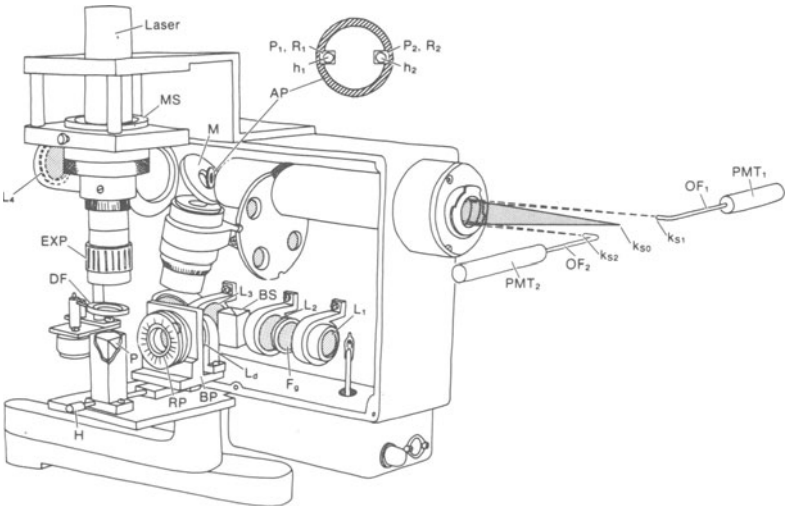

Figure 19–5. Fundus camera based bidirectional LDV system. See text for details. (From Riva, C.E., B.L. Petrig, R.D. Shonat, and C.J. Pournaras. Appl Optics 28:1078–1083, 1989.)

The laser beam is attenuated in intensity by a neutral density filter (DF) mounted on a rotary solenoid, deflected horizontally by a prism (P), and transmitted through a rotatable biprism (RP) with continuously variable refractive power and a lens (L_d, focal length 54 mm). It is then deflected into the illumination system of the fundus camera by a cube beamsplitter (BS) placed between lenses L_2 and L_3. RP lies in a plane conjugated to the pupil of the subject's eye. RP and L_d are mounted on a baseplate (BP) that, using handle (H), can be moved precisely along the optical axis to focus the laser beam at the retina (range −4 to +4 diopters). The beam propagates along an axis parallel to the optical axis of RP and L_d at a distance of 5.5 mm. A mechanical system (MS) allows its eccentric rotation around the axis so that the operator can direct it at the appropriate location of the subject's pupil within the annulus of light produced by the fundus illumination of the cornea. Accurate aiming of the beam at any location of the retina is achieved by rotating the RP and varying the refractive power of the prism. Conceptually, this has the same effect as if the laser beam could be pivoted around a point within the pupil and aimed at any retinal location. The fundus is illuminated in green light by inserting an appropriate filter (F_g), such as Kodak No 57A, between lenses L_1 and L_2.

Bidirectional light-collecting system

This system collects the scattered laser light and focuses it in the retinal image plane of the fundus camera. The two scattering directions are extracted from the scattered light by means of the following optical scheme: In a plane

conjugated to the subject's pupil and lying just behind the hole in the mirror (M), a circular aperture (AP) (10.5 mm in diameter) has been inserted. At the periphery of AP, two small prisms (P_1, P_2) have been mounted along a diameter. These prisms cover two holes (h_1, h_2, 2 mm in diameter), which are themselves covered by red filters (R_1, R_2, Kodak No 29). The laser beams transmitted through h_1 and h_2 are the scattered beams $\vec{\mathbf{K}}_1$ and $\vec{\mathbf{K}}_2$. These beams can be identified in the retinal image plane from the rest of the incident light which is focused at k_{s0}, the image of the incident laser focus at the retina, because P_1 and P_2 shift their locations in this plane by approximately 0.5 mm in opposite directions (figure 19–5, points k_{s1} and k_{s2}). AP can be rotated to align the scattering plane with the direction of the vessel to set $\cos\beta$ in equation 19.10 equal to unity. Two optical fibers (OF_1, OF_2, 400 μm in diameter), bent at 90°, collect the light at k_{s1} and k_{s2} and guide it to photomultipliers PMT_1 and PMT_2 (Hamamatsu R1463), respectively. Each fiber and its corresponding PMT have been mounted on a x-y microstage. The operator observes the fundus through a 10x eyepiece and places the tip of the fibers on k_{s1} and k_{s2}. Detecting the scattered laser light in the image plane of the camera prevents detection of laser light scattered by the ocular media and fundus structures different from the RBCs and vessel wall at the measurement site.

The fixation target is the exit of a 50 μm optical fiber that can be moved precisely in x-y-z directions behind lens L_4 (for precise positioning and focusing at the subject's retina). The fiber is illuminated by a helium–neon laser (not shown). The target appears as a speckled pattern and the subject is asked to fixate at one of the speckles.

With this optical scheme, V_{max} is calculated from the formula [19]

$$V_{max} = \frac{\lambda l}{nd} \Delta^* f_{max}, \tag{19.11}$$

where l (mm) is the axial length of the eye and d (mm) the distance between the centers of the images, at the cornea, of the holes h_1 and h_2, projected in the pupil. With $\lambda = 6328 \cdot 10^{-7}$ m (helium–neon laser), $n = 1.336$ = index of refraction of the vitreous, and choosing for d the maximum possible value of 2.3 mm that is achievable with the Topcon fundus camera, equation 19.11 becomes

$$V_{max}(\text{mm/s}) = 0.21\ e\Delta^* f_{max}(\text{kHz}). \tag{9.12}$$

Equation 19.12 is valid for emmetropic eyes and those with axial ametropia, the most common form of ametropia. It shows that the only ocular measurement required to determine V_{max} is the axial length of the eye, a measurement that can be performed routinely by A-scan ultrasonography.

Other bidirectional LDV systems

Laser delivery and bidirectional direction optical systems have been adapted to slit-lamp biomicroscopes [14,18]. Although, in principle, they offer the

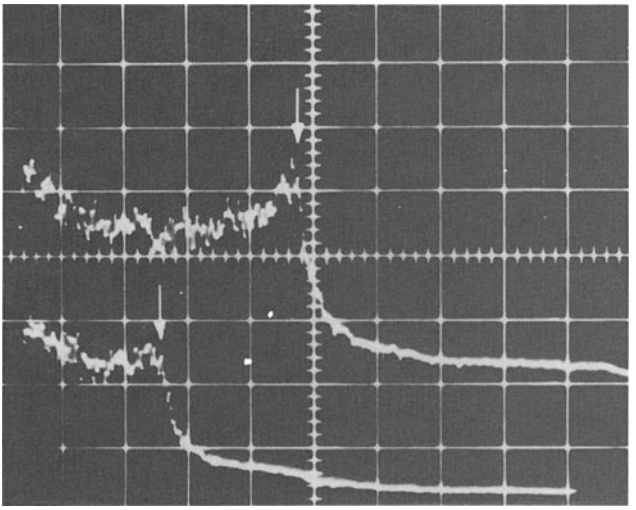

Figure 19–6. Doppler shift power spectra (DSPS) from 0.3 μm polystyrene spheres suspended in water flowing through a 200 μm internal diameter glass capillary tube. The tube was mounted in the focal plane of a Topcon model eye. Arrows indicate the cutoff frequencies, Δf_1 and Δf_2.

advantage of larger scattering angles than those obtainable with fundus cameras, the system presently in use [18] is adequate only for measurements of vessels making an angle of 70° or less with the horizontal. For bigger angles, the scattering angle becomes too small to provide accurate velocity measurements. This system could be improved by enabling rotation of the detection system to align the plane containing both scattering directions with the direction of the velocity vector at the site of LDV measurements. Another disadvantage of these slit-lamp LDV systems is that they require placing a contact lens on the cornea of the tested eye, with the risk of producing corneal abrasion.

EXPERIMENTAL VERIFICATION

Illustration of the bidirectional LDV technique: flow of polystyrene spheres in small tubes

Through a capillary tube (diameter = 200 μm) placed on the retinal plane of a Topcon model eye, polystyrene spheres (diameter = 0.3 μm) suspended in water, were passed at known V_{max}. The incident laser beam was focused at the center of the tube. The DSPS recorded for the two scattering directions are shown in figure 19–6. They are characterized by very sharp cutoffs from which V_{max} can be accurately determined. The increase in spectral power in the region of the cutoff frequency is due to the nonuniform illumination of the tube by the laser beam, which was smaller than the tube internal dia-

meter. As a result, the faster particles received more light than the slower ones close to the vessel wall.

Doppler-shift power spectra from blood in retinal vessels

Equation 19.12 is based on a model that assumes single scattering of the incident laser light by the RBCs. The validity of this assumption, however, may be questionable in the context of previous studies that demonstrate a predominance of multiple scattering when visible light interacts with whole blood. A blood layer of 100 μm has a calculated optical depth of approximately 0.9 at $\lambda = 0.63$ μm, a value for which multiple scattering is important [21]. At this wavelength, the photon mean free pathlength is only 7 μm [22], which is comparable to the diameter of an RBC. Thus for retinal vessels with diameters typically between 50 and 200 μm, photons would be expected to have undergone a great number of scattering events and consequently of Doppler shifts before being detected.

DSPS recorded from retinal vessels generally do not exhibit the ideal rectangular shape, and the cutoffs are usually less clear than those from polystyrene spheres, particularly so for the DSPS from the large retinal vessels. The sharpness of the cutoffs can be improved by recording the DSPS in short timespans, i.e., less than 0.2 sec [17]. Recent studies in cats [22] have shown that ideal rectangular shape can be obtained from vessels less than approximately 120 μm diameter if one can prevent detection of light that has been doubly transmitted through the vessels. In this case, the predominant process is single backscattering. For vessels bigger than about 120 μm, single backscattering becomes less predominant than multiple backscattering, with ensuing degradation of the quality of the cutoffs.

The cat retina offers the unique opportunity to record DSPS arising from two different scattering processes. Double forward scattering is predominant when the incident laser beam is focused on a retinal vessel coursing in front of the tapetum, a highly reflecting layer (figure 19–7). Laser light transmitted through such a vessel is retransmitted through it after reflection at the tapetum. This doubly forward transmitted light involves predominatly multiple scattering of light by the RBCs. Laser light detected from these vessels is depolarized, and the corresponding DSPS appear to have an exponential shape (figure 19–8A). This shape does not vary with the scattering angle. Such DSPS conform to the theory of Bonner and Nossal [23], in which multiple scattering is dominant.

In the lower part of the cat's eye, the retinal vessels course in front of a heavily pigmented layer that absorbs nearly all the incident laser light transmitted through the vessel. Only light backscattered by the RBCs and vessel wall can reach the photodetectors. In this case, the detected light maintains most of the polarization of the incident light. The DSPS have the rectangular shape and a sharp cutoff that varies with the scattering angle as expected from the Doppler formula (figure 19–8B). The detected light mainly consists

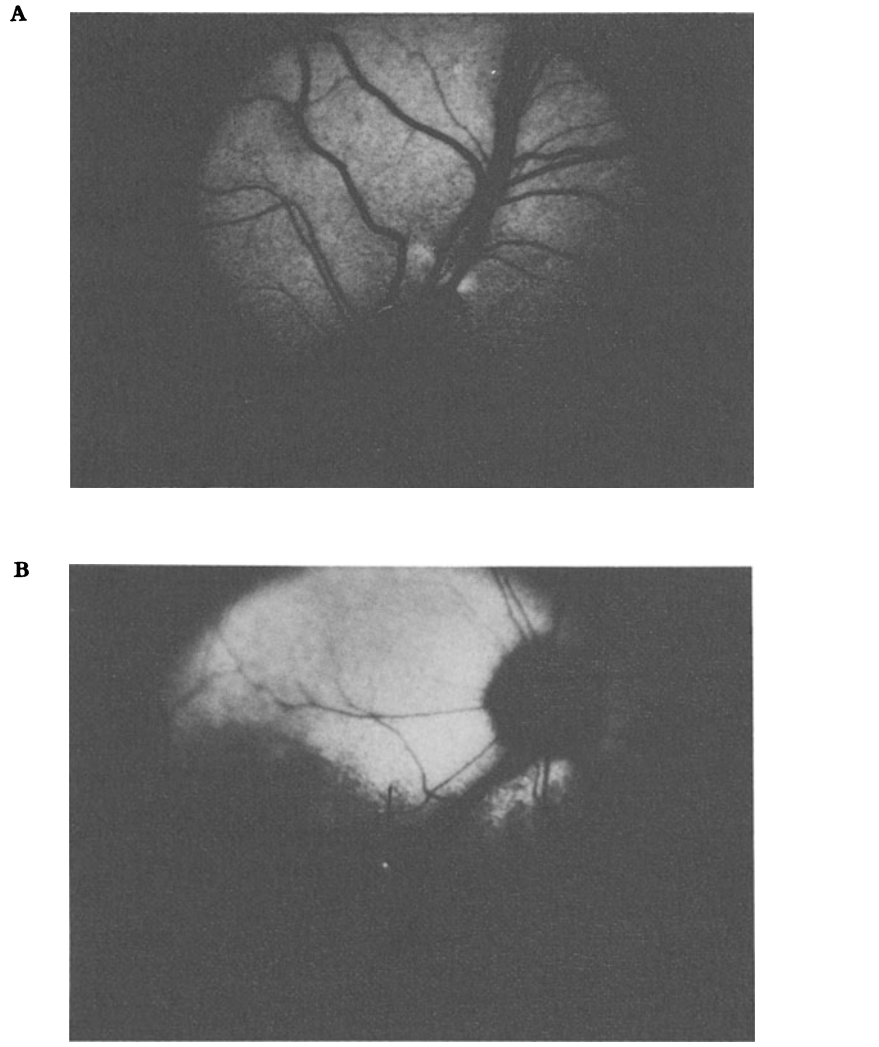

Figure 19–7. Photograph of the fundus of a cat. The superior part of the fundus (A) is the region of the retina containing the highly light-reflecting tapetum, while the inferior part (B) contains the strongly light-absorbing pigment. A laser beam focused on a vessel in front of the tapetum (arrow) appears highly diffuse due to a second transmission of the light through the vessel after reflection at the tapetum (A). In contrast, the image (arrow) of a beam focused on a vessel in front of the highly light-absorbing pigment is sharp and is predominatly due to light backscattered by the red blood cells (B). (From Riva, C.E., B.L. Petrig, R.D. Shonat, and C.J. Pournaras. Appl Optics 28:1078–1083, 1989.)

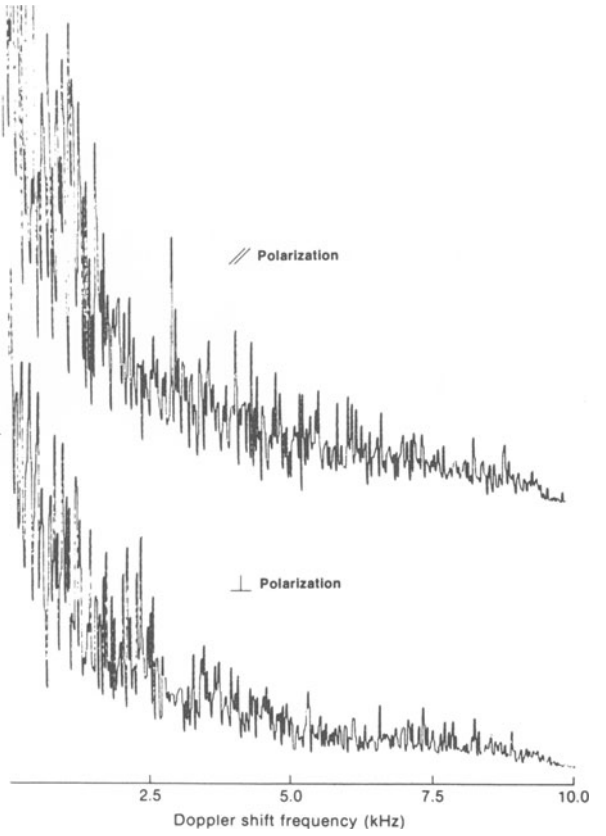

Figure 19–8A. Doppler shift power spectra (DSPS) obtained from a vein in the tapetal region of the cat retina. For the upper DSPS, the scattered light was detected in the same plane of polarization (//) as the incident light. For the lower DSPS, these polarizations were perpendicular (⊥). Light transmitted through the blood column is highly reflected and some of it is retransmitted through the blood. This doubly transmitted light represents predominantly multiply scattered light. (From Riva, C.E., B.L. Petrig, R.D. Shonat, and C.J. Pournaras. Appl Optics 28:1078–1083, 1989.)

of singly backscattered light, or if one uses the expression introduced by Stern [24], of pseudo-singly backscattered light. These results imply that for vessels with diameters up to at least 120 μm, multiple backscattering has a negligible effect on the DSPS.

DSPS from human retinal vessels

In order to test the performance of the model-derived cutoffs, we compared $\Delta^* f_{max}$ values determined from the same DSPS pairs by the computer algorithm and by the trained examiner. One hundred and six pairs of DSPS

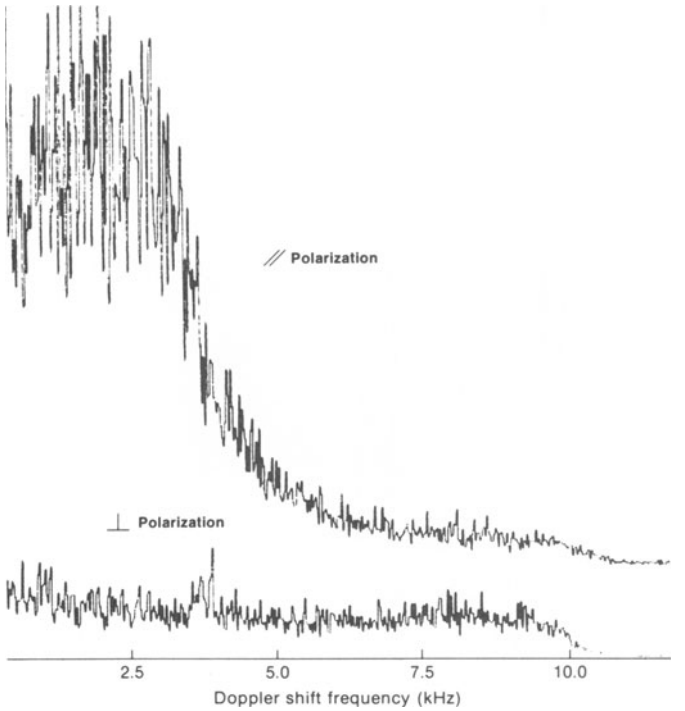

Figure 19–8B. DSPS from a vein in the pigmented region of the cat's retina. Notice the disappearance of the spectral power associated with red blood cell motion when the polarization of the scattered light is perpendicular (⊥) to that of the incident light. For vessels above the pigment, only the light backscattered by the blood column reaches the detector. Light transmitted through this column is totally absorbed by the pigment behind the vessel. (From Riva, C.E., B.L. Petrig, R.D. Shonat, and C.J. Pournaras. Appl Optics, 28:1078–1083, 1989.)

were obtained from volunteers to establish this comparison. A typical pair of DSPS is shown in figure 19–9A. Data from different-size veins were used to include a large range of cutoff frequency values. The correlation between both methods is excellent, as shown in figure 19–9B. The computer model analysis yields values slightly higher than the observer (+10, +4, and +1.7% at 5, 10, and 15 kHz, respectively).

Retinal LDV in animals and human subjects

The precision and short-term reproducibility of the LDV technique is best demonstrated by a recording of $\Delta^* f_1 \propto V_{max}$ obtained from a retinal arteriole in an anesthetized miniature pig (figure 19–10A), in which the eye was immobilized by sutures at the limbus. After a short period of air breathing, the animal was given 100% oxygen to breathe. A unidirectional

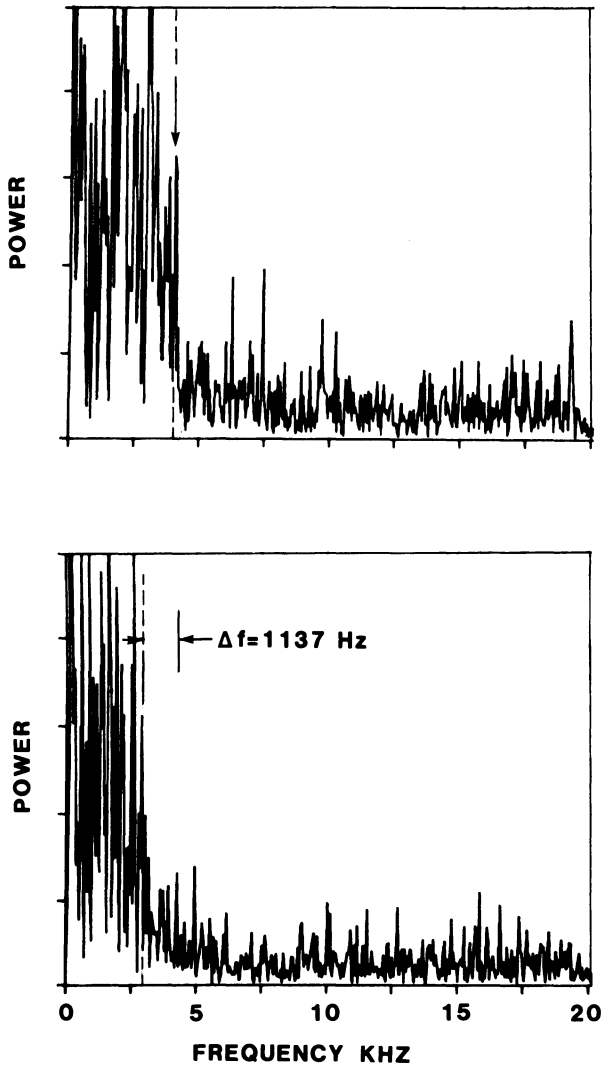

Figure 19–9A. A pair of DSPS from a retinal artery of a normal human subject. Both spectra were recorded simultaneously during diastole. Time window: 0.1 second. Frequency range: 0–20 kHz. The cutoff frequencies are indicated by arrows. (From Riva, C.E., J.E. Grunwald, S.H. Sinclair, and B.L. Petrig. 1985. Invest Ophthal Vis Sci 26:1124–1132.)

LDV signal was recorded on magnetic tape and subsequently played back at $\frac{1}{8}$ the recording speed and analyzed by means of the Masscomp MC5500 system. In the unfiltered version of the output Δf_1 signal, one observes the presence of large differences between the systolic and diastolic Δf_1, from

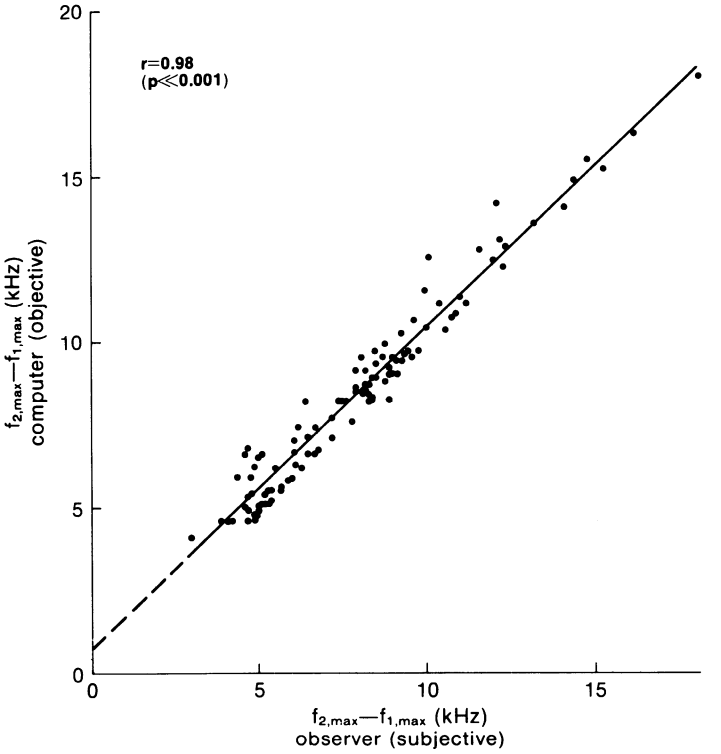

Figure 19–9B. Correlation between cutoff frequency determined by visual inspection of the DSPS and by computer. ($f_{2,max} - f_{1,max} = \Delta^* f_{max}$)

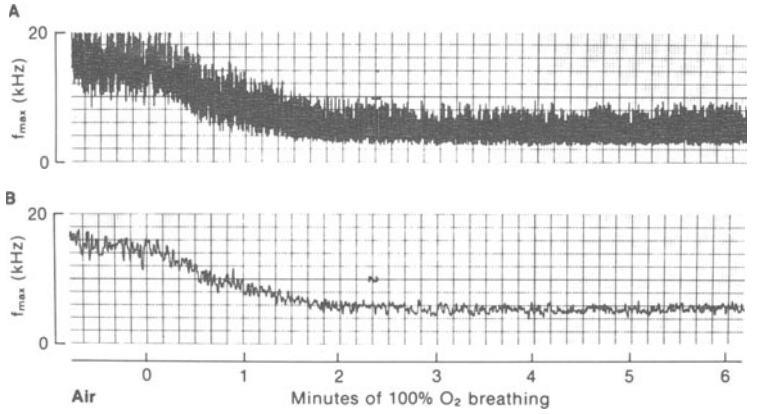

Figure 19–10. Recording of relative blood velocity, f_{max} (= Δf, in text), in a retinal artery of an anesthetized miniature pig when the breathing gas mixture is changed from air to 100% oxygen. The diastolic and systolic variation of the velocity (A) and the time average of this relative velocity (B) are presented. After about two minutes of inhaling pure oxygen, a new equilibrium is reached at a value 60%–72% below baseline. (From Petrig, B.L., and C.E. Riva. 1988. Appl Optics 27:1126–1134.)

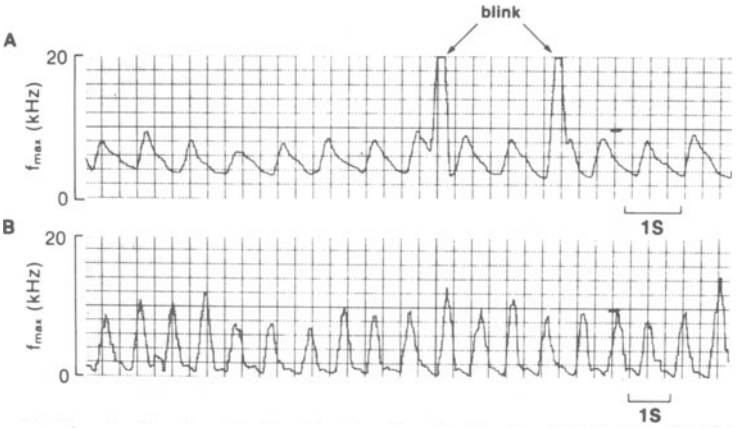

Figure 19–11. Relative red blood cell velocity in a human retinal artery at rest (A) and at an intraocular pressure elevated to a value close to diastolic ophthalmic artery pressure by means of a scleral suction cup (B). The velocity at diastole is reduced to about zero, while the same at systole is increased over its baseline value, suggesting that the retinal vasculature is counteracting the change in perfusion pressure. Nevertheless, time-average velocity is decreased. (From Petrig, B.L., and C.E. Riva. 1988. Appl Optics 27:1126–1134.

which one can determine the velocity pulsatility. By averaging Δf_1, a smooth recording of the time course of relative V_{max} is obtained (figure 19–10B). This example demonstrates that LDV can provide precise, continuous measurement of rapid blood velocity transient in animals.

Measurements performed in a healthy human subject with good target fixation, at resting and elevated intraocular pressure also demonstrate a stable diastolic V_{max} (figure 19–11). Figure 19–12 shows the effect of an acute elevation of the intraocular pressure, induced with a scleral suction cup on absolute V_{max} in a retinal vein of a normal volunteer. V_{max} was obtained in real time. The baseline shows some fluctuations around a value of 1.5 cm/sec. When the intraocular pressure is raised to 38 mmHg, V_{max} drops to around 0.5 cm/sec. At an intraocular pressure equal to that of the diastolic blood pressure in the ophthalmic artery, V_{max} is practically down to zero. After the suction is removed, V_{max} jumps to 2.5 cm/sec and then returns to baseline value within approximately one minute.

These examples demonstrate the potential of LDV for investigating retinal blood flow regulation in response to various physiological stimuli. Since this topic is beyond the scope of this chapter, we will only mention that a number of articles have reported on the effect of hyperoxia [25,26], acute raise of blood pressure [27], acute raise of intraocular pressure [28], and changes in retinal illumination [29,30] on retinal blood flow in normal subjects using LDV.

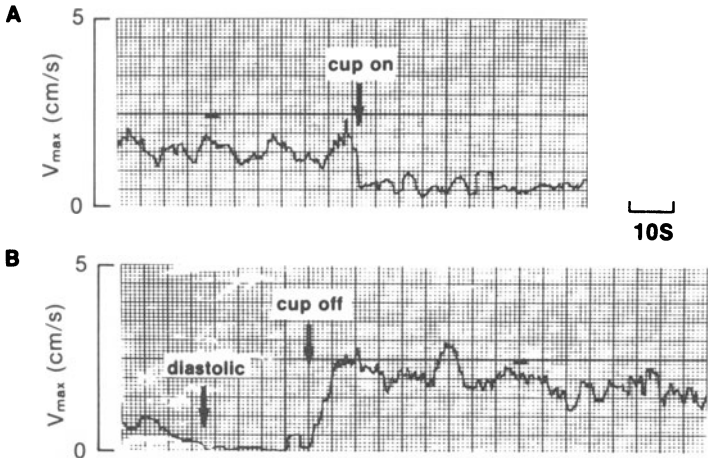

Figure 19–12. Effect of acute elevation of intraocular pressure (IOP) on blood velocity in a human retinal vein. On-line absolute measurements of V_{max} are shown before and after an acute IOP increase induced by suction cup (A) and before and after releasing the suction (B). V_{max} decreases from approximately 1.5 to 0.5 cm/sec after pressure elevation to 38 mmHg (A). Raising the IOP to diastolic (B) causes V_{max} to approach zero. After the cup is released, V_{max} quickly increases to 2.5 cm/sec and returns to baseline after approximately one minute. (From Petrig, B.L., and C.E. Riva. 1988. Appl Optics 27:1126–1134.)

CLINICAL APPLICATIONS

Investigation of the ocular circulation provides information on the impact and extent of ocular and systemic diseases on the visual system. Measurements of the hemodynamic changes that occur in different ocular diseases are important because they may lead to a better understanding of the pathophysiology involved. Knowledge of these changes may help us devise better treatment modalities and test the effect of surgical and pharmacological treatment on the ocular circulation.

Diabetes mellitus is one of the main causes of visual impairment. One of the earliest events occuring in this disease is retinal venous dilatation (figure 19–13A), which is later accompanied by vascular occlusion [31]. Other hemodynamic alterations also take place. Blood velocity measured in major retinal veins and arteries of eyes of diabetics is significantly slower than that of age-matched normal individuals [32] (figure 19–13B). This decrease is probably due to closure of some retinal capillaries and rheological changes. Retinal blood flow, however, is not significantly different from normal (figure 19–13C). The mechanism by which blood flow is maintained normal remains to be established. Blood flow pulsatility, $1 - \frac{V_{max,diast}}{V_{max,syst}}$ on the other hand, is increased in severe diabetic retinopathy, probably as a consequence of the vasodilatation [33].

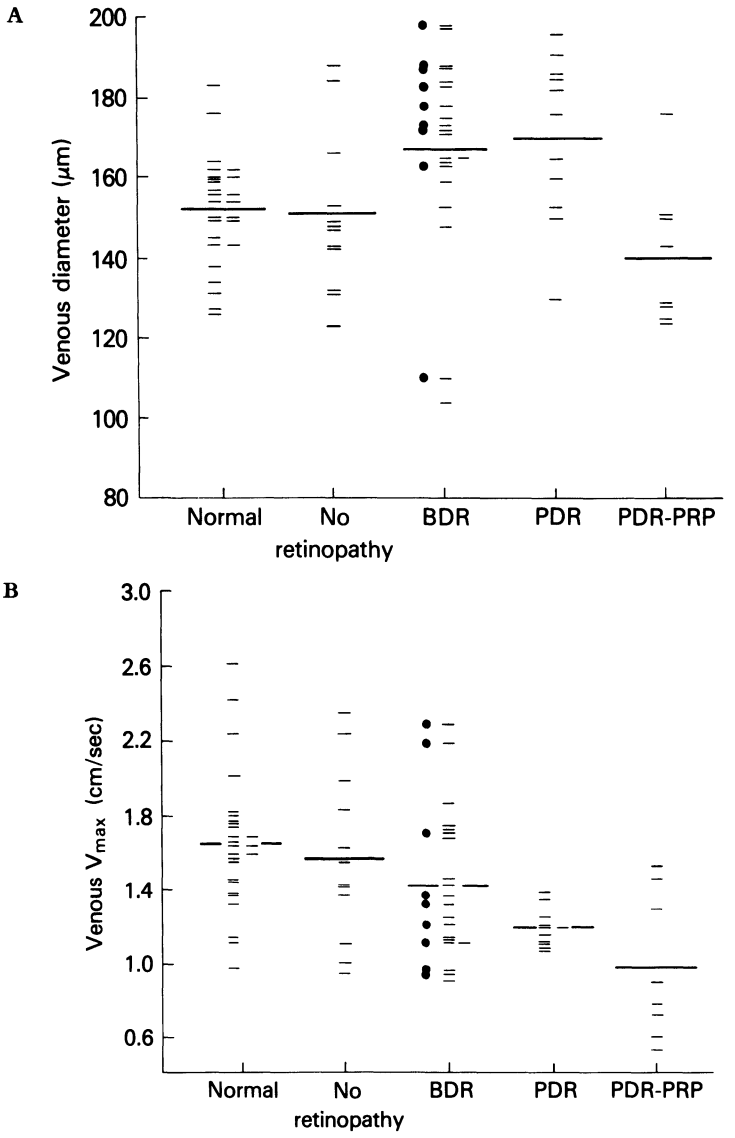

Figure 19–13. A. Diameter of main superior or inferior temporal retinal veins of normal subjects and patients with diabetes (various degrees of retinopathy). BDR indicates patients with background retinopathy; PDR, patients with proliferative retinopathy; and PDR-PRP, patients with PDR treated by panretinal photocoagulation. B. V_{max} measured at the site of diameter measurements. C. Volumetric blood flow rate, Q, obtained using the relationship $Q = \frac{V_{max}}{1.6} \times \pi D^2/4$. Large horizontal bars represent the average value for each group. In BDR, results marked with dot correspond to eyes with severe background retinopathy. (From Grunwald, J.E., C.E. Riva, S.H. Sinclair, A.J. Brucker, and B.L. Petrig. 1986. Arch Ophthalmol 104:991–996.)

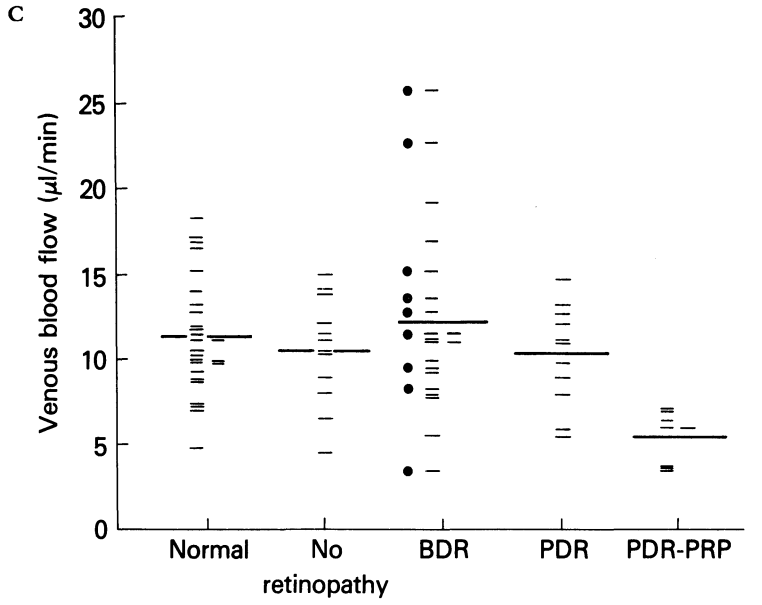

Figure 19–13. (Continued)

Because blood flow is maintained close to normal values in the diabetic retina, it is important to investigate the regulatory capacity of the retinal circulation. A convenient way to test this capacity is to stress the retinal circulation by having subjects breathe 100% oxygen at atmospheric pressure for five minutes and measure the change in blood flow (hyperoxia response). In the normal subject, this maneuver decreases blood flow by about 60% [25]. This response is abnormal in diabetic patients and diminishes in magnitude with the progression of diabetic retinopathy (figure 19–14) [34]. Interestingly, it improves following laser panretinal photocoagulation therapy [35] (figure 19–14, PDR–PRP). This abnormal response may be related to the retinal hypoxia and ischemia that presumably are present in the diabetic retina with retinopathy. Its improvement following photocoagulation is probably due to the improvement in oxygen supply to the remaining retina due to the treatment [35]. Eyes that showed regression of neovascular proliferation after photocoagulation had a more normal regulatory response than those in which proliferation continued [36]. It is possible that retinal hypoxia was not fully relieved by treatment in the latter cases.

Another LDV investigation in diabetic patients has shown that retinal blood flow is elevated in poorly controlled diabetics with high blood-glucose levels [37]. However, normalizing blood glucose by insulin administration reduces retinal blood flow and improves the hyperoxia response. These hemodynamic and regulatory changes could play a role in the development

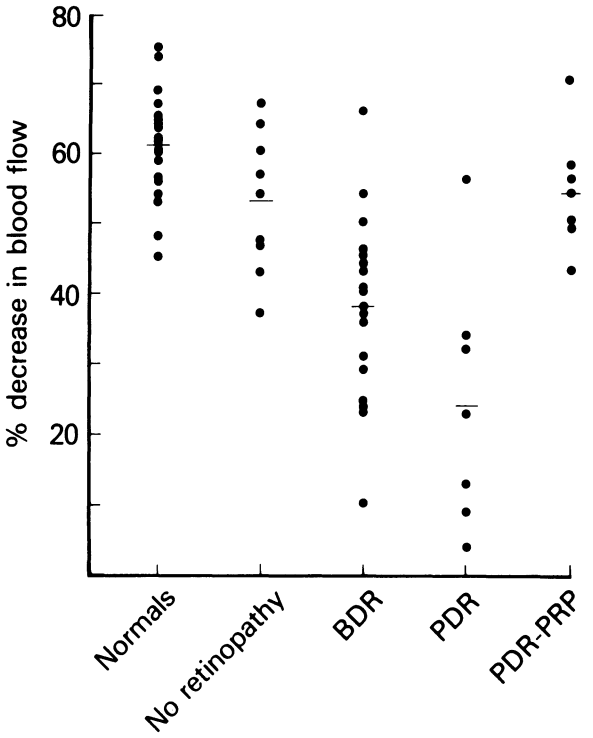

Figure 19–14. Percent decrease in blood flow at five minutes of 100% oxygen breathing in normal subjects and diabetic patients. Horizontal bars represent the average for each group of subjects. (From Grunwald, J.E., C.E. Riva, A.J. Brucker, S.H. Sinclair, and B.L. Petrig. 1984. Ophthalmology 91:1447–1452.)

of retinal ischemia and the appearance of nerve fiber layer infarcts described in patients following the institution of strict diabetic metabolic control.

LDV can also been used to determine the effect of pharmacological agents on retinal blood flow. For example, administration of topical 0.5% timolol maleate, a drug widely used for the treatment of glaucoma, was found, two hours after the instillation of the drug, to increase blood velocity and blood flow by an average of 11% and 13%, respectively [38].

Other retinal blood flow LDV studies performed on a limited number of patients have included measurements in patients with retinal vein occlusion [39], ocular hypertension [40] and scleral buckling procedures [41].

FUTURE DIRECTIONS FOR RETINAL LDV

As indicated earlier, the signal-to-noise ratio of the DSPS increases linearly with the retinal irradiance of the laser light. It is therefore advantageous to use as much light as possible within the limit imposed by the guidelines on

maximum permissible levels of retinal irradiance. Assuming that photodetectors of similar sensitivity are used, these guidelines show that there is considerable advantage to using lasers in the near-infrared region of the spectrum. At such wavelengths, the maximum permissible exposure for continuous illumination is at least 20 times higher than at the wavelength of the helium–neon laser [42]. The feasibility of LDV measurements in the near-infrared has been demonstrated recently [20]. Diode lasers with collimating optics have been used at wavelengths of 750, 785, and 810 nm.

Routine clinical applications of the LDV technique will require improvements in speed and automation of the LDV recordings to minimize cost and patient fatigue and to maximize the number of vessels that can be measured. Automated data collection and analysis reduce the number of people needed to obtain the desired information and ensure standardization of the technique. Clearly, stabilization of the laser beam on a given measurement site would considerably decrease the measurement time. Another approach that does not require stabilization of the laser beam is to use computer algorithms that identify those times during which the laser beam is appropriately centered on the vessel and to extract only those V_{max} values recorded during this time. Such algorithms are being developed [16].

LDV MEASUREMENTS FROM THE OPTIC NERVE AND CHOROID

The application of LDV to the study of hemodynamics in the optic nerve head tissue was first proposed by Riva, Feke, and Loebl [43] subsequent to the pioneering article by Stern [44] who proposed using LDV to measure blood flow in the tissue of the skin. Riva et al. [43] detected all the scattered light reaching the entrance pupil of the camera with a single optical fiber to record DSPS from discrete sites of the optic nerve head tissue. The beam from a helium–neon laser was focused onto areas approximately 200 μm in diameter, where no discrete blood vessels were visible when the optic nerve was observed in red free light. Figure 19–15 displays a typical DSPS recorded from the temporal rim of the nerve head of a normal volunteer, at normal intraocular pressure (IOP). Most of the spectral power is concentrated below 300 Hz. The shape of the DSPS recorded from normal volunteers could be best fitted by a log $\alpha/\Delta f$ function, where $\alpha = 2 V_{max}/\lambda$, according to the theoretical model of Stern and Lappe [45]. This model assumes that RBC speeds are distributed uniformly up to a value V_{max} and are equal to zero for $V > V_{max}$ and that the scattering by the RBCs and tissue is isotropic. Furthermore, the detection of the DSPS is achieved by heterodyne mixing of light scattered from the tissue (reference beam, local oscillator) with light scattering by the RBCs.

The spectral power at frequencies below 50 Hz was generally not used for determining the logarithmic fit because it was found to be affected by eye motion. Values of α obtained from normal volunteers lead to estimates of V_{max} of the order of 0.12 to 0.2 mm/sec, suggesting that the scattered light

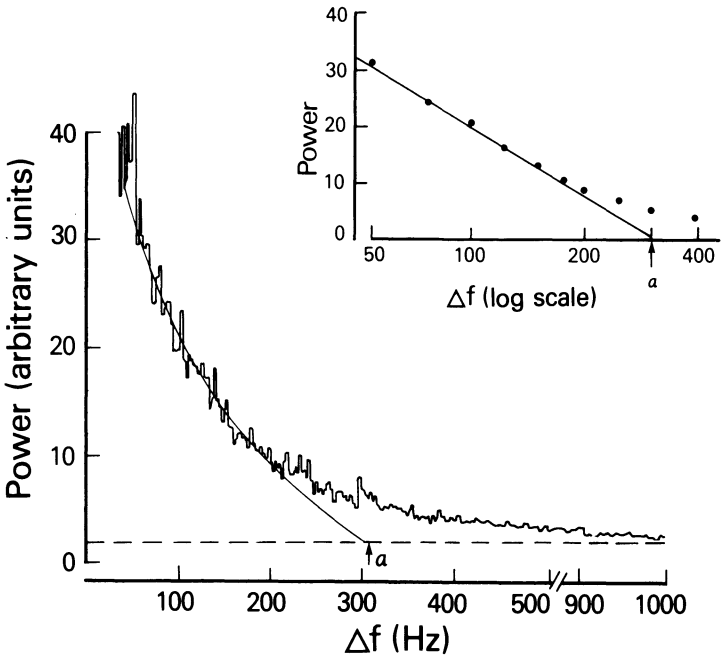

Figure 19–15. DSPS from the temporal rim of the optic nerve head of a normal subject and its logarithmic fit. The baseline is determined by the shot-noise level of the photodetector. α is the frequency at which the logarithmic fit (solid line) intersects the baseline (dashed line) and is proportional to the speed of the red blood cells. Inset: DSPS replotted on a semilogarithmic scale to evaluate the frequency at which the data points depart from a straight line. (From Riva, C.E., J.E. Grunwald, and S.H. Sinclair. 1982. Invest Ophthalmol 82:241–248.)

is detected predominantly from RBCs flowing in the microvessels of the optic nerve tissue.

Illustration of the technique: effect of increased intraocular pressure

Figure 19–16 shows the effect on the DSPS of sudden, acute increases of the intraocular pressure (IOP) from normal value (15 mmHg) to various IOPs, plotted as a function of $\log(\alpha/\Delta f)$ [46]. Recording time of each DSPS was 20 seconds, except for the DSPS recorded at systolic pressure (6 seconds). With IOP elevation, the speed of the RBCs decreased markedly. Most of the spectral power of the DSPS recorded at systolic pressure is probably due to eye motion.

If the IOP is rapidly increased above normal, kept approximately constant for a few minutes and then rapidly decreased below normal, α varies as shown in figure 19–17. With IOP elevation, the speed decreases markedly. It then increases toward normal and reaches a constant level within approximately 2–3 minutes, while the IOP is still elevated. Release of the pressure

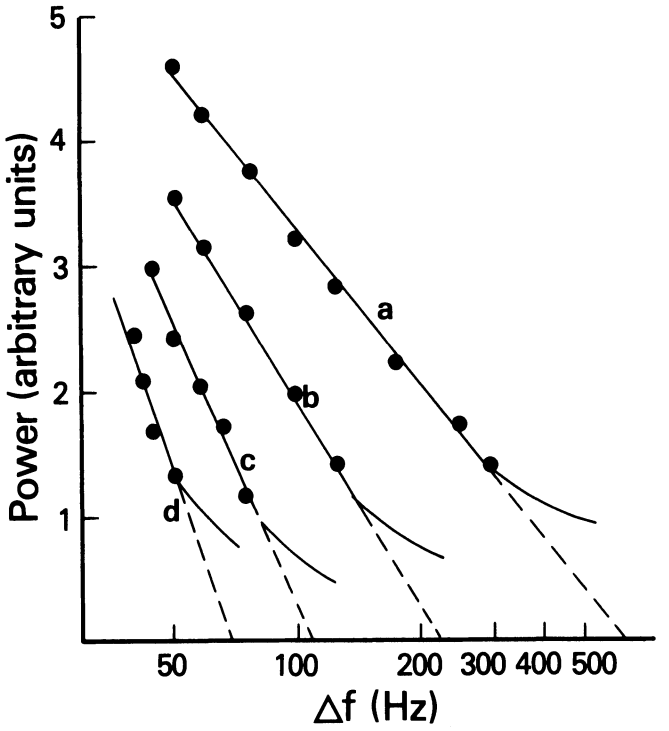

Figure 19–16. Effect of acute increases in intraocular pressure (IOP) on DSPS from optic nerve head. The DSPS are plotted as a function of logΔf. Curve (a) corresponds to normal IOP, (b) to 38 mmHg, and (c) and (d) to diastolic and systolic ophthalmic artery pressure, respectively. (From Riva, C.E., J.E. Grunwald, and S.H. Sinclair. 1982. Invest Ophthalmol 82:241–248.)

causes a rapid drop of the IOP that is accompanied by a marked increase in RBC speed above baseline. Within minutes, however, the speed returns to normal. The 45% increase in speed occurring between 15 seconds and 3 minutes after the step elevation of the IOP in spite of a 15% decrease in perfusion pressure (ophthalmic artery pressure minus IOP), represents an autoregulatory response of the optic nerve head circulation. Similarly, the decrease in speed occuring after release of the pressure cup (between 7 and 9 minutes) strongly suggests the presence of an autoregulatory response because the magnitude of this response (25%) cannot be due to the 4% decrease in perfusion pressure ocurring during this interval of time.

With this technique, the value of α depends upon the choice of the frequency range used in fitting a logarithmic function to the recorded curve. Because eye movements give rise to spectral components in the DSPS up to about 50 Hz, the frequency range to determine α must start at a frequency above this value. This limitation prevents measuring low flows with accur-

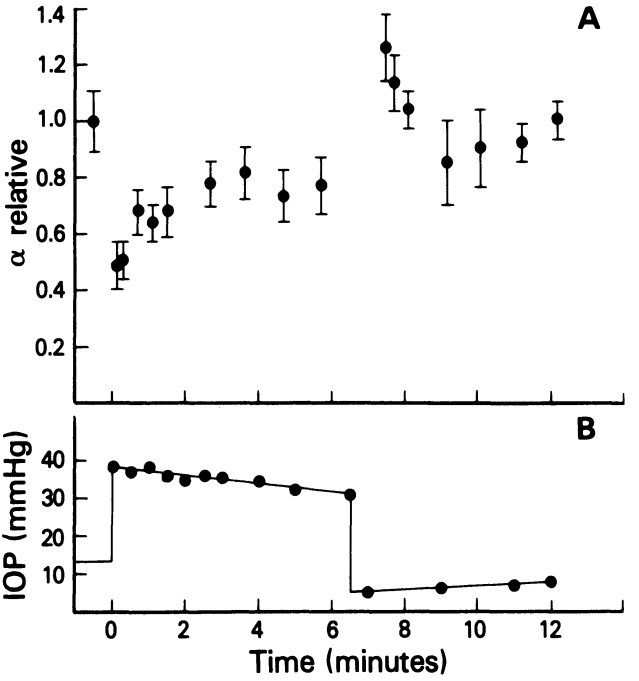

Figure 19–17. A. Relative variation of α, as a function of time, when the IOP is varied, as shown in (B). Error bars are ±1 S.D. calculated from data obtained from identical experiments conducted in the same normal subject on three separate occasions. (From Riva, C.E., J.E. Grunwald, and S.H. Sinclair. 1982. Invest Ophthalmol 82:241–248.)

acy. For instance, at high intraocular pressure most of the spectral power is below 50 Hz.

Previously, investigators using LDV for the optic nerve head have concentrated their efforts only on the changes in velocity of the red blood cells [46,47]. The laser-Doppler signal, however, contains additional information on the volume of blood contained in the illuminated tissue. To obtain recordings of blood flow by combining velocity and volume measurements, we have adapted the TSI LaserFlo instrument (Blood Perfusion Monitor, BPM403) to the LDV fundus camera [48]. Figure 19–18 shows preliminary measurements obtained from the optic nerve head tissue of a cat under two conditions: CO_2 breathing (figure 19–18A) and transient bilateral carotid occlusion (figure 19–18B). An optical detecting fiber was placed approximately 150 μm away from the illumination spot of the incident beam (helium–neon laser).

Potentially, the most important clinical application of this technique is in the field of glaucoma, a disease that affects a large number of elderly people and that manifests itself by gradual and irreversible loss of vision. The

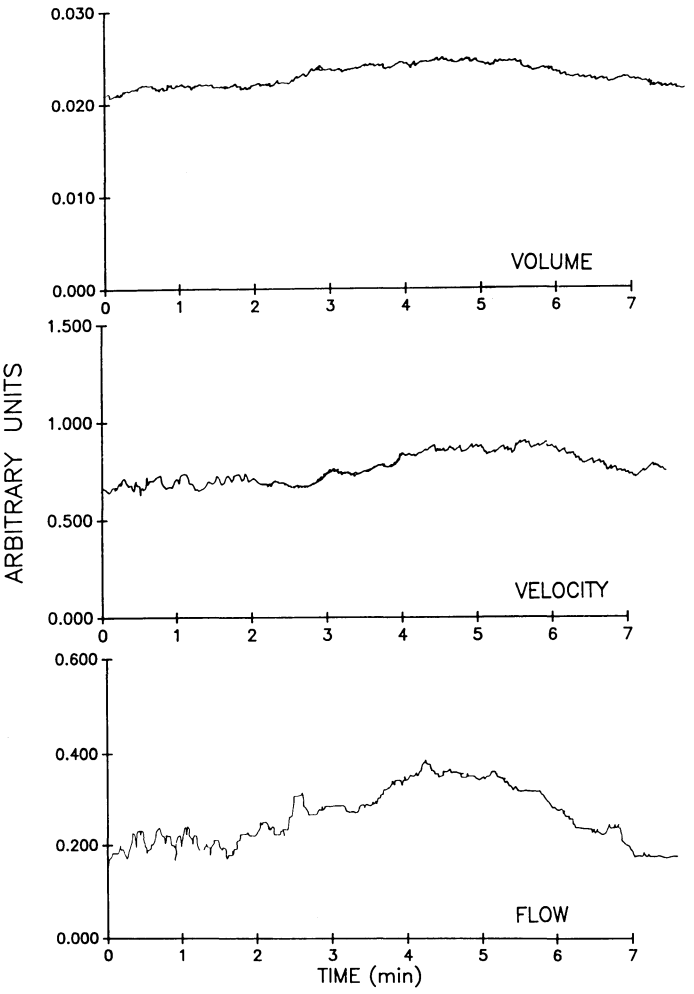

Figure 19–18A. Continuous recording of volume, velocity, and flow from the optic nerve head of the cat during approximately four minutes of CO_2 breathing followed by a return to normal air. CO_2 was started at time zero.

pathogenesis of this disease is still controversial, and the role of the circulation in the optic nerve head is not clear. An objective, precise, and noninvasive technique is needed to clarify the role of optic nerve head blood flow in this disease.

Rhythmic variations in optic nerve head and choroidal blood flow

Continuous recordings of the velocity, volume and flow of blood in the optic nerve head of anesthetized minipigs using the TSI LaserFlo instrument showed rhythmic variations of these parameters at a frequency of approx-

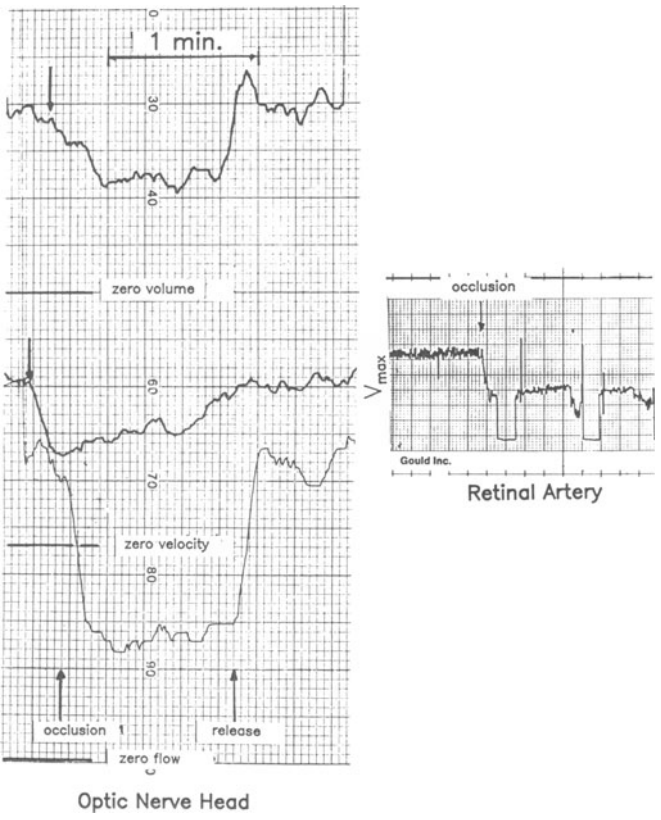

Figure 19–18B. Continuous recording of volume, velocity, and flow of blood from the optic nerve head and of V_{max} in a retinal artery of the cat during transient bilateral carotid occlusion.

imately 3 cycles/min (figure 19–19A). Interestingly, the variations in velocity and volume were always out of phase, with a phase difference of approximately 180°. [49]. These oscillatory variations are probably associated with the rhythmical, active vasomotion reported previously by others [50,51]. Similar oscillations were also observed in the choroidal circulation of the minipig, as shown in figure 19–19B, when a near-infrared (785 nm) laser beam was focused on an individual choroidal vessel. These recordings demonstrate that the laser-Doppler technique has the potential to become a useful tool for the study of vasomotion in the microcirculation of nervous tissue.

ACKNOWLEDGMENTS

The research described in this chapter has been supported by grants R01 EY-01303 and EY03242 from the National Eye Institute, by the Whitaker Foundation, Camp Hill, PA 17011, the Pennsylvania Lions Sight Conser-

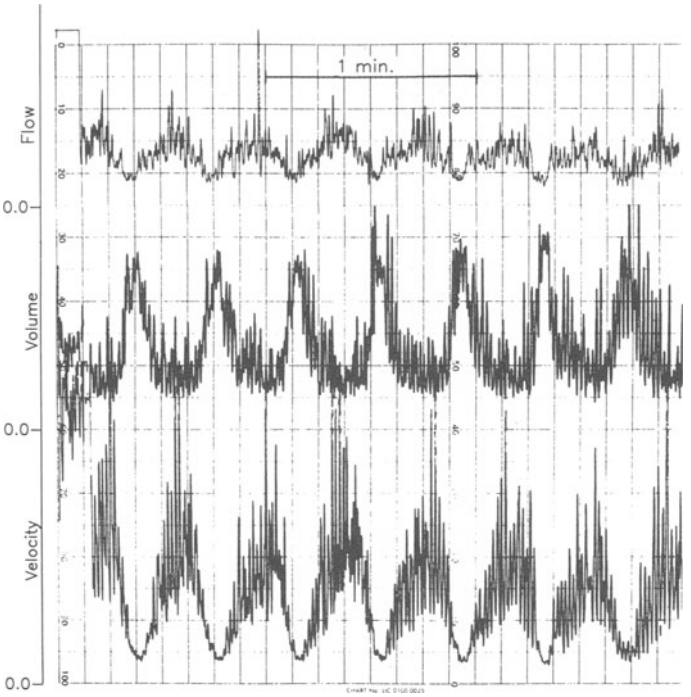

Figure 19–19A. Spontaneous rhythmic variations of the velocity, volume, and flow of blood in the optic nerve head microcirculation of an anesthetized minipig. The flow parameters are given in arbitrary units. Details on the anesthetic agents are given in [26]. Nominal area of recording was about 150 μm in diameter. The faster fluctuations are due to the heart cycle.

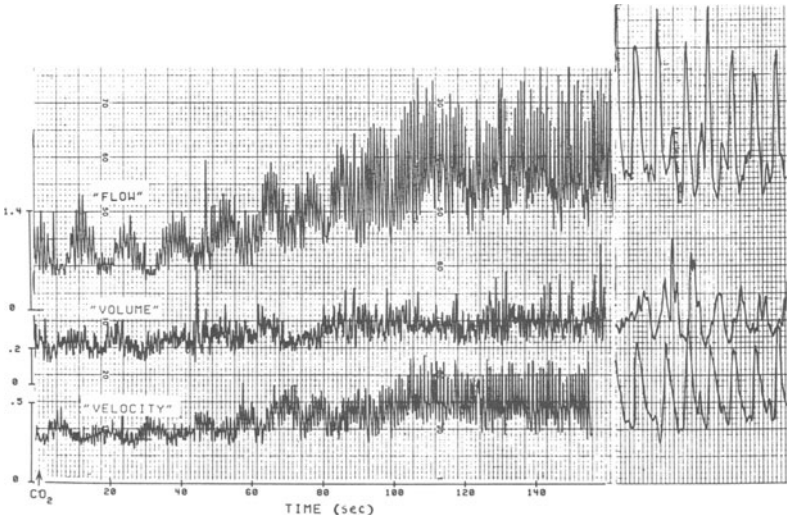

Figure 19–19B. Same type of rhythmic variations as in figure 19–19a but measured in a choroidal vessel of an anesthetized minipig during the breathing of CO_2. The time scale represents seconds. To the right of the picture, the fluctuations are shown on an expanded time scale to demonstrate the shape of the fluctuations due to the heart cycle (period of about one second). The laser beam used for the recordings in figures 19–19A and 19–19B was from a

vation and Eye Research Foundation, Inc., and the Vivian Simkins Lasko Retinal Vascular Research Fund.

REFERENCES

1. Riva, C.E., G.T. Timberlake, and G.T. Feke. 1979. Laser Doppler technique for measurement of eye movement. Appl Optics 18:2486–2490.
2. Zeimer, R., J.T. Wilenski, M.F. Goldberg, and S.A. Solin. 1981. Noninvasive measurement of optic nerve-head compliance by laser Doppler velocimetry. J Opt Soc Am [A] 71:499–501.
3. Alm, A., and A. Bill. 1975. The ocular circulation. In Adler's Physiology of the Eye—Clinical Application, Moses, R.A., ed. St. Louis: CV Mosby, p 210.
4. Hickam, J.B., and R. Frayser. 1966. Studies of the retinal circulation in man: Observation on vessel diameter, arteriovenous oxygen difference, and mean circulation time. Circulation 33:302–316.
5. Bulpitt, C.J., and C.T. Dollery. 1971. Estimation of retinal blood flow by measurement of the mean circulation time. Cardiovasc Res 5:406–412.
6. Riva, C.E., G.T. Feke, and I. Ben-Sira. 1978. Fluorescein dye-dilution technique and retinal circulation. Am J Physiol 234(3) (Heart Circ Physiol 3(3)):H315–H322.
7. Flower, R.W. 1972. Infrared absorption angiography of the choroid and some observations on the effect of high intraocular pressures. Am J Ophthalmol 74:600–614.
8. Riva, C.E., B. Ross, and G. Benedek. 1972. Laser Doppler measurements of blood flow in capillary tubes and retinal arteries. Invest Ophthalmol Vis Sci 11:936–944.
9. Tanaka, T., C.E. Riva, and I. Ben-Sira. 1974. Blood velocity measurements in human retinal vessels. Science 186:830–831.
10. Riva, C.E., and B.L. Petrig. Retinal blood flow: Laser Doppler velocimetry and blue field simulation technique. In New Developments in Noninvasive Studies to Evaluate Ocular Function, Masters, B., ed. New York: Springer-Verlag, in press.
11. Feke, G.T., and C.E. Riva. 1978. Laser Doppler measurements of blood velocity in human retinal vessels. J Opt Soc Am 68:526–531.
12. Benedek, G. 1969. Optical mixing spectroscopy, with applications to problems in physics, chemistry, biology and engineering. In Polarisation, Matiere et Rayonnement, volume jubilaire en l'honneur d'Alfred Kastler, French Physical Society, ed. Paris: Presses Universitaires de France, pp 49–84.
13. Lastovka, J.B. 1967. Light mixing spectroscopy and the spectrum of light scattered by thermal fluctuations in liquids. Ph.D. Thesis, Massachusetts Institute of Technology.
14. Riva, C.E., G.T. Feke, B. Eberli, and V. Benary. 1979. Bidirectional LDV system for absolute measurement of retinal blood speed. Appl Optics 18:2302–2306.
15. Riva, C.E., J.E. Grunwald, S.H. Sinclair, and B.L. Petrig. 1985. Blood velocity and volumetric flow rate in human retinal vessels. Invest Ophthalmol Vis Sci 26:1124–1132.
16. Petrig, B.L., and C.E. Riva. 1988. Retinal laser Doppler velocimetry: Towards its computer assisted clinical use. Appl Optics 27:1126–1134.
17. Riva, C.E., and G.T. Feke. 1981. Laser Doppler velocimetry in the measurement of retinal blood flow. In Current Laser Technology in Medicine and Surgery, Goldman, L., ed. New York: Springer, pp 135–161.
18. Feke, G.T., D.G. Goger, H.T. Tagawa, and F.C. Delori. 1987. Laser Doppler technique for absolute measurement of blood speed in retinal vessels. IEEE Trans Biomed Eng BME-34:673–680.
19. Riva, C.E., J.E. Grunwald, S.H. Sinclair, and K. O'Keefe. 1981. Fundus camera based retinal laser Doppler velocimeter. Appl Optics 20:117–120.
20. Riva, C.E., B.L. Petrig, and J.E. Grunwald. 1987. Near infrared retinal laser Doppler velocimetry. Lasers Ophthalmol 1:211–215.
21. Van de Hulst, H.C. 1957. Light Scattering by Small Particles. New York: Wiley.
22. Riva, C.E., R.D. Shonat, B.L. Petrig, and C.J. Pournaras. 1989. Scattering process in LDV from retinal vessels. Appl Optics.
23. Bonner, R., and R. Nossal. 1981. Model for laser Doppler measurements of blood flow in tissue. Appl Optics 21:2097–2107.
24. Stern, M.D. 1985. Laser Doppler velocimetry in blood and multiply scattering fluids: Theory Appl Optics 24:1968–1986.

25. Riva, C.E., J.E. Grunwald, and S.H. Sinclair. 1983. Laser Doppler velocimetry study of the effect of pure oxygen breathing on retinal blood flow. Invest Ophthalmol Vis Sci 24:47–51.
26. Riva, C.E., C.J. Pournaras, and M. Tsacopoulos. 1986. Regulation of local oxygen tension and blood flow in the inner retina during hyperoxia. J Appl Physiol 61(2):592–598.
27. Robinson, F., C.E. Riva, J.E. Grunwald, B.L. Petrig, and S.H. Sinclair. 1986. Retinal blood flow autoregulation in response to an acute increase in blood pressure. Invest Ophthalmol Vis Sci 27:722–726.
28. Riva, C.E., J.E. Grunwald, and B.L. Petrig. 1986. Autoregulation of human retinal blood flow. An investigation with laser Doppler velocimetry. Invest Ophthalmol Vis Sci 27:1706–1712.
29. Feke, G.T., R. Zuckerman, G.T. Green, and J.J. Weiter. 1983. Response of human retinal blood flow to light and dark. Invest Ophthalmol Vis Sci 24:136–141.
30. Riva, C.E., J.E. Grunwald, and B.L. Petrig. 1983. Reactivity of the human retinal circulation to darkness: A laser Doppler velocimetry study. Invest Ophthalmol Vis Sci 24:737–740.
31. Kohner, E.M. 1975. Dynamic changes in the microcirculation of diabetics as related to diabetic microangiopathy. Acta Med Scand Suppl 578:41–47.
32. Grunwald, J.E., C.E. Riva, S.H. Sinclair, A.J. Brucker, and B.L. Petrig. 1986. Laser Doppler velocimetry study of retinal circulation in diabetes mellitus. Arch Ophthalmol 104:991–996.
33. Feke, G.T., H. Tagawa, A. Yoshida, D.G. Goger, J.J. Weiter, S.M. Buzney, and J.W. McMeel. 1985. Retinal circulatory changes related to retinopathy progression in insulin dependent diabetes mellitus. Ophthalmology 92:1517–1522.
34. Grunwald, J.E., C.E. Riva, A.J. Brucker, S.H. Sinclair, and B.L. Petrig. 1982. Altered retinal vascular response to 100% oxygen breathing in diabetes mellitus. Ophthalmology 89:757–762.
35. Grunwald, J.E., C.E. Riva, A.J. Brucker, S.H. Sinclair, and B.L. Petrig. 1986. Effect of panretinal photocoagulation on retinal blood flow in proliferative diabetic retinopathy. Ophthalmology 93:590–595.
36. Grunwald, J.E., Brucker, A.J., Petrig, B.L., and Riva, C.E. 1989. Retinal blood flow regulation and the clinical response to panretinal photocoagulation in proliferative diabetic retinopathy. Opthamology 96:1518–1522.
37. Grunwald, J.E., C.E. Riva, D.B. Martin, A.R. Quint, and P.A. Epstein. 1987. Effect of an insulin-induced decrease in blood glucose on the human diabetic retinal circulation. Ophthalmology 94:1614–1620.
38. Grunwald, J.E. 1986. Effect of topical timolol on the human retinal circulation. Invest Ophthalmol Vis Sci 27:1713–1719.
39. Green, J.G., G.T. Feke, D.G. Goger, and J.W. McMeel. 1983. Clinical application of laser Doppler technique for retinal blood flow studies. Arch Ophthalmol 101:971–974.
40. Grunwald, J.E., C.E. Riva, and D.M. Kozart. 1988. Retinal circulation during spontaneous rise of intraocular pressure. Br J Ophthalmol 72:754–758.
41. Yoshida, A., G.T. Feke, J.G. Green, D.G. Goger, M. Matsuhashi, A.E. Jalkh, and J.W. McMeel. 1983. Retinal circulatory changes after scleral buckling procedures. Am J Ophthalmol 95:182–188.
42. Delori, F.C., J.S. Parker, and M.A. Mainster. 1980. Light levels of fundus photography and fluorescein angiography. Vision Res 20:1099–1104.
43. Riva, C.E., G.T. Feke, and M. Loebl. 1976. Laser Doppler measurement of blood flow in the fundus of the human eye. Proceedings of the 1976 Electro-Optical System Design/ International Laser Conference. Chicago: Industrial and Scientific Management, pp 142–147.
44. Stern, M.D. 1975. In vivo evaluation of microcirculation by coherent light scattering. Nature 254:56–58.
45. Stern, M.D., and D.L. Lappe. 1978. Method and apparatus for measurement of blood flow using coherent light. U.S. Patent No 4, 109, 647.
46. Riva, C.E., J.E. Grunwald, and S.H. Sinclair. 1982. Laser Doppler measurement of relative blood velocity in the human optic nerve head. Invest Ophthalmol Vis Sci 22:241–248.
47. Sebag, J., G.T. Feke, F.C. Delori, and J.J. Weiter. 1985. Anterior optic nerve blood flow in experimental optic atrophy. Invest Ophthalmol Vis Sci 26:1415–1422.
48. Riva, C.E., R.D. Shonat, and B.L. Petrig. 1989. Noninvasive investigation of the optic

nerve head circulation. In Noninvasive Assessment of the Visual System, 1989 Technical Digest Series, vol. 7. Washington, DC: Optical Society of America, pp 158–161.
49. Riva, C.E., C.J. Pournaras, C.L. Poitry-Yamate, and B.L. Petrig. 1989. Evidence for spontaneous rhythmic flow changes in the optic nerve head, retinal and choroidal circulations. Invest Ophthalmol Vis Sci Suppl 30:137.
50. Salerud, E.G., T. Tenland, G.E. Nilsson, and P.A. Oberg. 1983. Rhythmical variations in human skin blood flow. Int J Microcirc Clin Exp 2:91–102.
51. Colantuoni, A., S. Bertuglia, and M. Intaglietta. 1984. Quantitation of rhythmic diameter changes in arterial microcirculation. Am J Physiol 246 (Heart Circ Physiol 15):H508–H517.

GLOSSARY

ABSORPTION CROSS SECTION. The ratio of the power (in watts) absorbed by a particle to the light intensity (watts per m^2) incident on the absorbing particle. The absorption cross section usually has units of area and is a measure of the probability that light will be absorbed in the apparent geometric area of interest, e.g., 0.1 μm^2 for a red blood cell exposed to 800 nm light. As used in chapter 2, Σa is the cross section summed over the number of particles per unit volume of tissue, so it has the units of inverse length.

AUTOCORRELATION FUNCTION. A technique for comparing a signal at one instant with itself at another time. The autocorrelation function is the mean value of the product of the intensity of a signal at any instant with its intensity at a later time. The autocorrelation function is often used for detecting deterministic data masked by a random background but, in the case of dynamic light scattering, is used to obtain a measure of the random movements of scattering centers. Information discerned by autocorrelation analysis in the time domain is equivalent to information obtained by spectral analysis as a function of frequency.

BEAT FREQUENCY. The difference frequency that occurs when two waves with different frequencies are added. In laser-Doppler flowmetry, the beat frequency is very often the difference between the frequency of a Doppler-shifted wave and a nonshifted wave that has the same frequency as

the light source. However, it also may represent the difference between the frequencies of two waves, each of which has been shifted in frequency because of photon interactions with moving cells.

COHERENCE. The existence of a correlation between the phases of two or more waves, so that interference effects may be produced between them. See also *Spatial Coherence* and *Temporal Coherence.*

COHERENT LIGHT. Radiant electromagnetic energy of the same, or almost the same, wavelength, and with definite phase relationships between different points in the field.

COMMON-MODE REJECTION. The ability of an electronic circuit (very often a differential amplifier) to suppress a signal present on two inputs. This technique can be effective in reducing correlated noise common to both inputs, but it is ineffective in reducing random noise.

CW LASER. A laser that operates continuously (CW = continuous wave), the opposite of a pulsed or modulated laser. CW lasers typically exhibit a high degree of spatial or temporal coherence.

EQUIVALENT SPHERE. A perfect sphere with the same volume as a non-spherical particle such as a red blood cell. Such abstractions are used in light-scattering theories because the scattering from a perfect sphere can be described by simple mathematical expressions, whereas that from red blood cells requires complex anaytical forms of uncertain reliability.

FIRST MOMENT OF A FREQUENCY SPECTRUM. The sum of the products obtained by multiplying each frequency by the probability of a fluctuation occurring at that frequency. This quantity provides the mean frequency of Doppler-shifted and unshifted components.

GRADED-INDEX FIBER. Optical fiber in which the index of refraction of the core varies radially so as to minimize the temporal dispersion and interference among different light paths within the fiber.

INTENSITY AUTOCORRELATION FUNCTION. See *Autocorrelation Function.*

ISOTROPIC. Having the ability to scatter light equally in all diretions.

MONOCHROMATIC. Light having a single frequency or wavelength is said to have a single color or to be monochromatic.

OPTICAL PATHLENGTH. The distance a photon travels in a medium. As used here, the optical pathlength or photon pathlength is the mean distance a detected photon travels within the tissue.

QUASI-ELASTIC SCATTERING. Light scattering in which energy is conserved but that results in a change in momentum, so that the wave vector after scattering differs from that of the incident radiation.

RBC PATHLENGTH. A measure of microcirculatory tortuosity that relates the product of red blood cell concentration and mean RBC speed to volumetric flow. It is the equivalent mean distance that an RBC travels within the volume sampled by the laser light.

RMS CONVERTER. A detection principle often used in the measurement of random signals. The signal is first squared in a nonlinear element and then averaged to form the mean value. Finally, the square root of the averaged value is taken (RMS = root-mean-square).

SCATTERED FIELD. The electromagnetic field caused by light scattering from dipoles induced by the incident radiation; in other words, the radiation field generated by secondary dipoles in a region excited by an incident electromagnetic wave (light beam). The dipoles oscillate with the same frequency as the incident field, and the secondary radiation is generally scattered in all directions.

SCATTERING CROSS SECTION. The ratio of the power (in watts) scattered in all directions to the light intensity incident on the scattering particle. The scattering cross section usually has units of area and is a measure of the probability that light will be scattered in the apparent geometric area of interest, e.g., 40 μm^2 for a red blood cell exposed to 800 nm light. As used in chapter 2, Σ_{sc} is the cross section summed over the number of particles per unit volume of tissue, so it has the units of inverse length.

SCATTERING LENGTH. The mean distance between scattering events.

SPATIAL COHERENCE. If an optical field is spatially coherent, the intensity at all points in the medium can be determined if the intensity at one point is known.

SPECKLE PATTERN. An interference pattern created by a large number of monochromatic waves with different phase relations. The pattern consists of randomly distributed bright and dark spots. At the points where the rays are in phase, they enhance each other, producing a local high intensity. However, at points where the rays have opposite phase relations, they cancel each other, and the result is a dark spot.

SQUARE LAW DETECTOR. A nonlinear photodetector (such as a photomultipler tube) in which a photocurrent is produced proportional to the square of the total electric field falling on the photosensitive surface of the device.

STEP-INDEX FIBER. An optical fiber with a uniform refractive index within the core (which is higher than that of the cladding). In such fibers, temporal dispersion and interference effects among different light paths are much larger than for graded-index fibers.

TEMPORAL COHERENCE. A property of most laser beams in which the

field at one time determines the field at that point for subsequent times within an interval known as the coherence time.

VECTOR. The representation of a quantity having magnitude and direction. The motions of electromagnetic waves and red blood cells can be represented by vectors.

WAVE VECTOR. A vector that describes the propagation of light. See also *Vector.*

WOLLASTON PRISM. A polarizing prism used for separation of differently polarized beams. This type of prism gives a symmetrical deviation of the beams leaving the prism.

MANUFACTURERS OF LASER-DOPPLER BLOOD FLOWMETERS

Advance Company, Ltd.
5–7, Nihonbashi-Kobunacho-Chuo-ku
Tokyo 103, JAPAN
Phone: +81–3–664–6271
Telex J27687 CYRAX
Fax: +81–3–667–9523

Biomedical Science, Inc.
2–7, Awagasaki, Kanzawa
Ishikawa 920–02, JAPAN
Phone: +81–762 38 9528
Fax: +81–762 38 9790

Canon Inc.
53, Imaikarni-cho, Nakahara-ku, Kawasaki
Kanagawa 211, JAPAN
Phone: +81–44 733 3520
Telex: 3842738 CANONK J
Fax: +81–44 733 5051
Note: Available only in Japan

DIODOPP
Applied Laser Technology
Ceresstraat 2
5721 ZK ASTEN
P.O. Box 150
5700 AD ASTEN
The Netherlands
Phone: 4936–5885

Medpacific Corporation*
6701 Sixth Avenue South
Seattle, Washington, USA 98108
Phone: 206 763–9177
Telex: 32–8891
Note: No longer manufacturing

Perimed*
Box 5607
Stockholm, Sweden S 114 86
Phone: +46–8–22 25 40
Telex: 14375 STURES

Perimed, Inc.*
800 Centennial Avenue
Piscataway, New Jersey, USA 08855–1327
Phone: (201) 457–9111
Fax: (201) 457–8301

Perimed UK, Ltd
31 Pinecroft Road
Ipswich, Suffolk IPI 6BW
United Kingdom
Phone: 44 (473) 24 12 14
Fax: 44–473211508

TSI Incorporated*
500 Cardigan Road
Box 64394
St. Paul, Minnesota, USA 55164
Phone: 612 483–0900
Telex: 6879024
Fax: 612 481–1220

* Manufacturer whose flowmeter is described in this book.

INDEX